ISOTOPIC GEOCHEMISTRY OF NATURAL GAS

EDITED BY: Yunyan Ni, Qinhong Hu, Maowen Li, Tongwei Zhang and Deyu Gong
PUBLISHED IN: Frontiers in Earth Science

frontiers Research Topics

frontiers

ISSN 1664-8714
ISBN 978-2-83250-360-7
DOI 10.3389/978-2-83250-360-7

About Frontiers

Frontiers is more than just an open-access publisher of scholarly articles: it is a pioneering approach to the world of academia, radically improving the way scholarly research is managed. The grand vision of Frontiers is a world where all people have an equal opportunity to seek, share and generate knowledge. Frontiers provides immediate and permanent online open access to all its publications, but this alone is not enough to realize our grand goals.

Frontiers Journal Series

The Frontiers Journal Series is a multi-tier and interdisciplinary set of open-access, online journals, promising a paradigm shift from the current review, selection and dissemination processes in academic publishing. All Frontiers journals are driven by researchers for researchers; therefore, they constitute a service to the scholarly community. At the same time, the Frontiers Journal Series operates on a revolutionary invention, the tiered publishing system, initially addressing specific communities of scholars, and gradually climbing up to broader public understanding, thus serving the interests of the lay society, too.

Dedication to Quality

Each Frontiers article is a landmark of the highest quality, thanks to genuinely collaborative interactions between authors and review editors, who include some of the world's best academicians. Research must be certified by peers before entering a stream of knowledge that may eventually reach the public - and shape society; therefore, Frontiers only applies the most rigorous and unbiased reviews.
Frontiers revolutionizes research publishing by freely delivering the most outstanding research, evaluated with no bias from both the academic and social point of view. By applying the most advanced information technologies, Frontiers is catapulting scholarly publishing into a new generation.

What are Frontiers Research Topics?

Frontiers Research Topics are very popular trademarks of the Frontiers Journals Series: they are collections of at least ten articles, all centered on a particular subject. With their unique mix of varied contributions from Original Research to Review Articles, Frontiers Research Topics unify the most influential researchers, the latest key findings and historical advances in a hot research area! Find out more on how to host your own Frontiers Research Topic or contribute to one as an author by contacting the Frontiers Editorial Office: frontiersin.org/about/contact

ISOTOPIC GEOCHEMISTRY OF NATURAL GAS

Topic Editors:
Yunyan Ni, Research Institute of Petroleum Exploration and Development (RIPED), China
Qinhong Hu, University of Texas at Arlington, United States
Maowen Li, SINOPEC Petroleum Exploration and Production Research Institute, China
Tongwei Zhang, University of Texas at Austin, United States
Deyu Gong, Research Institute of Petroleum Exploration and Development (RIPED), China

Citation: Ni, Y., Hu, Q., Li, M., Zhang, T., Gong, D., eds. (2022). Isotopic Geochemistry of Natural Gas. Lausanne: Frontiers Media SA.
doi: 10.3389/978-2-83250-360-7

Table of Contents

frontiers | Frontiers in Earth Science

TYPE Editorial
PUBLISHED 15 September 2022
DOI 10.3389/feart.2022.1013940

OPEN ACCESS

EDITED AND REVIEWED BY
Martyn Tranter,
Aarhus University, Denmark

*CORRESPONDENCE
Yunyan Ni,
niyy@petrochina.com.cn

SPECIALTY SECTION
This article was submitted to Geochemistry, a section of the journal Frontiers in Earth Science

RECEIVED 08 August 2022
ACCEPTED 12 August 2022
PUBLISHED 15 September 2022

CITATION
Ni Y, Hu Q, Li M, Zhang T and Gong D (2022), Editorial: Isotopic geochemistry of natural gas.
Front. Earth Sci. 10:1013940.
doi: 10.3389/feart.2022.1013940

Editorial: Isotopic geochemistry of natural gas

Yunyan Ni[1]*, Qinhong Hu[2], Maowen Li[3], Tongwei Zhang[4] and Deyu Gong[1]

[1]PetroChina Research Institute of Petroleum Exploration and Development, Beijing, China, [2]Department of Earth and Environmental Sciences, University of Texas at Arlington, Arlington, VA, United States, [3]Sinopec Petroleum Exploration and Production Research Institute, Beijing, China, [4]Bureau of Economic Geology, University of Texas at Austin, Austin, TX, United States

KEYWORDS

China, natural gas, shale gas, helium, CO_2, isotope geochemistry, natural gas

Editorial on the Research Topic
Isotopic geochemistry of natural gas

After decades of development guided by coal-derived gas theories, China's natural gas exploration has made significant progress, with natural gas becoming an important component of China's energy supply mix. With an increasing demand for clean energy, China's annual domestic gas production has increased from 130×10^9 m^3 in 2014 to 209×10^9 m^3 in 2021. China has also changed from a gas-poor country to a major gas-producing country. Eight years have passed since four Research Topic were published on natural gas in Chinese sedimentary basins: three on natural gas geochemistry in the journals of *Organic Geochemistry* (2005; 2014) and *Energy, Exploration & Exploitation* (2014), and another on the geology of giant gas fields in China in the journal of *Marine and Petroleum Geology* (2008). Drilling targets for natural gas exploration have been becoming very complex, extending from conventional traps to more unconventional "continuous" accumulations and to deep-and-ultra-deep seated petroleum plays. More efficient and cost-effective exploration and development of such resources put forward higher requirements for gas research, including the aspects of isotope geochemistry.

As suggested by Professor Jinxing Dai, Member of the Chinese Academy of Sciences, we organized this thematic Research Topic on Isotope Geochemistry of Natural Gas. It contains 13 articles, covering four broad themes: gas-source correlation of conventional natural gas; isotopic geochemistry and origin of unconventional gas (shale gas and tight gas); geochemistry of non-hydrocarbon gases (CO_2, He, etc.); and geological controls on hydrocarbon gas occurrence. The Issue introduces important progress and achievements that have been made in natural gas geochemistry and exploration in China over the past several years.

Three articles focus on the molecular composition and isotopic geochemistry of conventional natural gases, by presenting the latest results in the Sichuan, Tarim, and Junggar basins, respectively. A scheme of natural gas classification was developed, with case studies illustrating the complexity in the chemical composition and hence the origin of natural gases in different basins. Results indicate that four types of gases occur in the

Junggar Basin, whereas the Middle Triassic Leikoupo Formation in the Sichuan Basin hosts natural gases derived from either sapropelic or humic organic matter.

The past several years have been a successful period for China in developing shale gas resource in tectonically relative complex regions, and has made China the first country outside of North America to achieve large-scale economic shale gas development. With the discovery and development of giant shale gas fields such as Fuling, Changning-Weiyuan, and Zhaotong, China's shale gas production reached 22.9×10^9 m^3 or slightly more than 10% of total domestic gas production in 2021. Three articles in this Issue are devoted to the in-depth discussion of shale gas geochemistry and origin of the Upper Ordovician-Lower Silurian Wufeng-Longmaxi formations, using stable carbon, hydrogen, and mercury isotopes.

Helium is an important strategic resource and has great significance for national energy security. With a total of three articles, this Issue has made comprehensive and in-depth studies of the helium gas geochemistry in the Ordos and Bohai Bay Basins. Results from both basins indicate that helium is of a crustal origin, and is likely derived from the radioactive decay of U and Th in the rocks and minerals, with no significant contribution from atmospheric or mantle-derived helium. Geological factors controlling the potential of large helium gas accumulation are explored in the context of deep sedimentary strata and deep geofluids. The occurrence and origin of non-hydrocarbon gases, such as CO_2 and tight gas, and light hydrocarbon gas are also discussed.

Natural gas has attracted more and more attention as the main clean energy resource in the global transition to green energy. With the exploration and development of natural gas resources increasingly targeting fields that are unconventional, in greater burial depth, or with greater stratigraphic complexity, the isotope gas geochemistry is expected to play a more important role in helping exploration geologists and development engineers to understand the gas systems, and come up with creative solutions for cost-effective and sustainable development. Results presented in this thematic Research Topic will certainly provide an excellent source of references for those involved in upper stream natural gas research and production, particularly for those who are working in tectonically complex basins.

Author contributions

All authors listed have made a substantial, direct, and intellectual contribution to the work and approved it for publication.

Conflict of interest

YN and DG were employed by PetroChina Research Institute of Petroleum Exploration and Development.

The remaining authors declare that the research was conducted in the absence of any commercial or financial relationships that could be construed as a potential conflict of interest.

Publisher's note

frontiers in Earth Science

ORIGINAL RESEARCH
published: 28 January 2022
doi: 10.3389/feart.2021.823319

Geochemical Characteristics and Origin of Tight Gas in Member Two of the Upper Triassic Xujiahe Formation in Western Sichuan Depression, Sichuan Basin, SW China

Xiaoqi Wu[1,2], *Quanyou Liu*[1,3]*, *Yingbin Chen*[1,2], *Jun Yang*[1,2], *Huasheng Zeng*[1,2] and *Huaji Li*[4]

[1]State Key Laboratory of Shale Oil and Gas Enrichment Mechanisms and Effective Development, Beijing, China, [2]Wuxi Research Institute of Petroleum Geology, Petroleum Exploration and Production Research Institute, Wuxi, China, [3]Petroleum Exploration and Production Research Institute, Beijing, China, [4]Exploration and Production Research Institute, Southwest Branch Company, Chengdu, China

Natural gas in the tight sandstone reservoirs in Member two of the Upper Triassic Xujiahe Formation in the Western Sichuan Depression of the Sichuan Basin has complex geochemical characteristics, and the origin and source of the tight gas are revealed based on the geochemical analysis and comparison in this study. The tight gas has the dryness coefficient of 0.950–0.994, which is positively correlated with the CH_4 content. The gaseous alkanes display positive carbon isotopic series, with the $\delta^{13}C_1$ and $\delta^{13}C_2$ values ranging from –35.6‰ to –30.3‰ and from –29.1‰ to –21.0‰, respectively, and the δD_1 values range from –176‰ to –155‰. Genetic identification based on the carbon and hydrogen isotopic compositions indicates that a small amount of tight gas is typically coal-derived gas, whereas most of the tight-gas samples have experienced mixing by oil-associated gas. Geochemical comparisons suggest that the tight gas displays distinct differences with the typical oil-associated gas in Member four of the Middle Triassic Leikoupo Formation in the Chuanxi gas field and the typical coal-derived gas in Member five of Xujiahe Formation in the Xinchang gas field. It is also apparently different from the typical coal-derived gas in Member two of Xujiahe Formation in both Zhongba and Qiongxi gas fields. Among the tight gas in Member two of the Xujiahe Formation from the Western Sichuan Depression, the coal-derived gas is generated mainly by the humic mudstone in the Upper Triassic Ma'antang and Xiaotangzi formations, with assistance of the humic mudstone in Member two of the Xujiahe Formation, whereas the oil-associated gas is derived from the sapropelic limestone in the Ma'antang Formation.

Keywords: tight gas, geochemical characteristics, genetic types, gas source, xujiahe formation

OPEN ACCESS

Edited by:
Deyu Gong,
Research Institute of Petroleum Exploration and Development (RIPED), China

Reviewed by:
Xiaofeng Wang,
Northwest University, China
Haifeng Gai,
Guangzhou Institute of Geochemistry (CAS), China

***Correspondence:**
Quanyou Liu
qyouliu@sohu.com

Specialty section:
This article was submitted to Geochemistry, a section of the journal Frontiers in Earth Science

Received: *27 November 2021*
Accepted: *24 December 2021*
Published: *28 January 2022*

Citation:
Wu X, Liu Q, Chen Y, Yang J, Zeng H and Li H (2022) Geochemical Characteristics and Origin of Tight Gas in Member Two of the Upper Triassic Xujiahe Formation in Western Sichuan Depression, Sichuan Basin, SW China. Front. Earth Sci. 9:823319. doi: 10.3389/feart.2021.823319

1 INTRODUCTION

Tight-gas reservoirs refer to the tight sandstone fields or traps which accumulate commercial natural gas, and they can be divided into continuous-type and trap-type (Dai et al., 2012a). As one important type of unconventional natural gas, tight gas has made a crucial contribution to the rapid increase of both the yields and reserves of natural gas in China. The proven reserves of tight gas in China reached

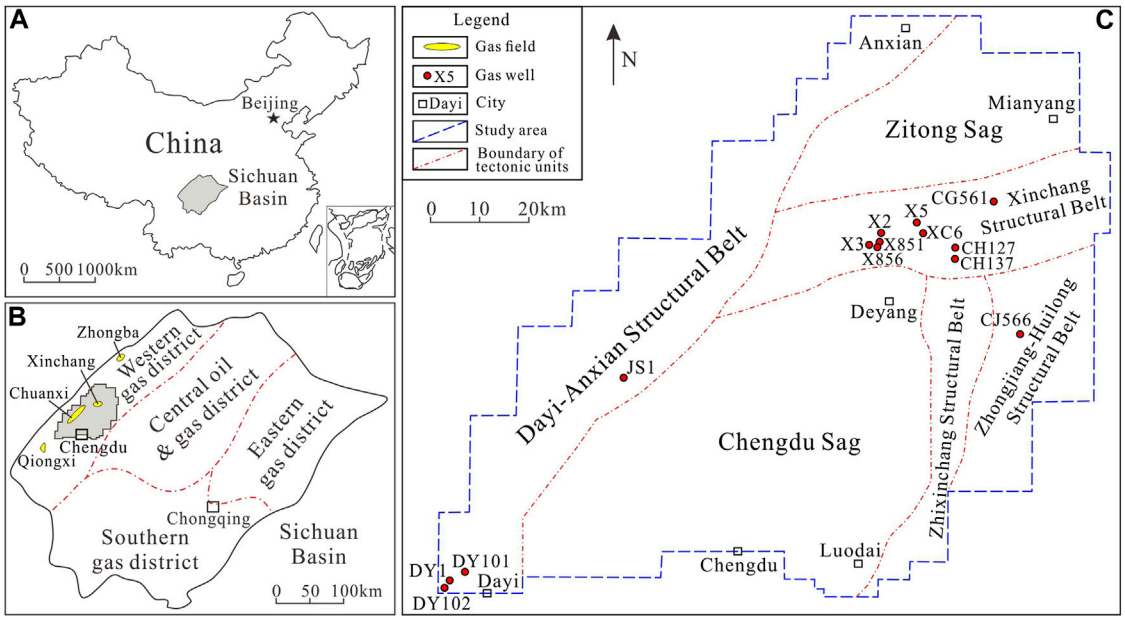

FIGURE 1 | The position of the Sichuan Basin in China **(A)**, the location of the depression in the Sichuan Basin **(B)**, and distribution of gas wells and structural units in the Western Sichuan Depression **(C)**.

3.0109×10^{12} m^3 by the end of 2010, which accounted for 39.2% of the total gas reserves (Dai et al., 2012a).

The Sichuan Basin is one of the important onshore petroliferous basins in China, and the exploration fields include terrigenous and marine strata (Dai et al., 2009; Dai et al., 2012b; Liu et al., 2012; Liu et al., 2013; Liu et al., 2014; Liu et al., 2016), with the former consisting of tight sandstone reservoirs in both the Upper Triassic Xujiahe Formation (T_3x) and Jurassic strata. The Zhongba gas field in Member two of the Xujiahe Formation (T_3x^2), located in the western Sichuan Basin, is the first tight-gas field discovered in China (Dai et al., 2014). Several giant tight-gas fields (e.g., Xinchang, Guang'an, Hechuan, and Anyue) with proven reserves exceeding 10×10^9 m^3 have been revealed during the gas exploration in the Xujiahe Formation of the Sichuan Basin (Dai et al., 2014).

The Western Sichuan Depression (WSD) is situated in the western Sichuan Basin, and the gas exploration has achieved successive breakthroughs in the Middle Triassic to Jurassic strata (Wu et al., 2017; Wu et al., 2020a; Wu et al., 2020b). The Member two of the Middle Triassic Xujiahe Formation (T_3x^2) has attracted wide attention due to the favorable exploration potential. The proven reserves of T_3x^2 in the Xinchang gas field from WSD are 121.12×10^9 m^3 (Dai, 2016), and the Zhongba and Qiongxi gas fields have also been discovered in the adjacent areas (Dai et al., 2012b).

The origin and source of tight gas in different strata of the Sichuan Basin have been extensively studied based on geochemical analysis, and the tight gas in the T_3x and Jurassic strata is considered as typical coal-derived gas and sourced mainly from the T_3x coal-measure source rocks (Dai et al., 2009; Dai et al., 2012b; Ni et al., 2014a; Ni et al., 2014b; Wu et al., 2017; Dai et al., 2018; Wu et al., 2019). The T_3x^2 gas from WSD displays complex geochemical characteristics, which are significantly different from the typical coal-derived gas from other members of T_3x. The authors intend to conduct geochemical analysis of the main components and stable carbon and hydrogen isotopes of the T_3x^2 gas from WSD, in order to reveal the genetic types and source of the gas as well as the differences with other reservoirs in the same area.

2 GEOLOGICAL SETTING

The Sichuan Basin is developed on the basis of the Upper Yangtze Craton in SW China (**Figure 1A**), covering an area of 180×10^3 km^2. It is the third largest petroliferous basin in China and superimposed by a marine craton and a terrigenous foreland basin. The annual gas yield in 2020 reaches 56.5×10^9 m^3, making it become the most productive petroliferous basin in China (Zhang, 2021). It consists of four exploration districts based on the structural units, i.e., Western, Eastern, and Southern gas districts, and Central oil and gas district (Dai et al., 2009).

The WSD is located in the central part of the Western gas district (**Figure 1B**), covering an area of 10×10^3 km^2. It is generally divided into four structural belts (Dayi-Anxian, Xinchang, Zhixinchang, and Zhongjiang-Huilong) and two sags (Zitong and Chengdu) (**Figure 1C**). The commercial gas wells in the Member two of the Xujiahe Fm. (T_3x^2) are mainly situated in the Xinchang and Dayi-Anxian Structural Belts (**Figure 1C**). The Qiongxi and Zhongba gas fields have been discovered in natural gas exploration to the southwest and north of WSD, respectively (**Figure 1B**).

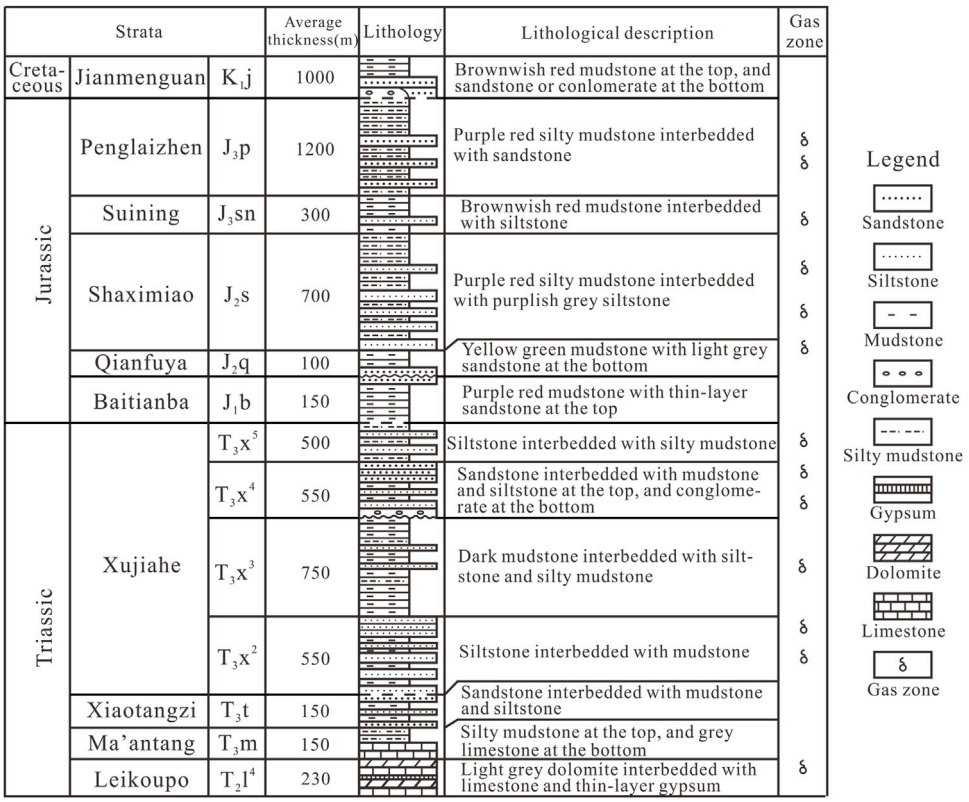

FIGURE 2 | Stratigraphic column of the Western Sichuan Depression, Sichuan Basin, China.

There are multiple gas-bearing layers in WSD, and the gas exploration has been conducted in Member four of the Middle Triassic Leikoupo Fm. (T_2l^4), Upper Triassic Xujiahe Fm. (T_3x), and Jurassic strata (**Figure 2**). The Xujiahe Fm. is commonly divided into six members bottom-up, i.e., Member 1 (T_3x^1) to Member 6 (T_3x^6), in which Member six is missing in the WSD due to weathering denudation, and Member one is generally divided into Xiaotangzi (T_3t) and Ma'antang (T_3m) formations (**Figure 2**). Member two of the Xujiahe Fm. (T_3x^2) consists of siltstone interbedded with mudstone, and it is conformably and disconformably contacted with the overlying Member three of T_3x and underlying T_3t, respectively.

3 SAMPLES AND ANALYTICAL METHODS

The T_3x^2 tight-gas samples in the WSD of the Sichuan Basin were collected from the wellheads using 5-cm-radius stainless steel cylinders with double valves, and the lines were flushed for 10–15 min in order to remove air contamination at first. A geochemical analysis of the gas samples was conducted at the Wuxi Research Institute of Petroleum Geology, Petroleum Exploration and Production Research Institute, SINOPEC.

The chemical composition of gas samples measured using an Agilent 7890A gas chromatograph (GC) equipped with a flame ionization detector and a thermal conductivity detector. Individual alkane gas components were separated using a capillary column (PLOT Al_2O_3 50 m × 0.53 mm × 25 μm). Helium was used as the carrier gas with a rate of 40 ml/min and unsplit stream sampling. The GC oven temperature was initially set at 40°C for 5 min, heating at a rate of 10°C/min to a final temperature of 180°C, which was held for 20 min.

The stable carbon isotopic composition of alkane gases was measured on a Finnigan MAT 253 mass spectrometer. The alkane gas components were initially separated using a fused silica capillary column (PLOT Q 30 m × 0.32 mm × 20 μm) with helium carrier gas at the flow rate of 10 ml/min. The gas was injected into the GC in the split injection model with the split ratio of 15:1. The oven temperature was ramped from 40°C to 180°C at a heating rate of 10°C/min, and the final temperature was held for 10 min. Each gas sample was measured in triplicate, and the results were averaged. Stable carbon isotopic values are reported in the δ notation in per mil (‰) relative to VPDB, and the measurement precision is estimated to be ±0.5‰ for $\delta^{13}C$.

The stable hydrogen isotopic composition of alkane gases was measured on a Thermo Scientific Delta V Advantage mass spectrometer (GC/TC/IRMS). The alkane gas components were separated on an HP-PLOT Q column (30 m × 0.32 mm × 20 μm) with helium carrier gas at 1.5 ml/min. The gas was injected into the GC in the split injection model with the split ratio of 15:1. The GC oven was initially held at 30°C for

TABLE 1 | Main components and stable carbon and hydrogen isotopic compositions of the T_3x^2 tight gas from the Western Sichuan Depression.

Tectonic units	Well	Components (%)						C_1/C_{1-4}	$\delta^{13}C$ (‰)			δD (‰)		
		CH_4	C_2H_6	C_3H_8	C_4H_{10}	N_2	CO_2		$\delta^{13}C_1$	$\delta^{13}C_2$	$\delta^{13}C_3$	δD_1	δD_2	δD_3
Dayi-Anxian Structural Belt	DY1	96.50	1.74	0.21	0.05	0.27	1.18	0.980	−32.0	−25.0	—	−160	—	—
	DY101	94.16	3.14	0.48	0.15	0.41	1.54	0.961	−31.8	−21.2	—	−163	—	—
	DY102	96.77	1.42	0.17	0.00	0.00	1.65	0.984	−32.7	−24.0	−24.9	−163	—	—
	JS1	96.68	0.51	0.04	0.04	0.69	1.94	0.994	−32.8	−25.3	−27.5	—	—	—
Xinchang Structural Belt	X2	97.28	0.83	0.07	0.02	0.23	1.53	0.991	−31.9	−28.3	—	−155	—	—
	X3	97.51	0.94	0.09	0.02	0.25	1.17	0.989	−31.4	—	—	−157	—	—
	X5	97.54	0.94	0.10	0.00	0.00	1.42	0.989	−31.6	−28.4	−28.2	−166	—	—
	X8-1H	97.27	0.80	0.08	0.00	0.55	1.28	0.991	−32.2	−26.7	−25.5	−159	−148	—
	X851	98.14	0.82	0.09	0.03	0.08	0.82	0.991	−30.3	−27.1	—	—	—	—
	X853	97.12	0.82	0.08	0.02	0.42	1.44	0.991	−31.2	−27.3	—	−159	—	—
	X856	97.45	0.81	0.07	0.02	0.63	0.94	0.991	−30.8	−29.1	−28.1	−157	−151	−115
	XC6	97.39	1.06	0.12	0.00	0.00	1.43	0.988	−31.9	−26.4	−26.8	−165	—	—
	CH127	97.18	0.83	0.07	0.02	0.65	1.11	0.991	−32.1	−26.8	−27.0	−163	−161	−123
	CH137	93.03	3.77	0.81	0.34	0.55	1.23	0.950	−34.5	−24.0	−21.4	−164	−125	—
	CG561	97.41	0.97	0.10	0.00	0.00	1.52	0.989	−32.9	−28.3	−27.8	−168	—	—
	CG561	93.69	3.96	0.56	0.22	0.37	1.04	0.952	−35.6	−22.7	−20.9	−176	−130	—
Zhongjiang-Huilong Structural Belt	CJ566	95.81	1.29	0.17	0.05	0.82	1.7	0.984	−33.7	−21.0	−19.8	—	—	—
	CJ566	95.86	1.75	0.23	0.09	0.36	1.60	0.979	−32.2	−22.1	—	−173	−110	—

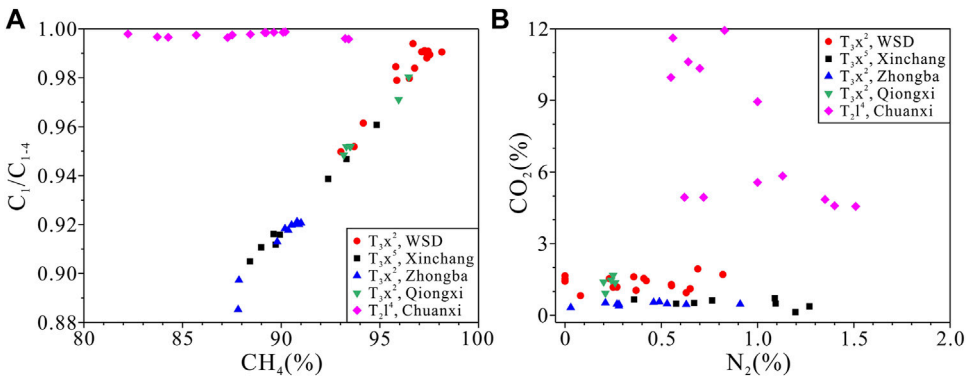

FIGURE 3 | The cross-plots of C_1/C_{1-4} versus CH_4% **(A)** and CO_2% versus N_2% **(B)**. The T_3x^2 gases of Zhongba and Qiongxi gas fields (Dai et al., 2012b), T_3x^5 gas from the Xinchang gas field (Wu et al., 2016), and T_2l^4 gas from the Chuanxi gas field (Wu et al., 2020b) are also plotted for comparative analysis and hereafter the same.

5 min, and then the temperature was programmed to 80°C at 8°C/min then heated to 260°C at 4°C/min where it was held for 10 min. Each gas sample was measured in triplicate, and the results were averaged. The measurement precision is estimated to be ±3‰ for δD with respect to VSMOW.

4 RESULTS

The chemical composition and stable isotopic compositions of the T_3x^2 tight gas from WSD are listed in **Table 1**. The previously published data of the T_3x^2 gases from Zhongba and Qiongxi gas fields (Dai et al., 2012b), T_3x^5 gas from the Xinchang gas field (Wu et al., 2016), and T_2l^4 gas from the Chuanxi gas field (Wu et al., 2020b) have also been collected for comparative analysis.

4.1 Main Components of Natural Gas

The T_3x^2 gas from WSD is mainly composed of CH_4, and the CH_4 content ranges from 93.03% to 98.14% with an average of 96.49%, whereas the heavy alkane (C_2–C_4) content ranges from 0.59% to 4.92% with an average of 1.72% (**Table 1**). The T_3x^2 gas from WSD is dry with the dryness coefficient (C_1/C_{1-4}) ranging from 0.950 to 0.994 (**Table 1**), and it displays a positive correlation between the CH_4 content and C_1/C_{1-4} ratio (**Figure 3A**), suggesting the effect of thermal maturity.

The non-hydrocarbon components of the T_3x^2 gas from WSD are predominantly CO_2 and N_2, with the contents ranging from 0.82% to 1.94% and from 0% to 0.82%, respectively (**Table 1**). The T_3x^2 gas is free of H_2S, and the correlation between CO_2 and N_2 contents is unobservable (**Figure 3B**).

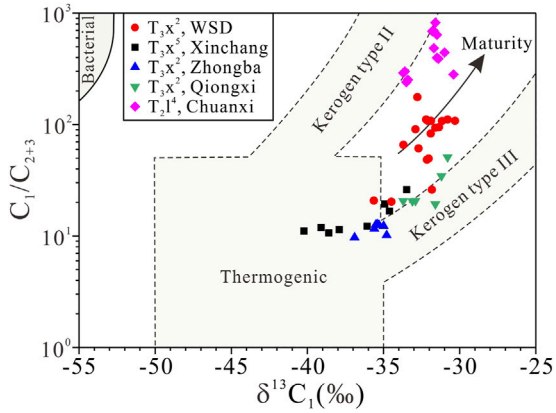

FIGURE 4 | The diagram of C_1/C_{2+3} versus $\delta^{13}C_1$ of the T_3x^2 gas from the Western Sichuan Depression (modified after Bernard et al., 1976).

4.2 Carbon Isotopes of Alkanes

The carbon isotopic value of CH_4 ($\delta^{13}C_1$) of T_3x^2 gas from WSD ranges from −35.6‰ to −30.3‰ with an average of −32.3‰, whereas the $\delta^{13}C_2$ value ranges from −29.1‰ to −21.0‰ with an average of −25.5‰ (**Table 1**). The gaseous alkanes mainly display positive carbon isotopic series (i.e., $\delta^{13}C_1 < \delta^{13}C_2 < \delta^{13}C_3$), with only a few samples possessing partial reversal between C_2H_6 and C_3H_8 ($\delta^{13}C_2 > \delta^{13}C_3$) (**Table 1**).

4.3 Hydrogen Isotopes of Alkanes

The hydrogen isotopic value of CH_4 (δD_1) of T_3x^2 gas from WSD ranges from −176‰ to −155‰ with an average of −163‰, whereas the δD_2 value ranges from −161‰ to −110‰ with an average of −138‰ (**Table 1**). The gas displays a positive hydrogen isotopic sequence between CH_4 and C_2H_6 (i.e., $\delta D_1 < \delta D_2$) (**Table 1**).

5 DISCUSSION

5.1 Genetic Types of Natural Gas

Biogenic gas consists of thermogenic gas and bacterial gas according to different mechanisms of gas generation, and the latter mostly has higher C_1/C_{2+3} ratios and lower $\delta^{13}C_1$ values (Bernard et al., 1976). The C_1/C_{2+3} ratios and $\delta^{13}C_1$ values of T_3x^2 gas from WSD range from 20.7 to 175.8 and from −35.6‰ to −30.3‰, respectively, suggesting the characteristics of thermogenic gas rather than bacterial gas (**Figure 4**). Thermogenic gas can be divided into coal-derived and oil-associated gases, which are generated by humic (kerogen type III) and sapropelic (kerogen type I/II) organic matters, respectively (Dai, 1992; Rooney et al., 1995; Liu et al., 2019). The Zhongba and Qiongxi T_3x^2 gases and Xinchang T_3x^5 gas follow the trend of natural gas from type III kerogen, suggesting the typical characteristics of coal-derived gas, whereas the Chuanxi T_2l^4 gas shares similar characteristics with natural gas from type II kerogen in the modified Bernard diagram (**Figure 4**). The T_3x^2 gas from WSD is mainly plotted between these two types of natural gas in the diagram (**Figure 4**), suggesting the characteristics of mixing gas, and it seems unlikely to be derived from single-type kerogen.

Coal-derived and oil-associated gases have different evolution trends in the correlation diagram between $\delta^{13}C_2$ and $\delta^{13}C_1$ values (Rooney et al., 1995), and oil-associated gas displays more negative $\delta^{13}C_2$ values than coal-derived gas under similar $\delta^{13}C_1$ values (**Figure 5A**). The Chuanxi T_2l^4 gas mainly follows the trend of oil-associated gas from type II kerogen in the Delaware/Val Verde Basin, whereas the Zhongba and Qiongxi T_3x^2 gases and Xinchang T_3x^5 gas follow the trend of coal-derived gas from type III kerogen in Niger Delta (**Figure 5A**). Several T_3x^2 gas samples from WSD are consistent with the coal-derived gas from type III kerogen in the diagram of $\delta^{13}C_2$ versus $\delta^{13}C_1$ values, whereas the other gas samples display the characteristics of oil-associated or mixing gas (**Figure 5A**), suggesting the complex features of the T_3x^2 gas.

The $\delta^{13}C_2$ and $\delta^{13}C_3$ values were considered to inherit the carbon isotopic compositions of original organic matter and thus could be used to identify the coal-derived and oil-associated gases (Dai et al., 2005). The geochemical statistics of natural gas in China indicated that the $\delta^{13}C_2$ values of coal-derived and oil-associated gases were commonly higher than −27.5‰ and lower than −29‰, respectively, whereas the $\delta^{13}C_3$ values were higher than −25.5‰ and lower than −27.0‰, respectively (Dai, 1999). The Zhongba and Qiongxi T_3x^2 gases and Xinchang T_3x^5 gas have consistent $\delta^{13}C_2$ and $\delta^{13}C_3$ values with typical coal-derived gas, whereas the only two T_2l^4 gas samples from the Chuanxi gas field display consistent $\delta^{13}C_2$ and $\delta^{13}C_3$ values with typical oil-associated gas (**Figure 5B**). Five gas samples in T_3x^2 reservoirs from WSD with relatively high $\delta^{13}C_2$ and $\delta^{13}C_3$ values display the characteristics of coal-derived gas, whereas the other gas samples are plotted in the transitional zone between oil-associated and coal-derived gas in **Figure 5B**, suggesting the characteristics of mixing gases.

Since the δD_1 values are associated with the types and thermal maturity of organic matter and water salinity (Liu et al., 2008; Schoell, 1980; Stahl, 1977), oil-associated gas and coal-derived gas generally follow different maturity trends in the correlation diagram between δD_1 and $\delta^{13}C_2$ values (**Figure 6**) (Wang et al., 2015). The Chuanxi T_2l^4 gas displays the characteristics of oil-associated gas with δD_1 values higher than −160‰, whereas the Zhongba and Qiongxi T_3x^2 gases and Xinchang T_3x^5 gas follow the trend of coal-derived gas in **Figure 6**. A positive correlation between δD_1 and $\delta^{13}C_2$ values is unobservable for the T_3x^2 gas from WSD, and most gas samples display the characteristics of mixing gas between typical oil-associated and coal-derived gases, with only five gas samples showing the characteristics of coal-derived gas (**Figure 6**). These indicate that most of the T_3x^2 gas samples from WSD follow the mixing trend rather than the maturity trend. Therefore, a small amount of the T_3x^2 gas from WSD is typically coal-derived gas, whereas most of the gas samples have experienced mixing by oil-associated gas.

The partial reversal of alkane carbon isotopes has been widely studied in China, and it can be attributed to mixing of abiogenic and biogenic gases, mixing of coal-derived and oil-associated

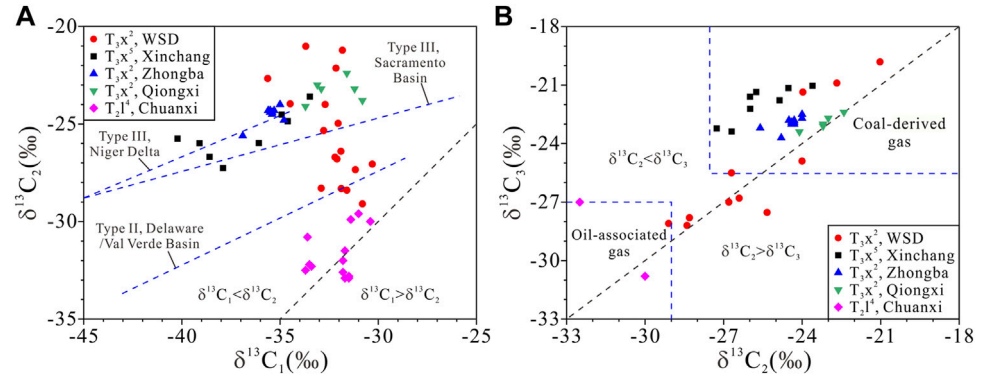

FIGURE 5 | The diagrams of $\delta^{13}C_2$ versus $\delta^{13}C_1$ **(A)** and $\delta^{13}C_3$ versus $\delta^{13}C_2$ **(B)**. The trends representing gases from Type III kerogen in Niger Delta and Type II kerogen in Delaware/Val Verde Basin **(A)** are after Rooney et al. (1995), and the trend for gas from Type III kerogen in Sacramento Basin **(A)** are after Jenden and Kaplan (1989). The ranges for coal-derived and oil-associated gases **(B)** are from Dai (1999).

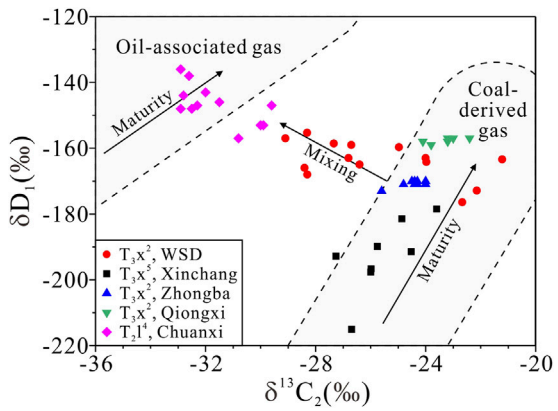

FIGURE 6 | Correlation diagram between δD_1 and $\delta^{13}C_2$ values of the T_3x^2 gas from the Western Sichuan Depression (modified after Wang et al., 2015).

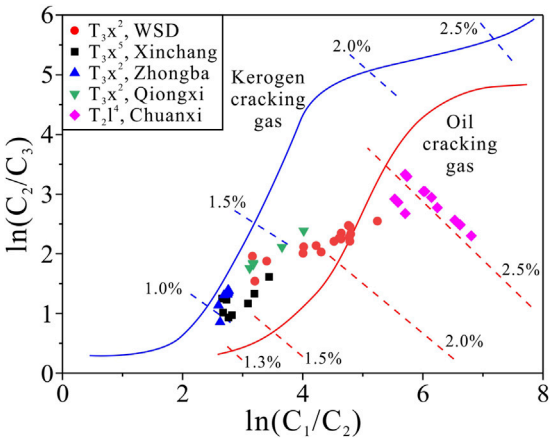

FIGURE 7 | The cross-plot of ln (C_2/C_3) versus ln (C_1/C_2) of the T_3x^2 gas from the Western Sichuan Depression (modified after Li et al., 2017).

gases, mixing of gases from the same types of source rocks with different maturity, or bacterial oxidation (Dai et al., 2004; Wu et al., 2014; Liu et al., 2019). Abiogenic gas or bacterial gas has not been found in WSD, and the mixing of abiogenic and biogenic gases or bacterial oxidation seems unlikely to happen. The mixing of coal-derived gas and oil-associated gas is demonstrated to be common in the T_3x^2 gas from WSD, and thus it is believed to be the main reason of partial $\delta^{13}C$ reversal between C_2H_6 and C_3H_8 ($\delta^{13}C_2 > \delta^{13}C_3$). The gas sample from Well JS1 displays a significantly heavier carbon isotope of C_2H_6 than that of C_3H_8 (**Table 1**). It is mainly caused by the extremely low $\delta^{13}C_3$ value (−27.5‰), which suggests the typical characteristics of oil-associated gas (**Figure 5B**). Therefore, the partial $\delta^{13}C$ reversal between C_2H_6 and C_3H_8 was attributed to mixing of coal-derived gas and oil-associated gas.

The coal-derived gas is commonly generated by humic organic matter (kerogen type III) through primary cracking of kerogen, whereas the oil-associated gas can be generated by both primary cracking of sapropelic kerogen (type II) and secondary cracking of oil, and the oil cracking gas accounts for nearly 80% of the total gas amount generated by sapropelic organic matter in the high-mature stage (Li et al., 2018). Natural gas in the marine strata of the Sichuan Basin is predominantly composed of oil-cracking gas (Hao et al., 2008; Liu et al., 2012; Liu et al., 2013; Liu et al., 2014). Theoretical and experimental studies indicate that kerogen cracking gas and oil cracking gas follow different evolution trends in the correlation diagram between ln (C_2/C_3) and ln (C_1/C_2) values (Prinzhofer and Huc, 1995; Li et al., 2017). The Chuanxi T_2l^4 oil-associated gas displays the characteristics of oil cracking gas (Wu et al., 2020b), whereas the coal-derived gas from the Zhongba and Qiongxi T_3x^2 and Xinchang T_3x^5 reservoirs primarily follows the trend of kerogen cracking gas (**Figure 7**). Three gas samples from the T_3x^2 reservoirs in WSD also follow the trend of kerogen cracking gas (**Figure 7**), and they have $\delta^{13}C_2$ values higher than −24.0‰ and display the characteristics of typical coal-derived gas in the correlation diagram between δD_1 and $\delta^{13}C_2$ values (**Figure 6**). Other gas samples from the T_3x^2 reservoirs in WSD are distributed closer

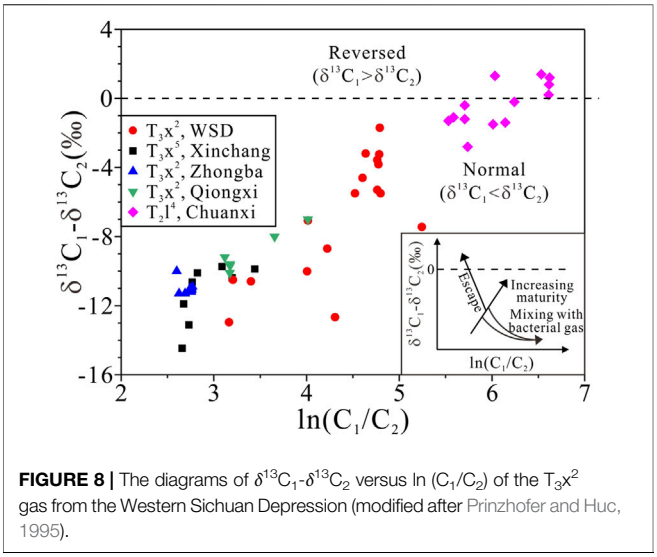

FIGURE 8 | The diagrams of $\delta^{13}C_1$-$\delta^{13}C_2$ versus ln (C_1/C_2) of the T_3x^2 gas from the Western Sichuan Depression (modified after Prinzhofer and Huc, 1995).

to the trend line of oil cracking gas in **Figure 7**; however, they are distinctly different from the oil cracking gas in the Chuanxi T_2l^4 reservoirs, which suggest that these T_3x^2 gas samples have experienced mixing by a significant amount of oil cracking gas. Therefore, the T_3x^2 tight gas from WSD are commonly mixed by oil cracking gas, except a few samples being typically coal-derived gas from kerogen cracking.

As indicated in **Figure 7**, the coal-derived gas in the T_3x^2 reservoirs from WSD seems to be mainly in the high-maturity stage with the maturity ranging from 1.3% to 1.7%, whereas the oil-associated gas reaches the over-mature stage with the maturity higher than 2.0%. The variance of the maturity may be attributed to the regional difference of potential source rocks, which was caused by different burial history and depth.

5.2 Gas—Source Correlation

5.2.1 Geochemical Comparison With the Chuanxi T_2l^4 Gas

The Chuanxi T_2l^4 gas is typical dry gas with the dryness coefficient (0.996–0.999) higher than the T_3x^2 gas from WSD (**Figure 3A**). The T_2l^4 gas is a sour gas with the H_2S content ranging from 0.59% to 4.90% (Wu et al., 2020b), and its CO_2 content (4.59%–15.25%) is apparently higher than the T_3x^2 gas from WSD (**Figure 3B**). These two gases share similar distribution ranges of $\delta^{13}C_1$ values; however, the Chuanxi T_2l^4 gas has higher C_1/C_{2+3} ratios (240–820) and thus the characteristics of oil-associated gas in the modified Bernard diagram (**Figure 4**), whereas the T_3x^2 gas from WSD displays the characteristics of mixing gas (**Figure 4**). The Chuanxi T_2l^4 gas has more negative $\delta^{13}C_2$ values (−32.9‰ to −29.6‰) and less negative δD_1 values (−157‰ to −136‰), resulting in different distribution characteristics with the T_3x^2 gas from WSD in **Figure 5A** and **Figure 6**. The larger ln (C_2/C_3), ln (C_1/C_2), and $\delta^{13}C_1$-$\delta^{13}C_2$ values of the Chuanxi T_2l^4 gas suggest higher thermal maturity than the T_3x^2 gas from WSD (**Figure 7**, **Figure 8**).

The Chuanxi T_2l^4 gas was demonstrated as typical oil-associated gas and derived mainly from the underlying Upper Permian source rocks (Wu et al., 2020b), and the gas pools were commonly distributed along the deep fault which directly or indirectly connected the reservoirs and the Permian strata (Wu et al., 2020a). The T_3x^2 gas from WSD is apparently different from typical oil-associated gas (**Figure 4**, **Figure 5A**, **Figure 6**), and the thermal maturity is significantly lower than the Chuanxi T_2l^4 gas (**Figure 7**, **Figure 8**). Therefore, the T_3x^2 gas from WSD displays few affinities with the Upper Permian source rocks.

5.2.2 Geochemical Comparison With the Xinchang T_3x^5 Gas

The Xinchang T_3x^5 gas is mainly wet gas with the dryness coefficient ranging from 0.905 to 0.961 (Wu et al., 2016), which is principally lower than that of the T_3x^2 gas from WSD (**Figure 3A**). The CO_2 content ranges from 0.13% to 0.70% and is also lower than that of the T_3x^2 gas from WSD (**Figure 3B**). The $\delta^{13}C_1$ and C_1/C_{2+3} values of the Xinchang T_3x^5 gas, ranging from −40.2‰ to −33.5‰ and from 10.7 to 26.0, respectively, are generally lower than the corresponding values of the T_3x^2 gas from WSD (**Figure 4**). This suggests a relatively lower thermal maturity of the Xinchang T_3x^5 gas. In the modified Bernard diagram (**Figure 4**), the Xinchang T_3x^5 gas follows the typical characteristics of coal-derived gas from type III kerogen, and it is different from the transitional or mixing characteristics of the T_3x^2 gas from WSD. The $\delta^{13}C_2$ and $\delta^{13}C_3$ values of the Xinchang T_3x^5 gas, concentrating from −27.3‰ to −23.6‰ and from −23.4‰ to −21.0‰, respectively, display differences with the wide distribution ranges of corresponding values of T_3x^2 gas from WSD (**Figure 5**). The Xinchang T_3x^5 gas has the δD_1 value ranging from −215‰ to −179‰, which is obviously lower than the T_3x^2 gas from WSD (**Figure 6**). Moreover, the relatively lower ln (C_2/C_3) and ln (C_1/C_2) values of the Xinchang T_3x^5 gas indicate its lower thermal maturity than the T_3x^2 gas from WSD (**Figure 7**, **Figure 8**).

The Xinchang T_3x^5 gas was demonstrated as typical coal-derived gas and mainly generated by the T_3x^5 source rocks (Wu et al., 2016). The T_3x^2 gas from WSD displays certain differences with typical coal-derived gas (**Figures 4**,**5**, **6**), and the thermal maturity is apparently higher than the Xinchang T_3x^5 gas (**Figures 7**, **8**). Consequently, the T_3x^2 gas from WSD displays few affinities with the T_3x^5 source rocks, and it is considered to be derived from source rocks with higher thermal maturity.

5.2.3 Geochemical Comparison With the Zhongba and Qiongxi T_3x^2 Gases

The Qiongxi T_3x^2 gas is mainly dry gas with the dryness coefficients between 0.948 and 0.980, whereas the Zhongba T_3x^2 gas is typical wet gas with the dryness coefficient ranging between 0.885 and 0.921 (Dai et al., 2012b). They are both apparently lower than the coefficient of the T_3x^2 gas from WSD (**Figure 3A**). The Qiongxi T_3x^2 gas has consistent CO_2 content (from 0.92% to 1.67%) with the T_3x^2 gas from WSD, whereas the Zhongba T_3x^2 gas displays an obviously lower CO_2 content (from 0.32% to 0.56%) than the T_3x^2 gas from WSD (**Figure 3B**).

Compared with the T_3x^2 gas from WSD, the Qiongxi T_3x^2 gas displays similar $\delta^{13}C_1$ values (ranging from −33.7‰ to −30.8‰) and overall lower C_1/C_{2+3} ratios (from 19.3 to 50.8), whereas the Zhongba T_3x^2 gas has apparently lower $\delta^{13}C_1$ values (ranging from −36.9‰ to −34.8‰) and C_1/C_{2+3} ratios (from 9.7 to 12.7)

(**Figure 4**). There are two gases that show the characteristics of coal-derived gas in the modified Bernard diagram (**Figure 4**). Their $\delta^{13}C_2$ values are distributed in the narrow ranges from −24.1‰ to −22.4‰ and from −25.6‰ to −24.0‰, respectively, whereas the δD_1 values range from −159‰ to −157‰ and from −173‰ to −170‰, respectively, with $\delta^{13}C_3$ values higher than −24‰ (Dai et al., 2012b). They also follow the typical characteristics of coal-derived gas in **Figure 5A,B** and **Figure 6** and displays certain differences with the T_3x^2 gas from WSD.

The Qiongxi and Zhongba T_3x^2 gases were demonstrated to be self-generated and self-accumulated in T_3x, i.e., they were mainly derived from the T_3x^1 coal–measure source rocks with assistance of T_3x^2 coal–measure source rocks (Zhu et al., 2011; Dai et al., 2012b; Liao et al., 2014). Affected by different largest burial depths, the present thermal maturity of T_3x^1 in the Zhongba gas field is slightly lower than that in the Qiongxi gas field and WSD (Jiang et al., 2012). This is consistent with the maturity difference indicated by the ln (C_2/C_3), ln (C_1/C_2), and $\delta^{13}C_1$-$\delta^{13}C_2$ values of the T_3x^2 gases in these areas (**Figures 7**, **8**). Therefore, the geochemical characteristics of the T_3x^2 gas from WSD match the thermal maturity of the *in-situ* T_3x^1 and T_3x^2 source rocks.

5.2.4 Source of the T_3x^2 Gas From WSD

The above geochemical analysis and genetic identification of natural gas indicate that the T_3x^2 gas from WSD is mainly coal-derived gas assisted by oil-associated gas, rather than typical coal-derived or oil-associated gas. Therefore, it is unreliable to calculate the thermal maturity by $\delta^{13}C_1$ values based on the $\delta^{13}C_1$-R_O empirical equations for typical coal-derived or oil-associated gas. According to the thermal maturity comparison indicated by geochemical characteristics of natural gas from different strata, the T_3x^2 gas from WSD displays apparently higher maturity than the overlying Xinchang T_3x^5 gas and lower maturity than the underlying Chuanxi T_2l^4 gas (**Figures 7**, **8**). The T_3x^2 gas from WSD is inferred to have consistent maturity with the T_3x^1 and T_3x^2 source rocks.

The T_3x source rocks in the Sichuan Basin were mainly developed in T_3x^1, T_3x^3, and T_3x^5, and a small amount of argillaceous source rocks was developed in T_3x^2, T_3x^4, and T_3x^6 (Dai et al., 2009; Wang et al., 2010; Cai and Yang, 2011; Dai et al., 2012b). T_3x^1 is commonly divided into Xiaotangzi (T_3t) and underlying Ma'antang (T_3m) formations, in which T_3t consists of sandstone interbedded with mudstone and siltstone, and T_3m is composed of silty mudstone at the top and grey limestone at the bottom (**Figure 2**). The kerogen-type indexes of T_3t and T_3m mudstone are less than 0 and consistent with those of the T_3x^2 mudstone, displaying the characteristics of typical type III kerogen, whereas the indexes of the T_3m limestone range from 23.75 to 50.5, displaying the characteristics of type II kerogen (Wang et al., 2010; Cai and Yang, 2011). The T_3m limestone from some areas in WSD displays certain hydrocarbon potential with the TOC contents higher than 0.5% (Yang et al., 2012). Therefore, among the T_3x^2 tight gas from WSD the coal-derived gas is generated mainly by the T_3t and T_3m mudstone with assistance of T_3x^2 mudstone, whereas the oil-associated gas is derived from the T_3m limestone.

6 CONCLUSION

The tight gas in Member two of the Upper Triassic Xujiahe Formation in the WSD of the Sichuan Basin is mainly composed of CH_4, with the CH_4 content ranging from 93.03% to 98.14%. The dryness coefficient of the tight gas is 0.950–0.994 and positively correlated with the CH_4 content. The gaseous alkanes display positive carbon isotopic series, with the $\delta^{13}C_1$ and $\delta^{13}C_2$ values ranging from −35.6‰ to −30.3‰ and from −29.1‰ to −21.0‰, respectively, and the δD_1 values range from −176‰ to −155‰.

According to the genetic identification based on the carbon and hydrogen isotopic compositions, a small amount of the tight gas is typically coal-derived gas, whereas most of the tight-gas samples have experienced mixing by oil-associated gas. Geochemical comparisons indicate that the tight gas displays distinct differences with the typical oil-associated and coal-derived gases in adjacent gas fields. Among the tight gas in Member two of the Xujiahe Formation from the WSD, the coal-derived gas is generated mainly by the humic mudstone in the Upper Triassic Ma'antang and Xiaotangzi formations, with assistance of the humic mudstone in Member two of the Xujiahe Formation, whereas the oil-associated gas is derived from the sapropelic limestone in the Ma'antang Formation.

DATA AVAILABILITY STATEMENT

The original contributions presented in the study are included in the article/Supplementary Material; further inquiries can be directed to the corresponding author.

AUTHOR CONTRIBUTIONS

XW: conceptulization, data curation, writing. QL: conceptulization, writing. YC: data curation, methodology. JY: methodology, investigation. HZ: sample collection, investigation. HL: investigation.

FUNDING

This work was funded by the National Natural Science Foundation of China (Grant Nos. 42172149, 41872122, U20B6001, and 42141021) and Strategic Priority Research Program of the Chinese Academy of Sciences (Class A) (Grant Nos. XDA14010402 and XDA14010404).

ACKNOWLEDGMENTS

The authors appreciate Jinxing Dai, Academician of Chinese Academy of Sciences, for the long-standing guidance of the relevant studies. We also appreciate QL for the valuable discussion and inspiration. The SINOPEC Southwest Branch Company and Key Laboratory for Hydrocarbon Accumulation Mechanism are acknowledged for the assistance on sample collection and geochemical analyses, respectively.

REFERENCES

Bernard, B. B., Brooks, J. M., and Sackett, W. M. (1976). Natural Gas Seepage in the Gulf of Mexico. *Earth Planet. Sci. Lett.* 31, 48–54. doi:10.1016/0012-821x(76)90095-9

Cai, X., and Yang, K. (2011). *Tight sandstone Gas Pools in the Xujiahe Formation, Western Sichuan Depression*. Beijing: Petroleum Industry Press.

Dai, J. (2016). *Giant Coal-Derived Gas Fields and Their Gas Sources in China*. Beijing: Science Press.

Dai, J. (1992). Identification and Distinction of Various Alkane Gases. *Sci. China (Series B)* 35, 1246–1257.

Dai, J., Ni, Y., Hu, G., Huang, S., Liao, F., Yu, C., et al. (2014). Stable Carbon and Hydrogen Isotopes of Gases from the Large Tight Gas fields in China. *Sci. China Earth Sci.* 57, 88–103. doi:10.1007/s11430-013-4701-7

Dai, J., Ni, Y., Qin, S., Huang, S., Peng, W., and Han, W. (2018). Geochemical Characteristics of Ultra-deep Natural Gas in the Sichuan Basin, SW China. *Pet. Exploration Dev.* 45, 619–628. doi:10.1016/s1876-3804(18)30067-3

Dai, J., Ni, Y., and Wu, X. (2012a). Tight Gas in China and its Significance in Exploration and Exploitation. *Pet. Exploration Dev.* 39, 277–284. doi:10.1016/s1876-3804(12)60043-3

Dai, J., Ni, Y., and Zou, C. (2012b). Stable Carbon and Hydrogen Isotopes of Natural Gases Sourced from the Xujiahe Formation in the Sichuan Basin, China. *Org. Geochem.* 43, 103–111. doi:10.1016/j.orggeochem.2011.10.006

Dai, J., Ni, Y., Zou, C., Tao, S., Hu, G., Hu, A., et al. (2009). Stable Carbon Isotopes of Alkane Gases from the Xujiahe Coal Measures and Implication for Gas-Source Correlation in the Sichuan Basin, SW China. *Org. Geochem.* 40, 638–646. doi:10.1016/j.orggeochem.2009.01.012

Dai, J., Qin, S., Tao, S., Zhu, G., and Mi, J. (2005). Development Trends of Natural Gas Industry and the Significant Progress on Natural Gas Geological Theories in China. *Nat. Gas Geosci.* 16, 127–142. doi:10.11764/j.issn.1672-1926.2005.02.127

Dai, J. (1999). Significant Advancement in Research on Coal-Formed Gas in China. *Pet. Exploration Dev.* 26, 1–10. cnki:sun:skyk.0.1999-03-000.

Dai, J., Xia, X., Qin, S., and Zhao, J. (2004). Origins of Partially Reversed Alkane δ 13 C Values for Biogenic Gases in China. *Org. Geochem.* 35, 405–411. doi:10.1016/j.orggeochem.2004.01.006

Hao, F., Guo, T., Zhu, Y., Cai, X., Zou, H., and Li, P. (2008). Evidence for Multiple Stages of Oil Cracking and Thermochemical Sulfate Reduction in the Puguang Gas Field, Sichuan Basin, China. *Bulletin* 92, 611–637. doi:10.1306/01210807090

Jenden, P. D., and Kaplan, I. R. (1989). Origin of Natural Gas in Sacramento Basin, California. *AAPG Bull.* 73, 431–453. doi:10.1306/44b49fc9-170a-11d7-8645000102c1865d

Jiang, X., Zeng, H., Zhu, J., and Cao, Q. (2012). Dynamic Evolution Simulation of the Upper Triassic Source Rocks in central Part of Western Sichuan Depression. *Oil Gas Geology.* 33, 545–551. doi:10.11743/ogg20120408

Li, J., Li, Z., Wang, X., Wang, D., Xie, Z., Li, J., et al. (2017). New Indexes and Charts for Genesis Identification of Multiple Natural Gases. *Pet. Exploration Dev.* 44, 535–543. doi:10.1016/s1876-3804(17)30062-9

Li, J., Ma, W., Wang, Y., Wang, D., Xie, Z., Li, Z., et al. (2018). Modeling of the Whole Hydrocarbon-Generating Process of Sapropelic Source Rock. *Pet. Exploration Dev.* 45, 461–471. doi:10.1016/s1876-3804(18)30051-x

Liao, F., Yu, C., Wu, W., and Liu, D. (2014). Stable Carbon and Hydrogen Isotopes of Natural Gas from the Zhongba Gasfield in the Sichuan Basin and Implication for Gas-Source Correlation. *Nat. Gas Geosci.* 25, 79–86. doi:10.11764/j.issn.1672-1926.2014.01.0079

Liu, Q., Dai, J., Li, J., and Zhou, Q. (2008). Hydrogen Isotope Composition of Natural Gases from the Tarim Basin and its Indication of Depositional Environments of the Source Rocks. *Sci. China Ser. D-earth Sci.* 51, 300–311. doi:10.1007/s11430-008-0006-7

Liu, Q., Jin, Z., Li, J., Hu, A., and Bi, C. (2012). Origin of marine Sour Natural Gas and Gas-Filling Model for the Wolonghe Gas Field, Sichuan Basin, China. *J. Asian Earth Sci.* 58, 24–37. doi:10.1016/j.jseaes.2012.07.007

Liu, Q., Wu, X., Wang, X., Jin, Z., Zhu, D., Meng, Q., et al. (2019). Carbon and Hydrogen Isotopes of Methane, Ethane, and Propane: A Review of Genetic Identification of Natural Gas. *Earth-Science Rev.* 190, 247–272. doi:10.1016/j.earscirev.2018.11.017

Liu, Q. Y., Worden, R. H., Jin, Z. J., Liu, W. H., Li, J., Gao, B., et al. (2014). Thermochemical Sulphate Reduction (TSR) versus Maturation and Their Effects on Hydrogen Stable Isotopes of Very Dry Alkane Gases. *Geochimica et Cosmochimica Acta* 137, 208–220. doi:10.1016/j.gca.2014.03.013

Liu, Q. Y., Worden, R. H., Jin, Z. J., Liu, W. H., Li, J., Gao, B., et al. (2013). TSR versus Non-TSR Processes and Their Impact on Gas Geochemistry and Carbon Stable Isotopes in Carboniferous, Permian and Lower Triassic marine Carbonate Gas Reservoirs in the Eastern Sichuan Basin, China. *Geochimica et Cosmochimica Acta* 100, 96–115. doi:10.1016/j.gca.2012.09.039

Liu, Q., Zhu, D., Jin, Z., Liu, C., Zhang, D., and He, Z. (2016). Coupled Alteration of Hydrothermal Fluids and thermal Sulfate Reduction (TSR) in Ancient Dolomite Reservoirs - an Example from Sinian Dengying Formation in Sichuan Basin, Southern China. *Precambrian Res.* 285, 39–57. doi:10.1016/j.precamres.2016.09.006

Ni, Y., Dai, J., Tao, S., Wu, X., Liao, F., Wu, W., et al. (2014a). Helium Signatures of Gases from the Sichuan Basin, China. *Org. Geochem.* 74, 33–43. doi:10.1016/j.orggeochem.2014.03.007

Ni, Y., Liao, F., Dai, J., Zou, C., Wu, X., Zhang, D., et al. (2014b). Studies on Gas Origin and Gas Source Correlation Using Stable Carbon Isotopes - A Case Study of the Giant Gas Fields in the Sichuan Basin, China. *Energy Exploration & Exploitation* 32, 41–74. doi:10.1260/0144-5987.32.1.41

Prinzhofer, A. A., and Huc, A. Y. (1995). Genetic and post-genetic Molecular and Isotopic Fractionations in Natural Gases. *Chem. Geology.* 126, 281–290. doi:10.1016/0009-2541(95)00123-9

Rooney, M. A., Claypool, G. E., and Moses Chung, H. (1995). Modeling Thermogenic Gas Generation Using Carbon Isotope Ratios of Natural Gas Hydrocarbons. *Chem. Geology.* 126, 219–232. doi:10.1016/0009-2541(95)00119-0

Schoell, M. (1980). The Hydrogen and Carbon Isotopic Composition of Methane from Natural Gases of Various Origins. *Geochimica et Cosmochimica Acta* 44, 649–661. doi:10.1016/0016-7037(80)90155-6

Stahl, W. J. (1977). Carbon and Nitrogen Isotopes in Hydrocarbon Research and Exploration. *Chem. Geology.* 20, 121–149. doi:10.1016/0009-2541(77)90041-9

Wang, D., Zeng, H., and Wang, J. (2010). Evaluation on Upper Triassic Hydrocarbon Source Rocks of Western Sichuan Depression, Sichuan Basin. *Pet. Geology. Exp.* 32, 192–195. doi:10.11781/sysydz201002192

Wang, X., Liu, W., Shi, B., Zhang, Z., Xu, Y., and Zheng, J. (2015). Hydrogen Isotope Characteristics of Thermogenic Methane in Chinese Sedimentary Basins. *Org. Geochem.* 83-84, 178–189. doi:10.1016/j.orggeochem.2015.03.010

Wu, X., Chen, Y., Zhai, C., Zhou, X., Liu, W., Yang, J., et al. (2020a). Gas Source and Exploration Direction of the Middle Triassic Leikoupo Formation in the Sichuan Basin, China. *J. Nat. Gas Geosci.* 5, 317–326. doi:10.1016/j.jnggs.2020.10.001

Wu, X., Liu, Q., Chen, Y., Zhai, C., Ni, C., and Yang, J. (2020b). Constraints of Molecular and Stable Isotopic Compositions on the Origin of Natural Gas from Middle Triassic Reservoirs in the Chuanxi Large Gas Field, Sichuan Basin, SW China. *J. Asian Earth Sci.* 204, 104589. doi:10.1016/j.jseaes.2020.104589

Wu, X., Liu, Q., Liu, G., and Ni, C. (2019). Genetic Types of Natural Gas and Gas-Source Correlation in Different Strata of the Yuanba Gas Field, Sichuan Basin, SW China. *J. Asian Earth Sci.* 181, 103906. doi:10.1016/j.jseaes.2019.103906

Wu, X., Liu, Q., Liu, G., Wang, P., Li, H., Meng, Q., et al. (2017). Geochemical Characteristics and Genetic Types of Natural Gas in the Xinchang Gas Field, Sichuan Basin, SW China. *Acta Geologica Sinica - English Edition* 91, 2200–2213. doi:10.1111/1755-6724.13458

Wu, X., Liu, Q., Tao, X., and Hu, G. (2014). Geochemical Characteristics of Natural from Halahatang Sag in the Tarim Basin. *Geochimica* 43, 477–488. doi:10.19700/j.0379-1726.2014.05.006

Wu, X., Wang, P., Liu, Q., Li, H., Chen, Y., Zeng, H., et al. (2016). The Source of Natural Gas Reservoired in the 5th Member of the Upper Triassic Xujiahe Formation in Xinchang Gasfield, the Western Sichuan Depression and its Implication. *Nat. Gas Geosci.* 27, 1409–1418. doi:10.11764/j.issn.1672-1926.2016.08.1409

Yang, J., Zhang, M., and Chen, X. (2012). Identification of Xu1 Member as Main Source Rock in Upper Triassic from West Sichuan Depression. *J. Yangtze Univ. (Natural Sci. Edition)* 9 (12), 41–43. doi:10.3969/j.issn.1673-1409(N).2012.12.013

Zhang, D. (2021). Development prospect of Natural Gas Industry in the Sichuan Basin in the Next Decade. *Nat. Gas Industry* 41, 34–45. doi:10.3787/j.issn.1000-0976.2021.08.004

Zhu, G., Zhang, S., Huang, H., Liang, Y., Meng, S., and Li, Y. (2011). Gas Genetic Type and Origin of Hydrogen Sulfide in the Zhongba Gas Field of the Western Sichuan Basin, China. *Appl. Geochem.* 26, 1261–1273. doi:10.1016/j.apgeochem.2011.04.016

Conflict of Interest: HL was employed by Exploration and Production Research Institute, Southwest Branch Company.

The remaining authors declare that the research was conducted in the absence of any commercial or financial relationships that could be construed as a potential conflict of interest.

Publisher's Note: All claims expressed in this article are solely those of the authors and do not necessarily represent those of their affiliated organizations, or those of the publisher, the editors, and the reviewers. Any product that may be evaluated in this article, or claim that may be made by its manufacturer, is not guaranteed or endorsed by the publisher.

frontiers in Earth Science

ORIGINAL RESEARCH
published: 04 February 2022
doi: 10.3389/feart.2022.823308

Geochemical Characteristics of Helium in Natural Gas From the Daniudi Gas Field, Ordos Basin, Central China

Quanyou Liu[1,2], Xiaoqi Wu[1,3], Huichong Jia[4], Chunhua Ni[1,3], Jianhui Zhu[1,3], Jiujun Miao[1,3], Dongya Zhu[1,2], Qingqiang Meng[1,2], Weilong Peng[1,2] and Huiyuan Xu[1,2]*

[1]State Key Laboratory of Shale Oil and Gas Enrichment Mechanisms and Effective Development, SINOPEC, Beijing, China, [2]Petroleum Exploration and Production Research Institute, SINOPEC, Beijing, China, [3]Wuxi Research Institute of Petroleum Geology, Petroleum Exploration and Production Research Institute, SINOPEC, Wuxi, China, [4]Exploration and Production Research Institute, North China Branch Company, SINOPEC, Zhengzhou, China

Helium-bearing gas is accumulated in the Lower Ordovician, Upper Carboniferous, and Lower Permian reservoirs of the Daniudi gas field in Ordos Basin, and the helium concentrations and isotopic compositions are investigated in order to reveal the abundance and origin of helium. Geochemical characteristics indicate that the natural gas from the Daniudi gas field has helium concentrations of 0.0271–0.1273%, with R/Ra ratios of 0.007–0.072. The $^{4}He/^{20}Ne$ ratios range from 848 to 17,000, which are substantially higher than the ratio of air or air saturated water. The proved helium reserves of the Daniudi gas field exceed $100 \times 10^{6}\ m^{3}$, suggesting an extra-large helium gas field. Helium in the field is of crustal origin and derived from the radioactive decay of U and Th in the rocks and minerals, with no significant contribution by atmospheric or mantle-derived helium. The natural gas in the Daniudi gas field displays the characteristics of typical crustal helium, which is consistent with the gases from cratonic basins (Ordos, Sichuan, and Tarim) in China, whereas the gases from rift basins (Songliao, Bohai Bay, and Subei) have experienced a significant addition of mantle-derived helium.

Keywords: helium, concentrations, isotopic compositions, Daniudi gas field, Ordos Basin

OPEN ACCESS

Edited by:
Deyu Gong,
Research Institute of Petroleum Exploration and Development (RIPED), China

Reviewed by:
Jian Cao,
Nanjing University, China
Yunpeng Wang,
Guangzhou Institute of Geochemistry (CAS), China

****Correspondence:***
Quanyou Liu
qyouliu@sohu.com

Specialty section:
This article was submitted to Geochemistry, a section of the journal Frontiers in Earth Science

Received: *27 November 2021*
Accepted: *10 January 2022*
Published: *04 February 2022*

Citation:
Liu Q, Wu X, Jia H, Ni C, Zhu J, Miao J, Zhu D, Meng Q, Peng W and Xu H (2022) Geochemical Characteristics of Helium in Natural Gas From the Daniudi Gas Field, Ordos Basin, Central China. Front. Earth Sci. 10:823308. doi: 10.3389/feart.2022.823308

INTRODUCTION

Helium (He) is an exhaustible natural resource with strategic values, and its unique physiochemical property leads it to an irreplaceable role in high-tech fields (Xu et al., 1998; Anderson, 2018). The development of science and technology made the application fields of helium become more and more extensive, causing the global demand of helium gas to increase annually by 4–6% (Zhao et al., 2012), and thus the shortage of helium supply existed for a long time. The leading locations for estimated helium resources in the world are the United States, Qatar, Algeria, and Russia, and their helium resources account for >90% of the world's total amount (Anderson, 2018). Helium resources in China are rare, with the supply basically relying on imports, and they have been poorly studied and explored to date. Therefore, the amounts of helium resources and reserves urgently need to be further evaluated (Tao et al., 2019; Chen et al., 2021).

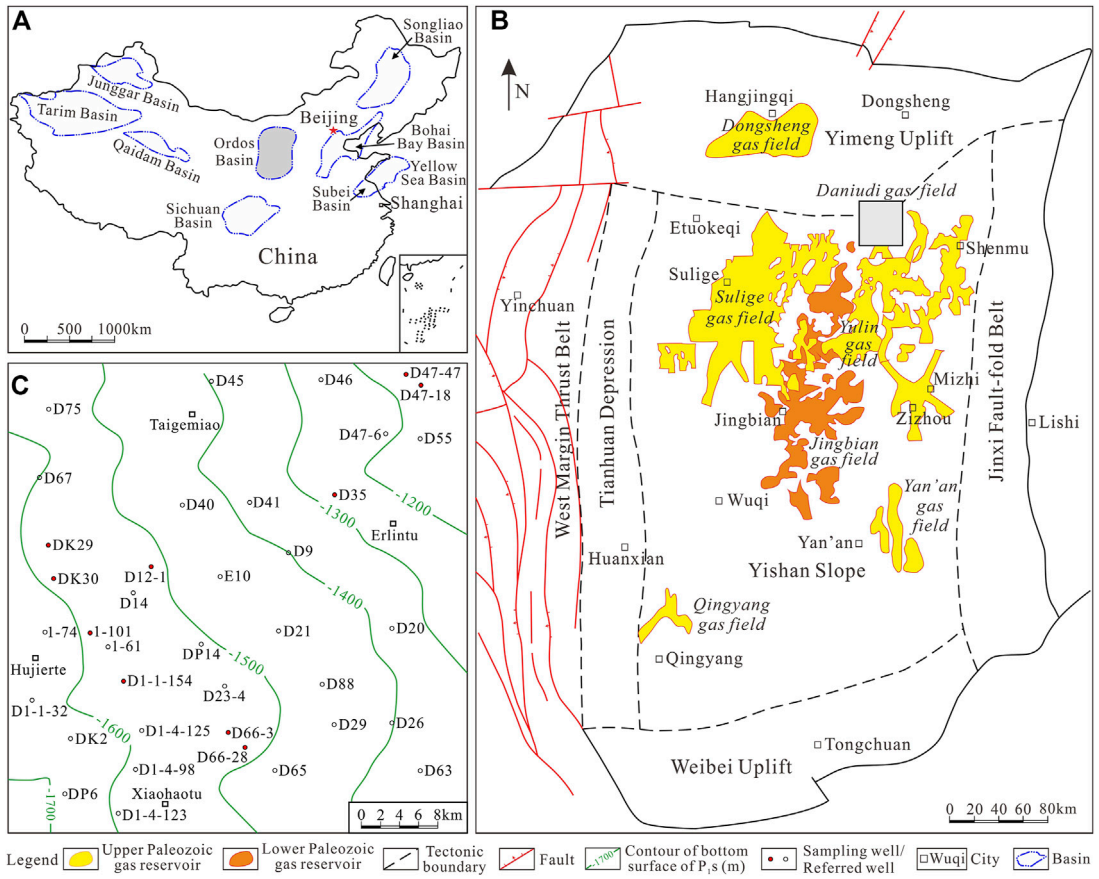

FIGURE 1 | The location of Ordos Basin in China **(A)**, location of the Daniudi gas field in the basin **(B)**, and distribution of gas wells in the gas field **(C)**.

Helium in natural gas has three different sources, including (1) atmospheric helium—being the helium in the air with a concentration of 5.24×10^{-6}, it was mainly produced from volcanic eruption, magma degassing, and rock weathering (Porcelli et al., 2002; Wang et al., 2020; Chen et al., 2021); (2) crustal helium—which is being generated by the radioactive decay of uranium (U) and thorium (Th) in crustal rocks and minerals (Oxburgh et al., 1986; Xu et al., 1998; Porcelli et al., 2002), and the production of crustal helium depends on the U and Th concentrations as well as the history of the rocks and minerals (Chen et al., 2021); and (3) mantle-derived helium—which is from mantle-derived volatiles and released into the sedimentary strata through magmatism and fault activities (O'Nions and Oxburgh, 1983; Poreda et al., 1986; Poreda et al., 1988; Xu et al., 1997; Anderson, 2000).

Helium commonly has two isotopes, *i.e.*, ^{3}He and ^{4}He, and the isotopic compositions of helium from different sources have certain differences. The ^{3}He/^{4}He ratio of air (Ra) is 1.4×10^{-6} (Mamyrin et al., 1970), whereas the ratios of crustal and mantle-derived helium are 2×10^{-8} and 1.1×10^{-5}, respectively (Lupton, 1983; Xu, 1996). The R/Ra ratios (R refers to the ^{3}He/^{4}He ratio of the samples) were commonly used to characterize helium isotopic compositions (Xu et al., 1995a; Ni et al., 2014), and they have played an important role in revealing mantle-derived magmatism (Sano et al., 1984; Poreda et al., 1988; Marty et al., 1989) and tectonic background (Xu et al., 1995a; Xu, 1997; Polyak et al., 2000; Ding et al., 2005) and tracing the origin and source of fluids in the petroleum system (Xu et al., 1995b; Dai et al., 2008; Ni et al., 2014; Dai et al., 2017; Zhang et al., 2019; Cao et al., 2020).

The only profitable way to produce helium at present is to extract from helium-bearing natural gas (Anderson, 2018; Tao et al., 2019), and the helium in natural gas pools is mainly crustal and mantle-derived (Xu et al., 1995a; Chen et al., 2021). Ordos Basin is a crucial petroliferous basin in China with an annual gas production of 46.496×10^{9} m^{3} in 2018, and it becomes the first Chinese basin with an annual gas production of over 40×10^{9} m^{3} (Dai et al., 2019). Helium-bearing gas with He% ≥0.05%, having potential industrial helium values, has been confirmed in the Sulige gas field in the basin (Dai et al., 2017). The Daniudi gas field is located in northern Ordos Basin with the proved gas reserves of 454.563×10^{9} m^{3} (Yang and Liu, 2014). Previous studies on the natural gas of the Daniudi gas field principally focused on genetic types and filling patterns (Liu et al., 2015; Wu et al., 2017a; Wu et al., 2017b), and less attention has been paid to helium. Therefore, the geochemical characteristics of helium for the Daniudi gas field were studied in this work based on the concentrations and isotopic compositions of helium and its relationship with neon and argon isotopes as well as the

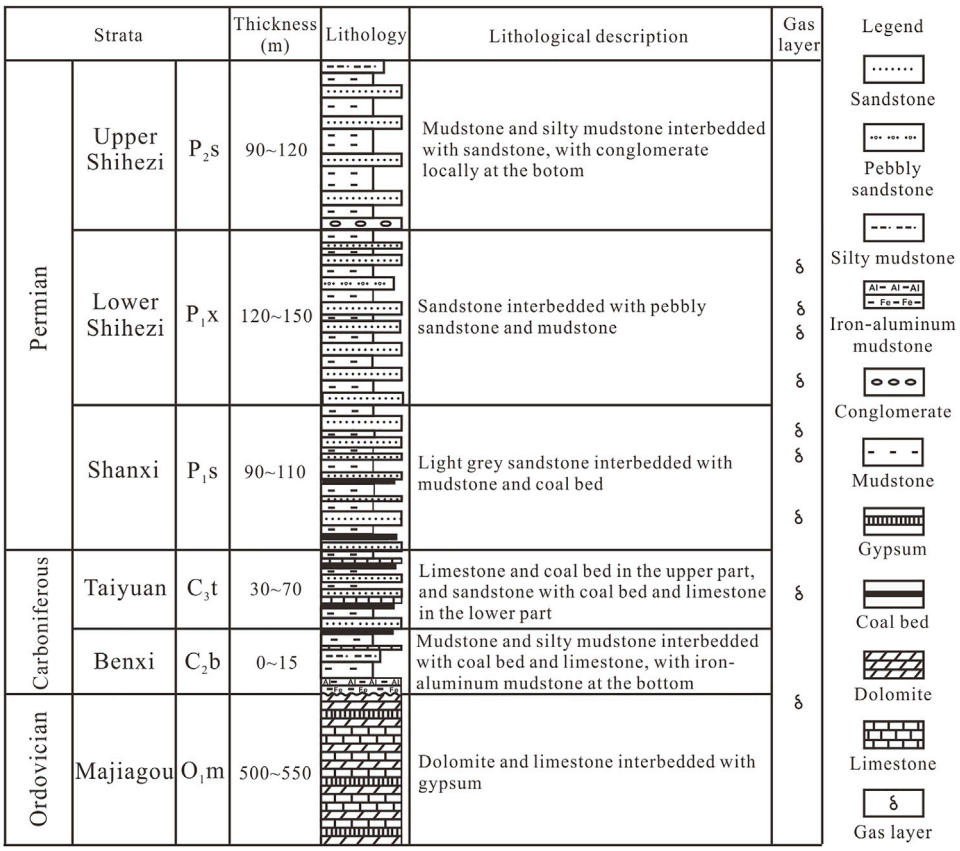

FIGURE 2 | Stratigraphic column of the Daniudi gas field, Ordos Basin.

relationship with CH_4 and CO_2 contents. The abundance and origin of helium were further investigated, which would provide scientific proofs for revealing helium enrichment mechanisms and evaluating the resource potential of helium.

GEOLOGICAL SETTING

Ordos Basin, a multicycle cratonic basin in central China (**Figure 1A**), tectonically belongs to the western margin of the North China Block, and it is the second largest sedimentary basin in China, covering an area of 37×10^4 km^2 (Yang and Pei, 1996). The basin is commonly divided into six secondary structural units (Yang et al., 2005), *i.e.*, Weibei Uplift, Yishan Slope, Yimeng Uplift, Tianhuan Depression, West Margin Thrust Belt, and Jinxi Fault–Fold Belt (**Figure 1B**). The exploration fields of conventional natural gas in Ordos Basin mainly include the Upper Paleozoic Carboniferous–Permian and Lower Paleozoic Ordovician strata. The natural gas of the discovered large gas fields is accumulated in the Carboniferous–Permian tight sandstone reservoirs in majority, except that the gas from the Jingbian gas field is mainly reservoired in marine carbonate rocks in the Lower Ordovician Majiagou Formation (Dai et al., 2005a; Liu et al., 2009; Liu et al., 2015; Dai, 2016).

The Daniudi gas field is located in the north margin of the Yishan Slope (**Figure 1B**), covering an area of 2,003.71 km^2 (Dai, 2016), and the strata dip gently to the southwest (**Figure 1C**). Natural gas in the field is mainly accumulated in the Upper Paleozoic tight sandstone reservoirs in the Carboniferous Taiyuan (C_3t), Lower Permian Shanxi (P_1s), and Lower Shihezi (P_1x) formations, and natural gas has also been discovered in carbonate reservoirs in the Lower Ordovician Majiagou Formation (O_1m) (**Figure 2**). The Upper Paleozoic (C_3t, P_1s, and P_1x) gas is mainly coal-derived gas and sourced from the C_3t-P_1s coal measures, and the regional caprocks of the gas pools are the stably distributed lacustrine mudstone and silty mudstone in the Upper Shihezi Formation (P_2s) (Liu et al., 2015; Wu et al., 2017a). However, the Lower Paleozoic (O_1m) gas is mixed by the Upper Paleozoic coal-derived gas and oil-associated gas from the O_1m source rocks (Wu et al., 2017b; Liu et al., 2015), and the main caprocks of the gas pools are the mudstone and iron–aluminum mudstone in the Benxi Formation (C_2b) (**Figure 2**).

SAMPLES AND ANALYTICAL METHODS

In this study, 20 gas samples from the O_1m, C_3t, P_1s, and P_1x reservoirs in the Daniudi gas field were collected directly from well heads. Double-ended stainless steel cylinders (5-cm radius, ~ 7,000-cm^3 volume) were used to collect the gas samples, and air

TABLE 1 | Noble gas concentrations and isotopic compositions of natural gas in the Daniudi gas field, Ordos Basin.

Well	Strata	CH_4 (%)	C_{2+} (%)	CO_2 (%)	^4He ($\times10^{-6}$)	^{20}Ne ($\times10^{-6}$)	^{40}Ar ($\times10^{-6}$)	$^3He/^4He$ ($\times10^{-8}$)	R/Ra	$^4He/^{20}Ne$	$^{40}Ar/^{36}Ar$	$CH_4/^3He$ ($\times10^9$)	$CO_2/^3He$ ($\times10^9$)
1-101	P_1x	97.19	2.55	0.25	586	0.122	52.9	3.976	0.028	4,803	797.0	41.7	0.107
2-1	P_1x	94.47	4.92	0.41	1,273	0.340	85.4	2.856	0.020	3,744	654.5	26.0	0.112
D66-28	P_1x	88.90	10.66	0.42	450	0.092	74.8	5.180	0.037	4,891	616.1	38.1	0.180
DK30	P_1x	94.39	5.17	0.42	459	0.027	52.4	6.440	0.046	17,000	1,163.9	31.9	0.141
D66-3	P_1x	97.52	2.38	0.09	421	0.158	66.5	2.660	0.019	2,665	514.0	87.1	0.081
DP14	P_1x	87.92	11.55	0.43	390	0.460	234.0	5.012	0.036	848	368.7	45.0	0.221
DK29	P_1x	88.70	10.57	0.55	371	ND	70.1	0.913	0.007	ND	537.5	261.9	1.621
D1-1-154	P_1x	90.54	8.30	1.14	394	0.161	90.2	2.618	0.019	2,447	547.5	87.8	1.108
2-47	P_1s	90.73	6.87	2.38	316	0.180	24.7	3.598	0.026	1756	1062.8	79.8	2.097
D1-4-107	P_1s	89.33	9.99	0.65	342	0.095	31.0	1.005	0.007	3,600	937.0	259.8	1.897
2-21	P_1s	89.15	9.93	0.90	376	ND	39.9	10.115	0.072	ND	2328.2	23.4	0.237
1-80	P_1s	88.92	10.26	0.80	381	0.089	48.3	2.688	0.019	4,281	945.1	86.8	0.783
2-45	P_1s	87.98	11.22	0.78	372	ND	44.1	1.226	0.009	ND	901.7	192.8	1.711
D12-1	P_1s	89.95	9.38	0.65	415	0.050	56.5	1.764	0.013	8,300	1038.4	122.9	0.889
D35	C_3t	90.33	7.56	1.98	287	0.164	69.5	2.940	0.021	1750	376.8	107.1	2.352
D23-4	C_3t	90.58	6.86	2.56	271	0.076	36.8	2.394	0.017	3,566	451.1	139.6	3.941
D47-18	C_3t	91.09	8.04	0.87	452	0.080	66.7	8.016	0.057	5,650	500.2	25.1	0.240
D35-22	C_3t	90.43	7.37	2.11	303	0.240	67.3	4.424	0.032	1,263	376.6	67.5	1.577
D47-47	C_3t	90.93	8.10	0.73	401	0.052	43.9	6.440	0.046	7,712	930.6	35.2	0.284
D66-38	O_1m	91.66	7.26	1.08	232	0.155	52.1	3.612	0.026	1,497	396.5	109.4	1.293

ND, no data.

contamination was removed by flushing the lines first for 15–20 min. The chemical composition of the main components and the stable carbon isotopic data for alkane gas were available from Liu *et al.* (2015) and Wu *et al.* (2017a). Noble gas concentrations and isotopic ratios were measured using a Noblesse SFT noble gas mass spectrometer at the Key Laboratory of Petroleum Resources Research, Chinese Academy of Sciences, in Lanzhou.

The gas was purified using a spongy titanium furnace at 800°C to remove active gases (C_1–C_4, N_2, CO_2, *etc.*) and then separated at a temperature ranging from 8 to 100 K using a cryogenic trap filled with activated charcoal. Noble gases were adsorbed in the trap at 8 K for 20 min, and He, Ne, and Ar gases were released for analysis at the temperature of 15, 50, and 100 K, respectively. ^4He isotope was analyzed using a Faraday collector, and ^3He was analyzed using an electric multiple detector. ^{20}Ne isotope was analyzed using a Faraday collector. ^{40}Ar and ^{36}Ar isotopes were analyzed using a Faraday cup. The volume of He, Ne, and Ar, respectively, was determined for the calibration of their concentration. The detailed analytical procedure can be seen in Cao *et al.* (2018).

The authors have also collected noble gas data from the Sichuan (Fan, 1999; Wu et al., 2013; Ni et al., 2014; Dai et al., 2017), Bohai Bay (Dai et al., 2005b; Zhang et al., 2008), Songliao (Liu et al., 2016), Subei (Xu et al., 1997; Liu et al., 2017), Tarim (Liu et al., 2018), and Ordos (Dai et al., 2017) basins for comparative analysis.

RESULTS

The He, Ne, and Ar concentrations and isotopic ratios of natural gas from the Daniudi gas field in Ordos Basin are listed in **Table 1**.

Helium Concentrations

The helium concentrations of natural gas from the Upper Paleozoic C_3t, P_1s, and P_1x reservoirs of the Daniudi gas field are in the ranges of 0.0271–0.0452, 0.0316–0.0415, and 0.0371–0.1273%, respectively, with the corresponding average values of 0.034% ($N = 5$), 0.0367% ($N = 6$), and 0.054% ($N = 8$) (**Table 1**; **Figure 3A**). One gas sample (Well D66-38) from the Lower Paleozoic O_1m reservoir displays a lower helium concentration of 0.0232% (**Table 1**; **Figure 3A**).

Helium Isotopic Compositions

The $^3He/^4He$ ratio of air (Ra) is generally considered as 1.4×10^{-6} (Mamyrin et al., 1970), whereas the $^3He/^4He$ ratios (R) of natural gas in the Daniudi gas field are in the range of (0.9128–10.115) $\times$ 10^{-8}, and thus the calculated R/Ra ratios of the gas range from 0.007 to 0.072 (**Table 1**). The R/Ra ratios of the C_3t, P_1s, and P_1x gases are in the ranges of 0.017–0.057, 0.007–0.072, and 0.007–0.046, with average values of 0.035, 0.024, and 0.026, respectively (**Table 1**). The O_1m gas sample has a R/Ra ratio of 0.026 (**Table 1**).

$^4He/^{20}Ne$ and $^{40}Ar/^{36}Ar$ Ratios

The $^4He/^{20}Ne$ ratios of the C_3t, P_1s, and P_1x gases from the Daniudi gas field are in the ranges of 1,263–7,712, 1,756–8,300, and 848–17,000, respectively, and the corresponding $^{40}Ar/^{36}Ar$ ratios are in the ranges of 376.6–930.6, 901.7–2,328.2, and 368.7–1,163.9, respectively (**Table 1**). The O_1m gas sample has $^4He/^{20}Ne$ and $^{40}Ar/^{36}Ar$ ratios of 1,499 and 396.5, respectively (**Table 1**).

$CH_4/^3He$ and $CO_2/^3He$ Ratios

The $CH_4/^3He$ ratios of the P_1x, P_1s, and C_3t gases from the Daniudi gas field are in the ranges of (26.0–261.9) $\times$ 10^9,

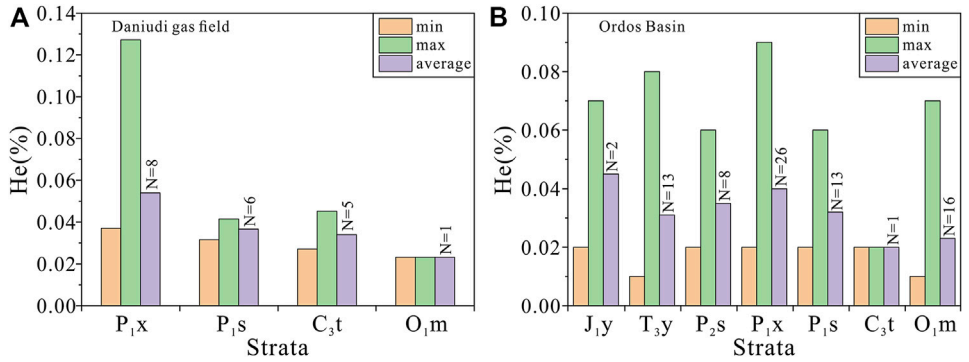

FIGURE 3 | Distribution of helium concentrations in natural gas from different strata in the Daniudi gas field **(A)** and Ordos Basin **(B)**. The data in **(B)** are from Dai *et al*. (2017).

(23.4–259.8) × 10^9, and (25.1–139.6) × 10^9, respectively, with corresponding average values of 77.4 × 10^9 (N = 8), 127.6 × 10^9 (N = 6), and 74.9 × 10^9 (N = 5) (**Table 1**). The $CO_2/^3He$ ratios of these gases are in the ranges of (0.081–1.621) × 10^9, (0.237–2.097) × 10^9, and (0.240–3.941) × 10^9, respectively, with corresponding average values of 0.446 × 10^9, 1.269 × 10^9, and 1.679 × 10^9 (**Table 1**). The O_1m gas sample has $CH_4/^3He$ and $CO_2/^3He$ ratios of 109.4 × 10^9 and 1.293 × 10^9, respectively (**Table 1**).

DISCUSSION

Helium Abundance in Natural Gas

Dai et al. (2017) have classified helium-bearing gas into five categories based on helium concentration, *i.e.*, helium extremely depleted (He% <0.005%), helium depleted (0.005% ≤He% <0.050%), helium general (0.050% ≤He% <0.150%), helium rich (0.150% ≤He% <0.500%), and helium extremely rich (He % ≥0.500%) gases. The natural gas from the Panhandle–Hugoton field in the US is helium-rich gas with an average helium concentration of 0.586% (Brown, 2019), and the gas from the Weiyuan gas field in Sichuan Basin in China is also helium-rich gas with an average helium concentration of 0.251% for 215 gas samples (Dai et al., 2017).

The natural gas in Ordos Basin is mainly accumulated in the P_1x, P_1s, C_3t, and O_1m reservoirs, and the statistics conducted by Dai *et al.* (2017) indicate that the average helium concentrations are 0.04, 0.032, 0.02, and 0.023%, respectively (**Figure 3B**). The gas is mainly helium-depleted gas with 0.005% ≤He% <0.050%, except for a small amount of gas samples being general gas with 0.050% ≤He% <0.150%. The helium concentrations of 20 gas samples from the Daniudi gas field are in the range of 0.0271–0.1273% (**Table 1**), in which 18 gas samples are helium depleted (0.005% ≤He% <0.050%), and the other two samples from the P_1x reservoirs (wells 1-101 and 2-1) are helium general (0.050% ≤He% <0.150%). The average helium concentration (0.0425%; **Table 1**) is consistent with the standard of helium-depleted gas, with no samples being helium rich or extremely rich.

According to the helium amount in the proved gas reserves, the helium-bearing gas fields can be classified into very small, small, medium, large, and extra-large gas fields, with helium reserves of <5 × 10^6 m^3, (5–25) × 10^6 m^3, (25–50) × 10^6 m^3, (50–100) × 10^6 m^3, and ≥100 × 10^6 m^3, respectively (Dai et al., 2017). The helium reserves of the Panhandle–Hugoton field in the US were 18 × 10^9 m^3 at the time of discovery (Brown, 2019), and the proved helium reserves of the Weiyuan gas field in Sichuan Basin and the Hetianhe gas field in Tarim Basin in China are 80 × 10^6 and 195.91 × 10^6 m^3, respectively (Tao et al., 2019), which imply that these three fields meet the standard of an extra-large helium gas field. The proved gas reserves of the Daniudi gas field are 454.563 × 10^9 m^3 (Yang and Liu, 2014), and the proved helium reserves are calculated as 193.19 × 10^6 m^3 according to the average helium concentration of 0.0425% (**Table 1**), which also meet the standard of an extra-large helium gas field.

The only profitable way to produce helium is believed to be by extracting from helium-bearing natural gas, and it was previously considered that helium concentrations were required to reach 0.1% (Tao et al., 2019; Chen et al., 2021). Helium was profitably produced as a byproduct of liquefied natural gas in Qatar, and the economically required helium concentrations can be as low as 0.04% (Anderson, 2018). The average helium concentration in natural gas from the Daniudi gas field is 0.0425% (**Table 1**), which meets the commercial requirement of helium production through the above-mentioned mechanism.

Origin of Helium

Helium in natural gas has three sources, and the typical $^3He/^4He$ ratios of atmospheric, crustal, and mantle-derived helium are 1.4 × 10^{-6} (Mamyrin et al., 1970), 2 × 10^{-8}, and 1.1 × 10^{-5} (Lupton, 1983; Xu, 1996), respectively. The calculated typical R/Ra ratios for crustal and mantle-derived helium are 0.014 and 7.9, respectively. Helium isotopic compositions have been widely used to trace the mantle-derived volatiles (Wakita and Sano, 1983; Oxburgh et al., 1986; Poreda et al., 1988; Xu et al., 1997). It is commonly considered that R/Ra >1 suggests the input of considerable mantle-derived helium, whereas R/Ra ≤0.1

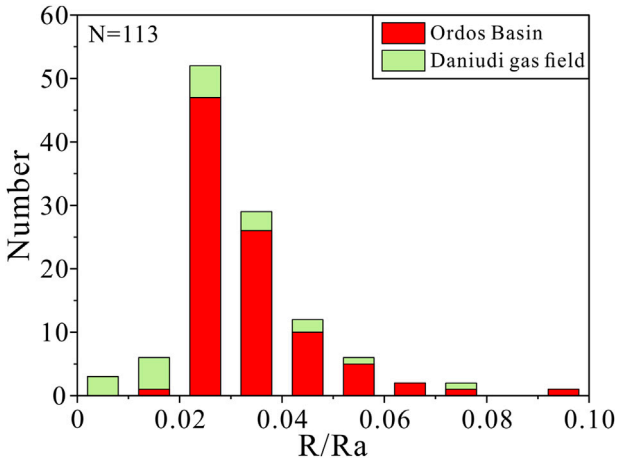

FIGURE 4 | Distribution of the R/Ra ratios of natural gas in Ordos Basin (Dai et al., 2017) and the Daniudi gas field.

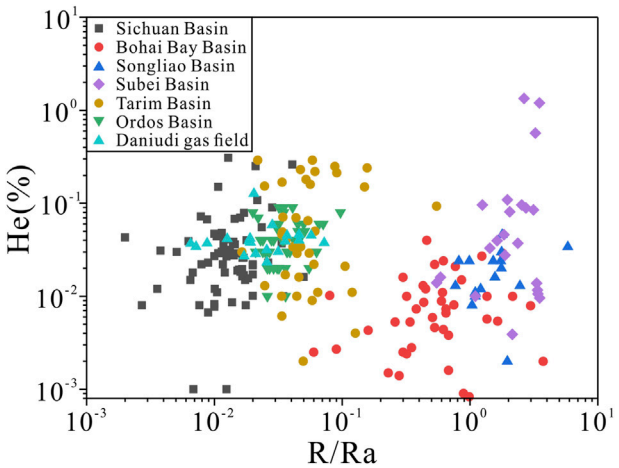

FIGURE 5 | Correlation of He (%) *versus* R/Ra of natural gas in the Daniudi gas field and typical petroliferous basins in China.

implies typical crustal helium (Xu et al., 1998; Li et al., 2017; Chen et al., 2021).

The study on helium isotopic compositions of natural gas in Chinese sedimentary basins indicated that the distribution pattern of $^{3}He/^{4}He$ ratios was controlled by the tectonic environment (Xu et al., 1995a). Both the Ordos and Sichuan basins belong to the central tectonic domain in China, with almost pure crustal helium (Xu et al., 1995a). Helium gas from the Sinian to Jurassic reservoirs in Sichuan Basin is of typical crustal origin (Ni et al., 2014). The R/Ra ratios of 113 gas samples from the basin are in the range of 0.002–0.05, with an average of 0.015, and a correlation between the R/Ra ratios and He concentrations is not observed (Wang et al., 2020).

The 93 gas samples from the Lower Ordovician Majiagou to Lower Jurassic Yan'an formations in Ordos Basin have R/Ra ratios of 0.0148–0.0974, with an average of 0.0334 (Dai et al., 2017). The R/Ra ratios for the Daniudi gas field range from 0.007 to 0.072 (**Table 1**), which are consistent with those for other areas of Ordos Basin (**Figure 4**). The R/Ra ratios for the different gas fields, including the Daniudi gas field, in the basin are lower than 0.1 (**Figure 4**), suggesting typical crustal origin with few mantle-derived helium, and the R/Ra ratios and He concentrations display few correlations (**Figure 5**). Therefore, helium in natural gas from the Daniudi gas field is supposed to be derived from the radioactive decay of U and Th in the rocks and minerals. Since the rocks and minerals in different strata, including P_1x, P_1s, and C_3t, contain various contents of U and Th, the radioactive decay of these U and Th could generate different concentrations of helium, and the generated helium could mix and accumulate in the reservoirs. Moreover, it is much easier for helium to migrate than alkane gas due to its smaller molecular. Therefore, it seems impossible to figure out where and which strata the rocks and minerals are from. Ordos Basin is a cratonic basin (Xu et al., 1995a; Dai et al., 2017) characterized by gentle structure and stable subsidence with a few faults or magmatism (Wu et al., 2017a). Natural gas from cratonic basins (*e.g.*, Sichuan, Ordos) in China has significantly lower R/Ra ratios than that from rift basins (*e.g.*, Bohai Bay) (**Figure 5**), indicating a few inputs of mantle-derived helium in the cratonic basins (Dai et al., 2017).

The He concentrations and R/Ra ratios of natural gas from different petroliferous basins in China are uncorrelated (**Figure 5**). The natural gas from Bohai Bay Basin has been contributed by a small amount of mantle-derived components, with R/Ra ratios and He concentrations commonly higher than 0.1 and lower than 0.1%, respectively (**Figure 5**). Although gases from the Subei and Songliao basins display a substantial contribution of mantle-derived helium with R/Ra ≥0.5, the He concentrations are generally lower than 0.1 (**Figure 5**). The natural gases from the Sichuan, Ordos, and Tarim basins are mainly of crustal origin, with R/Ra <0.1, and the He concentrations are principally lower than 0.1%, suggesting few differences with those for the Subei and Songliao basins (**Figure 5**). Therefore, the contribution of mantle-derived helium does not necessarily lead to the increase of He concentrations (**Figure 5**).

The natural gases from the Sinian and pre-Sinian strata in southern Sichuan Basin have high helium abundance compared to those from the other areas of the basin, suggesting an increase of crustal helium with time (Ni et al., 2014). However, the helium abundance of natural gas from different strata of the Daniudi gas field and other areas of Ordos Basin displays a few increase with time (**Figure 3B**), which indicates a little accumulation effect of crustal helium with time.

Helium Relationship With Argon and Neon Isotopes

Li *et al.* (2017) have proposed a diagram of $^{3}He/^{4}He$ *versus* $^{40}Ar/^{36}Ar$ to identify gases of crustal and mantle origins, which determines different participation degrees of mantle-derived components according to the $^{3}He/^{4}He$ ratios (**Figure 6**). The natural gas from Subei Basin generally has a higher $^{3}He/^{4}He$ ratio

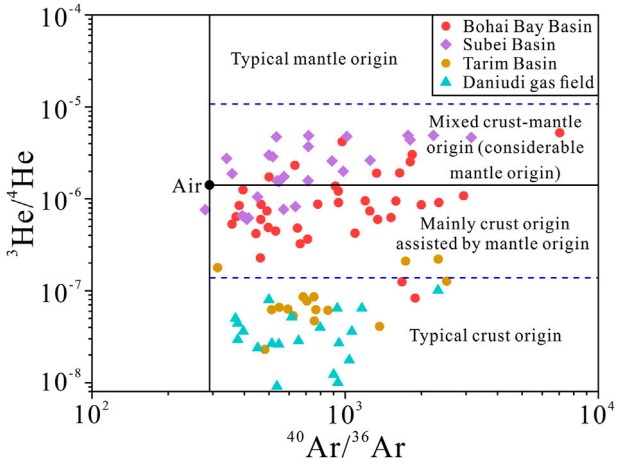

FIGURE 6 | Correlation of $^3He/^4He$ *vs.* $^{40}Ar/^{36}Ar$ of natural gas in the Daniudi gas field and typical petroliferous basins in China [modified after Li *et al.* (2017)].

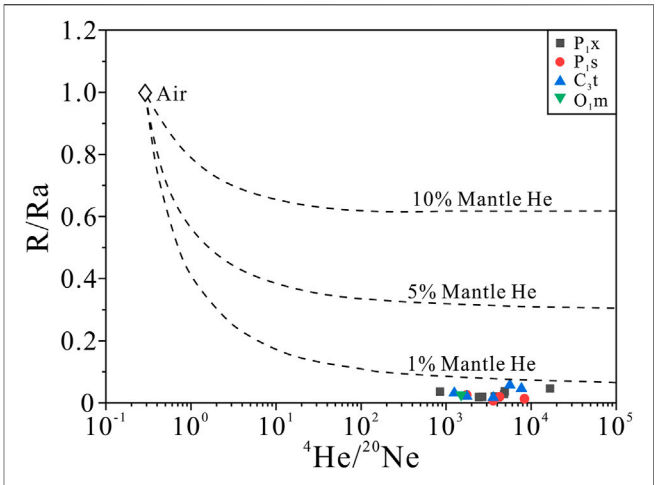

FIGURE 7 | Correlation of R/Ra *versus* $^4He/^{20}Ne$ of natural gas in the Daniudi gas field [modified after Zhang *et al.* (2019)].

than the air, *i.e.*, R/Ra >1, suggesting the mixed crust–mantle origin with considerable mantle helium (**Figure 6**). The natural gases from Bohai Bay Basin are mainly of crust origin assisted by mantle origin with R/Ra >0.1, and some of the gases are of mixed crust–mantle origin (with considerable mantle origin) with R/Ra >1 (**Figure 6**). The $^{40}Ar/^{36}Ar$ ratios for the Daniudi gas field in Ordos Basin range from 368.7 to 2,328.2 with R/Ra <0.1 (**Table 1**), suggesting a typical crust origin, and the $^3He/^4He$ and $^{40}Ar/^{36}Ar$ ratios are uncorrelated (**Figure 6**).

The $^4He/^{20}Ne$ ratios of natural gas from the Daniudi gas field range from 848 to 17,000 (**Table 1**), which are substantially higher than the ratio of air (0.318; Sano et al., 2013) or air-saturated water (ASW) (0.288, Kipfer et al., 2002). Therefore, atmospheric or ASW-derived helium has little contribution to natural gas in the field. The proportion of mantle-derived helium in the gas is less than 1% as indicated in the correlation diagram between R/Ra and $^4He/^{20}Ne$ ratios, which suggests the typical characteristics of crustal noble gas (**Figure 7**). Zhang *et al.* (2019) have used noble gases to trace ground water evolution and assessed helium accumulation in Weihe Basin in China, which provides an example for us to study the role of water in the migration of helium. It is a pity that we have not conducted such studies in the Daniudi gas field, and the present work only focused on the geochemical characteristics of helium in natural gas.

Helium Relationship With CH_4 and CO_2 Abundances

The CH_4 content of natural gas from the Daniudi gas field is in the range of 87.98–97.52%, with an average of 91.04%, whereas the CO_2 content is in the range of 0.09–11.22%, with an average of 0.96% (**Table 1**). Both the CH_4 and CO_2 contents have an insignificant correlation with the R/Ra ratios (**Figures 8A,B**), indicating that the origins of CH_4 and CO_2 are uncorrelated with the origin of He. Helium in natural gas from the Daniudi gas field is of crustal origin (**Figure 6**, **Figure 7**) and derived from the radioactive decay of U and Th in crustal rocks and minerals. The genetic identification of natural gas indicates that alkane gases, including CH_4, in the field are thermogenic and sourced from the direct or indirect thermal cracking of organic matters (Liu et al., 2015; Wu et al., 2017a; Wu et al., 2017b). CO_2 in natural gas from the Chinese cratonic basins (Sichuan and Ordos) commonly has contents lower than 5% (**Figure 8B**) and associated with the hydrocarbon generation process and decomposition of carbonates (Dai et al., 2017). However, natural gas from the rift basins (Bohai Bay, Subei, and Songliao) may have higher CO_2 contents of up to 100% (**Figure 8B**), and this CO_2 is of magmatic or mantle-derived origin (Dai et al., 2017). Therefore, the CO_2 contents and R/Ra ratios of natural gas from Chinese sedimentary basins generally have few correlations due to the different origins of CO_2 and He, except that only a few gas samples from rift basins (Bohai Bay, Subei, and Songliao) with both high CO_2 contents and R/Ra ratios were directly from magmatism or mantle degassing (**Figure 8B**).

The cross-plot of $CH_4/^3He$ *versus* R/Ra is conducive to constrain the possible crustal and magmatic source of natural gas (Poreda et al., 1986; Jenden et al., 1993; Ni et al., 2014; Dai et al., 2017). Ni *et al.* (2014) and Dai *et al.* (2017) have demonstrated that most gases from cratonic basins (Ordos, Sichuan, and Tarim) in China have $CH_4/^3He$ ratios mainly between 10^9 and 10^{12}, with R/Ra <0.1, suggesting a typical crustal origin, whereas the gases from rift basins (Bohai Bay, Songliao, and Subei) commonly display $CH_4/^3He$ ratios between 10^6 and 10^{11}, with R/Ra >0.1, indicating the incorporation of magmatic components (**Figure 9A**). The $CH_4/^3He$ ratios of natural gas from the Daniudi gas field are in the range of $(23.4–261.9) \times 10^9$ (**Table 1**), which are consistent with those from other areas of Ordos Basin (**Figure 9A**).

The $CO_2/^3He$ ratios of natural gas from magmatic systems are within a narrow range (10^9–10^{10}) compared with those of crustal fluids (10^5–10^{13}) (Ballentine et al., 2000). In the plot of $CO_2/^3He$ *versus* R/Ra, natural gas from active continental margins was explained by a two-component mixing between a crustal high-$CO_2/^3He$, low-R/Ra end-member and a magmatic low-$CO_2/^3He$, high-R/Ra end-member (Poreda et al., 1988). The varying $CO_2/^3He$ (3.0×10^7–1.3×10^{10}) and low R/Ra (0.002–0.035) ratios of natural

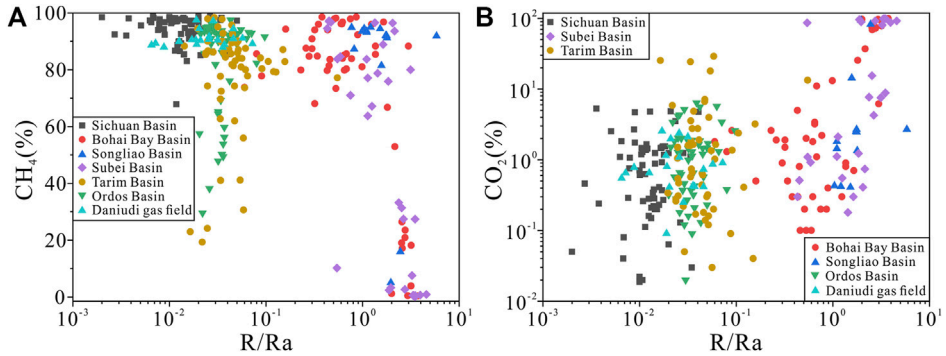

FIGURE 8 | Cross-plots of CH_4 (%) **(A)** and CO_2 (%) **(B)** *vs*. R/Ra of natural gas in the Daniudi gas field and typical petroliferous basins in China.

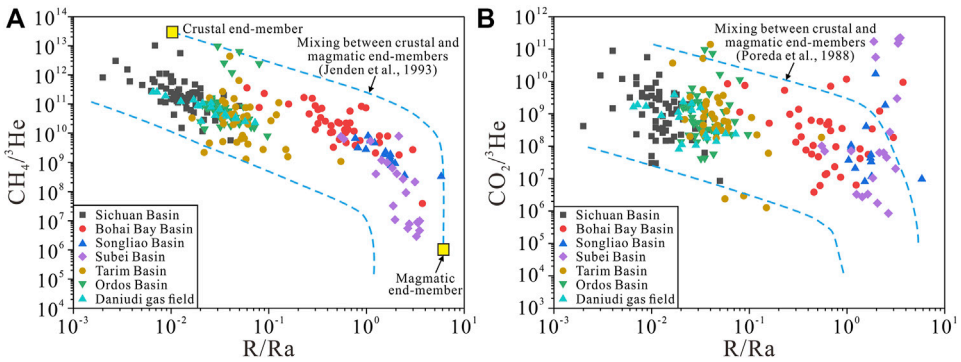

FIGURE 9 | Cross-plots of $CH_4/^3He$ *versus* R/Ra **(A)** and $CO_2/^3He$ *versus* R/Ra **(B)** of natural gas in the Daniudi gas field and typical petroliferous basins in China. Crustal end-member, magmatic end-member, and the mixing line in **Figure 1** are from Jenden *et al*. (1993), and the mixing line in **Figure 1** is from Poreda *et al*. (1988).

gas from eastern Sichuan Basin suggest a typical crustal origin (Wu et al., 2013). The $CO_2/^3He$ ratios of natural gas from the Daniudi gas field range from 0.081×10^9 to 3.941×10^9, with R/Ra <0.1 (**Table 1**), which are consistent with those from other areas in Ordos Basin (**Figure 9B**). The natural gases from cratonic basins (Ordos, Sichuan, and Tarim) in China display crustal characteristics of both $CO_2/^3He$ and R/Ra ratios, whereas those from rift basins (Songliao, Bohai Bay, and Subei) display the contribution of magmatic end-member (**Figure 9B**).

Moreover, it is noteworthy that the $CH_4/^3He$ ratio does not necessarily mean that the hydrocarbon gas is organic or inorganic since the CH_4 and He might be derived from the crust and the mantle, respectively (Dai et al., 2017). The $CO_2/^3He$ ratio may display similar features. Therefore, great attention has to be paid to only use these two parameters, and the identification of natural gas origin needs to be conducted based on comprehensive analyses of more parameters.

Future Prospects of Helium in Natural Gas in China

Helium is considered as an exhaustible natural resource with strategic values, and the replaceable role and wide application of helium determine that helium gas exploration needs more input and investment. The relevant studies on helium in natural gas in China mainly focused on the helium contents and isotopic compositions. However, the migration and accumulation mechanisms are weakly studied. The understandings of both origin and source of helium will be conducive to reveal the migration pathways and accumulation model. To accelerate the studies on the enrichment mechanisms of helium is an effective approach to find more helium resources.

CONCLUSION

The helium concentrations of natural gas from the Daniudi gas field in Ordos Basin are in the range of 0.0271–0.1273%, with an average helium concentration of 0.0425%. The $^3He/^4He$ ratios of the gas are in the range of $(0.9128–10.115) \times 10^{-8}$, and the calculated R/Ra ratios range from 0.007 to 0.072. The $^4He/^{20}Ne$ ratios are in the range of 848–17,000, with the $^{40}Ar/^{36}Ar$ ratios ranging from 368.7 to 2,328.2. The $CH_4/^3He$ and $CO_2/^3He$ ratios of the gas are in the ranges of $(23.4–261.9) \times 10^9$ and $(0.081–3.941) \times 10^9$, respectively.

The Daniudi gas field is an extra-large helium gas field with proved helium reserves of over 100×10^6 m^3. Helium from the

different strata of the field is of crustal origin, with R/Ra <0.1, and it is supposed to be derived from the radioactive decay of U and Th in the rocks and minerals, with little contribution by atmospheric or mantle-derived helium. The natural gases from cratonic basins (Ordos, Sichuan, and Tarim) in China display crustal helium characteristics, whereas those from rift basins (Songliao, Bohai Bay, and Subei) display the contribution of mantle-derived helium.

DATA AVAILABILITY STATEMENT

The original contributions presented in the study are included in the article/supplementary material. Further inquiries can be directed to the corresponding author.

AUTHOR CONTRIBUTIONS

QL contributed to conceptualization, data curation, and writing. XW contributed to data curation and writing. HJ contributed to conceptualization. CN contributed to data curation and methodology. JZ contributed to methodology and investigation. JM contributed to investigation. DZ contributed to methodology. QM contributed to investigation. WP contributed to data curation. HX contributed to investigation.

FUNDING

This work was funded by the National Natural Science Foundation of China (grant nos.: U20B6001, 42141021, 42172149, and 41872122) and the Strategic Priority Research Program of the Chinese Academy of Sciences (Class A) (grant nos. XDA14010402 and XDA14010404).

ACKNOWLEDGMENTS

The authors appreciate Prof. Jinxing Dai, academician of the Chinese Academy of Sciences, for the long-standing guidance on the relevant studies. The SINOPEC North China Branch Company is acknowledged for the assistance on sample collection.

REFERENCES

Anderson, D. L. (2000). The Statistics and Distribution of Helium in the Mantle. *Int. Geol. Rev.* 42, 289–311. doi:10.1080/00206810009465084

Anderson, S. T. (2018). Economics, Helium, and the U.S. Federal Helium Reserve: Summary and Outlook. *Nat. Resour. Res.* 27, 455–477. doi:10.1007/s11053-017-9359-y

Ballentine, C. J., Schoell, M., Coleman, D., and Cain, B. A. (2000). Magmatic CO_2 in Natural Gases in the Permian Basin, West Texas: Identifying the Regional Source and Filling History. *J. Geochem. Explor.* 69-70, 59–63. doi:10.1016/s0375-6742(00)00045-5

Brown, A. (2019). Origin of Helium and Nitrogen in the Panhandle-Hugoton Field of Texas, Oklahoma, and Kansas, United States. *AAPG Bull.* 103 (2), 369–403. doi:10.1306/07111817343

Cao, C., Zhang, M., Tang, Q., Yang, Y., Lv, Z., Zhang, T., et al. (2018). Noble Gas Isotopic Variations and Geological Implication of Longmaxi Shale Gas in Sichuan Basin, China. *Mar. Pet. Geol.* 89, 38–46. doi:10.1016/j.marpetgeo.2017.01.022

Cao, C., Zhang, M., Li, L., Wang, Y., Li, Z., Du, L., et al. (2020). Tracing the Sources and Evolution Processes of Shale Gas by Coupling Stable (C, H) and noble Gas Isotopic Compositions: Cases from Weiyuan and Changning in Sichuan Basin, China. *J. Nat. Gas Sci. Eng.* 78, 103304. doi:10.1016/j.jngse.2020.103304

Chen, J., Liu, K., Dong, Q., Wang, H., Luo, B., and Dai, X. (2021). Research Status of Helium Resources in Natural Gas and Prospects of Helium Resources in China. *Nat. Gas Geosci.* 32, 1436–1449. doi:10.11764/j.issn.1672-1926.2021.08.006

Dai, J., Li, J., Luo, X., Zhang, W., Hu, G., Ma, C., et al. (2005a). Stable Carbon Isotope Compositions and Source Rock Geochemistry of the Giant Gas Accumulations in the Ordos Basin, China. *Org. Geochem.* 36, 1617–1635. doi:10.1016/j.orggeochem.2005.08.017

Dai, J., Yang, S., Chen, H., and Shen, X. (2005b). Geochemistry and Occurrence of Inorganic Gas Accumulations in Chinese Sedimentary Basins. *Org. Geochem.* 36, 1664–1688. doi:10.1016/j.orggeochem.2005.08.007

Dai, J., Zou, C., Zhang, S., Li, J., Ni, Y., Hu, G., et al. (2008). Discrimination of Abiogenic and Biogenic Alkane Gases. *Sci. China Ser. D Earth Sci.* 51, 1737–1749. doi:10.1007/s11430-008-0133-1

Dai, J., Ni, Y., Qin, S., Huang, S., Gong, D., Liu, D., et al. (2017). Geochemical Characteristics of He and CO_2 from the Ordos (Cratonic) and Bohaibay (Rift) Basins in China. *Chem. Geol.* 469, 192–213. doi:10.1016/j.chemgeo.2017.02.011

Dai, J., Qin, S., Hu, G., Ni, Y., Gan, L., Huang, S., et al. (2019). Major Progress in the Natural Gas Exploration and Development in the Past Seven Decades in China. *Pet. Explor. Develop.* 46, 1100–1110. doi:10.1016/s1876-3804(19)60266-1

Dai, J. (2016). *Giant Coal-Derived Gas Fields and Their Gas Sources in China*. Beijing: Science Press.

Ding, W., Dai, J., Yang, C., Tao, S., and Hou, L. (2005). Helium Isotopic Compositions in Fluid Inclusions of the Gangxi Fault belt in the Huanghua Depression, Bohai Bay Basin. *Chin. Sci. Bull.* 50, 2621–2627. doi:10.1007/bf03183660

Fan, R. (1999). Origin and Migration of Natural Gas in the central Segment of Western Sichuan Depression: Evidence from Carbon Isotope Geochemistry. *Prog. Nat. Sci.* 9, 1126–1132.

Jenden, P. D., Hilton, D. R., Kaplan, I. R., and Craig, H. (1993). "Abiogenic Hydrocarbons and Mantle Helium in Oil and Gas fields," in *The Future of Energy Gases*. Editor D. G. Howell (Denver: U.S. Geological Survey), 31–56. U.S. Geological Survey Professional Paper.

Kipfer, R., Aeschbach-Hertig, W., Peeters, F., and Stute, M. (2002). Noble Gases in Lakes and Ground Waters. *Rev. Mineral. Geochem.* 47, 615. doi:10.2138/rmg.2002.47.14

Li, J., Li, Z., Wang, X., Wang, D., Xie, Z., Li, J., et al. (2017). New Indexes and Charts for Genesis Identification of Multiple Natural Gases. *Pet. Explor. Develop.* 44, 535–543. doi:10.1016/s1876-3804(17)30062-9

Liu, Q., Chen, M., Liu, W., Li, J., Han, P., and Guo, Y. (2009). Origin of Natural Gas from the Ordovician Paleo-Weathering Crust and Gas-Filling Model in Jingbian Gas Field, Ordos basin, China. *J. Asian Earth Sci.* 35, 74–88. doi:10.1016/j.jseaes.2009.01.005

Liu, Q., Jin, Z., Meng, Q., Wu, X., and Jia, H. (2015). Genetic Types of Natural Gas and Filling Patterns in Daniudi Gas Field, Ordos Basin, China. *J. Asian Earth Sci.* 107, 1–11. doi:10.1016/j.jseaes.2015.04.001

Liu, Q., Dai, J., Jin, Z., Li, J., Wu, X., Meng, Q., et al. (2016). Abnormal Carbon and Hydrogen Isotopes of Alkane Gases from the Qingshen Gas Field, Songliao Basin, China, Suggesting Abiogenic Alkanes? *J. Asian Earth Sci.* 115, 285–297. doi:10.1016/j.jseaes.2015.10.005

Liu, Q., Zhu, D., Jin, Z., Meng, Q., Wu, X., and Yu, H. (2017). Effects of Deep CO_2 on Petroleum and thermal Alteration: The Case of the Huangqiao Oil and Gas Field. *Chem. Geol.* 469, 214–229. doi:10.1016/j.chemgeo.2017.06.031

Liu, Q., Jin, Z., Li, H., Wu, X., Tao, X., Zhu, D., et al. (2018). Geochemistry Characteristics and Genetic Types of Natural Gas in central Part of the Tarim Basin, NW China. *Mar. Pet. Geol.* 89, 91–105. doi:10.1016/j.marpetgeo.2017.05.002

Lupton, J. E. (1983). Terrestrial Inert Gases: Isotope Tracer Studies and Clues to Primordial Components in the Mantle. *Annu. Rev. Earth Planet. Sci.* 11, 371–414. doi:10.1146/annurev.ea.11.050183.002103

Mamyrin, B. A., Anufrier, G. S., Kamensky, I. L., and Tolstikhin, I. N. (1970). Determination of the Isotopic Composition of Helium in the Atmosphere. *Geochem. Int.* 7, 498–505.

Marty, B., Jambon, A., and Sano, Y. (1989). Helium Isotopes and CO_2 in Volcanic Gases of Japan. *Chem. Geol.* 76, 25–40. doi:10.1016/0009-2541(89)90125-3

Ni, Y., Dai, J., Tao, S., Wu, X., Liao, F., Wu, W., et al. (2014). Helium Signatures of Gases from the Sichuan Basin, China. *Org. Geochem.* 74, 33–43. doi:10.1016/j.orggeochem.2014.03.007

O'Nions, R. K., and Oxburgh, E. R. (1983). Heat and Helium in the Earth. *Nature* 306, 429–431. doi:10.1038/306429a0

Oxburgh, E. R., O'Nions, R. K., and Hill, R. I. (1986). Helium Isotopes in Sedimentary Basins. *Nature* 324, 632–635. doi:10.1038/324632a0

Polyak, B. G., Tolstikhin, I. N., Kamensky, I. L., Yakovlev, L. E., Cheshko, A. L., and Marty, B. (2000). Helium Isotopes, Tectonics and Heat Flow in the Northern Caucasus. *Geochim. Cosmochim. Acta* 64, 1925–1944. doi:10.1016/s0016-7037(00)00342-2

Porcelli, D., Ballentine, C. J., and Wieler, R. (2002). An Overview of Noble Gas Geochemistry and Cosmochemistry. *Rev. Mineral. Geochem.* 47, 1–19. doi:10.2138/rmg.2002.47.1

Poreda, R. J., Jenden, P. D., Kaplan, I. R., and Craig, H. (1986). Mantle Helium in Sacramento basin Natural Gas wells. *Geochim. Cosmochim. Acta* 50, 2847–2853. doi:10.1016/0016-7037(86)90231-0

Poreda, R. J., Jeffrey, A. W. A., Kaplan, I. R., and Craig, H. (1988). Magmatic Helium in Subduction-Zone Natural Gases. *Chem. Geol.* 71, 199–210. doi:10.1016/0009-2541(88)90115-5

Sano, Y., Nakamura, Y., Wakita, H., Urabe, A., and Tominaga, T. (1984). Helium-3 Emission Related to Volcanic Activity. *Science* 224, 150–151. doi:10.1126/science.224.4645.150

Sano, Y., Marty, B., and Burnard, P. (2013). "Noble Gases in the Atmosphere," in *The Noble Gases as Geochemical Tracers*. Editor P. Burnard (Berlin, Heidelberg: Springer), 17–31. doi:10.1007/978-3-642-28836-4_2

Tao, X., Li, J., Zhao, L., Li, L., Zhu, W., Xing, L., et al. (2019). Helium Resources and Discovery of First Supergiant Helium reserve in China: Hetianhe Gas Field. *Earth Sci.* 44, 1024–1041. doi:10.3799/dqkx.2018.381

Wakita, H., and Sano, Y. (1983). 3He/4He Ratios in CH_4-Rich Natural Gases Suggest Magmatic Origin. *Nature* 305, 792–794. doi:10.1038/305792a0

Wang, X., Liu, W., Li, X., Liu, Q., Tao, C., and Xu, Y. (2020). Radiogenic Helium Concentration and Isotope Variations in Crustal Gas Pools from Sichuan Basin, China. *Appl. Geochem.* 117, 104586. doi:10.1016/j.apgeochem.2020.104586

Wu, X., Dai, J., Liao, F., and Huang, S. (2013). Origin and Source of CO_2 in Natural Gas from the Eastern Sichuan Basin. *Sci. China Earth Sci.* 56, 1308–1317. doi:10.1007/s11430-013-4601-x

Wu, X., Liu, Q., Zhu, J., Li, K., Liu, G., Chen, Y., et al. (2017a). Geochemical Characteristics of Tight Gas and Gas-Source Correlation in the Daniudi Gas Field, the Ordos Basin, China. *Mar. Pet. Geol.* 79, 412–425. doi:10.1016/j.marpetgeo.2016.10.022

Wu, X., Zhu, J., Ni, C., Li, K., Wang, Y., Hu, Y., et al. (2017b). Genetic Types and Sources of Lower Paleozoic Natural Gas in the Daniudi Gas Field, Ordos Basin, China. *Energy Explor. Exploit.* 35, 218–236. doi:10.1177/0144598716687932

Xu, S., Nakai, S. i., Wakita, H., Xu, Y., and Wang, X. (1995a). Helium Isotope Compositions in Sedimentary Basins in China. *Appl. Geochem.* 10, 643–656. doi:10.1016/0883-2927(95)00033-x

Xu, S., Nakai, S. i., Wakita, H., and Wang, X. (1995b). Mantle-derived noble Gases in Natural Gases from Songliao Basin, China. *Geochim. Cosmochim. Acta* 59, 4675–4683. doi:10.1016/0016-7037(95)00301-0

Xu, Y., Shen, P., Tao, M., and Liu, W. (1997). Geochemistry on Mantle-Derived Volatiles in Natural Gases from Eastern China Oil/gas Provinces (I). *Sci. China Ser. D Earth Sci.* 40, 120–129. doi:10.1007/bf02878370

Xu, Y., Shen, P., Liu, W., Tao, M., Sun, M., and Du, J. (1998). *Geochemistry of noble Gases in Natural Gas*. Beijing: Science Press.

Xu, Y. (1996). The Mantle noble Gas of Natural Gases. *Earth Sci. Front.* 3, 63–71.

Xu, Y. (1997). Helium Isotope Distribution of Natural Gases and its Structural Setting. *Earth Sci. Front.* 4, 185–190.

Yang, H., and Liu, X. (2014). Progress of Paleozoic Coal-Derived Gas Exploration in Ordos Basin, West China. *Pet. Explor. Develop.* 41, 129–137. doi:10.1016/s1876-3804(14)60017-3

Yang, J., and Pei, X. (1996). *Natural Gas Geology in China*, Vol. 4. Beijing: Petroleum Industry Press.

Yang, Y., Li, W., and Ma, L. (2005). Tectonic and Stratigraphic Controls of Hydrocarbon Systems in the Ordos basin: A Multicycle Cratonic basin in central China. *Bulletin* 89, 255–269. doi:10.1306/10070404027

Zhang, T., Zhang, M., Bai, B., Wang, X., and Li, L. (2008). Origin and Accumulation of Carbon Dioxide in the Huanghua Depression, Bohai Bay Basin, China. *Bulletin* 92, 341–358. doi:10.1306/10230706141

Zhang, W., Li, Y., Zhao, F., Han, W., Li, Y., Wang, Y., et al. (2019). Using noble Gases to Trace Groundwater Evolution and Assess Helium Accumulation in Weihe Basin, central China. *Geochim. Cosmochim. Acta* 251, 229–246. doi:10.1016/j.gca.2019.02.024

Zhao, H., Zhang, Y., and Li, C. (2012). Analysis of Supply and price System for Global Helium Gas. *Chem. Propellants Polymeric Mater.* 10, 91–96. doi:10.16572/j.issn1672-2191.2012.06.003

Conflict of Interest: QL, XW, HJ, CN, JZ, JM, DZ, QM, WP, and HX were employed by the company SINOPEC.

Publisher's Note: All claims expressed in this article are solely those of the authors and do not necessarily represent those of their affiliated organizations or those of the publisher, the editors, and the reviewers. Any product that may be evaluated in this article or claim that may be made by its manufacturer is not guaranteed or endorsed by the publisher.

frontiers in Earth Science

ORIGINAL RESEARCH
published: 21 February 2022
doi: 10.3389/feart.2022.809418

Mercury Isotopes in Shale Gas From Wufeng-Longmaxi Shale Formation of Sichuan Basin, Southern China: A Preliminary Investigation

Shunlin Tang[1], Yuxiang Ding[1], Guangyou Zhu[2]*, Xinbin Feng[3], Huaishun Zhang[1] and Penggao Li[1]*

[1]Institute of Resources and Environment, Henan Polytechnic University, Jiaozuo, China, [2]Research Institute of Petroleum Exploration and Development, PetroChina, Beijing, China, [3]State Key Laboratory of Environmental Geochemistry, Institute of Geochemistry, Chinese Academy of Sciences, Guiyang, China

A series of investigations have been conducted concerning the study of traditional stable isotopes and rare gas stable isotopes in natural gas. However, little is known regarding non-traditional stable isotopes of mercury in natural gas, especially in the development and utilization of shale gas in recent years. In fact, the presence of mercury in natural gas (including shale gas) provides a basis for research on mercury isotopes. Mercury was extracted from shale gas at the Wufeng-Longmaxi Formation in the YS108 block of the Zhaotong National shale gas demonstration area in the Sichuan Basin by using an acid potassium permanganate solution, followed by the analysis of mercury content and stable isotope composition. The mercury content in the marine shale gas at the Wufeng-Longmaxi Formation ranged from 171 to 2,906 ng/m^3, with an average of 1,551.08 ± 787.08 ng/m^3 (n = 37, 1 SD). The Δ^{199}Hg values of mercury stable isotopes range from 02‰ to 0.39‰, with an average of 22‰ ± 0.08‰ (n = 37, 1 SD); the δ^{202}Hg values range from –1.68‰ to –0.04‰, with an average of –0.87‰ ± 0.31‰ (n = 37, 1 SD), which are significantly different from the Δ^{199}Hg and δ^{202}Hg information of coalbed gas, but similar to the Δ^{199}Hg and δ^{202}Hg information of terrestrial oil-type gas and the Δ^{199}Hg in the main hydrocarbon-forming organic matter of lower organisms such as algae (t-test, $p > 0.05$). This indicates that terrestrial target strata with abundant algae or strata with positive Δ^{199}Hg are the target strata for the exploration of terrestrial oil and gas.

Keywords: mercury stable isotope, mass-independent fractionation, mercury content, shale gas, exploration target layer

OPEN ACCESS

Edited by:
Qinhong Hu,
University of Texas at Arlington, United States

Reviewed by:
Xiao Xianming,
China University of Geosciences, China
Hui Tian,
Guangzhou Institute of Geochemistry (CAS), China

****Correspondence:***
Shunlin Tang
tangshunlin@hpu.edu.cn
Guangyou Zhu
zhuguangyou@petrochina.com.cn

Specialty section:
This article was submitted to Geochemistry, a section of the journal Frontiers in Earth Science

Received: *05 November 2021*
Accepted: *17 January 2022*
Published: *21 February 2022*

Citation:
Tang S, Ding Y, Zhu G, Feng X, Zhang H and Li P (2022) Mercury Isotopes in Shale Gas From Wufeng-Longmaxi Shale Formation of Sichuan Basin, Southern China: A Preliminary Investigation. Front. Earth Sci. 10:809418. doi: 10.3389/feart.2022.809418

INTRODUCTION

As proposed by Ozerova (1983), the concentration of mercury (elemental mercury, Hg^0) reflects the origin of natural gas. Dai (1992) showed that Hg^0 concentrations are greater than 700 ng/m^3 in coalbed gas and less than 500 ng/m^3 in oil-type gas. However, Hg^0 concentrations vary significantly within a single gas field (Liu, 2013). As a result, the Hg^0 concentration alone is an imprecise estimate of the natural gas source.

Mercury is commonly found in oil and gas (including shale gas) and mainly exists in the form of elemental mercury, which provides a basis for the study of mercury isotopes. There are seven

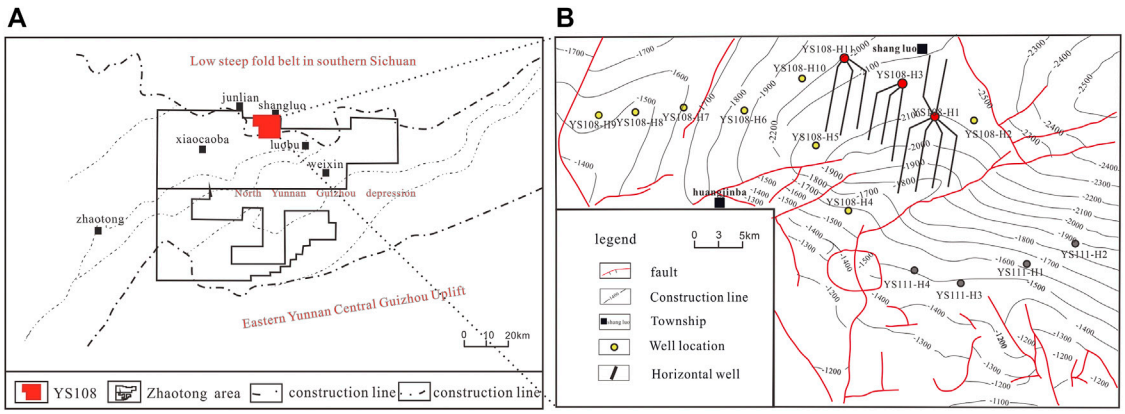

FIGURE 1 | Structural map of Zhaotong Demonstration Zone **(A)** and YS108 Block **(B)** [Figure A is modified according to Xu et al. (2019), and Figure B is modified according to Huang et al. (2019)]. In Figure B, the red wells are the sampling sites, and the horizontal wells of the related wells are drawn. The yellow and gray wells are other wells in the block.

stable isotopes of mercury: ^{196}Hg (0.15%), ^{198}Hg (9.97%), ^{199}Hg (16.87%), ^{200}Hg (23.10%), ^{201}Hg (13.18%),^{202}Hg (29.86%), and ^{204}Hg (6.87%). The relative mass difference between the isotopes was up to 4%. Mercury is the only identified heavy metal element that can undergo mass-dependent fractionation (MDF) and mass-independent fractionation (MIF). A series of important natural processes involved in the geochemical cycle of mercury, such as volatilization and evaporation (Lefticariu et al., 2011), oxidation/reduction (Foucher et al., 2009), microbial methylation/demethylation (Feng et al., 2010; Yin et al., 2013), photoreduction reactions (Bergquist and Blum, 2007; Kwon et al., 2020), and natural hydrothermal systems [(Smith et al., 2008; Stetson et al., 2009), can lead to significant mercury isotope mass-dependent fractionation. Photoreaction is the main natural process leading to the mass-independent fractionation of mercury stable isotopes (Bergquist and Blum, 2007; Kwon et al., 2020), where mercury isotopes are essential in tracing mercury sources and geochemical processes. Many studies have been conducted on mercury isotopes in organic matter correlated to oil and gas, such as algae and phytoplankton (Perrot et al., 2012; Tsui et al., 2012), invertebrates (Blum et al., 2014), lake sediments, marine sediments (Feng et al., 2010; Ma et al., 2013), terrestrial plants (Sun et al., 2017; Wang et al., 2017), lichens (Carignan et al., 2009), peat (Enrico et al., 2017; Enrico et al., 2016; Shi et al., 2011), coal (Biswas et al., 2008; Lefticariu et al., 2011; Sun et al., 2016), and soil (Foucher et al., 2009; Yin et al., 2013). The Hg isotopic ratios show promise as a method for distinguishing different sources of natural gas. Stable isotopes of mercury in oil-type gas and coalbed gas have been studied (Washburn et al., 2018; Tang et al., 2019); however, stable isotopes of mercury in shale gas have not yet been reported.

Shale gas, as a clean, efficient, and low-carbon unconventional natural gas, has multiple effects such as economy, society, and environment. The development and utilization of shale gas help achieve the goals of "carbon peak" and "carbon neutrality," which has become an important part of the energy structure of the world. The research object of this study is the existing shale gas in the Zhaotong Block of the Sichuan Basin. The mercury in shale gas was collected on-site, whereby we analyzed the mercury content and stable isotope composition of mercury in the samples. Further, we compared the mercury stable isotope compositions of oil-type gas and coalbed gas in previous studies. As such, we summarized, herein, the general characteristics of the mercury isotope composition of shale gas, and discussed the main material sources and exploration indicative significance of shale gas.

MERCURY CAPTURE AND ANALYSIS OF MERCURY CONTENT AND MERCURY ISOTOPE IN SHALE GAS

Geological Overview of Sampling Sites

The sampling site is located in the YS108 Block, Zhaotong National Shale Gas Demonstration Area, Sichuan Basin (**Figure 1**). The block is one of the first national shale gas demonstration zones in China and is an important part of commercial shale gas in China (Chen et al., 2019). The YS108 block is located in Gongxian County and Junlian County, Yibin City, Sichuan Province, adjacent to the Changning shale gas block, which is structurally located at the southern edge of the low-steep fold belt in the southern Sichuan Tai Depression and adjacent to the northern depression of Yunnan and Guizhou (**Figure 1A**). The main gas-producing zone is the upper Wufeng Formation of the Ordovician and lower Longmaxi Formation of Silurian, characterized by a buried depth of 2,000–2,500 m, and it is the main zone for shale gas horizontal well development in the block (**Figure 1B**). As a whole, it belongs to a set of black siliceous shale and organic-rich black carbonaceous shale

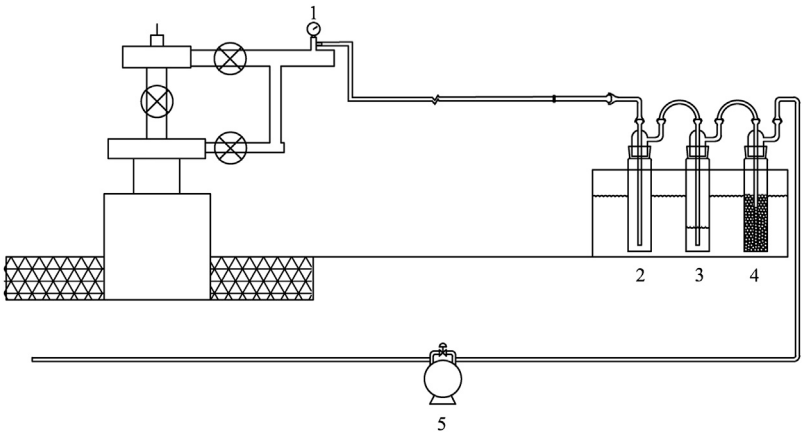

FIGURE 2 | Mercury capture device for shale gas [Description: 1. Sampling port; 2. Empty bottles; 3. Impact bottle with 4% (W/V) $KMnO_4$+1% (V/V) H_2SO_4 solution; 4. Impact bottle with color-changing silicone; 5. Gas flowmeter].

deposited in marine deepwater shelf subfacies, with large sedimentary thickness (30–40 m), high organic matter abundance, thermal evolution degree (TOC ≥2.0%, Ro: 2.0–3.5%), adequate gas content (3.0–4.6 m^3/t), adequate reservoir performance (Φ: 1.56–5.27%), and high compressibility (brittleness index: 44%–78%). The target formation has the characteristics of overpressure (pressure coefficient 1–1.9), and is a favorable shale gas development formation (Dai et al., 2014; Wang et al., 2016).

Sample Collection and Processing

The mercury in the shale gas of seven gas accumulation wells from three gas accumulation platforms in Block YS108 of Zhaotong National Shale Gas Demonstration Zone in Sichuan Basin was collected on-site, denoted as H1-3, H1-6, H3-1, H3-2, H11-1, H11-2, and H11-3 gas accumulation wells. A total of 37 samples of mercury capture fluid from shale gas were collected.

Mercury in shale gas is captured by potassium permanganate ($KMnO_4$) and sulfuric acid (H_2SO_4) mixture: Hg^0 in shale gas was oxidized to ionic form mercury and captured and retained in acidic potassium permanganate solution (**Figure 2**) by taking advantage of the strong oxidation and super absorption of mercury in acidic potassium permanganate solution, such that the acidic potassium permanganate solution was recovered as a sample for mercury content and mercury isotope analysis. In previous studies (Tang et al., 2019), we used three series of acid potassium permanganate cylinders to capture mercury in oil-type gas and coalbed gas, but laboratory simulations and mercury isotope tests found that Hg^0 is mainly enriched in the first impinger (the percentage of mercury content is 76%–97%), and the isotopic composition of total mercury is consistent with that of the solution of the first impinger. Therefore, we simplified the mercury capture device for shale gas, and the main body of the mercury capture device was composed of three impingers (Environmental Supply Company, United States, 500 ml for each sampling bottle) in series. The first impinger was an empty bottle for separating water vapor in shale gas, ensuring the concentration of acidic potassium permanganate mixture in the second impinger, mercury capture efficiency, and mercury capture time. The second impinger contained 100 ml of 4% (w/v) $KMnO_4$ and 1% (v/v) H_2SO_4. Hg^0 in shale gas was oxidized to ionic mercury and captured and retained in an acid potassium permanganate solution. The acid potassium permanganate solution was recovered as a sample for mercury content and mercury isotope analysis in shale gas. The third impinger contained approximately 100 mg of discolored silica gel, which was used to absorb the water vapor attached to the remaining gas to prevent its impact on the subsequent gas flowmeter. The three impingers were fixed in a cold-water tank.

To ensure the authenticity of mercury capture in shale gas, the used chemical reagents, drugs, impingers, and their connecting tubes need to be processed in advance, which requires a low blank value of mercury. Potassium permanganate was purchased from the United States (mercury content is <0.002 ng/ml), sulfuric acid is eminently pure (mercury content is <0.004 ng/ml), and the impinger and its connecting parts are borosilicate glass bottles purchased from the United States and have been subjected to high-temperature treatment in a muffle furnace. The purchased PTFE pipe was used to connect the pipe from the shale gas wellhead to the impinger. Before sampling, the entire sampling device was directly flushed with the original natural gas of the shale gas wellhead for approximately 3–5 min, and the acid potassium permanganate mercury-capturing mixture prepared on-site was quickly filled and connected to the whole device. Each sample captures 1 m^3 of mercury in shale gas, which ensures the representativeness of the capture shale gas and enriches enough mercury to meet the requirements of mercury isotope analysis. During the sampling process, the color of the

mercury capture liquid should always be purple. Once it becomes colorless, the sampling should be immediately stopped. The acidic potassium permanganate mixture was recovered as the sample, and the volume of the mixture and gas flowmeter data were recorded. After each sampling, the mercury capture solution was recovered, and the volume was recorded with a measuring cylinder and transferred to a borosilicate glass bottle. Approximately 0.5 ml of potassium dichromate solution (30%, w/v) was immediately added, sealed, numbered, and transported back to the laboratory for testing.

Analysis of Mercury Content

The mercury content of the captured mercury from acid potassium permanganate was determined by using the RA-915 M mercury meter and its liquid attachment. After the standard curve was plotted depicting the mercury standard solution, approximately 10 ml of acidic $KMnO_4$ solution sample was added to the centrifuge tube, and then approximately 0.5 ml of NH_2OH-HCl solution with a mass volume fraction of 15% was slowly added with a pipette. Shaking resulted in the captured mercury solution to be colorless and transparent, where 5 ml of the sample solution was added with a pipette to a 20% (w/v) $SnCl_2$ solution foaming bottle open on the left side of the liquid attachment. At this time, Hg^{2+} in the sample was reduced to Hg^0 and was pumped by the instrument to the right foaming bottle containing 30% NaOH solution (the purpose was to remove the volatile acidic gas in the sample and prevent the host from being corroded). Hg^0 was sent to the host of the mercury analyzer to determine the mercury content. The sampling process was powered by a constant-speed gas pump in the liquid attachment, and the average value of each sample was taken as the final result after two measurements (relative deviation less than 10%).

Analysis of Mercury Isotope

The mercury isotopic composition in the mercury capture solution was determined using multi-collector inductively coupled plasma mass spectrometry (MC-ICP-MS, Neptune Plus) at the Institute of Geochemistry, Chinese Academy of Sciences according to previous methods (Tang et al., 2017; Tang et al., 2019). The mercury concentration of the sample of mercury capture liquid to be diluted before the determination of mercury isotope was 0.5 ppb. A certain amount of mercury captured solution samples (calculated according to mercury content) with known mercury content were taken into a 15-ml centrifuge tube. At most, 0.5 NH_2OH-HCl (30%, w/v) was dropped into the solution to make it colorless and transparent, and the solution was then diluted to 15 ml with secondary distilled water. The mercury concentrations of the process standard solution NIST SRM3133 and the external standard NIST SRM3177 at the time of injection were configured to be 0.5 ppb. The mass fractionation of mercury isotopes is usually expressed by the thousandth fractionation (‰) of $\delta^{XXX}Hg$, where δ refers to the deviation between the sample mercury isotope ratio and the standard mercury isotope ratio (Blum and Bergquist, 2007). For better data comparison, NIST SRM3133 Hg is usually used as the standard (Blum, 2012). The calculation formula is as follows:

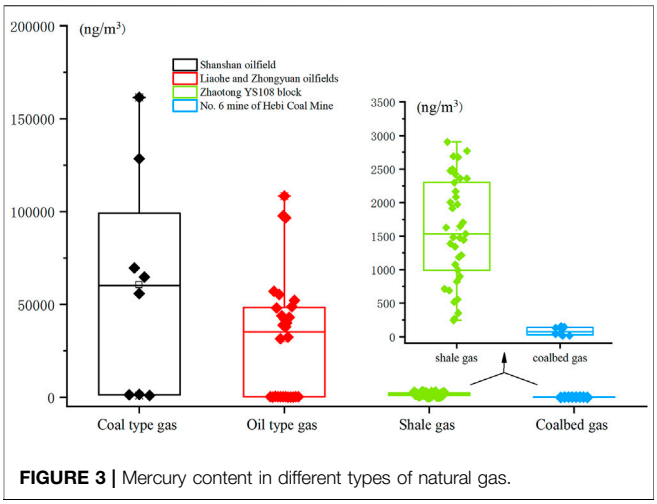

FIGURE 3 | Mercury content in different types of natural gas.

$$\delta^{XXX}Hg\,(‰) = \left[\left(\frac{^{XXX}Hg}{^{198}Hg_{sample}}\right)\Big/\left(\frac{^{XXX}Hg}{^{198}Hg_{NIST3133}}\right) - 1\right] \times 1000 \quad (1)$$

where XXX refers to 199, 200, 201, 202, and 204, respectively. The mass-independent fractionation of mercury isotopes is represented by $\Delta^{XXX}Hg$ (‰), which refers to the deviation between the measured and theoretical values. It is specifically calculated according to the following formula (Blum and Bergquist, 2007):

$$\Delta^{199}Hg = \delta^{199}Hg - (\delta^{202}Hg * 0.2520) \quad (2)$$

$$\Delta^{200}Hg = \delta^{200}Hg - (\delta^{202}Hg * 0.5024) \quad (3)$$

$$\Delta^{201}Hg = \delta^{201}Hg - (\delta^{202}Hg * 0.7520) \quad (4)$$

RESULTS AND DISCUSSION

Mercury Content in Shale Gas

The mercury content of shale gas in the YS108 block of the Zhaotong demonstration area is shown in **Figure 3** and **Supplementary Table S1** (Supporting Information). The mercury content of 37 shale gas samples ranged from 171 to 2,906 ng/m^3, with an average of 1,551.08 ± 787.08 ng/m^3 (n = 37, 1 SD). The mercury content in shale gas detected by Han et al. (2021) in the southern Sichuan Basin (mean: 1,420 ng/m^3) is consistent with that detected by Han et al. (2021), which is significantly lower than the average mercury content in the coal-formed gas of the Shanshan oilfield (Li, 2020) and the oil-type gas of the Liaohe oilfield, and higher than that in the coalbed gas of the Hebi Coal Mine (Tang et al., 2019). The overall mercury content demonstrates coal-formed

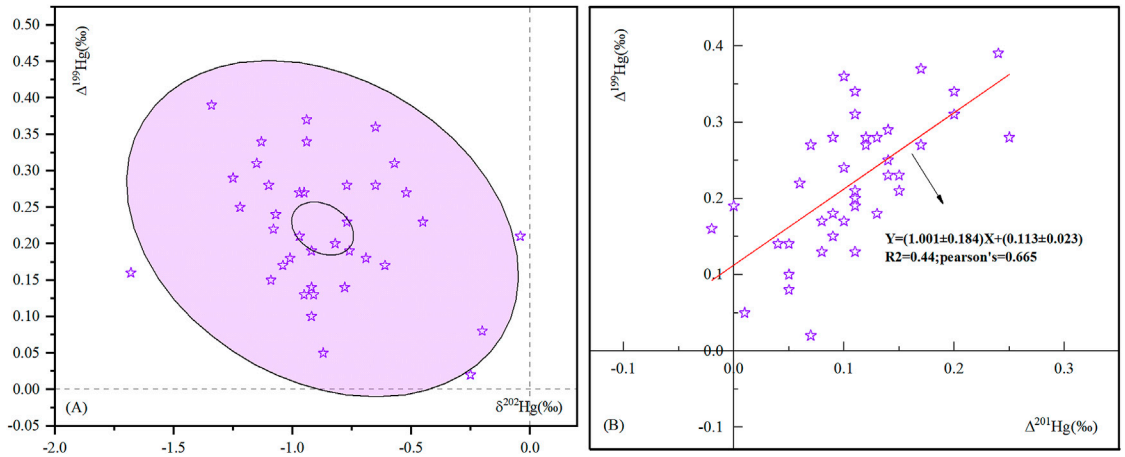

FIGURE 4 | Characteristics of shale gas Δ^{199}Hg and δ^{202}Hg **(A)** and Δ^{199}Hg and δ^{201}Hg **(B)**: The ellipse in Figure A shows the mean values of Δ^{199}Hg and δ^{202}Hg (inner ellipse) and 95% confidence level (outer ellipse).

gas > oil-type gas > shale gas > coalbed gas, but the mercury content varies by one to several orders of magnitude.

Natural gas can be divided into organic and inorganic gases according to genetic type, among which organic gas includes oil-type gas mainly from marine or lacustrine sapropelic and sapropelic to humic-type organic matter and oil-type gas that forms crude oil, and coal-formed gas mainly from terrestrial humic-type organic matter (Ni et al., 2019; Li et al., 2012a). According to the lithology of the reservoir, natural gas can be divided into coal-formed gas (including coalbed gas generated by coal seams and coal-formed gas, produced by coal seams but migrated to other coal seams or other reservoirs), shale gas, and tight sandstone gas (Liu, 2018). It is generally believed that mercury in natural gas is mainly derived from organic matter in gas source rocks or crude oil. During the thermal evolution of organic matter into hydrocarbons, mercury accumulates with natural gas in the form of volatile components. The mercury accumulation capacity of terrestrial organic matter (such as coal and dispersed humus) is relatively strong (Liu et al., 2020; Li et al., 2012b). The mercury content is relatively high; therefore, the mercury content in coal-formed gas is generally higher than that in oil-type gas, and the organic matter content in shale gas is relatively lower than that in coal-formed gas and oil-type gas; therefore, the mercury content is also relatively low (**Figure 3**). The mercury content in coalbed gas is the lowest in mine no. 6 of the Hebi coal mine, which is related to the low mercury content in the coal seam. The mercury content of shale gas in the YS108 block of the Zhaotong demonstration area is also lower than the average mercury content (6,840 ng/m^3) of over-mature marine gas (also oil-type gas) in the Sichuan Basin (Han et al., 2021).

In addition, the mercury content may be related to the state of natural gas occurrence. After the formation of alkane gas, it is stored in micron- or nanometer-sized reservoir pores in the form of free, adsorption, and dissolution (Gong et al., 2014). Mercury migrates with free natural gas in the form of steam during hydrocarbon generation. Coalbed gas and shale gas are self-generation and self-accumulation modes, respectively. About 70%–95% of coalbed gas exists in the adsorption state (Liu, 2018), the adsorption state of shale gas accounts for approximately 20%–85% of the total gas (Curtis, 2002; Montgomery et al., 2005), and the adsorption of shale gas at the Wufeng-Longmaxi Formation in Sichuan Basin accounts for approximately 40% (Li et al., 2018). Coal-formed gas and oil-type gas are mainly in the free state, CBM is mainly in the adsorption state, and shale gas has free and adsorbed gas. Therefore, the mercury content of coal-formed gas and oil-type gas is generally higher than that of shale gas and CBM, and the mercury content of CBM is the lowest. The mercury content in shale gas varies greatly between wells (**Supplementary Table S1**) mainly because of the maldistribution of organic matter in the source rock (Tian et al., 2014; Wu et al., 2016; Deng and Sun, 2019).

Characteristics of Mercury Isotope Composition in Shale Gas

The mercury isotopic composition of shale gas in the Zhaotong YS108 block is shown in **Figure 4**. The Δ^{199}Hg values (relative to NIST 3133) are positive (0.02‰–0.39‰), with an average of 22‰ ± 0.08‰ (n = 37,1 SD), which is consistent with the Hg-MIF values (Δ^{199}Hg: +0.05‰–+0.15‰, with an average of 0.12‰ ± 0.03‰) of the Wufeng-Longmaxi black shale in the Sichuan Basin reported by Shen et al. (2019), indicating that there is no evident mass-independent fractionation of mercury isotopes during gas formation from gas source rock to shale gas owning to the lack of exposure to light in the underground gas formation process leading to the MIF of the mercury stable isotope. Although some scholars have reported that the stable isotopes of mercury produce very small Hg-MIF under dark conditions (Zheng and Hintelmann, 2010) (Blum et al., 2014; Tang et al., 2019), photochemical reduction is believed to be the most important process causing Hg-MIF. Therefore, it is considered that the mass-independent fractionation of the stable isotope of mercury does not occur in the underground dark

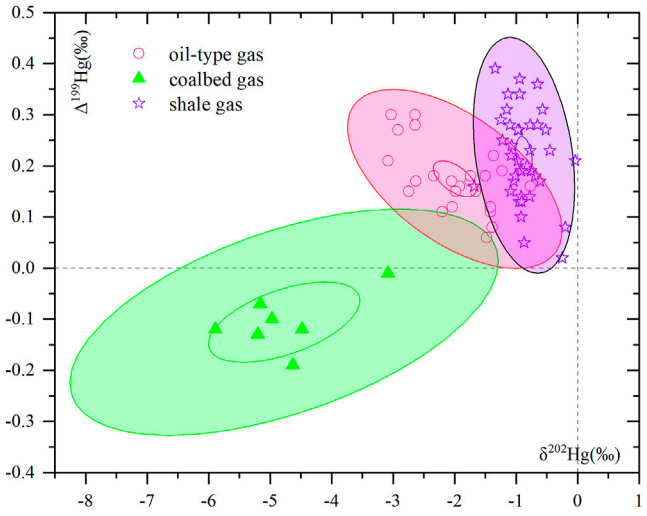

FIGURE 5 | Comparison of mercury isotopic composition in different types of natural gas: the data of oil-type gas and coalbed gas are quoted from the literature (Tang et al., 2019).

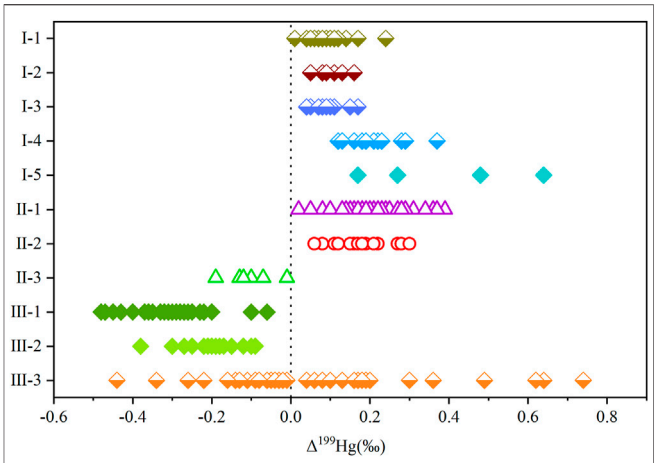

FIGURE 6 | Mercury isotopic composition information of shale gas and its hydrocarbon generating medium Δ^{199}Hg comparison, in which I-1 is Ordovician black shale [quoted from literature (Gong et al., 2017)], I-2 is Ordovician argillaceous limestone [quoted from literature (Shen et al., 2019; Gong et al., 2017)], I-3 is modern marine sediment [quoted from literature (Gehrke et al., 2009; Ogrinc et al., 2019)], I-4 is Arctic seawater [quoted from literature (Štrok et al., 2015)], I-5 is planktonic algae [quoted from literature (Perrot et al., 2012; Tsui et al., 2012)], II-1 is shale gas (this study), II-2 is continental oil-type gas [quoted from literature (Tang et al., 2019)] II-3 refers to coalbed gas [quoted from literature (Tang et al., 2019)], III-1 refers to leaves [quoted from literature (Demers et al., 2013; Zheng et al., 2016)], III-2 refers to litter on the Qinghai Tibet Plateau [quoted from literature (Wang et al., 2017)], and III-3 refers to freshwater sediments [quoted from literature (Gantner et al., 2009; Donovan et al., 2013; Sherman and Blum, 2013)].

environment of hydrocarbon generation, and the information characteristics of the mass-independent fractionation of the stable isotope of mercury in the organic matter of the gas source rocks are retained, which also indicates the main organic matter types of the gas source rocks. The δ^{202}Hg values in shale gas range from −1.68‰ to −0.04‰, with an average of −0.87‰ ± 0.31‰ (n = 37, 1 SD), and the δ^{202}Hg values in shale gas of the same formation range from −2.5‰ to −1.0‰ with an average value of −1.36‰ ± 0.34‰, n = 22, 2 SD) (Shen et al., 2019), but relatively positive, indicating that shale gas is more enriched in heavy isotopes of mercury than its source rock. Laboratory studies have demonstrated that many redox reactions involving Hg cause MDF including abiotic and biotic processes (Kritee et al., 2018; Wiederhold et al., 2010; Jiskra et al., 2012; Zheng et al., 2019); therefore, this study does not describe all geochemical processes that contribute to the mass fractionation of mercury isotopes.

It is generally believed that the nuclear volume effect (NVE) (Schauble, 2007) and magnetic isotope effect (MIE) (Buchachenko et al., 2007) are the main mechanisms for the generation of mercury stable isotope mass-independent fractionation (MIF), and the two can be effectively distinguished by the ratio of Δ^{199}Hg/Δ^{201}Hg. The ratio of MIFΔ^{199}Hg/Δ^{201}Hg caused by NVE was greater than 1.6, such as the mercury-thiol complex (Δ^{199}Hg/Δ^{201}Hg = 1.54) and mercury reduction process caused by abiotic action under dark conditions (Δ^{199}Hg/Δ^{201}Hg = 1.5–1.6) (Wiederhold et al., 2010; Zheng and Hintelmann, 2010) and elemental mercury volatilization (Δ^{199}Hg/Δ^{201}Hg = 2.0) (Estrade et al., 2009). The ratio of Δ^{199}Hg/Δ^{201}Hg of MIF caused by MIE is 1–1.36, such that the photoreduction reaction of Hg^{II}_{aq} Δ^{199}Hg/Δ^{201}Hg = 1.0 (Bergquist and Blum, 2007; Zheng and Hintelmann, 2009) and the photodegradation of methylmercury Δ^{199}Hg/Δ^{201}Hg = 1.36 (Bergquist and Blum, 2007). The mercury in the studied shale gas sample Δ^{199}Hg/Δ^{201}Hg = 1.001 ± 0.18 (**Figure 4B**) indicates that the main mechanism for the occurrence of MIF in the mercury isotope in shale gas is MIE caused by Hg^{II}_{aq} photoreduction reaction, which also indicates that the mercury in shale gas undergoes the photoreduction reaction of Hg^{2+} in water before deposition.

Comparison of Mercury Isotope Composition in Shale Gas, Oil-Type Gas, and Coalbed Gas

There are relatively few studies on mercury isotopes in natural gas (Tang et al., 2019; Washburn et al., 2018), and the development and utilization of mercury isotopes in shale gas in recent years have not been reported. **Figure 5** summarizes the results of shale gas and Tang et al. (2019) on mercury isotopes in oil-type gas and coalbed gas.

The Δ^{199}Hg of shale gas in the Zhaotong YS108 block is positive and similar to that of oil-type gas in the Liaohe oilfield and Zhongyuan oilfield, and δ^{202}Hg is also consistent (**Figure 5**), indicating that they have similar sources of mercury and types of organic matter. The Δ^{199}Hg range of shale gas in the Zhaotong YS108 block is 0.02‰–0.39‰, with an average of 0.22‰ ± 0.08‰ (n = 37, 1 SD). The gas source rock is deep-sea sedimentary shale, and its hydrocarbon-forming organic matter is mainly rich in algae and low phytoplankton, and algae is the only confirmed lower plant

with positive Δ^{199}Hg at present (**Figure 6**, Perrot et al., 2012; Tsui et al., 2012). This is similar to the positive value in Δ^{199}Hg of Ordovician black shale (Gong et al., 2017), Ordovician argillaceous limestone (Shen et al., 2019; Gong et al., 2017), and modern marine sediments (Gehrke et al., 2009; Ogrinc et al., 2019), which is also consistent with the positive value for Δ^{199}Hg of marine shale gas and continental oil-type gas (Tang et al., 2019), but it is significantly different from the negative Δ^{199}Hg value of coalbed gas and modern higher plants (**Figure 6**). Therefore, the isotopic composition of mercury in shale gas most likely retains that of hydrocarbon-forming algae and lower plankton. In fact, approximately 90% of the mercury in the ocean originates from atmospheric mercury deposition (Mason et al., 2012). Most of the mercury exists in the form of dissolved Hg^{2+} ions or other mercury oxides that are easily soluble in seawater. Algal organic matter is rich in −SH, which is thermodynamically favorable for the rapid uptake and accumulation of inorganic Hg^{2+} in seawater (Fitzgerald and Lamborg, 2014; Le Faucheur et al., 2014), allowing algae to reach a higher mercury concentration level. After algal death, the deposition of algal debris transfers mercury from surface waters to deeper waters and sediments, and the process is analogous to a "biological pump" of mercury (Hirner et al., 1990; Li et al., 2012b; Verburg et al., 2014). The average Hg content in algal organic matter in Arctic lake sediments before 1800 was as high as 159–776 μg/kg (n = 24), which is 2–39 times higher than that in the sediments, demonstrating the "biological pump" mechanism of algal cleaning of mercury in seawater (Outridge et al., 2019). Shale gas reservoirs in the Wufeng-Longmaxi Formation in the study area are mainly formed in a shelf retention environment with limited water circulation and are dominated by black carbonaceous shale and siliceous shale with rich organic matter content (Wu et al., 2016). Organic components such as planktonic algae, acritarch, bacteria, and animal detritus such as graptolite, chitin, and sponge needles have been observed in shales (Tengger et al., 2017; Nie et al., 2019). Ma et al. (2020) conducted hydrocarbon-generating thermal simulation experiments on shales and graptolites with different maturities in the upper Ordovician and lower Silurian and found that hydrocarbon-rich and fat-rich organic matter such as algae and acritarch are the main organic matter for shale gas generation. With an increase in burial depth and formation temperature, mercury in the complex and adsorbed state of algae organic matter gradually desorbed under thermal action and migrated to oil and gas reservoirs or oil reservoirs in the form of steam (Peng et al., 2019). Therefore, the Δ^{199}Hg information in shale gas and the Δ^{199}Hg of the main hydrocarbon-forming organic matter—algae (0.17‰–0.64‰, with an average of 0.39 ± 0.21‰, n = 4,1 SD) (Perrot et al., 2012; Tsui et al., 2012)—showed no significant difference (t-test, $p > 0.05$) and all values are positive, which also indicates that $\Delta 1^{99}$Hg in marine crude oil is similar to that of algae.

The oil-type gas in the Liaohe and Zhongyuan oilfields is formed by the evolution of source rocks in continental lakes or delta sedimentary environments. The source rocks, herein, are continental dark mudstone and shale (E2-3s) of the Eocene Shahejie Formation. The sources of mercury in lakes and oceans are significantly different: atmospheric mercury deposition is the main entry pathway of mercury in pelagic sediments, while lake or delta sedimentary environments receive various forms of mercury from various sources, such as mercury dissolved in catchment runoff, tributaries, and adsorbed and fixed in particulate matter and sediments (Fitzgerald and Lamborg, 2014). There exist both higher plant and animal sources of mercury, as well as planktonic sources of mercury such as algae in lake and river delta sedimentary environments (Outridge et al., 2007).

The Δ^{199}Hg values of freshwater sediments have both positive and negative values (**Figure 6** III-3; Donovan et al., 2013; Gantner et al., 2009; Sherman and Blum, 2013), but in the continental oil-type gas, we studied Δ^{199}Hg as positive (**Figure 6** II-2, Tang et al., 2019). As mentioned earlier, algae are the only lower plants with positive Δ^{199}Hg that have been confirmed so far, and the continental oil-type gas and mercury present in them are mainly derived from source rocks. Therefore, it is believed that the main hydrocarbon-forming organic matter of continental oil-type gas cannot come from higher plants but are mainly derived from plankton such as algae that self-accumulate in the sedimentary environment of the source rock. This also makes the Δ^{199}Hg between shale gas in the Zhaotong YS108 block and oil-type gas in the Liaohe and Zhongyuan oilfields (Δ^{199}Hg:0.06‰–0.30‰, mean 0.17‰ ± 0.06‰, n = 24, 1 SD) positive, showing no significant difference. The above results also indicate that the main organic matter of continental crude oil is abundant algae and other plankton in lake or delta environments, and Δ^{199}Hg is positive. Therefore, continental oil and gas exploration can find algae-rich target strata or delineate the target strata with a positive Δ^{199}Hg value. For example, most of the planktonic and algal fossils have been found in the source rocks of the continental oilfields in China, such as the Shengli, Maling, and Wangchang oilfields (Liu, 2018).

The Δ^{199}Hg of shale gas in the Zhaotong YS108 block, oil-type gas from the Liaohe oilfield, and Zhongyuan oilfield is significantly different from that of coalbed gas in mine no. 6 of the Hebi Coal Mine (**Figure 5**). The coal seam in mine no. 6 of the Hebi coal mine is the continental coal seam of the Permian fluvial and lacustrine facies. The main coal-forming organic matter was terrestrial higher plants, and the Δ^{199}Hg was negative (**Figure 6**). Therefore, the mercury Δ^{199}Hg (−0.19‰ to −0.01‰, −0.11‰ ± 0.06‰, n = 7, 1 SD) in coalbed gas was also negative. Δ^{199}Hg is significantly different from that of shale gas and oil-type gas.

CONCLUSION

The mercury content of marine shale gas in the YS108 block of Zhaotong demonstration area ranges from 171 to 2,906 ng/m^3, with an average of 1,551.08 ± 787.08 ng/m^3 (n = 37,1 SD). The Δ^{199}Hg values of mercury isotopes range from 0.02‰ to 0.39‰, with an average of 0.22‰ ± 0.08‰ (n = 37, 1 SD), and the δ^{202}Hg values range from −1.68‰ to −0.04‰, with an average of

−0.87‰ ± 0.31‰ (n = 37, 1 SD), which are significantly different from the Δ^{199}Hg and δ^{202}Hg values of coalbed gas, but not significantly different from the Δ^{199}Hg and δ^{202}Hg values of terrestrial oil-type gas. We can use it as an indicator to search for algae-rich continental strata or delineate the strata with positive Δ^{199}Hg as exploration targets.

DATA AVAILABILITY STATEMENT

The original contributions presented in the study are included in the article/**Supplementary Material**, Further inquiries can be directed to the corresponding authors.

AUTHOR CONTRIBUTIONS

ST: conceived the idea for this study and provided manuscript guidance; GZ: assisted in sample collection and manuscript revision; YD and ST: data analysis, manuscript writing and revision; XF, HZ and PL: helped supervise the projects. All authors listed have made a contribution to the work and approved it for publication.

FUNDING

This research was supported by the National Natural Science Foundation of China (41573006 and 41372360) and the CNPC (China National Petroleum Corporation) Scientific Research and Technology Development Project (Grant No. 2021DJ05).

ACKNOWLEDGMENTS

We thank Gaoen Wu of State Key Laboratory of Environmental Geochemistry, Chinese Academy of Sciences, for assistance in measuring Hg isotopes. We thank the editor and reviewers for their thoughtful comments, which significantly improved the quality of this paper.

SUPPLEMENTARY MATERIAL

The Supplementary Material for this article can be found online at: https://www.frontiersin.org/articles/10.3389/feart.2022.809418/full#supplementary-material

REFERENCES

Bergquist, B. A., and Blum, J. D. (2007). Mass-Dependent and -Independent Fractionation of Hg Isotopes by Photoreduction in Aquatic Systems. *Science* 318 (5849), 417–420. doi:10.1126/science.1148050

Biswas, A., Blum, J. D., Bergquist, B. A., Keeler, G. J., and Xie, Z. (2008). Natural Mercury Isotope Variation in Coal Deposits and Organic Soils. *Environ. Sci. Technol.* 42 (22), 8303–8309. doi:10.1021/es801444b

Blum, J. D. (2012). "Applications of Stable Mercury Isotopes to Biogeochemistry," in *Handbook of Environmental Isotope Geochemistry: Vol I*. Editor M. Baskaran (Berlin, Heidelberg: Springer Berlin Heidelberg), 229–245. doi:10.1007/978-3-642-10637-8_12

Blum, J. D., and Bergquist, B. A. (2007). Reporting of Variations in the Natural Isotopic Composition of Mercury. *Anal. Bioanal. Chem.* 388 (2), 353–359. doi:10.1007/s00216-007-1236-9

Blum, J. D., Sherman, L. S., and Johnson, M. W. (2014). Mercury Isotopes in Earth and Environmental Sciences. *Annu. Rev. Earth Planet. Sci.* 42 (1), 249–269. doi:10.1146/annurev-earth-050212-124107

Buchachenko, A. L., Ivanov, V. L., Roznyatovskii, V. A., Artamkina, G. A., Vorob'ev, A. K., and Ustynyuk, Y. A. (2007). Magnetic Isotope Effect for Mercury Nuclei in Photolysis of Bis(p-Trifluoromethylbenzyl)mercury. *Dokl. Phys. Chem.* 413, 39–41. doi:10.1134/S0012501607030013

Carignan, J., Estrade, N., Sonke, J. E., and Donard, O. F. X. (2009). Odd Isotope Deficits in Atmospheric Hg Measured in Lichens. *Environ. Sci. Technol.* 43 (15), 5660–5664. doi:10.1021/es900578v

Chen, Z., Cui, J., Ren, Z., Jiang, S., Liang, X., Wang, G., et al. (2019). Geochemistry, Paleoenvironment and Mechanism of Organic-Matter Enrichment in the Lower Silurian Longmaxi Formation Shale in the Sichuan Basin, China. *Acta Geol. Sin-engl.* 93 (3), 505–519. doi:10.1111/1755-6724.13868

Curtis, J. B. (2002). Fractured Shale-Gas Systems. *AAPG Bull.* 86 (11), 1921–1938. doi:10.1306/61EEDDBE-173E-11D7-8645000102C1865D

Dai, J. X. (1992). Identification of Various Alkane Gases. *Sci. China* 35 (10), 1246–1257.

Dai, J. X., Zou, C. N., Liao, S. M., Dong, D. Z., Ni, Y. Y., Huang, J. L., et al. (2014). Geochemistry of the Extremely High thermal Maturity Longmaxi Shale Gas, Southern Sichuan Basin. *Org. Geochem.* 74, 3–12. doi:10.1016/j.orggeochem.2014.01.018

Demers, J. D., Blum, J. D., and Zak, D. R. (2013). Mercury Isotopes in a Forested Ecosystem: Implications for Air-Surface Exchange Dynamics and the Global Mercury Cycle. *Glob. Biogeochem. Cy.* 27 (1), 222–238. doi:10.1002/gbc.20021

Deng, Y., and Sun, T. (2019). Discussion on the Symbiotic Relationship between High Quality Source Rocks and Large Oilfields. *China Offshore Oil Gas* 31 (5), 1–8. doi:10.11935/j.issn.1673-1506.2019.05.001

Donovan, P. M., Blum, J. D., Yee, D., Gehrke, G. E., and Singer, M. B. (2013). An Isotopic Record of Mercury in San Francisco Bay Sediment. *Chem. Geol.* 349-350, 87–98. doi:10.1016/j.chemgeo.2013.04.017

Enrico, M., Le Roux, G., Heimbürger, L., Van Beek, P., Souhaut, M., Chmeleff, J., et al. (2017). Holocene Atmospheric Mercury Levels Reconstructed from Peat Bog Mercury Stable Isotopes. *Environ. Sci. Technol.* 51 (11), 5899–5906. doi:10.1021/acs.est.6b05804

Enrico, M., Roux, G. L., Marusczak, N., Heimbürger, L., Claustres, A., Fu, X., et al. (2016). Atmospheric Mercury Transfer to Peat Bogs Dominated by Gaseous Elemental Mercury Dry Deposition. *Environ. Sci. Technol.* 50 (5), 2405–2412. doi:10.1021/acs.est.5b06058

Estrade, N., Carignan, J., Sonke, J. E., and Donard, O. F. X. (2009). Mercury Isotope Fractionation during Liquid–Vapor Evaporation Experiments. *Geochim. Cosmochim. Acta* 73 (10), 2693–2711. doi:10.1016/j.gca.2009.01.024

Feng, X. B., Foucher, D., Hintelmann, H., Yan, H. Y., He, T. R., and Qiu, G. L. (2010). Tracing Mercury Contamination Sources in Sediments Using Mercury Isotope Compositions. *Environ. Sci. Technol.* 44 (9), 3363–3368. doi:10.1021/es9039488

Fitzgerald, W. F., and Lamborg, C. H. (2014). "11.4 - Geochemistry of Mercury in the Environment," in *Treatise on Geochemistry*. Editors H. D. Holland and K. K. Turekian. Second Edition (Oxford: Elsevier), 91–129. doi:10.1016/b978-0-08-095975-7.00904-9

Foucher, D., Ogrincand Hintelmann, H. (2009). Tracing Mercury Contamination from the Idrija Mining Region (Slovenia) to the Gulf of Trieste Using Hg Isotope Ratio Measurements. *Environ. Sci. Technol.* 43 (1), 33–39. doi:10.1021/es801772b

Gantner, N., Hintelmann, H., Zheng, W., and Muir, D. C. (2009). Variations in Stable Isotope Fractionation of Hg in Food Webs of Arctic Lakes. *Environ. Sci. Technol.* 43 (24), 9148–9154. doi:10.1021/es901771r

Gehrke, G. E., Blum, J. D., and Meyers, P. A. (2009). The Geochemical Behavior and Isotopic Composition of Hg in a Mid-pleistocene Western Mediterranean Sapropel. *Geochim. Cosmochim. Acta* 73 (6), 1651–1665. doi:10.1016/j.gca.2008.12.012

Gong, Q., Wang, X. D., Zhao, L. S., Grasby, S. E., Chen, Z. Q., Zhang, L., et al. (2017). Mercury Spikes Suggest Volcanic Driver of the Ordovician-Silurian Mass Extinction. *Sci. Rep.* 7 (1). doi:10.1038/s41598-017-05524-5

Gong, X. F., He, J. X., Wu, C. K., Yang, J., Li, K., Li, D., et al. (2014). Basic Geological and Geochemical Characteristics of Unconventional Natural Gas Resources in China. Mar. *Geol. Quat. Geol.* 34 (05), 95–105. doi:10.3724/SP.J.1140.2014.05095

Han, Z. X., Gou, Y. X., Li, J., Gou, S. G., Tian, W. N., and Huang, H. (2021). Content Distribution Characteristics and Genetic Analysis of Mercury in the Natural Gas from Sichuan Basin. *Nat. Gas Geosci.* 32 (03), 356–362. doi:10.11764/j.issn.1672-1926.2020.11.014

Hirner, A. V., Kritsotakis, K., and Tobschall, H. J. (1990). Metal-organic Associations in Sediments—I. Comparison of Unpolluted Recent and Ancient Sediments and Sediments Affected by Anthropogenic Pollution. *Appl. Geochem.* 5 (4), 491–505. doi:10.1016/0883-2927(90)90023-X

Huang, X. Q., Wang, J. J., Du, Y., Li, L., and Zhang, Z. (2019). Discussion on Development Mode of Smaller Well Spacing and Tridimensional Development in the YS108 Block, Zhaotong National Shale Gas Demonstration Area. *Nat. Gas Geosci.* 30 (04), 557–565. doi:10.11764/ji.ssn1672-1926.2018.12.018

Jiskra, M., Wiederhold, J. G., Bourdon, B., and Kretzschmar, R. (2012). Solution Speciation Controls Mercury Isotope Fractionation of Hg(II) Sorption to Goethite. *Environ. Sci. Technol.* 46 (12), 6654–6662. doi:10.1021/es3008112

Kritee, K., Motta, L. C., Blum, J. D., Tsui, M. T., and Reinfelder, J. R. (2018). Photomicrobial Visible Light-Induced Magnetic Mass Independent Fractionation of Mercury in a Marine Microalga. *ACS Earth Space Chem.* 2 (5), 432–440. doi:10.1021/acsearthspacechem.7b00056

Kwon, S. Y., Blum, J. D., Yin, R. S., Tsui, M. T., Yang, Y. H., and Choi, J. W. (2020). Mercury Stable Isotopes for Monitoring the Effectiveness of the Minamata Convention on Mercury. *Earth-sci. Rev.* 203, 103111. doi:10.1016/j.earscirev.2020.103111

Le Faucheur, S., Campbell, P. G. C., Fortin, C., and Slaveykova, V. I. (2014). Interactions between Mercury and Phytoplankton: Speciation, Bioavailability, and Internal Handling. *Environ. Toxicol. Chem.* 33 (6), 1211–1224. doi:10.1002/etc.2424

Lefticariu, L., Blum, J. D., and Gleason, J. D. (2011). Mercury Isotopic Evidence for Multiple Mercury Sources in Coal from the Illinois Basin. *Environ. Sci. Technol.* 45 (4), 1724–1729. doi:10.1021/es102875n

Li, J., Han, Z. X., Yan, Q. T., Wang, S. Y., Ge, S. G., and Wang, C. Y. (2012a). Genesis of Mercury in Natural Gas of Chinese Gas Fields. *Nat. Gas Geosci.* 23 (3), 413–419. doi:10.11764/j.issn.1672-1926.2012.03.413

Li, J., Xie, S. L., Feng, J., Li, Y. H., and Chen, L. (2012b). Heavy Metal Uptake Capacities by the Common Freshwater green Alga Cladophora Fracta. *J. Appl. Phycol.* 24 (4), 979–983. doi:10.1007/s10811-011-9721-0

Li, Q. W., Pang, X. Q., Tang, L., Chen, G., Shao, X. H., and Jia, N. (2018). Occurrence Features and Gas Content Analysis of marine and continental Shales: A Comparative Study of Longmaxi Formation and Yanchang Formation. *J. Nat. Gas Sci. Eng.* 56, 504–522. doi:10.1016/j.jngse.2018.06.019

Li, Z. P. (2020).Preliminary Study on Mercury Content and Mercury Isotopes in Coal-Derived Gas and Terrestrial Oil-type Gas in Xinjiang. [dissertation/master's thesis]. jiaozuo: Henan Polytechnic University.

Liu, G. D. (2018). *Petroleum Geology*. Beijing: Petroleum Industry Press.

Liu, Q. Y. (2013). Mercury Concentration in Natural Gas and its Distribution in the Tarim Basin. *Sci. China Earth Sci.* 56 (8), 1371–1379. doi:10.1007/s11430-013-4609-2

Liu, Q. Y., Peng, W. L., Li, J., and Wu, X. Q. (2020). Source and Distribution of Mercury in Natural Gas of Major Petroliferous Basins in China. *Sci. China Earth Sci.* 63 (5), 643–648. doi:10.1007/s11430-019-9596-6

Ma, J., Hintelmann, H., Kirk, J. L., and Muir, D. C. G. (2013). Mercury Concentrations and Mercury Isotope Composition in lake Sediment Cores from the Vicinity of a Metal Smelting Facility in Flin Flon, Manitoba. *Chem. Geol.* 336, 96–102. doi:10.1016/j.chemgeo.2012.10.037

Ma, Z. L., Shen, B. J., Pan, A. Y., TenggerNing, C. X., and Zheng, L. J. (2020). Shale Gas Genesis and Carbon Isotope Inversion Mechanism of Wufeng Longmaxi Formation in Sichuan Basin -- Understanding from thermal Simulation experiment. *Pet. Geol. Exp.* 42 (03), 428–433. doi:10.11781/sysydz202003428

Mason, R. P., Choi, A. L., Fitzgerald, W. F., Hammerschmidt, C. R., Lamborg, C. H., Soerensen, A. L., et al. (2012). Mercury Biogeochemical Cycling in the Ocean and Policy Implications. *Environ. Res.* 119, 101–117. doi:10.1016/j.envres.2012.03.013

Montgomery, S. L., Jarvie, D. M., Bowker, K. A., and Pollastro, R. M. (2005). Mississippian Barnett Shale, Fort Worth basin, north-central Texas: Gas-Shale Play with Multi–Trillion Cubic Foot Potential. *AAPG Bull* 89 (02), 155–175. doi:10.1306/09170404042

Ni, Y. Y., Liao, F. R., Gong, D. Y., Jiao, L. X., Gao, J. L., and Yao, L. M. (2019). Stable Carbon and Hydrogen Isotopic Characteristics of Natural Gas from Taibei Sag, Turpan-Hami Basin, NW China. *Pet. Explor. Dev.* 46 (3), 531–542. doi:10.1016/S1876-3804(19)60033-9

Nie, H. K., Jin, Z. J., Sun, C. X., He, Z. L., Liu, G. X., and Liu, Q. Y. (2019). Organic Matter Types of the Wufeng and Longmaxi Formations in the Sichuan Basin, South China: Implications for the Formation of Organic Matter Pores. *Energy Fuels* 33 (9), 8076–8100. doi:10.1021/acs.energyfuels.9b01453

Ogrinc, N., Hintelmann, H., Kotnik, J., Horvat, M., and Pirrone, N. (2019). Sources of Mercury in Deep-Sea Sediments of the 481 Mediterranean Sea as Revealed by Mercury Stable Isotopes. *Sci. Rep.* 9 (1), 11626. doi:10.1038/s41598-019-48061-z

Outridge, P. M., Sanei, H., Stern, G. A., Hamilton, P. B., and Goodarzi, F. (2007). Evidence for Control of Mercury Accumulation Rates in Canadian High Arctic Lake Sediments by Variations of Aquatic Primary Productivity. *Environ. Sci. Technol.* 41 (15), 5259–5265. doi:10.1021/es070408x

Outridge, P. M., Stern, G. A., Hamilton, P. B., and Sanei, H. (2019). Algal Scavenging of Mercury in Preindustrial Arctic Lakes. *Limnol. Oceanogr.* 64 (4), 1558–1571. doi:10.1002/lno.11135

Ozerova, N. (1983). New Mercury Ore belt in Western Europe. *Int. Geol. Rev.* 25 (9), 1095–1100. doi:10.1080/00206818309466806

Peng, W. L., Liu, Q. Y., Feng, Z. Q., Fang, C. C., Gong, D. Y., Li, P., et al. (2019). First Discovery and Significance of Liquid Mercury in a Thermal Simulation Experiment on Humic Kerogen. *Energy Fuels* 33 (3), 1817–1824. doi:10.1021/acs.energyfuels.8b03294

Perrot, V., Pastukhov, M. V., Epov, V. N., Husted, S., Donard, O. F., and Amouroux, D. (2012). Higher Mass-independent Isotope Fractionation of Methylmercury in the Pelagic Food Web of Lake Baikal (Russia). *Environ. Sci. Technol.* 46 (11), 5902–5911. doi:10.1021/es204572g

Schauble, E. A. (2007). Role of Nuclear Volume in Driving Equilibrium Stable Isotope Fractionation of Mercury, Thallium, and Other Very Heavy Elements. *Geochim. Cosmochim. Acta* 71 (9), 2170–2189. doi:10.1016/j.gca.2007.02.004

Shen, J., Algeo, T. J., Chen, J. B., Planavsky, N. J., Feng, Q. L., Yu, J. X., et al. (2019). Mercury in marine Ordovician/Silurian Boundary Sections of South China Is Sulfide-Hosted and Non-volcanic in Origin. *Earth Planet. Sci. Lett.* 511, 130–140. doi:10.1016/j.epsl.2019.01.028

Sherman, L. S., and Blum, J. D. (2013). Mercury Stable Isotopes in Sediments and Largemouth Bass from Florida Lakes, USA. *Sci. Total Environ.* 448, 163–175. doi:10.1016/j.scitotenv.2012.09.038

Shi, W. F., Feng, X. B., Zhang, G., Ming, L. L., Yin, R. S., Zhao, Z. Q., et al. (2011). High-precision Measurement of Mercury Isotope Ratios of Atmospheric Deposition over the Past 150 Years Recorded in a Peat Core Taken from Hongyuan, Sichuan Province, China. *Sci. Bull.* 56 (9), 877–882. doi:10.1007/s11434-011-4396-0

Smith, C. N., Kesler, S. E., Blum, J. D., and Rytuba, J. J. (2008). Isotope Geochemistry of Mercury in Source Rocks, mineral Deposits and spring Deposits of the California Coast Ranges, USA, Earth Planet. *Sci. Lett.* 269 (3), 399–407. doi:10.1016/j.epsl.2008.02.029

Stetson, S. J., Gray, J. E., Wanty, R. B., and Macalady, D. L. (2009). Isotopic Variability of Mercury in Ore, Mine-Waste Calcine, and Leachates of Mine-Waste Calcine from Areas Mined for Mercury. *Environ. Sci. Technol.* 43 (19), 7331–7336. doi:10.1021/es9006993

Štrok, M., Baya, P. A., and Hintelmann, H. (2015). The Mercury Isotope Composition of Arctic Coastal Seawater. *C. R. Geosci.* 347 (7-8), 368–376. doi:10.1016/j.crte.2015.04.001

Sun, L., Lu, B., Yuan, D., Hao, W., and Zheng, Y. (2017). Variations in the Isotopic Composition of Stable Mercury Isotopes in Typical Mangrove Plants of the

Jiulong Estuary, SE China. *Environ. Sci. Pollut. Re.* 24 (2), 1459–1468. doi:10.1007/s11356-016-7933-1

Sun, R. Y., Sonke, J. E., and Liu, G. L. (2016). Biogeochemical Controls on Mercury Stable Isotope Compositions of World Coal Deposits: A Review. *Earth-sci. Rev.* 152, 1–13. doi:10.1016/j.earscirev.2015.11.005

Tang, S. L., Feng, C. H., Feng, X. B., Zhu, J. M., Sun, R. Y., Fan, H. P., et al. (2017). Stable Isotope Composition of Mercury Forms in Flue Gases from a Typical Coal-Fired Power Plant, Inner Mongolia, Northern China. *J. Hazard. Mater.* 328, 90–97. doi:10.1016/j.jhazmat.2017.01.014

Tang, S. L., Zhou, Y. P., Yao, X. J., Feng, X. B., Li, Z. P., and Wu, G. N. (2019). The Mercury Isotope Signatures of Coalbed Gas and Oil-type Gas: Implications for the Origins of the Gases. *Appl. Geochem.* 109, 104415. doi:10.1016/j.apgeochem.2019.104415

Tengger, B., Shen, B. J., Yu, L. J., Yang, Y. F., Zhang, W. T., Tao, C., et al. (2017). Mechanisms of Shale Gas Generation and Accumulation in the Ordovician Mechanisms of Shale Gas Generation and Accumulation in the Ordovician Wufeng-Longmaxi Formation, Sichuan Basin, SW China. *Petrol. Explor. Dev.* 44 (01), 69–78. doi:10.1016/S1876-3804(17)30009-5

Tian, J. C., Liu, W. W., Wang, F., Chen, R., and Lin, X. B. (2014). Heterogeneity of the Paleozoic Tight sandstone Reservoirs in Gaoqiao Area of Ordos Basin. *Oil Gas Geol.* 35 (02), 183–189. doi:10.11743/ogg20140202

Tsui, M. T., Blum, J. D., Kwon, S. Y., Finlay, J. C., Balogh, S. J., and Nollet, Y. H. (2012). Sources and Transfers of Methylmercury in Adjacent River and forest Food Webs. *Environ. Sci. Technol.* 46 (20), 10957–10964. doi:10.1021/es3019836

Verburg, P., Hickey, C. W., and Phillips, N. (2014). Mercury Biomagnification in Three Geothermally-Influenced Lakes Differing in Chemistry and Algal Biomass. *Sci. Total Environ.* 493 (sep.15), 342–354. doi:10.1016/j.scitotenv.2014.05.097

Wang, X., Luo, J., Yin, R. S., Yuan, W., Lin, C. J., Sommar, J., et al. (2017). Using Mercury Isotopes to Understand Mercury Accumulation in the Montane Forest Floor of the Eastern Tibetan Plateau. *Environ. Sci. Technol.* 51 (2), 801–809. doi:10.1021/acs.est.6b03806

Wang, Z., Li, X. Q., Zhang, J. Z., Xu, H. W., Wang, G., Zhou, B., et al. (2016). Longmaxi Formation Shale Gas Geochemical Features Comparison between Different Blocks in Sichuan Basin. *Coal Geol. China.* 28 (02), 22–27. doi:10.1016/j.jngse.2015.11.045

Washburn, S. J., Blum, J. D., Johnson, M. W., Tomes, J. M., and Carnell, P. J. (2018). Isotopic Characterization of Mercury in Natural Gas via Analysis of Mercury Removal Unit Catalysts. *ACS Earth Space Chem.* 2 (5), 462–470. doi:10.1021/acsearthspacechem.7b00118

Wiederhold, J. G., Cramer, C. J., Daniel, K., Infante, I., Bourdon, B., and Kretzschmar, R. (2010). Equilibrium Mercury Isotope Fractionation between Dissolved Hg(II) Species and Thiol-Bound Hg. *Environ. Sci. Technol.* 44 (11), 4191–4197. doi:10.1021/es100205t

Wu, K. Y., Zhang, T. S., Yang, Y., Liang, X., Zhou, S. Y., and Zhang, C. (2016). Geological Characteristics of Wufeng-Longmaxi Shale-Gas Reservoir in the Huangjinba Gas Field, Zhaotong National Shale Gas Demonstration Area. *Geol. China.* 43 (01), 275–287. doi:10.12029/gc20160120

Xu, Z. Y., Liang, X., Lu, H. L., Zhang, J. H., Shu, H. L., Xu, Y. J., et al. (2019). Structural Deformation Characteristics and Shale Gas Preservation Conditions in the Zhaotong National Shale Gas Demonstration Area along the Southern Margin of the Sichuan Basin.china. *Nat. Gas Ind.* 39 (10), 22–31. doi:10.1016/j.ngib.2019.10.004

Yin, R. S., Feng, X. B., Wang, J, X., Bao, Z. D., Yu, B., and Chen, J. B. (2013). Mercury Isotope Variations between Bioavailable Mercury Fractions and Total Mercury in Mercury Contaminated Soil in Wanshan Mercury Mine, SW China. *Chem. Geol.* 336, 80–86. doi:10.1016/j.chemgeo.2012.04.017

Zheng, W., Demers, J. D., Lu, X., Bergquist, B. A., Anbar, A. D., Blum, J. D., et al. (2019). Mercury Stable Isotope Fractionation during Abiotic Dark Oxidation in the Presence of Thiols and Natural Organic Matter. *Environ. Sci. Technol.* 53 (4), 1853–1862. doi:10.1021/acs.est.8b05047

Zheng, W., and Hintelmann, H. (2009). Mercury Isotope Fractionation during Photoreduction in Natural Water Is Controlled by its Hg/DOC Ratio. *Geochim. Cosmochim. Acta* 73 (22), 6704–6715. doi:10.1016/j.gca.2009.08.016

Zheng, W., and Hintelmann, H. (2010). Nuclear Field Shift Effect in Isotope Fractionation of Mercury during Abiotic Reduction in the Absence of Light. *J. Phys. Chem. A.* 114 (12), 4238–4245. doi:10.1021/jp910353y

Zheng, W., Obrist, D., Weis, D., and Bergquist, B. A. (2016). Mercury Isotope Compositions across North American Forests. *Glob. Biogeochem. Cy.* 30 (10), 1475–1492. doi:10.1002/2015GB005323

Conflict of Interest: Author GZ was employed by the company PetroChina.

The remaining authors declare that the research was conducted in the absence of any commercial or financial relationships that could be construed as a potential conflict of interest.

Publisher's Note: All claims expressed in this article are solely those of the authors and do not necessarily represent those of their affiliated organizations, or those of the publisher, the editors, and the reviewers. Any product that may be evaluated in this article, or claim that may be made by its manufacturer, is not guaranteed or endorsed by the publisher.

frontiers in Earth Science

METHODS
published: 24 February 2022
doi: 10.3389/feart.2022.862677

Helium Signatures of Natural Gas From the Dongpu Sag, Bohai Bay Basin, Eastern China

Chunhua Ni[1,2], Xiaoqi Wu[1,2], Quanyou Liu[2,3], Dongya Zhu[2,3], Fan Yang[1,2], Qingqiang Meng[2,3], Huiyuan Xu[2,3], Shutang Xu[4] and Tianwu Xu[4]*

[1]Wuxi Research Institute of Petroleum Geology, Petroleum Exploration and Production Research Institute, SINOPEC, Wuxi, China, [2]State Key Laboratory of Shale Oil and Gas Enrichment Mechanisms and Effective Development, SINOPEC, Beijing, China, [3]Petroleum Exploration and Production Research Institute, SINOPEC, Beijing, China, [4]Exploration and Production Research Institute, Zhongyuan Oilfield Branch, SINOPEC, Zhengzhou, China

The Dongpu Sag is one of the important areas for oil and gas exploration in the Bohai Bay Basin, eastern China, and natural gas from different strata in the sag contain a certain amount of helium, with the geochemical characteristics and the implications being weakly studied. Based on the analyses of the helium contents and isotopic ratios ($^3He/^4He$, $^{40}Ar/^{36}Ar$, $CH_4/^3He$, and $CO_2/^3He$) of natural gas, the abundance and origin of helium as well as the correlation with CH_4 and CO_2 are investigated. The results indicate that, natural gas samples from the Dongpu Sag display the helium contents of 0.0031–0.0217% and $^3He/^4He$ ratios of 0.148×10^{-7}–11.986×10^{-7}, and the $CH_4/^3He$ and $CO_2/^3He$ ratios range from 3.7×10^9 to 1.8263×10^{12} and from 0.05×10^9 to 35.04×10^9, respectively. Natural gas in the sag is helium depleted and extremely depleted, with the average helium content of 0.0133%. The helium reserves in the total gas reserves are 18.38×10^6 m^3, meeting the standard of small helium gas field. The helium is mainly crustal which has been mixed by a small amount of mantle-derived helium, whose proportion ranges from 0.01% to 10.72% with an average of 2.39%. Helium-related isotopic ratios of natural gas from the Dongpu Sag are consistent with those from other areas of the Bohai Bay Basin, suggesting crust-mantle mixed sources. Several gas samples from members 2 and 3 of the Shahejie Fm. contain an insignificant amount of mantle-derived helium, displaying the characteristics consistent with natural gas from typical cratonic basins.

Keywords: Dongpu Sag, helium content, helium isotopic compositions, argon isotopic ratios, Bohai Bay basin

OPEN ACCESS

Edited by:
Deyu Gong,
Research Institute of Petroleum Exploration and Development (RIPED), China

Reviewed by:
Hao Zou,
Chengdu University of Technology, China
Shu Tao,
China University of Geosciences, China

****Correspondence:***
Quanyou Liu
qyouliu@sohu.com

Specialty section:
This article was submitted to Geochemistry, a section of the journal Frontiers in Earth Science

Received: *26 January 2022*
Accepted: *10 February 2022*
Published: *24 February 2022*

Citation:
Ni C, Wu X, Liu Q, Zhu D, Yang F, Meng Q, Xu H, Xu S and Xu T (2022) Helium Signatures of Natural Gas From the Dongpu Sag, Bohai Bay Basin, Eastern China. Front. Earth Sci. 10:862677. doi: 10.3389/feart.2022.862677

INTRODUCTION

Geochemical characteristics of natural gas are fundamental to reveal the origin, source, and alteration processes of natural gas (Wu et al., 2017; Gong et al., 2018, Gong et al., 2019; Liu et al., 2019). As a noble gas with strategic values, helium has played an unreplaceable role in the high-tech fields considering the unique physicochemical properties (Xu et al., 1998; Anderson, 2018). Global helium demand increases by 4%–6% annually (Zhao et al., 2012), and it exceeds the supply for a long time. The discovered helium resources in the world are mainly concentrated in the U.S., Qatar, Algeria, and Russia, and their resources account for over 90% of the global resources (Anderson, 2018). Helium resource in China is relatively scarce, and the helium supply basically rely on imports (Tao et al., 2019; Chen et al., 2021; Peng et al., 2022). Helium is weakly

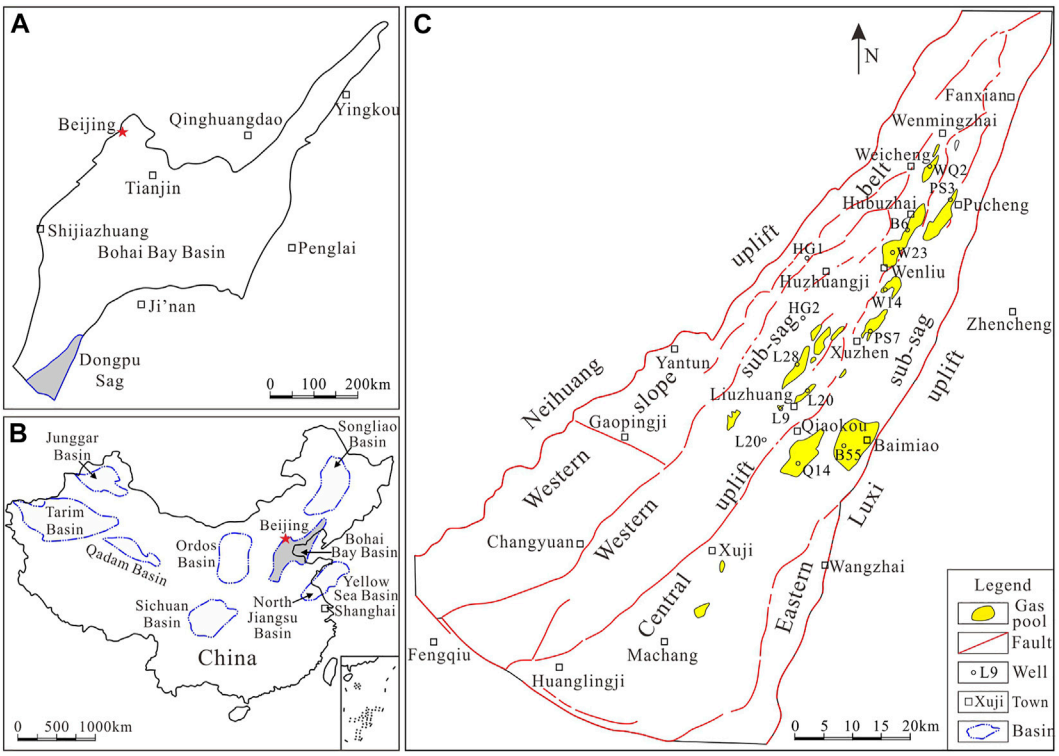

FIGURE 1 | The locations of the Dongpu Sag **(A)** and Bohai Bay Basin **(B)** and the distribution of gas reservoirs in the Dongpu Sag **(C)**.

explored in China, which demands further evaluation of helium resources and reserves. Since the helium content in the atmosphere is as low as 5.24×10^{-6} (Porcelli et al., 2002), helium extraction from helium-bearing natural gas is the only approach to industrially produce helium (Anderson, 2018; Tao et al., 2019; Chen et al., 2021).

Helium in natural gas includes three types, i.e., atmospheric helium, crustal helium, and mantle-derived helium (Xu et al., 1998; Anderson, 2018; Chen et al., 2021; Poreda et al., 1986, Poreda et al., 1988; Wang et al., 2020), and helium from gas pools in China are dominated by crustal and mantle-derived helium (Chen et al., 2021; Xu et al., 1995a). There are two stable isotopes of helium, i.e., ^{3}He and ^{4}He, and helium from different sources displays significantly different isotopic compositions. The R/Ra ratios (R and Ra refer to the ^{3}He/^{4}He ratio of the sample and the atmosphere, respectively) are commonly applied to describe the helium isotopic compositions (Xu et al., 1995a; Ni et al., 2014). The Ra value is generally considered as 1.4×10^{-6} (Mamyrin et al., 1970), and typical mantle-derived and crustal helium have the ^{3}He/^{4}He ratios (R) of 1.1×10^{-5} (Xu, 1996; Lupton, 1983) and 0.01 (Jenden et al., 1993), respectively. Helium isotopic ratios have been widely used in revealing the mantle-derived magmatism (Poreda et al., 1988; Marty et al., 1989) and tectonic setting (Xu et al., 1995a; Ding et al., 2005; Polyak et al., 2000) as well as tracing fluid origin and source in petroliferous system (Xu et al., 1995b; Dai et al., 2008, 2017; Ni et al., 2014; Zhang et al., 2019; Cao et al., 2020).

The Bohai Bay Basin is an vital rift petroliferous basin in eastern China. Under the effect of the Cenozoic magmatism, natural gas in the basin generally contain a certain amount of mantle-derived helium, and the helium content can be up to 0.26% (Dai et al., 2017), displaying commercial values. The Mesozoic-Cenozoic natural gas from the Huanghua Depression and the fluid inclusions around the Gangxi fault in the basin commonly display the incorporation of mantle-derived helium with the R/Ra ratios as high as 3.74, and the anomaly of mantle-derived helium is demonstrated to be controlled by the fault (Ding et al., 2005; Zhang et al., 2008). The Dongpu Sag is one of the crucial structural unis in the Bohai Bay Basin, and previous studies on natural gas mainly focused on the distribution characteristics, genetic types, filling models, and accumulation conditions (Lyu and Jiang, 2017; Chang et al., 2005; Jiao et al., 2006; Li and Chen, 2015; Liu et al., 2017a; Ni et al., 2015; Wang et al., 2011). Wang et al. (2011) have conducted preliminary discussion on the noble gas helium. Therefore, the authors intend to analyze the helium contents and isotopic ratios of natural gas from different strata of the Dongpu Sag, and discuss the abundance and origin of helium as well as the correlation with CH_4 and CO_2, aiming to provide scientific proofs for revealing the enrichment mechanism and resource potential of helium in natural gas.

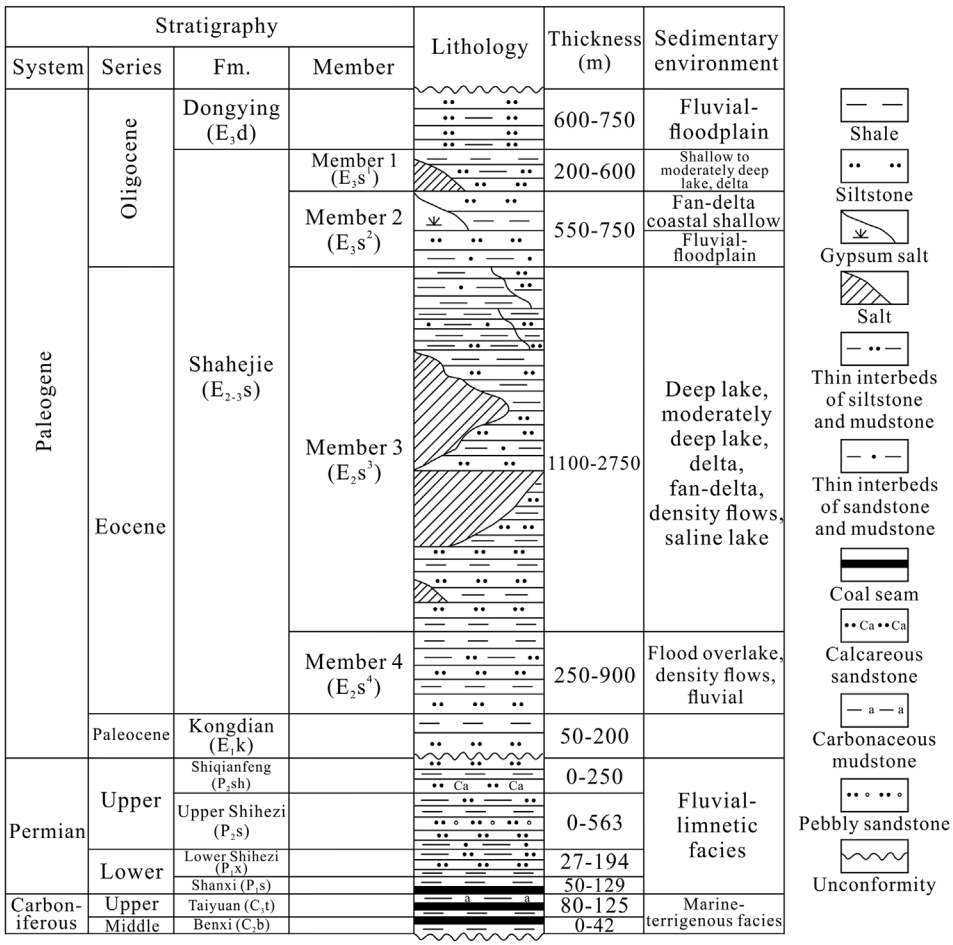

FIGURE 2 | Stratigraphic column of the Dongpu Sag, Bohai Bay Basin (Modified after Lyu and Jiang, 2017).

GEOLOGICAL SETTING

The Bohai Bay Basin, covering an area of 200×10^3 km^2, is located in eastern China (**Figures 1A,B**), and it is developed on the Mesoproterozoic-Neoproterozoic cratonic basement and superimposed by the Carboniferous-Permian coal measures and Mesozoic-Cenozoic rift layers (Dai et al., 2017). The nearly NE-trending Dongpu Sag is situated in southwestern Bohai Bay Basin (**Figure 1C**), and it covers an area of 5,300 km^2 narrowing northward (Liu et al., 2017b). The basement fault activities in the rift period result in the structural framework of "two sub-sag, one uplift, and one slope" in the sag (**Figure 1C**). Four structural units, i.e., Eastern sub-sag, Central uplift, Western sub-sag, and Western slope belt, have been developed eastward (Ni et al., 2015).

The Eocene strata in the Dongpu Sag can be downward divided into Dongying Fm. (E_3d), Shahejie Fm. ($E_{2\text{-}3}$s), and Kongdian Fm. (E_1k), in which the Shahejie Fm. can be further divided into four members downward (E_3s^1, E_3s^2, E_2s^3, and E_2s^4) (**Figure 2**). The underlying Carboniferous-Permian strata include Shiqianfeng Fm. (P_2sh), Upper Shihezi Fm. (P_2s), Lower Shihezi Fm. (P_1x), Shanxi Fm. (P_1s), Taiyuan Fm. (C_3t), and Benxi Fm. (C_2b) (Lyu and Jiang, 2017). Several Eocene tight sandstone gas reservoirs have been discovered in the Wenliu, Qiaokou, and Baimiao areas in the sag (**Figure 1**), and the Well HG2 in the Huzhuangji area has revealed gas accumulation in the Upper Permian reservoirs. Natural gas in the sag is demonstrated to be derived from two sets of main source rocks, i.e., the Eocene (E_3s^1 and E_2s^3) and Upper Paleozoic source rocks (P_1s and C_3t) (Lyu and Jiang, 2017; Wang et al., 2018; Liu et al., 2017a; Ni et al., 2015).

SAMPLES AND ANALYTICAL METHODS

19 gas samples from the E_3s^2, E_2s^3, E_2s^4, and Upper Permian reservoirs in the Dongpu Sag in the Bohai Bay Basin have been collected using stainless steel bottles with double valves. Geochemical analyzes of natural gas have been conducted in the SINOPEC Key Laboratory of Hydrocarbon Accumulation, and chemical compositions of natural gas are analyzed by Varian CP-3800 gas chromatograph. The contents and isotopic ratios of helium and argon are measured by Noblesse noble gas isotope mass spectrometer, and the detailed measuring processes refer to Cao et al. (2018).

TABLE 1 | Helium and argon contents and isotopic compositions of natural gas from the Dongpu Sag, Bohai Bay Basin.

Areas	Wells	Strata	CH_4 (%)	C_{2-5} (%)	CO_2 (%)	N_2 (%)	Helium ($\times10^{-6}$)	Argon ($\times10^{-6}$)	$^3He/^4He$ ($\times10^{-7}$)	R/Ra	$^{40}Ar/^{36}Ar$	$CH_4/^3He$ ($\times10^9$)	$CO_2/^3He$ ($\times10^9$)	Proportion of mantle-derived helium (%)
Wenliu	W108-4	E_2s^4	94.81	2.80	1.80	0.61	130	79.3	2.719	0.194	1965.3	26.8	0.51	2.33
	W23-40	E_2s^4	95.69	2.44	1.28	0.60	135	85.5	2.891	0.206	1,589.5	24.5	0.33	2.49
	W109-1	E_2s^4	95.42	2.40	1.59	0.59	132	94.9	2.904	0.207	1,116.2	24.9	0.41	2.50
	W72-462	E_2s^3	82.35	15.86	1.58	0.20	31	11.4	0.148	0.011	757.8	1826.3	35.04	0.01
	W13-353	E_2s^3	81.03	16.52	1.97	0.49	49	43.8	0.194	0.014	487.2	847.0	20.59	0.05
	WC194	E_3s^2	92.97	4.32	1.60	1.03	94	64	0.191	0.014	690.8	516.7	8.89	0.05
Hubuzhai	B17-2	E_2s^4	93.57	3.45	1.76	1.18	202	122	2.680	0.191	736.9	17.3	0.33	2.30
	B6	E_2s^4	92.87	3.82	2.29	1.03	183	73.2	2.732	0.195	2028.8	18.6	0.46	2.35
	B1-2	E_2s^4	93.00	3.93	2.10	0.94	171	78.6	2.970	0.212	1787.0	18.3	0.41	2.56
	B1-7	E_2s^4	93.12	4.15	1.84	0.88	168	77.6	2.693	0.192	1784.4	20.6	0.41	2.31
Xuji	X14-33	E_2s^3	90.65	6.49	1.98	0.88	133	69.2	3.089	0.221	1,191.9	22.1	0.48	2.67
Qiaokou	Q102	E_2s^3	59.78	7.08	1.00	32.08	48	29.8	0.318	0.023	677.7	392.3	6.56	0.16
Liuzhuang	L20-10	E_3s^2	92.54	4.59	1.88	1.00	93	101	2.534	0.181	758.6	39.3	0.80	2.17
	L9-6	E_3s^2	95.38	1.49	2.26	0.87	98	83.8	2.072	0.148	996.2	47.0	1.11	1.75
	L9-6	E_3s^2	95.52	1.69	1.87	0.90	91	78.9	2.388	0.171	915.4	44.0	0.86	2.04
Baimiao	BC20-1	E_3s^2	90.96	6.38	1.19	1.46	204	189	11.986	0.856	1,133.6	3.7	0.05	10.72
	BC52	E_2s^3	88.60	9.23	1.32	0.85	162	114	8.052	0.575	770.0	6.8	0.10	7.16
Huzhuangji	HG2	P_2sh	90.88	1.36	6.18	1.55	188	263	1.107	0.079	3,270.4	43.7	2.97	0.88
	HG2-1	P_2s	91.74	2.16	5.32	0.64	217	195	1.093	0.078	747.3	38.7	2.24	0.86

RESULTS

The helium and argon concentrations and isotopic ratios of natural gas from the Dongpu Sag in the Bohai Bay Basin are listed in **Table 1**.

Helium Contents

The E_3s^2, E_2s^3, E_2s^4, and Upper Permian gas samples from the Dongpu Sag display the helium contents of 0.0091–0.0204%, 0.0031–0.0162%, 0.0130–0.0202%, and 0.0188–0.0217%, respectively, with the average contents of 0.0116% (N = 5, N refers to the number of samples), 0.0085% (N = 5), 0.0160% (N = 7), and 0.0202% (N = 2), respectively (**Table 1**; **Figure 3A**). Helium contents in natural gas from different strata are lower than 0.05%, which is consistent with the results of other areas in the Bohai Bay Basin according to previous studies (**Figure 3B**).

Helium and Argon Isotopic Ratios

The $^3He/^4He$ ratios for natural gas from different strata in the Dongpu Sag range from 0.148×10^{-7} to 11.986×10^{-7} (**Table 1**).

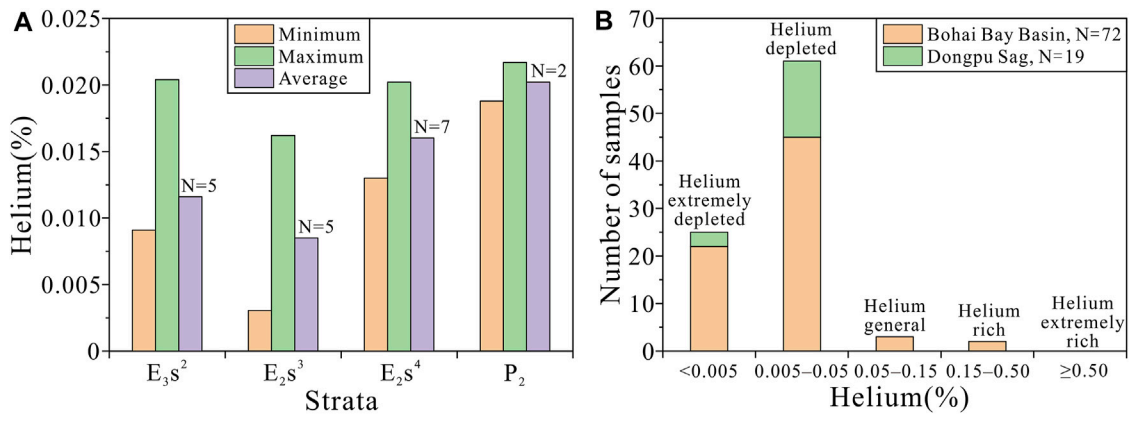

FIGURE 3 | Distribution of helium contents in natural gas from different strata in the Dongpu Sag **(A)** and the comparison with those from the Bohai Bay Basin **(B)**. Data for gas samples in the Bohai Bay Basin are from Zhang et al. (2008) and Dai et al. (2017).

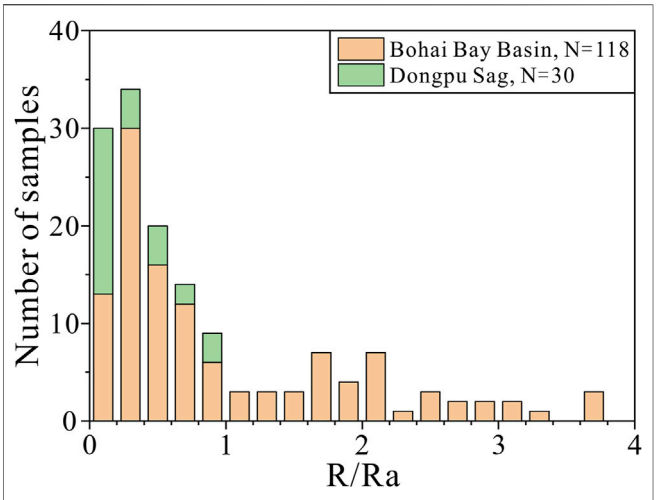

FIGURE 4 | Distribution of R/Ra ratios of natural gas from the Dongpu Sag. Data for gas samples in the Bohai Bay Basin are from Zhang et al. (2008) and Dai et al. (2017), and partial data for gas samples from the Dongpu Sag are from Wang et al. (2011).

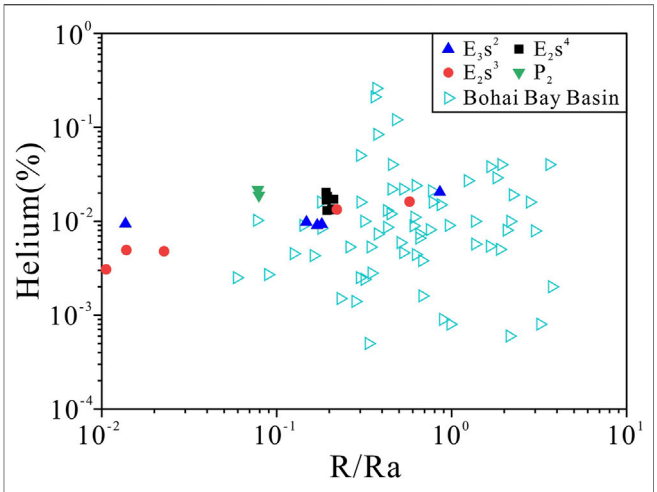

FIGURE 5 | Correlation between helium contents and R/Ra ratios of natural gas from the Dongpu Sag. Data for gas samples in the Bohai Bay Basin are from Zhang et al. (2008) and Dai et al. (2017).

The R/Ra values of the E_3s^2, E_2s^3, E_2s^4, and Upper Permian natural gas are 0.014–0.856, 0.011–0.575, 0.191–0.212, and 0.078–0.079, respectively, with the average values of 0.274 (N = 5), 0.169 (N = 5), 0.200 (N = 7), and 0.079 (N = 2), respectively (**Table 1**). The R/Ra ratios of natural gas from different strata are lower than 1 (**Table 1**; **Figures 4**, **5**). The $^{40}Ar/^{36}Ar$ ratios range from 487.2 to 3,270.4 (**Table 1**), which are significantly higher than that in the air (295.5, Allègre et al., 1987).

$CH_4/^3He$ and $CO_2/^3He$ Ratios

The $CH_4/^3He$ ratios for the E_3s^2, E_2s^3, E_2s^4, and Upper Permian natural gas from the Dongpu Sag are (3.7–516.7) × 10^9, (6.8–1826.3) × 10^9, (17.3–26.8) × 10^9, and (38.7–43.7) × 10^9, respectively (**Table 1**), with the average values of 130.1 × 10^9, 618.9 × 10^9, 21.6 × 10^9, and 41.2 × 10^9, respectively. The corresponding $CO_2/^3He$ ratios are (0.05–8.89) × 10^9, (0.10–35.04) × 10^9, (0.33–0.51) × 10^9, and (2.24–2.97) × 10^9, respectively (**Table 1**), with the average values of 2.34 × 10^9, 12.56 × 10^9, 0.41 × 10^9, and 2.61 × 10^9, respectively.

DISCUSSION

Helium Abundance in Natural Gas

Natural gas commonly includes five categories according to different helium contents, i.e., extremely depleted (Helium% < 0.005%), helium depleted (0.005% ≤ Helium% < 0.050%), helium general (0.050% ≤ Helium% < 0.150%), helium rich (0.150% ≤ Helium% < 0.500%), and helium extremely rich (Helium% ≥ 0.500%) gases (Dai et al., 2017). The average helium content of natural gas from the Panhandle-Hugoton gas field in the U.S. is 0.586% (Brown, 2019), suggesting the characteristics of helium extremely rich gas. Natural gas from the Weiyuan gas field in the Sichuan Basin in China display the average helium content of 0.251% for 215 gas samples (Dai et al., 2017), and helium contents of natural gas from the Hetianhe gas field in the Tarim Basin range from 0.30% to 0.37% (Tao et al., 2019), both suggesting helium rich gas.

The helium contents of natural gas from the Bohai Bay Basin range from 0.0005% to 0.26% with an average of 0.0197% (Zhang et al., 2008; Dai et al., 2017), which are mainly helium depleted and extremely depleted gases. Among the 72 gas samples from the basin, only 3 and 2 samples reach the standard of helium general and rich gases, respectively (**Figure 3B**). Natural gas from the Dongpu Sag has the helium contents ranging from 0.0031% to 0.0217% averaging 0.0133%. Natural gas from different strata is helium depleted and extremely depleted rather than helium rich despite various contents of heliumAlthough natural gas from different strata vary in helium contents, the gas is helium depleted and extremely depleted rather than helium rich (**Table 1**; **Figure 3**). Helium contents of natural gas from the Dongpu Sag are significantly lower than those from the Sichuan Basin, and this may be derived from the differences of helium source and accumulation mechanism.

Based on the helium amount in the natural gas reserves, helium gas fields can be divided into very small, small, medium, large, and extra large gas fields, with the corresponding helium reserves of <5 × 10^6 m^3, (5–25) × 10^6 m^3, (25–50) × 10^6 m^3, (50–100) × 10^6 m^3, and ≥100 × 10^6 m^3, respectively (Dai et al., 2017). The helium amounts in the Panhandle-Hugoton gas field in the U.S. were about 18,000 × 10^6 m^3 at the time of discovery (Brown, 2019), and the total proved helium reserves in the Hetianhe gas field in the Tarim Basin in China are 195.91 × 10^6 m^3, both being extra large helium gas field. The proved gas reserves in the Dongpu Sag are 138.2 × 10^9 m^3 with the average helium content of 0.0133%. The calculation based on these two parameters indicates that the proved helium reserves in the sag are 18.38 × 10^6 m^3, which suggest a small helium gas field. This indicates that natural gas in the Dongpu Sag displays a low helium abundance with a considerable total amount.

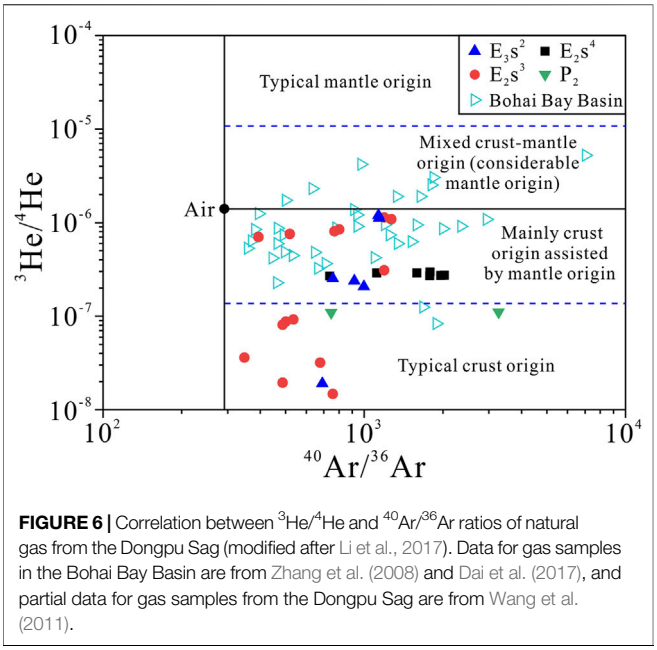

FIGURE 6 | Correlation between ^{3}He/^{4}He and ^{40}Ar/^{36}Ar ratios of natural gas from the Dongpu Sag (modified after Li et al., 2017). Data for gas samples in the Bohai Bay Basin are from Zhang et al. (2008) and Dai et al. (2017), and partial data for gas samples from the Dongpu Sag are from Wang et al. (2011).

Extraction from helium-bearing natural gas is the only approach to industrially produce helium, and the lower abundance limit for industrially valuable helium reservoirs was commonly believed to be 0.1% (Tao et al., 2019; Chen et al., 2021). Since the boiling point of helium is significantly lower than that of methane, during the process of compressing natural gas to produce liquefied natural gas (LNG) by some countries such as Qatar, helium is relatively enriched in the residual gas which is the by-product of producing LNG (Tao et al., 2019). The required helium contents for helium production by this approach can be as low as 0.04% (Anderson, 2018). 8 of 72 gas samples from the Bohai Bay Basin display the helium contents no less than 0.04% (Zhang et al., 2008; Dai et al., 2017), meeting the required helium abundance to produce helium by LNG. Most gas samples from the Dongpu Sag and other areas in the Bohai Bay Basin display helium contents lower than 0.04%. However, the required helium abundance to produce helium from natural gas may further decrease as the technologies of helium separation and enrichment continuously improve, which makes the effective use of more helium resource possible in the future.

Origin of Helium

Helium in natural gas includes atmospheric, crustal, and mantle-derived helium, in which the typical mantle-derived helium displays the ^{3}He/^{4}He of 1.1×10^{-5} (Xu, 1996; Lupton, 1983) with the R/Ra ratio of 7.9, whereas the R/Ra ratio of typical crustal helium is about 0.01 (Jenden et al., 1993). Helium in natural gas reservoirs in China is mainly composed of crustal and mantle-derived helium (Xu et al., 1995a; Chen et al., 2021). The proportion of mantle-derived helium can be calculated on the basis of a two-endmember (crustal and mantle-derived) mixing model, and the calculation equation is as follows (Jenden et al., 1993).

$$\begin{aligned} He_{mantle}\% &= 100 \times (R_{sample} - R_{crust}) / (R_{mantle} - R_{crust}) \\ &= 100 \times \left[(R/Ra)_{sample} - (R/Ra)_{crust} \right] / \left[(R/Ra)_{mantle} \right. \\ &\quad \left. - (R/Ra)_{crust} \right] \end{aligned}$$

where R refers to the ^{3}He/^{4}He ratio.

The helium content in natural gas from the Dongpu Sag ranges from 31×10^{-6} to 217×10^{-6} (**Table 1**), which is significantly higher than that in the atmosphere (5.24×10^{-6}, Porcelli et al., 2002). The ^{40}Ar/^{36}Ar ratio ranges from 487.2 to 3,270.4 (**Table 1**; **Figure 6**) and is also significantly higher than the atmospheric value (295.5, Allègre et al., 1987). Therefore, natural gas in the Dongpu Sag is unlikely mixed by atmosphere. Calculation based on the R/Ra ratios of natural gas from different strata in the sag (**Table 1**) and the above-mentioned equation indicates that, the proportion of mantle-derived helium in the gas ranges from 0.01% to 10.72% with an average of 2.39%. The proportions of mantle-derived helium in several samples are less than 1%, suggesting representative characteristics of crustal helium (**Table 1**).

Helium isotopic compositions have been commonly used to trace mantle-derived volatiles (Poreda et al., 1988; Xu et al., 1997; Oxburgh et al., 1986). R/Ra < 0.1 generally suggests typical crustal source, and 0.1 ≤ R/Ra<1 suggests mixing by a small amount of mantle-derived helium, whereas R/Ra ≥ 1 indicates remarkable addition of mantle-derived helium (Xu et al., 1998; Chen et al., 2021; Li et al., 2017). Natural gas from different strata in the Sichuan Basin displays R/Ra ratios of 0.002–0.05 with an average of 0.015 (Wang et al., 2020), suggesting typical crustal helium (Ni et al., 2014). The R/Ra ratios of natural gas from the Bohai Bay Basin range from 0.059 to 3.74 (**Figure 5**) with an average of 1.013 (Zhang et al., 2008; Dai et al., 2017), indicating general mixing of mantle-derived helium by various degrees (**Figure 6**). The R/Ra ratios of natural gas from the Dongpu Sag range from 0.011 to 0.856 (**Table 1**), displaying the characteristics of mixing between crustal and mantle-derived helium. The R/Ra distribution is consistent with that for gas samples from other areas in the Bohai Bay Basin (**Figure 4**). In the correlation diagram between ^{3}He/^{4}He and ^{40}Ar/^{36}Ar ratios, 9 of 29 gas samples from the Dongpu Sag are of crustal origin, whereas the other samples are dominated by crustal helium and mixed by a small amount of mantle-derived helium (**Figure 6**). These are in accordance with the calculation results of the proportion of mantle-derived helium (**Table 1**).

The alkane gas in the Dongpu Sag is demonstrated to be derived from the organic matters in the $E_{2\text{-}3}s$ and C_3t-P_1s source rocks (Ni et al., 2015; Lyu and Jiang, 2017; Wang et al., 2018), however, the helium is believed to be derived from both the mantle and crustal decay of uranium (U) and thorium (Th) in the rocks. Since the rocks from different strata in the sag contain various contents of U and Th, it needs further study on which strata are the main source of crustal helium.

The Sinian and pre-Sinian gas in southern Sichuan Basin has higher helium abundances than natural gas from other areas of the basin, with the average helium content (0.24%) reaching the standard of commercial exploitation (Ni et al., 2014). The high content of helium in the ancient strata

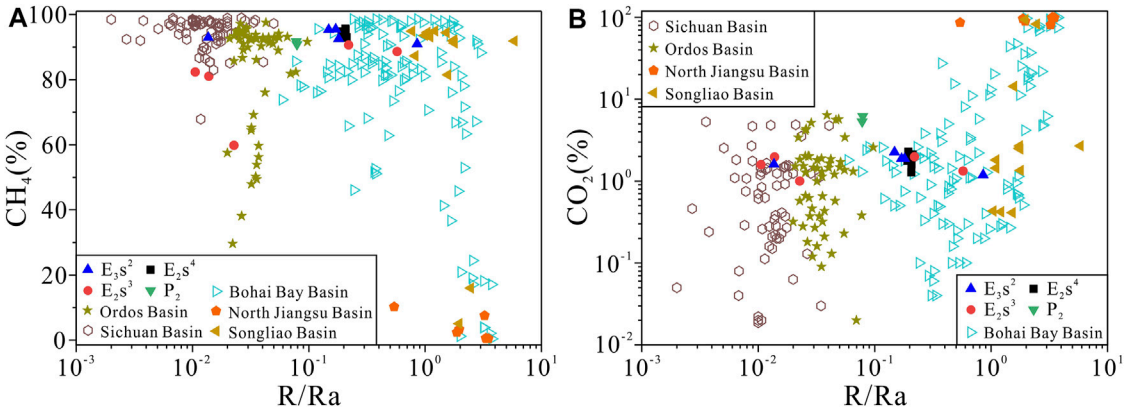

FIGURE 7 | Correlation diagrams of CH_4(%) versus R/Ra **(A)** and CO_2(%) versus R/Ra **(B)** of natural gas from the Dongpu Sag. Data for gas samples in the Bohai Bay Basin are from Zhang et al. (2008) and Dai et al. (2017), and those in the Sichuan Basin are from Dai et al. (2008), Ni et al. (2014), and Wu et al. (2013). Data for gas samples from the Ordos, North Jiangsu, and Songliao basins are from Dai et al. (2017), Liu et al. (2017a), and Liu et al. (2016), respectively.

suggests the accumulation of crustal helium with time (Ni et al., 2014), suggesting accumulation effect of helium derived from radioactive decay of U and Th in the rocks. Several gas wells in petroliferous basins in eastern China (e.g., Songliao and North Jiangsu) display the helium contents between 0.05 and 0.1%, and the proportions of mantle-derived helium range from 33.5% to 65.4% (Xu et al., 1997). These indicate that mantle-derived helium in sedimentary strata can form industrial accumulation (Xu et al., 1997). The helium contents and R/Ra ratios of natural gas from the Bohai Bay Basin display little positive correlation (**Figure 5**). Several gas samples have the helium contents higher than 0.05% with R/Ra ratios around 0.5, whereas the samples with higher R/Ra ratios does not display higher helium contents (**Figure 5**). This is probably associated with the various original contents of crustal helium in natural gas. Helium contents and R/Ra ratios of natural gas from the Dongpu Sag are positively correlated to some degree. Gas samples with R/Ra < 0.03 have helium contents lower than 0.01%, whereas those with R/Ra > 0.1 have helium contents generally higher than 0.01% (**Figure 5**). These indicate that the mixing of mantle-derived helium enhanced the helium abundance in natural gas to a certain extent. Moreover, the Upper Permian gas in the Dongpu Sag does not have remarkably higher helium contents than the $E_{2\text{-}3}s$ gas (**Figure 5**), which suggests that the accumulation effect of crustal helium with time is unobvious. The reservoirs in the Sichuan Basin are generally older than those in the Dongpu Sag, and thus the decay time of U and Th in the Sichuan Basin is supposed to be longer than that in the Dongpu Sag. Therefore, natural gas from the Sichuan Basin generally displays higher helium contents than that in the Dongpu Sag.

Since mantle-derived helium in sedimentary strata can form industrial accumulation (Xu et al., 1997), and crustal helium is favorable to be enriched in ancient strata (e.g., Sinian and pre-Sinian strata in southern Sichuan Basin) due to longer decay time of U and Th, helium is likely to accumulate more easily in ancient strata or along the deep faults which connect the mantle.

Correlation of Helium With CH_4 and CO_2

Helium in natural gas is generally accompanied with alkane gas (e.g., CH_4) and CO_2, and the association of geochemical characteristics and origin between helium and CH_4/CO_2 has attracted wide attention (Poreda et al., 1986; Dai et al., 2017; Liu et al., 2016; Liu et al., 2021). The CH_4 contents of natural gas from the Dongpu Sag are higher than 80% except one sample of 59.78% (**Table 1**). The CO_2 contents range from 1.0 to 6.18% (**Table 1**), and both CH_4 and CO_2 contents have unremarkable correlation with R/Ra ratios (**Figures 7A,B**). Natural gas from Chinese petroliferous basins display similar characteristics, and only a few gas samples from the North Jiangsu, Songliao, and Bohai Bay basins have experienced mixing by mantle-derived gas with high CO_2 contents and R/Ra ratios (**Figures 7A,B**). Dai et al. (2017) have demonstrated that, natural gas from the cratonic basins in central-western China (e.g., Sichuan and Ordos) has the CO_2 contents generally lower than 5%, and the CO_2 is considered to be derived from the hydrocarbon generation process and decomposition or erosion of carbonate rocks. Moreover, the gas from the rift basins in eastern China such as Bohai Bay Basin may have higher CO_2 content up to nearly 100%, and the CO_2 is mainly derived from volcanic-magmatic activities or being mantle-derived (Dai et al., 2017).

The correlation diagram between $CH_4/^3He$ and R/Ra ratios are commonly used to constrain natural gas from the crustal or magmatic/mantle source (Poreda et al., 1986; Jenden et al., 1993). Natural gas from cratonic basins in China (e.g., Sichuan, Ordos, and Tarim) is mainly of crustal origin with the $CH_4/^3He$ ratios of 10^{10}–10^{12} and R/Ra < 0.1 (Ni et al., 2014; Dai et al., 2017). However, the gas from rift basins (e.g., Bohai Bay and Songliao) displays the addition of mantle-derived components with $CH_4/^3He$ ratios mainly of 10^6–10^{11} and R/Ra > 0.1 (Ni et al., 2014; Dai et al., 2017). The $CH_4/^3He$ ratios of natural gas from different strata in the Dongpu Sag range from 3.7×10^9 to 1.8263×10^{12}

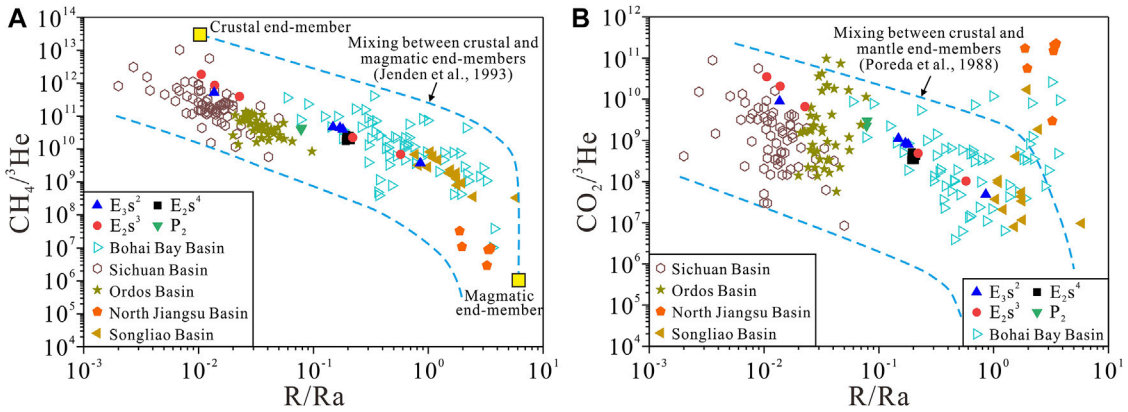

FIGURE 8 | Correlation diagrams of $CH_4/^3He$ versus R/Ra **(A)** and $CO_2/^3He$ versus R/Ra **(B)** of natural gas from the Dongpu Sag. The crustal and magmatic endmembers and crus-mantle mixing line in **Figure 7A** are from Jenden et al. (1993), whereas the crust-mantle mixing line in **Figure 7B** is from Poreda et al. (1988). Data for gas samples in the Bohai Bay Basin are from Zhang et al. (2008) and Dai et al. (2017), and those in the Sichuan Basin are from Dai et al. (2008), Ni et al. (2014), and Wu et al. (2013). Data for gas samples from the Ordos, North Jiangsu, and Songliao basins are from Dai et al. (2017), Liu et al. (2017b), and Liu et al. (2016), respectively.

(**Table 1**), which are mainly consistent with those from other areas in the Bohai Bay Basin and display the characteristics of crust-mantle mixing. The high $CH_4/^3He$ ratios and low R/Ra ratios for several E_3s^2 and E_2s^3 samples are consistent with those for natural gas from cratonic basins such as Sichuan Basin (**Figure 8A**).

Magmatic/mantle-derived fluids generally have low $CO_2/^3He$ ratios and high R/Ra ratios, whereas the crustal fluids have high $CO_2/^3He$ ratios and low R/Ra ratios, and the gas from active continental margins displays a two-endmember mixing trend in the correlation diagram between $CO_2/^3He$ and R/Ra ratios (Poreda et al., 1988). Natural gas from typical cratonic basins such as Sichuan and Ordos is crustal gas as indicated in the correlation diagram (Wu et al., 2013), whereas the gas from rift basins such as Bohai Bay displays the contribution of mantle-derived fluids (**Figure 8B**). The $CO_2/^3He$ ratios of natural gas from the Dongpu Sag range from 0.05×10^9 to 35.04×10^9 (**Table 1**), which are mainly consistent with those from other areas of the Bohai Bay Basin and display the characteristics of mixing by mantle-derived gas. Several E_3s^2 and E_2s^3 samples with relatively high $CH_4/^3He$ and $CO_2/^3He$ ratios show similar characteristics with natural gas from cratonic basins such as Sichuan, which display the characteristics of typical crustal gas (**Figures 8A,B**).

CONCLUSION

Natural gas from the Dongpu Sag in the Bohai Bay Basin in eastern China has the helium contents of 0.0031%–0.0217% averaging 0.0133%. The $^3He/^4He$, R/Ra, and $^{40}Ar/^{36}Ar$ ratios are 0.148×10^{-7}–11.986×10^{-7}, 0.011–0.856, and 487.2–3,270.4, respectively. The $CH_4/^3He$ and $CO_2/^3He$ ratios range from 3.7×10^9 to 1.8263×10^{12} and from 0.05×10^9 to 35.04×10^9, respectively.

The gas from the Dongpu Sag is helium depleted and extremely depleted, and the calculated helium amounts in the proved gas reserves are 18.38×10^6 m^3, suggesting a small helium gas field. Although the helium abundance is relatively low, the total amount of helium is considerable. The effective use of these helium resource may be probable with the continuous improvement of the technologies of helium separation and enrichment.

Helium in natural gas from the Dongpu Sag is mainly crustal and mixed by a small amount of mantle-derived helium, and the proportion of mantle-derived helium ranges from 0.01% to 10.72% averaging 2.39%. The isotopic compositions associated with helium indicate that, natural gas from the Dongpu Sag is mainly derived from mixing between crustal and mantle sources, which is in accordance with the gas from other areas of the Bohai Bay Basin. Several gas samples from members 2 and 3 of the Shahejie Fm. display unremarkable mixing by mantle-derived helium, and their characteristics are consistent with those of natural gas from cratonic basins in China.

DATA AVAILABILITY STATEMENT

The original contributions presented in the study are included in the article/Supplementary Material, further inquiries can be directed to the corresponding author.

AUTHOR CONTRIBUTIONS

CN: Conceptulization, Data curation, Writing. XW: Data curation, Writing. QL: Conceptulization, Writing. DZ: Data curation, Methodology. FY: Methodology, Investigation. QM: Investigation. HX: Methodology. SX: Investigation. TX: Investigation.

FUNDING

This work was funded by National Natural Science Foundation of China (Grant Nos: 42141021, 42172149, 41872122, U20B6001) and Strategic Priority Research Program of the Chinese Academy of Sciences (Class A) (Grant No. XDA14010404).

ACKNOWLEDGMENTS

The authors appreciate the SINOPEC Zhongyuan Branch Company for the assistance on sample and data collection. The SINOPEC Key Laboratory of Hydrocarbon Accumulation is acknowledged for the assistance on geochemical analyzes. We sincerely appreciate the constructive comments and suggestions proposed by the reviewers.

REFERENCES

Allègre, C. J., Staudacher, T., and Sarda, P. (1987). Rare Gas Systematics: Formation of the Atmosphere, Evolution and Structure of the Earth's Mantle. *Earth Planet. Sci. Lett.* 81 (2), 127–150. doi:10.1016/0012-821x(87)90151-8

Anderson, S. T. (2018). Economics, Helium, and the U.S. Federal Helium Reserve: Summary and Outlook. *Nat. Resour. Res.* 27 (4), 455–477. doi:10.1007/s11053-017-9359-y

Brown, A. (2019). Origin of Helium and Nitrogen in the Panhandle-Hugoton Field of Texas, Oklahoma, and Kansas, United States. *AAPG Bulletin* 103, 369–403. doi:10.1306/07111817343

Cao, C., Zhang, M., Tang, Q., Yang, Y., Lv, Z., Zhang, T., et al. (2018). Noble Gas Isotopic Variations and Geological Implication of Longmaxi Shale Gas in Sichuan Basin, China. *Mar. Pet. Geology.* 89, 38–46. doi:10.1016/j.marpetgeo.2017.01.022

Cao, C., Zhang, M., Li, L., Wang, Y., Li, Z., Du, L., et al. (2020). Tracing the Sources and Evolution Processes of Shale Gas by Coupling Stable (C, H) and noble Gas Isotopic Compositions: Cases from Weiyuan and Changning in Sichuan Basin, China. *J. Nat. Gas Sci. Eng.* 78, 103304. doi:10.1016/j.jngse.2020.103304

Chang, J., Li, X., He, J., Lv, H., Zhang, T., and Huang, Y. (2005). Researches on Characteristics of Geochemistry and Formation of Wengu 2 Well Natural Gas in Dongpu Depression. *Nat. Gas Geosci.* 16 (5), 608–611. doi:10.11764/j.issn.1672-1926.2005.05.608

Chen, J., Liu, K., Dong, Q., Wang, H., Luo, B., and Dai, X. (2021). Research Status of Helium Resources in Natural Gas and Prospects of Helium Resources in China. *Nat. Gas Geosci.* 32 (10), 1436–1449. doi:10.11764/j.issn.1672-1926.2021.08.006

Dai, J., Zou, C., Zhang, S., Li, J., Ni, Y., Hu, G., et al. (2008). Discrimination of Abiogenic and Biogenic Alkane Gases. *Sci. China Ser. D-earth Sci.* 51, 1737–1749. doi:10.1007/s11430-008-0133-1

Dai, J., Ni, Y., Qin, S., Huang, S., Gong, D., Liu, D., et al. (2017). Geochemical Characteristics of He and CO_2 from the Ordos (Cratonic) and Bohaibay (Rift) Basins in China. *Chem. Geology.* 469, 192–213. doi:10.1016/j.chemgeo.2017.02.011

Ding, W., Dai, J., Yang, C., Tao, S., and Hou, L. (2005). Helium Isotopic Compositions in Fluid Inclusions of the Gangxi Fault belt in the Huanghua Depression, Bohai Bay Basin. *Chin. Sci. Bull.* 50, 2621–2627. doi:10.1007/bf03183660

Gong, D., Li, J., Ablimit, I., He, W., Lu, S., Liu, D., et al. (2018). Geochemical Characteristics of Natural Gases Related to Late Paleozoic Coal Measures in China. *Mar. Pet. Geology.* 96, 474–500. doi:10.1016/j.marpetgeo.2018.06.017

Gong, D., Song, Y., Wei, Y., Liu, C., Wu, Y., Zhang, L., et al. (2019). Geochemical Characteristics of Carboniferous Coaly Source Rocks and Natural Gases in the Southeastern Junggar Basin, NW China: Implications for New Hydrocarbon Explorations. *Int. J. Coal Geology.* 202, 171–189. doi:10.1016/j.coal.2018.12.006

Jenden, P. D., Hilton, D. R., Kaplan, I. R., and Craig, H. (1993). "Abiogenic Hydrocarbons and Mantle Helium in Oil and Gas fields," in *The Future of Energy Gases*. Editor D. G. Howell (Denver: U.S. Geological Survey Professional Paper), 31–56.

Jiao, D., Wang, D., and Wu, X. (2006). Patterns of Natural Gas Accumulation and Enrichment in Dongpu Depression. *Oil Gas Geology.* 27 (6), 794–803. doi:10.11743/ogg20060610

Li, C., and Chen, F. (2015). Origin of the Natural Gas from Paleogene Shahejie Formation in the Qiaokou-Baimiao Areas of the Dongpu Depression, Bohai Bay Basin. *Nat. Gas Geosci.* 26 (11), 2114–2121. doi:10.11764/j.issn.1672-1926.2015.11.2114

Li, J., Li, Z., Wang, X., Wang, D., Xie, Z., Li, J., et al. (2017). New Indexes and Charts for Genesis Identification of Multiple Natural Gases. *Pet. Exploration Dev.* 44, 535–543. doi:10.1016/s1876-3804(17)30062-9

Liu, Q., Dai, J., Jin, Z., Li, J., Wu, X., Meng, Q., et al. (2016). Abnormal Carbon and Hydrogen Isotopes of Alkane Gases from the Qingshen Gas Field, Songliao Basin, China, Suggesting Abiogenic Alkanes. *J. Asian Earth Sci.* 115, 285–297. doi:10.1016/j.jseaes.2015.10.005

Liu, J., Jiang, Y., Zhang, Y., Xu, T., Mu, X., and Wan, T. (2017a). Genesis and Charge Difference of Paleogene Tight sandstone Gas in Dongpu Sag. *Acta Petrolei Sinica* 38 (9), 1010–1020. doi:10.7623/syxb201709003

Liu, Q., Zhu, D., Jin, Z., Meng, Q., Wu, X., and Yu, H. (2017b). Effects of Deep CO_2 on Petroleum and thermal Alteration: The Case of the Huangqiao Oil and Gas Field. *Chem. Geology.* 469, 214–229. doi:10.1016/j.chemgeo.2017.06.031

Liu, Q., Wu, X., Wang, X., Jin, Z., Zhu, D., Meng, Q., et al. (2019). Carbon and Hydrogen Isotopes of Methane, Ethane, and Propane: A Review of Genetic Identification of Natural Gas. *Earth-Science Rev.* 190, 247–272. doi:10.1016/j.earscirev.2018.11.017

Liu, Q., Wu, X., Zhu, D., Meng, Q., Xu, H., Peng, W., et al. (2021). Generation and Resource Potential of Abiogenic Alkane Gas under Organic-Inorganic Interactions in Petroliferous Basins. *J. Nat. Gas Geosci.* 6 (2), 79–87. doi:10.1016/j.jnggs.2021.04.003

Lupton, J. E. (1983). Terrestrial Inert Gases: Isotope Tracer Studies and Clues to Primordial Components in the Mantle. *Annu. Rev. Earth Planet. Sci.* 11, 371–414. doi:10.1146/annurev.ea.11.050183.002103

Lyu, X., and Jiang, Y. (2017). Genesis of Paleogene Gas in the Dongpu Depression, Bohai Bay Basin, East China. *J. Pet. Sci. Eng.* 156, 181–193. doi:10.1016/j.petrol.2017.05.021

Mamyrin, B. A., Anufrier, G. S., Kamensky, I. L., and Tolstikhin, I. N. (1970). Determination of the Isotopic Composition of Helium in the Atmosphere. *Geochem. Int.* 7, 498–505.

Marty, B., Jambon, A., and Sano, Y. (1989). Helium Isotopes and CO_2 in Volcanic Gases of Japan. *Chem. Geology.* 76, 25–40. doi:10.1016/0009-2541(89)90125-3

Ni, Y., Dai, J., Tao, S., Wu, X., Liao, F., Wu, W., et al. (2014). Helium Signatures of Gases from the Sichuan Basin, China. *Org. Geochem.* 74, 33–43. doi:10.1016/j.orggeochem.2014.03.007

Ni, C., Bao, J., Zhou, X., Xu, S., Xu, L., Xu, T., et al. (2015). Geochemical Characteristics and Types of Natural Gas from Well Hugu 2 in the Dongpu Sag of Bohai Bay Basin. *Pet. Geology. Exp.* 37 (6), 764–769 775. doi:10.11781/sysydz201506764

Oxburgh, E. R., O'Nions, R. K., and Hill, R. I. (1986). Helium Isotopes in Sedimentary Basins. *Nature* 324, 632–635. doi:10.1038/324632a0

Peng, W., Liu, Q., Zhang, Y., Jia, H., Zhu, D., Meng, Q., et al. (2022). The First Extra-large Helium-Rich Gas Field Identified in a Tight sandstone of the Dongsheng Gas Field, Ordos Basin, central China. *Sci. China Earth Sci.* (in press). doi:10.1360/SSTe-2021-0277

Polyak, B. G., Tolstikhin, I. N., Kamensky, I. L., Yakovlev, L. E., Cheshko, A. L., and Marty, B. (2000). Helium Isotopes, Tectonics and Heat Flow in the Northern Caucasus. *Geochimica et Cosmochimica Acta* 64, 1925–1944. doi:10.1016/s0016-7037(00)00342-2

Porcelli, D., Ballentine, C. J., and Wieler, R. (2002). An Overview of Noble Gas Geochemistry and Cosmochemistry. *Rev. Mineralogy Geochem.* 47, 1–19. doi:10.2138/rmg.2002.47.1

Poreda, R. J., Jenden, P. D., Kaplan, I. R., and Craig, H. (1986). Mantle Helium in Sacramento basin Natural Gas wells. *Geochimica et Cosmochimica Acta* 50, 2847–2853. doi:10.1016/0016-7037(86)90231-0

Poreda, R. J., Jeffrey, A. W. A., Kaplan, I. R., and Craig, H. (1988). Magmatic Helium in Subduction-Zone Natural Gases. *Chem. Geology.* 71, 199–210. doi:10.1016/0009-2541(88)90115-5

Tao, X., Li, J., Zhao, L., Li, L., Zhu, W., Xing, L., et al. (2019). Helium Resources and Discovery of First Supergiant Helium reserve in China: Hetianhe Gas Field. *Earth Sci.* 44, 1024–1041. doi:10.3799/dqkx.2018.381

Wang, S., Liu, H., Dong, H., Liu, J., Zhu, L., and Xu, B. (2011). Distribution and Origin of Natural Gas in Qiaokou-Baimiao Area, Dongpu Depression. *Fautl-Block Oil & Gas Field* 18 (2), 207–211.

Wang, K., Pang, X., Zhang, H., Zhao, Z., Su, S., and Hui, S. (2018). Characteristics and Genetic Types of Natural Gas in the Northern Dongpu Depression, Bohai Bay Basin, China. *J. Pet. Sci. Eng.* 170, 453–466. doi:10.1016/j.petrol.2018.06.080

Wang, X., Liu, W., Li, X., Liu, Q., Tao, C., and Xu, Y. (2020). Radiogenic Helium Concentration and Isotope Variations in Crustal Gas Pools from Sichuan

Basin, China. *Appl. Geochem.* 117, 104586. doi:10.1016/j.apgeochem.2020.104586

Wu, X., Dai, J., Liao, F., and Huang, S. (2013). Origin and Source of CO_2 in Natural Gas from the Eastern Sichuan Basin. *Sci. China Earth Sci.* 56, 1308–1317. doi:10.1007/s11430-013-4601-x

Wu, X., Ni, C., Liu, Q., Liu, G., Zhu, J., and Chen, Y. (2017). Genetic Types and Source of the Upper Paleozoic Tight Gas in the Hangjinqi Area, Northern Ordos Basin, China. *Geofluids* 2017, 1–14. doi:10.1155/2017/4596273

Xu, S., Nakai, S. i., Wakita, H., Xu, Y., and Wang, X. (1995a). Helium Isotope Compositions in Sedimentary Basins in China. *Appl. Geochem.* 10, 643–656. doi:10.1016/0883-2927(95)00033-x

Xu, S., Nakai, S. i., Wakita, H., and Wang, X. (1995b). Mantle-derived noble Gases in Natural Gases from Songliao Basin, China. *Geochimica et Cosmochimica Acta* 59, 4675–4683. doi:10.1016/0016-7037(95)00301-0

Xu, Y., Shen, P., Tao, M., and Liu, W. (1997). Geochemistry on Mantle-Derived Volatiles in Natural Gases from Eastern China Oil/gas Provinces (I). *Sci. China Ser. D-earth Sci.* 40, 120–129. doi:10.1007/bf02878370

Xu, Y., Shen, P., Liu, W., Tao, M., Sun, M., and Du, J. (1998). *Geochemistry of noble Gases in Natural Gas*. Beijing: Science Press.

Xu, Y. (1996). The Mantle noble Gas of Natural Gases. *Earth Sci. Front.* 3, 63–71. doi:10.3321/j.issn:1005-2321.1996.03.006

Zhang, T., Zhang, M., Bai, B., Wang, X., and Li, L. (2008). Origin and Accumulation of Carbon Dioxide in the Huanghua Depression, Bohai Bay Basin, China. *Bulletin* 92, 341–358. doi:10.1306/10230706141

Zhang, W., Li, Y., Zhao, F., Han, W., Li, Y., Wang, Y., et al. (2019). Using noble Gases to Trace Groundwater Evolution and Assess Helium Accumulation in Weihe Basin, central China. *Geochimica et Cosmochimica Acta* 251, 229–246. doi:10.1016/j.gca.2019.02.024

Zhao, H., Zhang, Y., and Li, C. (2012). Analysis of Supply and price System for Global Helium Gas. *Chem. Propellants Polymeric Mater.* 10 (6), 91–96. doi:10.16572/j.issn1672-2191.2012.06.003

Conflict of Interest: Authors CN, XW, QL, DZ, FY, QM, HX, SX and TX were employed by SINOPEC.

Publisher's Note: All claims expressed in this article are solely those of the authors and do not necessarily represent those of their affiliated organizations, or those of the publisher, the editors and the reviewers. Any product that may be evaluated in this article, or claim that may be made by its manufacturer, is not guaranteed or endorsed by the publisher.

frontiers in Earth Science

ORIGINAL RESEARCH
published: 28 February 2022
doi: 10.3389/feart.2022.843245

Geneses, Sources and Accumulation Process of Natural Gases in the Hinterland of the Junggar Basin

Dongming Zhi[1,2]*, *Xiaojun Wang*[1] and *Zhijun Qin*[1]

[1]Xinjiang Oilfield Company, PetroChina, Karamay, China, [2]Turpan-Hami Oilfield Company, PetroChina, Hami, China

The Junggar Basin is rich in natural gas resources, but it has hardly been explored, with the proven rate being less than 9.0%. Although the hinterland of the Junggar Basin has a favorable condition for natural gas accumulation, the complex gas sources cause great trouble in the selection of zones and belts for exploration. Based on the molecular composition and stable carbon and hydrogen isotope data of 95 natural gas samples from 72 wells in this area, combined with the characteristics of structural evolution history, burial history, hydrocarbon generation and expulsion history, and fluid inclusions, this paper clarified the geneses and sources of natural gas, identified the secondary alteration of natural gas, and restored the process of natural gas accumulation. Natural gas in the hinterland was divided into four types: Type I was oil-type gas from the Lower Permian Fengcheng Formation; Type II was coal-type gas derived from the Carboniferous source rock; Type III was the mixture of Type I and II gases, which constituted the major fraction of natural gases in the hinterland; and Type IV that referred to secondary microbial gas formed by the biodegradation of crude oil. During the Late Cretaceous, the Carboniferous and Fengcheng source rocks entered the gas generation peak and a series of natural gas reservoirs were formed. However, affected by the later tectonic movements, some gas reservoirs were damaged or adjusted, and natural gas leakage and biodegradation occurred. This study has shifted the focus of natural gas exploration in the study area from the petroleum system associated with the Middle Permian source rocks to that with the Lower Permian and Carboniferous source rocks, which is of great significance for natural gas exploration in the Junggar Basin. Further, it provides an example to identify the geneses and sources of natural gas under complex conditions based on integrated geological and geochemical assessments.

Keywords: Junggar Basin, natural gas, stable carbon isotope, stable hydrogen isotope, fluid inclusion, hydrocarbon accumulation process

OPEN ACCESS

Edited by:
Yunyan Ni,
Research Institute of Petroleum Exploration and Development (RIPED), China

Reviewed by:
Qingtao Wang,
Guangzhou Institute of Energy Testing, China
Jianping Chen,
Research Institute of Petroleum Exploration and Development (RIPED), China
Bin Cheng,
China University of Petroleum, Qingdao, China

***Correspondence:**
Dongming Zhi
dongming_zhi@126.com

Specialty section:
This article was submitted to Geochemistry, a section of the journal Frontiers in Earth Science

Received: *25 December 2021*
Accepted: *03 February 2022*
Published: *28 February 2022*

Citation:
Zhi D, Wang X and Qin Z (2022) Geneses, Sources and Accumulation Process of Natural Gases in the Hinterland of the Junggar Basin. Front. Earth Sci. 10:843245. doi: 10.3389/feart.2022.843245

1 INTRODUCTION

The Junggar Basin, a late Paleozoic–Cenozoic superimposed basin, is located in the north of Xinjiang Uyghur Autonomous Region in northwest China (**Figure 1A**), covering an area of about 130×10^3 km^2 (He et al., 2018; Cao et al., 2020; Xia et al., 2021). In 2017, the proven oil reserves and the annual oil production in the basin reached 33.6×10^8 and 12.88×10^6 t (Hu S. Y. et al., 2020; Zhi et al., 2021), respectively, making the Junggar Basin one of the most important oil

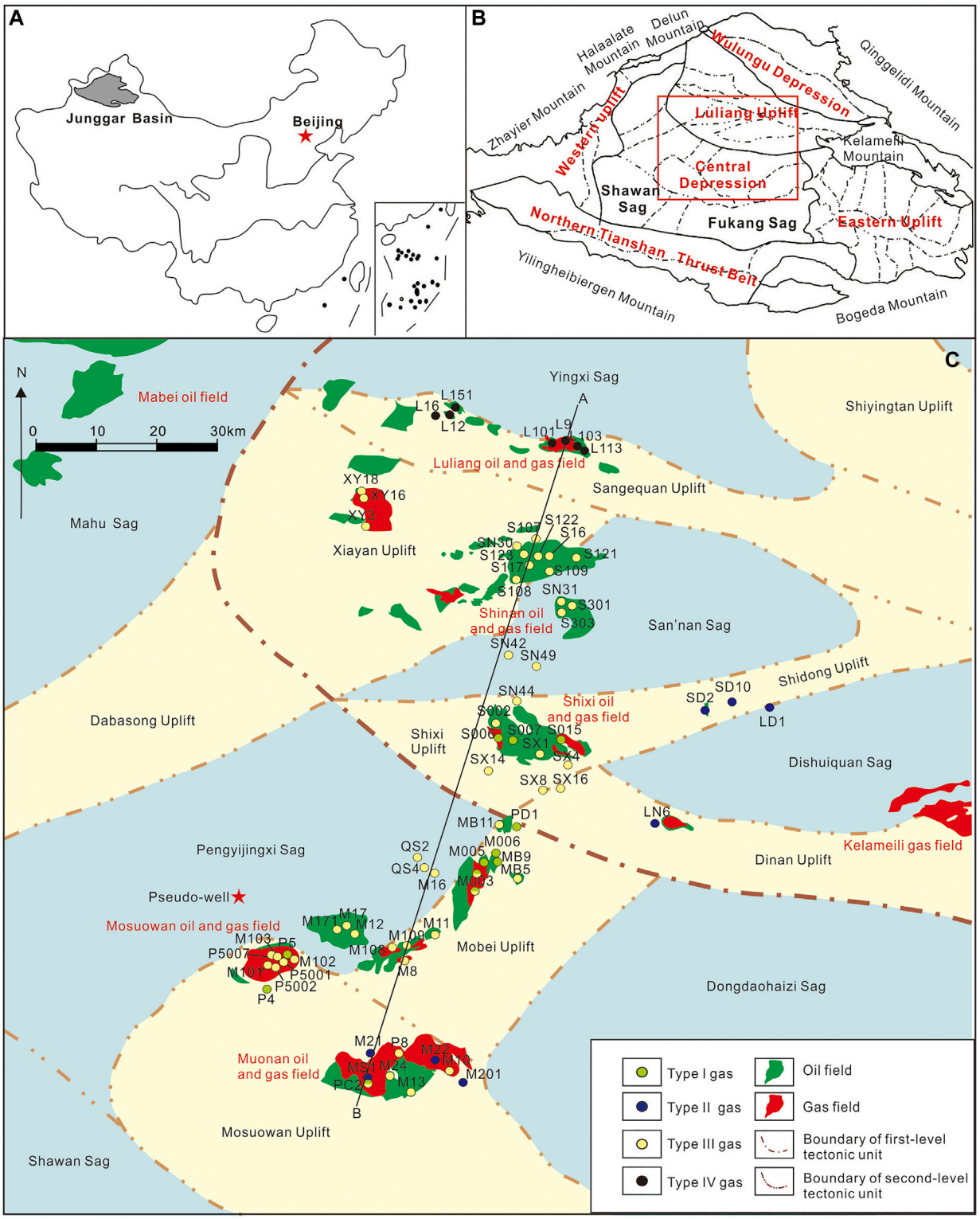

FIGURE 1 | Geological background in the hinterland of Junggar Basin. **(A)** Location of the Junggar Basin in China; **(B)** Characteristics of tectonic units in Junggar Basin; **(C)** Distribution of natural gas of different origins in the hinterland of Junggar Basin.

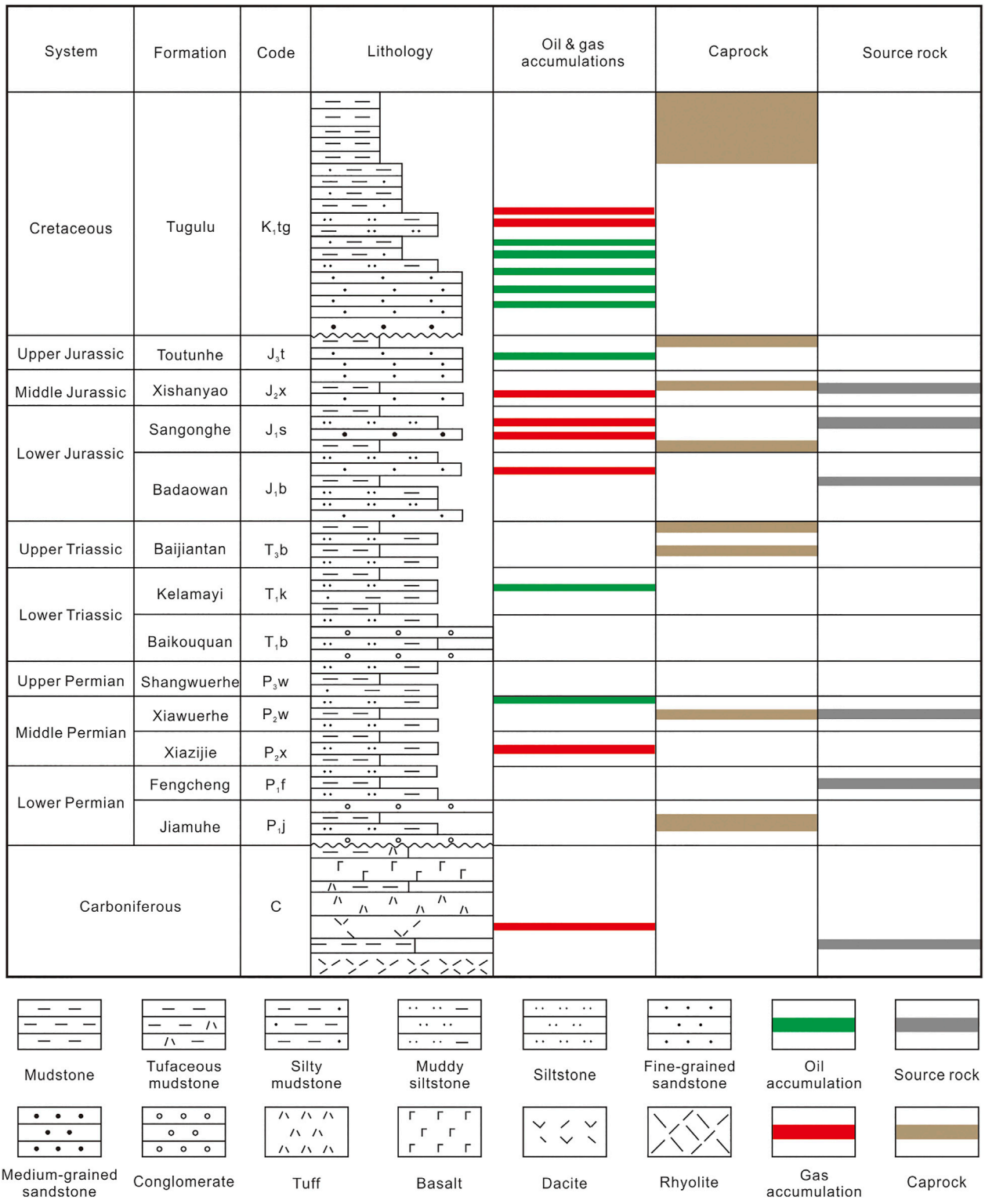

FIGURE 2 | Stratigraphic column in the hinterland of Junggar Basin.

production bases in China. In contrast, the proven natural gas reserves in the basin are only 209.25 × 109 m^3, which comes to less than 9% (Hu S. Y. et al., 2020).

At present, gas reservoirs in the Junggar Basin are mainly in the east (e.g., Kelameili and Wucaiwan gas fields), in the southern edge (e.g., Mahe and Hutubi gas fields), and in the northwestern edge (e.g., 561, 581, Ke 84, Jinlong 4 and Zhongjia 2 gas reservoirs) (Wang et al., 2013; Chen et al., 2014, Dai et al., 2016; Sun et al., 2016; Tao et al., 2016; Gong et al., 2018; Chen et al., 2019). The gas-producing reservoirs in the eastern region are mainly volcanic rocks characterized by strong heterogeneity and poor physical properties (Dai et al., 2016; Gong et al., 2019a, Gong et al., 2019b; Gong et al., 2021). The thermal evolution degree of source rocks in the northwestern region is relatively low, resulting in limited distribution range of gas sources kitchen (Chen et al., 2014; Tao et al., 2016). The southern edge has a complex structure, large reservoir burial depth, poor surface conditions, and increased development difficulty (Dai et al., 2016; Chen et al., 2019; Hu S. Y. et al., 2020). Such problems have hindered profitable exploration and development of natural gas in the Junggar Basin. Since 2007, the annual natural gas production in the Junggar Basin has been hovering at 2 × 109 m^3–3 × 109 m^3.

The total area of the hinterland is about 36 × 10^3 km^2. It is adjacent to the Pengyijingxi Sag in the west and Dishuiquan Sag in the east (**Figures 1B,C**). Four sets of source rocks developed in the study area, the Middle–Lower Jurassic Formation (J_{1-2}), Middle Permian Xiawuerhe Formation (P_2w), Lower Permian Fengcheng Formation (P_1f), and Carboniferous Formation (C), promising a favorable hydrocarbon source condition (**Figure 2**) (Cao et al., 2012; Wang et al., 2013). The gas layers are shallow (generally <4,000 m) and have conducive physical properties (Liu G et al., 2019) for rapidly building the production capacity. Thus, exploration and development of natural gas in the study area can have tremendous economic benefits. Although several gas-producing wells were drilled in this area (**Figure 1C**) (Cao et al., 2012), no significant reserves have been found yet. In 2019, Well QS2 drilled in the Qianshao Salient (**Figure 1C**) obtained high-yield industrial oil and gas flow in the Lower Jurassic Sangonghe Formation (J_1s), with a daily gas and oil production of 203.6 × 103 m^3 and 39.3 t, respectively. In 2020, 6.5 × 109 m^3 of proven geological reserves of natural gas were confirmed, shedding light on great potential for gas exploration in this area.

There are two main viewpoints on the geneses and sources of the natural gas in the hinterland: one proposed the gases were mainly derived from the J_{1-2} coaly source rock (Dai et al., 2009; Li et al., 2009), and the other argued that gases were derived from the P_2w lacustrine source rock (Cao et al., 2012; Sun et al., 2012; Gong et al., 2018). More significant disputes regarding the gas sources of different reservoirs also exist (Song, 1996; Wu et al., 2003; Liao et al., 2004; Li et al., 2011; Sun et al., 2012; Lu et al., 2014). There are several reasons for this diversity of perceptions. 1) Because the organic matter of the source rocks in J_{1-2}, P_2w, and Carboniferous are all humic types (Cao et al., 2012; Wang et al., 2013; Dai et al., 2016), the geochemical characteristics of the generated natural gas are difficult to distinguish. 2) The superimposition of the multiple sets of source rocks makes natural gas more likely to mix. 3) Because the Cenozoic, the Junggar Basin has tilted southward, resulting in the adjustment or destruction of early formed petroleum reservoirs (Xiang et al., 2015; Liu G et al., 2019). In addition, natural gas may suffer secondary alteration, which further increases the difficulty of gas source identification.

In addition to the three sets of humic source rocks, P_1f sapropelic lacustrine source rock was also developed in the study area (Wang et al., 2013; Cao et al., 2020). In the past, it was mainly considered as a set of oil source rocks (Cao et al., 2020; Xia et al., 2021). Recently, highly mature oil-type gas derived from the P_1f source rock was found in the southwest of the basin (Zhi et al., 2021). However, there is no systematic study on the gas generation potential of P_1f source rocks in the hinterland of the basin.

Given these problems, we systematically analyzed the molecular composition and stable carbon ($\delta^{13}C$) and hydrogen (δ^2H) isotope ratios of 95 natural gas samples in the hinterland of the Junggar Basin. It clarifies the geneses, sources, and secondary alteration of the natural gas. The natural gas accumulation process is rebuilt with the structural evolution history, burial history, hydrocarbon generation and expulsion history, and fluid inclusion characteristics in the study area. The research results are of great significance for natural gas exploration in the Junggar Basin and provide an example to identify the geneses and sources of natural gas under complex conditions based on integrated geological and geochemical information.

2 GEOLOGICAL SETTING

Located at the junction of three paleo-plates (i.e., Siberia, Tarim, and Kazakhstan), the Junggar Basin is composed of the Junggar massif and its surrounding fold belts (He et al., 2018). The basin is approximately rhombic on the plane, with the Qinggelidi Mountains and Kelameili Mountains in the northeast, the Zhayier Mountains, Halaalate Mountains, and Delun Mountains in the northwest, and the Yilingheibiergen Mountains and Bogeda Mountains in the south (**Figure 1B**). Based on the Permian paleo-structures, the Junggar Basin can be roughly divided into six first-order tectonic units (i.e., Central Depression, Wulungu Depression, Luliang Uplift, West Uplift, East Uplift, and Northern Tianshan thrust belt), and can be further subdivided into 44 secondary tectonic units (**Figure 1B**) (Gong et al., 2019a; Zhi et al., 2021). The study area is mainly located in the Luliang Uplift and the Central Depression (**Figures 1B,C**).

After the Hercynian (~268 Ma) tectonic movement, the Junggar Basin formed large uplifts and depressions dominated by NW- and NWW-striking directions under regional SN compression and collision (Hu et al., 2006; Qi et al., 2010). The study area began to take shape at this time. During the Yanshanian period (~200 Ma), large-scale uplifting occurred in the study area, and the J_{1-2} strata were denuded (Yang et al., 2002). Since then, the basin entered a stable

TABLE 1 | Molecular and stable carbon isotopes of natural gases in the central Junggar Basin.

Wells	Depth (m)	Formation	Molecular compositions (mol%)							$C_1/\Sigma C_{1-4}$	Stable carbon isotopes (‰, VPDB)				References	Gas type
			CH_4	C_2H_6	C_3H_8	*i*-C_4H_{10}	*n*-C_4H_{10}	N_2	CO_2		CH_4	C_2H_6	C_3H_8	C_4H_{10}		
S006	4,373	C	88.47	4.30	1.49	0.53	0.40	4.13	0.07	0.93	–41.6	–28.7	–25.9	–25.4	Li et al. (2009), Cao et al. (2012)	
S007	4,397	C	80.90	5.47	3.40	n.d.	n.d.	5.25	n.d.	0.90	–40.6	–30.2	–26.9	–26.8	This study	
S015	3,198	J_1s	80.13	9.41	3.38	0.81	0.82	4.60	0.10	0.85	–41.5	–29.0	–26.5	–25.9		
MB2	3,958	J_1s	90.64	3.61	1.22	n.d.	n.d.	2.61	0.30	0.95	–44.1	–29.4	–26.3	–26.6		
PD1	5,260–5,292	P_2w	74.28	7.59	4.95	2.48	1.44	5.53	0.50	0.82	–48.5	–31.7	–30.1	–29.3		
MB9	3,782	J_1s	84.56	5.75	2.67	1.06	0.84	1.71	1.29	0.89	–45.6	–31.5	–28.9	–28.1	Li et al. (2009), Cao et al. (2012)	
MB2	3,953	J_1s	90.60	3.50	1.17	n.d.	n.d.	2.88	0.25	0.95	–42.9	–30.0	–27.3	–27.0	This study	I
M003	3,910	J_1s	91.73	3.68	1.13	n.d.	n.d.	1.82	0.25	0.95	–41.3	–29.0	–27.4	–26.9		
M005	3,829	J_1s	91.24	3.66	1.17	n.d.	n.d.	2.29	0.25	0.95	–43.3	–29.3	–27.1	–26.8		
M005	3,895	J_1s	89.26	4.85	1.95	n.d.	n.d.	1.37	0.68	0.93	–44.1	–30.2	–27.7	–27.4	Li et al. (2009), Cao et al. (2012)	
PC2	5,122	J_1b	92.09	3.34	0.94	n.d.	n.d.	2.62	0.57	0.96	–38.4	–29.7	–28.2	–27.0	This study	
P4	4,514	J_1s	89.72	4.20	1.60	0.45	0.48	2.69	0.36	0.93	–43.9	–28.4	–27.7	–27.9		
P5	4,257	J_1s	87.49	4.49	1.86	0.65	0.55	3.25	0.57	0.92	–41.4	–28.0	–27.0	–27.4	Li et al. (2009), Cao et al. (2012)	
M006	3,760	J_1s	85.72	5.29	2.38	n.d.	n.d.	2.63	0.78	0.92	–39.5	–28.2	–28.0	–27.3	This study	
M21	4,351	J_1s	88.62	3.83	2.17	0.95	0.80	2.05	0.41	0.92	–33.4	–25.2	–25.6	–25.5	This study	
M21	5,115	J_1s	91.75	2.74	1.01	0.43	0.36	2.18	0.44	0.95	–31.8	–25.9	–25.4	–26.1		
M22	4,598	J_1s	92.19	3.10	0.87	0.29	0.25	2.60	0.12	0.95	–33.3	–25.9	n.d.	n.d.		
M201	4,574	J_1s	90.92	3.62	1.22	0.75		2.62	0.48	0.94	–34.1	–24.9	–24.4	–25.1	Cao et al. (2012)	
MS1	7,209	C	n.d.	n.d.	n.d.	n.d.	n.d.	n.d.	n.d.	n.d.	–32.4	–24.2	n.d.	n.d.	This study	
LN6	3,196	J_1s	83.59	3.55	2.20	0.98	1.29	4.72	0.07	0.91	–32.0	–28.0	–27.3	–27.5		II
LN6	2,997	K_1q	46.99	8.16	18.88	7.10	8.52	4.40	0.03	0.52	–33.4	–27.3	–25.0	–26.8		
LD1	4,161	C	93.82	1.82	0.46	0.12	0.15	3.37		0.97	–31.9	–27.0	–26.0	–26.1	Cao et al. (2012)	
SD2	2,679	K_1q	n.d.	n.d.	n.d.	n.d.	n.d.	n.d.	n.d.	n.d.	–32.1	–26.3	–24.0	–25.2	This study	
SD10	3,442	C	36.89	16.27	10.04	4.50	5.17	19.20	0.18	0.51	–32.0	–26.6	–24.4	–25.8	Cao et al. (2012)	
Min			36.89	1.82	0.46	0.12	0.15	2.05	0.03	0.51	–34.1	–28.0	–27.3	–27.5		
Max			93.82	16.27	18.88	7.10	8.52	19.20	0.48	0.97	–31.8	–24.2	–24.0	–25.1		
Average			78.10	5.39	4.61	1.89	2.36	5.14	0.25	0.84	–32.6	–26.1	–25.3	–26.0		
P5001	4,226	J_1s	83.27	4.62	1.62	0.57	0.45	7.32	0.81	0.92	–36.4	–29.7	–27.6	–27.9	This study	
P5002	4,220	J_1s	83.76	4.76	1.65	0.62	0.48	6.33	0.80	0.92	–37.1	–29.7	–27.6	–27.9		
P5007	4,216	J_1s	86.45	4.50	1.67	0.66	0.50	4.12	0.96	0.92	–35.7	–29.2	–27.9	–27.8		
M109	4,180	J_1s	91.97	4.16	1.10	0.50		1.81	0.22	0.94	–39.0	–24.7	–23.6	n.d.	Cao et al. (2012)	
XY3	2,692	J_1s	85.50	5.49	1.57	0.43	0.46	5.33	0.54	0.91	–34.7	–26.3	–25.6	–26.0		
XY16	2,521	J_2x	87.64	3.84	1.35	0.47	0.46	4.93	0.15	0.93	–35.0	–26.1	–24.2	–25.2	This study	
XY18	2,501	J_2x	87.40	4.16	1.60	0.60	0.51	3.93	0.30	0.93	–34.2	–26.8	–24.9	n.d.		III
XY18	2,503	n.d.	87.57	4.29	1.72	0.68	0.57	3.70	0.22	0.92	–34.3	–26.0	–25.6	–26.0		
SN31	2,606	K_1q	85.24	6.46	3.10	1.21	1.03	1.73	0.05	0.88	–34.8	–26.6	–25.6	–26.4	Li et al. (2009), Cao et al. (2012)	
S108	2,511	J_2t	86.22	6.02	2.77	1.07	0.91	1.55	0.16	0.89	–36.6	–26.7	–25.4	–25.3	This study	
S109	2,536	J_2t	n.d.	n.d.	n.d.	n.d.	n.d.	n.d.	n.d.	n.d.	–35.3	–26.8	–25.6	–26.4		
S116	2,476	J_2t	84.08	7.23	3.43	1.35	1.14	1.27	0.08	0.86	–35.3	–26.5	–25.7	–26.2		
S117	2,461	J_2t	90.99	4.28	1.44	0.41	0.46	1.58	0.03	0.93	–35.4	–27.1	–25.8	–26.3		

(Continued on following page)

TABLE 1 | (*Continued*) Molecular and stable carbon isotopes of natural gases in the central Junggar Basin.

Wells	Depth (m)	Formation	Molecular compositions (mol%)							$C_1/\Sigma C_{1-4}$	Stable carbon isotopes (‰, VPDB)				References	Gas type
			CH_4	C_2H_6	C_3H_8	*i*-C_4H_{10}	*n*-C_4H_{10}	N_2	CO_2		CH_4	C_2H_6	C_3H_8	C_4H_{10}		
S121	2,528	J_2t	85.04	6.47	3.09	1.26	1.05	1.38	0.04	0.88	–35.9	–27.3	–26.2	–26.7		
S122	2,446	J_2t	83.13	7.16	3.97	1.53	1.30	1.18	0.10	0.86	–35.6	–26.7	–25.6	–26.4		
S123	2,421	J_2t	84.36	7.22	2.90	1.08	0.04	1.92	0.63	0.88	–35.0	–26.7	–25.6	–26.4		
S301	2,607	K_1q	83.11	7.01	3.15	1.19	1.00	3.33	0.06	0.87	–35.0	–26.3	–24.9	–23.2	Li et al. (2009), Cao et al. (2012)	
S303	2,645	K_1q	84.13	6.98	3.24	1.30	1.07	1.64	0.03	0.87	–35.3	–26.2	–25.7	–26.2	This study	
SN44	2,862	K_1q	88.33	4.90	1.92	0.64	0.56	2.58	0.36	0.92	–35.1	–26.4	–24.6	–26.1	Cao et al. (2012)	
SX1	4,460	P_1j	80.39	5.69	3.53	n.d.	n.d.	5.94	n.d.	0.90	–35.3	–27.2	–26.6	–26.0	This study	
SX4	3,840	J_1b	87.74	4.65	2.38	1.11	0.87	2.40	0.00	0.91	–38.4	–26.9	–26.0	–26.1		
SX8	n.d.	J_1s	84.04	7.61	2.98	1.97		1.25	0.63	0.87	–34.4	–26.1	–24.7	–25.6	Cao et al. (2012)	
MB2	3,874	J_1s	88.49	4.66	1.85	0.60	0.55	2.69	0.53	0.92	–35.7	–26.8	–26.2	–26.4		
MB5	3,726	J_1s	88.16	5.19	1.73	n.d.	n.d.	2.71	0.00	0.93	–34.8	–26.9	–26.1	–26.3	This study	
M7	4,230	J_1s	89.31	3.30	0.97	0.38	0.27	4.64	0.64	0.95	–37.1	–25.5	–24.9	–25.6		
M8	4,230	J_1s	92.83	3.48	1.04	0.39	0.28	1.08	0.24	0.95	–35.8	–26.2	–25.4	–25.5	Cao et al. (2012)	
M11	4,148	J_1s	93.67	3.57	1.08	0.39	0.30	0.39	0.07	0.95	–34.9	–25.7	–25.1	–25.5	This study	
M11	4,136	J_1s	88.58	3.30	1.01	0.39	0.29	3.60	1.49	0.95	–35.2	–25.7	–25.1	–25.6	Li et al. (2009), Cao et al. (2012)	
M11	4,172	J_1s	91.82	3.86	1.33	0.41	0.36	1.65	0.27	0.94	–34.8	–27.1	–26.4	–26.6		
M7	4,223	J_1s	88.72	3.43	1.23	0.36	0.46	4.93	0.12	0.94	–35.2	–26.5	–25.8	–26.2	This study	
M8	4,263	J_1s	91.31	3.55	1.16	0.32	0.44	1.86	0.85	0.94	–34.3	–26.1	–25.2	–25.7	Li et al. (2009), Cao et al. (2012)	
M16	4,038	J_1s	87.44	5.62	1.77	0.50	0.40	2.69	0.62	0.91	–36.5	–26.5	–25.0	–26.3	Cao et al. (2012)	
M108	4,176	J_1s	87.34	4.64	2.05	0.84	0.74	2.53	0.66	0.91	–35.3	–25.7	–25.3	–25.8	Li et al. (2009), Cao et al. (2012)	
M17	4,158	J_1s	91.20	4.02	1.07	0.33	0.27	1.86	0.57	0.94	–36.9	–26.9	–25.6	–26.4	This study	
M17	4,190	J_1s	73.88	10.90	5.96	2.54	1.84	1.55	0.66	0.78	–35.9	–26.5	–24.4	–25.4		
M171	4,319	J_1s	87.65	4.69	1.98	0.79	0.64	2.59	0.58	0.92	–36.6	–26.6	–25.6	–26.2	Cao et al. (2012)	
M12	4,232	J_1s	80.44	6.96	4.14	1.52	1.20	3.25	0.66	0.85	–34.1	–27.3	–26.3	–26.6	Li et al. (2009), Cao et al. (2012)	
P8	4,363	J_1s	92.81	2.82	0.98	0.33	0.31	1.25	1.16	0.95	–34.0	–26.2	–26.3	–26.2	Cao et al. (2012)	
PC2	4,478	J_2x	n.d.	n.d.	n.d.	n.d.	n.d.	n.d.	n.d.	n.d.	–37.1	–26.9	–25.8	–26.3		
PC2	4,721	J_1s	93.41	2.74	1.33	n.d.	n.d.	1.92	0.43	0.94	–34.7	–26.8	–26.4	–25.5	This study	
M24	4,596	J_1s	91.32	3.48	1.25	0.37	0.47	2.27	0.12	0.94	–34.4	–26.8	–26.5	n.d.		
M10	4,564	J_1s	93.30	3.33	1.16	0.43	0.41	0.75	0.02	0.95	–35.3	–26.3	–25.9	–26.7		
M13	4,546	J_1s	93.30	3.33	1.16	0.84		0.75	0.02	0.95	–35.3	–26.3	–25.9	–26.7	Cao et al. (2012)	
SN49	2,773	K_1q	90.51	3.93	1.39	0.49	0.41	1.85	0.63	0.94	–35.3	–26.1	–24.6	–25.7		

(Continued on following page)

TABLE 1 | (*Continued*) Molecular and stable carbon isotopes of natural gases in the central Junggar Basin.

Wells	Depth (m)	Formation	Molecular compositions (mol%)							$C_1/\Sigma C_{1-4}$	Stable carbon isotopes (‰, VPDB)				References	Gas type
			CH_4	C_2H_6	C_3H_8	i-C_4H_{10}	n-C_4H_{10}	N_2	CO_2		CH_4	C_2H_6	C_3H_8	C_4H_{10}		
M101	4,204	J_1s	88.76	4.35	1.56	0.57	0.50	3.01	0.41	0.93	–36.8	–27.3	–26.3	–26.8	Li et al. (2009), Cao et al. (2012)	
M102	4,248	J_1s	88.13	4.70	1.92	0.65	0.56	2.71	0.52	0.92	–36.1	–27.5	–26.4	–26.5		
M103	4,249	J_1s	89.34	4.45	1.64	0.49	0.59	1.98	0.45	0.93	–35.3	–26.7	–25.9	–26.3	This study	
M103	4,252	J_1s	86.60	5.67	2.43	0.87	0.72	1.68	0.59	0.90	–37.4	–27.2	–26.5	–26.3		
S002	3,223	J_1s	82.37	6.15	2.91	1.13	0.78	6.12	0.01	0.88	–38.3	–26.7	–25.8	–26.3		
M003	3,968	J_1s	91.05	4.97	1.48	n.d.	n.d.	0.79	0.31	0.93	–37.8	–26.6	–24.7	–23.6	Cao et al. (2012)	
M003	3,975	J_1s	92.40	3.61	1.20	0.34	0.40	1.08	0.59	0.94	–36.3	–27.2	–25.6	–26.1	This study	
SX16	4,812–4,822	C	84.54	5.31	2.78	1.17	1.26	2.94	0.14	0.90	–36.2	–28.5	–27.5	n.d.		
SX14	3,483	J_1s	75.41	8.45	4.72	1.68	1.77	3.63	0.82	0.82	–37.0	–27.8	–27.2	–28.0	Cao et al. (2012)	
QS2	3,972–3,990	J_1s	91.18	4.31	1.47	0.54	0.40	1.09	0.45	0.93	–37.5	–27.5	–26.7	–27.3	This study	
QS2	3,980	J_1s	92.57	3.51	0.83	0.54	0.26	1.24	0.32	0.95	–37.6	–27.1	–26.8	–27.1		
QS2	3,989	J_1s	92.09	3.89	1.03	0.58	0.31	1.01	0.29	0.94	–37.4	–27.2	–26.6	–27.2		
QS4	4,003–4,026	J_1s	90.79	4.39	1.48	0.39	0.52	1.56	0.31	0.93	–37.8	–27.6	–26.7	–27.0		
M7	4,260	J_1s	89.99	3.33	1.15	0.36	0.35	3.65	0.50	0.95	–37.9	–27.9	–27.2	–27.7	Cao et al. (2012)	
MB11	3,708	J_1s	84.98	6.69	3.01	1.04	0.89	1.31	0.82	0.88	–37.1	–28.2	–26.8	–26.7	Li et al. (2009), Cao et al. (2012)	
S107	1,726	K_1h	90.93	4.41	1.39	0.35	0.47	1.55	0.00	0.93	–36.3	–26.2	–23.0	–25.6	This study	
S107	2,349	K_1q	91.06	4.86	1.42	0.36	0.44	1.27	0.00	0.93	–36.4	–26.5	–25.3	–26.0	Cao et al. (2012)	
SN30	1,875	K_1h	84.30	3.09	0.33	0.08	0.50	6.28	4.29	0.95	–37.6	–25.5	–16.4	–26.0	Li et al. (2009), Cao et al. (2012)	
SN42	1,623	K_1tg	87.07	5.04	1.72	1.10		4.29	0.19	0.92	–36.5	–25.6	–22.4	–23.6	Cao et al. (2012)	
L12	2,038	J_2x	93.32	2.66	0.89	0.09	0.43	1.82	0.64	0.96	–52.8	–32.4	–24.7	–26.7	This study	
L9	1,192	K_1tg	93.54	3.34	0.44	n.d.	n.d.	1.96	0.00	0.96	–50.1	–27.9	–14.8	–19.0	Li et al. (2009), Cao et al. (2012), Sun et al. (2012)	
L9	960	K_1tg	93.34	0.10	0.02	n.d.	n.d.	4.69	0.85	1.00	–49.9	–26.7	n.d.	n.d.	Cao et al. (2012)	IV
L102	1,014	K_1tg	95.89	0.09	0.04	n.d.	n.d.	3.55	0.43	1.00	–49.0	–26.3	–28.3	n.d.	Li et al. (2009), Cao et al. (2012), Sun et al. (2012)	
L103	1,228	K_1tg	94.99	0.14	0.00	0.00	0.00	4.79	0.08	1.00	–54.8	–24.5	n.d.	n.d.		
L113	1,832	K_1q	91.67	2.29	0.69	0.08	0.46	3.95	0.44	0.96	–46.0	–25.5	–17.8	–24.7		
L151	1,911	J_2x	92.33	1.68	1.41	0.70	1.61	0.90	0.26	0.94	–43.7	–25.4	–17.9	–24.5	This study	
L16	2,042	J_2x	85.41	3.82	1.69	0.57	0.57	7.01	0.43	0.93	–43.2	–26.3	–25.1	–26.1		

Note: n.d. = none data.

depositional period during which the early-formed structures were better preserved (Li et al., 2002; Hu et al., 2006). During the Himalayan period (~23 Ma), the basin's southern part subsided sharply (Liu Q et al., 2019). The structural amplitude in the study area gradually decreased with the high point moving northward. Only a series of low-

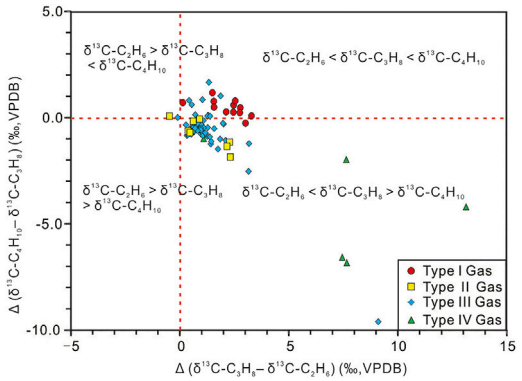

FIGURE 3 | The $\delta^{13}C$ distribution pattern of natural gas in the hinterland of Junggar Basin.

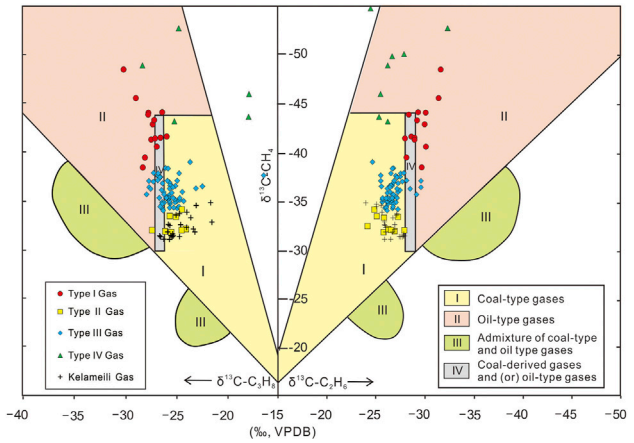

FIGURE 4 | Using the $\delta^{13}C\text{-}CH_4$–$\delta^{13}C\text{-}C_2H_6$–$\delta^{13}C\text{-}C_3H_8$ diagram to identify the genesis of natural gas in the hinterland of Junggar Basin (diagram modified after Dai et al., 1992, Dai et al., 2014).

amplitude bulges were retained (Qi et al., 2010; Cao et al., 2012) (**Figure 1C**).

The discovered natural gas in the study area is mainly distributed in the Sangequan, Xiayan, Shixi, Mobei, and Mosuowan Salients (**Figure 1C**). Gas producing zones are mainly in the Jurassic and Cretaceous sandstone reservoirs and Carboniferous volcanic reservoirs (**Figure 2**; **Table 1**). Four significant sets of reservoir–seal assemblages were developed in the study area: 1) the reservoir–seal assemblage with the Carboniferous volcanic weathering crust as reservoir and the Lower Permian mudstone as seal, 2) the reservoir–seal assemblage with glutenite in the Middle Permian Xiazijie Formation (P_2x) as a reservoir and the P_2w mudstone as seal, 3) the reservoir–seal assemblage with glutenite of the Lower Triassic Baikouquan Formation (T_1b) and Karamay Formation (T_2k) as reservoirs, and the mudstone of the Upper Triassic Baijiantan Formation (T_3b) as seal, and 4) the reservoir–seal assemblage composed of interbedded sandstone and mudstone

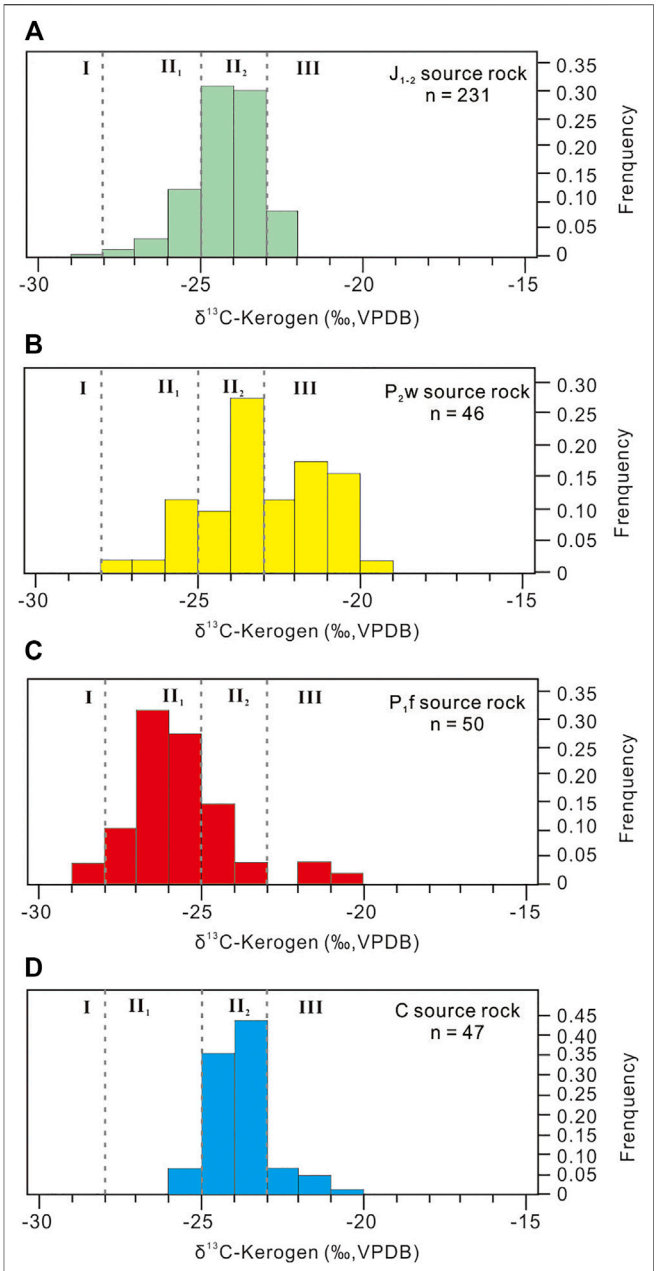

FIGURE 5 | Histogram of $\delta^{13}C_{kerogen}$ values of primary **(A)** $J_{1\text{-}2}$, **(B)** P_2w, **(C)** P_1f, and **(D)** C source rocks in the hinterland of Junggar Basin.

in the Jurassic and Cretaceous strata (**Figure 2**) (Cao et al., 2012; Liu Q et al., 2019).

3 SAMPLE AND METHODS

3.1 Sampling

Ninety-five natural gas samples were collected from 72 wells in the hinterland of the Junggar Basin, of which 55 samples were newly collected, and the rest were from the previous researches (Li et al., 2009; Cao et al., 2012; Sun et al., 2012). The planar

distribution positions and analysis results are shown in **Figure 1C** and **Table 1**. In addition, this study also conducted geochemical analysis of 437 source rock samples from 129 wells in the basin and on crude oil samples associated with natural gas.

3.2 Analytical Processes

3.2.1 Geochemical Analysis of Natural Gas

The geochemical analysis of the natural gas was conducted at the Experimental and Testing Institute of PetroChina Xinjiang Oilfield Company and Northwest Institute of Eco-Environment and Resources, Chinese Academy of Sciences. A Hewlett Packard 6890 II gas chromatograph (GC) was used for the analysis of the natural gas components. The hydrocarbon gas component was separated with capillary columns (Plot Al_2O_3 50 m × 0.53 mm). The furnace temperature of the GC was first set to be 30°C and held for 10 min. Then the temperature was ramped up to 180°C at a rate of 10°C/min. Stable carbon isotope analysis of alkane gas (C_1–C_4) was conducted with a Finnigan Mat Delta S mass spectrometer interfaced with an HP 6890II gas chromatograph. The alkane gas components (C_1–C_3) and CO_2 were separated by using a chromatographic column (Plot Q 30 m × 0.32 mm). The column heating process was as follows: the heating rate was 8°C/min at temperatures of 35–80°C; the temperature was then increased to 260°C at a heating rate of 5°C/min. The final temperature was held for 10 min. Each sample was analyzed three times with an accuracy of ±0.3‰ (VPDB).

The hydrogen isotopic compositions of natural gas were determined on a MAT253 isotopic mass spectrometer (Thermo Fisher Scientific) equipped with a Trace GC Ultra™ using the gas chromatography pyrolysis interface and the water removing device. Helium was used as the carrier gas and a 30 m × 0.32 mm × 20 μm HP–PLOT Q column was used with flow rate of 1.4 ml/min. The inlet temperature was set at 180°C. A split injection mode (split ratio 1:7) was used for the methane hydrogen isotope measurement and a splitless injection mode for the ethane and propane hydrogen isotopes. The initial temperature was 40°C and held for 5 min, then heated from 40 to 80°C at 5°C/min, from 80 to 140°C at 10°C/min and from 140 to 260°C at 30°C/min, respectively. The temperature of the pyrolysis oven was 1,450°C, and gaseous hydrocarbon components were transformed into C and H_2. The H_2 went into mass spectrometer to be measured. The δ^2H was calculated relative to VSMOW. The reproducibility and precision of hydrogen isotope value are less than ±3‰.

3.2.2 Geochemical Analysis of Oil

The GC analysis of oils was performed in an Agilent 7890A gas chromatograph fitted with a 60 m × 0.25 mm × 0.25 μm capillary column with nitrogen (99.999%) as the carrier gas. The GC oven temperature was initially held at 40°C for 10 min, then ramped from 40 to 70°C at 4°C/min and to 300°C at 8°C/min, and finally held at 300°C for 40 min.

The GC–MS analysis was performed in an Agilent 7890–5975C with the same column type as used in the GC analysis, but with helium (99.999%) as the carrier gas. During the GC–MS analysis, the GC oven temperature was initially held at 50°C for 1 min, then ramped to 120°C at 20°C/min, from 120 to 250°C at 4°C/min, and from 250 to 310°C at 3°C/min. Finally, it was held at 310°C for 30 min.

3.2.3 Basin Modelling

The burial and thermal histories of the source rocks in the study area were reconstructed using PetroMod software. The current heat flow and thermal conductivity values of the source rocks were adopted from previous studies (Wang et al., 2000a, Wang et al., 2000b; Qiu et al., 2000; Qiu et al., 2001; Qin, 2002). The vitrinite reflectance (Ro) values were calculated with the Easy%Ro model proposed by Sweeney and Burnham (1990). This model was proved to be applicable for a Ro range of 0.3%–4.6%.

3.2.4 Total Organic Carbon and Rock–Eval Analysis

The analyses were carried out at the China University of Petroleum (Beijing). The 146 rock samples were crushed to powder for total organic carbon (TOC) analysis (**Table 1**). The powdered samples were split into 200-mg sub-samples and treated with HCl at 60°C to remove the carbonates, then washed with distilled water to remove the HCl. The washed sub-samples were dried overnight at 50°C, and their carbon contents were determined using a LECO CS–230 analyzer.

For rock–eval pyrolysis, 100 g of each crushed rock sample was placed in the vessel of an OGE-II instrument. These samples were heated from 300 to 600°C in a helium atmosphere at a heating rate of 50°C/min, and their Rock–Eval parameters (S_1, S_2, and T_{max}) were measured. Here S_1 is the amount of free hydrocarbon that can be volatilized from the rock sample (mg HC/g rock), and S_2 is the amount of hydrocarbon produced by the cracking of organic matter (mg HC/g rock). T_{max} (°C) is the temperature at which the S_2 yield is maximized, which roughly estimates the thermal maturity of the sediment (Peters, 1986).

4 RESULTS

4.1 Molecular Compositions of the Natural Gas

The alkane content of the natural gas was relatively concentrated, ranging from 72.87% to 99.01% (95.30% on average) (**Table 1**), the majority of which was within 90%–100% (**Table 1**). The methane content varied significantly from 36.89% to 95.89% (87.16% on average), with its primary span being 80%–100%. Except for samples SD10 and LN6 (K_1q), whose methane content was only 36.89% and 44.99%, respectively, most samples had methane content higher than 70% (**Table 1**). The contents of heavy hydrocarbon (C_{2-4}) gas components in natural gas were 0.12%–42.66% (averaging 8.14%), and the dominant frequency was distributed between 0% and 20%. The samples with C_{2-4} gas contents were mainly distributed in the Shidong and Lunan Salients and sporadically distributed in the Mosuowan and Shixi Salients (**Table 1**). Natural gas's drying coefficient ($C_1/\sum C_{1-4}$) was 0.51–1.00 (0.91 on average) with a primary interval of 0.85–0.95. Dry gas ($C_1/\sum C_{1-4} > 0.95$) and wet gas ($C_1/\sum C_{1-4} < 0.95$) constituted 15.4% and 84.6% of the total data, respectively (**Table 1**).

The contents of non-hydrocarbon gases varied from 0.46% to 19.38% (averaging 3.45%) (**Table 1**). 78.9% of the samples have

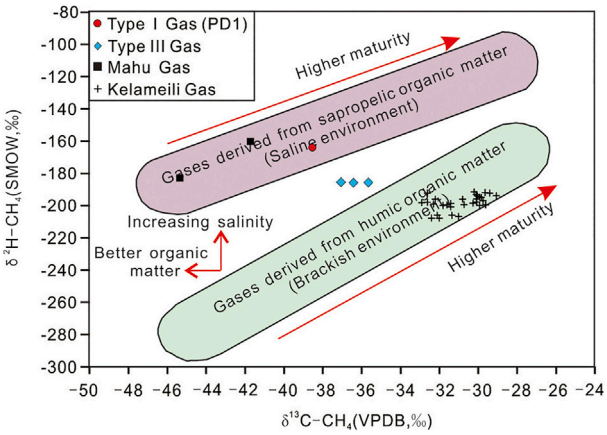

FIGURE 6 | The δ^{13}C-CH_4 vs. δ^2H-CH_4 plot of natural gas in the Junggar Basin (diagram modified after Wang et al., 2015).

non-hydrocarbon gas contents less than 5% (**Table 1**). Except for SD10, whose nitrogen content reached 19.20%, most samples had a nitrogen content of 0%–5% (3.00% on average) (**Table 1**). Carbon dioxide content was mainly between 0 and 1% (0.47% on average) (**Table 1**).

4.2 Stable Carbon Isotopic Composition of Natural Gas

Stable carbon isotopic compositions of methane (δ^{13}C-CH_4) varied broadly (from −54.8‰ to −31.8‰, −37.7‰ on average) with a primary interval of −45.0‰ to −30‰ (**Table 1**). Among them, the relatively ^{13}C-depleted samples (δ^{13}C-CH_4 < −45‰) were mainly distributed in the Luliang oil and gas field, while the relatively ^{13}C-enriched samples were mainly in the Lunan, Shidong, and Monan Salients (**Figure 1C**; **Table 1**). Stable carbon isotopic compositions of ethane (δ^{13}C-C_2H_6) ranged from −32.4‰ to −24.2‰ (−27.1‰ on average) with the dominant interval between −28‰ and −24.0‰. Among them, 78.9% of the samples have δ^{13}C-C_2H_6 ratios more than −28.0‰, and the samples with δ^{13}C-C_2H_6 < −28.0‰ are mainly distributed in the Mobei and Mosuowan Salients (**Figure 1C**; **Table 1**). Stable carbon isotopic compositions of propane (δ^{13}C-C_3H_8) varied from −30.1‰ to −14.8‰ (−25.6‰ on average), and their dominant frequency was between −28.0‰ and −24.0‰. Four samples (i.e., L9, SN30, L113, and L151) have the most ^{13}C-enriched δ^{13}C-C_3H_8 ratios (−14.8‰, −16.4‰, −17.8‰ and −17.9‰, respectively), presenting an apparent difference from the other samples (**Figure 1C**; **Table 1**).

Generally, the natural gas samples in the study area showed a distribution pattern of δ^{13}C-CH_4 < δ^{13}C-C_2H_6 < δ^{13}C-C_3H_8 (**Figure 3**; **Table 1**). The reversals between δ^{13}C-C_2H_6 and δ^{13}C-C_3H_8 ratios were only observed in L102, P8, and M21 (**Figure 3**; **Table 1**). Some samples have reversed carbon isotopic composition of propane and butane. Except for SN30, which had the maximum the $\Delta\delta^{13}$C-(C_4H_{10} − C_3H_8) ratio (9.6‰), most of other samples have ratios less than 1.0‰ (**Figure 3**; **Table 1**).

5 DISCUSSION

5.1 Geneses of the Natural Gas

The δ^{13}C ratios are the most common and practical tools to distinguish the genetic types of natural gas (Liu G. et al., 2019). Based on the δ^{13}C data of thousands of natural gas samples from major petroliferous basins around the world, (Dai et al., 1992, Dai et al., 2014) proposed a δ^{13}C-CH_4–δ^{13}C-C_2H_6–δ^{13}C-C_3H_8 genetic identification chart for natural gas. The natural gas in the study area can be divided into four types in the chart. Type I gas generally has relatively ^{13}C-depleted δ^{13}C ratios, with average δ^{13}C-CH_4, δ^{13}C-C_2H_6 and δ^{13}C-C_3H_8 values being −42.6‰, −29.5‰ and −27.5‰, respectively, falling within the domain of oil-type gas (**Figure 4**; **Table 1**). Type II and Type III gases generally had relatively ^{13}C-enriched δ^{13}C ratios, both falling in the domain of coal-type gas (**Figure 4**; **Table 1**). Although Type II and Type III gas had similar δ^{13}C ratios, they could still be distinguished from their δ^{13}C-CH_4 ratios. The δ^{13}C-CH_4 ratios of Type II gas were between −34.1‰ and −31.8‰, while those of Type III were between −39.0‰ and −34.0‰ (**Figure 4**; **Table 1**). The average value of the former was 3.4‰ more than that of the latter. Because the $C_1/\sum C_{1-4}$ ratios of these two types of natural gases were similar (mainly 0.90–0.95) (**Table 1**), their δ^{13}C-CH_4 difference was primarily affected by their distinct geneses, rather than the difference in maturities. The distribution position of Type IV gas in **Figure 4** was different from the other types of natural gases. Type IV gas had the most ^{13}C-depleted δ^{13}C-CH_4 value, and most of them were within the range of low mature oil-type gas (**Figure 4**). However, its $C_1/\sum C_{1-4}$ ratios were very high (0.97 on average, **Table 1**), significantly different from thermogenic gas, reflecting possible secondary alteration.

5.2 Sources of Natural Gas

5.2.1 Type I Gas

Four sets of source rocks were developed in the study area (i.e., J_{1-2}, P_2w, P_1f, and Carboniferous source rocks) (Cao et al., 2012; Wang et al., 2013). The J_{1-2}, P_2w, and Carboniferous source rocks are humic, characterized by kerogen types II_2–III with their carbon isotopic composition of kerogen ($\delta^{13}C_{kerogen}$) mainly varying from −26.0‰ to −20.0‰ (**Figure 5**). These source rocks primarily generate coal-type gases (Dai et al., 1992; Liu G. et al., 2019). The P1f source rock was deposited under a saline lacustrine environment, with algae and lower aquatic organisms as the primary organic input (Cao et al., 2020; Xia et al., 2021; Zhi et al., 2021). It is a set of oil-prone source rock characterized by kerogen type II_1 with their $\delta^{13}C_{kerogen}$ mainly varying from −28.0‰ and −24.0‰ (**Figure 5**). The Mahu super-giant oil field's petroleum in the Junggar Basin was mainly generated from the P_1f source rock (Wang et al., 2013; Cao et al., 2020). Besides oil, the P_1f source rock can also generate a considerable amount of oil-type gas. As discussed in **Section 5.1**, Type I gas was an oil-type gas with relatively ^{13}C-depleted δ^{13}C ratios (**Figure 4**; **Table 1**), which was generated from the P_1f source rock, the only sapropelic source rock in the study area.

This conclusion was supported by evidence from the δ^2H ratios of natural gas. Identical to δ^{13}C ratios, the δ^2H ratios of

TABLE 2 | Stable hydrogen isotopes of natural gases in the Junggar Basin.

Well name	Formation	Depth (m)	$\delta^{13}C$-CH_4 (VPDB,‰)	$\delta^{2}H$-CH_4 (VSMOW,‰)	References
H60	C	1,525.8	−41.7	−160	Dai et al. (1992)
W5153	T	3,221	−45.3	−183	
PD1	P_2w	5,278	−38.5	−164	This study
P5001	J_1s	4,225.75	−36.4	−186	
P5002	J_1s	4,220	−37.1	−185	
P5007	J_1s	4,216	−35.7	−186	
D403	C	3,915.45	−30.3	−198	
DX1707	C	3,620.25	−29.6	−192	
DX321	C	3,639	−29.9	−200	
DX1433	C	3,832.65	−30.1	−198	
DXHW178	C	4,000	−29.6	−199	
D405	C	3,707.3	−29.4	−192	
DXHW1851	C	3,568	−20.0	−201	
DX189	C	3,439	−32.4	−208	
DX1805	C	3,553.39	−29.9	−195	
DX1824	C	3,663.6	−32.3	−199	
DX1851	P_3wt	3,355.5	−31.6	−200	
DXHW1854	C	3,502	−31.4	−199	
DX1860	C	3,348.5	−31.0	−207	
DX1855	C	3,363	−31.4	−201	
DX1859	C	3,435.5	−32.1	−206	
DXHW1852	C	3,964	−32.9	−198	
DXHW184	C	4,338	−32.6	−192	
DX325	C	3,666.6	−31.8	−200	
DX184	C	3,558.45	−32.2	−196	
DX1823	C	3,621.65	−32.6	−198	
DX1827	C	3,685.45	−30.7	−199	
DX1826	C	3,717.3	−30.1	−193	
DX185	C	3,471	−32.0	−208	
DX1812	C	3,519.2	−30.8	−196	
DX186	C	3,416	−31.3	−206	
DX1430	C	3,762.95	−29.8	−197	
DX1426	C	3,787.45	−29.8	−195	
DXHW142	C	4,389	−30.2	−192	
DX1418	C	3,707.1	−29.1	−194	
DX1427	C	3,713	−30.0	−194	
DXHW143	C	4,297.5	−30.1	−196	

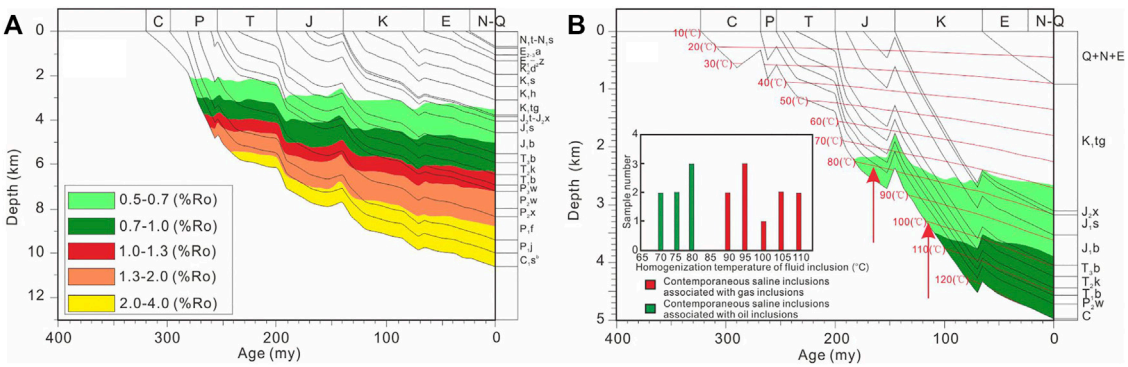

FIGURE 7 | Burial history and geothermal evolution history of **(A)** virtual well and **(B)** Well SX16 in the Pengyijingxi Sag.

alkane gases also have parent material inheritance (Schoell, 1980, Schoell, 1984; Ni et al., 2011). Under the same or similar thermal evolution conditions, the δ^2H ratios of the natural gas generated by marine or saline lacustrine source rocks are usually more enriched in ^2H (Liu et al., 2008a; Wang et al., 2015; Liu Q. et al., 2019). Therefore, the δ^2H ratios of alkane gas can be used to judge the geneses and sources of natural gas (Schoell, 1980; Wang et al., 2015). Gases from Well PD1 have

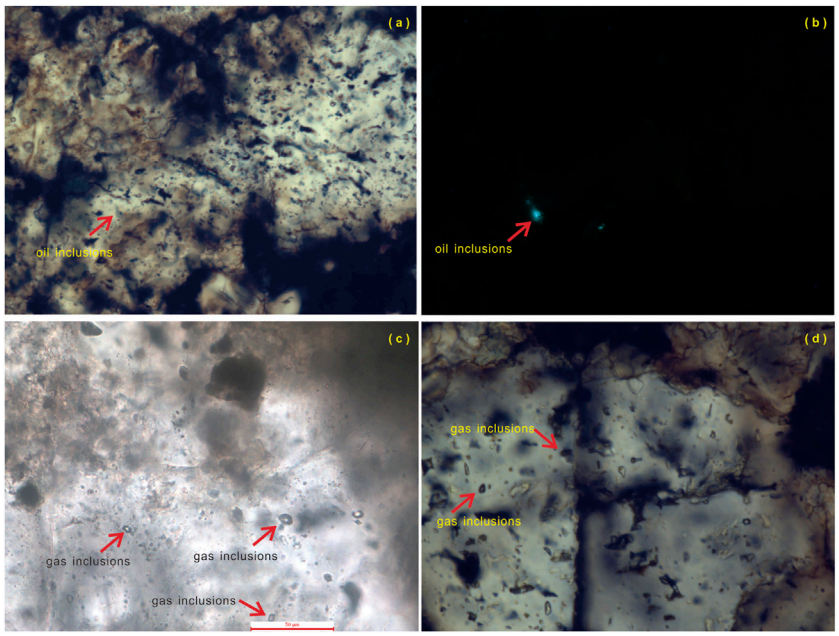

FIGURE 8 | Micrographs of fluid inclusions in the Carboniferous reservoir of Well SX16 (**(A,C,D)** under plane polarized light; **(B)** under fluorescence).

δ^2H-CH_4 and δ^{13}C-CH_4 ratios of −164‰ and −38.5‰, respectively, and was located within the distribution area of oil-type gas generated from the saline sapropelic source rock (Wang et al., 2015; **Figure 6**; **Table 2**). Two gas samples derived from the P_1f source rock in the Mahu Sag (Dai et al., 1992) were also located in this area (**Figure 6**; **Table 2**).

5.2.2 Type II Gas

As mentioned in **Section 5.1**, the Type II gas is a highly mature coal-type gas generated from the humic source rock. Unfortunately, however, three sets of humic source rocks (i.e., J_{1-2}, P_2w, and Carboniferous) developed in the study area (**Figure 5**), which brought added complications in identifying the gas source.

In northwestern China, the J_{1-2} source rock is a set of high-quality coaly source rock, and a large number of giant gas fields related to the J_{1-2} source rock were discovered (Dai et al., 2009, 2014). Some researchers once pointed out that the study area's natural gas was mainly generated from the J_{1-2} source rock (Dai et al., 2009; Li et al., 2009). In this study, the limiting thermal evolution conditions of the four sets of source rocks were simulated (**Figure 7A**) based on a pseudo well in the deepest part of the Pengyijingxi Sag (for well location see **Figure 1C**). When the Lower Jurassic Badaowan (J_1b) source rock reached the maximum burial depth, it was still in the immature–low mature stage (Ro = 0.5%–0.7%) (**Figure 7A**). In other words, this set of source rock in the study area has never entered the main oil generation window, let alone the main gas generation window. Therefore, the contribution of J_{1-2} source rock was excluded.

Type II gas from Wells MS1, SD2, and LD1 were produced from the Carboniferous reservoirs (**Table 1**). The P_2x was interbedded between the Carboniferous and P_2w with a thickness of approximately 200 m in Well MS1. Besides, the gas-producing zone was approximately 400 m lower from the top Carboniferous in Well MS1. Moreover, Permian strata were absent in the area where Well SD2 and Well LD1 were drilled. Therefore, it is inferred from geological conditions that the Type II gas was derived from the Carboniferous source rock rather than from the P_2w source rock. Previous studies have shown that the natural gas of the Kelameili gas field in the eastern Junggar Basin was generated from the Carboniferous source rock (Sun et al., 2016; Gong et al., 2019a, Gong et al., 2019b, Gong et al., 2021). It

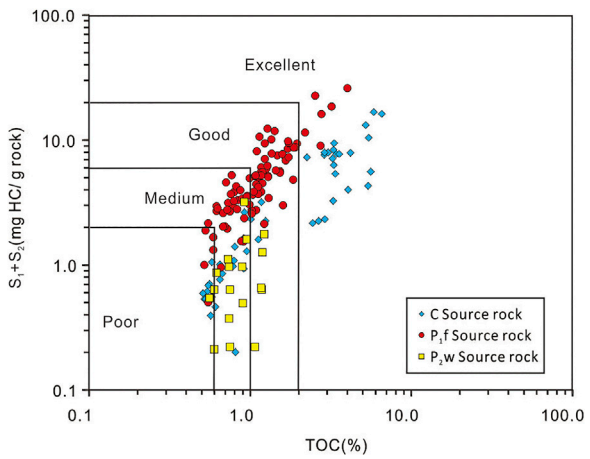

FIGURE 9 | The TOC vs. $S_1 + S_2$ plot of C, P_1f, and P_2w source rocks in the Junggar Basin.

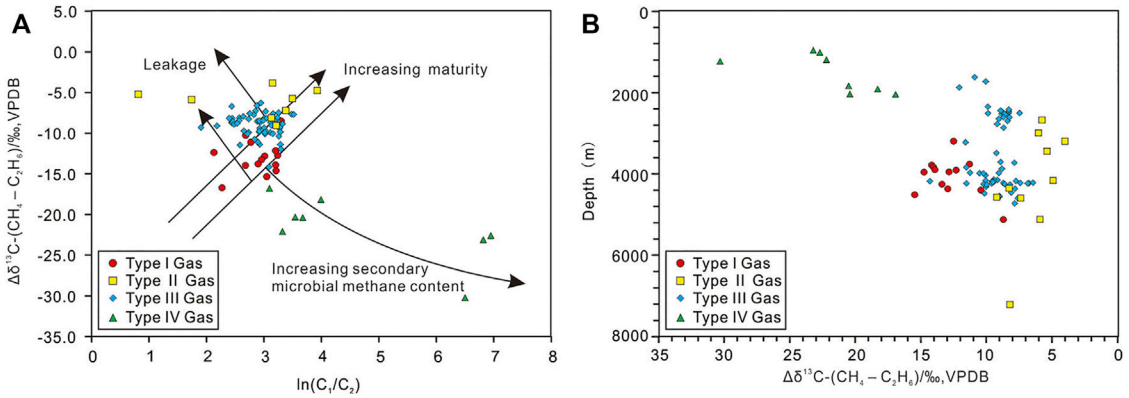

FIGURE 10 | Cross plots of **(A)** $\Delta\delta^{13}C\text{-}(CH_4 - C_2H_6)$ vs. $\ln(C_1/C_2)$ (the chart is modified after Prinzhofer and Huc, 1995), and **(B)** depth vs. $\Delta\delta^{13}C\text{-}(CH_4 - C_2H_6)$ of natural gas in the hinterland of Junggar Basin.

shared similar $\delta^{13}C$ ratios with the Type II gas (**Figure 4**), further supporting our conclusion.

5.2.3 Type III Gas

Generally, the $\delta^{13}C_{kerogen}$ values of P_2w source rocks were more enriched in ^{13}C than Carboniferous source rocks, although the former has a broader distribution range (**Figure 5**). The $\delta^{13}C_{kerogen}$ ratios revealed that the P_2w source rock has more terrigenous organic input and poorer kerogen type (Hunt et al., 1996). When the maturities of natural gas were similar (the $C_1/\sum C_{1-4}$ ratios were similar) (**Table 1**), the $\delta^{13}C\text{-}CH_4$ values of natural gas generated from the P_2w source rocks should theoretically be more enriched in ^{13}C than those generated from the Carboniferous source rocks (Liu et al., 2008b; Gai et al., 2018). However, the actual condition was just the opposite (**Figure 4**). We also noticed that a small number of P_2w source rock samples had relatively ^{13}C-depleted $\delta^{13}C_{kerogen}$ values (–28‰ to –25‰) (**Figure 5**). Thus, the contribution to Type III gas by P_2w source rock could not be totally excluded, entirely based on $\delta^{13}C_{kerogen}$ values (**Figure 5**).

However, evidence from the fluid inclusions further precluded the significant contribution from the P_2w source rock. SX16 was a high yield well drilled in 2011 in the study area (**Figure 1C**). The producing layer was the Carboniferous volcanic rocks, and the daily gas production was 86.27 × 103 m^3. Abundant oil and gas inclusions and associated contemporaneous brine inclusions were detected in the calcite-filled fractures in the producing interval (**Figure 8**). Through microscopic observation, one period of oil charging and one period of gas charging were identified. The oil inclusions mainly emitted blue or blue-green fluorescence (**Figures 8A,B**). Most natural gas inclusions are circular/oval-shaped and appear black under transmitted light with no fluorescence (**Figures 8C,D**). The homogenization temperature of the brine inclusions associated with natural gas inclusions ranged from 92.7 to 106.6°C. Combined with the thermal evolution history of Well SX16, the natural gas filling period was mainly the Late Cretaceous (**Figure 7B**). At that time, the deepest P_2w source rock in the Pengyijingxi Sag

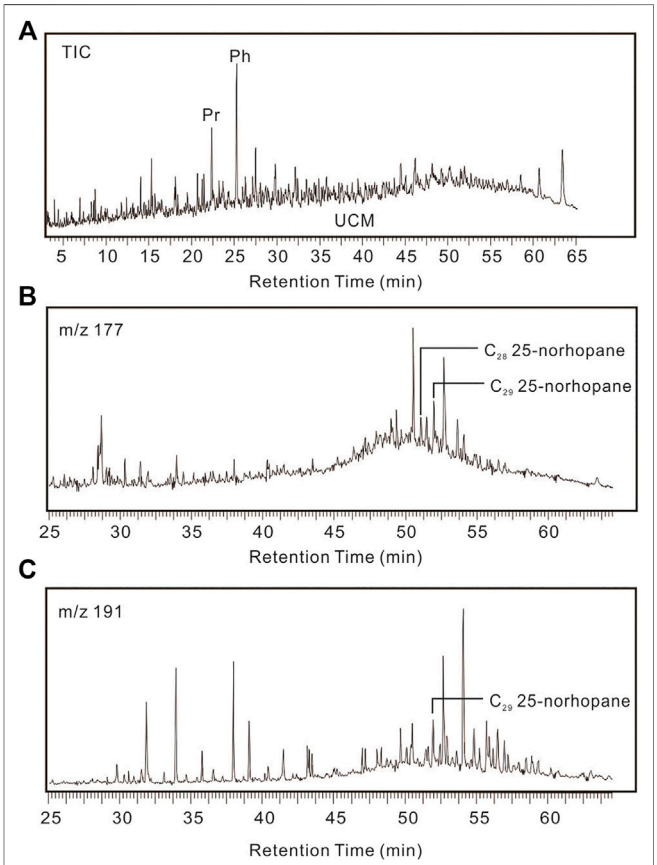

FIGURE 11 | Biomarker characteristics of crude oil associated with Type IV gas in Well L103. **(A)** TIC; **(B)** *m/z* 177; **(C)** *m/z* 191.

was still in the main oil generation window (Ro = 1.0%–1.3%) and had not entered the gas generation stage (**Figure 7A**). On the contrary, the P_1f and Carboniferous source rocks had entered a high mature–overmature stage in the deep part of the sag (**Figure 7A**). They could have generated a large amount of natural gas, which accumulated in suitable traps.

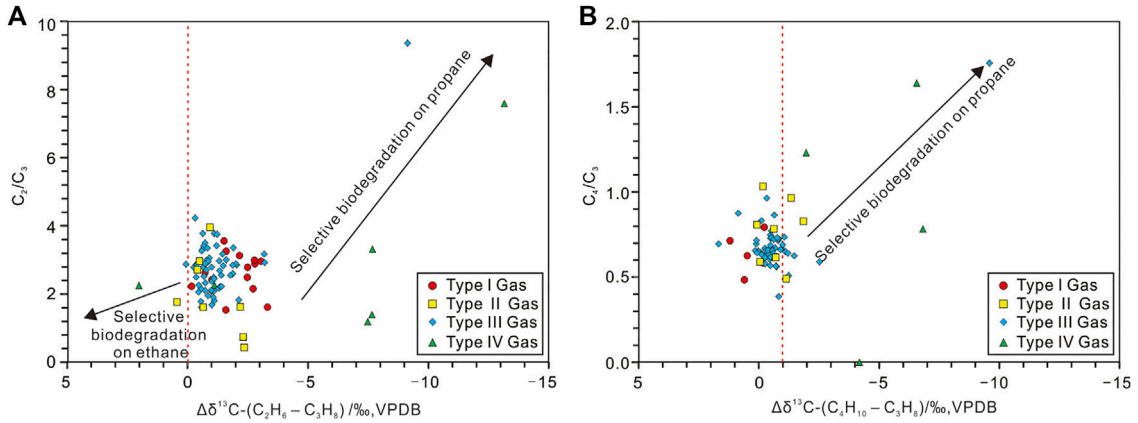

FIGURE 12 | Cross plots of **(A)** $\Delta\delta^{13}C\text{-}(C_2H_6 - C_3H_8)$ vs. C_2/C_3 and **(B)** $\Delta\delta^{13}C\text{-}(C_4H_{10} - C_3H_8)$ vs. C_4/C_3 of natural gas in the hinterland of Junggar Basin.

Therefore, type III gas was most likely a mixture of natural gases generated from the P_1f and Carboniferous source rocks.

In addition, the TOC, $S_1 + S_2$, and hydrogen index (HI) of P_2w source rock were 0.1%–1.2% (0.5% on average), 0.08–3.16 mg HC/g rock (0.82 mg HC/g rock on average), and 7–103 mg HC/g TOC (53 mg HC/g TOC on average), respectively, indicating poor source rock–non-source rock (**Figure 9**). The P_2w source rock had a hydrocarbon generation capacity far inferior to P_1f and Carboniferous source rocks (**Figure 9**). Thus, it did not have the potential to form a large-scale natural gas field (reservoir).

Based on the hypotheses, it was believed that Type III gas was a mixture of natural gas generated from the Carboniferous and P_1f source rocks. The mixing gas (Type III) had $\delta^{13}C\text{-}CH_4$ values between Type I and Type II gases (**Figure 4**; **Table 1**). The $\delta^{13}C$ ratios of C_{2-4} of Type III gas were relatively ^{13}C-enriched, similar to those of Type II natural gas (**Figure 4**; **Table 1**). Under similar maturity, the oil-type gas usually had a lower content of C_{2-4} than the coal-type gas (Dai et al., 1992; Whiticar, 1994; Liu Q et al., 2019), causing the $\delta^{13}C$ ratios of C_{2-4} gas in type III to be closer to those in type II, rather than in Type I gas.

The evidence from hydrogen isotopes further confirmed our conclusion. The $\delta^2H\text{-}CH_4$ values of three samples from Peng5 gas field were −186‰, −185‰ and −186‰, respectively (**Figure 6**; **Table 2**), which was significantly different from those of gases generated from the fresh (humic) source rocks such as Carboniferous or P_2w (Wang et al., 2013). The three samples were located in the transitional area between the coal-type gas (from fresh humic source rock) and oil-type gas (from saline sapropelic source rock) (**Figure 6**). Considering the number and planar distribution of the samples, the Type III natural gas constituted the main part of the natural gas in the hinterland.

However, recent researches indicated that Well JT 1 in the Shawan Sag has encountered high-quality P_2w source rocks with their TOC, HI and $\delta^{13}C_{kerogen}$ being 4.15%, 671 mg HC/g TOC and −28.6‰, respectively (Zhi et al., 2021; Gong et al., 2022). Thus, the locally developed high-quality P_2w source rocks cannot be excluded in the hinter land of Junggar Basin. Since the P_2w source rock has entered condensate-generating period in the Pengyijingxi Sag nowadays (**Figure 3A**), it may also made some contribution to the Type III gas.

5.2.4 Type IV Gas

Compared with the $\delta^{13}C$ ratio of C_{2-4} gas, methane is generally more sensitive to the change of maturity (Stahl and Carey, 1975; Dai et al., 1992; Berner and Faber 1996). Thus, the $\Delta\delta^{13}C\text{-}(CH_4 - C_2H_6)$ ratio is often used to reflect the maturity of natural gas (Prinzhofer and Huc, 1995; Dai et al., 2014; Wu et al., 2019). For primary thermogenic gas, the increase of $\Delta\delta^{13}C\text{-}(CH_4 - C_2H_6)$ reflected the increase of maturity. However, with the increase of $\Delta\delta^{13}C\text{-}(CH_4 - C_2H_6)$, the $\ln(C_1/C_2)$ of Type IV gas showed a decreasing trend, which was not in line with the characteristics of primary thermogenic gas (**Figure 10A**).

We believe that Type IV gas was mainly a secondary microbial gas. Natural gas generated via bacterial alteration of organic matter is called primary microbial gas, whose $\delta^{13}C\text{-}CH_4$ values are generally lower than −55‰ to −60‰ (James and Burns, 1984). The $\delta^{13}C\text{-}CH_4$ of Type IV natural gas was more enriched in ^{13}C than this threshold (**Table 1**). Secondary microbial gas refers to the natural gas formed by the biodegradation (anaerobic biodegradation in most cases) of crude oil (Head et al., 2003; Etiope et al., 2009; Milkov, 2010; Milkov, 2011). Generally, secondary microbial gas has the following characteristics: 1) $\delta^{13}C\text{-}CO_2$ > +2‰; 2) Natural gas is associated with biodegraded crude oil; 3) $\delta^{13}C\text{-}CH_4$ = −55‰ to −35‰; 4) High methane content; 5) Low reservoir temperature (<70–90°C); 6) The reservoirs are mostly sandstone formations with high porosity and permeability; and 7) The reservoirs are usually characterized by normal pressures with poor sealing conditions (Bernard et al., 1992; Milkov, 2010; Milkov, 2011).

The crude oil associated with Type IV gas is generally subjected to biodegradation (**Figure 11**). The 25-norhopanes are formed by the loss of methyl group at C–10 position of hopanes *via* the alteration of microorganisms (Seifert and Moldowan, 1979). Their appearance has been widely used as a sign of severe biodegradation to crude oil (Moldowan et al., 1984; Tian et al., 2012). In the study area, abundant C_{28} and C_{29} 25-norhopane were detected in the *m/z* 177 mass

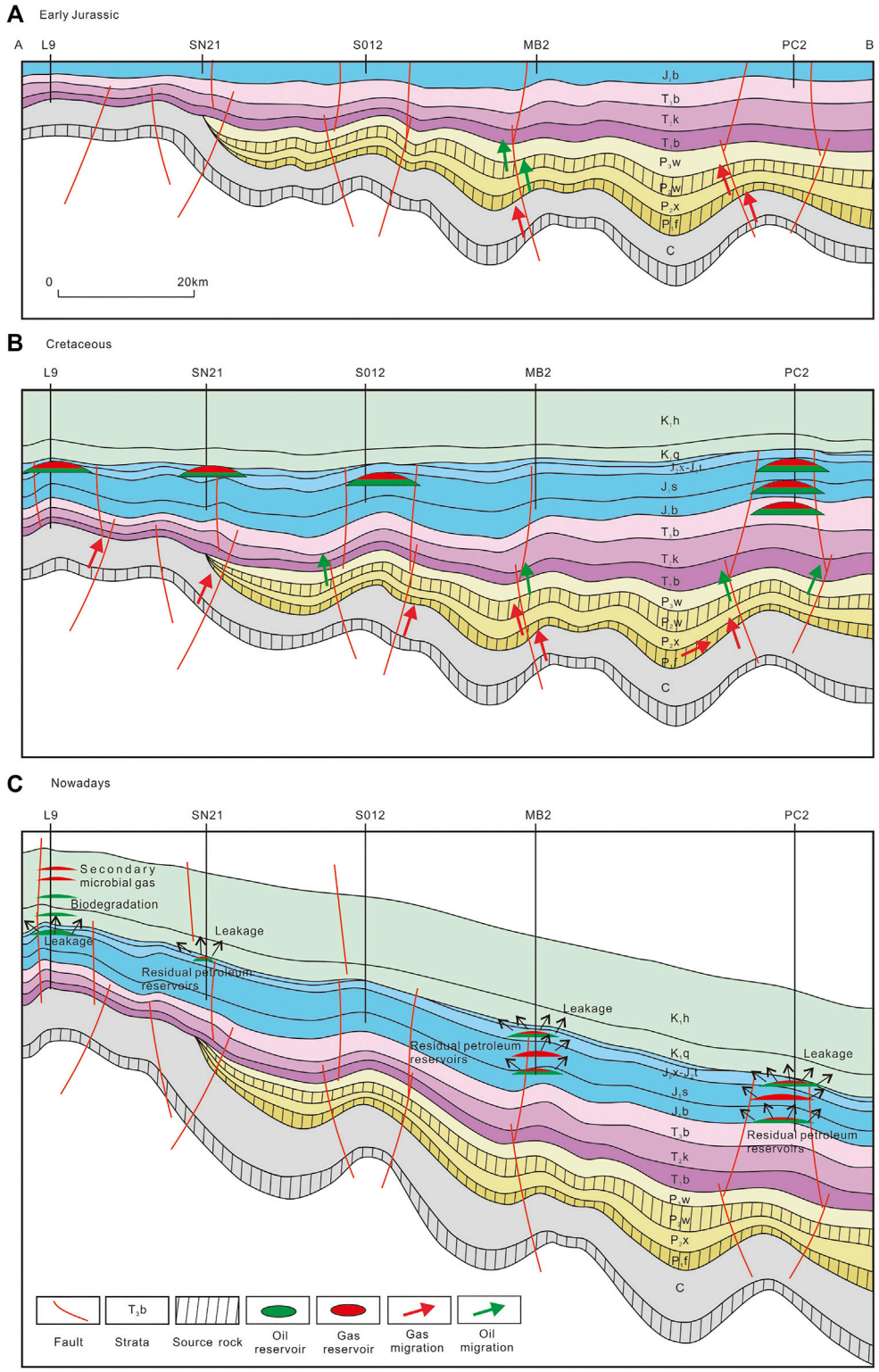

FIGURE 13 | Accumulation model of natural gas in **(A)** early Jurassic, **(B)** Cretaceous, and **(C)** nowadays in the hinterland of Junggar Basin.

chromatogram of crude oil associated with the Type IV gas, indicating that the crude oil had suffered severe biodegradation (**Figure 11**). In addition, when crude oil was subjected to biodegradation, the compounds with strong resistance to biodegradation formed bulges (i.e., unresolved complex mixtures, UCM) in gas

chromatography of saturated hydrocarbons or FID diagram (Killops and Al-Juboori, 1990; Gouch et al., 1992; Hu S. Z. et al., 2020). Noticeable UCM bulges were observed in the FID diagram in the current samples, which also reflected the biodegradation of crude oil (**Figure 11**).

The δ^{13}C-CH_4 and $C_1/\sum C_{1-4}$ ratios of Type IV gas were −54.8‰ to −43.2‰ (−48.7‰) and 0.93–1.0 (0.97 on average), respectively, which are well in accordance with those of the typical secondary microbial gas (**Table 1**). The gas-producing zones of Type IV gas had favorable physical properties, with their porosity and permeability being 20.7%–31.0% (24.9% on average) and 313 × 10^{-3} μm^2–4,760 × 10^{-3} μm^2 (1,180.6 × 10^{-3} μm^2 on average), respectively. All gas-producing zones had normal pressures, with the formation pressure coefficients (obtained by the DST test) being 0.77–1.04 (0.92 on average). The burial depths of the producing zones were 960–2,041.5 m. Assuming the current surface temperature was 20°C and the geothermal gradient was 22.3°C/km (Qiu, 2002; Wang et al., 2013), the current formation temperatures were 41.4–65.5°C (**Figure 10B**; **Table 1**). Although δ^{13}C-CO_2 data were not obtained in this study, considering other characteristics, the Type IV gas was identified as a secondary microbial gas in this study。

It should be noted that laboratory simulation and field examples showed that the main component of the pure secondary microbial gas was methane, and the content of C_{2-4} gas was extremely low (Pallasser, 2000; Milkov and Dzou, 2007; Jones et al., 2008). However, a certain amount of C_{2-4} gas components were found in Type IV natural gas (**Table 1**), indicating the gases were also mixed with a small amount of thermogenic gas.

5.3 Secondary Alteration of Natural Gas

5.3.1 Biodegradation

Bacteria may alter C_{1-4} gaseous hydrocarbons in gas reservoirs (Davis, 1967; Whiticar, 1994; Clayton et al., 1997; Pallasser, 2000). In most cases, the alteration on C_{2-4} gas components tends to be more prominent (James and Burns, 1984). The selective degradation of a specific gas component by bacteria will reduce its relative content. At the same time, as ^{12}C is less stable than ^{13}C, it is often degraded first, resulting in a more ^{13}C-enriched δ^{13}C ratio of natural gas (Dai et al., 1992; Galimov, 2006). The carbon isotopic reversal of ethane and propane were observed in natural gas in Wells L102 and M11, with $\Delta\delta^{13}$C-(C_2H_6 – C_3H_8) values being 2.0 and 0.08‰, respectively (**Figure 12A**). Meanwhile, the C_2/C_3 ratios of the two samples were relatively low, at 2.25 and 1.76, respectively (**Figure 12A**). The above characteristics inferred that the ethane was selectively degraded by bacteria.

Similarly, some samples had significant carbon isotopic reversal between propane and butane [$\Delta\delta^{13}$C-(C_4H_{10} – C_3H_8) < 1‰], accompanied by a decrease in C_4/C_3 ratio (**Figure 12B**). The propane in this part of the natural gas was selectively degraded by bacteria. This process also resulted in the abnormal decrease of $\Delta\delta^{13}$C-(C_2H_6 – C_3H_8) (<−5‰) and the increase of C_2/C_3 in these natural gas (**Figure 13A**; **Table 1**). We noted differences in the degraded gas components in different samples, which may be caused by different types of bacterial strains involved in the degradation processes (Connan et al., 1996; Wilkes et al., 2000; Gong et al., 2017). Moreover, some natural gas samples also displayed δ^{13}C-C_3H_8 and δ^{13}C-C_4H_{10} inversion, but the amplitude was relatively small (<1‰), and the C_4/C_3 ratio had not increased significantly (**Figure 12B**). The carbon isotopic reversal of these samples was more likely caused by the mixing of natural gas with different maturity or different geneses (Dai et al., 2004; Liu et al., 2016).

5.3.2 Gas Leakage

Gas leakage often occurs in the reservoir when the sealing condition is poor. In this case, the gases in the leakage phase will be rich in methane, and its δ^{13}C ratios tend to be depleted in ^{13}C (Prinzhofer and Huc, 1995). In contrast, the residual gas in the reservoir tends to show lower C_1/C_2 ratio and higher δ^{13}C-CH_4 values [decreasing δ^{13}C-(CH_4 – C_2H_6) values] (Prinzhofer and Huc, 1995). As shown in **Figure 10A**, considerable part of natural gas in the study area deviated from the evolution trend of primary thermogenic gas and showed the characteristics of residual phase gas after leakage. Thus, the leakage process reflected a poor preservation condition of gas reservoirs in the study area, and intense modifications occurred after the formation of these reservoirs. Wells LN6 and SD10 are two typical examples. The extremely low C_1/C_2 values in natural gases (**Table 1**) indicated that the two gas reservoirs had been completely destroyed after reconstruction. Furthermore, the oil test data showed that LN6 and SD10 only produced more than 100 m^3 of natural gas per day, which also confirmed our analysis.

5.4 Gas Accumulation Process

From the Late Permian to the Early Triassic, the Carboniferous and P_1f source rocks in the Penyijingxi Sag became mature successively (**Figure 6B**). During the Jurassic, the P_1f source rock had entered the stage of generating condensate/wet gas, while the Carboniferous source rock began generating dry gas (**Figure 7A**). The early natural gas reservoirs were formed at that time. It is speculated that gases derived from the Carboniferous source rock account for most (**Figure 13A**). During the same time, the P_2w source rock was still in the early stage of the oil generation window (**Figure 7A**), which corresponded to the early crude oil filling reflected by fluid inclusions (**Figure 7B**).

During the Late Cretaceous, the P_1f source rock also entered the gas generating peak. The generated oil-type gas and the coal-type gas from the Carboniferous source rock constituted the main body of natural gas in the hinterland of the Junggar Basin (**Figure 13B**). The process corresponded to the second stage of natural gas filling reflected by fluid inclusions (**Figure 7B**). At that time, the P_2w source rock entered the late stage of the oil generation window and was still dominated by oil generation (**Figure 7A**).

During the Himalayan period, the Junggar Basin totally tilted southward, resulting in different degrees of adjustment or destruction of early formed petroleum reservoirs (**Figure 13C**). This process resulted in a widespread leakage in gas reservoirs in the hinterland (**Figure 10A** and **Figure 13C**). Meanwhile, some oil reservoirs suffered severe biodegradation (**Figure 13C**), with the residual crude oil generally rich in 25-norhopane (**Figure 11**).

During the biodegradation process, a large amount of secondary microbial gas (Type IV gas) was formed, and the latter accumulated in suitable traps (**Figure 13C**).

6 CONCLUSION

Four types of natural gas have been identified in the hinterland of the Junggar Basin. The Type I gas was derived from the P_1f saline lacustrine source rock in the Pengyijingxi Sag. It had relatively ^{13}C-depleted $\delta^{13}C$ ratios with an average $C_1/\Sigma C_{1-4}$ value of 0.92. The δ^2H ratios of Type I gas were enriched in ^2H. Type II gas was coal-type gas derived from the Carboniferous source rock. It had relatively ^{13}C-enriched $\delta^{13}C$ ratios with $C_1/\Sigma C_{1-4}$ values mainly varying from 0.90 to 0.95. The Type III natural gas was a mixture of Type I and Type II gases, which constituted the main part of the natural gas in the study area. The Type IV gas was a secondary microbial gas generally occurring in the shallow reservoirs (960–2,041.5 m), with the $\delta^{13}C$-CH_4 values and $C_1/\Sigma C_{1-4}$ ratios being −54.8‰ to −43.2‰ and 0.96, respectively. Abundant 25-norhopane and UCM bulges were found in its associated crude oil. One period of oil charging and one period of gas charging were identified in the study area. The homogenization temperature range of the latter was 92.7–106.6°C, corresponding to the gas generation peak of P_1f and Carboniferous source rocks (Late Cretaceous). Affected by the late tectonic movements, some gas reservoirs were damaged and adjusted, and natural gas leakage and biodegradation widely occurred.

The research results shifted the focus of natural gas exploration in the study area from the petroleum systems associated with the P_2w source rocks to those associated with the P_1f and Carboniferous source rocks. This is of great significance for natural gas exploration in the Junggar Basin. When the geochemical characteristics alone cannot accurately determine the gas genesis, the geological characteristics of the gas reservoir can often be used as an effective auxiliary tool.

DATA AVAILABILITY STATEMENT

The original contributions presented in the study are included in the article/supplementary material, further inquiries can be directed to the corresponding author.

AUTHOR CONTRIBUTIONS

DZ: Conceptualization, Resources, Project administration; XW: Writing Original Draft, Formal analysis; ZQ: Writing Original Draft, Formal analysis, Methodology.

FUNDING

This work is funded by Chinese National Natural Science Foundation (No. 41802177).

REFERENCES

Bernard, F. P., Connan, J., and Magot, M. (1992). "Indigenous Microorganisms in Connate Water of Many oil Fields: A New Tool in Exploration and Production Techniques," in 67th Annual Technical Conference and Exhibition of the Society of Petroleum Engineers, Washington, DC, October, 1992. (Washington, DC: SPE Paper), 467–476.

Berner, U., and Faber, E. (1996). Empirical Carbon Isotope/maturity Relationships for Gases from Algal Kerogens and Terrigenous Organic Matter, Based on Dry, Open-System Pyrolysis. *Org. Geochem.* 24, 947–955. doi:10.1016/s0146-6380(96)00090-3

Cao, J., Wang, X., Sun, P. a., Zhang, Y., Tang, Y., Xiang, B., et al. (2012). Geochemistry and Origins of Natural Gases in the central Junggar Basin, Northwest China. *Org. Geochem.* 53, 166–176. doi:10.1016/j.orggeochem.2012.06.009

Cao, J., Xia, L., Wang, T., Zhi, D., Tang, Y., and Li, W. (2020). An Alkaline lake in the Late Paleozoic Ice Age (LPIA): A Review and New Insights into Paleoenvironment and Petroleum Geology. *Earth-Science Rev.* 202, 103091. doi:10.1016/j.earscirev.2020.103091

Chen, Z., Cao, Y., Ma, Z., and Zhen, Y. (2014). Geochemistry and Origins of Natural Gases in the Zhongguai Area of Junggar Basin, China. *J. Pet. Sci. Eng.* 119, 17–27. doi:10.1016/j.petrol.2014.05.007

Chen, J., Wang, X., Ni, Y., Xiang, B., Liao, F., Liao, J., et al. (2019). Genetic Type and Source of Natural Gas in the Southern Margin of Junggar Basin, NW China. *Pet. Exploration Development* 46, 482–495. doi:10.1016/s1876-3804(19)60029-7

Clayton, C. J., Hay, S. J., Baylis, S. A., and Dipper, B. (1997). Alteration of Natural Gas during Leakage from a North Sea Salt Diapir Field. *Mar. Geology.* 137, 69–80. doi:10.1016/s0025-3227(96)00080-1

Connan, J., Lacrampe-Coulome, G., and Magot, M. (1996). "Origin of Gases in Reservoirs," in *Proceedings of the 1995 International Gas Research Conference*. Editor D. Dolenc (Rockville: Government Institutes), 21–62.

Dai, J. X., Pei, X. G., and Qi, H. F. (1992). *Natural Gas Geology of China*. Beijing: Petroleum Industry Press, 46–50. (in Chinese with English abstract).

Dai, J., Xia, X., Qin, S., and Zhao, J. (2004). Origins of Partially Reversed Alkane δ 13 C Values for Biogenic Gases in China. *Org. Geochem.* 35, 405–411. doi:10.1016/j.orggeochem.2004.01.006

Dai, J., Zou, C., Li, J., Ni, Y., Hu, G., Zhang, X., et al. (2009). Carbon Isotopes of Middle-Lower Jurassic Coal-Derived Alkane Gases from the Major Basins of Northwestern China. *Int. J. Coal Geology.* 80, 124–134. doi:10.1016/j.coal.2009.08.007

Dai, J., Gong, D., Ni, Y., Huang, S., and Wu, W. (2014). Stable Carbon Isotopes of Coal-Derived Gases Sourced from the Mesozoic Coal Measures in China. *Org. Geochem.* 74, 123–142. doi:10.1016/j.orggeochem.2014.04.002

Dai, J. X., Zou, C. N., Li, W., and Hu, G. Y. (2016). *Giant Coal-Derived Gas Fields and Their Gas Sources in China*. New York: Academic Press.

Davis, J. B. (1967). *Petroleum Microbiology*. Amsterdam: Elsevier.

Etiope, G., Feyzullayev, A., Milkov, A. V., Waseda, A., Mizobe, K., and Sun, C. H. (2009). Evidence of Subsurface Anaerobic Biodegradation of Hydrocarbons and Potential Secondary Methanogenesis in Terrestrial Mud Volcanoes. *Mar. Pet. Geology.* 26, 1692–1703. doi:10.1016/j.marpetgeo.2008.12.002

James, A. T., and Burns, B. J. (1984). Microbial Alteration of Subsurface Natural Gas Accumulations. *Am. Assoc. Petroleum Geol. Bull.* 68, 957–960.

Gai, H., Tian, H., and Xiao, X. (2018). Late Gas Generation Potential for Different Types of Shale Source Rocks: Implications from Pyrolysis Experiments. *Int. J. Coal Geology.* 193, 16–29. doi:10.1016/j.coal.2018.04.009

Galimov, E. M. (2006). Isotope Organic Geochemistry. *Org. Geochem.* 37, 1200–1262. doi:10.1016/j.orggeochem.2006.04.009

Gong, D., Ma, R., Chen, G., Ma, W., Liao, F., Fang, C., et al. (2017). Geochemical Characteristics of Biodegraded Natural Gas and its Associated Low Molecular Weight Hydrocarbons. *J. Nat. Gas Sci. Eng.* 46, 338–349. doi:10.1016/j.jngse.2017.07.027

Gong, D., Li, J., Ablimit, I., He, W., Lu, S., Liu, D., et al. (2018). Geochemical Characteristics of Natural Gases Related to Late Paleozoic Coal Measures in China. *Mar. Pet. Geology.* 96, 474–500. doi:10.1016/j.marpetgeo.2018.06.017

Gong, D., Song, Y., Wei, Y., Liu, C., Wu, Y., Zhang, L., et al. (2019a). Geochemical Characteristics of Carboniferous Coaly Source Rocks and Natural Gases in the Southeastern Junggar Basin, NW China: Implications for New Hydrocarbon Explorations. *Int. J. Coal Geology.* 202, 171–189. doi:10.1016/j.coal.2018.12.006

Gong, D. Y., Lan, W. F., Xiang, H., Ding, J., Wu, W. A., and Hu, Z. L. (2019b). Genetic Types and Origins of Natural Gases from the Eastern Junggar basin. *J. China Univ. Mining Technology* 48 (01), 142–152. (in Chinese with English abstract).

Gong, D. Y., Wang, X. L., Zhou, C. M., Zheng, M. L., Jiang, W. L., and Wu, W. A. (2021). Discovery of Large-Scale Carboniferous Source Rocks and Natural Gas Exploration Potential in the Southeast of Junggar Basin. *Acta Petrolei Sinica* 42, 836–852. (in Chinese with English abstract).

Gong, D. Y., Zhao, C. Y., He, W. J., Zhao, L., Kong, Y. M., Ma, L. Y., et al. (2022). Genetic Types and Exploration Potential of Natural Gas at Northwestern Margin of Junggar Basin. *Oil Gas Geology.* 43, 162–175. (in Chinese with English abstract).

Gouch, M. A., Rhead, M. M., and Rowland, S. J. (1992). Biodegradation Studies of Unresolved Complex Mixtures of Hydrocarbons: Model UCM Hydrocarbons and the Aliphatic UCM. *Org. Geochem.* 18, 17–22. doi:10.1016/0146-6380(92)90139-o

He, D. F., Zhang, L., Wu, S. T., Li, D., and Zhen, Y. (2018). Tectonic Evolution Stages and Features of the Junggar Basin. *Oil Gas Geol.* 39, 845–861. (in Chinese with English abstract).

Head, I. M., Jones, D. M., and Larter, S. R. (2003). Biological Activity in the Deep Subsurface and the Origin of Heavy Oil. *Nature* 426, 344–352. doi:10.1038/nature02134

Hu, S. Y., Wei, Y. J., Dong, D. Z., Li, F., and Wang, Y. M. (2006). Control of Fault Activity on Hydrocarbon in central Junggar Basin. *Acta Petrolei Sinica* 27, 1–7. (in Chinese with English abstract).

Hu, S. Y., Wang, X. J., Cao, Z. L., Li, J. Z., Gong, D. Y., and Xu, Y. (2020). Formation Conditions and Exploration Direction of Large and Medium Gas Reserviors in the Junggar Basin, NW China. *Petrol. Explor. Dev.* 47 (1), 1–13. doi:10.1016/s1876-3804(20)60045-3

Hu, S. Z., Li, S. F., Wang, J. H., and Cao, J. (2020). Origin of Unresolved Complex Mixtures (UCMs) in Biodegraded Oils: Insights from Artificial Biodegradation Experiments. *Fuel* 231, 53–60.

Hunt, J. M. (1996). *Petroleum Geochemistry and Geology* 2 edition. San Francisco: W.H. Freeman.

Jones, D. M., Head, I. M., Gray, N. D., Adams, J. J., Rowan, A. K., Aitken, C. M., et al. (2008). Crude-oil Biodegradation via Methanogenesis in Subsurface Petroleum Reservoirs. *Nature* 451, 176–180. doi:10.1038/nature06484

Killops, S. D., and Al-Juboori, M. A. H. A. (1990). Characterisation of the Unresolved Complex Mixture (UCM) in the Gas Chromatograms of Biodegraded Petroleums. *Org. Geochem.* 15, 147–160. doi:10.1016/0146-6380(90)90079-f

Li, Z. H., Tang, L. J., Ding, W. L., and Yao, S. P. (2002). Fault Characteristic Analysis for the Hinterland of Junggar Basin. *Petrol. Explor. Dev.* 29, 40–42. (in Chinese with English abstract).

Li, J., Jiang, Z., Luo, X., Wang, D., and Han, Z. (2009). Geochemical Characteristics of Coalmeasure Source Rocks and Coal-Derived Gas in Junggar Basin, NW China. *Pet. Exploration Development* 36, 365–374.

Li, L., Chen, S. J., Yang, D. S., Lu, J. G., Zhao, K. B., and Xu, H. M. (2011). Petroleum Origin and Source in Shidong Area, Junggar Basin. *Pet. Geology. Exp.* 33, 536–538. (in Chinese with English abstract).

Liao, J. D., Wang, X. L., Xiang, B. L., Cheng, X. S., Liu, C. M., Ling, Y., et al. (2004). Oil and Gas Origin and Reservoir Analyses of Mosuowan Region in Junggar Basin. *Nat. Gas Industry* 24, 15–18. (in Chinese with English abstract).

Liu, Q., Dai, J., Li, J., and Zhou, Q. (2008a). Hydrogen Isotope Composition of Natural Gases from the Tarim Basin and its Indication of Depositional Environments of the Source Rocks. *Sci. China Ser. D-earth Sci.* 51, 300–311. doi:10.1007/s11430-008-0006-7

Liu, Q., Qin, S., Li, J., Liu, W., Zhang, D., Zhou, Q., et al. (2008b). Natural Gas Geochemistry and its Origins in Kuqa Depression. *Sci. China Ser. D-earth Sci.* 51, 174–182. doi:10.1007/s11430-008-5003-3

Liu, Q., Dai, J., Jin, Z., Li, J., Wu, X., Meng, Q., et al. (2016). Abnormal Carbon and Hydrogen Isotopes of Alkane Gases from the Qingshen Gas Field, Songliao Basin, China, Suggesting Abiogenic Alkanes? *J. Asian Earth Sci.* 115, 285–297. doi:10.1016/j.jseaes.2015.10.005

Liu, G., Wei, Y. Z., Chen, G., Jia, K. F., Gong, D. Y., Wang, F., et al. (2019). Genetic Mechanism and Distribution Characteristics of Jurassic–Cretaceous Secondary Reservoirs in the Hinterland of Junggar Basin. *Acta Petrolei Sinica* 35, 914–927. (in Chinese with English abstract).

Liu, Q., Wu, X., Wang, X., Jin, Z., Zhu, D., Meng, Q., et al. (2019). Carbon and Hydrogen Isotopes of Methane, Ethane, and Propane: A Review of Genetic Identification of Natural Gas. *Earth-Science Rev.* 190, 247–272. doi:10.1016/j.earscirev.2018.11.017

Lu, J. G., Chen, Y. Y., Wang, L., Yao, Y. T., Chen, S. J., Yang, D. S., et al. (2014). Origin and Source of Oil and Gas in Lunan Area of Junggar Basin. *Acta Petrolei Sinica* 35, 429–438. (in Chinese with English abstract).

Milkov, A. V., and Dzou, L. (2007). Geochemical Evidence of Secondary Microbial Methane from Very Slight Biodegradation of Undersaturated Oils in a Deep Hot Reservoir. *Geol* 35, 455–458. doi:10.1130/g23557a.1

Milkov, A. V. (2010). Methanogenic Biodegradation of Petroleum in the West Siberian basin (Russia): Significance for Formation of Giant Cenomanian Gas Pools. *Bulletin* 94, 1485–1541. doi:10.1306/01051009122

Milkov, A. V. (2011). Worldwide Distribution and Significance of Secondary Microbial Methane Formed during Petroleum Biodegradation in Conventional Reservoirs. *Org. Geochem.* 42, 184–207. doi:10.1016/j.orggeochem.2010.12.003

Moldowan, J. M., Seifert, W. K., Arnold, E., and Clardy, J. (1984). Structure Proof and Significance of Stereoisomeric 28,30-bisnorhopanes in Petroleum and Petroleum Source Rocks. *Geochimica et Cosmochimica Acta* 48, 1651–1661. doi:10.1016/0016-7037(84)90334-x

Ni, Y. Y., Ma, Q. S., Ellis, G., Dai, J. X., Katz, B., Zhang, S. C., et al. (2011). mFundamental Studies on Kinetic Isotope Effect (KIE) of Hydrogen Isotope Fractionation in Natural Gas Systems. *Geochimica et Cosmochimica Acta* 75, 2270–2696. doi:10.1016/j.gca.2011.02.016

Pallasser, R. J. (2000). Recognising Biodegradation in Gas/oil Accumulations through the δ 13 C Compositions of Gas Components. *Org. Geochem.* 31, 1363–1373. doi:10.1016/s0146-6380(00)00101-7

Peters, K. E. (1986). Guidelines for Evaluating Petroleum Source Rock Using Programmed Pyrolysis. *AAPG Bull.* 70, 318–329. doi:10.1306/94885688-1704-11d7-8645000102c1865d

Prinzhofer, A. A., and Huc, A. Y. (1995). Genetic and post-genetic Molecular and Isotopic Fractionations in Natural Gases. *Chem. Geology.* 126, 281–290. doi:10.1016/0009-2541(95)00123-9

Qi, X. F., Wu, X. Z., and Liu, D. G. (2010). The Deep Structural Features and Hydrocarbon prospect in Hinterland of Junggar Basin. *Xinjiang Pet. Geology.* 31, 111–114. (in Chinese with English abstract).

Qiu, N. S., Zha, M., and Wang, X. L. (2000). Simulation of Geothermal Evolution History in Junggar Basin. *Xinjing Pet. Geol.* 21, 39–41. (in Chinese with English abstract).

Qiu, N. S., Wang, X. L., Yang, H. B., and Xiang, Y. (2001). The Characteristics of Temperature Distribution in the Junggar Basin. *Chin. J. Geology.* 36, 350–358. (in Chinese with English abstract).

Qiu, N. S. (2002). Characters of thermal Conductivity and Radiogenic Heat Production Rate in Basins of Northwest China. *Chin. J. Geology.* 37, 196–206. (in Chinese with English abstract).

Schoell, M. (1980). The Hydrogen and Carbon Isotopic Composition of Methane from Natural Gases of Various Origins. *Geochimica et Cosmochimica Acta* 44, 649–661. doi:10.1016/0016-7037(80)90155-6

Schoell, M. (1984). Recent Advances in Petroleum Isotope Geochemistry. *Org. Geochem.* 6, 645–663. doi:10.1016/0146-6380(84)90086-x

Seifert, W. K., and Michael Moldowan, J. (1979). The Effect of Biodegradation on Steranes and Terpanes in Crude Oils. *Geochimica et Cosmochimica Acta* 43, 111–126. doi:10.1016/0016-7037(79)90051-6

Song (1996). *The Geological Characteristics of Natural Gas Accumulations in the Junggar Basin*. Beijing: Petroleum Industry Press. (in Chinese).

Stahl, W. J., and Carey, B. D. (1975). Source-rock Identification by Isotope Analyses of Natural Gases from fields in the Val Verde and Delaware Basins, West Texas. *Chem. Geology.* 16, 257–267. doi:10.1016/0009-2541(75)90065-0

Sun, P. A., Wang, X. L., Tang, Y., Wan, M., and Cao, J. (2012). Geochemical Constraints on the Multiple Origins of Shallow-Buried Natural Gases in the Junggar Basin. *Geochimica* 41, 109–121. (in Chinese with English abstract).

Sun, P. a., Wang, Y., Leng, K., Li, H., Ma, W., and Cao, J. (2016). Geochemistry and Origin of Natural Gas in the Eastern Junggar Basin, NW China. *Mar. Pet. Geology.* 75, 240–251. doi:10.1016/j.marpetgeo.2016.04.018

Sweeney, J. J., and Burnham, A. K. (1990). Evaluation of a Simple Model of Vitrinite Reflectance Based on Chemical Kinetics. *AAPG (Am. Assoc. Pet. Geol. Bull.* 74, 1559–1570. doi:10.1306/0c9b251f-1710-11d7-8645000102c1865d

Tao, K., Cao, J., Wang, Y., Ma, W., Xiang, B., Ren, J., et al. (2016). Geochemistry and Origin of Natural Gas in the Petroliferous Mahu Sag, Northwestern Junggar Basin, NW China: Carboniferous marine and Permian Lacustrine Gas Systems. *Org. Geochem.* 100, 62–79. doi:10.1016/j.orggeochem.2016.08.004

Tian, H., Cheng, P., Zhou, Q., Xiao, X., and Wilkins, R. W. T. (2012). A Complete Series of C31-C34 25-norbenzohopanes in the Devonian and Jurassic Bitumen Sands, NW Sichuan Basin. *Org. Geochem.* 45, 1–6. doi:10.1016/j.orggeochem.2012.01.003

Wang, S. J., Hu, S. B., and Wang, J. Y. (2000a). The Characteristics of Heat Flow and Geothermal fields in Junggar Basin. *Chin. J. Geophys.* 43, 771–779. (in Chinese with English abstract). doi:10.1002/cjg2.98

Wang, S., Hu, S., Li, T., Wang, J., and Zhao, W. (2000b). Terrestrial Heat Flow in Junggar Basin, Northwest China. *Chin.Sci.Bull.* 45, 1808–1813. doi:10.1007/bf02886273

Wang, X. L., Zhi, D. M., Wang, Y. T., Chen, J. P., and Qin, Z. J. (2013). *Organic Geochemistry of Source Rocks and Hydrocarbons in the Junggar Basin*. Beijing: Petroleum Industry Press. (in Chinese).

Wang, X., Liu, W., Shi, B., Zhang, Z., Xu, Y., and Zheng, J. (2015). Hydrogen Isotope Characteristics of Thermogenic Methane in Chinese Sedimentary Basins. *Org. Geochem.* 83-84, 178–189. doi:10.1016/j.orggeochem.2015.03.010

Whiticar, M. J. (1994). "Correlation of Natural Gases with Their Sources," in *The Petroleum System – from Source to Trap*. Editors L. Magoon and W. Dow (AAPG Memoir 60), 261–284.

Wilkes, H., Boreham, C., Harms, G., Zengler, K., and Rabus, R. (2000). Anaerobic Degradation and Carbon Isotopic Fractionation of Alkylbenzenes in Crude Oil by Sulphate-Reducing Bacteria. *Org. Geochem.* 31, 101–115. doi:10.1016/s0146-6380(99)00147-3

Wu, X. H., Yin, H. S., and Wang, C. S. (2003). Oil and Gas Sources from the Luliang Oil Field in the Junggar Basin, Xinjiang. *Sediment. Geology. Tethyan Geology.* 23, 96–102. (in Chinese with English abstract).

Wu, X., Liu, Q., Liu, G., and Ni, C. (2019). Genetic Types of Natural Gas and Gas-Source Correlation in Different Strata of the Yuanba Gas Field, Sichuan Basin, SW China. *J. Asian Earth Sci.* 181, 103906. doi:10.1016/j.jseaes.2019.103906

Xia, L., Cao, J., Hu, W., Zhi, D., Tang, Y., Li, E., et al. (2021). Coupling of Paleoenvironment and Biogeochemistry of Deep-Time Alkaline Lakes: A Lipid Biomarker Perspective. *Earth-Science Rev.* 213, 103499. doi:10.1016/j.earscirev.2020.103499

Xiang, B., Zhou, N., Ma, W., Wu, M., and Cao, J. (2015). Multiple-stage Migration and Accumulation of Permian Lacustrine Mixed Oils in the central Junggar Basin (NW China). *Mar. Pet. Geology.* 59, 187–201. doi:10.1016/j.marpetgeo.2014.08.014

Yang, Y. T., Wang, S. J., Pei, D. H., and Xing, Y. (2002). An Analysis of Deep Hydrocarbon Accumulation Conditions and Exploratory Realms in the Heartland of Junggar Basin. *Explor. Dev.* 29, 32–34. (in Chinese with English abstract).

Zhi, D., Song, Y., Zheng, M., Qin, Z., and Gong, D. (2021). Genetic Types, Origins, and Accumulation Process of Natural Gas from the Southwestern Junggar Basin: New Implications for Natural Gas Exploration Potential. *Mar. Pet. Geology.* 123, 104727. doi:10.1016/j.marpetgeo.2020.104727

Conflict of Interest: Authors DZ, XW, and ZQ were employed by the company Xinjiang Oilfield Company. Author DZ was employed by the company Turpan-Hami Oilfield Company.

Publisher's Note: All claims expressed in this article are solely those of the authors and do not necessarily represent those of their affiliated organizations, or those of the publisher, the editors and the reviewers. Any product that may be evaluated in this article, or claim that may be made by its manufacturer, is not guaranteed or endorsed by the publisher.

frontiers | Frontiers in Earth Science

ORIGINAL RESEARCH
published: 13 April 2022
doi: 10.3389/feart.2022.879959

The Volume and Geochemical Characteristics of Desorption Gases From Wufeng–Longmaxi (O_3w-S_1l) Shale in the Xishui Area, North Guizhou, China

Shuyong Shi[1,2,3], *Yunpeng Wang*[1,2]*, *Yu Sun*[1,2,3] *and Huijuan Guo*[1,2,3]

[1]State Key Laboratory of Organic Geochemistry, Guangzhou Institute of Geochemistry, Chinese Academy of Sciences, Guangzhou, China, [2]CAS Center for Excellence in Deep Earth Science, Chinese Academy of Sciences, Guangzhou, China, [3]College of Earth Science and Planetary Sciences, University of Chinese Academy of Sciences, Beijing, China

OPEN ACCESS

Edited by:
Yunyan Ni,
Research Institute of Petroleum Exploration and Development (RIPED), China

Reviewed by:
Quanyou Liu,
SINOPEC Petroleum Exploration and Production Research Institute, China
Guodong Zheng,
Northwest Institute of Eco-Environment and Resources (CAS), China

***Correspondence:**
Yunpeng Wang
wangyp@gig.ac.cn

Specialty section:
This article was submitted to Geochemistry, a section of the journal Frontiers in Earth Science

Received: 20 February 2022
Accepted: 07 March 2022
Published: 13 April 2022

Citation:
Shi S, Wang Y, Sun Y and Guo H (2022) The Volume and Geochemical Characteristics of Desorption Gases From Wufeng–Longmaxi (O_3w-S_1l) Shale in the Xishui Area, North Guizhou, China. Front. Earth Sci. 10:879959. doi: 10.3389/feart.2022.879959

The Upper Ordovician–Lower Silurian Wufeng–Longmaxi (O_3w-S_1l) shale is widely distributed in the Xishui area, north Guizhou, China. However, the potential and characteristics of shale gases in the Xishui area are not well evaluated, which has limited the exploration of shale gas in this area. In this study, we collected 14 fresh core samples of Wufeng–Longmaxi Formations from Well XK-3 and conducted gas desorption experiments to evaluate the potential of shale gas resources in the Xishui area. After analyzing the chemical and isotopic composition of desorption gases, the origin and genesis of the shale gas were systematically studied. Our results show that the volume of desorption gases varies from 2.14 m^3/t to 6.01 m^3/t, with a mean value of 4.12 m^3/t, showing great potential for shale gas in this area. The positive correlation between total organic carbon (TOC) and desorption gas volume indicates that organic matter provides the main pore volume for shale gas preservation. The desorption gases are very dry, which are mainly composed of methane (99.64‰–99.74%) with a very low content of ethane, and no nitrogen, carbon dioxide, and hydrogen sulfide are detected. Based on geochemical diagrams, the desorption gases are identified as oil-associated thermogenic gases. The carbon isotopic values of methane and ethane display reversal distribution, due to the mixing of primary gases from kerogen cracking and the secondary gases from retained oil cracking and further possible cracking of heavy gaseous hydrocarbons (C_3H_8—C_5H_{12}) at higher thermal maturity (Ro > 2.00%). After comparing with Jiaoshiba, Changning, Weiyuan, and Dingshan areas, the carbon isotopic values of shale gases of Wufeng–Longmaxi shale also show different features at different areas, which are mainly controlled by the thermal maturity levels of the shale.

Keywords: Wufeng–Longmaxi (O_3w-S_1l) shale, desorption gases, thermogenic origin, shale gas, isotopic reversal, thermal maturity

INTRODUCTION

Shale gas is mostly stored in nanoscale pores of shale with abundant organic matter in the forms of absorbed and free states (Ross and Bustin, 2008; Gao, 2015). The Upper Ordovician Wufeng Formation and the Lower Silurian Longmaxi Formation are considered the most favorable layers for shale gas exploration and development in China (Dai et al., 2020). In recent years, China had discovered several giant shale gas fields such as Jiaoshiba, Weiyuan, Changning, and Fushun (Dai et al., 2014; Dong et al., 2018). Up to 2019, the explored reserves of marine shale gas had reached 1.8×10^{12} m^3, with an annual production of approximately 145×10^8 m^3/a in China (Zou et al., 2020). In the past 5 y, north Guizhou has caused widespread attention for shale gas exploration (Yi and Gao, 2015; Zhang et al., 2015; Zhao et al., 2015; He et al., 2020). In 2016, commercial shale gas was discovered in Well AY-1 in Anchang anticline, Zheng'an area, and the mean production reached about 95×10^3 m^3/day (Liu Y. et al., 2018). In 2017, shale gas with industrial values was also discovered in the Dingshan area (Wei et al., 2020). From the angle of the geological structure, Jiaoshiba, Changning, Dingshan, and Xishui anticlines are distributed along with the same geological structure; however, the potential of shale gas in the Xishui area is not well evaluated. One key question is the preservation of gases in the low burial thin shale layer like the Xishui area. Another question is whether there are obvious differences in geochemical and isotopic compositions in such a shallow thin shale layer in comparison with deep thick shale layers in other areas. Another observation is whether there exists carbon isotopic reversal for methane and ethane in this area, which is commonly observed in higher maturated marine shale gas in the world (Dai et al., 2014; Liu et al., 2021). In order to investigate the shale gas potential in the Xishui area, Wells XK-1, XK-2, and XK-3 were drilled by the Chinese Academy of Sciences in 2017 and 2018. Compared with Jiaoshiba and Changning areas, it is found that the Xishui area is not the depositional center of Wufeng–Longmaxi shale, and the thickness of high-quality shale is also thin (less than 30 m) due to the influence of Qianzhong paleo-uplift to the south (Yi and Gao, 2015; Zhang et al., 2016). Although the burial depth of Wufeng–Longmaxi shale is shallower than 700 m in this area, the volume of desorption gases is greater than 1 m^3/t, which indicates the shale gas in these three wells have reached industrial standard (Shi et al., 2019; Sun et al., 2020). However, the geochemical and isotopic characteristics of shale gas in this area are also not well studied. In this study, 14 fresh core samples of Wufeng–Longmaxi shale from Well XK-3, Xishui area, north Guizhou, were collected with the drilling of well, and chemical and isotopic composites of the desorption gases were analyzed. The shale gas potential, gas origin, and the cause of carbon isotopic reversal were discussed after comparing with shale gas samples of Wufeng–Longmaxi shale from other areas in the Sichuan Basin.

GEOLOGICAL BACKGROUND

The Xishui area is tectonically located in the transition zone between north Guizhou and the southeast Sichuan Basin (**Figure 1**), belonging to the upper part of the Yangtze block (Zhao A. et al., 2017). Because of the collision of the Yangtze block and Cathaysian block, a restricted anoxic depositional environment was formed during the period from the Late Ordovician to Early Silurian in north Guizhou (Wu et al., 2014). The Wufeng–Longmaxi shale was deposited due to two events of transgression in the periods of Late Ordovician and Early Silurian (He et al., 2020; Liu et al., 2021). The shale is distributed in the northern Guizhou area and the whole Sichuan Basin due to the influence of Qianzhong paleo-uplift (Yi and Gao, 2015; Zhang et al., 2016). The thickness of high-quality shale gradually becomes thicker from south to north, which is estimated at around 30 m in the Xishui area (Zhao A. et al., 2017; Zhao Z. et al., 2017). The regional stratigraphy of this area is shown in **Figure 2**. It can be seen that the exposed strata of the Xishui anticline include Cambrian, Ordovician, Lower Silurian, Permian, Triassic, Jurassic, and Cretaceous. From **Figure 2**, it is clear that there exist multiple unconformities in the stratigraphy, indicating the Xishui area mainly experienced four geological movements, such as Guangxi movement, Dongwu movement, Indosinian movement, and Himalayan movement. The Middle-Upper Silurian, Devonian, and Carboniferous are missing due to the erosion event related to the Guangxi movement (Yuan et al., 2013; Chen et al., 2014). Since the Late Cretaceous, the Xishui area suffered intense folding and denudation caused by the Himalayan movement. The NE–SW Xishui anticline was formed in this period, and many faults were developed in the core part of the anticline (**Figure 1**). In the Xishui area, the lithology of the Wufeng Formation is mainly composed of dark carbonaceous mudstone. The Longmaxi Formation can be divided into two members. The lower part is mainly composed of siliceous shale, carbonaceous shale, and calcareous shale with abundant graptolite and pyrite, while the upper part is composed of gray silty mudstone and argillaceous limestone (**Figure 2**). Well XK-3 is located in the core part of the Lintanchang dome-shaped anticline, and the complete well depth is 663 m (**Figure 1**). The thickness of high-quality shale with a TOC value of more than 2.00% is about 20 m, in which the Wufeng Formation is around 5 m and the Guanyinqiao Member is only around 34 cm.

METHODS

The desorption gas was measured using specially designed equipment mainly composed of a sealed aluminum connected with a U-shaped glass tube. The fresh shale core samples were taken while drilling, put into the sealed aluminum immediately, and the saturated salt solution was filled into cans as quickly as possible. The desorption gas was released into a U-shaped glass tube, which is also filled with saturated salt solution, by a plastic conduit. Then, the desorption gas volume in a U-shaped glass tube can be measured using the labeled scale meter. The desorption gas volume (m^3/t) at standard conditions can be calculated using the following equation:

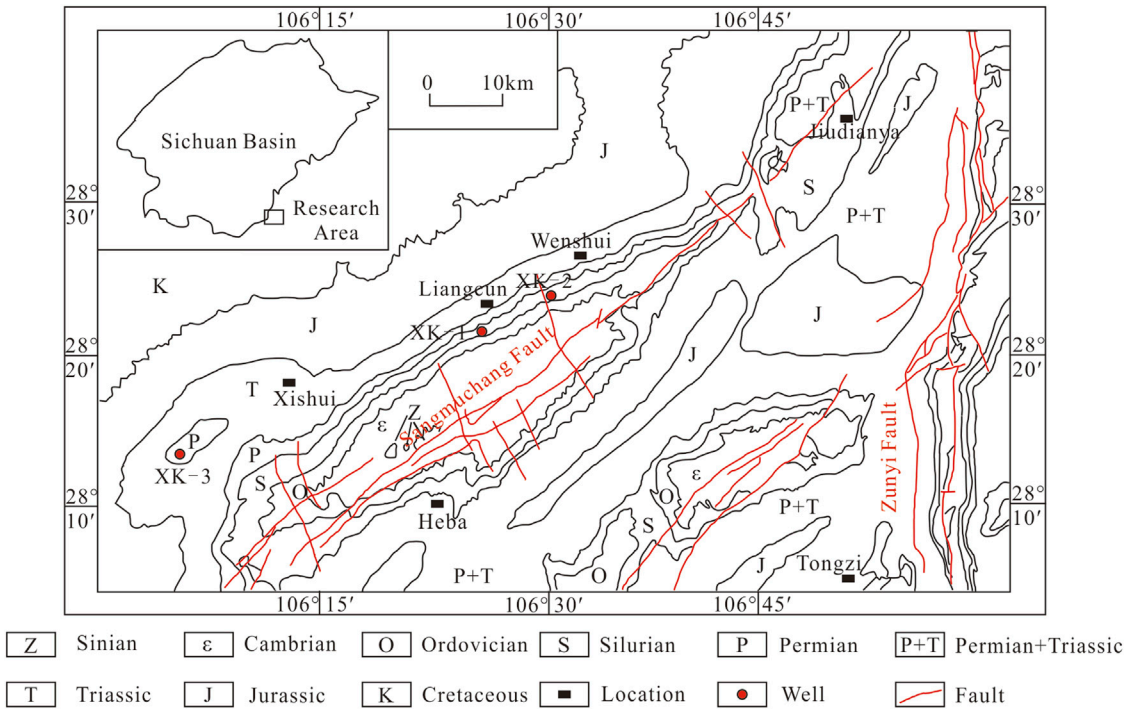

FIGURE 1 | Geological map of the Xishui area, north Guizhou, with the location of Well XK-3 (figure modified from Shi et al., 2019).

$$V_{de} = (PV)/(P_0 * M_{shale}), \quad (1)$$

where V_{de} is the desorption gas volume (m^3/t) at standard conditions (P_0 = 0.1 Mpa, 25°C), V is the desorption gas volume in U-shaped glass tube and aluminum can, P is the pressure of the desorption gas in U-shaped glass, P_0 is the standard atmospheric pressure (P_0 = 0.1 Mpa), and M_{shale} is the quantity of shale (t).

The chemical composition of desorption gas samples was analyzed by Agilent 6890N GC equipped with a flame ionization detector and a thermal conductivity detector. Carbon isotopic ($\delta^{13}C$) analysis of gases was analyzed using Isochrom GC-IRMS with the precision of ±0.5‰. Hydrogen isotopic ($\delta^{2}H$) analysis of gases was analyzed using IsoPrime GC-IRMS, with a precision of ±5‰.

Total organic carbon (TOC) was measured by using the LECO CS-800 analyzer, and the carbonates were removed by the hydrochloric acid (HCl) before measuring. The mineral compositions were analyzed using an Olympus X-ray Powder Diffraction (XRD) analyzer with CoKα radiation, and the powder was analyzed with a 2θ value from 5° to 55°.

The burial and thermal histories of Well XK-3 were built by PetroMod software. The first step of basin modeling is the basic input data, including stratigraphy (lithology, thickness, and age), tectonic events (unconformities, erosion, and age), and boundary conditions (paleo-water depth, heat flow, and sediment–water interface temperature) (Yao and Wang, 2016). Subsequently, the temperature and thermal maturation were calculated mainly based on burial depth and heat flow. Finally, the results of thermal maturity were required to be calibrated by the measured values. As shown in **Figure 5B**, the calculated thermal maturity from the Easy%Ro model (Sweeney and Burnham, 1990) was consistent with measured values.

RESULTS

TOC and Mineral Composition of Shale

The results of total organic carbon and mineral compositions of 14 samples are listed in **Table 1**. The total organic carbon of studied 14 samples varies from 1.39% to 7.22%, with a mean value of 4.48%. All shale samples mainly consist of quartz, feldspar, clay minerals, calcite, dolomite, and a lower content of pyrite. All samples are clay-rich, and the content of clay minerals varies from 19.8% to 54.5%, with a mean value of 35.9%. The content of quartz varies from 21.1% to 64.4%, with a mean value of 38.7%. The positive correlation between TOC and the content of quartz can be observed (**Figure 3A**), which may indicate that the quartz is mainly of biogenic origin (Guo, 2014; Liang et al., 2016).

Gas Volume and Molecular Composition of Desorption Gases

The results of desorption experiments show that the gas volume ranges from 2.14 m^3/t to 6.01 m^3/t, with a mean value of 4.12 m^3/t (**Table 2**). All samples show the gas volume exceeds 1 m^3/t, which

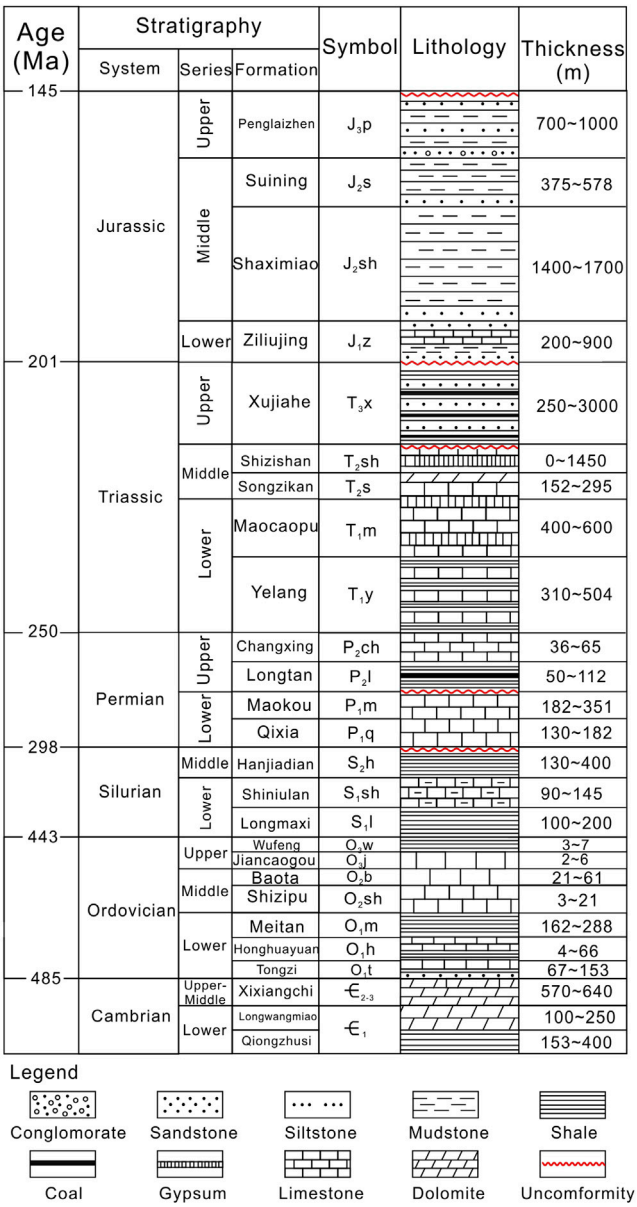

FIGURE 2 | Stratigraphic column in the Xishui area, north Guizhou.

indicates it reaches the industrial standard. The positive correlation between TOC and gas volume (**Figure 3B**) indicates that the organic matter provides the main pore volume for the preservation of shale gas. The molecular composition of desorption gases is dominantly hydrocarbon gases, in which methane and ethane meanly account for 99.70% (99.64‰–99.74%) and 0.30% (0.26‰–0.36%), respectively, and no carbon dioxide, hydrogen sulfide, and nitrogen are detected. The lower wetness of shale gas from Wufeng–Longmaxi shale is very common in Sichuan Basin and its adjacent areas, such as Changning, Jiaoshiba, and Weiyuan areas (Dai et al., 2014; Feng et al., 2016).

Isotopic Composition of Desorption Gas

The carbon isotopic results (**Table 2**) show that the methane carbon isotopic values ($\delta^{13}C\text{-}CH_4$) of desorption gases range from −37.41‰ to 31.21‰, with a mean value of −33.70‰. The ethane carbon isotopic values ($\delta^{13}C\text{-}C_2H_6$) range from −37.90‰ to −35.47‰, with a mean value of −36.27‰. The carbon isotopic values of desorption gases show an obvious

TABLE 1 | TOC and mineral composition of 14 shale samples from Well XK-3, Xishui area, north Guizhou.

Sample ID	Strata	Depth (m)	TOC (%)	Quartz (%)	Feldspar (%)	Clay minerals (%)	Calcite (%)	Dolomite (%)	Pyrite (%)
sxc-1	S_1l	641.5	1.22	25.0	20.0	48.9	4.1	—	2.0
sxc-2	S_1l	643.4	3.69	22.4	18.9	49.0	4.7	2.4	2.6
sxc-3	S_1l	644.4	3.88	23.8	17.9	45.5	6.9	2.9	3.0
sxc-4	S_1l	646.2	4.45	37.7	17.1	34.7	4.7	3.2	2.6
sxc-5	S_1l	647.5	4.23	36.2	18.2	33.4	5.8	3.6	2.8
sxc-6	S_1l	649.3	4.60	43.2	17.1	29.8	4.4	3.5	2.0
sxc-7	S_1l	650.6	4.23	44.6	15.8	31.1	4.1	2.9	1.5
sxc-8	S_1l	651.6	5.17	42.4	17.0	31.8	4.8	4.0	—
sxc-9	S_1l	653.6	5.44	53.6	12.5	23.0	5.0	4.8	1.1
sxc-10	S_1l	655.0	5.38	43.7	19.2	30.2	4.0	2.9	—
sxc-11	S_1l	656.7	7.07	48.6	19.5	26.2	2.9	2.8	—
sxc-12	O_3w	658.0	5.72	64.4	7.3	19.8	5.3	3.2	—
sxc-13	O_3w	659.4	2.37	21.1	12.9	54.5	4.4	3.9	3.2
sxc-14	O_3w	660.7	5.25	34.4	17.0	44.5	—	4.1	—

Clay minerals = chlorite + illite.
— not detected.

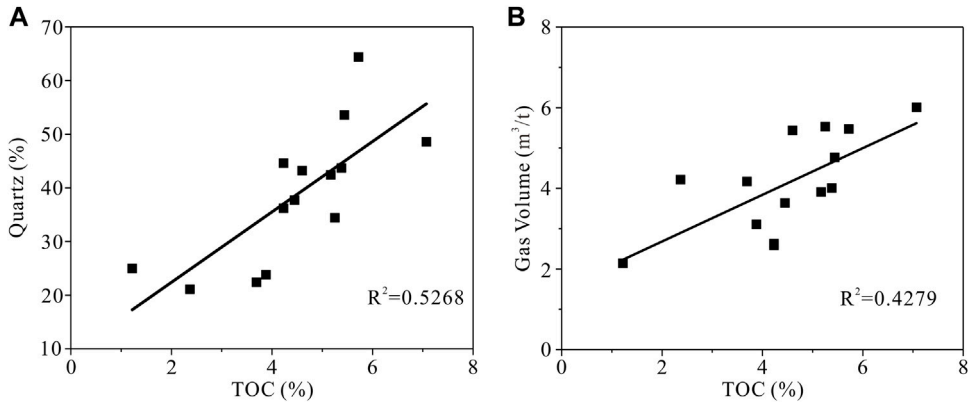

FIGURE 3 | Total organic carbon vs. quartz **(A)** and total organic carbon vs. desorption gas volume **(B)** of 14 samples of Wufeng–Longmaxi shale from Well XK-3.

reversal distribution (**Figure 4A**, $\delta^{13}C\text{-}CH_4 > \delta^{13}C\text{-}C_2H_6$), which is similar to other areas, such as Changning, Weiyuan, Jiaoshiba, and Dingshan in the Sichuan Basin (Dai et al., 2014; Dai et al., 2016; Feng et al., 2016; Yang et al., 2017; Zhong et al., 2019). **Figure 4B** shows that shale gas samples of Well XK-3 fall in the post-rollover zone with the wetness lower than 1.2%, suggesting an extremely high maturity (Dai et al., 2014). In addition, the $\delta^2H\text{-}CH_4$ (‰) values range from −157.07‰ to −159.99‰, with a mean value of −154.37‰, which is similar to Weiyuan (with a mean value of 141.50‰), Jiaoshiba (with a mean value of 148.95‰), and Changning (with a mean value of 148.00‰) areas.

Burial and Thermal Histories of Well XK-3

For discussing the origin of desorption gas, we also built the geological model of Well XK-3 by using PetroMod software with the constrain of measured maturity data (Ro%) from publications (Zhao et al., 2015; Guo et al., 2016). The results of burial and thermal histories of Wufeng–Longmaxi shale from Well XK-3 are shown in **Figure 5** (Zhao et al., 2015; Guo et al., 2016). It can be seen that Wufeng–Longmaxi shale of Well XK-3 experienced four stages of deep burial and uplift. The shale in Well XK-3 experienced a long-term erosion caused by Guangxi movement in the Late Silurian and the burial depth of Wufeng–Longmaxi shale is shallow (<1,500 m), when the temperature of Wufeng–Longmaxi shale is about 70°C and the maturity (Ro%) of the shale is about 0.40%, showing an immature stage. During the Permian period, there was short-term quick erosion due to the Dongwu movement (approximately 259 Ma). At that period, the burial depth of Wufeng–Longmaxi shale was also lower than 1,500 m, the temperature was approximately 90°C, and the maturity (Ro %) was about 0.50%, which was still in the immature stage. After the Dongwu movement, the Wufeng–Longmaxi shale of Well XK-3 entered into a long-term continuous deep burial stage and a short-term erosion related to the Indosinian

TABLE 2 | Gas volume and geochemical characteristics of desorption gases from Well XK-3, Xishui area, north Guizhou.

Sample ID	Depth (m)	Strata	TOC (%)	Gas volume (m^3/t)	CH_4 (%)	C_2H_6 (%)	$\delta^{13}C$-CH_4 (‰)	$\delta^{13}C$-C_2H_6 (‰)	$\delta^{2}H$-CH_4 (‰)
scx-1	641.5	S_1l	1.22	2.14	99.74	0.26	−33.20	−35.47	−156.04
scx-2	643.4	S_1l	3.69	4.17	99.64	0.36	−32.50	−35.98	−161.00
scx-3	644.4	S_1l	3.88	3.11	99.70	0.30	−33.90	−36.09	−156.38
scx-4	646.2	S_1l	4.45	3.64	99.68	0.32	−34.73	−35.60	−154.00
scx-5	647.5	S_1l	4.23	2.63	99.69	0.31	−33.79	−36.69	−152.15
scx-6	649.3	S_1l	4.60	5.44	99.70	0.30	−34.28	−36.70	−153.64
scx-7	650.6	S_1l	4.23	2.59	99.68	0.32	−37.12	−37.90	−152.05
scx-8	651.6	S_1l	5.17	3.91	99.74	0.26	−33.95	−36.11	−151.85
scx-9	653.6	S_1l	5.44	4.77	99.72	0.28	−34.21	−36.31	−152.53
scx-10	655.0	S_1l	5.38	4.01	99.73	0.27	−31.58	−35.87	−150.99
scx-11	656.7	S_1l	7.07	6.01	99.70	0.30	−31.41	−36.17	−153.95
scx-12	658.0	O_3w	5.72	5.47	99.74	0.26	−33.79	−36.59	−157.04
scx-13	659.4	O_3w	2.37	4.22	99.71	0.29	−33.38	−36.43	−153.81
scx-14	660.7	O_3w	5.25	5.53	99.68	0.32	−33.98	−35.93	−155.76

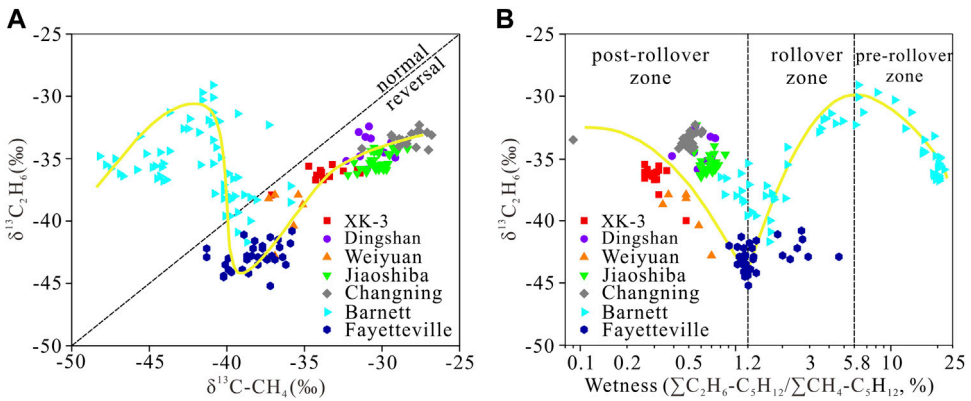

FIGURE 4 | Plot of $\delta^{13}C$-CH_4 vs. $\delta^{13}C$-C_2H_6 **(A)** and the wetness vs. $\delta^{13}C$-C_2H_6 **(B)** of shale gases from different areas. Data sources: the Dingshan gas field (Zhong et al., 2019); (2) the Weiyuan gas field (Dai et al., 2014); (3) the Jiaoshiba gas field (Dai et al., 2016; Yang et al., 2017); (4) the Changning gas field (Dai et al., 2016; Feng et al., 2016); (5) the Barnett shale in the Fort Worth Basin (Zumberge et al., 2012); and (6) the Fayetteville shale in the Arkoma Basin (Zumberge et al., 2012).

movement occurred during the Late Triassic period. Meanwhile, the temperature and maturity (Ro%) of Wufeng–Longmaxi shale increased with the burial depth. Since the middle Triassic (approximately 235 Ma), the Wufeng–Longmaxi shale has been in the main oil stage (Ro = 0.70–1.00%); the burial depth was more than 2,700 m, and the temperature was about 120°C. Subsequently, the shale entered into the wet gas stage at the Late Jurassic (Ro > 1.30%, approximately 150 Ma) and dry gas stage at the early stage of Late Cretaceous (Ro > 2.00%, approximately 100 Ma), successively. The burial depth of Wufeng–Longmaxi reached the maximum depth (approximately 5,500 m) at the Late Cretaceous. At the same time, the temperature of the Wufeng–Longmaxi shale in Well XK-3 reached 190°C, and the maturity of the shale reached the current level (around 2.21%). Then, the shale of Well XK-3 uplifted and was eroded because of the Himalayan movement. Currently, the burial depth of Wufeng–Longmaxi shale in this area is about 650 m, and the temperature is about 37°C.

DISCUSSION

Origin of Desorption Gases

Whiticar's diagrams (Whiticar, 1999) could be used to determine the origin of natural gases based on the chemical and isotopic compositions of natural gases. As **Figure 6A** shows, shale gases from Well XK-3, Dingshan, Changning, Weiyuan, and Jiaoshiba are of thermogenic origin, which is different from the gases from Barnett and Fayetteville shales. The $\delta^{13}C$-CH_4 vs. $CH_4/(C_2H_6+C_3H_8)$ diagram (**Figure 6B**) shows that shale gases from Barnett and Fayetteville shales fall into the type II zone. On the contrary, shale gases from Well XK-3, Dingshan, Changning, and Jiaoshiba areas almost fall into the zone shifting from the typical type II kerogen gases, except for the Weiyuan area. This phenomenon may be caused by the extremely high content of methane and heavier carbon isotopic value at a relatively higher thermal maturity stage (Ro > 2.00%) (Liu et al., 2016; Yang et al., 2017). The $\delta^{13}C$-C_2H_6 values could be used to classify two types of natural gases. Dai (2011) proposed that natural gases with $\delta^{13}C$-C_2H_6 < −28.5‰ are oil-associated gases, while the

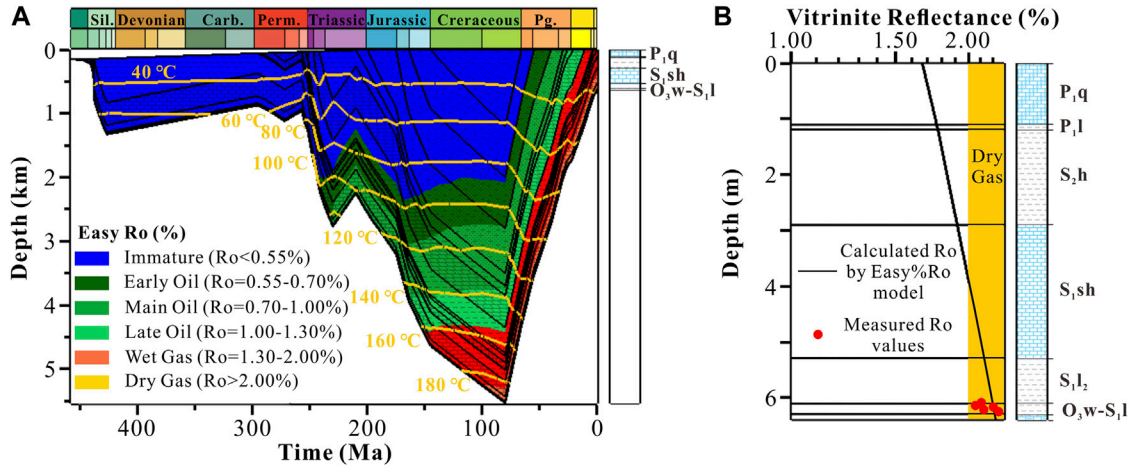

FIGURE 5 | Burial and thermal histories of Wufeng–Longmaxi shale of Well XK-3 **(A)** and thermal model calibration **(B)**.

gases with $\delta^{13}C\text{-}C_2H_6 > -29‰$ are coal-derived gases. Although there are some different viewpoints regarding this threshold (Milkov et al., 2020), a range of −27.0‰ to −29.0‰ for $\delta^{13}C\text{-}C_2H_6$ value is acceptable for distinguishing oil-derived gases. As shown in **Table 2**, the $\delta^{13}C\text{-}C_2H_6$ values of the gas samples are between −37.90‰ and −35.47‰, suggesting that the desorption gases of Wufeng–Longmaxi shale from Well XK-3 are oil-associated gases, which is similar to other areas in the Sichuan Basin (**Figure 4**).

Causes of the Carbon Isotopic Reversal in Well XK-3

The carbon isotopic reversal is commonly observed in Wufeng–Longmaxi shale gas in the Sichuan Basin (**Figure 4A**). Previous studies interpreted and summarized the following causes of this phenomenon: 1) mixing gases with different thermal maturity (Hao and Zou, 2013; Xia et al., 2013; Liu Q. et al., 2018; Zhao et al., 2019); 2) redox reactions with transition metals and water (Burruss and Laughrey, 2010; Feng et al., 2016); 3) depressurization during uplifting (Milkov et al., 2020); and 4) thermochemical sulfate reduction (Hao et al., 2008; Liu et al., 2019).

In order to discuss the cause of carbon isotopic reversal in this area, we recovered the generation history of hydrocarbons of Wufeng–Longmaxi shale of Well XK-3 with consideration of oil secondary cracking based on Pepper's hydrocarbon generation kinetics (Pepper and Corvi, 1995), and the results are shown in **Figure 7**. During the relatively lower maturity stage (Ro < 1.00%), a considerable amount of gases was mainly from kerogen cracking, and no or little retained oil cracking before oil cracking (**Figure 7**). $\delta^{13}C$ increased with the carbon number, and the carbon isotopic distribution was normal (**Figures 4A**, **7**; $\delta^{13}C\text{-}CH_4 < \delta^{13}C\text{-}C_2H_6$); thus, the carbon isotopic reversal was not observed due to the same origin of gases. With the increase in thermal maturity and burial depth, the open system was gradually converted into a closed system. When thermal maturity (Ro%) reached over 1.00% (165 Ma, T = 160°C), the retained oil started cracking (**Figures 5A**, **7**). The retained oil was mainly cracked and converted into wet gases and generated lighter $\delta^{13}C\text{-}C_2H_6$ values (Liu Q. et al., 2018). As a result, $\delta^{13}C\text{-}C_2H_6$ becomes lighter due to the mixing of gases from kerogen cracking and retained oil cracking (Dai et al., 2017; Liu Q. et al., 2018). Although $\delta^{13}C\text{-}CH_4$ also becomes lighter, the extent of change for $\delta^{13}C\text{-}CH_4$ is not as obvious as $\delta^{13}C\text{-}C_2H_6$ (**Figure 4A**). The main reason causing isotopic reversal is that the retained oil mainly cracked into wet gases with a little methane, and methane was mainly from kerogen cracking (Xia et al., 2013). During this stage, $\delta^{13}C\text{-}C_2H_6$ becomes more negative with the increase in thermal maturity, and reversal carbon isotopic distribution ($\delta^{13}C\text{-}CH_4 > \delta^{13}C\text{-}C_2H_6$) occurs with increasing contribution of wet gases from retained oil cracking (**Figure 4**). Therefore, we proposed that mixing gases from kerogen and retained oil cracking might be the main reason for the carbon isotopic reversal in this area.

Differences and Causes of Carbon Isotopic Values in the Sichuan Basin

In this study, we also collected carbon isotopic data of Wufeng–Longmaxi shale gas from Changning, Weiyuan, Dingshan, and Jiaoshiba areas. Although the values of $\delta^{13}C\text{-}CH_4$ and $\delta^{13}C\text{-}C_2H_6$ for shale gas are distributed in the reversal zone, we still found that there existed differences in the carbon isotopic values of shale gases in different areas, Sichuan Basin (**Figure 8**). The mean values of $\delta^{13}C\text{-}CH_4$ are −36.21‰ in Weiyuan (Dai et al., 2014), −33.70‰ in Well XK-3, −30.73‰ in Dingshan (Zhong et al., 2019), −30.59‰ in Jiaoshiba (Dai et al., 2016; Yang et al., 2017), and −28.34‰ in Changning (Feng et al., 2016), respectively. The mean values of $\delta^{13}C\text{-}C_2H_6$ are −39.31‰ in Weiyuan (Dai et al., 2014), −36.27‰ in Well XK-3, −34.09‰ in Dingshan (Zhong et al., 2019), −35.09‰ in Jiaoshiba (Dai et al., 2016; Yang et al., 2017), and −33.44‰ in Changning (Feng et al., 2016), respectively. As shown in **Figure 8**, the carbon isotopic values of Well XK-3 and Weiyuan are lighter than those of the other areas, and gases from Changning show

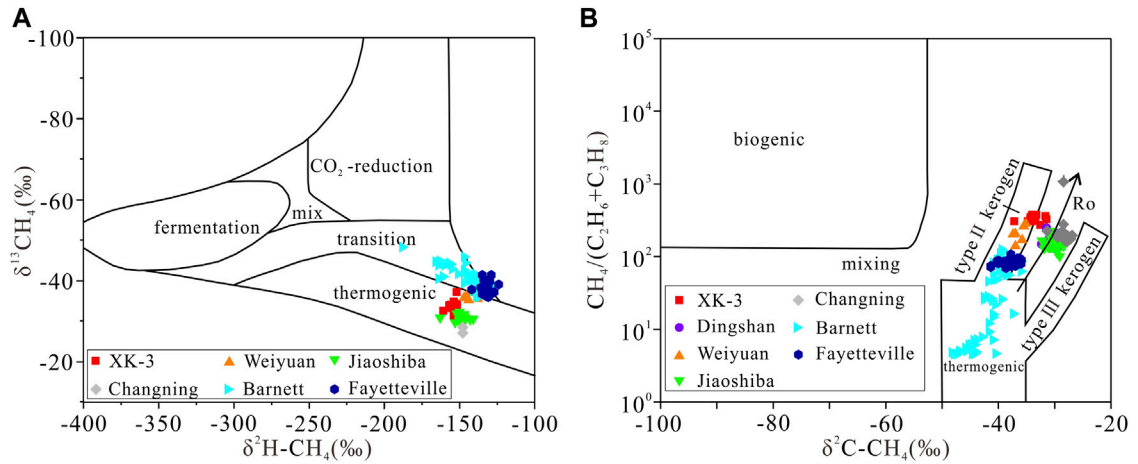

FIGURE 6 | Plot of δ^2H-CH_4 vs. δ^{13}C-CH_4 **(A)** and δ^{13}C-CH_4 vs. $CH_4/(C_2H_6+C_3H_8)$ **(B)** of shale gases from different areas (modified from Whiticar 1999). Data sources: (1) the Dingshan gas field (Zhong et al., 2019); (2) the Weiyuan gas field (Dai et al., 2014); (3) the Jiaoshiba gas field (Dai et al., 2016; Yang et al., 2017); (4) the Changning gas field (Dai et al., 2016; Feng et al., 2016); (5) the Barnett shale in the Fort Worth Basin (Zumberge et al., 2012); and (6) the Fayetteville shale in the Arkoma Basin (Zumberge et al., 2012).

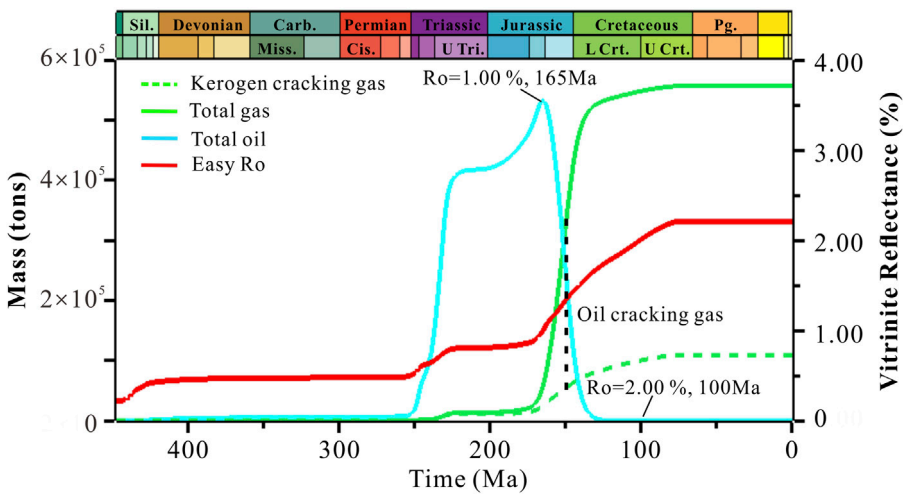

FIGURE 7 | Generation history of hydrocarbons of Wufeng–Longmaxi shale of Well XK-3, Xishui area, north Guizhou.

the heaviest carbon isotopic values for both methane and ethane. We regard that this difference may be controlled by thermal maturity. The current maturities of Wufeng–Longmaxi shale from Weiyuan, Xishui, Dingshan, Jiaoshiba, and Changning are 2.00%–2.20% (Feng et al., 2016), 1.80%–2.20% (Zhao A. et al., 2017), 2.14%–2.24% (Wei et al., 2017), 2.50%–2.80% (Feng et al., 2018), and 2.50%–3.00% (Chen et al., 2017), respectively. It is obvious that there exists a positive correlation between δ^{13}C-CH_4 or δ^{13}C-C_2H_6 and thermal maturity (**Figure 8**).

The generation history of Wufeng–Longmaxi shale of Well XK-3 shows the retained oil stopped cracking into gases when thermal maturity reached 2.00% (**Figures 5A**, **7**, approximately 100 Ma, T = 185°C). The current thermal maturity of Wufeng–Longmaxi shale is over 2.00%, which indicates that Wufeng–Longmaxi shale had experienced the stage of retained oil cracking into wet gases. It is worth noting that gaseous hydrocarbons are still generated and increased when thermal maturity is greater than 2.00% (**Figure 7**). This increasing part of generated gases might be from kerogen cracking because the cracking of retained oil is stopped. Meanwhile, heavier gaseous hydrocarbons are further cracked and converted to lighter gaseous hydrocarbons, and this process is also controlled by thermal maturity (Hao and Zou, 2013; Liu Q. et al., 2018). The current maturity (Ro%) values of Wufeng–Longmaxi shale in Changning and Jiaoshiba areas are higher than those in Xishui,

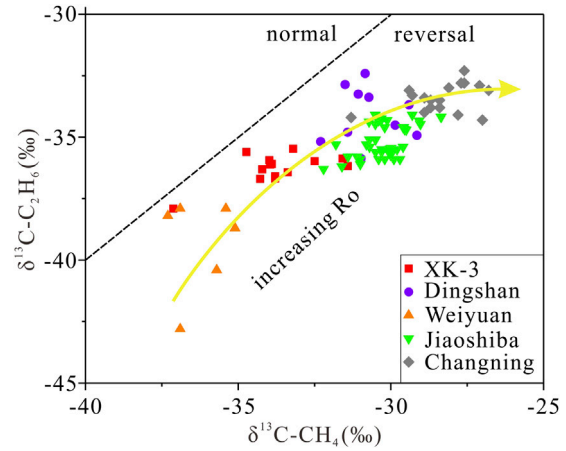

FIGURE 8 | Plot of $\delta^{13}C$-CH_4 vs. $\delta^{13}C$-C_2H_6 of shale gases of Longmaxi shale in different areas, Sichuan Basin. Data sources: (1) the Dingshan gas field (Zhong et al., 2019); (2) the Weiyuan gas field (Dai et al., 2014); (3) the Jiaoshiba gas field (Dai et al., 2016; Yang et al., 2017); and (4) the Changning gas field (Dai et al., 2016; Feng et al., 2016).

Weiyuan, and Dingshan areas. It may indicate that Wufeng–Longmaxi shale in Changning areas experienced a longer period of heavier gases cracking into lighter gases. Thus, the carbon isotopic values of shale gases in Changning and Jiaoshiba are heavier than those of other areas.

CONCLUSION

The gas desorption experiments on 14 fresh core samples of Wufeng–Longmaxi Formations collected from Well XK-3 show the volume of desorption gases varies from 2.14 m^3/t to 6.01 m^3/t, with a mean value of 4.12 m^3/t, suggesting great potential of shale gas resources for Wufeng–Longmaxi shale in the Xishui area, north Guizhou. Our results indicate that the shallow and thin shale still enjoys the high capability of gas resources. From the angle of the regional structure, the belt along the Jiaoshiba, Changning, Dingshan, and Xishui anticlines is the most prospective exploration target for further exploration of shale gas. The positive relationship between desorption gas volume and TOC indicates that organic matter can provide more pore volume for shale gas storage. The desorption gases are typically dry gases, which are mainly composed of methane (99.64%–99.74%), with a little ethane (0.26%–0.36%) and no detected nitrogen, carbon dioxide, and hydrogen sulfide. The desorption gases are thermogenic origin and oil-associated gases. The carbon isotopic reversal is mainly caused by the mixing of gases from kerogen primary cracking and retained oil secondary cracking. The further cracking of heavy gaseous hydrocarbons during higher thermal maturity (Ro > 2.00%) may lead to the carbon isotopic differences of shale gases from Wufeng–Longmaxi shale in different areas, Sichuan Basin. The difference of geochemical and isotopic compositions in such a shallow thin shale layer is the maturation of the gases in comparison with deep thick shale layers in other areas, which should cause the attention for further studies and explorations.

DATA AVAILABILITY STATEMENT

The raw data supporting the conclusion of this article will be made available by the authors, without undue reservation.

AUTHOR CONTRIBUTIONS

YW and HG presented the idea and conceived this study. SS, YS, and YW designed the field works and experiments. SS and YS performed the experiments. SS, YW and HG interpreted the data and wrote the manuscript.

FUNDING

This study was supported by the Strategic Priority Research Program of the Chinese Academy of Sciences (XDA14010103, XDB10010300), the National Natural Science Foundation of China (No. 41702151), and the National Science and Technology Major Project of China (No. 2017ZX05008-002-030).

ACKNOWLEDGMENTS

The authors thank Prof. Xiao Li and Dr. Guanfang Li, Institute of Geology and Geophysics, Beijing, China, to assist with core sample collection. We also thank the editor and reviewers for their critical and constructive comments, which have improved this manuscript significantly. This is contribution No.IS-3156 from GIGCAS.

REFERENCES

Burruss, R. C., and Laughrey, C. D. (2010). Carbon and Hydrogen Isotopic Reversals in Deep basin Gas: Evidence for Limits to the Stability of Hydrocarbons. *Org. Geochem.* 41, 1285–1296. doi:10.1016/j.orggeochem.2010.09.008

Chen, X., Fan, J., Chen, Q., Tang, L., and Hou, X. (2014). Toward a Stepwise Kwangsian Orogeny. *Sci. China Earth Sci.* 57 (3), 379–387. doi:10.1007/s11430-013-4815-y

Dai, J. (2011). Significance of the Study on Carbon Isotopes of Alkane Gases. *Nat. Gas Industry.* 31 (12), 1–6. doi:10.3787/j.issn.1000-0976.2011.12.001

Dai, J., Dong, D., Ni, Y., Hong, F., Zhang, S., Zhang, Y., et al. (2020). Some Essential Geological and Geochemical Issues about Shale Gas Research in China. *Nat. Gas Geosci.* 31 (6), 745–760. doi:10.11764/j.issn.1672-1926.2020.05.016

Dai, J., Ni, Y., Gong, D., Feng, Z., Liu, D., Peng, W., et al. (2017). Geochemical Characteristics of Gases from the Largest Tight Sand Gas Field (Sulige) and Shale Gas Field (Fuling) in China. *Mar. Pet. Geology.* 79, 426–438. doi:10.1016/j.marpetgeo.2016.10.021

Dai, J., Zou, C., Dong, D., Ni, Y., Wu, W., Gong, D., et al. (2016). Geochemical Characteristics of marine and Terrestrial Shale Gas in China. *Mar. Pet. Geology.* 76, 444–463. doi:10.1016/j.marpetgeo.2016.04.027

Dai, J., Zou, C., Liao, S., Dong, D., Ni, Y., Huang, J., et al. (2014). Geochemistry of the Extremely High thermal Maturity Longmaxi Shale Gas, Southern Sichuan Basin. *Org. Geochem.* 74, 3–12. doi:10.1016/j.orggeochem.2014.01.018

Dong, D., Shi, Z., Guan, Q., Jiang, S., Zhang, M., Zhang, C., et al. (2018). Processes, Challenges and Prospects of Shale Gas Exploration in Wufeng-Longmaxi Reservoirs in the Sichuan Basin. *Nat. Gas Industry* 38 (4), 8. doi:10.3787/j.issn.1000-0976.2018.04.008

Feng, W., Wang, F., Guan, J., Zhou, J., Wei, F., Dong, W., et al. (2018). Geologic Structure Controls on Initial Productions of Lower Silurian Longmaxi Shale in south China. *Mar. Pet. Geology.* 91, 163–178. doi:10.1016/j.marpetgeo.2018.01.001

Feng, Z., Liu, D., Huang, S., Wu, W., Dong, D., Peng, W., et al. (2016). Carbon Isotopic Composition of Shale Gas in the Silurian Longmaxi Formation of the Changning Area, Sichuan Basin. *Pet. Exploration Develop.* 43 (5), 1–9. doi:10.11698/PED.2016.05.0010.1016/s1876-3804(16)30092-1

Gao, B. (2015). Geochemical Characteristics of Shale Gas from Lower Silurian Longmaxi Formation in the Sichuan Basin and its Geological Significance. *Nat. Gas Geosci.* 26 (6), 1173–1182. doi:10.11764/j.issn.1672-1926.2015.06.1173

Guo, S., Guo, J., Liu, C., Zhang, L., Guo, X., and Xiao, P. (2016). Shale Gas Accumulation Potential of Lower Silurian Longmaxi Formation in Northern Guizhou. *J. Cent. South Univ. (Science Technology)* 47 (6), 1973–1980. doi:10.11817/j.issn.1672-7207.2016.06.021

Guo, X. (2014). Rules of Two-Factor Enrichment for Marine Shale Gas in Southern China-Understanding from the Longmaxi Formation. *Acta Geologica Sinica* 88 (7), 1209–1218. doi:10.1111/1755-6724.12347

Hao, F., Guo, T., Zhu, Y., Cai, X., Zou, H., and Li, P. (2008). Evidence for Multiple Stages of Oil Cracking and Thermochemical Sulfate Reduction in the Puguang Gas Field, Sichuan Basin, China. *Bulletin* 92 (5), 611–637. doi:10.1306/01210807090

Hao, F., and Zou, H. (2013). Cause of Shale Gas Geochemical Anomalies and Mechanisms for Gas Enrichment and Depletion in High-Maturity Shales. *Mar. Pet. Geology.* 44, 1–12. doi:10.1016/j.marpetgeo.2013.03.005

He, Y., Xiang, K., An, Y., Yi, C., Yang, Z., and Yu, N. (2020). Geological Characteristics and Favorable Areas Prediction of Shale Gas in Wufeng-Longmaxi Formation in Zheng'an Area of North Guizhou. *Geol. Survery China* 7 (3), 21–29. doi:10.19388/j.zgdzdc.2020.0303

Liang, C., Jiang, Z., Cao, Y., Wu, M., Guo, L., and Zhang, C. (2016). Deep-water Depositional Mechanisms and Significance for Unconventional Hydrocarbon Exploration: A Case Study from the Lower Silurian Longmaxi Shale in the southeastern Sichuan Basin. *Bulletin* 100 (05), 773–794. doi:10.1306/02031615002

Liu, Q., Jin, Z., Wang, X., Yi, J., Meng, Q., Wu, X., et al. (2018a). Distinguishing Kerogen and Oil Cracked Shale Gas Using H, C-Isotopic Fractionation of Alkane Gases. *Mar. Pet. Geology.* 91, 350–362. doi:10.1016/j.marpetgeo.2018.01.006

Liu, Q., Li, P., Jin, Z., Liang, X., Zhu, D., Wu, X., et al. (2021). Preservation of Organic Matter in Shale Linked to Bacterial Sulfate Reduction (BSR) and Volcanic Activity under marine and Lacustrine Depositional Environments. *Mar. Pet. Geology.* 127, 104950. doi:10.1016/j.marpetgeo.2021.104950

Liu, Q., Wu, X., Wang, X., Jin, Z., Zhu, D., Meng, Q., et al. (2019). Carbon and Hydrogen Isotopes of Methane, Ethane, and Propane: A Review of Genetic Identification of Natural Gas. *Earth-Science Rev.* 190, 247–272. doi:10.1016/j.earscirev.2018.11.017

Liu, Y., Zhang, J., Ren, J., Liu, Z., Huang, H., and Tang, X. (2016). Stable Isotope Geochemistry of the Nitrogen-Rich Gas from Lower Cambrian Shale in the Yangtze Gorges Area, South China. *Mar. Pet. Geology.* 77, 693–702. doi:10.1016/j.marpetgeo.2016.07.020

Liu, Y., Zhang, J., Zhang, P., Liu, Z., Zhao, P., Huang, H., et al. (2018b). Origin and Enrichment Factors of Natural Gas from the Lower Silurian Songkan Formation in Northern Guizhou Province, south China. *Int. J. Coal Geology.* 187, 20–29. doi:10.1016/j.coal.2018.01.004

Milkov, A. V., Faiz, M., and Etiope, G. (2020). Geochemistry of Shale Gases from Around the World: Composition, Origins, Isotope Reversals and Rollovers, and Implications for the Exploration of Shale Plays. *Org. Geochem.* 143, 103997. doi:10.1016/j.orggeochem.2020.103997

Pepper, A. S., and Corvi, P. J. (1995). Simple Kinetic Models of Petroleum Formation. Part I: Oil and Gas Generation from Kerogen. *Mar. Pet. Geology.* 12 (3), 291–319. doi:10.1016/0264-8172(95)98381-e

Ross, D. J. K., and Bustin, R. M. (2008). Characterizing the Shale Gas Resource Potential of Devonian-Mississippian Strata in the Western Canada Sedimentary basin: Application of an Integrated Formation Evaluation. *Bulletin* 92 (1), 87–125. doi:10.1306/09040707048

Shangbin, C., Yanming, Z., Si, C., Yufu, H., Changqing, F., and Junhua, F. (2017). Hydrocarbon Generation and Shale Gas Accumulation in the Longmaxi Formation, Southern Sichuan Basin, China. *Mar. Pet. Geology.* 86, 248–258. doi:10.1016/j.marpetgeo.2017.05.017

Shi, S., Sun, Y., Guo, H., Deng, R., Cheng, C., and Wang, Y. (2019). Geochemical and thermal Evolution of Wufeng-Longmaxi Shale and its prospect in the Xishui Area, North Guizhou. *Geochimica* 48 (6), 567–579. doi:10.19700/j.0379-1726.2019.06.005

Sun, J., Xiao, X., Wei, Q., Cheng, P., Tian, H., and Wu, Y. (2020). Gas in Place and its Controlling Factors of the Shallow Longmaxi Shale in the Xishui Area, Guizhou, China. *J. Nat. Gas Sci. Eng.* 77, 1–11. doi:10.1016/j.jngse.2020.103272

Sweeney, J. J., and Burnham, A. K. (1990). Evaluation of a Simple Model of Vitrinite Reflectance Based on Chemical Kinetics. *AAPG Bull.* 74 (10), 1559–1570. doi:10.1306/0c9b251f-1710-11d7-8645000102c1865d

Wei, X., Liu, Z., Wang, Q., Wei, F., and Yuan, T. (2020). Analysis and Thinking of the Difference of Wufeng-Longmaxi Shale Gas Enrichment Conditions between Dingshan and Jiaoshiba Areas in southeastern Sichuan Basin. *Nat. Gas Geosci.* 31 (8), 1041–1050. doi:10.11764/j.issn.1672-1926.2020.02.011

Wei, X., Zhao, Z., Wang, Q., Liu, Z., Zhou, M., and Zhang, H. (2017). Comprehensive Evaluation on Geological Conditions of the Shale Gas in Upper Ordovician Wufeng Formation-Lower Silurian Longmaxi Formation in Dingshan Area, Qijiang, Southeastern Sichuan. *Geol. Rev.* 63 (1), 153–164. doi:10.16509/j.georeview.2017.01.014

Whiticar, M. J. (1999). Carbon and Hydrogen Isotope Systematics of Bacterial Formation and Oxidation of Methane. *Chem. Geology.* 161, 219–314. doi:10.1016/s0009-2541(99)00092-3

Wu, Y., Fan, T., Zhang, J., Jiang, S., Li, Y., Zhang, J., et al. (2014). Characterization of the Upper Ordovician and Lower Silurian Marine Shale in Northwestern Guizhou Province of the Upper Yangtze Block, South China: Implication for Shale Gas Potential. *Energy Fuels* 28 (6), 3679–3687. doi:10.1021/ef5004254

Xia, X., Chen, J., Braun, R., and Tang, Y. (2013). Isotopic Reversals with Respect to Maturity Trends Due to Mixing of Primary and Secondary Products in Source Rocks. *Chem. Geology.* 339, 205–212. doi:10.1016/j.chemgeo.2012.07.025

Yang, R., He, S., Hu, Q., Hu, D., and Yi, J. (2017). Geochemical Characteristics and Origin of Natural Gas from Wufeng-Longmaxi Shales of the Fuling Gas Field, Sichuan Basin (China). *Int. J. Coal Geology.* 171, 1–11. doi:10.1016/j.coal.2016.12.003

Yao, X., and Wang, Y. (2016). Assessing Shale Gas Resources of Wufeng-Longmaxi Shale (O3w-S1l) in Jiaoshiba Area, SE Sichuan (China) Using Petromod I: Burial and thermal Histories. *Pet. Sci. Technol.* 34 (11-12), 1000–1007. doi:10.1080/10916466.2016.1176041

Yi, T., and Gao, D. (2015). Characteristics and Distribution Pattern of Shale Gas Reservoir in Longmaxi Formation in Guizhou Province. *Coal Geology. Exploration* 43 (3), 22–32. doi:10.3969/j.issn.1001-1986.2015.03.005

Yuan, Y., Sun, D., li, S., and Lin, J. (2013). Caledonian Erosion Thickness Reconstruction in the Sichuan Basin. *Chin. J. Geology.* 48 (3), 581–591.

Zhang, P., Zhang, J., Huang, Y., Tang, X., Wang, Z., and Peng, J. (2015). Characteristics and Gas Content Evaluation of Wufeng-Longmaxi Formation Shale in Well Xiye-1. *Resour. Industries* 17 (4), 48–55. doi:10.13776/j.cnki.resourcesindustries.20150514.012

Zhang, P., Zhang, J., Liu, H., and Huang, Y. (2016). Accumulation Conditions of Shale Gas from Lower Silurian Longmaxi Formation in Guizhou. *J. Cent. South Univ. (Science Technology)* 47 (9), 3085–3092. doi:10.11817/j.issn.1672-7207.2016.09.024

Zhao, A., Yu, Q., Lei, Z., Tan, J., Zhou, W., Zhao, G., et al. (2017a). Geological and Microstructural Characterization of the Wufeng-Longmaxi Shale in the Basin-Orogen Transitional Belt of North Guizhou Province, China. *j nanosci nanotechnol* 17 (9), 6026–6038. doi:10.1166/jnn.2017.14522

Zhao, L., He, Y., Yang, P., Chen, H., and An, Y. (2015). Characteristics of Lower Palaeozoic Hydrocarbon Source Strata and a Primary Study of the Shale Gas Accumulation in Northern Guizhou Province. *Geology. China* 42 (6), 1931–1943.

Zhao, W., Zhang, S., He, K., Zeng, H., Hu, G., Zhang, B., et al. (2019). Origin of Conventional and Shale Gas in Sinian-Lower Paleozoic Strata in the Sichuan

Basin: Relayed Gas Generation from Liquid Hydrocarbon Cracking. *Bulletin* 103 (6), 1265–1296. doi:10.1306/11151817334

Zhao, Z., Li, R., Feng, W., Yu, Q., Yang, H., and Zhu, L. (2017b). Enrichment Conditions and Favorable Zone Prediction of Wufeng–Longmaxi Shale Gas Reservoirs in the Northern Yunnan–Guizhou Provinces, China. *Nat. Gas Industry* 37 (12), 26–34. doi:10.3787/j.issn.1000-0976.2017.12.004

Zhong, C., Qin, Q., Fan, C., and Hu, D. (2019). Geochemical Characteristics of Shale Gas and its Response to thermal Maturity (Ro) in the Longmaxi Formation, Dingshan Area, Southeast Sichuan. *Pet. Sci. Technol.* 37 (11), 1270–1278. doi:10.1080/10916466.2018.1558241

Zou, C., Pan, S., Jing, Z., Gao, J., Yang, Z., Wu, S., et al. (2020). Shale Oil and Gas Revolution and its Impact. *Acta Petrolei Sinica* 41 (1), 1–12. doi:10.7623/syxb202001001

Zumberge, J., Ferworn, K., and Brown, S. (2012). Isotopic Reversal ('rollover') in Shale Gases Produced from the Mississippian Barnett and Fayetteville Formations. *Mar. Pet. Geology.* 31 (1), 43–52. doi:10.1016/j.marpetgeo.2011.06.009

Conflict of Interest: The authors declare that the research was conducted in the absence of any commercial or financial relationships that could be construed as a potential conflict of interest.

frontiers | Frontiers in Earth Science

ORIGINAL RESEARCH
published: 26 April 2022
doi: 10.3389/feart.2022.857876

Carbon Dioxide and its Carbon Isotopic Composition of Natural Gas in the Sichuan Basin, SW China

Jinxing Dai[1], Yunyan Ni[1], Quanyou Liu[2]*, Xiaoqi Wu[2], Cong Yu[1], Deyu Gong[1], Feng Hong[1], Yanling Zhang[1] and Zengmin Yan[1]*

[1]Research Institute of Petroleum Exploration and Development, PetroChina, Beijing, China, [2]Petroleum Exploration and Production Research Institute, SINOPEC, Beijing, China

The Sichuan Basin, covering an area of 180 × 10^3 km^2, has the following advantages in natural gas geology: The sedimentary rocks are 6,000–12,000 m thick with high maturity of source rocks, and nine sets of primary gas source rocks are developed in the basin with a gas–oil ratio of 80:1, and thus it is a gas basin. The remaining recoverable reserves of conventional and unconventional natural gas are up to 13.6404 × 10^{12} m^3. Multiple gas-bearing systems are developed with 25 conventional and tight oil and gas producing layers and 135 discovered gas fields, and the total proved geological reserves and cumulative production of natural gas by the end of 2019 were 5.7966 × 10^{12} m^3 and 648.8 × 10^9 m^3, respectively. The CO_2 components and the correlation with relevant parameters for 243 samples from 22 gas fields indicate that CO_2 in the Sichuan Basin display the following two characteristics: (1) Relatively low CO_2 content of 0.02%–22.90% with an average of 2.96%, which guaranteed the commerciality of natural gas exploration and production; (2) cratonic CO_2, which is characterized by low CO_2 contents (<5%) and low R/Ra ratios (<0.24). According to the $\delta^{13}C_{CO2}$ values and the relationship with R/Ra, $\delta^{13}C_1$, CO_2 contents, and wetness coefficient (W) for 263 gas samples, the $\delta^{13}C_{CO2}$ values display three characteristics: (1) The highest $\delta^{13}C_{CO2}$ value (10.4‰) in China is found in the Fuling shale gas field, which extends the interval values from previous −39‰–7‰ to −39‰–10.4‰. (2) The $\delta^{13}C_{CO2}$ values can be applied to identify the CO_2 origin of natural gas in the Sichuan Basin: type A, organic origin from thermal decomposition of organic matter, with an average $\delta^{13}C_{CO2}$ value of −12.8‰ and average wetness coefficient of 7.8% for 44 samples; type B, organic origin from thermal cracking of organic matter, with an average $\delta^{13}C_{CO2}$ value of −15.7‰ and average wetness coefficient of 1.30% for 34 samples; type C, inorganic origin from thermal decomposition or organic acid dissolution of carbonate rocks or minerals, with an average $\delta^{13}C_{CO2}$ value of −1.8‰ and average wetness coefficient of 0.85% for 175 samples. (3) $\delta^{13}C_{CO2}$>$\delta^{13}C_{CH4}$. This is a common characteristic shared by all geological age (from Z_2dn to J_2s) gas reservoirs and various gas types (coal-derived gas, oil-associated gas, and shale gas).

Keywords: Sichuan Basin, carbon dioxide, $\delta^{13}CCO_2$, origin, geochemical characteristics

OPEN ACCESS

Edited by:
Fang-Zhen Teng,
University of Washington,
United States

Reviewed by:
Ziqi Feng,
China University of Petroleum (East China), China
Shikha Sharma,
West Virginia University, United States

****Correspondence:***
Yunyan Ni
niyy@petrochina.com.cn
Quanyou Liu
qyliu@sohu.com

Specialty section:
This article was submitted to Geochemistry, a section of the journal Frontiers in Earth Science

Received: *19 January 2022*
Accepted: *10 March 2022*
Published: *26 April 2022*

Citation:
Dai J, Ni Y, Liu Q, Wu X, Yu C, Gong D, Hong F, Zhang Y and Yan Z (2022) Carbon Dioxide and its Carbon Isotopic Composition of Natural Gas in the Sichuan Basin, SW China. Front. Earth Sci. 10:857876. doi: 10.3389/feart.2022.857876

1 INTRODUCTION

The Sichuan Basin is a large superimposed basin developed on the basis of craton, with an area of about 180×10^3 km^2. The basin has developed sedimentary rocks with a thickness of 6,000–12,000 m. It is a basin with the most developed source rock series in China, especially gas source rocks (nine sets) due to its high thermal maturity (**Figure 1**), which makes it a basin enriched in both conventional and unconventional gas resources. The remaining recoverable resources of conventional and unconventional natural gas amounted to 13.6404×10^{12} m^3 (Li et al., 2019). By the end of 2019, the total proved geological reserves of the basin had reached 5.7966×10^{12} m^3. The cumulative gas production is 648.8×10^9 m^3, but the cumulative oil production is very low, 7.296×10^6 t, so the gas oil equivalent ratio is up to 80:1 (Dai et al., 2021). The basin has many gas-bearing layers and they overlap to form multiple gas-bearing systems, including 25 conventional and tight oil and gas producing layers (18 marine facies) and two shale gas producing layers (**Figure 1**). It is the basin with the most industrial oil and gas layers found so far in China (Dai et al., 2018; Dai, 2019). By the end of 2019, 135 gas fields had been discovered in the basin (**Figure 2**). There are 27 large gas fields with reserves more than 30.0×10^9 m^3, among which Anyue gas field is the largest. Anyue gas field is also the largest carbonate gas field in China, with a proved geological reserve of 1.1709×10^{12} m^3 and a gas production of 12.013×10^9 m^3 by the end of 2019 (Dai et al., 2021). In the 13th century, the Sichuan Basin developed the world's first gas field—Ziliujing gas field (Meyerhoff, 1970; Dai, 1981). Fryklund and Stark (2020) pointed out that when the cumulative gas production exceeded five billion barrels of oil equivalent (793.166×10^9 m^3 gas), sedimentary basins with remaining recoverable resources of at least five billion barrels of oil equivalent were regarded as super basins, which are called tier-one super basins. If it is slightly lower than these two indicators, it is called a tier-two super basin. Accordingly, since the

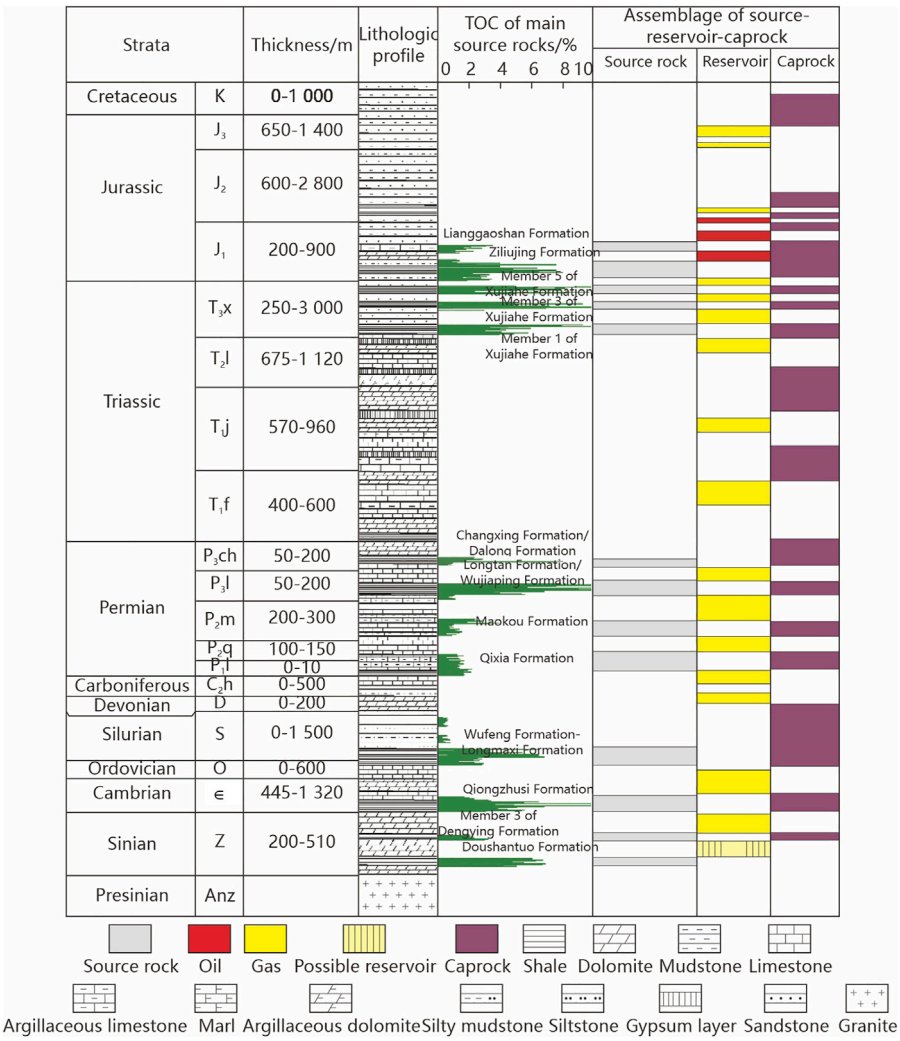

FIGURE 1 | Comprehensive histogram of source-reservoir-caprock in Sichuan Basin. T_3x-Upper Triassic Xujiahe Formation; T_2l-Middle Triassic Leikoupo Formation; T_1j-Lower Triassic Jialingjiang Formation; T_1f-Lower Triassic Feixianguan Formation; P_3ch-Upper Permian Changxing Formation; P_2m -Middle Permian Maokou Formation; P_2q-Middle Permian Qixia Formation; P_1l-Lower Permian Liangshan Formation; C_2h-Middle Carboniferous Huanglong Formation.

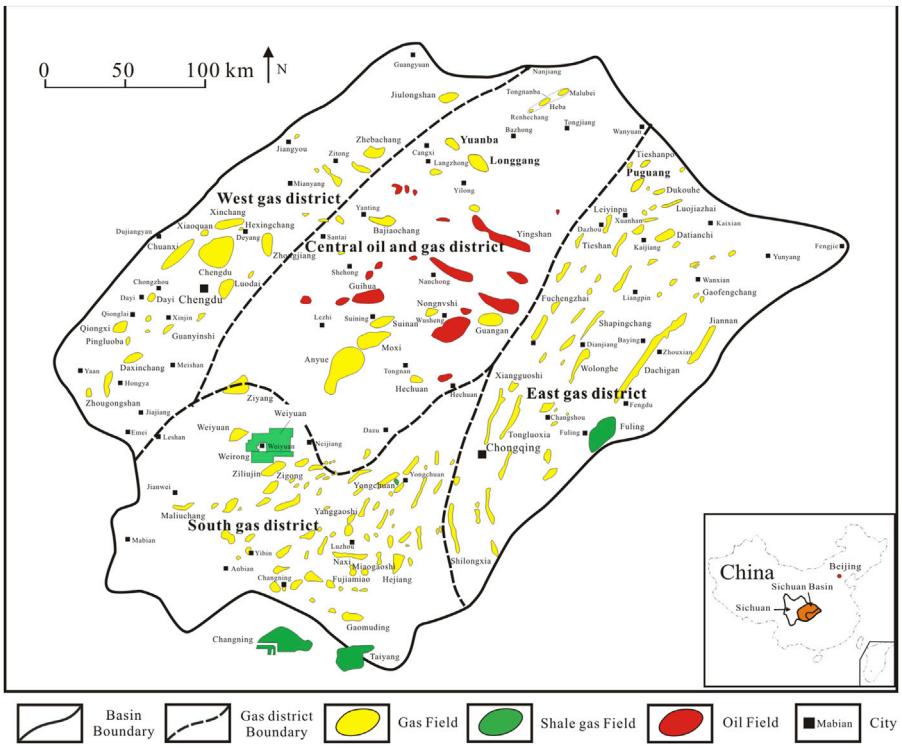

FIGURE 2 | Distribution of oil and gas fields in the Sichuan Basin (Modified after Ni et al., 2021).

remaining recoverable resources in the Sichuan Basin are 13.6404×10^{12} m^3, exceeding the index value of 793.166×10^9 m^3, while its cumulative gas production is 656.9×10^9 m^3, slightly lower than the index cumulative gas production, it can only be regarded as a tier-two super basin. Recently, Dai et al. (2021) claimed that according to the percentage of oil and gas in the cumulative total production, the oil and gas fields with an oil or gas ratio of 20–80% should be regarded as super oil and gas basins. Most super basins in the world fall into this class. When the proportion of oil is greater than 80%, it is called a super oil basin; when the proportion of gas exceeds 80%, it is called a super gas basin. The proportion of gas in the Sichuan Basin is 98.76% (Dai et al., 2021).

Natural gas more or less contains CO_2; generally, the content of CO_2 in natural gas is low. According to the analysis of 1,025 gas samples from 48 large gas fields in nine basins in China, the average CO_2 content is 3.58% (Dai, 2016). The CO_2 content in natural gas is low and is often widely distributed in cratonic basins with stable structures, such as the Ordos Basin and Sichuan Basin in China (Dai et al., 2017; Wu et al., 2017; Wu et al., 2020). However, there are also some natural gases with a high CO_2 content, which are often widely distributed in rift basins with intense tectonic activity, large fault zones, and volcanic activity zones in geological history or modern times (Dai et al., 2000; Dai et al., 2017). For example, the CO_2 content of Well Shuishen nine in Sanshui Basin in China reaches 99.55%. The CO_2 in natural gas after the volcanic period in the famous young volcanic area of Tengchong is 96.0%–96.9%. CO_2 is a greenhouse gas that pollutes the environment, so its high content will reduce the commercial value of natural gas exploration in the area. For example, the CO_2 content in natural gas from the exploration well in Lishui sag of the East China Sea extensional basin is high, which is 31%–98%, reducing the commercial interests of exploration (Diao, 2019).

Gas reservoirs can be classified according to the carbon dioxide content in the gas reservoir. Tang (1983) called a gas reservoir with CO_2 content of more than 80% to nearly 100% a CO_2 gas reservoir. Shen et al. (1991) called a gas reservoir a CO_2 gas reservoir when the content of carbon dioxide in the gas reservoir is greater than 85%. Dai et al. (2000) called a gas reservoir with CO_2 content of 90% to nearly 100% a CO_2 gas reservoir. The gas reservoir with a CO_2 content of 60%–90% is called a sub CO_2 gas reservoir; the gas reservoir with a CO_2 content of 15%–60% is called a high CO_2 gas reservoir; A gas reservoir with a CO_2 content of trace to 15% is called a CO_2-containing gas reservoir. There are many research studies on CO_2 gas reservoirs (fields) carried out at home and abroad (Muffler and White, 1968; Qi and Dai, 1981; Tang, 1983; Song, 1991; Dai et al., 2000). The imperial gas field in the Los Angeles Basin of the United States has been producing carbon dioxide since 1934–1954 with accumulated gas production of 18.4×10^6 m^3 (Muffler and White, 1968). China's proved CO_2 geological reserves at the end of 2019 amounted to 213×10^9 m^3, with a cumulative output of CO_2 gas of 12.75×10^9 m^3. At least 30 CO_2 gas fields (reservoirs) with industrial value have been found in the continental rift basins in eastern China, the continental shelf marginal basins in the East China Sea, and the northern South China Sea (Zhang et al., 2019).

The carbon isotope value of carbon dioxide ($\delta^{13}C_{CO2}$) is an important parameter to identify organic and inorganic carbon dioxide, which has been the research object of many scholars at

home and abroad. Shangguan and Zhang (1990) pointed out that CO_2 of metamorphic origin has $\delta^{13}C$ value similar to that of the sedimentary carbonate rocks, that is, −3‰ ~ +1‰, while mantle-derived CO_2 has $\delta^{13}C$ between −8.5‰ and −5‰. Shen et al. (1991) believed that inorganic CO_2 has $\delta^{13}C$>−7‰. For the quartz monzodiorite, equigranular granodiorite, and porphyritic granodiorite in granite in Fangshan District, Beijing, the $\delta^{13}C_{CO2}$ values were −3.8‰, −7.4‰, and −7.8‰, respectively (Zhen et al., 1987). Gould et al. (1981) believed that the $\delta^{13}C_{CO2}$ values of magmatic rock origin were generally −7 ± 2‰, although they were variable, while Pankina et al. (1978) believed that the $\delta^{13}C_{CO2}$ value is between −9.1‰ and 4.9‰. Moore et al. (1977) pointed out that the $\delta^{13}C_{CO2}$ value in basalt inclusions in the Middle Pacific ridge is −6.0‰ to −4.5‰. Dai et al. (1989); Dai et al. (1992); Dai et al. (2000) proposed a $\delta^{13}C_{CO2}$–CO_2 content identification diagram of organic origin and inorganic origin based on the compilation of 212 gas samples from China and more than 100 samples from Australia, Thailand, New Zealand, the Philippines, Canada, Japan, and the former Soviet Union. At the same time, it is pointed out that organic CO_2 has $\delta^{13}C$ value lower than −10‰, mainly in the range of −30‰ to −10‰; inorganic CO_2 has $\delta^{13}C$ value more than −8‰, mainly in the range of −8‰ to +3‰. Among inorganic carbon dioxide, those of carbonate rock metamorphism origin have $\delta^{13}C_{CO2}$ value close to that of the carbonate rock, about 0 ± 3‰; CO_2 of volcanic magmatic origin and mantle origin has $\delta^{13}C$ values mostly in the range of - 6 ± 2‰. At the same time, the $^3He/^4He$–$\delta^{13}C_{CO2}$ diagram (see **Section 3.1**) can be used to identify inorganic carbon dioxide of carbonate thermal metamorphic origin or magmatic and mantle origin (Etiope et al., 2011).

The study of CO_2 is far behind that of the alkane gas due to the following two reasons: 1. Alkane gas has very high economic values; thus, it attracts much research attention. 2. Alkane gases have similar chemical structure and chemical characteristics, which can provide more scientific information. However, CO_2 is an important greenhouse gas; its occurrence in natural gas not only impacts the commercial value of natural gas and potential environmental pollution but also has great significance on the gas origin and gas-source correlation research of the accompanied natural gases. The aim of this study is to investigate the geochemistry characteristics of CO_2 in the Sichuan Basin and further explore its formation mechanism, thus establishing a set of chemical and isotopic distinguishing parameters for CO_2 of different origins. In this study, we systematically analyzed the chemical and isotopic compositions of CO_2 from the Sichuan Basin, and published data of CO_2 from different strata and gas fields are also compared. Three different formation mechanisms of CO_2 are investigated, their typical carbon isotopic compositions are identified, and their relationship with hydrocarbon gases is discussed. The geochemical study of CO_2 has great significance for the research and exploration of natural gas in the Sichuan Basin.

2 ANALYTICAL METHODS

Stable carbon isotopic compositions were determined on a Thermo Delta V mass spectrometer in the PetroChina Research Institute of Petroleum Exploration and Development. The mass spectrometer was interfaced with a Thermo Trace GC Ultra gas chromatograph (GC). Individual hydrocarbon gas components (C_1–C_4) and CO_2 were separated on a gas chromatograph using a fused silica capillary column (PLOT Q 27.5 m × 0.32 mm × 10 μm), which were then converted into CO_2 in a combustion interface, and finally injected into the mass spectrometer. The temperature of the GC oven rises from 33 to 80°C at 8°C/min, then to 250°C at 5°C/min, and the final temperature was maintained for 10 min. Gas samples were analyzed in triplicate, and the stable carbon isotopic values were reported in the δ-notation in per mil (‰) relative to Vienna Peedee Belemnite (VPDB), and the analytical precision is ±0.3‰.

3 RESULTS AND DISCUSSION

3.1 Cratonic CO_2 With Low Content in Natural Gas

Supplementary Tables S1, S2 show the geochemical parameters of natural gas from 22 gas fields in Sichuan Basin. By analyzing 243 CO_2 components and their relationship with relevant parameters, the compositional characteristics of CO_2 can be obtained.

The CO_2 content of 243 gas fields ranges from 0.02% (Xinchang gas field X21-h, Dachiganjing gas field G31, Weiyuan gas field Wei202, and Fuling gas field JY6-2) to 22.90% (Yuanba gas field YB101), with an average content of 2.96%, which is lower than the average CO_2 content of 3.58% (Dai et al., 2016) of 1,025 gas samples from 48 large gas fields developed in China (**Supplementary Tables S1, S2**, **Figure 3**). The low CO_2 content in Sichuan Basin reduces the risk of natural gas exploration and development.

According to the CO_2-R/Ra diagram (**Figure 4**) (Dai et al., 2017), CO_2 in cratonic basin (expressed as cratonic CO_2) is characterized by low CO_2 content (generally <5%) and small variation of R/Ra ratio (<0.24), while CO_2 in rift basin (expressed as rift CO_2) is characterized by large variation of CO_2 content (0.0n%– > 95%) and large variation of R/Ra (0.0n–n). A total of 41 samples with CO_2 and R/Ra values from **Supplementary Tables S1, S2** all fall into C_1 (Ordos Basin) and C_2 (Sichuan Basin) cratonic areas, indicating that the CO_2 from **Supplementary Tables S1, S2** belongs to cratonic CO_2. The rest 202 samples in **Supplementary Tables S1, S2** have CO_2 values but no R/Ra values. According to the research work by Ni et al. (2014), the average value of R/Ra in the Sichuan Basin is only 0.016, so the rest 202 samples without R/Ra data are also cratonic CO_2.

3.2 Characteristics of Carbon Isotope of Carbon Dioxide ($\delta^{13}C_{CO2}$)

3.2.1 Heaviest Carbon Isotope of Carbon Dioxide in China

The interval value of $\delta^{13}C_{CO2}$ of natural gas in the Sichuan Basin ranges from −25.4‰ (Yuanba gas field, Y11 well) to +10.4‰ (Fuling gas field, JY47-3 well), and the main frequency peak is

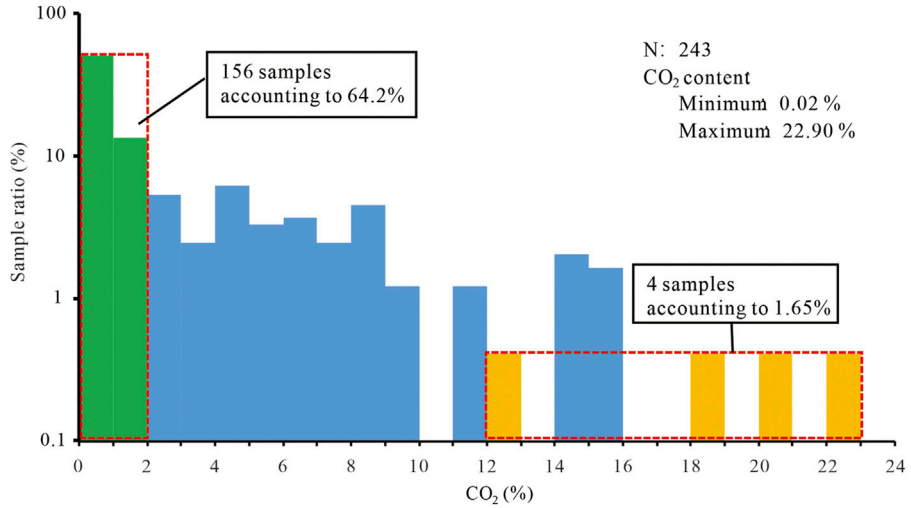

FIGURE 3 | Distribution frequency of CO_2 content of natural gas in the Sichuan Basin.

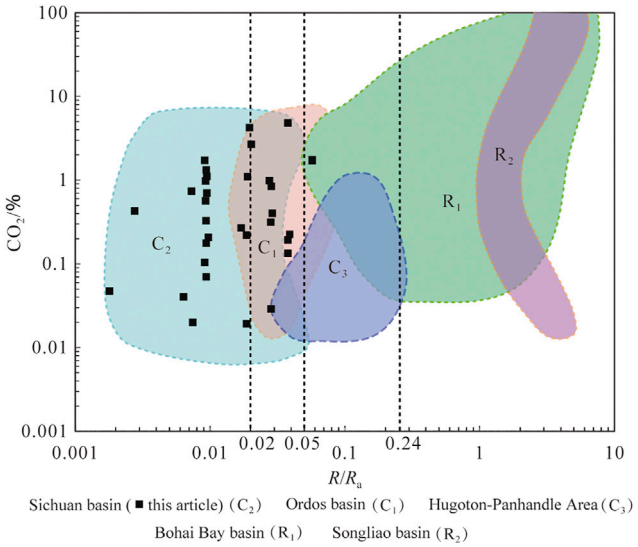

FIGURE 4 | Comparison of CO_2-R/Ra between cratonic basin and rift basin (Modified after Dai et al., 2017).

between −6‰ and +2‰ (**Supplementary Tables S1, S2**, **Figure 5**). 30 years ago, Dai et al. (1992) pointed out that the $\delta^{13}C_{CO2}$ value of natural gas in China ranged from −39‰ to +7‰. In the past 30 years, the author analyzed $\delta^{13}C_{CO2}$ values of 102 samples. Combined with 508 published $\delta^{13}C_{CO2}$ values by other researchers (He, 1995; Fu et al., 2004; Liao et al., 2012; Liu D et al., 2016; Liu et al., 2018; Deng et al., 2018; Zhang et al., 2018a; Xu et al., 2018; Zhang et al., 2018b; Zhang S. et al., 2018; Li, et al., 2018; Diao, 2019; She et al., 2021; Wei et al., 2021), about 610 samples in total are investigated, which are distributed in Songliao, Bohai Bay, Sanshui, Ordos, Sichuan, Tarim, East China Sea, and Yinggehai–Qiongnan basins. Among them, only five samples have $\delta^{13}C_{CO2}$ values higher than 7‰, ranging from 7.8‰ to 8.9‰ (Xu et al., 2018). Therefore, at present, the $\delta^{13}C_{CO2}$ value of 10.4‰ in Well JY47-3 in this study should be the highest in China. Thus, in China, the variation range of $\delta^{13}C_{CO2}$ value should be −39‰ to +10.4‰, which is lower than that of the world whose interval value of the $\delta^{13}C_{CO2}$ ranges from −42‰ to +27‰ (Barker, 1983). Therefore, the $\delta^{13}C_{CO2}$ interval value of China, both high and low, still has the potentiality of extension.

3.2.2 Carbon Isotopic Identification Parameters of CO_2

The $\delta^{13}C$ values have usually been used to identify the CO_2 origins such as organic *versus* inorganic and also sub-categories of them (**Table 1**). Parameters such as $\delta^{13}C_{CO2}$–CO_2 (Dai et al., 1992) (**Figure 6**), $\delta^{13}C_{CO2}$–R/Ra (Etiope et al., 2011), and $\delta^{13}C_{CO2}$–$\delta^{13}C_1$ (Milkov and Etiope, 2018) have been widely used. It can be seen from **Table 1** and **Figure 6** that the $\delta^{13}C_{CO2}$ value of inorganic CO_2 is higher than that of organic CO_2. This is because the original $\delta^{13}C$ of organic CO_2 is relatively low, and the original $\delta^{13}C$ of inorganic CO_2 is relatively high (**Table 2**). Due to the carbon isotopic inheritance, the carbon isotopic composition of organic and inorganic CO_2 gases is mainly affected by the carbon isotopic value of their precursors.

When the $\delta^{13}C_{CO2}$ value < −10‰ (a few < −8‰), the carbon dioxide belongs to organic origin, including gas samples from Guang'an, Bajiaochang, Zhongba, Wenxingchang, Wolonghe, Dachiganjing, Zhangjiachang, Bandong, Xiangguosi, and Weiyuan gas fields, and Xujiahe Formation gas reservoir of Longgang gas field, Jurassic Formation gas reservoir of Xinchang gas field, and Triassic Formation gas reservoir of Anyue gas field (**Supplementary Table S1**, **Table 1**, and **Figure 6**). CO_2 of organic origin can be divided into several sub-categories (**Supplementary Table S1**, **Table 1** and **Figure 7**). Among the abovementioned 13 gas fields, gases in the Guang'an, Bajiaochang, and Zhongba gas fields, Jurassic Formation gas reservoir in Xinchang gas field, and Triassic Formation gas reservoir in Anyue gas field are thermogenic wet gas (oil-

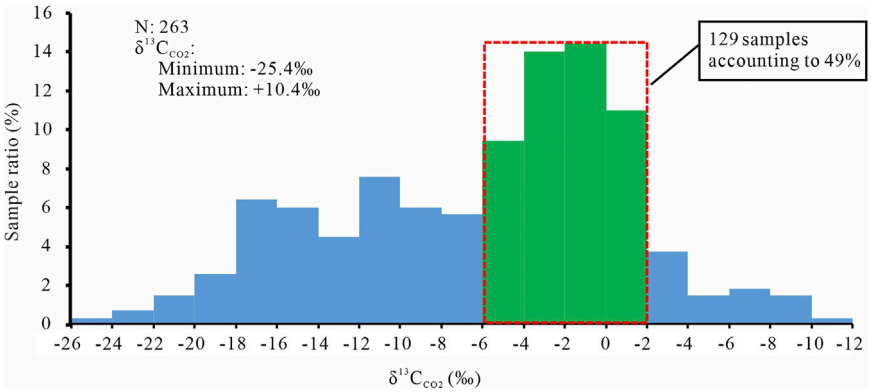

FIGURE 5 | Distribution frequency of the carbon isotopes of CO_2 in the Sichuan Basin.

TABLE 1 | Carbon isotopic composition of carbon dioxide of different origins.

$\delta^{13}C$ of inorganic CO_2			$\delta^{13}C$ of organic CO_2			References
Upper mantle degassing	**Volcano magma origin**	**Carbonate mineral thermal metamorphism or organic acid dissolution**	**Causes of microbial degradation**	**Origin of thermal degradation of organic matter**	**Organic matter cracking origin**	
−7–5‰						Hoefs (1978)
−8–4‰						Javoy et al. (1978)
−5.3–4.6‰						Cornides (1993)
	−9.1–4.9‰	−3.5‰ to +3.5	< −20‰			Pankina et al. (1978)
		−3–1‰				Shangguan and Zhang (1990)
	−7‰					Sano et al. (2008)
				−15–25‰		Hunt (1979)
		−3.7 to +3.7‰			−15–9‰	Zhu and Wu (1994)
−6 ± 2‰		0 ± 3‰				Dai et al. (1996)
>−8‰, mainly fall between −8‰ and +3			<−10‰, mainly fall between −10 and 30‰			
−8–4‰	−10–4‰	−4–4‰		−25–15‰	<−20‰	Liu et al. (2016)

associated thermogenic gas, OA). The wetness (W) of 37 gas samples varies between 3.2% and 17.7%, with an average value of 7.8%, and the $\delta^{13}C_{CO2}$ values of 44 gas samples range from −6.2‰ to −22.6‰, with an average of −12.8‰. The thermal maturity Ro% value of gas source rocks of Xujiahe Formation in Guang'an gas field, Zhongba gas field, and Bajiaochang gas field is between 0.88% and 1.15% (Dai et al., 2016), which also proves that the carbon dioxide in these gas fields is of thermogenic origin. Among them, there are individual wells showing a $\delta^{13}C_{CO2}$ value of inorganic origin, that is, Well Jiao49 has a $\delta^{13}C_{CO2}$ value of −6.2‰, which is inorganic CO_2 formed by dissolution of carbonates through organic acid, such as Well Pu1 in Ordos Basin, whose $\delta^{13}C_{CO2}$ value of −6.39‰ results from the dissolution of carbonates by organic acid (Dai et al., 1992).

CO_2 in Wenxingchang gas field, Xujiahe Formation gas reservoir of Longgang gas field, Wolonghe gas field, Dachiganjing gas field, Zhangjiachang gas field, Bandong gas field, Xiangguosi gas field, and Weiyuan gas field are of cracking origin. The $\delta^{13}C_{CO2}$ value of 34 gas samples fall between −23.4 and −10.3‰, with an average of −15.7‰. The wetness of 33 gas samples ranges from 0.08% to 7.04%, with an average of 1.30%. Alkane gas accompanied with CO_2 of thermogenic origin is often dry gas, which also proves that CO_2 is of thermogenic origin. It can be seen from **Figure 7** that there are only thermogenic CO_2 (in the area of OA) and cracking CO_2 (in the area of LMT) among the biogenic gas in the Sichuan Basin, and no microbial degradation type CO_2 (EMT).

In addition to the abovementioned thermal decomposition and cracking CO_2, in **Supplementary Table S1**, among Xujiahe Formation gas reservoir and Leikoupo Formation gas reservoir of Xinchang gas field, Western Sichuan gas field, Qiongxi gas field, Pingluoba gas field, Leikoupo Formation gas reservoir of Longgang gas field, Feixianguan Formation gas reservoir, Changxing Formation gas reservoir, and Permian gas reservoir of Yuanba gas field, Feixianguan Formation gas reservoir of Puguang gas field, and Longwangmiao Formation gas reservoir and Dengying Formation gas reservoir of Anyue gas field, the

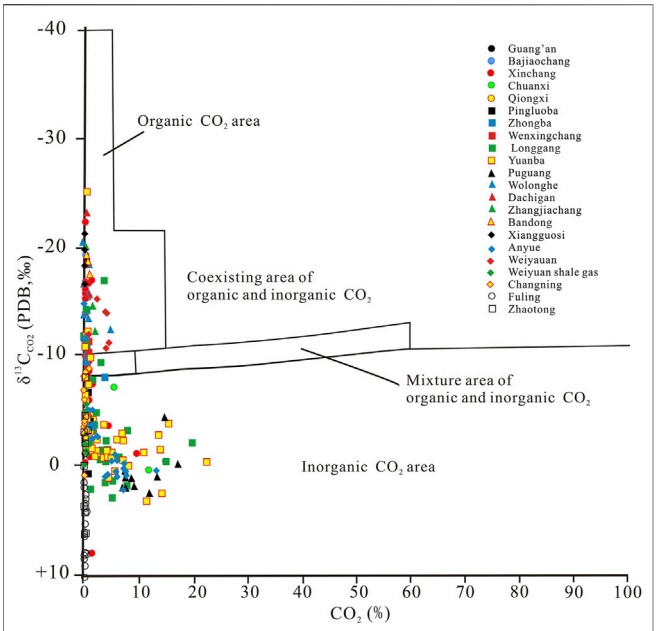

FIGURE 6 | Identification of CO_2 origin of natural gas in the Sichuan Basin (Dai et al., 1996).

majority is dry gas. Based on the analysis of 120 gas samples, the $\delta^{13}C_{CO2}$ value ranges from 8.1 to 17.2‰, with an average of 2.4‰. According to the analysis of 118 gas samples, the gas wetness is 0.02%–11.5%, with an average value of 1.02%. **Supplementary Table S2** shows the $\delta^{13}C_{CO2}$ values of shale gas from Weiyuan, Changning, Fuling, and Zhaotong shale gas fields. According to the analysis of 55 gas samples, the $\delta^{13}C_{CO2}$ value ranges from −9.2‰ (well N211) to 10.4‰ (well JY47-3), with an average value of 0.42‰. According to the analysis of 54 gas samples, the gas wetness ranges from 0.28% to 0.79% with an average of 0.47%. It can be seen from **Table 1** and **Figure 6** that CO_2 in the abovementioned gas fields is of inorganic origin.

According to the genetic type, inorganic CO_2 can be subdivided into upper mantle degassing, volcanic magmatic source, and thermal metamorphism or organic acid dissolution of carbonate rocks (minerals) (**Table 1**). The shale gas is characterized by $\delta^{13}C_1 > \delta^{13}C_2 > \delta^{13}C_3$, belonging to the secondary negative carbon isotope series (Dai et al., 2016). For the Marcellus shale gas, which has the largest annual production, when the gas wetness (W) is less than 1.49%–1.57%, the secondary negative carbon isotope series appear (Jenden et al., 1993). The gas wetness of the four shale gas fields in **Supplementary Table S2** is between 0.28% (well NH3-6) and 0.79% (well JY12-2), so they all have negative carbon isotope series. The negative carbon isotope series only occur in the thermogenic gas in the over-mature area, and the R_O% of the gas source rocks is greater than 2%. As shown in **Supplementary Table S2**, the R_O% value of Wufeng–Longmaxi shale in Changning, Zhaotong, and Fuling shale gas fields fall in the range of 2.1%–3.85% (Dai et al., 2014; Guo and Zeng, 2015; Dai et al., 2016; Liu S et al., 2016; Feng et al., 2020). Since the shale of Wufeng–Longmaxi formations is rich in carbonate minerals (Dai et al., 2014; Dai et al., 2016; Feng et al., 2020) and is at the over-mature stage, these two factors together led to inorganic CO_2 from thermal metamorphism of carbonate minerals. **Figure 8** clearly shows that the CO_2 from the four shale gas fields is of inorganic origin related to carbonate minerals. However, the $\delta^{13}C_{CO2}$ values of the four shale gas fields in **Figure 7** mainly fall in the thermogenic area (LMT), so the $\delta^{13}C_{CO2}$ value in **Figure 7** is in the range of −8‰ to 10‰, which should be classified as inorganic CO_2 from thermal metamorphism of carbonate minerals.

Calcareous sandstone is widely distributed in the fourth member of Xujiahe Formation (T_3x^4) in Western Sichuan depression, and carbonate rock debris accounts for more than 50% of calcium debris (Lin et al., 2007; Lin et al., 2012). Calcareous sandstone is also developed in the third member of Xujiahe Formation (T_3x^3) in the Yuanba area. Carbonate debris which is dissolved by organic acid is discharged during the compaction of mudstone in the third member of Xujiahe Formation in the late diagenetic stage of Xujiahe Formation (Ma, 2012), forming organic acid dissolved CO_2 in inorganic carbonate rocks of Xujiahe Formation in Yuanba gas field (Dai et al., 2013). However, according to **Supplementary Table S1**, Xujiahe Formation gas reservoir of Yuanba gas field is characterized by dry gas, with gas wetness mainly between 0.39% and 1.51%, and $\delta^{13}C_{CO2}$ value between −7.5‰ and 0.5‰, so CO_2 in Xujiahe Formation gas reservoir of Yuanba gas field should also include CO_2 derived from the thermal metamorphism of carbonate mineral. The Xujiahe Formation gas reservoirs of Pingluoba gas field and Qiongxi gas field are similar to Yuanba gas reservoir with dry natural gas, so the

TABLE 2 | $\delta^{13}C$ values of various carbon-bearing materials (Dai et al., 2000).

Type of carbon	Carbon-bearing materials	$\delta^{13}C$ (‰)
Organic carbon	Chinese oil	−34.57 to −23.50
	Chinese coal	−30.80 to −21.54
	Chinese mudstone kerogen	−30.86 to −19.38
	Chinese carbonate rock kerogen	−35.04 to −24.34
	Terrestrial plants and animals	Mean to −25.5
	Marine organisms (including plankton)	−22 to −9.0
Inorganic carbon	Diamond	−9 to −2
	Marine inorganic carbon	−1.0 to +2.0
	Dissolved carbon in fresh water	−11.0 to −5.0
	Dolomite	−2.29 to +2.66
	Marine limestone	−9.0 to +6.0
	Nonmarine limestone	−8.0 to −3.0

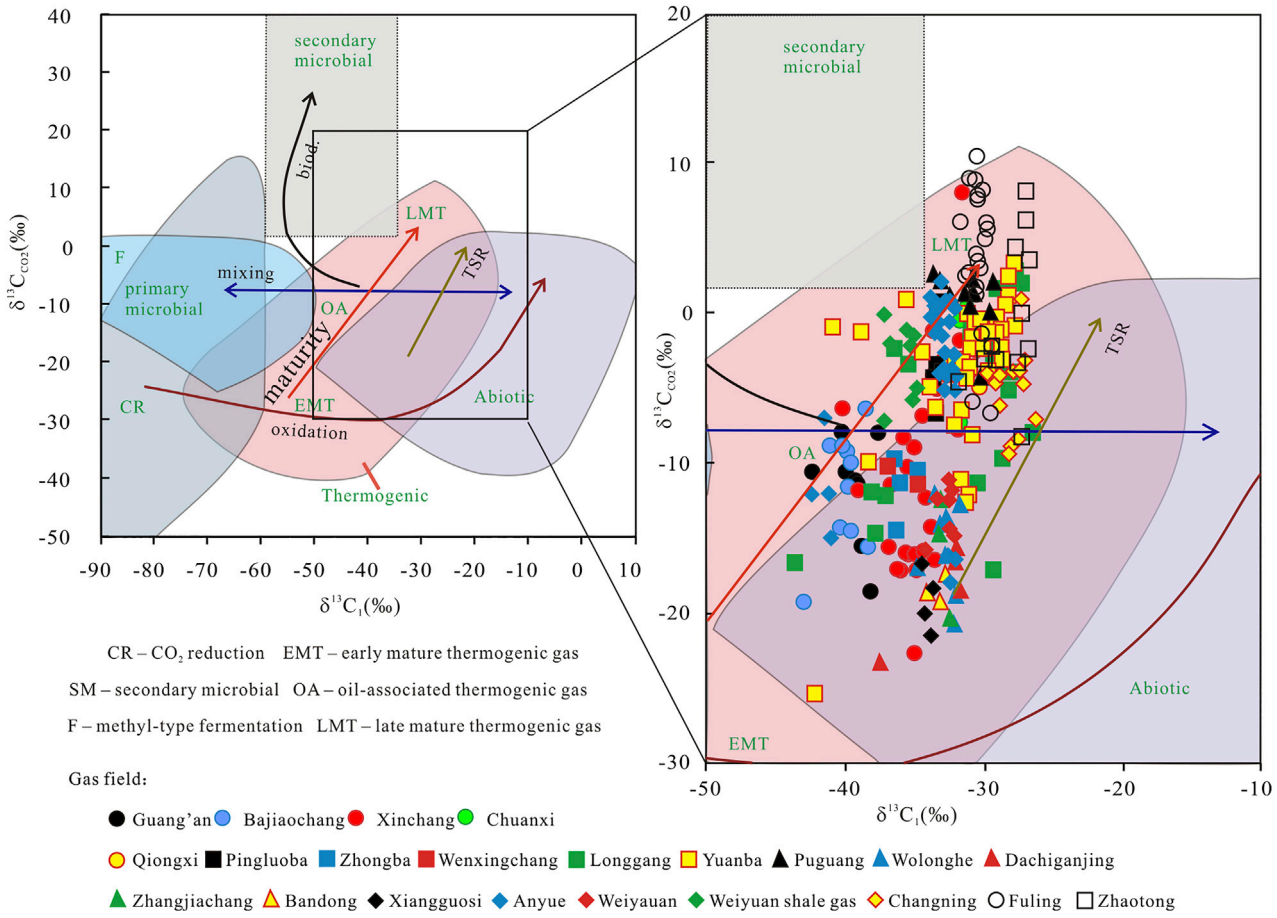

FIGURE 7 | Plot of $\delta^{13}C_1$–$\delta^{13}C_{CO2}$ of natural gases from gas fields in the Sichuan Basin (Modified after Milkov and Etiope, 2018).

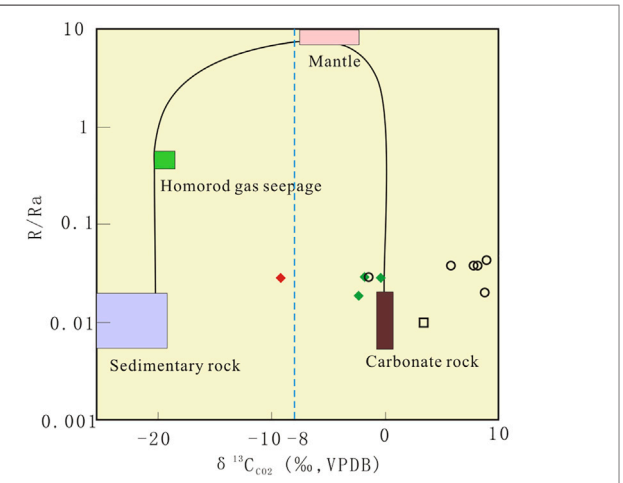

FIGURE 8 | Comparison diagram of natural gas R/Ra–$\delta^{13}C_{CO2}$ in the Sichuan Basin (Modified after Etiope et al., 2011).

CO_2 in these gas fields should also originate from thermal metamorphism of carbonate minerals.

In **Supplementary Table S1**, the Leikoupo Formation gas reservoir of Xinchang gas field, Leikoupo Formation gas reservoir of Longgang gas field, Feixianguan Formation gas reservoir, Changxing Formation gas reservoir, and Leikoupo Formation gas reservoir of Yuanba gas field, Feixianguan Formation gas reservoir and Changxing Formation gas reservoir of Puguang gas field, and Longwangmiao and Dengying (Z_2dn) formations gas reservoirs of Anyue gas field are characterized by carbonate rock reservoir and dry natural gas. Therefore, they should also produce carbonate mineral thermal metamorphism type of CO_2.

3.2.3 $\delta^{13}C_{CO2} > \delta^{13}C_1$

Figure 9 shows the carbon isotope of coexisting carbon dioxide and methane from the 22 gas fields, which shows a wide range of $\delta^{13}C_{CO2}$ (35.8‰) but a relatively narrow range of $\delta^{13}C_1$ (17.2‰). They are characterized by $\delta^{13}C_{CO2} > \delta^{13}C_1$, which is found in all geological age (from Z_2dn to J_2s) gas reservoirs and various gas types (coal-derived gas, oil-associated gas, and shale gas). The

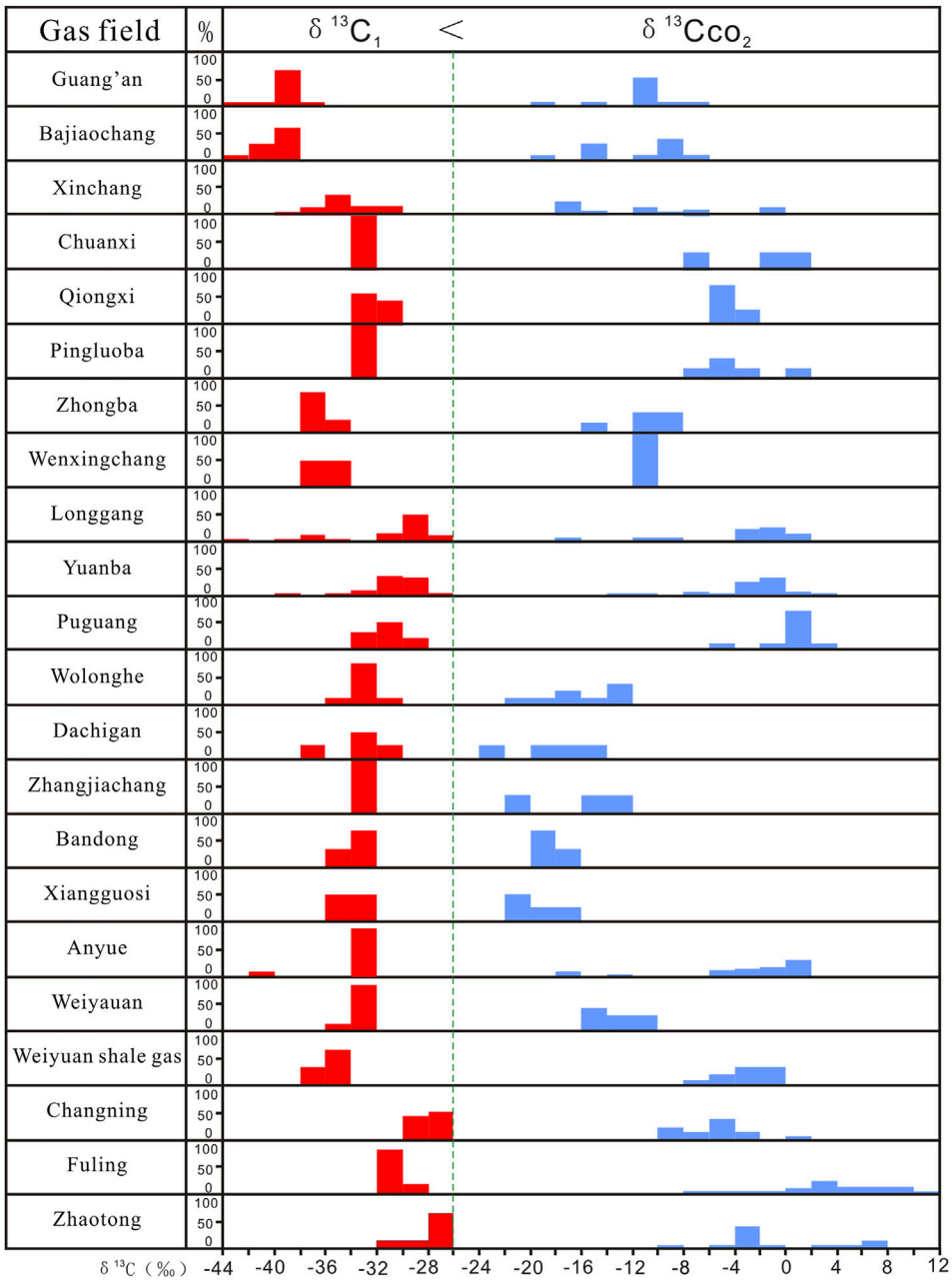

FIGURE 9 | Comparison of carbon isotopic value of methane and CO_2 in natural gas from the Sichuan Basin.

difference between $\delta^{13}C_{CO2}$ and $\delta^{13}C_1$ ($\delta^{13}C_{CO2\text{-}CH4}$) for individual gas samples varies between 11.4‰ (Wolonghe gas field) and 40.9‰ (Fuling shale gas field), with an average of 27.0‰ (n = 261).

Carbon isotopic changes of CH_4 and CO_2 mainly result from the different sources. Sources of methane mainly include bacterial, thermogenic, and inorganic. Bacterial methane is normally generated at low temperature and depleted in ^{13}C ($\delta^{13}C$ < −50‰), thermogenic methane is formed at elevated temperatures by decomposition or cracking of organic matter and generally characterized by −50‰<$\delta^{13}C$ < −30‰, and inorganic methane derived from mantle degassing or reactions at high temperatures is enriched in ^{13}C ($\delta^{13}C$ > −30‰). As discussed previously, sources of carbon dioxide mainly include thermogenic and inorganic. CO_2 formed through the decomposition or cracking of organic matter is relatively depleted in ^{13}C (<−10‰, mainly of −10‰ to −30‰), while CO_2 derived from mantle degassing, volcanic magmatic source, and thermal metamorphism or organic acid dissolution of carbonate rocks (minerals) are much more enriched in ^{13}C (>−8‰, mainly of −8‰~+3‰).

As shown in **Figure 10**, $\delta^{13}C_{CO2}$ varies between −25.4‰ and 10.4‰, with an average of −5.8‰ (n = 263), while $\delta^{13}C_1$ varies

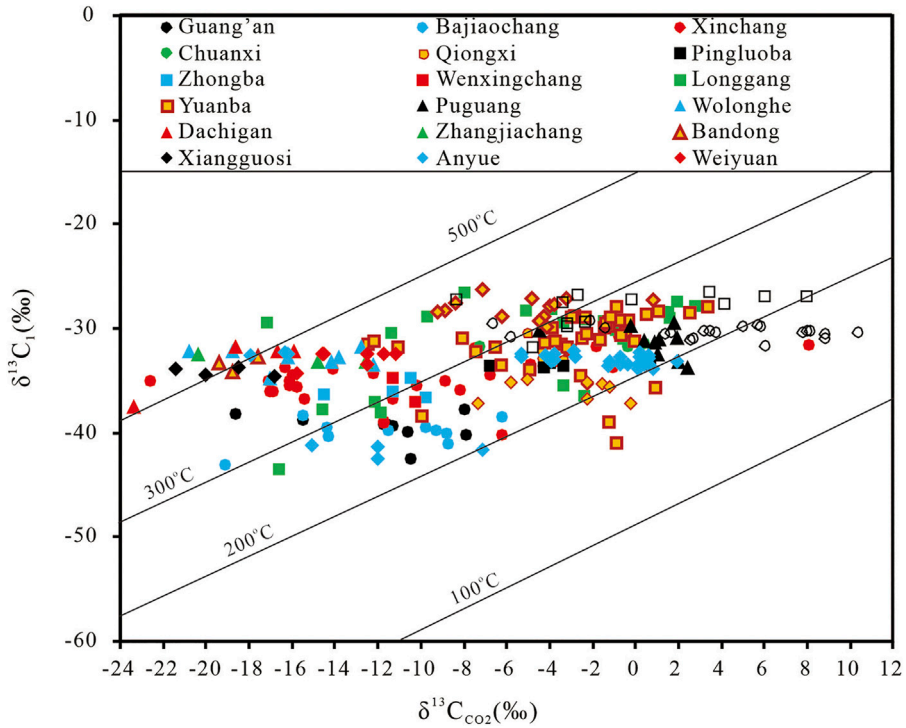

FIGURE 10 | Plot of $\delta^{13}C$ values of CO_2 and coexisting CH_4. Isotherms for hypothetical isotopic equilibrium are from Richet et al. (1977).

between −43.5‰ and −26.3‰, with an average of −32.8‰ ($n = 261$). The variation range of CO_2 (35.8‰) is nearly twice that of CH_4 (17.2‰). According to the $\delta^{13}C$ values of methane, alkane gases from these 22 gas fields all belong to thermogenic gas. In contrast, sources of CO_2 include both organic and inorganic. Organic CO_2 commonly has carbon isotopic composition lower than −10‰, and the lowest $\delta^{13}C_{CO2}$ value of −25.4‰ is found in the Yuanba gas field. Since thermogenic methane has $\delta^{13}C_1<\delta^{13}C_{CO2}$, the carbon isotopic difference between thermogenic methane and organic CO_2 ($\delta^{13}C_{CO2\text{-}CH4}$) is relatively small, and the smallest carbon isotopic difference of 11.4‰ is found in the Wolonghe gas field. Since inorganic CO_2 is characterized by much heavier carbon isotopic compositions ($\delta^{13}C_{CO2}>-8$‰), the carbon isotopic difference between thermogenic methane and inorganic CO_2 ($\delta^{13}C_{CO2\text{-}CH4}$) will be bigger, and the biggest carbon isotopic difference of 40.9‰ is found in the Fuling shale gas field. CO_2 generated from the thermos-metamorphic process of carbonates is enriched in ^{13}C. As in the CO_2–calcite system, carbon isotope fractionation will cause the enrichment of ^{13}C in CO_2 at high temperature; therefore, CO_2 produced by decarbonation reactions will be more enriched in ^{13}C than that in the original carbonates (Giustini et al., 2013). $\delta^{13}C$ of Phanerozoic seawater is generally stable, and the Phanerozoic low magnesium calcite shells have $\delta^{13}C$ values of −2 to +6‰ (Veizer et al., 1999; Dong et al., 2021). $\delta^{13}C$ values of carbonate cement of sandstone from the Silurian Formation in southeast Sichuan vary from −1.90‰ to 4.78‰ with an average value of 1.42‰ ($n = 14$) (An et al., 2015). However, positive carbon isotopic excursion of both shales and limestones has been found in the Late Ordovician Hirnantian stage in North America (Orth et al., 1986; BergstrÖM et al., 2006), Europe (Brenchley et al., 1994; Marshall et al., 1997), and China (Wang et al., 1997; Fan et al., 2009). The positive carbon isotopic excursion can be up to 5–7‰ in the Hirnantian limestones (Qing and Veizer, 1994; Marshall et al., 1997). A recent study found that diffusive migration of shale gas occurs in the southern Sichuan Basin (Ni et al., 2021). Therefore, if assuming an infinite reservoir of C compared with CO_2 generated by decarbonation and the CO_2 decarbonated does not isotopically fractionate on its way to the surface in the absence of water, metamorphic reactions between carbonate and silicate occur at 600 °C (Muffler and White, 1968), and the produced CO_2 will be enriched in ^{13}C by about +2.6‰ compared with that of $CaCO_3$ (Ohmoto and Rye, 1979). Then, it will produce a gas with $\delta^{13}C$ around 4‰, and if considering the carbon isotopic excursion, it will be around 10‰ (Giustini et al., 2013). While in the presence of water, metamorphic reactions between carbonate and silicate begin with T > 200°C (Muffler and White, 1968), and the produced CO_2 will be enriched in ^{13}C by 1.3‰ at a temperature around 250°C (Ohmoto and Rye, 1979). Then, it will produce a gas with $\delta^{13}C$ around 2.7‰, and if considering the carbon isotopic excursion, it will be around 9‰ (Giustini et al., 2013).

4 GEOLOGICAL IMPLICATIONS

The three types of CO_2 gases are characterized by different geochemical characteristics and different reservoir types, and distributed in different sedimentary basins. Type A organic CO_2, generated from the thermal decomposition of organic matter, was mainly formed in the craton basin, where organic matter was

controlled by thermal evolution. The CO_2 content and carbon isotope composition were different at different stages of thermal evolution, but the CO_2 abundance was generally relatively low, such as the Upper Paleozoic gas reservoir in Ordos Basin. Type B organic CO_2 was formed through the cracking of organic matter or hydrocarbons at higher thermal maturity. For example, CO_2 in the over-mature coal-derived gas from the Kuqa depression in the Tarim basin was mainly formed through the cracking of organic matter. Thermal cracking of crude oil in the marine gas reservoirs can also form cracking CO_2 of organic origin such as the CO_2 in the Tazhong and Tabei deep natural gas. Type C inorganic CO_2 has complex sources and pathways, including the thermal metamorphism or thermal decomposition of deep carbonates, organic acid dissolution, TSR, and mantle degassing. High temperature is required for the thermal metamorphism or thermal decomposition of deep carbonates such as the CO_2-rich gas reservoirs in Yinggehai Basin. CO_2 formed through the organic acid dissolution is mainly distributed in the gas reservoirs where TSR occurs such as the Ordovician marine facies Jianbian gas field in the Ordos Basin and the marine gas reservoirs in Sichuan Basin. Inorganic mantle-derived CO_2 is mainly controlled by deep faults such as Fangshen two and Songnan gas reservoirs in Songliao Basin and Huangqiao gas reservoir in Subei Basin. The content of inorganic CO_2 varies widely. Generally, the content of deep mantle-derived CO_2 is more than 60%, while the content of carbonate decomposition and organic acid dissolution depends on gas reservoir temperature and source supply. In short, different geological backgrounds and evolutionary histories will form different types of CO_2, and their content is also very different.

5 CONCLUSION

The Sichuan Basin is a large superimposed basin developed on the basis of craton, with an area of about 180×10^3 km^2. It has excellent geological conditions for natural gas development: ① The thickness of sedimentary rocks is 6,000–12,000 m, the maturity of source rocks is high, there are nine sets of main gas source rocks, and the equivalent ratio of gas to oil production is 80:1, so it is a gas basin. ② It is rich in conventional and unconventional gas resources, and the remaining recoverable resources of conventional and unconventional natural gas amounts to 13.6404×10^{12} m^3. The total proved geological reserves of natural gas was 5.7966×10^{12} m^3, and the cumulative gas production of the basin was 648.8×10^9 m^3 by the end of 2019. ③ There are many gas-bearing formations and systems, including 25 conventional and tight oil and gas producing formations (18 marine facies) and two shale gas–producing formations. ④ A total of 135 gas fields had been discovered by the end of 2019. Anyue gas field, the largest gas field and the largest carbonate gas field in China, had proved geological reserves of 1.1709×10^{12} m^3, with an annual output of 120×10^8 m^3 in 2019.

Carbon dioxide composition of CO_2 in Sichuan Basin is characterized by two features: ① The content of carbon dioxide is low. Based on 243 CO_2 components collected from 22 gas fields, the content ranges from 0.02% to 22.90%, with an average value of 2.96%, which is lower than the average value of 3.58% of 1025 CO_2 components in 48 large gas fields developed in China. ② Carbon dioxide in cratonic basins is featured with a combination of a low CO_2 content (generally <5%) and a low R/Ra ratio (<0.24), while carbon dioxide in rift basins is typically characterized by large variation of the CO_2 content (0.0n% – > 95%) and large variation of the R/Ra ratio (0.0n – n).

Based on the $\delta^{13}C_{CO2}$ values of 263 samples in Sichuan Basin and their correlation with R/Ra, $\delta^{13}C_1$, CO_2 content, and gas wetness, it is observed that $\delta^{13}C_{CO2}$ has three characteristics: ① $\delta^{13}C_{CO2}$ (10.4‰) in Fuling shale gas field was found to be the highest in China, making the interval value of $\delta^{13}C_{CO2}$ of China expand from −39‰–7‰ to −39–10.4‰. ② According to the $\delta^{13}C_{CO2}$ value, three types of CO_2 were identified: A. organic CO_2 formed by the thermal decomposition of organic matter. The $\delta^{13}C_{CO2}$ values of 44 samples range from −6.2 to −22.6‰, with an average value of −12.8‰, and the gas wetness of 37 samples ranges from 3.2% to 17.7%, with an average of 7.8%; B. organic CO_2 formed by the cracking of organic matter. The $\delta^{13}C_{CO2}$ values of 34 samples range from −10.3‰ to −23.4‰, with an average value of −15.7‰, and gas wetness of 33 samples ranges from 0.08% to 7.04%, with an average value of 1.30%; C. inorganic CO_2 formed by the dissolution of carbonates through metamorphism or organic acid. $\delta^{13}C_{CO2}$ values of 175 samples range from −17.2 to 10.4‰, with an average value of −1.8‰, and gas wetness of 172 samples ranges from 0.02% to 11.5%, with an average value of 0.85%; ③ $\delta^{13}C_{CO2} > \delta^{13}C_1$, which is a characteristic shared by all geological age (from Z_2dn to J_2s) gas reservoirs and various gas types (coal-derived gas, oil-associated gas, and shale gas).

DATA AVAILABILITY STATEMENT

The original contributions presented in the study are included in the article/**Supplementary Material**, further inquiries can be directed to the corresponding author.

AUTHOR CONTRIBUTIONS

JD: manuscript writing and design, data collection. YN: manuscript writing and revision, sample analyses. QL: manuscript revision and data collection. XW, CY and DG: manuscript revision. FH, YZ and ZY: manuscript preparation.

FUNDING

This study is funded by the National Key Research and Development Projects of China (Grant No. 2019YFC1805505), the PetroChina Scientific Research and Technology Development Project (2017D-5008-08), and the National Natural Science Foundation of China (Grant Nos.: U20B6001, 42172149, and 42141021).

SUPPLEMENTARY MATERIAL

The Supplementary Material for this article can be found online at: https://www.frontiersin.org/articles/10.3389/feart.2022.857876/full#supplementary-material

REFERENCES

An, Q., Huang, D., and Zhu, Z. (2015). Carbon and Oxygen Isotope Geochemistry for Carbonate Cement of the Lower Silurian Xiaoheba Formation Sandstone in Southeast Sichuan-West Hunan. *Acta Geologica Sichuan* 35 (1), 157–160.

Barker, C. (1983). *Petroleum Generation and Occurrence for Exploration Geologists*. Testbook of OGCI.

BergstrÖM, S. M., Saltzman, M. M., and Schmitz, B. (2006). First Record of the Hirnantian (Upper Ordovician) $\delta^{13}C$ Excursion in the North American Midcontinent and its Regional Implications. *Geol. Mag.* 43 (5), 657–678.

Brenchley, P. J., Marshall, J. D., Carden, G. A. F., Robertson, D. B. R., Long, D. G. F., Meidla, T., et al. (1994). Bathymetric and Isotopic Evidence for a Short-Lived Late Ordovician Glaciation in a Greenhouse Period. *Geology* 22 (4), 295–298. doi:10.1130/0091-7613(1994)022<0295:baiefa>2.3.co;2

Cao, B., Mz, C., Lla, B., Ywb, D., Zla, B., Dab, L., et al. (2020). Tracing the Sources and Evolution Processes of Shale Gas by Coupling sTable (C, H) and noble Gas Isotopic Compositions: Cases from Weiyuan and Changning in Sichuan Basin, China. *J. Nat. Gas Sci. Eng.* 78. doi:10.1016/j.jngse.2020.103304

Chen, Z., Chen, L., Wang, G., Zou, C., Jiang, S., Si, Z., et al. (2020). Applying Isotopic Geochemical Proxy for Gas Content Prediction of Longmaxi Shale in the Sichuan Basin, China. *Mar. Pet. Geology*. 116 (C8), 104329. doi:10.1016/j.marpetgeo.2020.104329

Cornides, I. (1993). Magmatic Carbon Dioxide at the Crust's Surface in the Carpathian Basin. *Geochem. J.* 27, 241–249. doi:10.2343/geochemj.27.241

Dai, J., Chen, J., Zhong, N., Pang, X., and Qin, S. (2003). *Large Gas fields and Their Gas Sources in China*. Beijing: Science Press, 37–44.

Dai, J. (1981). Geographical Distribution of Oil and Gas Discovered in Ancient China. *Oil & Gas Geology*. 2 (3), 292–299.

Dai, J. (2016). *Giant Coal-Derived Gas fields and Their Gas Sources in China*. Beijing: Science Press, 180–186. 210-214, 241-254.

Dai, J., Liao, F., and Ni, Y. (2013). Discussions on the gas source of the Triassic Xujiahe Formation tight sandstone gas reservoirs in Yuanba and Tongnanba, Sichuan Basin: An answer to Yinfeng et al. *Pet. Exploration Dev.* 40 (2), 250–256. doi:10.1016/s1876-3804(13)60033-6

Dai, J., Ni, Y., Huang, S., Gong, D., Liu, D., Feng, Z., et al. (2016). Secondary Origin of Negative Carbon Isotopic Series in Natural Gas. *J. Nat. Gas Geosci.* 1 (1), 1–7. doi:10.1016/j.jnggs.2016.02.002

Dai, J., Ni, Y., Liu, Q., Wu, X., Gong, D., Hong, F., et al. (2021). Sichuan Super Gas basin in Southwest China. *Pet. Exploration Dev.* 48 (6), 1–8. doi:10.1016/s1876-3804(21)60284-7

Dai, J., Ni, Y., Qin, S., Huang, S., Gong, D., Liu, D., et al. (2017). Geochemical Characteristics of He and CO 2 from the Ordos (Cratonic) and Bohaibay (Rift) Basins in China. *Chem. Geology*. 469, 192–213. doi:10.1016/j.chemgeo.2017.02.011

Dai, J., Ni, Y., Qin, S., Huang, S., Peng, W., and Han, W. (2018). Geochemical Characteristics of Ultra-deep Natural Gas in the Sichuan Basin, SW China. *Pet. Exploration Dev.* 45 (4), 619–628. doi:10.1016/s1876-3804(18)30067-3

Dai, J., Pei, X., and Qi, H. (1992). *Natural Gas Geology of China·Volume 1*. Beijing: Petroleum Industry Press, 46–50.

Dai, J., Qi, H., and Hao, S. (1989). *Survey of Natural Gas Geology*. Beijing: Petroleum Industry Press, 30–42.

Dai, J., Song, Y., and Dai, C. (2000). *Conditions Governing the Formation of Abiogenic Gas and Gas Pools in Eastern China*. Beijing, New York. 1-4, 19-23, 42-60, 73-200.

Dai, J., Song, Y., and Dai, C. (1996). Geochemistry and Accumulation of Carbon Dioxide Gases in China. *AAPG Bull.* 80 (10), 1615–1626. doi:10.1306/64eda0d2-1724-11d7-8645000102c1865d

Dai, J. (2019). The Four Major Onshore Gas Provinces in China. *Nat. Gas Oil* 37 (2), 1–6.

Dai, J., Zou, C., Liao, S., Dong, D., Ni, Y., Huang, J., et al. (2014). Geochemistry of the Extremely High thermal Maturity Longmaxi Shale Gas, Southern Sichuan Basin. *Org. Geochem.* 74, 3–12. doi:10.1016/j.orggeochem.2014.01.018

Deng, Y., Hu, G., and Zhao, C. (2018). Geochemical Characteristics and Origin of Natural Gas in Changxing-Feixianguan Formtions from Longgang Gas Field in the Sichuan Basin, China. *Nat. Gas Geosci.* 29 (6), 892–907.

Diao, H. (2019). Sources of Natural Gas and Carbon Dioxide in Lishui Sag, East China Sea Basin. *Shanghai Land Resour.* 40 (4), 101–105.

Dong, Q., Hu, Z., and Chen, S. (2021). Isotope Geochemical Responses and Their Geological Significance of Changxing-Feixianguan Formation Carbonates, Northeastern Sichuan Basin. *Oil Gas Geology*. 42 (6), 1307–1320.

Etiope, G., Baciu, C. L., and Schoell, M. (2011). Extreme Methane Deuterium, Nitrogen and Helium Enrichment in Natural Gas from the Homorod Seep (Romania). *Chem. Geology*. 280, 89–96. doi:10.1016/j.chemgeo.2010.10.019

Fan, J. X., Peng, P. A., and Melchin, M. J. (2009). Carbon Isotopes and Event Stratigraphy Near the Ordovician–Silurian Boundary, Yichang, South China. *Palaeogeogr. Palaeoclimatol. Palaeoecol.* 276 (1), 160–169. doi:10.1016/j.palaeo.2009.03.007

Fan, R., Zhou, H., and Cai, K. (2005). Carbon Istopic Geochemistry and Origin of Natural Gas in Southern Part of the Western Sichuan Depression. *Acta Geoscientica Sinica* 26 (2), 157–162.

Feng, Z., Hao, F., Dong, D., Zhou, S., and Li, Z. (2020). Geochemical Anomalies in the Lower Silurian Shale Gas from the Sichuan Basin, China: Iosights from a Rayleigh-type Fractionation Model. *Org. Geochem.* 142. doi:10.1016/j.orggeochem.2020.103981

Fryklund, B., and Stark, P. (2020). Super Basins-New Paradigm for Oil and Gas Supply. *Bulletin* 104 (12), 2507–2519. doi:10.1306/09182017314

Fu, X., Li, C., Wang, X., and Hao, J. (2004). Forming Conditions of CO_2 Gas Reservoir in Sanshui Basin. *Nat. Gas Geosci.* 15 (4), 428–431.

Giustini, F., Blessing, M., Brilli, M., Lombardi, S., Voltattorni, N., and Widory, D. (2013). Determining the Origin of Carbon Dioxide and Methane in the Gaseous Emissions of the San Vittorino plain (Central Italy) by Means of Stable Isotopes and noble Gas Analysis. *Appl. Geochem.* 34, 90–101. doi:10.1016/j.apgeochem.2013.02.015

Gould, K. W., Hart, G. N., and Smith, J. W. (1981). Technical Note: Carbon Dioxide in the Southern Coalfields N.S.W.—A Factor in the Evolution of Natural Gas Potential. *Proceeding Australas. Inst. Mining Metall.* 279, 41–42.

Guo, T., and Zeng, P. (2015). The Structural and Preservation Conditions for Shale Gas Enrichment and High Productivity in the Wufeng-Longmaxi Formation, Southeastern Sichuan Basin. *Energy Exploration & Exploitation* 33 (3), 259–276. doi:10.1260/0144-5987.33.3.259

Guo, X., and Guo, T. (2012). *Theory and Exploration Practice of Puguang and Yuanba Giant Gas Field in Platform Margin*. Beijing: Science Press.

He, J. (1995). Preliminary Study on CO_2 Natural Gas in Yinggehai Basin. *Nat. Gas Geosciences* 29 (6), 1–12.

Hoefs, J. (1978). Some Peculiarities in the Carbon Isotope Composition of "Juvenile Carbon": sTable Isotopes in the Earth Science. *DSIR Bull.* 200, 181–184.

Hu, G., Yu, C., Gong, D., Tian, X., and Wu, W. (2014). The Origin of Natural Gas and Influence on Hydrogen Isotope of Methane by TSR in the Upper Permian Changxing and the Lower Triassic Feixianguan Formations in Northern Sichuan Basin, SW China. *Energy Exploration & Exploitation* 32, 139–158. doi:10.1260/0144-5987.32.1.139

Hunt, J. M. (1979). *Petroleum Geochemistry and Geology*. San Francisco: W. H. Freeman.

Javoy, M., Pineau, F., and Iiyama, I. (1978). Experimental Determination of the Isotopic Fractionation between Gaseous CO_2 and Carbon Dissolved in Tholeiitic Magma. *Contr. Mineral. Petrol.* 67, 35–39. doi:10.1007/bf00371631

Jenden, P. D., Drazan, D. J., and Kaplan, I. R. (1993). Mixing of Thermogenic Natural Gas in Northern Appalachian Basin. *AAPG Bull.* 77 (6), 980–998. doi:10.1306/bdff8dbc-1718-11d7-8645000102c1865d

Li, D., Li, W., and Wang, Z. (2007). The Natural Gas Genesis Type and Gas-Source at Analysis of Guang'an Gas Field in the Middle of Sichuan Basin. *Geology. China* 34 (5), 829–836.

Li, J., Li, J., Li, Z., Zhang, C., Cui, H., and Zhu, Z. (2018). *Characteristics and Genetic Types of the Lower Paleozoic Natural Gas, Ordos Basin*. Marine & Petroleum Geology, 89106–89119.

Li, J., Zheng, M., Guo, Q., and Wang, S. (2019). *Forth Assessment for Oil and Gas Resource*. Beijing: Petroleum Industry Press, 203–270.

Li, P., Hao, F., Guo, X., Zou, H., Yu, X., and Wang, G. (2015). Processes Involved in the Origin and Accumulation of Hydrocarbon Gases in the Yuanba Gas Field,

Sichuan Basin, Southwest China. *Mar. Pet. Geology*. 59, 150–165. doi:10.1016/j.marpetgeo.2014.08.003

Liao, F., Wu, X., and Huang, S. (2012). Geochemical Characteristics of CO_2 Gases in Eastern China and the Distribution Patterns of Their Accumulations. *Acta Petrologica Sinica* 28 (3), 939–948.

Lin, X., Liu, L., and Wei, L. (2007). Prediction of Calcarenaceous sandstone Gas-Bearing Reservoir in the 4th Member, Xujiahe Formation in Fenggu Area, West Sichuan basin. *J. Southwest Pet. Univ.* 29 (4), 82–84.

Lin, Y., Wu, S., Xu, Z., and Ni, Y. (2012). Controlling Factors for T3x4 Calcarenaceous sandstone in Fenggu Structure, Western Sichuan Basin. *Nat. Gas Geosci.* 23 (4), 691–699.

Liu, D., Zhang, W., Kong, Q., Feng, Z., Fang, C., and Peng, W. (2016). Lower Paleozoic Source Rocks and Natural Gas Origins in Ordos Basin, NW China. *Pet. Exploration Dev.* 43 (4), 540–549. doi:10.1016/s1876-3804(16)30069-6

Liu, Q., Jin, Z., Li, H., Wu, X., Tao, X., Zhu, D., et al. (2018). Geochemistry Characteristics and Genetic Types of Natural Gas in central Part of the Tarim Basin, NW China. *Mar. Pet. Geology*. 89, 91–105. doi:10.1016/j.marpetgeo.2017.05.002

Liu, S., Lu, X., Hong, F., Fu, X., San, X., Wei, L., et al. (2016). *Accumulation Mechanisms and Distribution Patterns of CO_2-containing Natural Gas Reservoirs in the Songliao Basin*. Beijing: Science Press. 6-12、41-47.

Ma, R. (2012). Main Controlling Factors of Gas Accumulation in the Calcarenaceous sandstone Reservoirs in the 3rd Member of the Xujiahe Formation in the YB Area. *Nat. Gas Industry* 38 (8), 56–62.

Marshall, J. D., Brenchley, P. J., Mason, P., Wolff, G. A., Astini, R. A., Hints, L., et al. (1997). Global Carbon Isotopic Events Associated with Mass Extinction and Glaciation in the Late Ordovician. *Palaeogeogr. Palaeoclimatol. Palaeoecol.* 132 (1), 195–210. doi:10.1016/s0031-0182(97)00063-1

Meyerhoff, A. A. (19701969). Developments in Mainland China. *AAPG Bull.* 54 (8), 1949. doi:10.1306/5d25cbd1-16c1-11d7-8645000102c1865d

Milkov, A. V., and Etiope, G. (2018). Revised Genetic Diagrams for Natural Gases Based on a Global Dataset of >20,000 Samples. *Org. Geochem.* 125, 109–120. doi:10.1016/j.orggeochem.2018.09.002

Moore, J. G., Backelder, N., and Cunningham, C. G. (1977). CO_2 Filled Vesicle in Mid-ocean basalt. *J.Valcano. Gestherm. Res.* 2, 309. doi:10.1016/0377-0273(77)90018-x

Muffler, F. J. P., and White, D. E. (1968). Origin of CO_2 in the Salton Sea Geothermal System, southeastern California. *U.S.A. XXIII International Geol. Congress* 17, 185–194.

Ni, Y., Dai, J., Tao, S., Wu, X., Liao, F., Wu, W., et al. (2014). Helium Signatures of Gases from the Sichuan Basin, China. *Org. Geochem.* 74, 33–43. doi:10.1016/j.orggeochem.2014.03.007

Ni, Y., Yao, L., and Liao, F. (2021). Geochemical Comparison of the Deep Gases from the Sichuan and Tarim Basins, China. *Front. Earth Sci.* 9, 1–22. doi:10.3389/feart.2021.634921

Ohmoto, H., and Rye, R. O. (1979). "Isotope of Sulfur and Carbon," in *Geochemistry of Hydrothermal Deposits*. Editor H. L. Barnes (New York: John Wiley & Sons), 509–567.

Orth, C. J., Gilmore, J. S., Quintana, L. R., and Sheehan, P. M. (1986). Terminal Ordovician Extinction: Geochemical Analysis of the Ordovician/Silurian Boundary, Anticosti Island, Quebec. *Geol* 14 (5), 433–436. doi:10.1130/0091-7613(1986)14<433:toegao>2.0.co;2

Pankina, R. G., Mekhtiyeva, V. L., and Guriyeva, S. M. (1978). Origin of CO_2 in Petroleum Gases (From the Isotopic Composition of Carbon). *Int. Geology. Rev.* 21 (5), 535–539.

Qi, H., and Dai, J. (1981). Discussion on Distribution and Origin of the Gas Pools Containing High Percentage of Carbon Dioxide of China. *Pet. Exploration Dev.* 2, 34–42.

Qin, S., Yang, Y., Lu, F., Zhou, H., and Li, Y. (2016). The Gas Origin in Changxi-Feixianguan Gas Pools of Longgang Gas Field in Sichuan Basin. *Nat. Gas Geosci.* 27 (1), 41–49.

Qing, H., and Veizer, J. (1994). Oxygen and Carbon Isotopic Composition of Ordovician Brachiopods: Implications for Coeval Seawater. *Geochimica et Cosmochimica Acta* 58 (20), 4429–4442. doi:10.1016/0016-7037(94)90345-x

Richet, P., Bottinga, Y., and Javoy, M. (1977). A Review of Hydrogen, Carbon, Nitrogen, Oxygen, Sulphur, and Chlorine Stable Isotope Fractionation Among Gaseous Molecules. *Annu. Rev. Earth Planet. Sci.* 5, 65–110. doi:10.1146/annurev.ea.05.050177.000433

Sano, Y., Urabe, A., Wakita, H., Chiba, H., and Sakai, H. (2008). Chemical and Isotopic Compositions of Gases in Geothermal Fluids in Iceland. *Geochemical J. GJ* 19 (3), 135–148.

Shangguan, Z., and Zhang, P. (1990). *Active Faults in Northwestern Yunnan Province*. Beijing: Seismology Press, 162–164.

She, J., Li, K., Zhang, H., Shabbiri, K., Hu, Q., and Zhang, C. (2021). The Geochemical Characteristics, Origin, Migration and Accumulation Modes of Deep Coal-Measure Gas in the West of Linxing Block at the Eastern Margin of Ordos Basin. *Nat. Gas Sci.* Engi. doi:10.1016/j.jngse.2021.103965

Shen, P., Xu, Y., Wang, X., Liu, D., Shen, Q., and Liu, W. (1991). Studies on Geochemical Characteristics of Gas Source Rocks and Natural Gas and Mechanism of Genesis of Gas. *Lan Zhou. Gansu Sci. TechnologyPress*, 120–121.

Song, Y. (1991). Origin of the Natural Gas in Wanjinta Reservoir of the Songliao Basin. *Nat. Gas Industry* 11 (1), 17–21.

Tang, Z. (1983). Geologic Characteristics of Natural Carbon Dioxide Gas Pool and its Utilization. *Nat. Gas Industry* 3 (3), 22–26.

Tao, S., Zou, C., Tao, X., Huang, C., Zhang, X., Gao, X., et al. (2009). Study on Fluid Inclusion and Gas Accumulation Mechanism of Xujiahe Formation of Upper Triassic in the Central Sichuan Basin. *Bull. Mineralogy, Pet. Geochem.* 28 (1), 2–11.

Veizer, J., Ala, D., and Azmy, K. (1999). $^{87}Sr/^{86}Sr$, $\delta^{13}C$ and $\delta^{18}O$ Evolution of Phanerozoic Seawater. *Chem. Geology*. 161 (1), 59–88. doi:10.1016/s0009-2541(99)00081-9

Wang, K., Chatterton, B. D. E., and Wang, Y. (1997). An Organic Carbon Isotope Record of Late Ordovician to Early Silurian marine Sedimentary Rocks, Yangtze Sea, South China: Implications for CO2 Changes during the Hirnantian Glaciation. *Palaeogeogr. Palaeoclimatol. Palaeoecol.* 132 (1), 147–158. doi:10.1016/s0031-0182(97)00046-1

Wei, G., Xie, Z., Song, J., Yang, W., Wang, Z., Li, J., et al. (2015). Features and Origin of Natural Gas in the Sinian–Cambrian of central Sichuan Paleo-Uplift, Sichuan Basin, SW China. *Pet. Exploration Dev.* 42 (6), 702–711. doi:10.1016/s1876-3804(15)30073-2

Wei, J., Wang, Y., Wang, G., Wei, Z., and He, W. (2021). Geochemistry and Shale Gas Potential of the Lower Permian marine-continental Transitional Shales in the Eastern Ordos Basin. *Energy Exploration & Exploitation* 39 (3), 738–760. doi:10.1177/0144598720979242

Wu, X., Liu, Q., Chen, Y., Zhai, C., Ni, C., and Yang, J. (2020). Constraints of Molecular and Stable Isotopic Compositions on the Origin of Natural Gas from Middle Triassic Reservoirs in the Chuanxi Large Gas Field, Sichuan Basin, SW China. *J. Asian Earth Sci.* 204. doi:10.1016/j.jseaes.2020.104589

Wu, X., Liu, Q., Liu, G., and Ni, C. (2019). Genetic Types of Natural Gas and Gas-Source Correlation in Different Strata of the Yuanba Gas Field, Sichuan Basin, SW China. *J. Asian Earth Sci.* 181, 103906. doi:10.1016/j.jseaes.2019.103906

Wu, X., Liu, Q., Liu, G., Wang, P., Li, H., Meng, Q., Chen, Y., and Zeng, H. (2017). Geochemical characteristics and genetic types of Natural Gas in the Xinchang Gas Field, Sichuan Basin, SW China. *Acta Geologica Sinica - English Edition* 91 (6), 2200–2213. doi:10.1111/1755-6724.13458

Xu, H., Zhou, W., Cao, Q., Xiao, C., Zhou, Q., Zhang, H., et al. (2018). Differential Fluid Migration Behaviour and Tectonic Movement in Lower Silurian and Lower Cambrian Shale Gas Systems in China Using Isotope Geochemistry. *Mar. Pet. Geology*. 89, 47–57. doi:10.1016/j.marpetgeo.2017.03.027

Yin, F., Liu, R., and Qin, H. (2013). About Origin of Tight sandstone Gas: To Discuss with Academician Dai Jinxing. *Pet. Exploration Dev.* 40 (1), 125–128. doi:10.1016/s1876-3804(13)60016-6

Zhang, M., Tang, Q., Cao, C., Lv, Z., Zhang, T., Zhang, D., et al. (2018b). Molecular and Carbon Isotopic Variation in 3.5 Years Shale Gas Production from Longmaxi Formation in Sichuan Basin, China. *Mar. Pet. Geology*. 89, 27–37. doi:10.1016/j.marpetgeo.2017.01.023

Zhang, M., Tang, Q., and Cao, C. (2018a). Oxygen Hydrogen and Carbon Isotope Studies for Fangshan Granitic Intrusion. *Acta Petrologica Sinica* 3 (3), 13–22.
Zhang, S., He, K., Hu, G., Mi, J., Ma, Q., Liu, K., et al. (2018c). Unique Chemical and Isotopic Characteristics and Origins of Natural Gases in the Paleozoic marine Formations in the Sichuan Basin , SW China: Isotope Fractionation of Deep an High Mature Carbonate Reservoir Gases. *Mar. Pet. Geology*. 89, 68–82.
Zhang, S., Hu, G., and Liu, S. (2019). *Chinese Natural Gas Formation and Distribution*. BeijingPetroleum Industry Press, 143–146.
Zhen, S., Huang, F., Jiang, C., and Zheng, S. (1987). Oxygen Hydrogen and Cabon Istope Studies for Fangshan Granitic Intrusion. *Acta Petrologica Sinica* 3 (3), 13–22.
Zhu, Y., and Wu, X. (1994). *Geological Studying of Carbon Dioxide*. Lan Zhou: Lan Zhou University Press, 1–13.

Conflict of Interest: Authors JD, YN, CY, DG, FH, YZ, and ZY were employed by the company PetroChina. Authors QL and XW were employed by the company SINOPEC.

The authors declare that the research was conducted in the absence of any commercial or financial relationships that could be construed as a potential conflict of interest.

Publisher's Note: All claims expressed in this article are solely those of the authors and do not necessarily represent those of their affiliated organizations, or those of the publisher, the editors, and the reviewers. Any product that may be evaluated in this article, or claim that may be made by its manufacturer, is not guaranteed or endorsed by the publisher.

frontiers | Frontiers in Earth Science

ORIGINAL RESEARCH
published: 08 June 2022
doi: 10.3389/feart.2022.885860

Geochemical Characteristics of Catalytic Hydrogenation of Low-Mature Kerogen Under Deep Fluids

Xiaowei Huang[1,2,3], *Zhijun Jin*[1,2,4]*, *Quanyou Liu*[1,2,4]*, *Qingqiang Meng*[2,4], *Dongya Zhu*[2,4], *Lu Wang*[1,2], *Jiayi Liu*[2,4], *Panpan Zhang*[2,3] and *Jingbin Wang*[2,3,4]

[1]Institute of Energy, Peking University, Beijing, China, [2]State Key Laboratory of Shale Oil and Gas Enrichment Mechanisms and Effective Development, SINOPEC, Beijing, China, [3]School of Energy Resources, China University of Geosciences (Beijing), Beijing, China, [4]Petroleum Exploration and Production Research Institute, SINOPEC, Beijing, China

There is increasingly valued attention on whether the matter and energy carried in the deep fluids can significantly change the hydrocarbon (HC) generation of low-mature source rocks. Previous studies suggest that the upward movement of deep fluids to sedimentary basins will change the HC generation evolution mode of low-mature source rocks, and the matter and energy carried by the fluid will transform the evolution process as transient events. However, there is a lack of quantitative evaluation of the specific changes of gaseous HC generation in the process of modification. In this study, the effect of deep fluids on HC generation and evolution of low maturity source rocks were quantitatively studied through simulation experiments of the gold tube closed system. We quantitatively selected hydrogen and catalysts ($ZnCl_2$ and MoS_2) to conduct catalytic hydrogenation of kerogen and explore the quantitative effects of deep fluids on HC generation in low-mature source rocks. Through the experimental results, it is found that catalytic hydrogenation has significant changes in a HC generation transformation of organic matter (OM). With the increase of catalytic hydrogenation reaction intensity, the maximum gaseous HC generation yield is 3.16–3.24 times that of the control groups without hydrogenation. In the relatively low-temperature stage (<400°C), the competitive hydrogenation effect occurs and the drying coefficient is high. After the high-temperature stage, a large amount of hydrogen participates in the reaction, which significantly promotes the increase of gaseous HCs and decreases the drying coefficient. $ZnCl_2$ or MoS_2 can change the relative content ratio of isomerism and isomorphism of butane and pentane, suggesting that cationic catalysis plays a greater role. In the reaction process, OM plays the most important role in the contribution to HC generation, exogenous hydrogen is more likely to participate in HC generation reaction than water and has the potential contribution to HC generation in Fischer-Tropsch synthesis (FFT) under catalytic conditions. The results of this study effectively verify that exogenous hydrogen and metal elements in deep fluids significantly modify the thermal evolution of low-mature source rocks, and enhance the HC generation potential in the high-temperature stage.

Keywords: simulation experiment, catalytic hydrogenation, gaseous yield, Xiamaling formation, FTT synthesis

OPEN ACCESS

Edited by:
Tongwei Zhang,
University of Texas at Austin,
United States

Reviewed by:
Dionysis Foustoukos,
Geophysical Laboratory (CIS),
United States
Shuai Yin,
Xi'an Shiyou University, China

***Correspondence:**
Zhijun Jin
jinzj1957@pku.edu.cn
Quanyou Liu
qyouliu@sohu.com

Specialty section:
This article was submitted to Geochemistry, a section of the journal Frontiers in Earth Science

Received: *28 February 2022*
Accepted: *23 May 2022*
Published: *08 June 2022*

Citation:
Huang X, Jin Z, Liu Q, Meng Q, Zhu D, Wang L, Liu J, Zhang P and Wang J (2022) Geochemical Characteristics of Catalytic Hydrogenation of Low-Mature Kerogen Under Deep Fluids. Front. Earth Sci. 10:885860. doi: 10.3389/feart.2022.885860

1 INTRODUCTION

The deep fluids carry a lot of matter and energy as the transport link between the interior and exterior of the sedimentary basin, which play a key role in the HC generation evolution of the young and low-mature HC source in the sedimentary basin has been paid much attention (Jin et al., 2002,2004; Meng et al., 2010; Liu et al., 2016, 2018). As one of the major components of deep fluids, hydrogen is widely distributed in geological strata (Sherwood-Lollar et al., 2014; Meng et al., 2015; Etiope, 2017; Guelard et al., 2017; Etiope and Whiticar, 2019; Bougault et al., 2019; Klein et al., 2019; Klein et al., 2020). Meanwhile, there are lots of metal elements in the deep fluids (e.g., Mg, Fe, Mn, Zn, and Mo) (Tivey, 2007; Resing et al., 2015).

For the study on HC promotion by adding H_2, Jin et al. (2004) found that deep hydrogen-rich fluids can promote HC generation of source rocks. Meng et al. (2015) confirmed that deep hydrogen-rich fluids can activate and increase the HC regeneration of ancient source rocks. Liu et al. (2016) found deep fluids can make a contribution to inorganic methane by Fischer-Tropsch synthesis in Songliao Basin, China. Huang et al. (2021) verified that H_2 plays a dominant role in the contribution of sufficient deep hydrogen-rich fluid to the HC promotion of high-mature kerogen. Meanwhile, the effects of transition metals on HC generation of OM have been widely studied (Mango, 1996; Mango and Hightower, 1997; Medina et al., 2000; Lewan et al., 2008; He et al., 2011; Ma et al., 2018). Transition metals can significantly promote the decomposition of OM and generate methane-rich gas, and the content of gas products was similar to the composition of natural gas through simulation experiments with the addition of transition metal Ni or NiO, and the transition metal elements play a major role in natural gas generation through catalytic action (Mango, 1996; Mango and Hightower, 1997). He et al. (2011) analyzed the catalytic mechanism of MoS_2 in two aspects through a simulation control experiment: the generation of H_2S through MoS_2 reduction can trigger the free radical reaction of HCs, and the Lewis acid site provided by the transition metal Mo can promote the homolysis of H_2 to generate H free radical, and promote the catalytic HC generation of OM. Ma et al. (2018) showed that pyrite plays a catalytic role by converting into pyrrhotite and monovalent sulfur, which can reduce the isomerization degree and promote the generation of saturated HCs. However, previous studies have not determined the synergistic reaction and quantitative transformation evaluation of hydrogen and catalysts in catalytic hydrogenation reaction of low-mature source rocks. In the simulation experimental study of catalytic hydrogenation of low mature HC source rocks, it is difficult to accurately quantify the gaseous reactant hydrogen, and there are few quantitative studies on the comparison of reaction participation degree, which makes it difficult to accurately quantify and evaluate the contribution of hydrogen to HC generation.

Therefore, the effects of external hydrogen sources and catalysts on HC generation of low-mature source rocks were investigated with the gold tube closed system experimental reaction system. It was believed that HC generation transformation of low-mature source rocks by deep fluids was an "instantaneous event" in geological history, catalytic hydrogenation effects on the yield of gaseous products confirmed further potential of HC generation in low-maturity marine I-type kerogen in the quantitative hydrogenation process.

2 EXPERIMENTAL SAMPLES AND METHODS

2.1 Experimental Samples

The low-maturity source rock samples selected in the experiment were taken from the bottom of the Middle Proterozoic Xiamaling Formation (Fm.) in the Xiahuayuan section in Northern China. The lithologic character is argillaceous limestone with strong HC generation capacity, low thermal maturity and retain abundant early HC generation parent materials (Sun et al., 2003; Zhang et al., 2007; Xie et al., 2013; Guo et al., 2014). The rock samples were washed with deionized water to remove surface impurities, then left to dry in a fume hood and ground to 200 mesh powder particles using a grinder. The mixed solvent of CH_2Cl_2 and HCOOH with a volume ratio of 9:1 was used to extract the rock samples for 72 h by the soxhlet extraction method. After that, the extracted powder was treated with HCl acid at a constant temperature of 80°C for 8 h to remove carbonate minerals, and then the remaining powder was washed with deionized water to pH = 7.0 to remove HCl acid. Then the powder was treated with the mixed solution of HCl and HF with a 1:1 volume ratio for 8 h, and acid treatment was performed to remove the excess inorganic minerals. After that, the powder was washed with deionized water to pH = 7.0 and dried in a fume cabinet to evaporate the excess water to finish kerogen preparation.

The catalyst $ZnCl_2$ powder is produced by Aladdin Reagent Company with a purity of 99.95%. MoS_2 powder is produced by Aldrich Chemical Reagent Company with a purity of 99.00%. The particle sizes of the two reagents were both 200 mesh, which reached the purity standard of experimental analysis. Deionized water was prepared in the laboratory. H_2 was stored in the gas cylinder with 5% molar volume He as the internal standard gas.

The basic geochemical data of the prepared kerogen samples were analyzed, Rock-eval and Vitrinite reflectance Ro parameters were tested to determine the content of HC and other elements in OM and the amount of reactants in a quantitative experiment. The kerogen is type I, and the thermal maturity (Ro) is 0.63%. The total organic carbon (TOC) content is 88.0% with purification. Tmax is 433°C, and pyrolysis parameter S1 is 2.22 mgHC/g ker. S2 = 342.12 mgHC/g ker, S3 = 34.74 mg HC/g ker, hydrogen index (HI) = 389, oxygen index (OI) = 39, which are typical low evolution hydrogen-rich kerogen.

2.2 Experimental Method

The experimental work was carried out in the State Key Laboratory of Organic Geochemistry, Guangzhou Institute of Geochemistry, Chinese Academy of Sciences. Sample loading involves quantitative loading of solid, liquid, and gaseous three-phase samples. For the quantitative loading steps of solid and liquid samples in the control group with H2 addition, specific

experimental methods of predecessors were mainly referred to (Liu and Tang, 1998; Huang et al., 2021). The reactants were 24.00 mg kerogen powder, 24.00 mg deionized water, 2.40 mg catalyst powder, and 0.60 mg H2. After completing the above sample loading, the gold tubes are placed into the high-temperature reactor and heated. The heating program is set to reach each predetermined temperature point in 2 h and then heated for 72 h. There are four experimental samples of different control groups with each set at six temperature points, 300°C, 350°C, 375°C, 400°C, 450°C, 500°C, and 550°C. The pressure in the simulation experiment was set at 500bar, and the abnormal pressure change in the heating reactor was controlled within ±1bar. Experimental group IA is kerogen + deionized water + $ZnCl_2$; group IIA is kerogen + deionized water + MoS_2; group IIIA is kerogen + deionized water + $ZnCl_2$+H_2; group IVA is kerogen + deionized water + MoS_2+H_2.

The gold tubes were removed from the reactor and cleaned after heating, then the gold tube was slowly placed into a custom-made vacuum glass tube connected to the Agilent 6890N full-component gas chromatography (GC) modified by Wasson ECE Instrumentation company from the US. The GC consists of two TCD detectors and one FID detector. The detection column is a Paraplot Q capillary column (25 m × 0.32 mm × 10 μm). The heating procedure was to set at the initial temperature at 50°C for 3 min, then raised to 190°C at a rate of 25°C/min and kept for 5 min (Wang et al., 2020; Huang et al., 2021).

3 RESULTS

The simulation experiment results show that the total yield of gas components in all groups has a rising trend with increasing temperature. The detected organic components were divided into $C_{1\sim5}$, and the inorganic components were divided into CO_2 and H_2. The total gas production rate of group IA starts from 46.78 m^3/t at the initial temperature of 300°C and reaches the maximum yield of 561.99 m^3/t at the maximum temperature of 550°C. The total gas production rate of group IIA starts from 46.19 m^3/t at the initial temperature of 300°C, and the maximum gas yield was 441.75 m^3/t at 550°C. Between 300 and 375°C, the total gas yield under the action of MoS_2 was slightly higher than that under the action of $ZnCl_2$. After 400°C, the total gas yield under the action of $ZnCl_2$ was significantly higher than that under the action of MoS_2. In groups IIIA and IVA, the total gas yield (H_2 yield not calculated) was 44.36 m^3/t and 29.87 m^3/t at 300°C, respectively. The yield increased significantly with the temperature increase. At 550°C, the maximum yields are 1,283.85 m^3/t and 1,064.92 m^3/t, which are 2.3 and 2.4 times of the maximum yields of IA and IIA groups without H_2 groups, respectively. Moreover, the effect of $ZnCl_2$ on the increase of total gas yield is greater than that of MoS_2. Compared with groups IA and IIA, the CO_2 yield of the control group was significantly reduced after adding the H_2 reaction. The alkane yield shows a decreasing trend at 300–400°C and is mainly inhibited at a low temperature. After 450°C, the alkane yield increases greatly. Alkanes yield is significantly affected by temperature change, while CO_2 yield is insignificant at 300°C–450°C and significant at a higher temperature.

The total gaseous HC yield distribution of $\sum C_{1\text{-}5}$ increased from the initial low-temperature to the high-temperature stage and reached the maximum at 550°C. The initial temperature yield of total gaseous HCs in group IA is 1.52 m^3/t and the maximum yield is 366.67 m^3/t. The initial temperature yield of total gaseous HCs in group IIA is 2.73 m^3/t and the maximum yield is 298.13 m^3/t. The maximum yield of total gaseous HCs in groups IA and IIA increases steadily with the temperature increase. The initial temperature yield of total gaseous HCs in group IIIA is 9.91 m^3/t, and the maximum yield is 1,158.59 m^3/t. The initial yield of total gaseous HCs in group IVA is 7.67 m^3/t, and the maximum yield is 966.60 m^3/t. The maximum yield of $\sum C_{1\text{-}5}$ increases with the increase of temperature in IIIA and IVA groups. The maximum yields of hydrogenated groups IIIA and IVA are 3.16 and 3.24 times that of groups IA and IIA without H_2, respectively (**Figure 1A**).

The distribution of C_1 changes from low temperature to high temperature, and the total gaseous HC yield increases continuously (**Figure 1B**), reaching its maximum value at 550°C. The initial temperature yield of total gaseous HCs in group IA is 1.06 m^3/t and the maximum yield is 365.34 m^3/t. The initial temperature yield of total gaseous HCs in experimental group IIA is 1.94 m^3/t and the maximum yield is 294.27 m^3/t. The maximum yield C_1 in groups IA and IIA increases relatively gently with the increase of temperature. The initial temperature yield of total gaseous HCs in group IIIA was 7.07 m^3/t, and increase with the increase of temperature, the maximum yield was 1,029.01 m^3/t. The initial temperature yield of total gaseous HCs in group IVA was 5.72 m^3/t, and the maximum yield was 938.48 m^3/t. And the yield of total gaseous HCs was increased with the increase of temperature. In groups IIIA and IVA, the maximum yield C_1 increased significantly with the increasing temperature. The maximum yield of hydrogenated groups IIIA and IVA are 2.82 and 3.19 times that of groups IA and IIA without H_2.

In terms of the distribution of C_2 yield (**Figure 1C**), the C_2 yield of IA and IIA groups increased from the initial temperature of 300°C–450°C, respectively, and reached the maximum yield at 450°C, which decreased from 450 °C to 550°C. The maximum yield of C_2 was 59.79 m^3/t (450°C) and 61.05 m^3/t (450°C), respectively. There was no significant difference in the temperature change curve of C_2 yield under $ZnCl_2$ and MoS_2. The maximum yields of C_2 in IIIA and IVA groups were 378.73 m_3/t (500°C) and 283.01 m^3/t (500°C), which were 6.33 and 4.64 times higher than those in IA and IIA groups with only catalyst, respectively. During the reaction process, the addition of exogenous H_2 inhibited the increase of C_2 yield in the range of about 300°C–410°C, and the ethane yield increased rapidly with the temperature rising from about 410°C. The participation of H_2 in the reaction at high temperature delayed the peak temperature point of C_2 HC generation, and the increase of C_2 yield under $ZnCl_2$ was larger than MoS_2.

The C_3 yields of IA and IIA groups showed an overall increasing trend from the initial temperature of 300°C–450°C, respectively, and reached the maximum yield between 400°C and 450°C, after which the yield decreased with the increase of temperature. The maximum C_3 yields were 14.84 m^3/t (400°C)

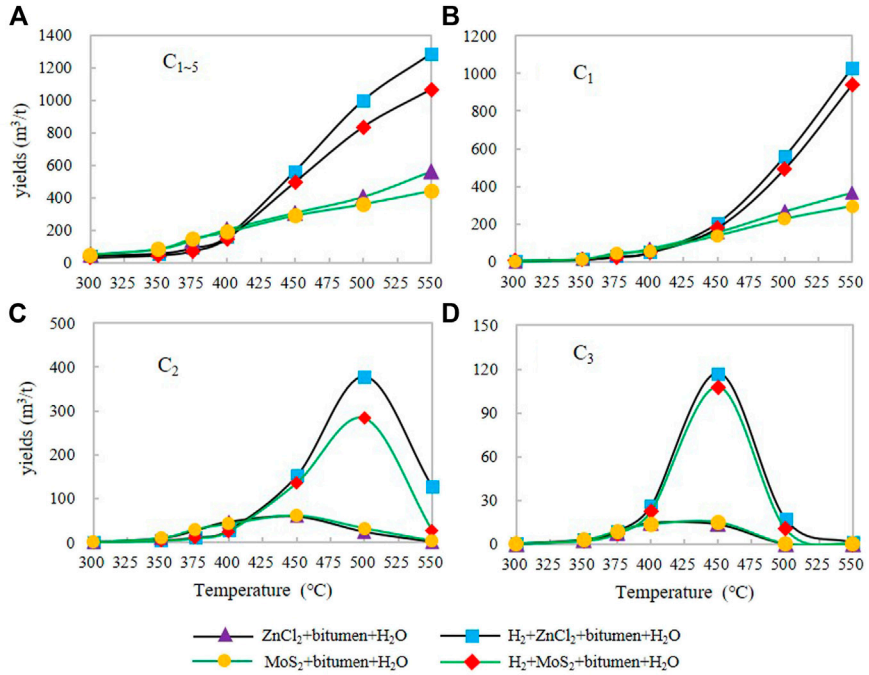

FIGURE 1 | The yield characteristics of $C_{1\sim5}$**(A)**, C_1**(B)**, C_2**(C)**, C_3**(D)** under different catalytic hydrogenation control conditions of the closed system.

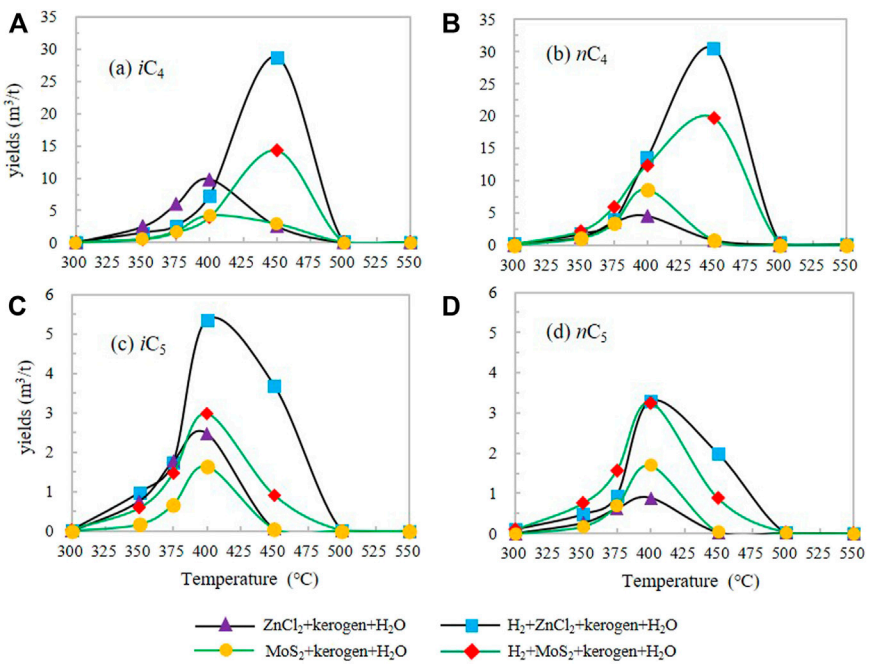

FIGURE 2 | The yield characteristics of iC_4**(A)**, nC_4**(B)**, iC_5**(C)**, nC_5**(D)** under different catalytic hydrogenation control conditions of the closed system.

and 14.95 m^3/t (450°C), respectively. In groups IIIA and IVA, the maximum C_3 yields were 117.16 m^3/t (500°C) and 107.55 m^3/t (500°C), respectively (**Figure 1D**), which were 7.89 and 7.19 times higher than those of the IA and IIA groups without H_2 addition, respectively. The addition of exogenous H_2 inhibited the increase of C_3 yield from 300°C to 375°C and increased significantly after 400°C. The participation of H_2 in the reaction at high temperature delayed the peak temperature of C_3 HC generation, and the

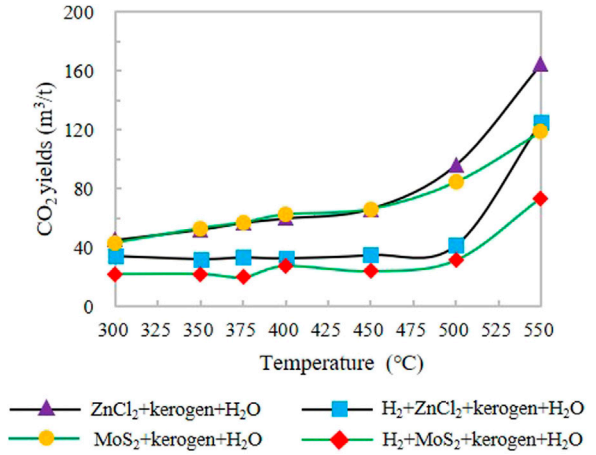

FIGURE 3 | Change in CO_2 yield simulated under different catalytic hydrogenation control conditions of the closed system.

increase of C_3 yield under $ZnCl_2$ was greater than that under MoS_2. The addition of exogenous H_2 inhibited the growth of C_3 yield from 300°C to 375°C and significantly increased C_3 yield after 400°C.

The change of iC_4 yield in IA and IIA groups increased from the initial temperature first, reaching the maximum yield of 3.62 m^3/t and 1.67 m^3/t at 400°C, respectively, and then decreased rapidly with the increase of temperature. The maximum yield of iC_4 in IIIA and IVA groups was 25.04 m^3/t (450°C) and 11.99 m^3/t (450°C), respectively, which were 6.92 and 7.18 times of the maximum yield in I and II groups without H_2 (**Figure 2A**).

The nC_4 yield in groups IA and IIA increased from the initial temperature and reached the maximum yield at 400°C, and then decreased with the increase of temperature. The maximum yield of nC_4 was 3.85 m^3/t (400°C) and 4.29 m^3/t (400°C), respectively. After the H_2 reaction was added in groups IIIA and IVA, the maximum yield of nC_4 was 22.75 m^3/t (450°C) and 23.71 m^3/t (450°C) (**Figure 2B**), which are 5.91 and 5.53 times of that in groups IA and IIA without H_2, respectively. The addition of exogenous H_2 delayed the peak of HC generation of i/nC_4 to the high-temperature point and significantly increased the yield of iC_4 and nC_4, among which, the effect of promoting the yield of nC_4 was greater than that of iC_4.

The variation of iC_5 yield of groups IA and IIA increased from the initial temperature first, and reached the maximum yield in the range of 400°C–450°C. After that, the yield decreased with the increase of temperature. Maximum yields of iC_5 were 0.69 m^3/t (400°C) and 0.81 m^3/t (400°C), respectively. The maximum yields of iC_5 in groups IIIA and IVA were 3.22 m^3/t (400°C) and 2.43 m^3/t (400°C), respectively, which were 4.67 and 3.00 times higher than those in IA and IIA groups without H_2 addition, respectively.

For n-pentane nC_5 (**Figure 2D**), nC_5 production in groups IA and IIA firstly increased from the initial temperature of 300°C, and reached the maximum yield of 0.36 m^3/t and 0.97 m^3/t at 400°C, respectively. After that, the yield decreased rapidly with the increase of temperature. The maximum yield of nC_5 was 2.82 m^3/t (450°C) and 4.33 m^3/t (450°C) in groups IIIA and IVA after H_2 reaction, which was 7.83 and 4.46 times of that in groups IA and IIA, respectively. The addition of exogenous H_2 significantly promoted the increase of HC generation yield of i/nC_5 and delayed the peak temperature of HC generation of i/nC_5. Among them, the HC increasing effect of nC_5 is greater than that of iC_5.

CO_2 production increases continuously from the initial temperature to the high-temperature stage, and reaches its maximum value at 550°C. The minimum CO_2 yield in groups IA and IIA was 45.21 m^3/t (300°C) and 43.44 m^3/t (300°C), and the maximum CO_2 yield was 164.65 and 119.02 m^3/t (550°C), respectively (**Figure 3**). The minimum CO_2 yields of groups IIIA and IVA were 34.47 m^3/t (350°C) and 22.18 m^3/t (350°C), which were 0.76 and 0.51 times of the minimum CO_2 yields of IA and IIA groups without H_2 addition, respectively. The maximum CO_2 yields were 125.30 m^3/t and 73.72 m^3/t, respectively, which were 0.76 and 0.62 times higher than those of IA and IIA without H_2. The comparison of the experimental results shows that the addition of H_2 leads to a significant decrease in CO_2 yield, and the CO_2 yield remains stable with the change of temperature between 300°C and 550°C.

H_2 production distribution of gaseous products in groups IA and IIA increased continuously from low temperature to high temperature, reaching the maximum at 550°C (**Figure 4**). The maximum H_2 production of groups IA and IIA were 30.67 m^3/t and 24.60 m^3/t, respectively. The results show that H_2 generation is significantly promoted by the addition of catalyst. Compared with MoS_2, $ZnCl_2$ has a greater effect on H_2 yield, with an average of 1.2 times. Combined with the study on the catalytic hydrogenation of highly mature kerogen (Huang et al., 2021), the main H element of H_2 generation comes from OM itself. The H_2 yields of groups IIIA and IVA are the amount of consumption involved in the reaction. All the H_2 yield changes show one positive linear relationship between ln (H_2) and temperature.

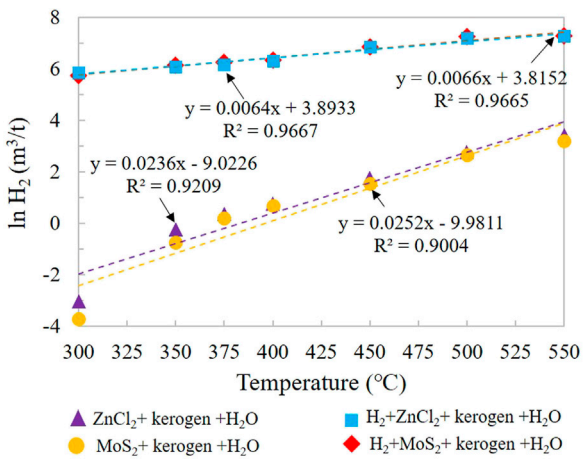

FIGURE 4 | Change in H_2 yield simulated under different catalytic hydrogenation control conditions of the closed system.

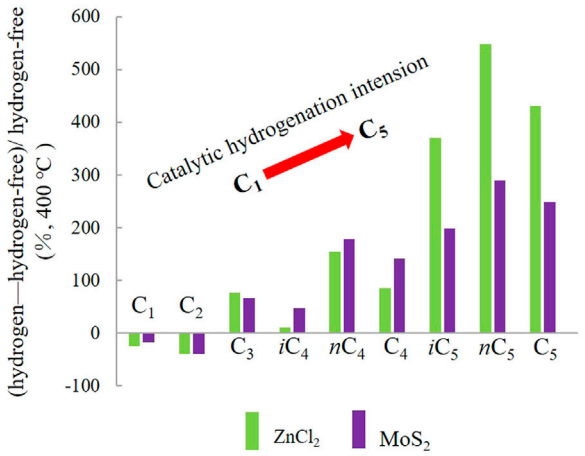

FIGURE 5 | Comparison of C_{1-5} production under $ZnCl_2$ and MoS_2 at 400 °C in closed system.

4 DISCUSSION

4.1 H_2 Contribution on Gaseous HC Generation

4.1.1 HC Generation Promotion

During the low-temperature stage (300°C–400°C), the gaseous HC yields of the H_2 groups are lower than those of the H_2-free groups under the catalysis for the low-mature kerogen. For example, the results at 400°C (**Figure 5**) show that, under the action of $ZnCl_2$ and MoS_2, the C_1 yields after the H_2 reaction increased by 17.49 m^3/t and 9.57 m^3/t, respectively, accounting for 25.0% and 16.6% of the C_1 yield of the groups without H_2, respectively. C_2 yields increased by 19.03 m^3/t and 16.52 m^3/t, accounting for 39.8% and 38.9% of those with H_2-free groups, respectively. The C_3 yield increased by 11.45 m^3/t and 9.12 m^3/t, accounting for 77.2% and 67.0% of C_3 yield without the H_2 groups, respectively. The yield variation of C_4 and C_5 was similar to that of C_3. Compared with C_3, the yield increased more after exogenous H_2 was involved in the reaction. This is due to the joint determination of the bond energy of the macromolecular groups of kerogen and the activation energy provided by the outside. As the bond energy of different HC groups in kerogen decreases with the increase of C number, the reaction is less affected by the external energy and catalytic action at the relatively low-temperature stage, which leads to preferential fracture of long-chain alkyl groups to generate shorter HCs (Dai, 2014). At the same time, under the condition of mass conservation of total active carbon, the content of active C involved in the synthesis of small molecules such as C_1, C_2, and C_3 decreased, resulting in a significant decrease in the yield of gaseous light HCs compared with adding H_2 groups. Therefore, HC generation at low-temperature is mainly controlled by pyrolysis of organic components of low-mature kerogen. In high-temperature phase, the kerogen is affected by external energy and catalytic increases gradually, under the effect of catalyst and H_2, the gaseous HC production rate increases significantly, and increase of CH_4 as the most stable HC molecule, its yield increase composite generated by kerogen cracking itself and other C_{2+} hydrogenation cracking from the combined impact of the contrast experiment under the same condition of, the methane yield under $ZnCl_2$ is higher than MoS_2. For C_{2+} gaseous HCs, the bond energy of gaseous HC groups decreases with the increasing carbon number (e.g., -C_5<-C_4<-C_3<-C_2), which promote the C_{2+} groups to react with H_2 preferentially, resulting in the significant increasing yields of the C_{2+} HCs.

4.1.2 Drying Coefficient

The catalytic hydrogenation takes prominent effects on the drying coefficient ($C_1/\sum C_{1-5}$). All the experimental group values of $C_1/\sum C_{1-5}$ showed a trend of decreasing, and then increasing with higher temperatures (**Figure 6**). In IA and IIA groups, $C_1/\sum C_{1-5}$ decreased firstly and then increased from low temperature to high temperature, $C_1/\sum C_{1-5}$ decreased from initial temperature (300°C) about 0.70 and 0.71 to the minimum temperature 0.50 (350°C) and 0.47 (350°C), respectively, and $C_1/\sum C_{1-5}$ increased from 350°C to 375°C. After 400°C, $C_1/\sum C_{1-5}$ values increase continuously under the participation of $ZnCl_2$ and MoS_2 and reach the maximum $C_1/\sum C_{1-5}$ values of 1.00 and 0.99 at 550°C. $C_1/\sum C_{1-5}$ was more significant than $ZnCl_2$ under MoS_2 catalysis.

The $C_1/\sum C_{1-5}$ of groups IIIA and IVA, in which exogenous H_2 and catalyst were involved in the reaction together, firstly decreased and then increased from the initial low temperature to the high-temperature stage, continuously decreased from 0.71 to 0.75, respectively, and decreased to the minimum value of 0.39 and 0.38 at 450°C, respectively. The continuous increase of C_1 produced by catalytic hydrocracking of kerogen or C_{2+} component and the decrease of C_{2+} component yield resulted in a rapid increase of $C_1/\sum C_{1-5}$, reaching the maximum values of 0.89 and 0.97 at 550°C, respectively.

The $C_1/\sum C_{1-5}$ values of the XML Fm. with H_2 increased from 300 to 375°C, while the $C_1/\sum C_{1-5}$ values of the Yurtus Fm. with H_2 decreased (Huang et al., 2021). It indicates that this is caused by

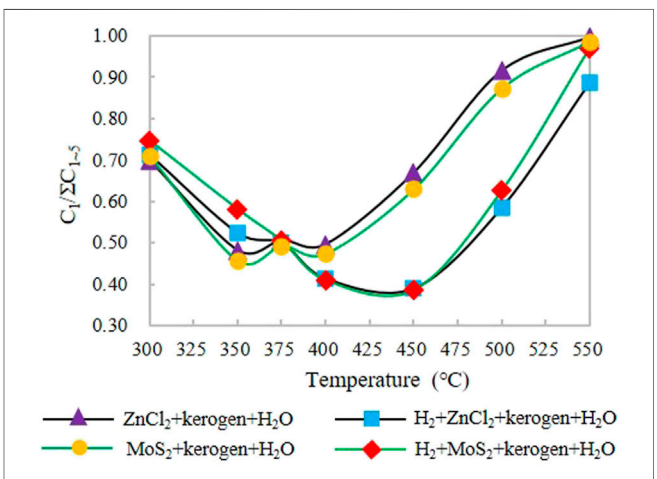

FIGURE 6 | Characteristics of $C_1/\sum C_{1-5}$ contrast under different catalytic hydrogenation.

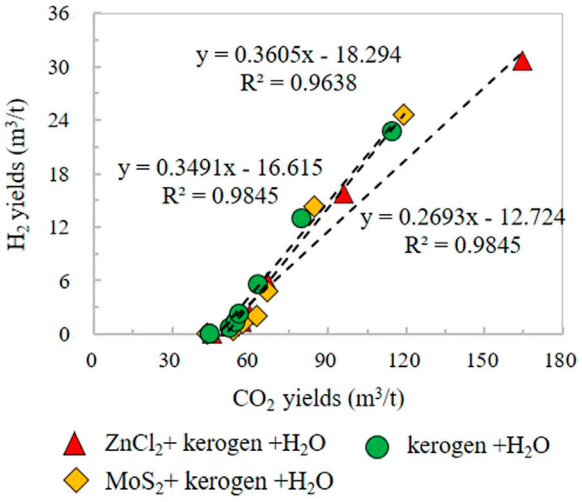

FIGURE 7 | Correlation changes of the synergistic yields between H_2 and CO_2.

the structural differences between the two kerogens. Both Xiamaling Fm. and Yurtus Fm. develop Marine type I kerogens in ancient layers, while Xiamaling Fm. is low-mature kerogens with aliphatic branch chains and heteroatomic groups (Sun et al., 2003; Guo et al., 2014). At the same time, the gaseous HC production rate also decreased after the H_2 addition reaction, which was speculated to be due to the binding reaction of exogenous H_2 with the upper branch chain of low-mature kerogen molecule or other heteroatomic groups, which inhibited the generation of gaseous HC. After 375°C, hydrogenation increases the gaseous HC yield more significantly, promotes the generation of C_{2+}, and increases the temperature point at which $C_1/\sum C_{1\text{-}5}$ reaches the minimum value, which is mainly due to the early generation of the addition reaction of exogenous H_2. Furthermore, the drying coefficient of the product decreased significantly, and the temperature of the minimum drying coefficient was delayed relative to that of the H_2 groups.

4.2 Contribution of Different Hydrogen Sources to HC Generation

In the simulated reaction experiment of kerogen with only water or catalyst in Xiamaling Fm., there was a good linear positive correlation between CO_2 and H_2 yields, H_2 (catalyst free) = 0.3491CO_2-16.615, R^2 = 0.9845. H_2 (MoS_2) CO_2 = 0.3605 18.294, R^2 = 0.9638; H_2 ($ZnCl_2$) = 0.2693CO_2-12.724, R^2 = 0.9845 (**Figure 7**). The above results indicate that H element in the H_2 and the C element in CO_2 are homologous, and both come from OM itself. Compared with the reaction change equation of the Yurtus Fm., the slope is larger, and the intercept value of the horizontal axis is significantly smaller than that of the Yurtus Fm., which indicating the low-mature kerogen has stronger pyrolysis capacity than that of high-mature kerogen. Under the same temperature and pressure conditions, the low-mature Xiamaling kerogen is more likely to generate more H_2.

By comparing the yield changes of lnH_2 and temperature of the Xiamaling Fm. under the action of catalyst, it was found that lnH_2 = 0.0252T-9.9811, R^2 = 0.9004 under the action of MoS_2; lnH_2 = 0.0236T-9.0226, R^2 = 0.9209 under $ZnCl_2$ catalysis. Temperature (T) and lnH_2 under the each catalyst showed good positive correlation linear characteristics and high fitting degree (**Figure 4**). Although the amount of H_2 produced by the low-mature kerogen of Xiamaling Fm. is larger than that of the high-mature kerogen of Yurtus Fm., the contribution of $ZnCl_2$ or MoS_2 to the catalytic action of Xiamaling Fm. is relatively smaller, and the difference of $ZnCl_2$ and MoS_2 in the catalytic effect of Xiamaling Fm. kerogen is also significantly smaller than that of Yurtus kerogen. It is speculated that the molecular structure of kerogen at the low-mature stage is more developed than that of alkane at the high-mature stage, and the bond energy is smaller. Therefore, the activation energy reduced by external catalysis has relatively little influence on H_2 generation from pyrolysis. In addition, in the adding H_2 groups, the linear relationship between lnH_2 and T under MoS_2 catalysis is lnH_2 = 0.0066T + 3.8152, R^2 = 0.9665. The linear relationship between lnH_2 and T under $ZnCl_2$ catalysis is lnH_2 = 0.0064T + 3.8933, R^2 = 0.9667, both of which also have a good linear relationship. At the initial temperature of 300°C, the minimum consumption of exogenous H_2 is 457.81 m^3/t, which is more easily involved in the catalytic hydrocracking reaction of Kerogen in the Xiamaling Fm. than H_2O. However, the actual participation amount of H_2 in this series of reactions was significantly smaller than that of high-mature kerogen, suggesting that the molecular structure of Kerogen in The Yurtus Fm. was higher in aromatization and contained lower HI abundance, leading to the need for more exogenous hydrogen to participate in the catalytic cracking reaction.

Therefore, the difference in consumption of hydrogen generation and H_2 participation in catalytic pyrolysis of kerogen with different maturity, as well as the lower yield of $C_{1\sim4}$ in the initial low-temperature stage of catalytic H_2 addition reaction in the Xiamaling Fm. than that in the reaction without H_2 addition, indicated that H element in Xiamaling kerogen itself would participate in the reaction prior to external H_2.

4.3 Different Effects Under Catalytic Hydrogenation

4.3.1 i/n Ratio Changes

As for the comparison of C_4 and C_5 in the Xiamaling Fm., the comparison of iC_4/nC_4 and iC_5/nC_5 at the same temperature showed that the i/n under the catalytic action of $ZnCl_2$ is larger than that under the action of MoS_2, and the ratio was significantly reduced with the H_2 reaction. The iC_4/nC_4 ratios of the products formed only under $ZnCl_2$ or MoS_2 catalysts from the initial temperature are 0.63–2.10 (N = 6, Ave. = 1.13) and 0.35–1.84 (N = 6, Ave. = 0.76), respectively (**Figure 8A**). The average ratio of iC_4/nC_4 in $ZnCl_2$ is about 1.49 times that in MoS_2, indicating that Zn^{2+} catalyzes iC_4 more strongly than Mo^{2+} and S^{2-}. In the adding H_2 groups, the iC_4/nC_4 ratios of $ZnCl_2$ and MoS_2 are 0.39–1.10 (N = 6, Ave. = 0.57) and 0.03–0.51 (N = 6, Ave. = 0.26),

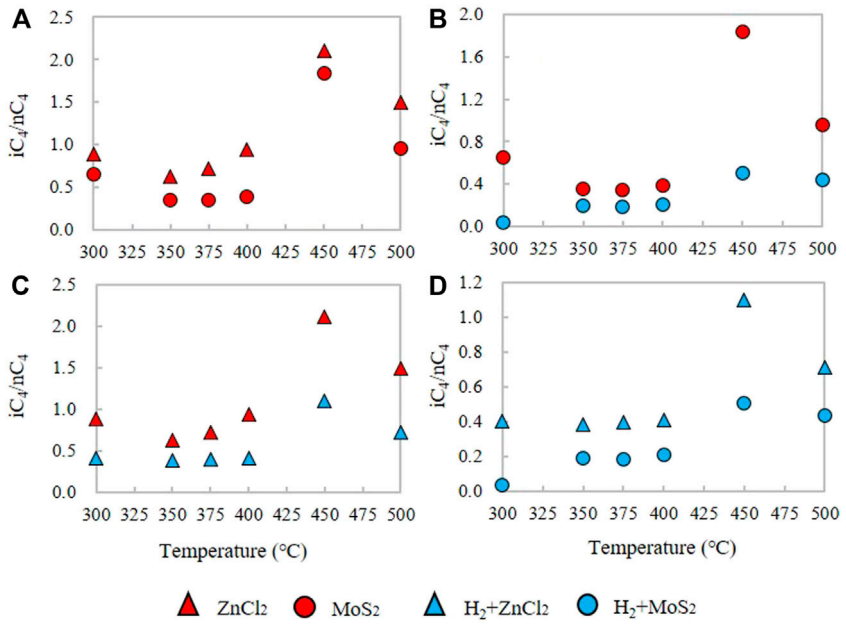

FIGURE 8 | Comparison of the iC_4/nC_4 alkane ratio under the $ZnCl_2$, MoS_2, H_2+$ZnCl_2$, and H_2+MoS_2 conditions for the kerogen in closed system.

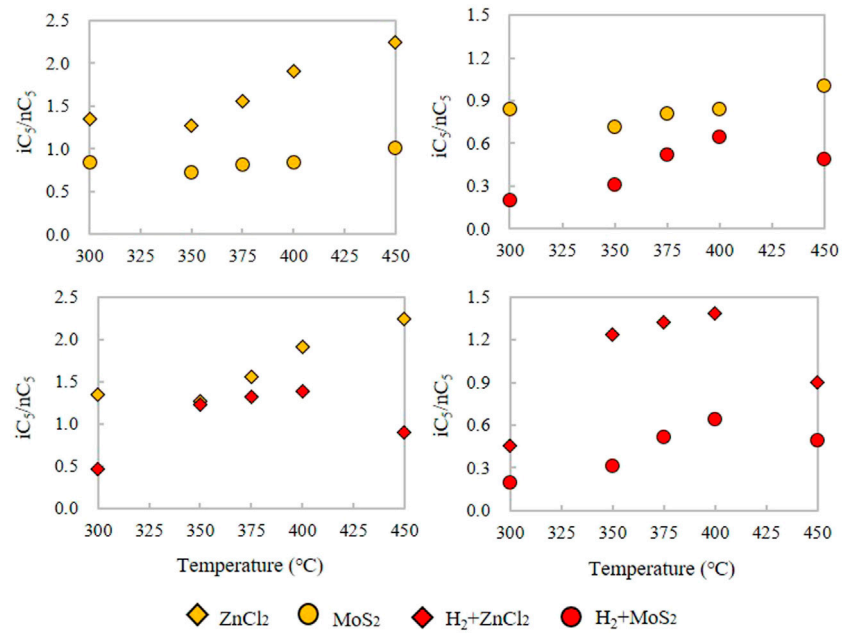

FIGURE 9 | Comparison of the iC_5/nC_5 alkane ratio under the $ZnCl_2$, MoS_2, H_2+$ZnCl_2$, and H_2+MoS_2 conditions for the kerogen in closed system.

respectively (**Figure 8D**). The iC_4/nC_4 values under $ZnCl_2$ were about 2.19 times higher than those under MoS_2. At the same time, the H_2 groups under $ZnCl_2$ and MoS_2 are 0.34 and 0.31 of the iC_4/nC_4 ratio of the control groups without H_2 (**Figure 8b~c**). For iC_5 and nC_5, the iC_5/nC_5 ratios are 1.27–2.25 (N = 5, Ave. = 1.67) and 0.72–1.01 (N = 5, Ave. = 0.84) under the catalytic action of $ZnCl_2$ and MoS_2, respectively. The value of iC_5/nC_5 under $ZnCl_2$ is about 1.98 times that under MoS_2, indicating that the change of iC_5 and nC_5 yield is affected more by Zn ion than Mo ion (**Figure 9A**). The iC_5/nC_5 ratio of H_2 reaction with $ZnCl_2$ and MoS_2 are 0.46–1.38 (N = 5, Ave. = 1.06) and 0.20–0.65 (N = 5, Ave. = 0.43), respectively (**Figure 9D**). The iC_5/nC_5 value under $ZnCl_2$ is about 2.47 times that under MoS_2. Meanwhile, the H_2 groups added by $ZnCl_2$ and MoS_2 are 0.63 and 0.51 of

the control groups iC_5/nC_5 without H_2, respectively (**Figure 9b~c**).

Therefore, the addition of exogenous H_2 changes the original pyrolysis evolution model of low-mature kerogen. As the C-C bond energy of gas component iC_m is greater than that of nC_m (Wang et al., 2011; Dai, 2014), it is easier to promote the generation of normal gaseous alkanes in the catalytic H_2 addition reaction, which preferentially promotes the increase of the yield of normal alkanes. In addition, the i/n ratio decreases significantly in the catalytic hydrogenation reaction. Meanwhile, the small molecule HC yield decreased significantly in the reaction catalyzed by H_2 addition of low-mature kerogen at a relatively low temperature.

4.3.2 FTT Synthesis May Occurduring Catalytic Hydrogenation Reaction

Large amounts of inorganic C_1 is formed through FTT synthesis reaction, and the estimated reaction temperatures can be less than 140°C in geologic settings (Young et al., 2017; Morrill et al., 2018; Etipe and Whiticar, 2019). The CO_2 yields are inhibited by the addition of exogenous H_2 during the reaction. For the gaseous HCs, the activation carbon source with low bond energy preferentially participates in the generation of long-chain carbon products with lower bond energy in the reaction stage at low temperature, resulting in the relatively insufficient generation of gaseous HCs with small molecular weight and affecting the pyrolysis and release of small molecular alkanes. At the high-temperature stage, the cracking degree of catalytic H_2 reaction is strengthened, resulting in a large increase in gaseous products. Decarboxylation is required in combination with Lewis acid catalytic mode. An important influencing factor of catalytic hydrogenation is determined by the abundance of oxygen-containing groups in the OM, which can promote more CO_2 production to participate in the FTT synthesis reaction. More gaseous HCs (mainly C_1) are generated, which has a certain increasing effect on the HCs. The decarboxylation corresponds to the HC increasing effect in OM mainly accompanied by Fischer-Tropsch synthesis contribution. In the kerogen reaction groups of Xiamaling Fm. (**Figure 3**), the change of CO_2 production is similar to that of the high-mature kerogen series (Huang et al., 2021), and the reduction range of CO_2 production decreases, which may be due to the high HI content of the formation increasing the alkane gas production. The yield of the hydrogenation groups does not increase significantly between 300°C and 500°C, revealing the consumption of CO_2 under FTT synthesis.

CONCLUSION

Catalytic hydrogenation plays an important role in the HC generation for the low-mature source rocks. Compared with the low-temperature state, the exogenous H_2 begins to participate in the catalytic pyrolysis reaction of kerogen in large quantities at the relatively high-temperature stage (≥400°C), promoting the increase of gaseous HC production. The maximum gaseous HC yield increases by about 3.2 times. The catalytic H_2 reaction significantly reduces the drying coefficient of natural gas at the relatively high-temperature stage and participates in FTT synthesis adding H_2 under the action of the catalyst. Through the comparison of the composition and isotope characteristics of gaseous products, the catalytic hydrogenation effect of $ZnCl_2$ on immature kerogen is better than MoS_2 under the same conditions, and mainly through cation action. It is revealed that exogenous H_2 and metal ions carried by the deep fluid have significant HC promotion effects on the yield of gaseous products under the catalytic hydrogenation condition.

DATA AVAILABILITY STATEMENT

The original contributions presented in the study are included in the article/Supplementary Material, further inquiries can be directed to the corresponding authors.

AUTHOR CONTRIBUTIONS

XH: Data curation, writing. ZJ: Conceptulization, writing. QL: Investigation, conceptulization. QM: Data curation, methodology. DZ: Methodology, investigation. LW: Investigation. JL: Methodology. PZ: Data curation. JW: Investigation.

FUNDING

This work was funded by National Key R&D Program of China (2019YFA0708504), National Natural Science Foundation of China (42172168, 41625009), and Strategic Priority Research Program of the Chinese Academy of Sciences (Class A) (XDA14010402 and XDA14010404).

ACKNOWLEDGMENTS

All the authors are grateful to Prof. Jinzhong Liu and Hong Lu for their experimental advice and sample assistance to support this study. We also thank. Dr. Qiang Wang and Yong Li for their laboratory help to improve the quality of the experimental results.

REFERENCES

Dai, J. (2014). *Natural Gas Geology and Geochemistry*, 6. Beijing: Petroleum Industry Press, 198–211.

Etiope, G. (2017). Abiotic Methane in Continental Serpentinization Sites: an Overview. *Procedia Earth Planet. Sci.* 17, 9–12. doi:10.1016/j.proeps.2016.12.006

Etiope, G., and Whiticar, M. J. (2019). Abiotic Methane in Continental Ultramafic Rock Systems: towards a Genetic Model. *Appl. Geochem.* 102, 139–152. doi:10.1016/j.apgeochem.2019.01.012

Guélard, J., Beaumont, V., Rouchon, V., Guyot, F., Pillot, D., Jézéquel, D., et al. (2017). Natural H2in Kansas: Deep or Shallow Origin? *Geochem. Geophys. Geosyst.* 18 (5), 1841–1865. doi:10.1002/2016gc006544

Guo, L. N., Ke, B. L., Liu, Q. J., Lin, H. L., Yin, T. Y., Lin, T. Y., et al. (2014). Shale Gas Organic Geochemistry Characteristic of the Mesoproterozoic Xiamaling Formation in Western Beijing Area. *Amr* 998-999, 1452–1457. doi:10.4028/www.scientific.net/amr.998-999.1452

He, K., Zhang, S., Mi, J., Chen, J., and Cheng, L. (2011). Mechanism of Catalytic Hydropyrolysis of Sedimentary Organic Matter with MoS2. *Pet. Sci.* 8 (02), 134–142. doi:10.1007/s12182-011-0126-0

Huang, X., Jin, Z., Liu, Q., Meng, Q., Liu, J., and Liu, J. (2021). Catalytic Hydrogenation of Post-mature Hydrocarbon Source Rocks under Deep-Derived Fluids: An Example of Early Cambrian Yurtus Formation, Tarim Basin, NW China. *Front. Earth Sci.* 9, 626111.

Jin, Z., Zhang, L., Yang, L., and Hu, W. (2004). A Preliminary Study of Mantle-Derived Fluids and Their Effects on Oil/gas Generation in Sedimentary Basins. *J. Pet. Sci. Eng.* 41 (1–3), 45–55. doi:10.1016/s0920-4105(03)00142-6

Jin, Z., Zhang, L., and Yang, L. (2002). Preliminary Study on Geochemical Characteristics of Fluids in Deep Sedimentary Basins and Hydrocarbon Accumulation Effect. *J. Earth Sci.* 27 (6), 659–665. doi:10.3321/j.issn:1000-2383.2002.06.001

Kissin, Y. V. (1987). Catagenesis and Composition of Petroleum: Origin of N-Alkanes and Isoalkanes in Petroleum Crudes. *Geochimica Cosmochimica Acta* 51 (9), 2445–2457. doi:10.1016/0016-7037(87)90296-1

Klein, F., Tarnas, J. D., and Bach, W. (2020). Abiotic Sources of Molecular Hydrogen on Earth. *Elements* 16 (1), 19–24. doi:10.2138/gselements.16.1.19

Liu, J., and Tang, Y. (1998). Kinetics of Early Methane Generation from Green River Shale. *Chin. Sci. Bull.* 43 (22), 1908–1912. doi:10.1007/bf02883470

Liu, Q., Dai, J., Jin, Z., Li, J., Wu, X., Meng, Q., et al. (2016). Abnormal Carbon and Hydrogen Isotopes of Alkane Gases from the Qingshen Gas Field, Songliao Basin, China, Suggesting Abiogenic Alkanes? *J. Asian Earth Sci.* 115, 285–297. doi:10.1016/j.jseaes.2015.10.005

Liu, Q., Zhu, D., Meng, Q., Liu, J., Wu, X., Zhou, B., et al. (2018). The Scientific Connotation of Oil and Gas Formations under Deep Fluids and Organic-Inorganic Interaction[J]. *Sci. China Earth Sci.* 62 (3), 507–528. doi:10.1007/s11430-018-9281-2

Lollar, B. S., Onstott, T. C., Lacrampe-Couloume, G., and Ballentine, C. J. (2014). The Contribution of the Precambrian Continental Lithosphere to Global H2 Production. *Nature* 516 (7531), 379–382. doi:10.1038/nature14017

Ma, X., Zheng, G., Sajjad, W., Xu, W., Fan, Q., Zheng, J., et al. (2018). Influence of Minerals and Iron on Natural Gases Generation during Pyrolysis of Type-III Kerogen. *Mar. Petroleum Geol.* 89, 216–224. doi:10.1016/j.marpetgeo.2017.01.012

Mango, F. D., and Hightower, J. (1997). The Catalytic Decomposition of Petroleum into Natural Gas. *Geochimica Cosmochimica Acta* 61 (24), 5347–5350. doi:10.1016/s0016-7037(97)00310-4

Mango, F. D. (1996). Transition Metal Catalysis in the Generation of Petroleum and Natural Gas. *Geochem. Cosmochim. Acta.* 56 (1), 553–555. doi:10.1016/0016-7037(92)90153-a

McCollom, T. M. (2016). Abiotic Methane Formation during Experimental Serpentinization of Olivine. *Proc. Natl. Acad. Sci. U.S.A.* 113 (49), 13965–13970. doi:10.1073/pnas.1611843113

Morrill, P., Cumming, E. A., Rietze, A., Morissey, L. S., Cook, M., Rhim, J. H., et al. (2018). *Sourcing Dissolved Methane from the Tablelands, Gros Morne National Park, NL, CAN: A Terrestrial Site of Serpentinization*. Boston: Goldschmidt Abstract 1816.

Qingqiang, M., Yuhua, S., Jianyu, T., Qi, F., Jun, Z., Dongya, Z., et al. (2015). Distribution and Geochemical Characteristics of Hydrogen in Natural Gas from the Jiyang Depression, Eastern China. *Acta Geol. Sin. - Engl. Ed.* 89 (5), 1616–1624. doi:10.1111/1755-6724.12568

Resing, J. A., Sedwick, P. N., German, C. R., Jenkins, W. J., Moffett, J. W., Sohst, B. M., et al. (2015). Basin-scale Transport of Hydrothermal Dissolved Metals across the South Pacific Ocean. *Nature* 523 (7559), 200–203. doi:10.1038/nature14577

Sun, X., Chen, J., Liu, W., and Zhang, S. (2003). Hydrothermal Venting on the Seafloor and Formation of Organic-Rich Sediments-Eevidence from the Neoproterozoic Xiamaling Formation, North China. *Geol. Rev.* 49 (6), 588–595.

Tivey, M. (2007). Generation of Seafloor Hydrothermal Vent Fluids and Associated Mineral Deposits. *Oceanogr* 20 (1), 50–65. doi:10.5670/oceanog.2007.80

Wang, Q., Jia, W., Yu, C., Song, J., Zhang, H., Liu, J., et al. (2020). Potential of Light Oil and Condensates from Deep Source Rocks Revealed by the Pyrolysis of Type I/II Kerogens after Oil Generation and Expulsion. *Energy fuels.* 34 (8), 9262–9274. doi:10.1021/acs.energyfuels.0c00553

Wang, X., Liu, W., Xu, Y., and Zheng, J. (2011). Influences of Water Media on the Hydrogen Isotopic Composition of Natural Gas/methane in the Processes of Gaseous Hydrocarbon Generation and Evolution. *Sci. China Earth Sci.* 54 (9), 1318–1325. doi:10.1007/s11430-011-4195-0

Xie, L., Sun, Y., Yang, Z., Chen, J., Jiang, A., Zhang, Y., et al. (2013). Evaluation of Hydrocarbon Generation of the Xiamaling Formation Shale in Zhangjiakou and its Significance to the Petroleum Geology in North China. *Sci. China Earth Sci.* 56, 444–452. doi:10.1007/s11430-012-4538-5

Young, E. D., Kohl, I. E., Lollar, B. S., Etiope, G., Rumble, D., III, Li, S., et al. (2017). The Relative Abundances of Resolved l2CH2D2 and 13CH3D and Mechanisms Controlling Isotopic Bond Ordering in Abiotic and Biotic Methane Gases. *Geochimica Cosmochimica Acta* 203, 235–264. doi:10.1016/j.gca.2016.12.041

Zhang, S., Zhang, B., Bian, L., Jin, Z., Wang, D., and Chen, J. (2007). The Xiamaling Oil Shale Generated through Rhodophyta over 800 Ma Ago. *Sci. China Ser. D.* 50, 527–535. doi:10.1007/s11430-007-0012-1

Conflict of Interest: The authors declare that the research was conducted in the absence of any commercial or financial relationships that could be construed as a potential conflict of interest.

Publisher's Note: All claims expressed in this article are solely those of the authors and do not necessarily represent those of their affiliated organizations, or those of the publisher, the editors and the reviewers. Any product that may be evaluated in this article, or claim that may be made by its manufacturer, is not guaranteed or endorsed by the publisher.

frontiers | Frontiers in Earth Science

ORIGINAL RESEARCH
published: 14 June 2022
doi: 10.3389/feart.2022.881762

The Effect of Thermochemical Sulphate Reduction on the Carbon Isotope Ratio of Individual Light Hydrocarbons Associated With Natural Gas

Guoyi Hu[1], Jinhao Guo[1], Lianjie Tian[1], Xiaoqi Wu[2], Jin Su[1], Zhisheng Li[1] and Chenchen Fang[1]*

[1]Research Institute of Petroleum Exploration and Development, PetroChina, Beijing, China, [2]Wuxi Research Institute of Petroleum Geology, Petroleum Exploration and Production Research Institute, Sinopec, Wuxi, China

To understand the effect of thermochemical sulphate reduction (TSR) on the stable carbon isotopes of light hydrocarbons (LHs) associated with natural gas, 15 gases with varying H_2S content from Ordovician reservoir of the Tazhong gas field (TZ-I) in Tarim Basin and Triassic Leikoupo reservoir of the Zhongba gas field (ZB) in Sichuan Basin were collected. Based on the data from molecular components and stable carbon isotope ratios of the C_1-C_4 alongside the individual LHs (C_6-C_7) in these gases, the origin of natural gas and the effect of TSR on the stable carbon isotope ratio of individual LHs were studied. The $\delta^{13}C$ in ethane (<−28‰), LHs (<−26‰) and the composition distribution characteristic of C_6-C_7 indicated that the gases were oil-associated gases. Moreover, the gas sourness index, defined as $H_2S/(H_2S+\sum C_n)$ demonstrated that the gases from the TZ-I and ZB gas fields were in the early liquid-hydrocarbon-involved and heavy-hydrocarbon-gas-dominated TSR stages, respectively. The comparison of stable carbon isotope ratios of the LHs between the two gas fields revealed that TSR exhibited a complex effect on the carbon isotope values of LHs, but only little effect on 2-methylpentane (2-MP) and 3-methylpentane (3-MP). The $\delta^{13}C$ values of benzene (BEN) and toluene (TOL) were -28.3‰ and -29.4‰ in the TZ-I and -27.7‰ and -28.1‰ in the ZB gas field. The stable carbon isotope ratios of BEN and TOL in ZB gas field exhibited more enriched ^{13}C than those in TZ-I gas field, likely driven by TSR. Meanwhile, cycloalkanes, such as methyl cyclopentane (MCP), cyclohexane (CH), and methylcyclohexane (MCH), enriched ^{13}C with TSR process and displayed a greater trend than aromatic compounds, about 2‰. Therefore, the influence of TSR on the carbon isotopes of individual LHs should be considered while using the stable carbon isotope ratio of cycloalkanes, BEN, and TOL to identify the genetic type and source of marine natural gas, especially at the cross plot ($\delta^{13}C$ = −24‰) of coal-derived gas and oil-associated gas.

Keywords: light hydrocarbons, carbon isotope, thermochemical sulfate reduction, natural gas, Zhongba gas field, Tazhong|gas field

OPEN ACCESS

Edited by:
Tongwei Zhang,
University of Texas at Austin,
United States

Reviewed by:
Weichao Wu,
Stockholm University, Sweden
Amzad Hussain Laskar,
Physical Research Laboratory, India

****Correspondence:***
Guoyi Hu
huguoyi69@petrochina.com.cn

Specialty section:
This article was submitted to Geochemistry, a section of the journal Frontiers in Earth Science

Received: *23 February 2022*
Accepted: *04 May 2022*
Published: *14 June 2022*

Citation:
Hu G, Guo J, Tian L, Wu X, Su J, Li Z and Fang C (2022) The Effect of Thermochemical Sulphate Reduction on the Carbon Isotope Ratio of Individual Light Hydrocarbons Associated With Natural Gas. Front. Earth Sci. 10:881762. doi: 10.3389/feart.2022.881762

INTRODUCTION

Table A1 Table Light hydrocarbons (LHs) associated with gas contain abundant geochemical information, so they have been widely used to determine the genetic type and origin of natural gas (Hu et al., 1990; Dai, 1993; Mango, 1997; Tassi et al., 2012; Hu et al., 2018). In particular, the iso/normal alkane ratio, normal heptane (nC_7), methylcyclohexane (MCH), and total dimethylcyclopentane (DMCP) ternary diagram are usually utilized to identify the type of organic source. Moreover, the nC_7 and isoheptane indices are often used to indicate maturity (Thompson, 1983). The ratios of iso-alkanes to n-alkanes (iC_5/nC_5, 3-MP/nC_6) have been applied to identify the extent of biodegradation (Welte et al., 1982; BeMent et al., 1995; George et al., 2002). Among isomers, these isotopic distributions are strong evidences indicating that the formation of these gasoline-range hydrocarbons is intricately linked to the isotopic signature of the precursor molecules from which they are derived (Whiticar and Snowdon, 1999). The carbon isotopes of individual LHs associated with natural gas are an effective tool for identifying the origin of natural gas. It mainly focuses on identifying coal-derived gas and oil-associated gas by using the carbon isotopic composition of benzene (BEN), toluene (TOL), CH and MCH (Jiang et al., 2000; Li et al., 2003; Dai et al., 2005; Hu et al., 2008). Jiang et al. (2000) have reported that the carbon isotopes of BEN and TOL in the LHs of natural gas are mainly influenced by the type of organic matter, while the thermal evolution and migration effect have only minor influence. In particular, Li et al. (2003) have argued that the carbon isotope of TOL is associated with the type of organic matter in the source rocks. Thus, the correlation of gas with the source rocks can be determined based on examination of the carbon isotopes of TOL in natural gas and source rocks. Hu et al. (2008) have analyzed the individual LHs isotope of abundant typical coal-derived/oil-associated gas samples from the Tarim and Ordos Basins in China and further proposed that the carbon isotopes of CH and MCH can be also utilized to identify coal-derived and oil-associated gases. The coal-derived gases with $\delta^{13}C_{CH}$ > -24‰ and $\delta^{13}C_{MCH}$ > -24‰, the oil-associated gases are opposite. Therefore, $\delta^{13}C_{CH}$ = -24‰ and $\delta^{13}C_{MCH}$ = -24‰ can be also used as cut-off plot to identify coal-derived gas and oil-associated gas.

The carbon isotopes of individual LHs are not only affected by the type of organic matter but also by secondary processes such as biodegradation and evaporation. During biodegradation, the straight chain is less abundant in ^{13}C than cycloalkanes and aromatics, whereas ^{12}C is preferentially consumed, thereby enriching each residual LH molecule in ^{13}C (George et al., 2002; Vieth and Wilkes, 2006). The $\delta^{13}C_{final\text{-}initial}$ of individual LHs in the C_6-C_8 range >1‰ mainly occurs when evaporative losses of individual LHs are >70%. However, nearly complete absence of stable carbon isotopic fractionation has been previously reported for cycloalkanes (Xiao et al., 2012). TSR, thermochemical sulphate reduction is the thermally driven reaction of sulphate (anhydrite) with hydrocarbon producing combinations of H_2S, carbonate minerals (e.g., calcite, $CaCO_3$), CO_2, elemental sulphur and water (Worden and Smalley, 1996). The TSR would preferentially consume the ^{12}C of C_5-C_8 individual LHs that are more enriched in ^{13}C, such as the $\delta^{13}C$ LHs of the crude oil, which increased up to 10‰ by TSR in the Western Canadian Sedimentary Basin. Isoalkanes, cycloalkanes and aromatics were more diagnostic for TSR and oil-source correlation than normal alkanes (Whiticar and Snowdon, 1999). Owing to the increasing H_2S concentration in carbonate gas reservoir was strongly associated with decreasing hydrocarbon content, Worden and Smalley (1996) used a gas souring index (GSI) to characterize the extent of TSR. Heavy hydrocarbon gas is preferentially consumed in the TSR process. Thus, the drying coefficient of natural gas affected by TSR is often reported to be high (Liu et al., 2013). Research on the carbon isotopes of individual hydrocarbons, associated with natural gas by TSR often focuses on low-molecular-weight gaseous hydrocarbons (C_1-C_4) (Hao et al., 2008). Thus far, only a few studies have used the carbon isotope ratios of LHs associated with gas as indicators of TSR. The gases from the TZ-I gas field in the Tarim Basin and the ZB gas field in the Sichuan Basin originated from marine source rocks and have been affected by TSR (Cai et al., 2001; Zhu et al., 2011; Cai et al., 2015).

This study evaluates the TSR process by using carbon isotope fractionation of LHs based on 15 gas-producing samples from TZ-I and ZB gas fields (Tarim and Sichuan Basin, China). To this end, the composition, stable carbon isotope of C_1 to C_4, quantification, and the individual compound-specific carbon isotopes of C_6-C_7 LHs were determined. The main objectives of this study are (a) to determine the molecular composition characteristics of C_1-C_4 and C_6-C_7 LHs for marine gas from the gas fields of TZ-I in the Tarim Basin and ZB in the Sichuan Basin; (b) to measure the individual compound-specific carbon isotopes of the C_1-C_4 and C_6-C_7 LHs; (c) to elucidate the genetic type, oil-cracking stage and TSR degree of the gases by the relative content, $\delta^{13}C$ of C_1-C_4 and LHs as well as GSI from these two gas fields (d) to examine the effect of TSR on the carbon isotopes of individual LHs.

TABLE A1 | The light hydrocarbon of C_6–C_7.

Compound	Abbreviation
2-methylpentane	2-MP
3-methylpentane	3-MP
normal-hexane	nC_6
methylcyclopentane	MCP
benzene	BEN
cyclohexane	CH
dimethylcyclopentane	DMCP
normal-heptane	nC_7
methylcyclohexane	MCH
toluene	TOL

GEOLOGICAL SETTING

The Tazhong area is an essential oil and gas exploration target in the Tarim Basin. The TZ-I gas field is located on the northern slope of the Tazhong Uplift in the Tarim Basin, between the central horst zone and Tazhong No. 1 fault zone, as shown in **Figure 1A**. The area of the field is ~264.54 km^2. It is the deepest

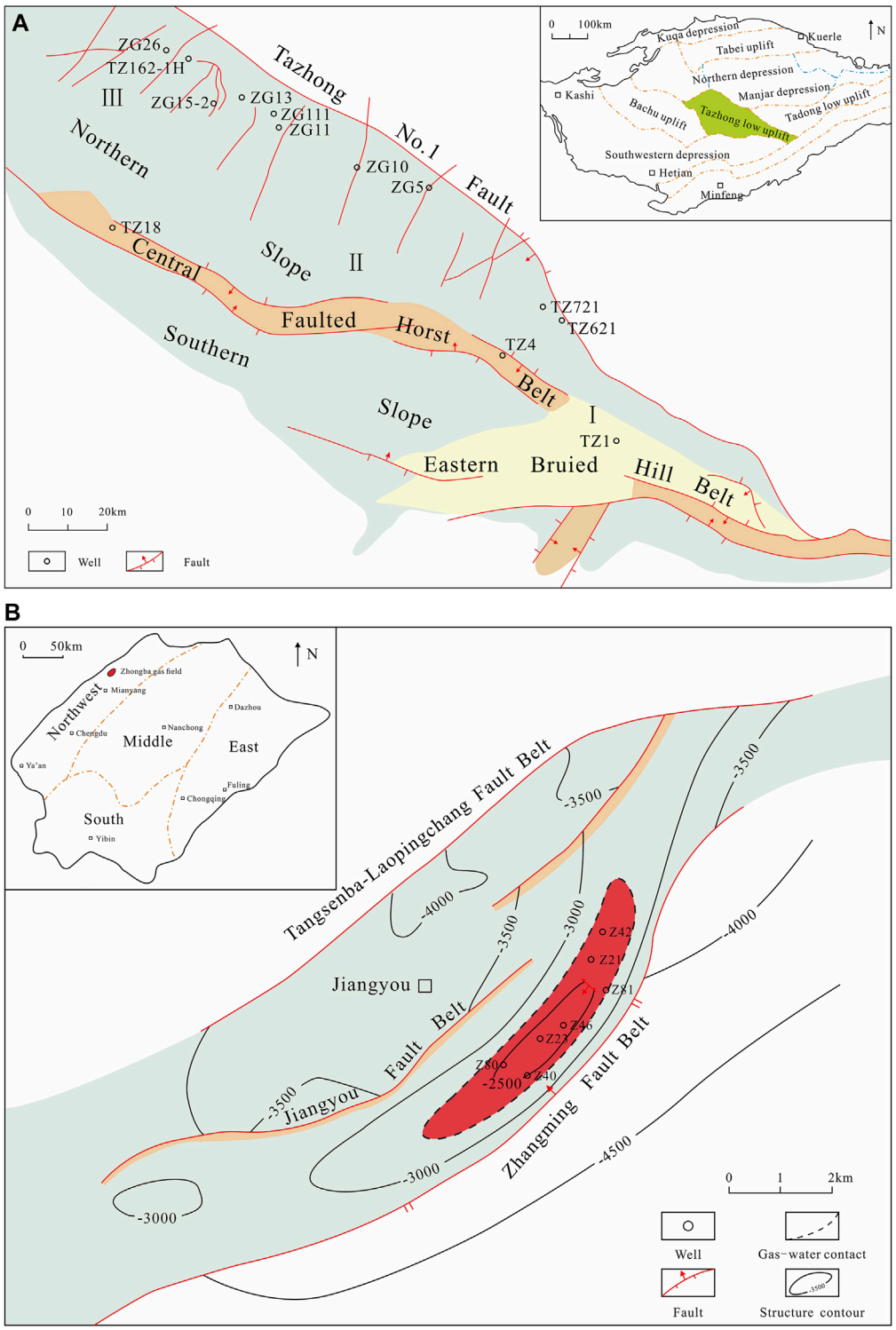

FIGURE 1 | Sketch maps showing the location of the TZ-I gas field in Tarim basin **(A)** (modified after Wu et al., 2014 and Guan et al., 2020) and ZB gas field in Sichuan basin **(B)** (modified from Zhu et al., 2011).

and oldest large reef-shoal complex condensate gas reservoir discovered in the Tarim Basin. The TZ-I gas field is divided into three zones ordered by the F82 and F14 horst zones. Zone I mainly represents a margin reef-bank condensate gas reservoir and buried hill dolomite condensate gas reservoir in the Lianglitage Formation platform. Zone II is mainly a fracture-

vuggy condensate gas reservoir in the Ordovician Lianglitage Formation and Yingshan Formation. At last, Zone III is the fracture-vuggy reservoir of the Yijianfang Formation (Guan et al., 2020). The buried depth of the three main Ordovician exploitation reservoirs ranges from 4,500 to 7,000 m, while the average buried depth exceeds 5,000 m. The height of the gas column and fluid distribution are controlled by the reservoir growth depth, rather than by the local structure and closure height, with a salient water body but no unified gas-water interface within (Wang et al., 2013; Zhou, 2013). The reservoir features various lithologies and hydrocarbon storage types. The former includes bioclastic, clastic, and reef limestones, and the latter embraces numerous modified pore holes, caves, and fissures. Moreover, the reservoir features physical properties with a porosity of 1.8%–4.1%, with an average of 2.3%, and permeability in the 0.01–452 md range (average estimate = 53 md) (Yang et al., 2007). The natural gas contains 17.5×10^4 to 18.4 $\times$ 10^4 mg/m^3 of hydrogen sulphide. The reservoir water belongs to the $CaCl_2$ type, with an average density and pH value of 1.09 g/cm^3 and 6.87, respectively. These phenomena confirmed good water preservation conditions and relatively weak groundwater activity. The Cambrian and lower Ordovician are composed of thick dolomites with intercalated dark mudstones and shales, which arguably represents the main source rocks (Cai et al., 2009). Besides, the ^{13}C of crude oil from Ordovician reservoir in TZ area (from −31.5‰ to −30.5‰) is consistent with the ^{13}C of kerogen from Cambrian source rock (−31.0‰ to −28.0‰), indicating that the condensate oil and gases derived from Cambrian and lower Ordovician source rocks. The TZ-I fault is an important conducting pathway for oil and gas (Zhao et al., 2009). It is located in the northern margin of the Tazhong low uplift and extends over 200 km. Also, it represents the boundary between the Tazhong low uplift and the Manjar Depression. The TZ-I fault is also the circulation channel of deep hydrothermal fluid with dissolution. The broken rock in the fracture zone receives bidirectional dissolution of atmospheric fresh water and deep hydrothermal fluid. Meanwhile, Karst fracture-vuggy reservoirs are distributed mostly along the strike-slip fault zone. The fault zone is the main factor, governing the fracture-vuggy carbonate reservoir.

The ZB gas field is a NE trending nose structure, located in a low anticline in the front fold belt of Longmen Mountain in the northwestern Sichuan Basin (**Figure 1B**) (Zhu et al., 2011). The gas field is composed of the Xuer gas reservoir of the Triassic Xujiahe Formation (T_3x^2) and Leisan gas reservoir of the Leikoupo Formation (T_2l^3). The Leikoupo Formation comprises a set of marine strata. The buried depth of the Leikoupo gas reservoir ranges from 3,140 to 3,510 m. It virtually represents a compound trap, composed of an anticline and fault-screened structure and a fracture-pore edge type water gas reservoir. The unified original gas-water interface altitude is -2,871 m, the gas-bearing area is 13.4 km^2, the gas-bearing height is 473 m, and the proven reserve is 86.3×10^8 m^3. The original formation pressure of the gas reservoir is 35.3 MPa, and the formation temperature is 86.1°C. The lithology of the reservoir is gray fine crystal dolomite, powdery crystal dolomite, algal debris, and sand debris dolomite of the Lower Leisan Formation. The acid insoluble matter content is <1%, and the thickness is ~100 m. The reservoir was stable in the transverse direction, and the average effective thickness of the gas reservoir was 74.2 m. The main type of storage and permeability space is represented by pinholes, with an effective porosity of 2%–4% (average = 5.4%). The permeability varies from 0.01 md to 35.04 md, and the average water saturation is 39.4%. Natural gas contains hydrogen sulphide and a high content of heavy hydrocarbons. Natural gas mainly originates from marine Cambrian or Permian sapropelic source rocks (Liao et al., 2014). The stable carbon isotope of condensate oil associated with gas from T_2l^3 in ZB gas field varied slightly from −31.5‰ to −31.8‰ also indicated the gases from type II kerogen. The Leikoupo Formation continued to descend and is buried deeply in the Lower Cretaceous, and the maximum thickness of the residual strata of the Lower Cretaceous in northwest Sichuan reached over 1,700 m. It has been previously estimated that the buried depth of the Leisan reservoir in the ZB gas field is >4,000 m, and the paleogeothermal temperature is >200°C. During the deep burial process, which lasted ~70–80 million years from the Early Cretaceous to Tertiary, crude oil was thermally cracked into natural gas. Some of the pores of the Leisan algae sand-debris pinhole dolomite are filled with black and brown bitumen, thereby, physically suggesting petroleum cracking. Given the high temperature, driven by deep burial, the anhydrite contained in the Leikoupo Formation dissolved in the formation water and produced sulphate, which reacted with hydrocarbon gas in the gas reservoir to produce hydrogen sulphide (the sulfuric acid content in the formation water of the Zhongba Leisan strata reached 712–1,109 g/L). Consequently, the hydrogen sulphide content in Zhongba Leisan gas reservoir is as high as 4.95%–8.34%. On one hand, the structural deformation of Zhongba in the late Himalayan period exacerbated the fractures of the reservoir, which was conducive to the seepage of natural gas and obtaining high-production gas wells. On the other hand, the structural trap area and closure were dwindled, fluid potential energy was changed, gas-water interface was adjusted, part of natural gas was lost, and the other part of natural gas reacted with formation water sulphate to generate hydrogen sulphide under the action of thermal catalysis. Moreover, the content of hydrocarbon gas was weakened, and the gas reservoir was somehow damaged.

SAMPLING AND ANALYTIC METHODS

Sampling

Fifteen gas samples were collected at the wellheads of commercial gas production wells using 15 stainless steel cylinders with double valves. First, the cylinder was flushed for 15–20 min to remove air contamination. Second, eight gases were sampled from the TZ-I gas field and seven gases were sampled from the ZB gas field. Note that the pressure inside the cylinder was kept as high as 1–5 MPa.

Analytic Methods

Gas composition, carbon isotope of C_1-C_4 and CO_2, as well as chemical and isotopic compositions of the LHs were analysed. All

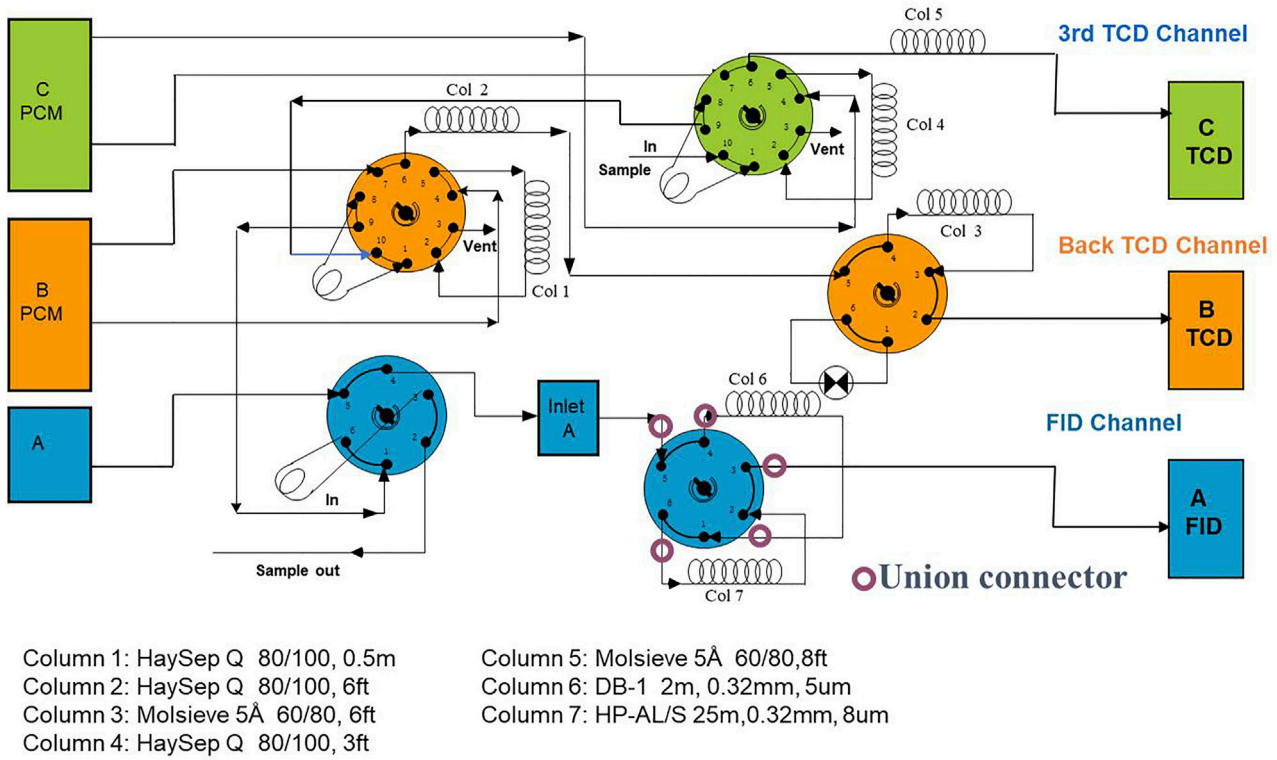

FIGURE 2 | Configuration of Agilent 7890B gas chromatograph (GC) with 5 valves, 7 columns and 3 detectors for analyzing hydrocarbon and non-hydrocarbon components of natural gas.

the sample preparation and measurements were finished in the Key Laboratory of Petroleum Geochemistry at the Research Institute of Petroleum Exploration and Development of PetroChina. The individual hydrocarbon and non-hydrocarbon components of natural gas were identified and quantified using an Agilent 7890B gas chromatograph (GC), equipped with a flame ionisation detector (FID), and two thermal conductivity detectors (TCD). The configuration of Agilent 7890B as shown in **Figure 2**. Helium was used as the carrier gas for the FID and the first TCD. The proportion of N_2, CO_2, and H_2S was detected by the first TCD, and the second TCD only measured the proportion of He which was carried by nitrogen as the carrier gas. All the carrier gas were high purity He (99.9995%) and N_2 (99.9999%). The inlet temperature was set at 150°C. The initial oven temperature was initially set at 35°C for 5 min, then programmed to 100°C at 10°C/min, and finally to 200°C at 20°C/min. The external standard gases indicated the GC had a precision of better than ±0.3 mol% for each component.

Carbon isotopic compositions of the gases were analysed using a Thermo Delta V mass spectrometry interfaced to a Thermo gas chromatograph *via* a combustion interface. Individual gaseous hydrocarbon compounds were separated using a PQ capillary column. Temperatures of the inlet and the oxidation oven were set at 200°C and 980°C, respectively. The gas chromatograph temperature started at 33°C and was kept steady for 5 min, then programmed to rise from 33°C to 80°C at 8°C/min, from 80 to 170°C at 5°C/min, and finally from 170°C to 250°C at 6°C/min. Every sample was analysed at least twice. The stable carbon isotopic values are reported in the δ-notation in per mil (‰) relative to the Vienna Peedee Belemnite standard (VPDB), and the reproducibility for $\delta^{13}C$ measurement is ±0.5‰. The calibrated standard values of the oil-derived gas in ‰ relative to VPDB in our laboratory are $\delta^{13}C_1 = -43.61 \pm 0.09‰$, $\delta^{13}C_2 = -40.24 \pm 0.10‰$ and $\delta^{13}C_3 = -33.79 \pm 0.09‰$. The assigned values are fundamentally traceable to the international carbon isotope standard of VPDB (Dai et al., 2012).

Furthermore, LHs were analysed on a HP5890A gas chromatography with a PONA capillary column. The components were collected with a liquid nitrogen cold trap for 10 min, and the eluting hydrocarbons were detected using a FID at 300°C. The initial oven temperature was maintained at 30°C for 15 min, ramped up to 70°C at a rate of 1.5°C/min and then to 280°C at 2.5°C/min. The standard test mixture contained 53 compounds (i-butane to normal octane). Note that the LH analysis of the test mixture was performed before the analysis of the study samples to ensure the sample analysis quality and comparability of analytical samples at different time periods.

The carbon isotopic compositions of the individual LHs were determined *via* gas chromatography–combustion-isotope ratio monitoring mass spectrometry by freezing the GC column in a cold trap filled with liquid nitrogen. Note that precise and explicit analytical methods were introduced in details in Hu and Zhang (2011). The Thermo Trace GC Ultra gas chromatograph connected to MAT 253 isotopic mass spectrometer (Thermo

TABLE 1 | The molecular composition and stable carbon isotope of natural gas from the TZ- I and ZB gas fields.

Gas fields	Well	Strata	Depth/m	Composition/%												$\delta^{13}C$/‰, VPDB			
				CH_4	C_2H_6	C_3H_8	*i*-C_4	*n*-C_4	C_1-C_4	Dryness	N_2	CO_2	He	H_2S	GSI	CH_4	C_2H_6	C_3H_8	CO_2
TZ-I	ZG162-1H	O_I	6,094.83–6,780	85.3	4.1	1.6	0.4	0.7	92.0	0.93	4.6	3.3	0.04	0.1	0.12	-47.3	-36.4	-30.8	-2.2
	ZG26	O_{II}	6,085.5–6,295	77.7	4.2	5.2	1.7	1.9	90.7	0.86	5.9	3.3	0.05	0.0	0.02	-49.0	-37.0	-32.5	-1.8
	ZG15-2	O_I	5,918.5–6,155	76.4	8.6	4.3	1.0	1.7	91.9	0.83	6.3	1.7	0.04	0.1	0.13	-51.5	-38.4	-32.2	n.d.
	ZG13	O_{II}	6,458–65,504	75.5	10.4	5.2	1.1	2.4	94.5	0.80	1.2	4.2	0.03	0.1	0.12	-49.9	-37.0	-32.0	-5.2
	ZG111	O_{II}	6,008–6,250	88.2	4.4	1.7	0.5	0.7	95.5	0.92	1.7	2.4	0.04	0.4	0.46	-46.7	-33.0	-29.6	n.d.
	ZG11	O_{II}	6,165–6,631.1	89.4	3.6	1.4	0.4	0.7	95.6	0.94	1.9	1.7	0.04	0.8	0.83	-47.5	-35.6	-28.5	-11.9
	TZ721	O_I	5,355.5–5,505	93.8	0.5	0.2	0.0	0.1	94.7	0.99	0.9	4.4	0.04	0.0	0.01	-42.1	-35.6	-31.0	n.d.
	TZ621	O_I	4,851–4,885	91.1	1.7	0.7	0.2	0.3	94.0	0.97	3.4	2.6	0.04	0.0	0.04	-38.2	-34.1	-31.7	-3.0
		Average		84.7	4.7	2.5	0.7	1.1	93.6	0.90	3.2	2.9	0.04	0.2	0.22	-46.5	-35.9	-31.0	-4.8
ZB	Z46	T_2^3	3,134.51	83.4	1.6	0.5	0.1	0.3	85.9	0.97	1.7	5.1	0.04	7.2	7.72	-34.2	-29.3	-27.5	-4.9
	Z40	T_2^3	3,121.7	82.7	1.5	0.5	0.1	0.2	85.1	0.97	2.0	5.2	0.04	7.6	8.21	-34.5	-28.1	-26.9	-4.6
	Z42	T_2^3	3,358.75	82.5	1.6	0.6	0.2	0.3	85.2	0.97	1.6	5.4	0.06	7.7	8.28	-33.5	-28.2	-27.0	-4.4
	Z80	T_2^3	3,120	83.0	1.6	0.5	0.2	0.3	85.4	0.97	2.5	4.2	0.05	7.8	8.35	-34.4	-28.4	-28.6	-5.4
	Z81	T_2^3	3,231.7	84.4	1.4	0.4	0.1	0.2	86.6	0.97	1.5	4.9	0.04	7.0	7.45	-34.2	-28.6	-26.8	-4.6
	Z21	T_2^3	3,303	82.2	1.6	0.5	0.2	0.3	84.8	0.97	2.5	4.9	0.06	7.8	8.45	-33.7	-28.0	-26.5	-4.1
	Z23	T_2^3	3,100	83.3	1.6	0.5	0.1	0.3	85.9	0.97	2.3	4.5	0.04	7.3	7.86	-35.1	-28.0	-26.7	-3.9
		Average		83.1	1.6	0.5	0.2	0.3	85.6	0.97	2.0	4.9	0.05	7.5	8.04	-34.2	-28.4	-27.1	-4.6

n.d., not detected.

Fischer Scientific) *via* a micro-combustion furnace and water-removal assembly. The carrier gas was helium, and the inlet temperature was 200°C. The amount of sample injected is 1–10 ml, and the components were collected with cold trap for 5 min. The initial oven temperature was held at 30°C for 15 min and then programmed to 70°C at 1.5°C/min, then rose from 70°C to 160°C at 3°C/min, finally from 160°C to 250°C at 5 °C/min. The final temperature was held for 20 min. A mixture of standards of n-alkanes from A. Schimmelmann of Indiana University was measured two times before sample testing. Every sample was analysed at least twice. The stable carbon isotopic values were calibrated relative to the PeeDee Belemnite Standard (V-PDB) with an error of less than 0.5‰.

RESULTS

Molecular Composition of Natural Gas

The molecular compositions of the gases from the TZ-I and ZB gas fields are shown in **Table 1**. All the natural gases were dominated by methane, ranging from 75.5% to 93.8% (average = 83.9%). The total contents of C_1-C_4 alkane gases ranged from 84.8% to 95.6% (average = 89.8%). However, some remarkable differences of the alkane gas compositions in the TZ-I and ZB gas fields were identified. The contents of all alkane gases in the TZ-I gas field were higher than those in the ZB gas field. The content in the TZ-I gas field ranged from 90.7% to 95.6% (average = 93.6%) and from 84.8% to 86.6% (average = 85.6%) in the ZB gas field. The gas dryness coefficient, defined as $C_1/(C_1$-$C_4)$, exhibited strong variations (0.80–0.99) with the averages of 0.90 and 0.97 for TZ-I and ZB gas fields, respectively (**Table 1**). The alkane gas composition in the TZ-I gas field strongly with the content of methane from 75.5% to 93.8% and mostly wet gases, $C_1/(C_1$-$C_4) < 0.95$, except the wells TZ621 and TZ721 (**Figure 3A**). The gases in the ZB gas field slightly varied with the concentration of methane from 82.2% to 84.4% and were found to be very dry (the dryness coefficient = ~0.97).

The content of non-hydrocarbon gases exhibited strong variability (4.4%–15.2%) except for noble gas, helium. Notably, greater differences were identified between the gases in the TZ-I and ZB gas fields (**Figure 3B**). In general, non-hydrocarbon gas exhibits high concentration in the ZB gas field, compared with that in the TZ-I gas field. The gas in the TZ-I gas field was mainly composed of N_2 (3.2% on average) and CO_2 (2.9%), while the H_2S contents were extremely low from 0.01% to 0.80%, regardless of the content variation of methane. Meanwhile, in the ZB gas field, the H_2S content was found to be fairly homogeneous, from 7.0% to 7.8%, and the highest (7.5% on average) among non-hydrocarbon gases, followed by CO_2 (4.9% on average) and N_2 (2.0% on average). Besides, the gas souring index (GSI) in the ZB gas field (from 7.45 to 8.45 with an average of 8.04) is greater than that in the TZ-I gas field (from 0.01 to 0.83 with a mean of 0.22).

Carbon Isotope of Gaseous Alkanes

The carbon isotopic compositions of the individual components of the gases in the TZ-I and ZB gas fields are listed in **Table 1**. The

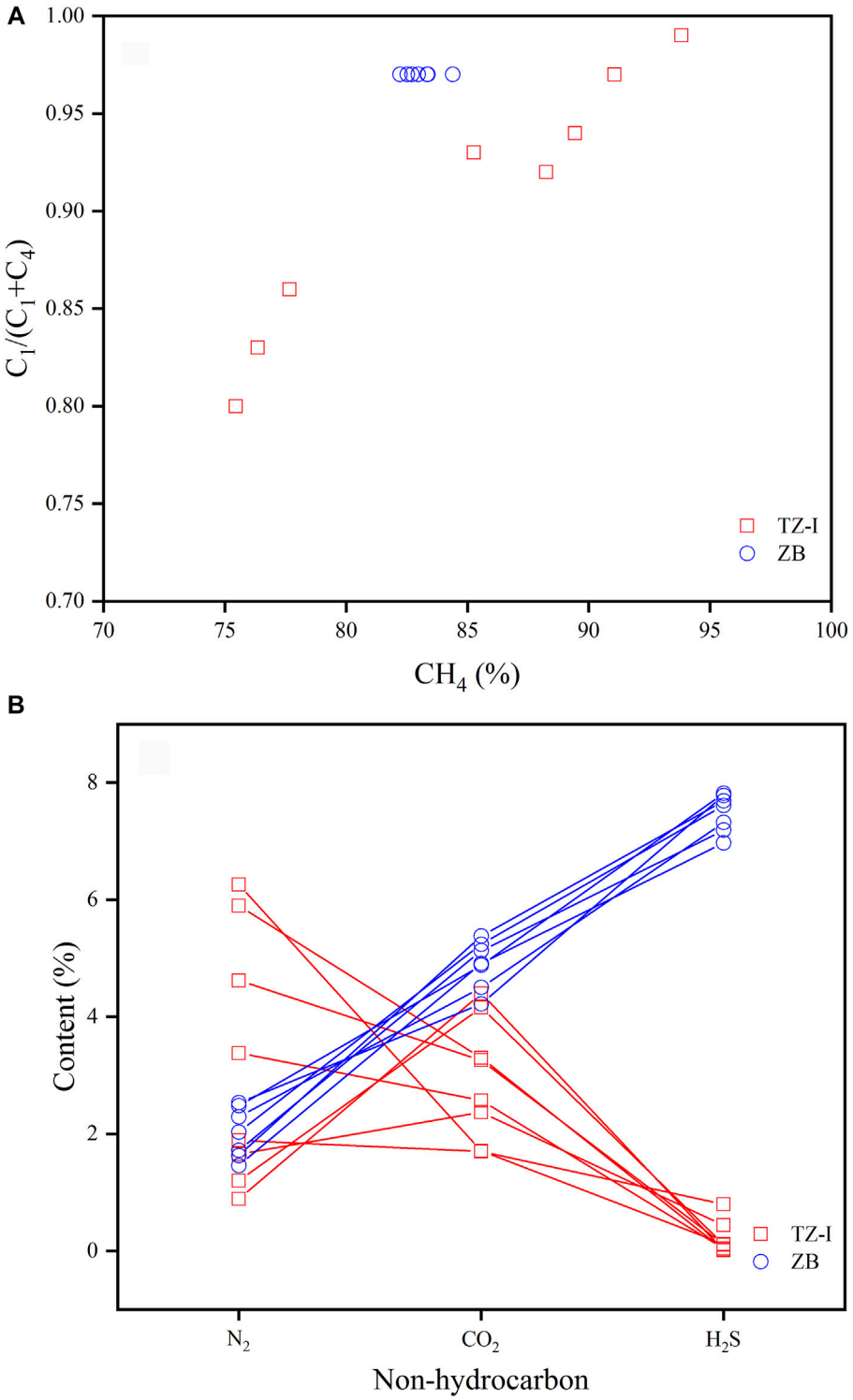

FIGURE 3 | The correlation of $C_1/C_{1\text{-}4}$-CH_4% **(A)** and N_2%-CO_2%-H_2S% **(B)** of natural gases in the TZ-I and ZB gas fields.

methane carbon isotope composition ranged from −51.5‰ to −33.5‰ (average = −40.8‰). The $\delta^{13}C$ value of ethane ranged from −38.4‰ to −28.0‰ (average = −32.4‰), and that of propane ($\delta^{13}C_3$) ranged from −32.5‰ to −26.5‰. **Figure 3** shows that all the gas samples exhibited a normal stable carbon isotope trend for C_1–C_3 alkanes ($\delta^{13}C_1 < \delta^{13}C_2 < \delta^{13}C_3$). However, the carbon isotopes of the natural gas components in the two gas fields significantly varied (**Table 1**;

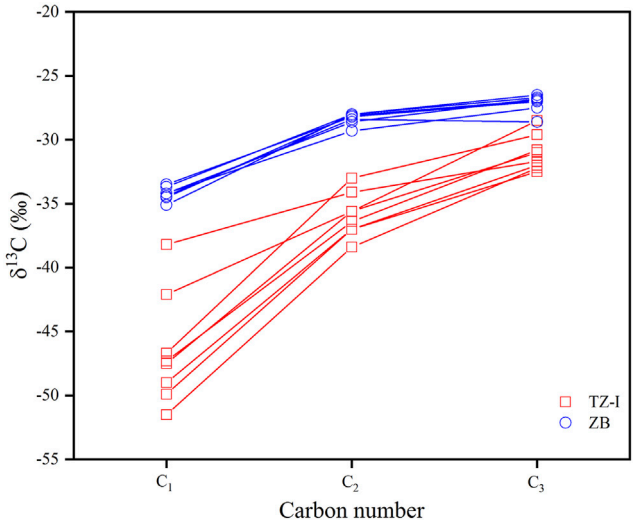

FIGURE 4 | Relationship between $\delta^{13}C$ and carbon number of gases in the TZ-I gas field and the ZB gas field.

Figure 4). The carbon isotopes of the natural gas components in the TZ-I gas field were found to be very light. In particular, the $\delta^{13}C_1$ ranged from −51.5‰ to −38.2‰ (average = −46.5‰), $\delta^{13}C_2$ ranged from -38.4‰ to -33.0‰ (average = −35.9‰), and $\delta^{13}C_3$ ranged from −32.5‰ to −28.5‰ (average = -31.0‰). The carbon isotopes of natural gas components in the ZB gas field were relatively heavy, whereas $\delta^{13}C_1$ ranged from −35.1‰ to −33.5‰ (average = -34.2‰), $\delta^{13}C_2$ ranged from −29.3‰ to −28.0‰ (average = −28.4‰), and $\delta^{13}C_3$ ranged from −28.6‰ to −26.5‰ (average = −27.1‰). The $\delta^{13}C_1$, $\delta^{13}C_2$, $\delta^{13}C_3$ values in the ZB gas field exceeded 12.3‰, 7.5‰, and 3.9‰, respectively, compared to those in the TZ-I gas field. The CO_2 carbon isotope in some samples was also measured. It was found that the $\delta^{13}C$ values ranged from -11.9‰ to −1.8‰, thereby indicating that the carbon isotope variation of CO_2 in the two gas fields was very high. The $\delta^{13}C_{CO2}$ in the TZ gas field widely ranged from −11.9‰ to −1.8‰, whereas in the ZB gas field presented a slightly vary from −5.4‰ to −3.9‰.

Molecular Variability of C_6-C_7 LHs

The molecular variability of the C_6-C_7 LHs, associated with the gases in the TZ-I and ZB gas fields is shown in **Table 2** and **Figures 6A,B**. The gases in the two gas fields were notably characterized by the high content of normal and isoalkanes. Among the C_6-C_7 compounds, the relative contents of normal and isoalkanes ranged from 60.5% to 85.9% (average = 71.6%) higher than that of cycloalkanes and aromatics, respectively (**Table 2**). Meanwhile, the concentration of normal and isoalkanes in the ZB gas fields was lower than TZ-I gas field, about 10% (**Figure 6A**). The content of nC_7 was found to be highest among nC_7, DMCP, and MCH, it ranged from 44.1% to 70.5% (average = 54.6%). However, the abundance of DMCP and MCH were somewhat low, with the average estimates of 15.4% and 30.0%, respectively. Furthermore, there were some differences in the compositions of nC_7, DMCP, and MCH compounds. Specifically, the relative nC_7 content in the TZ-I gas field was significantly higher than that in the ZB gas field (**Figure 6B**). In contrast, the relative contents of DMCP and MCH in the ZB gas field were higher than those of the TZ-I field.

Isotope Variability

The compound-specific carbon isotopic compositions of the C_6-C_7 hydrocarbons of the 15 gas samples measured to examine their isotopic characteristics, the response to TSR and origin. Given the co-elution or insufficient partition of adjacent hydrocarbon components and low abundance, only nine compounds were analysed from isotope ratio perspective. The carbon isotope compositions of the nine compounds of the various samples

TABLE 2 | The relative contents of C_6-C_7 light hydrocarbons of natural gases from the TZ-I and ZB gas fields.

Gas fields	Well	Strata	Depth/m	C_6-C_7/GC area, %					C_7/GC area, %		
				Normal alkane	Isoalkane	Normal and isoalkanes	Cycloalkane	Aromatic	Heptane	Dimethyl cyclopentane	Methyl cyclohexane
TZ-I	ZG162-1H	O_{II}	6,094.83–6,780	45.9	32.5	78.5	13.7	7.8	70.5	8.3	21.2
	ZG26	O_{III}	6,085.5–6,295	41.1	38.4	79.5	15.1	5.4	67.7	8.9	23.4
	ZG15-2	O_{II}	5,918.5–6,155	40.5	39.3	79.8	14.6	5.6	64.2	12.9	22.9
	ZG13	O_{III}	6,458–6,550.36	38.3	47.6	85.9	10.8	3.3	58.2	21.3	20.5
	ZG111	O_{III}	6,008–6,250	41.2	33.9	75.1	18.0	6.9	65.3	9.2	25.6
	ZG11	O_{III}	6,165–6,631.1	39.0	34.0	72.9	19.2	7.9	57.8	12.6	29.6
	TZ721	O_I	5,355.5–5,505	37.3	32.8	70.1	17.0	12.9	60.7	13.2	26.1
	TZ621	O_I	4,851–4,885	38.2	35.9	74.2	18.1	7.7	59.4	14.3	26.3
		Average		40.2	36.8	77.0	15.8	7.2	63.0	12.6	24.4
ZB	Z46	T_2l^3	3,134.5	31.4	35.1	66.5	22.3	11.2	46.6	18.8	34.6
	Z40	T_2l^3	3,121.7	32.2	38.8	71.0	16.8	12.2	44.3	22.1	33.6
	Z42	T_2l^3	3,358.8	32.9	39.0	71.9	20.4	7.7	44.6	20.8	34.6
	Z80	T_2l^3	3,120	31.8	32.4	64.2	25.1	10.7	45.6	17.8	36.6
	Z81	T_2l^3	3,231.7	30.6	30.5	61.1	25.8	13.1	44.1	16.6	39.3
	Z21	T_2l^3	3,303	31.2	31.6	62.7	25.6	11.7	44.6	17.4	38.1
	Z23	T_2l^3	3,100	29.6	30.9	60.5	25.2	14.3	45.0	17.0	38.0
		Average		31.4	34.0	65.4	23.0	11.5	45.0	18.6	36.4

TABLE 3 | Individual light hydrocarbons carbon isotope of fifteen gases from the TZ-I and ZB gas fields.

Gas fields	Well	Strata	Depth/m	$\delta^{13}C$‰(VPDB)								
				2-MP	3-MP	nC_6	MCP	BEN	CH	nC_7	MCH	TOL
TZ-I	ZG162-1H	O_{II}	6,094.83–6,780	-28.8	-29.0	-29.4	-28.0	-28.1	*-29.5*	-30.1	-31.0	-28.5
	ZG26	O_{III}	6,085.5–6,295	-29.6	-29.6	-30.9	-29.7	-29.1	*-30.2*	-30.7	-31.5	-30.1
	ZG15-2	O_{II}	5,918.5–6,155	-28.9	-28.9	-29.8	-28.6	-29.3	*-31.0*	-30.9	-31.5	-29.5
	ZG13	O_{III}	6,458–6,550.36	-28.6	-29.4	-30.3	-30.0	-28.1	*-30.8*	-30.3	-32.3	-29.6
	ZG111	O_{III}	6,008–6,250	-28.4	-29.8	-29.5	-30.9	-29.0	*-31.9*	-30.9	-32.6	-30.5
	ZG11	O_{III}	6,165–6,631.1	-27.8	-28.4	-28.7	-29.1	-27.7	*-29.2*	-29.9	-29.8	-28.5
	TZ721	O_I	5,355.5–5,505	-28.1	-28.6	n.d.	-30.1	-28.6	*-29.0*	-30.2	-30.6	-30.0
	TZ621	O_I	4,851–4,885	-28.5	-28.9	-30.5	-28.7	-26.8	*-30.1*	-30.8	-32.3	-28.1
		Average		-28.6	-29.1	-29.9	-29.4	-28.3	*-30.2*	-30.5	-31.5	-29.4
ZB	Z46	T_2l^3	3,134.5	-28.3	-28.6	-27.8	-26.6	-27.9	*-27.2*	-30.8	-27.4	-28.1
	Z40	T_2l^3	3,121.7	-29.1	-28.7	-28.2	-27.0	-28.1	*-28.8*	-30.1	-28.1	-28.2
	Z42	T_2l^3	3,358.8	-27.5	-28.1	n.d.	-27.0	-27.9	-27.4	-30.5	-28.0	-28.0
	Z80	T_2l^3	3,120	-28.1	-28.0	-26.7	-26.5	-27.4	-27.6	-30.1	-28.0	-28.1
	Z81	T_2l^3	3,231.7	-28.8	-28.4	-25.8	-26.6	-27.8	-27.8	-30.2	-28.2	-28.2
	Z21	T_2l^3	3,303	-28.2	-28.7	n.d.	-27.8	-28.0	-28.4	-29.8	-29.0	-28.3
	Z23	T_2l^3	3,100	-28.9	-30.0	-28.7	-28.2	-27.0	-28.0	-28.4	-27.5	-28.0
		Average		-28.4	-28.6	-27.4	-27.1	-27.7	-27.9	-30.0	-28.0	-28.1

n.d., not detected.

are listed in **Table 3**. Despite slight offsets of single compounds between the different samples, all the compounds were generally enriched in ^{12}C. The carbon isotopes of branched alkanes 2-MP, 3-MP, nC_6, and nC_7 were relatively light. They ranged from −29.6‰ to −27.5‰, −30.0‰ to −28.0‰, −30.9‰ to −5.8‰ and −30.9‰ to −28.4‰, respectively. The carbon isotopes of cycloalkanes, such as MCP, CH, and MCH, somewhat differed in the two gas fields. Their carbon isotopes were relatively light in the TZ-I gas field with the average estimates of −29.4‰, −30.2‰, and −31.5‰, respectively. Meanwhile, the average values of the ZB gas field were −27.1‰, −27.9‰, and −28.0‰, respectively. The average difference was more significant than 2‰, while the difference in carbon isotopes of light aromatic BEN and TOL was rather minor. Specifically, the average values of carbon isotopes of BEN were found to be −28.3‰ and −27.7‰ in the TZ-I and ZB gas fields, respectively with only 0.6‰ differences. However, the differences were identified in the carbon isotopes of TOL; in average, the TZ-I gas field was 1.3‰ lighter than the ZB gas field.

DISCUSSION

Genetic Type of Gases

The molecular and isotopic variability of the C_1-C_4 and C_6-C_7 LHs can indicate the genetic type (oil-associated or coal-derived, primary cracking, or secondary cracking) of natural gas (Stahl and Carey, 1975; Dai et al., 2005; Hu et al., 2008). Bernard et al. (1978) have already utilized the $C_1/(C_2+C_3)$ ratio and $\delta^{13}C$ of methane (Bernard diagram) to elucidate the origin and possible process of gas generation. The $\delta^{13}C_1$ versus $\delta^{13}C_2$ cross plot is typically used to classify the origin and maturity trends of natural gas (Jenden et al., 1988; Rooney et al., 1995; Berner and Faber, 1996; Tilley and Muehlenbachs, 2013). Numerous empirical studies of gas carbon isotope geochemistry, conducted in the Chinese sedimentary basins, have suggested a threshold of $\delta^{13}C_2$ (−28‰) can be used to differentiate the origin of thermogenic gases. Generally, thermogenic gases, generated from sapropelic source rocks (oil-associated gas) are characterised by $\delta^{13}C_2$ values lighter than −28‰, whereas ethane and propane derived from humic source rocks (coal-derived gas) own carbon isotopic values heavier than -28‰ (Dai et al., 1992, Liang, et al., 2002; Dai et al., 2005; Xiao et al., 2008). The majority of the gases were plotted in the lower area of the cross plot of $\delta^{13}C_1$ vs. $\delta^{13}C_2$, $\delta^{13}C_2 < -28$‰, whereas the gases from the TZ-I gas field exhibited relatively lighter $\delta^{13}C_2$ values than those from ZB gas field (**Figure 5**). The difference between the two gas fields coincided with oil-associated gas or type II kerogen maturity trends (Jenden et al., 1988; Rooney et al., 1995; Tilley and Muehlenbachs, 2013). Therefore, we suggested that the heavier $\delta^{13}C_2$ of ZB gas field may be caused by the increasing process of thermal. Although some of the $\delta^{13}C_2$ of the gas originated from type III kerogen was < −28‰, methane, ethane, and propane carbon isotope distributions in these gases exhibited negative carbon isotope characteristics ($\delta^{13}C_1 > \delta^{13}C_2 > \delta^{13}C_3$) and were distributed in the over-mature area of source rocks (Dai et al., 2016). Different with the unusual gases, the carbon isotopes of the natural gas in the TZ-I and ZB gas fields were relatively light and presented a positive sequence distribution (**Figure 4**). This finding indicates that the natural gas in the TZ-I and ZB gas fields was derived from the Type II kerogen and not from the Type III kerogen in the over-mature stage.

The molecular composition and isotopic ratio of C_6-C_7 LHs can unravel the genetic type and source of natural gas. The ternary diagram of nC_7, DMCP, and MCH is also useful for distinguishing coal-derived gases from oil-associated gases (Hu et al., 1990; Dai, 1993; Hu et al., 2008). Hu et al. (2008) have already proposed that coal-derived gas typically contains >50% MCH among nC_7, DMCP, and MCH. The ternary composition

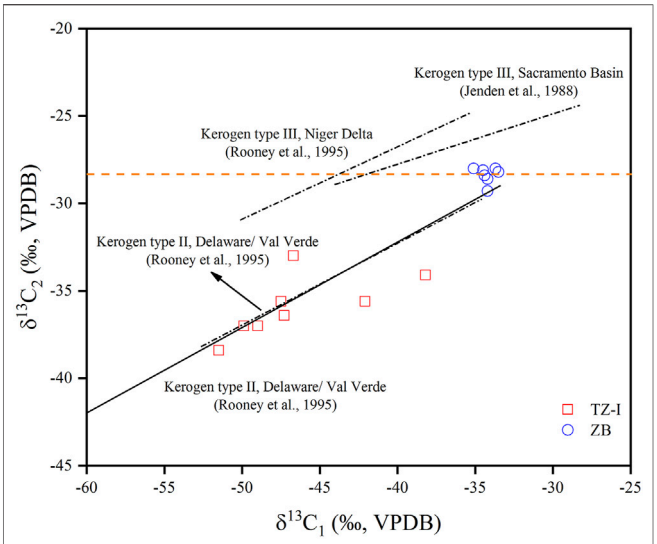

FIGURE 5 | $\delta^{13}C_1$ verse $\delta^{13}C_2$ cross plot of natural gases from TZ-I and ZB gas fields. Also shown are the maturity trend of type II kerogen (Rooney et al., 1995; Tilley and Muehlenbachs, 2013) and type III kerogen (Jenden et al., 1988; Rooney et al., 1995).

diagram of C_6-C_7 n-alkanes, isoalkanes, and cycloalkanes can be also widely used to identify the origin of natural gas (Hu et al., 2008). The relative content of C_6-C_7 normal and isoalkanes in the oil-associated gas was >30%, coal-derived gas was opposite. As shown in **Figure 6A**, the gases from the TZ-I and ZB gas fields were located in the area of oil-associated gas. In the ternary diagram of nC_7, DMCP and MCH, all of the gases from the TZ-I and ZB gas fields were also located in oil-associated gas areas (**Figure 6B**), thereby suggesting that these gases originated from the type II kerogen. Stable carbon isotope information, carried by the LHs, associated with oils and gas can be applied to elucidate the secondary alteration, origin, and correlation of oil and gas (Rooney et al., 1995; Whiticar and Snowdon, 1999; George et al., 2002; Li et al., 2003; Dai et al., 2005; Hu et al., 2008). Jiang et al. (2000) have already argued that the carbon isotopes of BEN and TOL are mainly affected by the type of organic matter, rather by thermal evolution and migration. Hence, the isotope ratio of light aromatic compound can be used to reflect the type of organic matter. Hu et al. (2008) have proposed the identification index of coal-derived gas and oil-associated gas by studying the carbon isotopes of BEN, TOL, CH, and MCH in light hydrocarbon from typical sedimentary basins in China. Generally, the carbon isotopes of BEN, TOL, CH, and MCH in the coal-derived gas are heavier. Specifically, $\delta^{13}C_{BEN}$ = −23‰, $\delta^{13}C_{TOL}$ = −24‰, $\delta^{13}C_{CH}$ = −24‰, and $\delta^{13}C_{MCH}$ = −24‰ can be used as cut-off points for the identification of oil-associated gas and coal-derived gas. As shown in **Figures 7A,B**, the gases from the TZ-I and ZB gas fields were located in the area of oil-associated gas, thereby indicating that these gases were sourced from type II kerogen.

The molecular components and individual carbon isotopes of C_1-C_4 and LHs demonstrated that the gases from TZ-I gas field in Tarim Basin and ZB gas field in Sichuan Basin sourced from sapropelic source rocks or type II kerogen. Our findings are consistent with the results of Wu et al. (2014) and Liao et al. (2014) on the gas genetic types.

Stage of Oil Cracking Gas

The generation of oil-associated gas by sapropelic organic matter can be further divided into kerogen cracking (primary cracking) gas and oil cracking (secondary cracking) gas. Numerous geochemistry studies aimed to distinguish between these two gases which generated from the thermal degradation (Behar et al., 1992; Prinzhofer and Huc, 1995; Lorant et al., 1998; Prinzhofer and Rocha (2000)). The chemical composition and stable carbon isotope characteristics of natural gas indicated that kerogen cracking gas and oil cracking gas can be identified. The cracking experiments, conducted by Hill et al. (2003) have already indicated that oil cracking gas in a closed system exhibited a low dryness index and $\delta^{13}C_1$ value. At a similar pyrolysis temperature, the $\delta^{13}C_1$ value of the kerogern cracking gas was heavier than that of the oil cracking gas due to the differences of precursors (Tian et al., 2007). Behar et al. (1992) have demonstrated that the C_1/C_2 and C_2/C_3 ratios followed different variation trends in the process of kerogen cracking and oil cracking. On this basis, the different variation tendencies in the ln (C_1/C_2)–ln (C_2/C_3) plot can be used to identify kerogen cracking and oil cracking gases (Prinzhofer and Huc, 1995). However, these parameters are not applicable for TZ gas fields (Wu et al., 2014). Lorant et al. (1998) and Prinzhofer et al. (2010) further suggested a quantitative ($\delta^{13}C_2$-$\delta^{13}C_3$) -(C_2/C_3) plot to classify kerogen cracking and oil cracking gases. Note that the gases from the TZ-I and ZB gas fields are barely located in the area of the primary cracking except minor samples (**Figure 8**). Tian et al. (2007) have reported that as the pyrolysis temperature increased, the $\delta^{13}C_1$ values of oil cracking gases decreased in the early cracking stage and then increased. The $\delta^{13}C_2$-$\delta^{13}C_3$ values of the gases in the TZ-I gas field ranged from −7.1‰ to −3.4‰, and the carbon isotopes of ethane (average = −35.9‰) and propane (average = −31.0‰) are very light. Furthermore, the C_2/C_3 values were relatively small, ranging from 0.81 to 2.64, although there were a certain amount of C_2 and C_3 (**Table 1**). This indicates that the gases in the TZ-I gas field were the early product of the secondary cracking of oil. **Figure 8** shows that the gases of ZB gas field are in the transition zone between the NSO compounds and crude oil cracking gas due to the smaller values of $\delta^{13}C_2$-$\delta^{13}C_3$ (from -1.8‰ to 1.2‰) compared to the TZ-I gas field. However, the gases in this gas field were drier with extremely low concentration of C_{2+} and more enrich ^{13}C in methane, demonstrating the maturity of the natural gas was higher than of the TZ-I gas field. The quite homogeneous heavier carbon isotope of ethane and propane also suggest that the gases undergo similar high thermal evolution. Therefore, it is reasonable to suggest that the natural gas in the ZB gas field may have mainly originated from the late cracking of oil or secondary cracking of wet gas rather than the NSO. Generally,

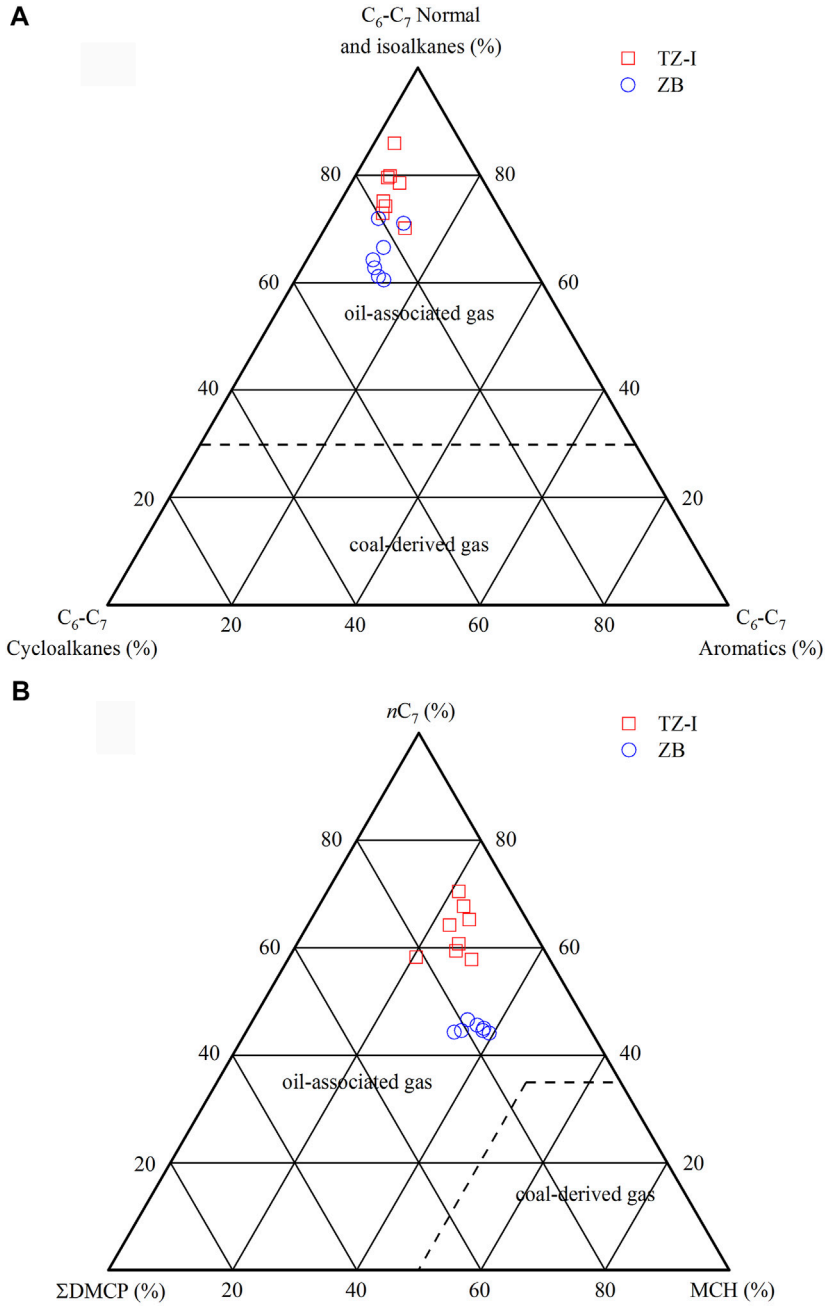

FIGURE 6 | Ternary diagram of C_6–C_7 normal and isoalkane, cycloalkane, aromatic **(A)** and ternary diagram of nC_7, DMCP and MCH **(B)** in the TZ-I and ZB gas fields (modified from Hu et al., 2008).

the gases in the ZB gas field have experienced more actively oil cracking than those in TZ-I gas field.

Thermochemical Sulphate Reduction Degree

In most cases, TSR represents the only source that contributes high concentrations of H_2S to the deeply buried gas reservoirs (Orr, 1977; Worden and Smalley, 1996; Mougin et al., 2007; Hao et al., 2008). Worden et al. (1995) combined the gas source index (GSI), defined as $H_2S/(H_2S + \sum C_n)$, with total hydrocarbon gases to characterize the extent of TSR. Under the premise of sufficient sulfate concentration in reservoir, Hao et al. (2008) further proposed the three-stage TSR series corresponding to liquid-hydrocarbon-involved TSR, heavy-hydrocarbon-gas-dominated TSR and the methane-dominated TSR stage, respectively. In brief, the hydrocarbons are consumed and transformed to CO_2, H_2S, carbonate mineral if thermochemical sulphate reduction occurs in economic carbonate reservoir.

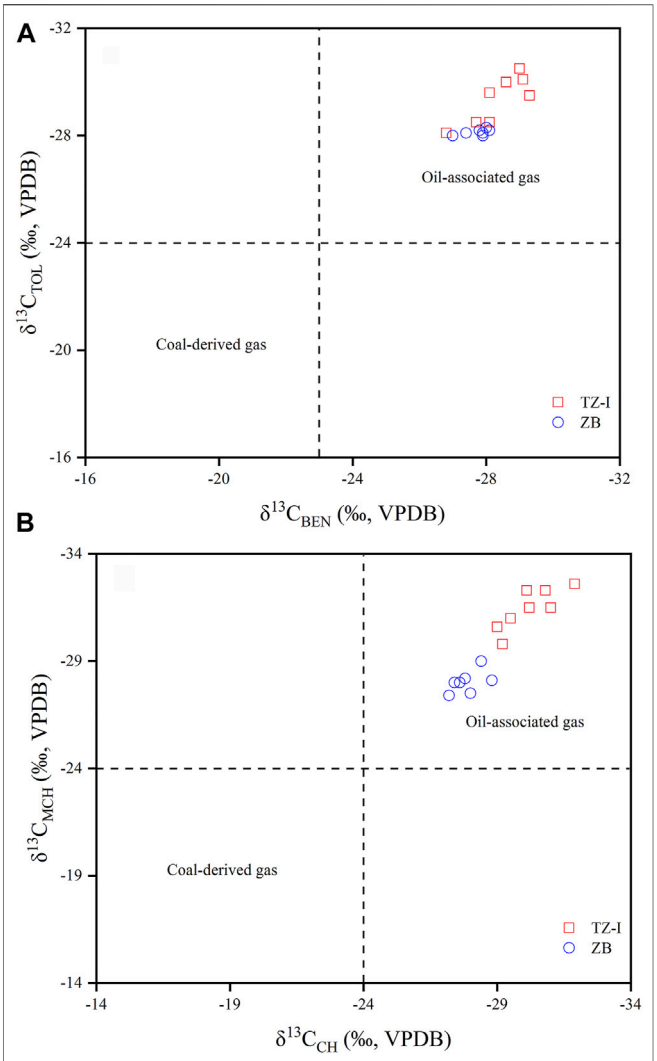

FIGURE 7 | $\delta^{13}C_{BEN}$ verse $\delta^{13}C_{TOL}$ **(A)**, $\delta^{13}C_{CH}$ verse $\delta^{13}C_{MCH}$ **(B)** cross plots of natural gases from TZ-I and ZB gas fields (modified from Hu et al., 2008).

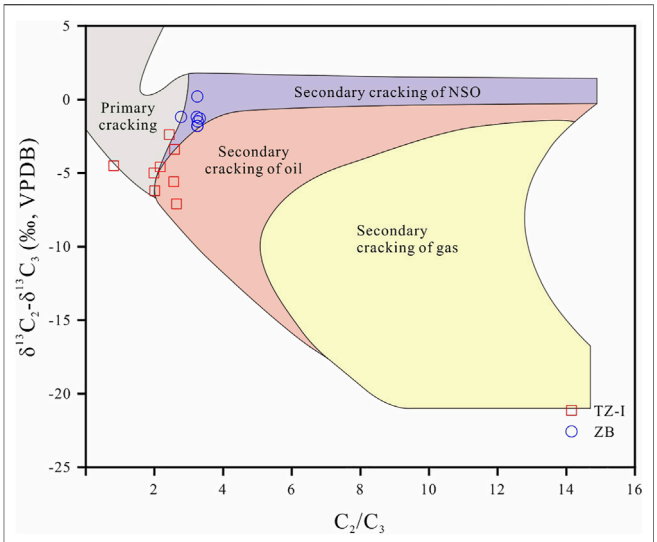

FIGURE 8 | The ($\delta^{13}C_2$-$\delta^{13}C_3$) and C_2/C_3 cross plot of natural gases from the TZ-I and ZB gas fields (Based on Prinzhofer et al., 2010).

Generally, the carbon isotope of CO_2 from TSR should be lighter due to the degradation of hydrocarbons.

Both the TZ-I and ZB gas fields have experienced TSR (Zhu et al., 2011; Cai et al., 2015), but the extent of the impact may have varied. The H_2S content of the gas in the TZ-I gas field was very low (<0.2%), and even in the gas with high maturity (TZ721 and TZ261 wells with dryness coefficients of >0.95), the content of H_2S was <0.05% (**Table 1**). Potentially, liquid-hydrocarbon-involved TSR did not significantly contribute to H_2S, which was found in the reservoirs (Hao et al., 2008). The concentration of total hydrocarbon gases in TZ-I gas field was still greater than 90%, implicitly demonstrating that the natural gases (C_1-C_4) rarely undergo heavy-hydrocarbon-gas-dominated or methane-dominated TSR (**Figure 9A**). Besides the disorder content relationship between CO_2 and GSI, a great discrepancy in the carbon isotope of CO_2 (from −11.9‰ to −2.8‰), suggesting that the CO_2 is controlled by other factors rather than a by-product of TSR (**Figure 9B**). Wu et al. (2014) suggested that the CO_2 with high $\delta^{13}C$ value in the natural gases were generated by mixing inorganic and organic CO_2. Some case studies (Krouse et al., 1988; Rooney et al., 1995; Worden and Smalley, 1996; Hao et al., 2008; Cai et al., 2015) and oxidation experiments (Pan et al., 2006) have suggested that the TSR affects the carbon isotope compositions of hydrocarbon gas to increase $\delta^{13}C$ of methane and ethane with increasing GSI. **Figures 9C,D** show that the carbon isotopes of methane and ethane in the TZ-I gas field were very light, and the carbon isotope ratios were rarely controlled by GSI, which was slightly affected by the TSR. The molecular compositions and isotopic characteristics all show that the gases in TZ-I gas field may be in the early liquid-hydrocarbon-involved TSR stage.

The gases of ZB gas field displayed high content H_2S (**Table 1**), and Zhu et al. (2011) suggested that TSR was most likely responsible for the occurrence of H_2S. The dryness coefficient of the gases in the ZB gas field was 0.97, with very low heavy hydrocarbon gas (**Table 1**). Besides, the decreasing content of total hydrocarbon gases was linearly associated with rising GSI (**Figure 9A**). These phenomena strongly showed that the methane, ethane and propane of the gases in the ZB gas field had been altered or consumed by TSR. Hence, there should be a certain amount of lighter CO_2 by hydrocarbon oxidation. The invariable content and very homogeneous carbon isotope of CO_2 in the ZB gas field indicated that the CO_2 was derived from a similar reaction or source, but its isotope was heavier beyond typical organic origin. Carbon dioxide in the ZB gas field may be mixed gas that is generated from TSR and carbonate decomposition under acidic conditions. Moreover, Worden and Smalley (1996) have indicated that elemental sulphur is an essential product of reactions between C_{2+} hydrocarbon gases and sulphate. The ^{12}C-rich C_{2+} gases were preferentially lost due to the weaker bond strengths of ^{12}C hydrocarbons (Krouse et al., 1988; Worden and Smalley, 1996). This phenomenon, in turn, triggers an increase in ^{13}C of ethane with increasing GSI. Elemental sulphur was only observed in sour gas reservoirs (Zhu et al., 2011), and the $^{13}C_2$ of associated gas is very

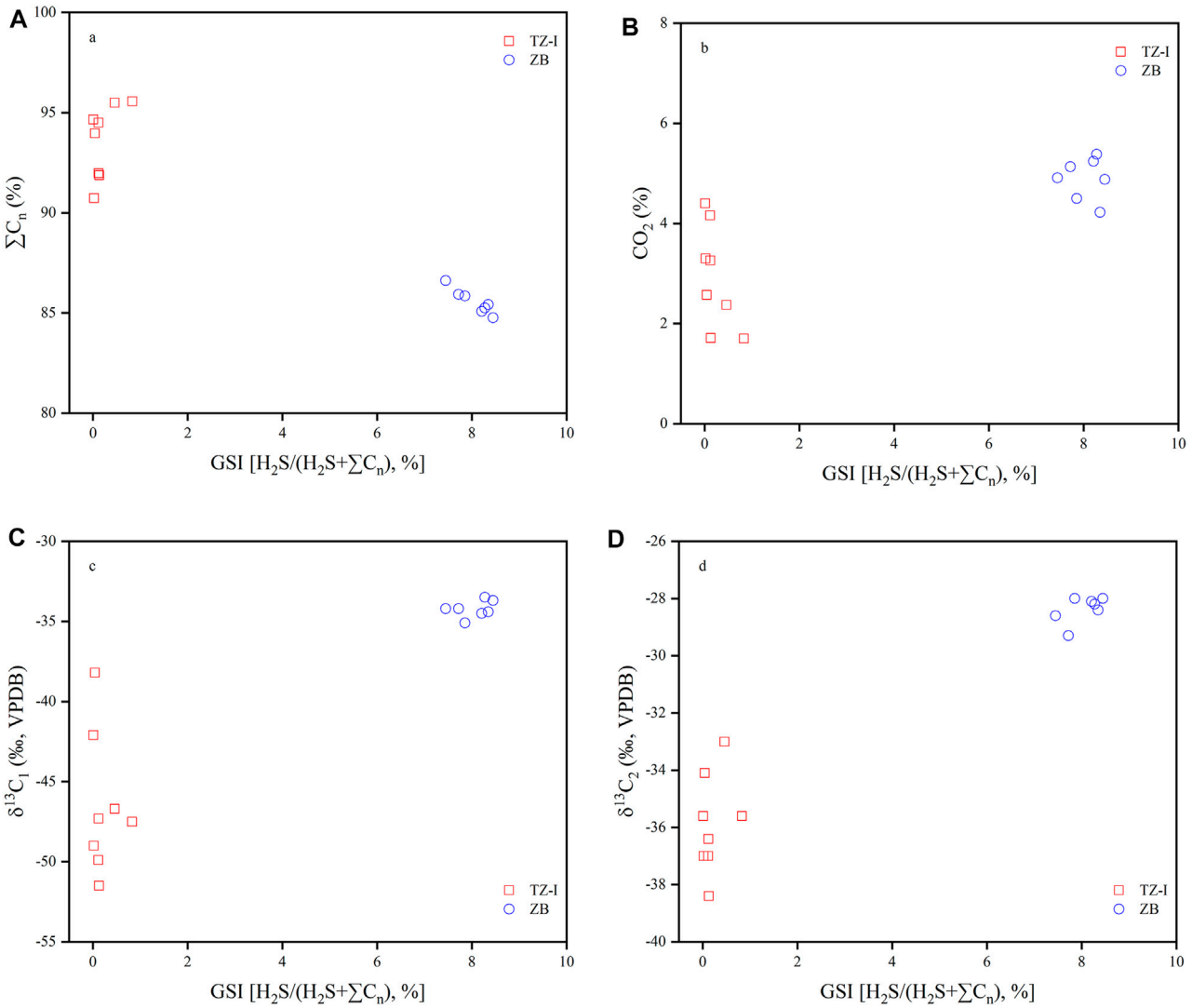

FIGURE 9 | Variation of $\sum C_n$ **(A)**, CO_2 **(B)**, $\delta^{13}C_1$ **(C)** and $\delta^{13}C_2$ **(D)** with gas souring index (GSI) for natural gases in the TZ-I and ZB gas fields, GSI = $H_2S/(H_2S+\sum C_n)$.

heavy. These findings further suggested that thermochemical sulphate reduction occurs in C_{2+}. As shown in **Figures 9C,D**, the $^{13}C_1$ has no significant variation with GSI, but the $^{13}C_2$ increasing enriched ^{13}C with the ascend of GSI. These characteristics were consistent with those of the heavy-hydrocarbon-gas-dominated TSR proposed by Hao et al. (2008) and indicated that methane-dominant TSR has barely happened yet. Therefore, the degree of TSR in the ZB gas field is in the stage of heavy-hydrocarbon-gas-dominated TSR and significantly differs from that in the TZ-I gas field. The latter was in the stage of the early liquid-hydrocarbon-involved TSR.

Effects of TSR on Carbon Isotope of Individual LHs

Whiticar and Snowdon (1999) have proposed that the carbon isotope ratios of the gasoline-range fraction (C_5-C_8) in Brazeau River condensate samples were strongly affected by TSR, the isotopic discrepancy among affected and unaffected specific compound even up to 10‰. In general, this induced the enrichment in ^{13}C for most compounds in TSR condensates relative to the samples less affected or unaffected by TSR (Rooney et al., 1995; Whiticar and Snowdon, 1999). Notably, the gases in the ZB and TZ-I gas fields were in different stages of TSR. Specifically, the gas in the TZ-I gas field was in the stage of the early liquid-hydrocarbon-involved TSR. Meanwhile, the gas in the ZB gas field was in the heavy-hydrocarbon-gas-dominated TSR. The carbon isotopes of individual LHs, associated with the gases in these two gas fields, indicated that TSR exerted a complex effect on the carbon isotopes of these individual LHs. Meanwhile, rather minor effect on the branch chain compounds 2-MP and 3-MP is identified. For instance, the $\delta^{13}C$ value of 2-MP in the TZ-I gas field was −28.6‰ on average, and that of the ZB gas field was

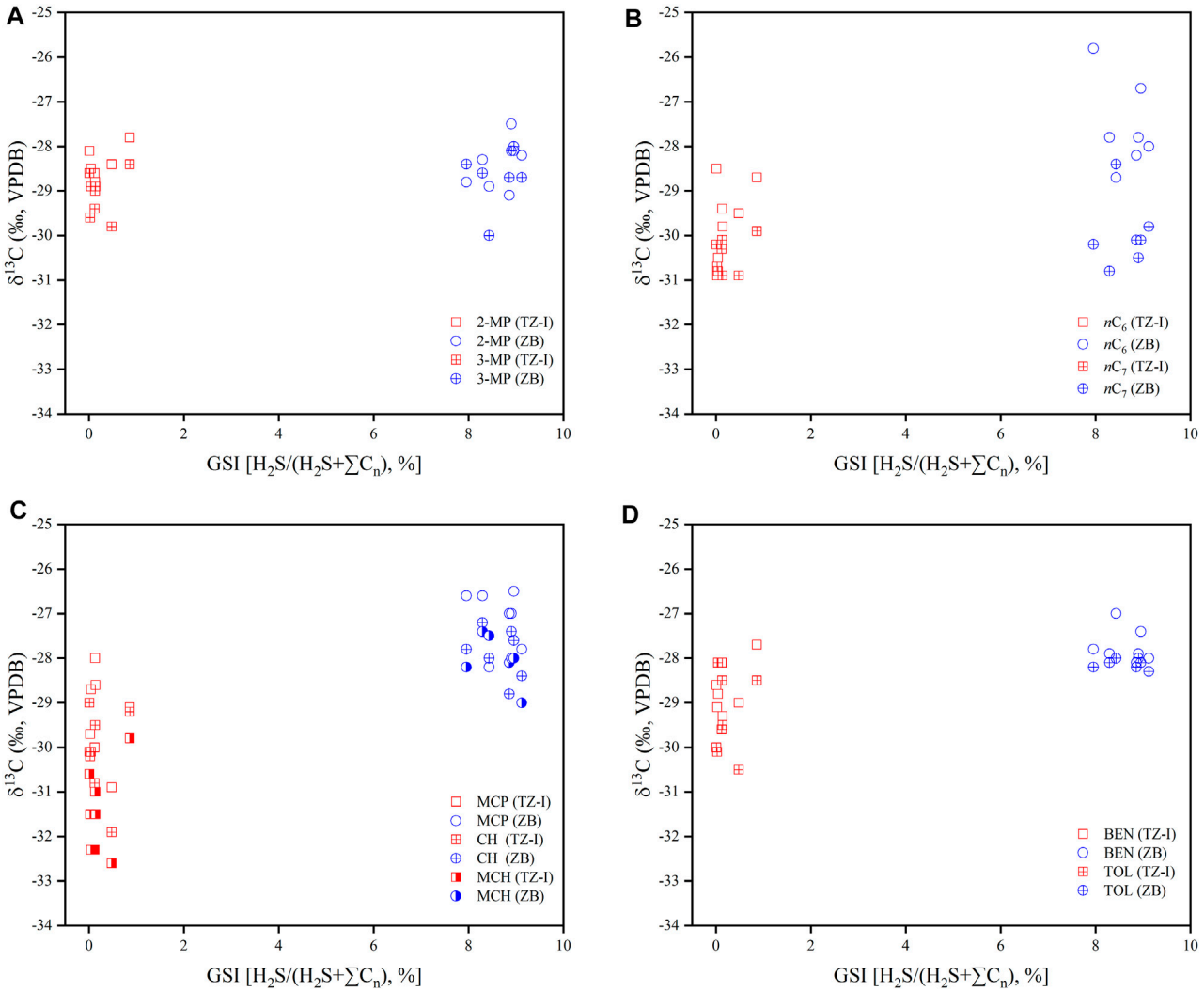

FIGURE 10 | The cross plot of $H_2S/(H_2S+\sum C_n)$ and ^{13}C for individual LHs [**(A)** 2-MP and 3-MP, **(B)** nC_5 and nC_6, **(C)** MCP, CH and MCH, **(D)** BEN and TOL] in the TZ-I and ZB gas fields.

−28.4‰. Thus, there was a slight difference (**Figure 10A**), which does not agree with the results from Whiticar and Snowdon (1999). They argued that TSR has a significant influence on the carbon isotopes of individual LHs. This disagreement was probably driven by the degree of TSR influence on the carbon isotopes of the individual LHs. During the liquid-hydrocarbon-involved and heavy-hydrocarbon-gas-dominated TSR stages, the TSR slightly affected the carbon isotopes of the individual LHs. For normal alkanes, there was also little effect by TSR (**Figure 10B**). However, for BEN and TOL carbon isotopes, it had been previously reported that maturity had little effect and was a good indicator for determining natural gas genetic types and gas sources (Li et al., 2003; Hu et al., 2008). The mean $\delta^{13}C$ values of BEN and TOL in the TZ-I gas field were −28.6‰ and −29.4‰, respectively, while those in the ZB gas field were −27.7‰ and −28.1‰, respectively. The comparative analysis of the two gas fields indicated that different degrees of TSR also slightly affected the carbon isotopes of BEN and TOL, about 1‰ (**Figure 10D**). Some relatively great differences in $\delta^{13}C$ for cyclocalkanes (2‰) were identified in these two gas fields, such as MCP, CH, and MCH (**Figure 10C**; **Table 3**). In the TZ-I gas field, the $\delta^{13}C$ values for MCP, CH, and MCH were −29.4‰, −30.2‰, −31.5‰ on average, respectively. As seen, they were more enriched ^{12}C than that in the ZB gas field during the hydrocarbon-gas-dominant TSR. Moreover, TSR was found to cause variations in the carbon isotopes of BEN and TOL, as well as cycloalkanes (**Figures 10C,D**). The carbon isotope of the above compound will be heavier with the TSR process. However, these variations were much lower than those of Whiticar and Snowdon (1999). The mechanism which caused the carbon isotope distribution discrepancy of normal, isoalkanes, cycloalkanes and aromatic compounds will be the focus on further research. Overall, the influence of TSR on the carbon isotopes of individual LHs should be considered, while using these carbon isotope indices to identify the

genetic type and source of marine natural gas, especially at the cut-off point ($\delta^{13}C$ = −24‰) of coal-derived gas and oil-associated gas.

CONCLUSION

The components and stable carbon isotope ratios of the C_1-C_4 and the individual LHs (C_6-C_7) in the gases from the TZ-I and ZB gas fields were used to examine the genetic type, oil cracking gas stage, TSR degree, and effects of TSR on carbon isotope of individual LHs. The main findings of this study are summarised below.

1) The $^{13}C_2$ of gases from the TZ-I gas field in Tarim Basin and ZB gas field in Sichuan Basin were always enriched ^{12}C (<-28.0‰), whereas the gases from the TZ-I gas field exhibited relatively lighter $\delta^{13}C_2$ values than those from the ZB gas field. The relative content of C_6-C_7 normal and iso-alkanes was found to be much greater than 30%. The gases were also located in the oil-associated area of the ternary diagram of C_7 LHs, which was similar to the distribution of C_6-C_7 LHs.The concentration of heptane was highest. The $\delta^{13}C_{BEN}$ and $\delta^{13}C_{TOL}$, $\delta^{13}C_{CH}$, and $\delta^{13}C_{MCH}$ values were < −26‰. These findings indicated that the gases in the TZ-I and ZB gas fields originated from the type II kerogen and were oil-associated gases.
2) The gases from the TZ-I and ZB gas fields were oil-cracking gases. It was demonstrated that the gas in the TZ-I gas field was in the early stage of oil cracking. The dryness coefficient of the gas in the ZB gas field was 0.97 and $\delta^{13}C_2$ value was higher than that in the TZ-I gas field. Meanwhile, the gas from the ZB gas field may have originated mainly from the secondary cracking stage of oil and wet gas.
3) The GSI value of gas from the TZ-I gas field was found to be very low, with quite a few heavy hydrocarbon gases and relatively lighter $\delta^{13}C_1$ and $\delta^{13}C_2$. This magnitude was somehow driven by TSR, and the gas may be in the early liquid carrier-involved TSR stage. The gas in the ZB gas field contained high contents of H_2S and CO_2 and lower C_{2+}. The carbon isotope of ethane becomes heavier as GSI increased. It was shown that the degree of TSR in the ZB gas field was in the heavy-hydrocarbon-gas-dominated TSR stage.
4) During the liquid-hydrocarbon-involved and heavy-hydrocarbon-gas-dominated TSR stages, the TSR slightly affected the carbon isotopes of individual LHs. Notably, TSR had a negligible effect on the branch chain compounds 2-MP and 3-MP and slightly affected on aromatic compound BEN and TOL. Meanwhile, greater effects (2‰) on carbon isotopes were identified for cycloalkanes such as MCP, CH, and MCH. The mechanism that caused these different phenomena will be the core for further research. To conclude, the carbon isotopes of individual LHs should be considered while using these indices to identify the genetic type and source of marine natural gas.

DATA AVAILABILITY STATEMENT

The original contributions presented in the study are included in the article/supplementary material, further inquiries can be directed to the corresponding author.

AUTHOR CONTRIBUTIONS

GH: manuscript writing. JG, LT, JS, and CF: manuscript discussion. XW: assistance in sample collection. ZL: assistance in sample analysis. All authors contributed to the article and approved the submitted version.

FUNDING

The first funding is a study about reservoir-forming rule and key exploration technology of large gas field which was funded by Petrochina Science and Technology Projects, and the Contract Number is 2021DJ0601. The second funding is a study on the carbon isotope composition and geochemical significance of light hydrocarbons in natural gas from the Sichuan Basin, and it was supported by National Natural Science Foundation of China (42172149).

ACKNOWLEDGMENTS

We thank Professor Jinxing Dai for long-standing help and associated Professor Wenlong Zhang for experiment help from the PetroChina Research Institute of Petroleum Exploration and Development.

REFERENCES

Behar, F., Kressmann, S., Rudkiewicz, J., and Vandenbroucke, M. (1992). Experimental Simulation in a Confined System and Kinetic Modelling of Kerogen and Oil Cracking. *Org. Geochem.* 19 (1-3), 173–189. doi:10.1016/0146-6380(92)90035-v

BeMent, W. O., Levey, R. A., and Mango, F. D. (1995). "The Temperature of Oil Generation as Defined with C7 Chemistry Maturity Parameter (2,4-Dmp/2,3-DMP Ratio)," in *Organic Geochemistry: Developments and Applications to Energy, Climate, Environment and Human History* (Donostian-San Sebastian: European Association of Organic Geochemists), 505–507.

Bernard, B. B., Brooks, J. M., and Sackett, W. M. (1978). Light Hydrocarbons in Recent Texas Continental Shelf and Slope Sediments. *J. Geophys. Res.* 83 (C8), 4053. doi:10.1029/jc083ic08p04053

Berner, U., and Faber, E. (1996). Empirical Carbon Isotope/maturity Relationships for Gases from Algal Kerogens and Terrigenous Organic Matter, Based on Dry, Open-System Pyrolysis. *Org. Geochem.* 24 (10-11), 947–955. doi:10.1016/s0146-6380(96)00090-3

Cai, C., Hu, G., Li, H., Jiang, L., He, W., Zhang, B., et al. (2015). Origins and Fates of H2S in the Cambrian and Ordovician in Tazhong Area: Evidence from Sulfur Isotopes, Fluid Inclusions and Production Data. *Mar. and Petroleum Geol.* 67, 408–418. doi:10.1016/j.marpetgeo.2015.05.007

Cai, C., Hu, W., and Worden, R. H. (2001). Thermochemical Sulphate Reduction in Cambro-Ordovician Carbonates in Central Tarim. *Mar. and Petroleum Geol.* 18 (6), 729–741. doi:10.1016/s0264-8172(01)00028-9

Cai, C., Zhang, C., Cai, L., Wu, G., Jiang, L., Xu, Z., et al. (2009). Origins of Palaeozoic Oils in the Tarim Basin: Evidence from Sulfur Isotopes and Biomarkers. *Chem. Geol.* 268 (3-4), 197–210. doi:10.1016/j.chemgeo.2009.08.012

Dai, J. (1993). Identification of Coal Formed Gas and Oil Type Gas by Light Hydrocarbons. *Petroleum Explor. Dev.* 20 (5), 26–32. (in Chinese with English abstract).

Dai, J., Li, J., Luo, X., Zhang, W., Hu, G., Ma, C., et al. (2005). Stable Carbon Isotope Compositions and Source Rock Geochemistry of the Giant Gas Accumulations in the Ordos Basin, China. *Org. Geochem.* 36 (12), 1617–1635. doi:10.1016/j.orggeochem.2005.08.017

Dai, J., Ni, Y., Huang, S., Gong, D., Liu, D., Feng, Z., et al. (2016). Secondary Origin of Negative Carbon Isotopic Series in Natural Gas. *J. of Nat. Gas Geoscience* 1 (1), 1–7. doi:10.1016/j.jnggs.2016.02.002

Dai, J., Song, Y., Chen, K., Hong, F., and &Fan, G. (1992). Characteristics of Carbon Isotopes of Organic Alkane Gases in Petroliferous Basins of China. *J. of Petroleum Sci. and Eng.* 7 (3-4), 329–338.

Dai, J., Xia, X., Li, Z., Coleman, D. D., Dias, R. F., Gao, L., et al. (2012). Inter-laboratory Calibration of Natural Gas Round Robins for δ2H and δ13C Using Off-Line and On-Line Techniques. *Chem. Geol.* 310-311, 49–55. doi:10.1016/j.chemgeo.2012.03.008

George, S. C., Boreham, C. J., Minifie, S. A., and Teerman, S. C. (2002). The Effect of Minor to Moderate Biodegradation on C 5 to C 9 Hydrocarbons in Crude Oils. *Org. Geochem.* 33 (12), 1293–1317. doi:10.1016/s0146-6380(02)00117-1

Guan, B., Zhang, C., Li, S., Han, J., Zhao, L., and Xiong, C. (2020). Three-stage Reservoir Unit Description and Benefit Development of Fracture-Controlled Cave Carbonate Reservoirs in Tazhong Uplift, Tarim Basin. *Nat. Gas. Geosci.* 31 (12), 1766–1778. (in Chinese with English abstract). doi:10.11764/j.issn.1672-1926.2020.04.009

Hao, F., Guo, T., Zhu, Y., Cai, X., Zou, H., and Li, P. (2008). Evidence for Multiple Stages of Oil Cracking and Thermochemical Sulfate Reduction in the Puguang Gas Field, Sichuan Basin, China. *Bulletin* 92 (5), 611–637. doi:10.1306/01210807090

Hill, R. J., Tang, Y., and Kaplan, I. R. (2003). Insights into Oil Cracking Based on Laboratory Experiments. *Org. Geochem.* 34 (12), 1651–1672. doi:10.1016/s0146-6380(03)00173-6

Hu, G., Li, J., and Li, J. (2008). Preliminary Study on the Origin Identification of Natural Gas by Parameters of Light Hydrocarbon. *Sci. China Ser. D Earth Sci.* 51 (S1), 131–139. doi:10.1007/s11430-008-5017-x

Hu, G., Li, J., Xie, Z., and Yu, C. (2018). *Geochemistry of Light Hydrocarbons Associated with Natural Gas*. Beijing: Petroleum Industry Press. (in Chinese with English abstract).

Hu, G., and Zhang, S. (2011). Characterization of Low Molecular Weight Hydrocarbons in Jingbian Gas Field and its Application to Gas Sources Identification. *Energy Explor. Exploitation* 29 (6), 777–795. doi:10.1260/0144-5987.29.6.777

Hu, T., Ge, B., and Zhang, Y. (1990). The Development and Application of Fingerprint Parameters for Hydrocarbons Absorbed by Source Rocks and Light Hydrocarbon in Natural Gas. *Petroleum Explor. Dev.* 12 (4), 375–379. (in Chinese with English abstract).

Jenden, P., Newell, K., Kaplan, I., and Watney, W. (1988). Composition and Stable-Isotope Geochemistry of Natural Gases from Kansas, Midcontinent, U.S.A. *Chem. Geol.* 71 (1-3), 117–147. doi:10.1016/0009-2541(88)90110-6

Jiang, Z., Luo, X., Li, Z., Zhang, Y., and Pang, X. (2000). Carbon Isotope Composition of Benzene and Toluene as a New Index for Correlation of Gases with Their Source Rocks. *Geochemica* 29 (4), 410–415. (in Chinese with English abstract). doi:10.19700/j.0379-1726.2000.04.015

Krouse, H. R., Viau, C. A., Eliuk, L. S., Ueda, A., and Halas, S. (1988). Chemical and Isotopic Evidence of Thermochemical Sulphate Reduction by Light Hydrocarbon Gases in Deep Carbonate Reservoirs. *Nature* 333 (6172), 415–419. doi:10.1038/333415a0

Li, J., Luo, X., Li, Z. S., Jiang, Z., Hu, G., and Xie, Z. (2003). Carbon Isotope Value of Toluene as a New Index for Correlation of Gases with Their Source Rocks. *Nat. Gas. Geosci.* 14 (3), 177–180. (in Chinese with English abstract). doi:10.11764/j.issn.1672-1926.2003.03.117

Liang, D., Zhang, S., Zhao, M., and Wang, F. (2002). Hydrocarbon Sources and Stages of Reservoir Formation in Kuqa Depression, Tarim Basin. *Chin. Sci. Bull.* 47 (S1), 62–70. doi:10.1007/bf02902820

Liao, F., Yu, C., Wu, W., and Liu, D. (2014). Stable Carbon and Hydrocarbon Isotopes of Natural Gas from the Zhongba Gas Field in the Sichuan Basin and Implication for Gas-Source Correlation. *Nat. Gas. Geosci.* 25 (1), 79–86. (in Chinese with English abstract). doi:10.11764/j.issn.1672-1926.2014.01.0079

Liu, Q. Y., Worden, R. H., Jin, Z. J., Liu, W., Li, J., Gao, B., et al. (2013). TSR Versus Non-TSR Processes and Their Impact on Gas Geochemistry and Carbon Stable Isotopes in Carboniferous, Permian and Lower Triassic Marine Carbonate Gas Reservoirs in the Eastern Sichuan Basin, China. *Geochim. Cosmochim. Acta* 100 (1), 96–115.

Lorant, F., Prinzhofer, A., Behar, F., and Huc, A. (1998). Carbon Isotopic and Molecular Constraints on the Formation and the Expulsion of Thermogenic Hydrocarbon Gases. *Chem. Geol.* 147 (3-4), 249–264. doi:10.1016/s0009-2541(98)00017-5

Mango, F. (1997). The Light Hydrocarbons in Petroleum: a Critical Review. *Org. Geochem.* 26 (7-8), 417–440. doi:10.1016/s0146-6380(97)00031-4

Mougin, P., Lamoureux-Var, V., Bariteau, A., and Huc, A. (2007). Thermodynamic of Thermochemical Sulphate Reduction. *J. of Petroleum Sci. and Eng.* 58 (3-4), 413–427. doi:10.1016/j.petrol.2007.01.005

Orr, W. L. (1997). *Geologic and Geochemical Controls on the Distribution of Hydrogen Sulfide in Natural Gas: Advances in Organic Geochemistry: Madrid, Enadisma*, 571–597.

Pan, C., Yu, L., Lui, J., and Fu, J. (2006). Chemical and Carbon Isotopic Fractionations of Gaseous Hydrocarbons during Abiogenic Oxidation. *Earth and Planet. Sci. Lett.* 246 (1-2), 70–89. doi:10.1016/j.epsl.2006.04.013

Prinzhofer, A., and Rocha, M. (2000). Geochemical Characterization of Natural Gas: A Physical Multivariable Approach and its Applications in Maturity and Migration Estimates. *AAPG Bul.* 84, 1152–1172. doi:10.1306/a9673c66-1738-11d7-8645000102c1865d

Prinzhofer, A., Dos Santos Neto, E. V., and Battani, A. (2010). Coupled Use of Carbon Isotopes and Noble Gas Isotopes in the Potiguar Basin (Brazil): Fluids Migration and Mantle Influence. *Mar. and Petroleum Geol.* 27 (6), 1273–1284. doi:10.1016/j.marpetgeo.2010.03.004

Prinzhofer, A., and Huc, A. (1995). Genetic and Post-genetic Molecular and Isotopic Fractionations in Natural Gases. *Chem. Geol.* 126 (3-4), 281–290. doi:10.1016/0009-2541(95)00123-9

Rooney, M., Claypool, G., and Moses Chung, H. (1995). Modeling Thermogenic Gas Generation Using Carbon Isotope Ratios of Natural Gas Hydrocarbons. *Chem. Geol.* 126 (3-4), 219–232. doi:10.1016/0009-2541(95)00119-0

Stahl, W. J., and Carey, B. D. (1975). Source-rock Identification by Isotope Analyses of Natural Gases from Fields in the Val Verde and Delaware Basins, West Texas. *Chem. Geol.* 16 (4), 257–267. doi:10.1016/0009-2541(75)90065-0

Tassi, F., Bonini, M., Montegrossi, G., Capecchiacci, F., Capaccioni, B., and Vaselli, O. (2012). Origin of Light Hydrocarbons in Gases from Mud Volcanoes and CH4-Rich Emissions. *Chem. Geol.* 294-295, 113–126. doi:10.1016/j.chemgeo.2011.12.004

Tian, H., Xiao, X. M., Li, X. Q., Xiao, Z. Y., Shen, J. Q., and Liu, D. H. (2007). Comparison of Gas Generation and Carbon Isotope Fractionation of Methane From Marine Kerogen- and Crude Oil-Cracking Gases. *Geochimica* 36 (1), 71–77. (in Chinese with English abstract)

Thompson, K. F. M. (1983). Classification and Thermal History of Petroleum Based on Light Hydrocarbons. *Geochimica Cosmochimica Acta* 47 (2), 303–316. doi:10.1016/0016-7037(83)90143-6

Tilley, B., and Muehlenbachs, K. (2013). Isotope Reversals and Universal Stages and Trends of Gas Maturation in Sealed, Self-Contained Petroleum Systems. *Chem. Geol.* 339, 194–204. doi:10.1016/j.chemgeo.2012.08.002

Vieth, A., and Wilkes, H. (2006). Deciphering Biodegradation Effects on Light Hydrocarbons in Crude Oils Using Their Stable Carbon Isotopic Composition: A Case Study from the Gullfaks Oil Field, Offshore Norway. *Geochimica Cosmochimica Acta* 70 (3), 651–665. doi:10.1016/j.gca.2005.08.022

Wang, Z., Su, J., Zhu, G., Han, J., and Wang, Y. (2013). Characteristics and Accumulation Mechanism of Quasi-Layered Ordovician Carbonate Reservoirs in the Tazhong Area, Tarim Basin. *Energy Explor. Exploitation* 31 (4), 545–567. doi:10.1260/0144-5987.31.4.545

Welte, D. H., Kratochvil, H., Rullkötter, J., Ladwein, H., and Schaefer, R. G. (1982). Organic Geochemistry of Crude Oils from the Vienna Basin and an Assessment of Their Origin. *Chem. Geol.* 35, 33–68. doi:10.1016/0009-2541(82)90018-3

Whiticar, M. J., and Snowdon, L. R. (1999). Geochemical Characterization of Selected Western Canada Oils by C5–C8 Compound Specific Isotope Correlation (CSIC). *Org. Geochem.* 30 (9), 1127–1161. doi:10.1016/s0146-6380(99)00093-5

Worden, R., and Smalley, P. (1996). H_2S-producing Reactions in Deep Carbonate Gas Reservoirs: Khuff Formation, Abu Dhabi. *Chem. Geol.* 133 (1-4), 157–171. doi:10.1016/s0009-2541(96)00074-5

Worden, R. H., Smalley, P. C., and Oxtoby, N. H. (1995). Gas Souring by Thermochemical Sulfate Reduction at 140°C. *AAPG Bull.* 79, 854–863.

Wu, X., Tao, X., and Hu, G. (2014). Geochemical Characteristics and Genetic Types of Natural Gas from Tazhong Area in the Tarim Basin, NW China. *Energy Explor. Exploitation* 32 (1), 159–174. doi:10.1260/0144-5987.32.1.159

Xiao, Z., Xie, Z., Li, Z., and Ma, C. (2008). Isotopic Characteristics of Natural Gas of Xujiahe Formayion in Southern and Middle of Sichuan Basin. *Geochimica* 37 (3), 245–250. (in Chinese with English abstract). doi:10.19700/j.0379-1726.2008.03.007

Xiao, Q., Sun, Y., Zhang, Y., and Chai, P. (2012). Stable Carbon Isotope Fraction of Individual Light Hydrocarbons in the C6-C8 Range in Crude Oil as Induced by Natural Evaporation: Experimental Results and Geological Implications. *Org. Geochem.* 50, 44–56

Yang, H., Han, J., Chen, L., Wu, C., and Ji, Y. (2007). Characteristics and Patterns of Complex Hydrocarbon Accumulation in the Lower Paleozoic Carbonate Rocks of the Tazhong Paleouplift. *Oil and Gas Geology* 28 (6), 784–790. (in Chinese with English abstract)

Zhao, W., Zhu, G., Zhang, S., Zhao, X., Sun, Y., Wang, H., et al. (2009). Relationship between the Later Strong Gas-Charging and the Improvement of the Reservoir Capacity in Deep Ordovician Carbonate Reservoir in Tazhong Area, Tarim Basin. *Chin. Sci. Bull.* 54 (17), 3076–3089. doi:10.1007/s11434-009-0457-z

Zhou, X. (2013). Accumulation Mechanism of Complicated Deep Carbonate Reservoir in the Tazhong Area, Tarim Basin. *Energy Explor. Exploitation* 31 (3), 429–457. doi:10.1260/0144-5987.31.3.429

Zhu, G., Zhang, S., Huang, H., Liang, Y., Meng, S., and Li, Y. (2011). Gas Genetic Type and Origin of Hydrogen Sulfide in the Zhongba Gas Field of the Western Sichuan Basin, China. *Appl. Geochem.* 26 (7), 1261–1273. doi:10.1016/j.apgeochem.2011.04.016

Conflict of Interest: Authors GH, JG, LT, JS, ZL and CF were employed by the company PetroChina. Author XW was employed by the company Sinopec.

frontiers | Frontiers in Earth Science

ORIGINAL RESEARCH
published: 22 June 2022
doi: 10.3389/feart.2022.884445

A Comparison of the Geochemical Characteristics of Ultra-Deep Natural Gas in the Kuqa Foreland and Marine Craton Areas in the Tarim Basin, China

Cong Yu, Yunyan Ni, Jinxing Dai*, Yuanyuan He, Chenchen Fang and Fengrong Liao*

Research Institute of Petroleum Exploration and Development, Petrochina, Beijing, China

OPEN ACCESS

Edited by:
Jon Hawkings,
University of Pennsylvania,
United States

Reviewed by:
Dongya Zhu,
SINOPEC Petroleum Exploration and Production Research Institute, China
Shuai Yin,
Xi'an Shiyou University, China

****Correspondence:***
Yunyan Ni
niyy@petrochina.com.cn
Jinxing Dai
djx@petrochina.com.cn

Specialty section:
This article was submitted to Geochemistry, a section of the journal Frontiers in Earth Science

Received: *26 February 2022*
Accepted: *31 May 2022*
Published: *22 June 2022*

Citation:
Yu C, Ni Y, Dai J, He Y, Fang C and Liao F (2022) A Comparison of the Geochemical Characteristics of Ultra-Deep Natural Gas in the Kuqa Foreland and Marine Craton Areas in the Tarim Basin, China. Front. Earth Sci. 10:884445. doi: 10.3389/feart.2022.884445

This research analyzed the composition and hydrocarbon isotope geochemical characteristics of ultra-deep natural gas (buried deeper than 6000 m) in more than 130 wells in the Tarim Basin. Characteristics of the ultra-deep natural gas components in the Tarim Basin are as follows: natural gas in the Kuqa sandstone reservoir is developed as dry gas, with a high methane content (an average of 95.53%) and a low ethane content (an average of only 1.39%). The ultra-deep gas of the marine craton carbonate reservoirs in the North Tarim-Central Tarim-East Tarim area is developed as wet gas. It is mainly composed of methane ranging from 56.1% to 98.8%, with an average content of 76.36% and also contains a small amount of ethane amounting to 6.74%. CO_2 and H_2S contents of ultra-deep condensate gas in the Central Tarim area are high, with maximum values of 24.2% and 23.1%, respectively. Isotopic characteristics are as follows: $\delta^{13}C_1$ values of Kuqa natural gas are distributed between –36‰ and –25.3‰, with an average of –28.2‰, $\delta^{13}C_2$ values are distributed between –26.2‰ and –13.8‰, with an average of –18.3‰. Most gas samples in Kuqa area are developed with the reversal of carbon isotopic series as $\delta^{13}C_2 > \delta^{13}C_3$, and the $\delta^{13}C_{CO2}$ values are distributed between –19.5‰ and –10.3‰. The $\delta^{13}C_1$ values of ultra-deep gas in marine craton carbonate rocks are distributed between –54.4‰ and –33.3‰, with an average of –42.6‰. $\delta^{13}C_2$ values are distributed between –41.1‰ and –29.4‰, with an average of –33.8‰, and $\delta^{13}C_{CO2}$ values are distributed between –28.2‰–0.6‰. According to the identification chart, it can be seen that the ultra-deep gas in the sandstone reservoir of the Kuqa foreland is mainly coal-derived gas in the high over-mature stage, and the reversal of carbon isotopic series may be caused by the mixing of natural gas of the same type and different sources. The natural gas in carbonate reservoirs of marine craton is mainly oil-type gas with complex sources, including both kerogen cracking gas and oil cracking gas. CO_2 can be formed by organic and inorganic genesis. Inorganic CO_2 is most likely to be generated by the dissolution of carbonate rocks under acid formation water.

Keywords: natural gas isotope, gas source, carbon dioxide, kerogen cracking gas, oil cracking gas

INTRODUCTION

In Central and Western China's foreland areas, those strata ranging in depth from 4,000 to 6000 m are considered to be deep strata, while the strata with a depth of more than 6000 m are ultra-deep strata (Dai et al., 2018a). Ultra-deep strata in China are rich in oil and gas resources and are one of the most important development fields for China's petroleum industry in the future. China's onshore ultra-deep oil and gas resources are concentrated in "ultra-deep carbonate rocks," "ultra-deep clastic rocks" and "ultra-deep volcanic rocks," which are mainly found in the Tarim Basin, Sichuan Basin, Ordos Basin, Bohai Bay Basin, Songliao Basin and Junggar Basin. The Tarim Basin is underlain by ultra-deep clastic reservoirs and carbonate reservoirs. As a result, it is rich in ultra-deep gas resources accounting for 51% of the total gas resources in the entire basin (Yang, et al., 2019).

The Tarim Basin is a large superimposed basin with several Paleozoic-Cenozoic foreland areas superimposed on the margin of the Paleozoic craton basin. Tarim Basin is primarily developed with ultra-deep exploration fields in the foreland and marine craton areas of Kuqa region. The source rocks of the Kuqa petroleum system are mainly coal and lacustrine mudstone from Triassic and Jurassic, and the reservoirs are Jurassic-Quaternary sandstone and Paleogene dolomite. The source rocks of marine craton area are largely formed by mudstone and marl from Cambrian and Lower Ordovician, and the reservoirs are Lower Paleozoic carbonate (Liu, et al., 2020; Zhang, et al., 2021).

The Tarim Basin is mainly developed with typical ultra-deep large-scale oil and gas fields such as the Kelasu gas field in the Kuqa Depression, the Ordovician oil and gas field in Harahatang, and the North Tarim Uplift and large-scale Ordovician condensate gas field in Central Tarim (**Figure 1**). Natural gas is developed in different phases, such as gas-reservoir gas, associated gas and condensate gas. The sources of natural gas are complex, including coal-formed gas and oil-type gas. Oil-type gas can be divided into kerogen cracking gas and oil cracking gas (Huang, et al., 2016; Chen et al., 2018; Liu et al., 2019; Zhu et al., 2019). It is a natural geological reservoir for studying the geochemical characteristics of ultra-deep natural gas and identifying gas sources. In consideration of the general diversity of composition and hydrocarbon isotope characteristics in the ultra-deep gas of Tarim Basin and the difficulty of gas source identification, more

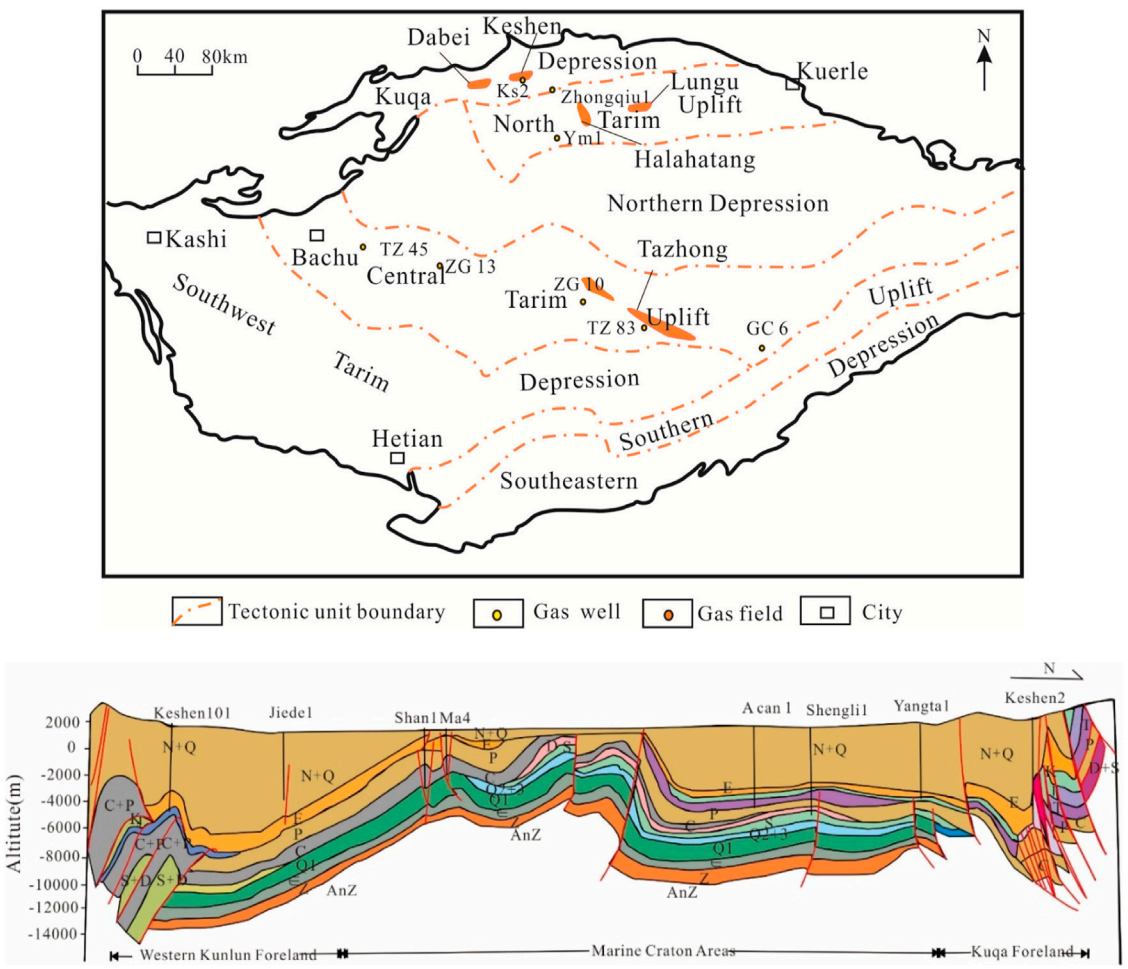

FIGURE 1 | Structural distribution map of Tarim Basin (the second map is according to Yang et al., 2019).

than 130 natural gas samples were collected in this research, including gas samples from the Cretaceous sandstone reservoirs of Keshen, Zhongqiu, Wushi, Bozi and Dabei in Kuqa foreland area, carbonate reservoirs of Harahatang, Lungu, Yingmaili and Luntai of marine craton area, Shunnan and Gucheng in East Tarim, and Ordovician reservoirs in Shunbei. According to the composition and hydrocarbon isotope of natural gas, the geochemical characteristics of sandstone gas in the foreland area and carbonate gas in craton area of Kuqa are compared, and alkane gas and CO_2 gas sources are identified. The comparison of the geochemical characteristics of natural gas in the Kuqa foreland area and the marine craton area is not only a deeper analysis of different oil and gas systems in Tarim, but also a deepening of the theory of ultra-deep natural gas source identification.

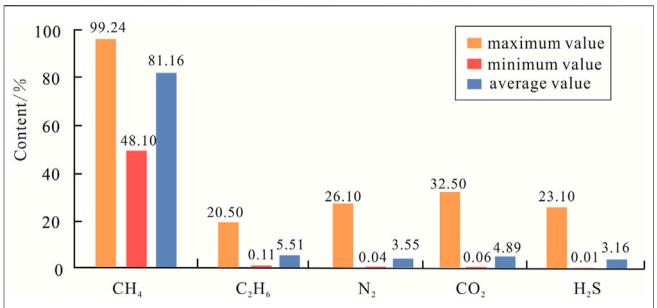

FIGURE 2 | Natural gas components in deep layers of Tarim (In addition to this article, data sources include Wang et al., 2014; Zhu, et al., 2014; Zhu, et al., 2015; Dai, et al., 2016; Liu, et al., 2018; Zhu, et al., 2018; Ma et al., 2021; Wei, et al., 2019; Li, et al., 2020)

EXPERIMENTAL METHODS

Natural gas component analysis was carried out on HP6890 chromatograph, using SGE-60 chromatographic column (50 m×0.25 mm×0.25 mm), the inlet temperature was 300°C, the carrier gas was nitrogen, the flow rate was 1 ml/min, and the split ratio was 50:1. The temperature program was raised from 30°C to 260°C, and the heating rate was 3°C/min.

The carbon isotope determination of natural gas components was carried out on the DeltapluxXL gas chromatography-combustion interface-isotope mass spectrometer (GC/C/IRMS) produced by Thermo Fisher. The chromatographic column is 30 m×320 μm PLOT Q, and the carrier gas flow rate is 2 ml/min. The temperature of the oxidation furnace is 960°C, the temperature of the reduction furnace is 650°C, the electron bombardment ion source, the electron energy is 120 eV, and the accelerating voltage is 3 kV. The heating program was an initial temperature of 30°C, constant temperature for 5 min, then increased to 80°C at 8°C/min, and then increased to 260°C at 4°C/min. Carbon isotope values are compared to the GBW 04405 reference, giving values relative to PDB with a standard deviation of ±0.3‰.

The instrument used for hydrogen isotope detection of natural gas components is the same MAT253 gas chromatography-thermal conversion interface-isotope mass spectrometer produced by Thermo Fisher Company. The chromatographic column is 30 m×320 μm PLOT Q, and the carrier gas flow rate is 2 ml/min. The temperature of the pyrolysis furnace is 1,450°C, the electron bombardment ion source, the electron energy is 90 eV, and the accelerating voltage is 10 kV. The heating program was an initial temperature of 40°C, a constant temperature of 5 min, and then the temperature was increased to 80°C at 8°C/min, and then increased to 260°C at 4°C/min.

RESULTS

Component Characteristics

After analyzing data from more than 130 wells, methane is absolutely dominant in the alkane gas of ultra-deep natural gas in Tarim Basin (**Figure 2**). Well Keshen 501, located in Keshen gas field of Kuqa, has highest methane content at 99.24%. 84% of the gas in Kuqa sandstone reservoir has a methane content of more than 95%. Well XK9C has the lowest methane content (48.1%). The natural gas in Well XK9C is associated gas generated from Halahatang carbonate rocks, North Tarim. The methane content of carbonate associated gas and condensate gas is less than 90% except for some gases of the Lungu, Shunnan and Gucheng gas reservoirs. The highest ethane content is 20.50% (Well HA701). The average ethane content of associated gas in Shunbei and North Tarim is relatively high, varying from 5.47% to 17.97%. The gas from the gas-reservoir in the East Tarim area has the lowest ethane content of only 0.11% (Well SN5). In addition, the ethane contents of natural gas in Kuqa, East Tarim and North Tarim reservoirs are relatively low. Well HA 701 has the highest propane content of 12.5%, and an average value of 2.68%. However, propane is not measured in some wells. Butane content in 23 wells is 0.

The non-hydrocarbon gas N_2 content is the highest at 26.10% (Well YM2), the lowest content at 0.04% (well SN7), and has an average content of 3.55%. CO_2 is developed with the highest content of 32.5% (Well LG351), the lowest content of 0.06% (Well GC12), and an average content of 4.89%. The average CO_2 contents in Central and East Tarim are 6.98% and 9.11%, respectively. The lowest CO_2 is developed in ultra-deep gas of Kuqa sandstone reservoir with an average of 1.2%. The H_2S is developed with the highest content of 23.1% (Well ZG6), the lowest content of 0.01% (Well ZG5), and an average of 3.16%. The gas wells with highest H_2S content are all located in the condensate gas area of Central Tarim.

As is shown in **Figure 3**, gas-reservoir gas is dominated by dry gas, with higher methane content than associated gas and condensate gas. Gas in the Cretaceous sandstone reservoir of the Kuqa foreland area is richer in methane than in the carbonate reservoir of marine craton in North and Central Tarim. The CO_2 and H_2S contents in ultra-deep condensate gas reservoirs of Central Tarim are high, with maximum values as high as 24.2% and 23.1%, respectively.

Characteristics of Carbon and Hydrogen Isotopes

Carbon Isotopic Composition of Alkane Gas

As is shown in **Figures 4**, **5**, Samples of the Cretaceous sandstone reservoir in the Kuqa foreland area were collected

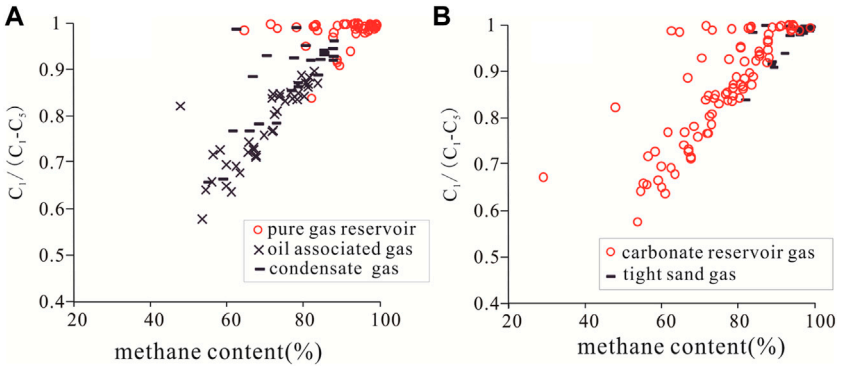

FIGURE 3 | C_1 (%)-$C_1/(C_1-C_5)$ of **(A)** natural gas in different states, **(B)** natural gas in different reservoirs of Tarim Basin.

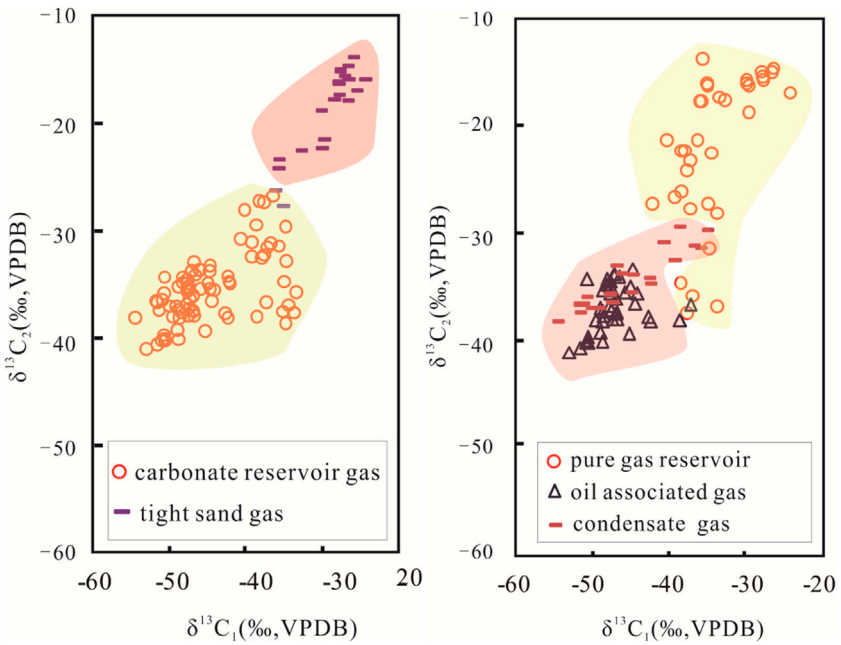

FIGURE 4 | $\delta^{13}C_1$-$\delta^{13}C_2$ of deep natural gas in different states and in different reservoirs of Tarim Basin.

from Keshen (21 samples), Zhongqiu (1 sample), Wushi (3 samples), Bozi (3 samples) and Dabei (4 samples). The $\delta^{13}C_1$ values are distributed between −36‰ and −25.3‰, with an average of −28.2‰, $\delta^{13}C_2$ values are distributed between −26.2‰ and −13.8‰, with an average of −18.3‰. The reversal of carbon isotopic series as $\delta^{13}C_2 > \delta^{13}C_3$ occurs in most gas samples.

Gas samples from the ultra-deep gas reservoir in marine craton of North Tarim-Central Tarim-East Tarim include natural gas from Shunnan and Gucheng of East Tarim, Harahatang, Lungu, Yingmaili and Luntai of North Tarim, Ordovician-Cambrian in Central Tarim, and gas from the Shunbei Ordovician carbonate reservoir.

Natural gas in the Ordovician carbonate reservoirs of Harahatang, Yingmaili and Luntai in North Tarim are associated gas, with the $\delta^{13}C_1$ value of −53‰ ~ −45.2‰, and an average $\delta^{13}C_1$ value of −48.3‰, with the $\delta^{13}C_2$ value of −40.2‰~−34.3‰, and an average $\delta^{13}C_2$ value of −37.9‰. Some gas samples are developed with the reversal of carbon isotopic series as $\delta^{13}C_2 > \delta^{13}C_3$ or $\delta^{13}C_3 > \delta^{13}C_4$. Natural gas in the Lungu area is developed from gas reservoirs, with the $\delta^{13}C_1$ value of −35.5‰ ~ −33.3‰, an average $\delta^{13}C_1$ value of −34.5‰, with the $\delta^{13}C_2$ value of −37.5‰ ~ −34.1‰, and an average $\delta^{13}C_2$ value of −35.7‰. It is noteworthy that 4 of the 6 samples are formed with the reversal of carbon isotopic series as $\delta^{13}C_1 > \delta^{13}C_2$.

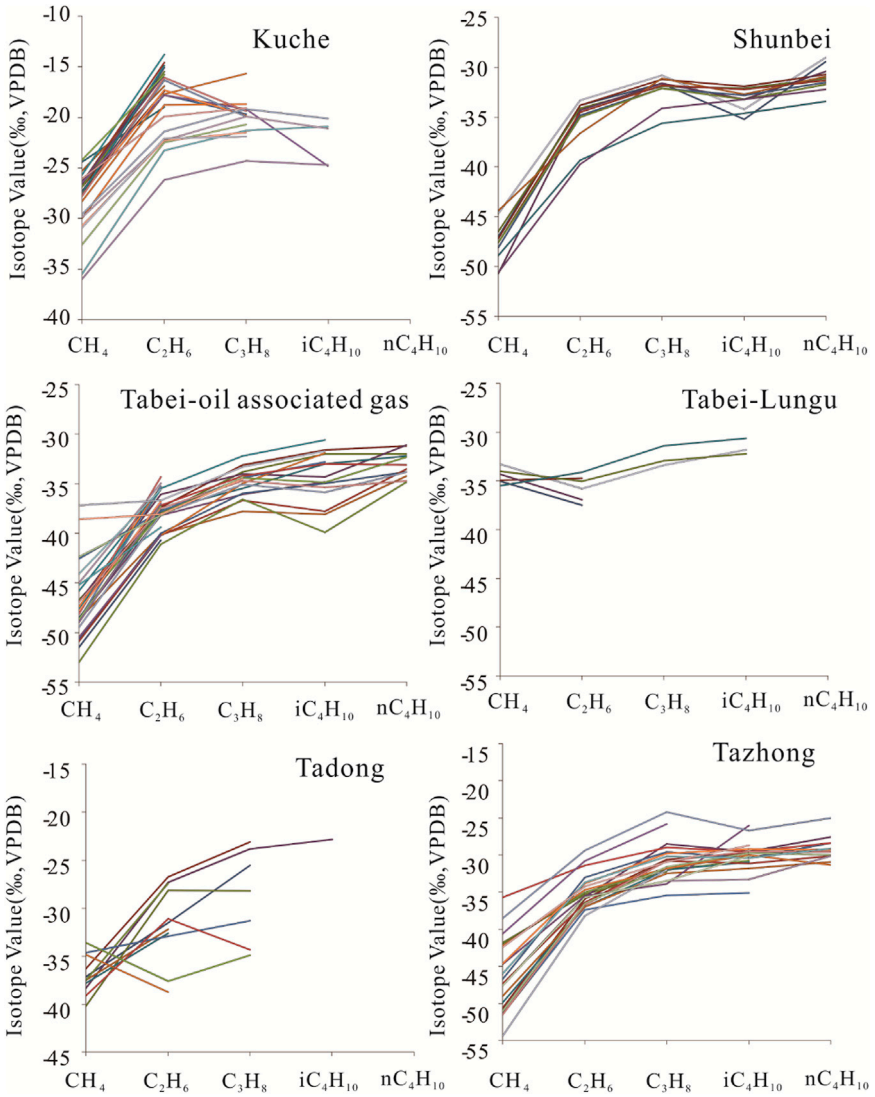

FIGURE 5 | Line chart of carbon isotope distribution of deep natural gas in Tarim.

The ultra-deep gas of the Ordovician carbonate reservoir in Central Tarim is condensate gas, with the $\delta^{13}C_1$ value of −54.4‰ ~ −34.8‰, an average $\delta^{13}C_1$ value of −45‰, with the $\delta^{13}C_2$ value of −38.2‰ ~ −29.7‰, and an average $\delta^{13}C_2$ value of −34.5‰. Most gas samples are formed with the reversal of carbon isotopic series as $\delta^{13}C_3 > \delta^{13}C_4$.

Natural gas in the Ordovician carbonate reservoirs of Shunnan and Gucheng in East Tarim is from gas reservoirs, with the $\delta^{13}C_1$ value of −40.2‰ ~ −33.6‰, an average $\delta^{13}C_1$ value of −36.9‰, with the $\delta^{13}C_2$ value of −37.6‰ ~ −26.7‰, and an average $\delta^{13}C_2$ value of −31.6‰. The gas from East Tarim is similar to that in North Tarim, with the reversal of $\delta^{13}C_1 > \delta^{13}C_2$ and $\delta^{13}C_2 > \delta^{13}C_3$.

Ultra-deep natural gas in the Shunbei Ordovician reservoir is developed as associated gas, with the $\delta^{13}C_1$ value of −50.7‰ ~ −44.7‰, an average $\delta^{13}C_1$ value of −47.6‰, the $\delta^{13}C_2$ value of −39.7‰ ~ −33.3‰ and an average $\delta^{13}C_2$ value of −35.4‰. Most gas samples are formed with the positive carbon isotope series as $\delta^{13}C_1 < \delta^{13}C_2 < \delta^{13}C_3 < \delta^{13}C_4$.

In summary, the carbon isotope values of methane and ethane in the ultra-deep gas of the Kuqa sandstone reservoir are higher than those in the carbonate reservoir. Compared with gas-reservoir gas, the carbon isotope values of methane and ethane in associated gas and condensate gas are low.

Hydrogen Isotope Characteristics of Alkane Gas

Natural gas in the sandstone reservoir of Keshen, Kuqa is developed with the $\delta^{13}D_1$ value of −155‰ ~ −149‰, and the $\delta^{13}D_2$ value of −105‰ ~ −92‰. The $\delta^{13}D_1$ values in the three gas samples of Shunnan carbonate gas reservoir in East Tarim are −134‰, −129‰ and −122‰, respectively. Condensate gas in Central Tarim is developed with the $\delta^{13}D_1$ value of −-206‰ ~ −162‰ and the $\delta^{13}D_2$ value of −145‰ ~ −103‰. The associated gas in North Tarim is developed with the $\delta^{13}D_1$ value of −262‰ ~

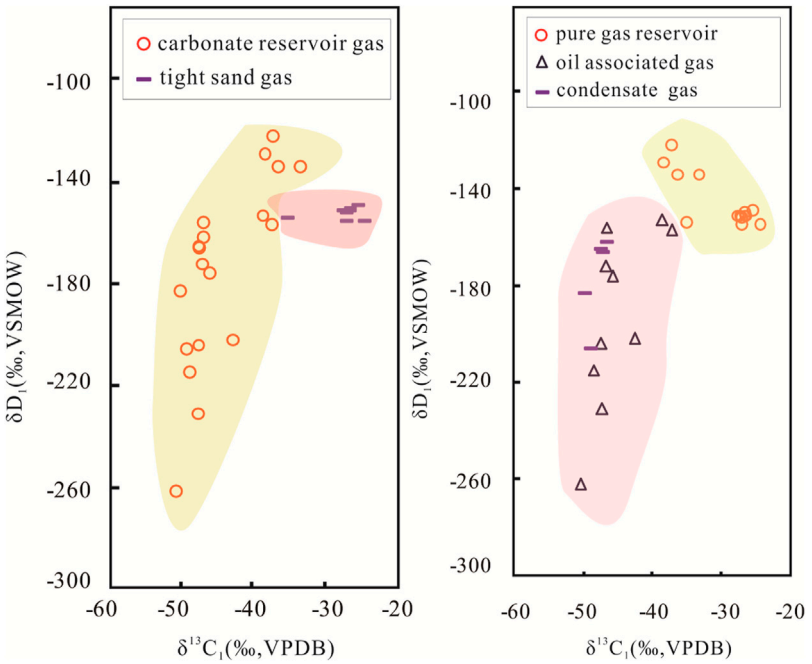

FIGURE 6 | $\delta^{13}C_1$-δD_1 of deep natural gas in different states and in different reservoirs of Tarim Basin.

−153‰, and the $\delta^{13}D_2$ value of −190‰ ~ −143‰. It can be seen from **Figure 6** that the distribution of hydrogen isotope values for methane is rather concentrated in the gas reservoirs of Keshen, Kuqa and Shunnan, East Tarim, whereas the distribution of hydrogen isotope values for other carbonate associated gas and condensate gas range widely.

Carbon Isotopic Composition of CO_2

It can be seen from **Table 1** and other data from references that the $\delta^{13}C_{CO2}$ values of deep natural gas in Tarim Basin are distributed in −30.2‰–0.6‰ range, while those in China as a whole range between −39‰ and 7‰. As a result, the $\delta^{13}C_{CO2}$ values of Tarim deep natural gas vary largely. The gas-reservoir gas in the sandstone reservoir of Keshen, Kuqa contains $\delta^{13}C_{CO2}$ values of −19.5‰ ~ −10.3‰, and an average value of −14.3‰, showing a centralized distribution, while the gas in carbonate reservoir has a wide distribution of $\delta^{13}C_{CO2}$ values, such as the condensate gas in Central Tarim with the $\delta^{13}C_{CO2}$ values from −30.2‰ to 0.6‰, showing the largest span in all regions.

DISCUSSION

Alkane Gas Generation

Putting the data of **Table 1** and other data from references into the genetic identification chart of natural gas, it can be seen that the gas samples from the sandstone gas reservoir in the Kuqa foreland area are coal-derived gas, while the ultra-deep natural gas samples in the marine craton area of Central Tarim-East Tarim-North Tarim are oil-type gas zone (**Figure 7**). Natural gas in each zone will now be discussed separately.

Gas-reservoir gas in the sandstone reservoir of the Kuqa foreland area is mainly developed in Keshen-Dabei area. The gas fields and gas reservoirs in Keshen and Dabei are all located in the Kelasu structural belt of Kuqa, which belong to the Kelasu gas field. The gas reservoirs are developed as high pressure and ultra-high pressure reservoirs, with high formation temperature and pressure, while the pressure coefficient is between 1.60 and 1.86. The gas reservoirs belong to normal-temperature gas reservoirs with the temperature in the middle part of 146–188°C (Yang, et al., 2019; Li, et al., 2020). The carbon isotopes of methane and ethane show the natural gas belongs to coal-derived gas in the highover mature stage, and some of the gas is developed with the reversal as $\delta^{13}C_2 > \delta^{13}C_3$. The possible reasons for the reversal of carbon isotope series are: ① isotope fractionation effect during the process of natural gas migration; ② oxidation of alkane gas component by bacteria; ③ mixing of organic gas and inorganic gas; ④ mixing of coal-derived gas and oil-type gas; ⑤ mixing of natural gas of the same type and different sources, or gas of the same source and different periods; ⑥ reversal of alkane gas under high temperature and high pressure (Yu, et al., 2013; Dai, et al., 2016; Liu, et al., 2018). The Kuqa foreland area mainly develops thick coal-bearing source rocks and high-quality mudstone source rocks. A small amount of oil was generated in the early stage at a shallow depth, while a large amount of oil was generated in the late stage at a greater depth (Wei, et al., 2019; Wang, et al., 2021). As a result, the influence of ①~④ can be eliminated. The most likely reason for reversal can be the mixing of natural gases of the same type (coal-derived gas) but from different sources. In addition, source rocks of the Keshen and Dabei gas fields have reached the over-mature stage. The gas reservoirs are under high pressure and high temperature, which

TABLE 1 | Geochemical data of natural gas deeper than 6000 m in the Tarim Basin.

Area	Gas field	Well	Strata	Reservior	Depth/m	Style	Gas component/%								$\delta^{13}C$ (‰),VPDB					
							CH_4	C_2H_6	C_3H_8	iC_4H_{10}	nC_4H_{10}	N_2	CO_2	H_2S	CH_4	C_2H_6	C_3H_8	iC_4H_{10}	nC_4H_{10}	CO_2
Kuqa	Keshen	KS101	K_1bs	Sandstone	6945–7160	Gas	99.23	0.43	0.04				0.30		−27.3	−16.3				
		KS201	K_1bs	Sandstone	6505–6700	Gas	98.05	0.54	0.04			0.54	0.83		−26.9	−17.4				
		KS203	K_1bs	Sandstone	6600–6685	Gas	98.31	0.55	0.04	0.01	0.01	0.72	0.30		−27.7	−16.3	−19.9			
		KS3-1	K_1bs	Sandstone	6805–6930	Gas	93.21	0.21	0.01			6.58			−26.6	−15.1				
		KS501	K_1bs	Sandstone	6370–6520	Gas	99.24	0.32	0.02				0.41		−24.4	−19				
		KS505	K_1bs	Sandstone	6660–6885	Gas	99.00	0.30	0.02			0.17	0.51		−25.3	-16.9				
		KS8	K_1bs	Sandstone	6860–6903	Gas	99.03	0.65	0.02			0.30			−27.5	−15.1				
		KS802	K_1bs	Sandstone	7222–7354	Gas	98.16	0.68	0.03			0.33	0.81		−26.5	−14.6				
		KS8-10	K_1bs	Sandstone	6968–7060	Gas	99.13	0.82	0.04						−26.9	−15.5				
		KS8-8	K_1bs	Sandstone	6800–6920	Gas	83.90	1.20	0.12				14.91		−26.4	−15.8				
		KS9	K_1bs	Sandstone	7445–7552	Gas	98.73	1.01	0.14	0.03	0.05				−27.5	−14.9				
		KS2	K_1bs	Sandstone	6573–6697	Gas	97.50	0.51	0.04	0.01	0.02	1.10	0.83		−28.3	−17.7	−15.7			
		KS5	K_1bs	Sandstone	6703–6742	Gas	97.40	0.27	0.01	0.02	0.97	1.36		−26.5	−17.8	−19.7			−15.8	
		KS2-1–1	K_1bs	Sandstone	6636–6785	Gas	97.000	0.530	0.040	0.008	0.005	1.58								
		KS2-1–6	K_1bs	Sandstone	6593–6710	Gas	97.500	0.550	0.040	0.009	0.005	1.17								
		KS2-2–4	K_1bs	Sandstone	6250–6708	Gas	97.000	0.540	0.040	0.018	0.009	1.48								
	Dabei	DB2	K_1bs	Sandstone	5541–5594	Gas	95.30	2.26	0.42	0.13	0.11	1.16	0.43							
		DB102	K_1bs	Sandstone	5425–5479	Gas	95.30	2.22	0.28	0.25	1.29	0.71		-30.7	−22.3	−21.5				
		DB201	K_1bs	Sandstone	932–6112	Gas	95.80	1.90	0.27	0.18	1.42	0.44		−30.9	−22.1	−21.9				
Tabei	Halahatang	XK4	O	Carbonate	6850.0	Oil-gas	69.70	12.20	6.39	1.21	1.69	5.31	0.92		−48.6	−38.2	−36.1	−34.8		−3.6
		XK902	O	Carbonate	6880.2	Oil-gas	67.20	11.90	8.11	1.74	2.51	5.05	1.95		−51.5	−40.7				
		XK9C	O	Carbonate	7011.7	Oil-gas	48.10	10.40	0.01	0.00	0.00	3.95	1.51		−46.8	−37.4	−33.1	−31.6	−31.2	−4.6
		XK7C	O	Carbonate	6956–7018	Oil-gas	72.22	5.75	3.37	0.96	1.64	2.34	10.74		−46.7	−38.0	−33.8	−32	−32	−4.8
		HA11	O	Carbonate	6748.0	Oil-gas	77.30	8.53	4.19	0.77	1.08	4.63	2.81		−46.9	−36.1	−34.0	−34.3	−31.1	−9.7
		HA12	O	Carbonate	6625.8	Oil-gas	73.30	12.00	3.26	0.64	0.92	5.41	3.91		−48.5	−37.7	−35.5	−33	−32.2	−7.9
		HA601	O	Carbonate	6637.6	Oil-gas	65.80	16.10	6.45	0.75	1.55	7.72	0.71		−48.7	−40.1	−37.8	−38.1	−34.2	−20.7
		HA7	O	Carbonate	6633.8	Oil-gas	62.40	18.90	6.07	0.71	1.56	5.52	4.10		−50.7	−40.0	−36.0	−35	−33.8	−8.4
		HA701	O	Carbonate	6588.0	Oil-gas	53.70	20.50	12.50	1.54	3.46	5.84	0.44		−50.9	−40.2	−36.7	−37.8	−33.5	−11.7
		HA9	O	Carbonate	6696.5	Oil-gas	58.50	16.30	4.35	0.37	0.83	3.79	15.60		−53.0	−41.1	−36.6	−39.9	−34.8	−2.6
		HA11	O	Carbonate	6658–6748	Oil-gas	67.17	10.44	7.14	1.88	3.16	3.71	2.79		−45.8	−35.5	−32.2	−30.6		
		HA702	O	Carbonate	6534.61–6688	Oil-gas	60.10	14.31	6.57	1.23	2.53	5.41	3.70		−50.5	−40.2	−35.0	−31.9		
		HA601-2	O	Carbonate	6556.08–6664.72	Oil-gas	63.45	14.71	9.27	1.71	2.96	3.34	1.87		−42.6	−37.8	−34.4	−32.8		
		HA601-6	O	Carbonate	6582–6671	Oil-gas	78.59	9.08	4.21	0.79	1.12	3.62	1.49		−47.5	−37.2	−34.2	−33	-33.1	
		HA702C	O	Carbonate	6594.06–6660	Oil-gas	60.02	15.96	9.84	1.64	3.26	3.59	2.40		−47.4	−38.0	−34.4	−34.9	−32.3	
	Lungu	LG351C	O	Carbonate	6448.5–6486.5	Gas	93.75	0.76	0.21	0.03	0.08	1.21	2.89		−33.3	−35.8	−33.4	−31.8		
		LG32	O	Carbonate	6185.48	Gas	94.30	0.56	0.12	0.03	0.06	4.24	0.53		−35.0	−37.5				−19.7
		LG34	O	Carbonate	6609.13	Gas	96.00	0.97	0.14	0.03	0.05	1.91	0.85		−34.9	-34.7				−19.6
		LG39	O	Carbonate	5690–5715	Gas									−34.0	−35.0	−32.9	−32.2		−4.4
		LG351	O	Carbonate	6539	Gas	64.70	0.56	0.15	0.03	0.09	0.95	32.50		−34.3	−36.9				−4.8
		LG100-11	O	Carbonate	5402.6–5483.0	Gas	91.50	2.11	0.81	0.37	0.21	2.16	1.99		−35.5	−34.1	−31.4	−30.6		−4.3
Tazhong	Tazhong	TZ45	O	Carbonate	6020–6150	Condensate	85.63	4.44	1.24			4.78	3.20		−54.4	−38.2	−32.0	−30.7		−0.4
		TZ86	O	Carbonate	6273–6320	Condensate	81.90	3.27	1.52	0.46	0.88	4.07	4.94	1.33	−46.0	−33.7	−30.2	−30.4	−29.1	−6.9
		TZ451	O	Carbonate	6090.5–6297	Condensate	84.12	6.34	2.41	0.51	0.81	5.07	0.17		−50.6	−35.9	−30.6	−29.7		
		TZ622	O	Carbonate	4,913.52–4,925	Condensate	91.39	1.17	0.41	0.32	2.72	3.57		-41.8	−35.3	−32.2				
		ZG11	O_{III}	Carbonate	6165–6631.1	Condensate	88.07	3.57	1.35	0.41	0.72	1.86	1.67		−47.5	−35.6	−28.5	−29.5	−27.6	−11.9
		ZG13	O_{III}	Carbonate	6458–6550.31	Condensate	72.98	10.03	5.05	1.03	2.32	1.16	4.02		−49.9	−37.0	−32.0	−30.9		−5.2
		ZG26	O_{III}	Carbonate	6085.5–6295	Condensate	55.39	13.90	8.97	1.68	2.87	11.63	3.23		−49.0	−37.0	−32.5	−31.8	−30.9	−1.8
		ZG111	O_{III}	Carbonate	6008–6250	Condensate	87.80	4.35	1.68	0.46	0.73	1.64	2.36		−46.7	−33.0	−29.6	−30.4	−28.4	
		ZG162-1H	O_{III}	Carbonate	6094.83–6780	Condensate	84.62	4.05	1.58	0.39	0.65	4.59	3.22		−47.3	−36.4	−30.8	−31.1	−30.1	−2.2
		ZS1	ϵ_1x	Carbonate	6597.53–6835.0	Condensate	78.30	0.50	0.14	0.05	0.07	2.55	14.40		−42.1	−35.0	−31.9	−30		−30.2
		ZS1	ϵ_2a	Carbonate	6439	Condensate	68.60	10.90	5.79	0.80	1.58	0.80	10.90		−44.7	−35.5	−33.9	−26		
		ZS1	ϵ_2a	Carbonate	6458	Condensate	78.30	0.47	0.14	0.05	0.07	2.55	14.40	3.90	−40.6					

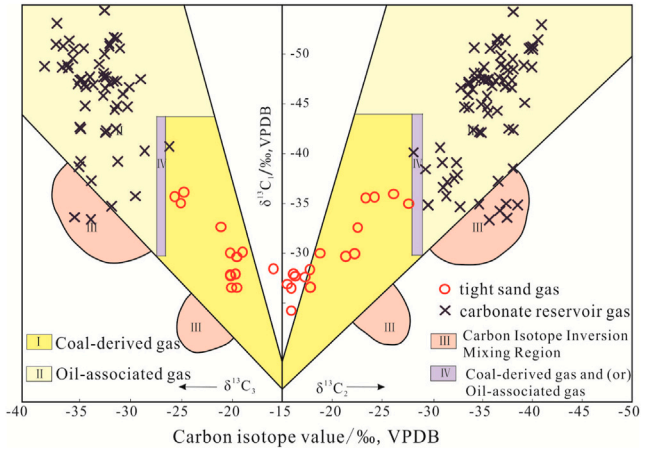

FIGURE 7 | $\delta^{13}C_1$-$\delta^{13}C_2$-$\delta^{13}C_3$ value of deep natural gas in Tarim.

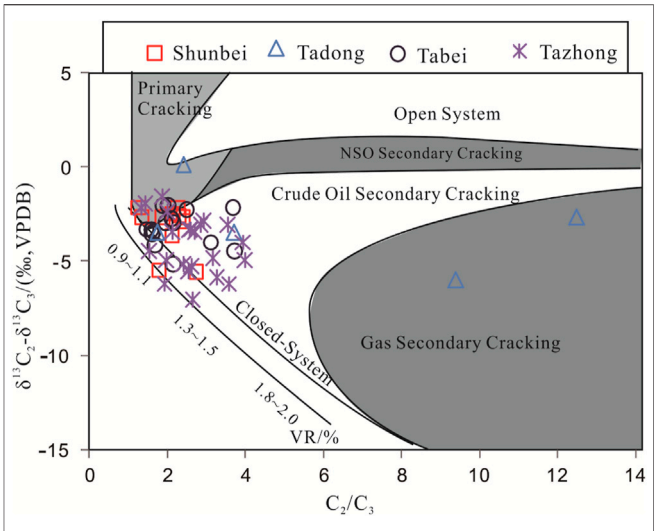

FIGURE 8 | C_2/C_3-($\delta^{13}C_2$-$\delta^{13}C_3$) of deep natural gas in Tarim. (base map according to Lorant et al., 1998)

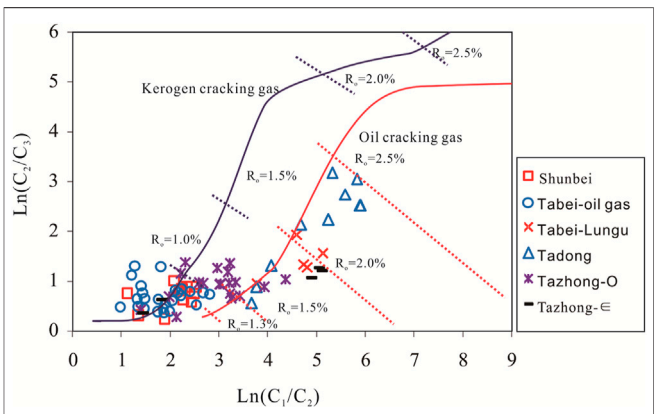

FIGURE 9 | Ln (C_1/C_2)-Ln (C_2/C_3) of deep natural gas in Tarim. (base map according to Li, et al., 2017)

may also cause the reversal of the ethane and propane carbon isotope series.

The deep natural gas in the marine craton of Central Tarim-East Tarim-North Tarim is developed as oil-type gas. Natural gas in marine craton is mainly composed of gas-reservoir gas, associated gas and condensate gas with diverse characteristics of components and hydrocarbon isotopes and complex sources. The Cambrian-Ordovician carbonate rocks in the marine craton can be divided vertically into upper, middle and lower oil and gas systems. The hydrocarbon-bearing layers in the upper oil and gas system are weathering crusts of the Lianglitage, Yijianfang, and Yingshan Formations of the Ordovician. The hydrocarbon-bearing layers in the middle oil and gas system are a deep Ordovician reservoir and Penglaiba Formation. And the hydrocarbon-bearing layers in the lower oil and gas system are Cambrian Xiaoerbulake Formation. At present, the upper system is highly explored and the main focus of this study (Yang, et al., 2019).

Previous studies argued that there are two types of gas sources in the marine craton area, one is the mature/high-mature wet gas from the Ordovician gas source, and the other is the over-mature dry gas from the Cambrian gas source. The high over-mature dry gas can be divided into kerogen cracking gas and oil cracking gas (Liu, et al., 2017; Dai et al., 2018b; Ni, et al., 2019; Ding, et al., 2020; Zhu, et al., 2020; Yan, et al., 2021; Zhao, et al., 2022). Now the natural gas will be discussed in each zone.

Central Tarim Area

Han et al. (2021) divided the condensate gas reservoirs in the Central Tarim Uplift of the Tarim Basin into primary gas and secondary gas reservoirs and believed that the primary condensate gas reservoirs in ultra-deep Lower Cambrian were mixed with kerogen cracking gas and oil cracking gas, which were mainly distributed across the eastern buried hill with few paleo-oil reservoirs, while the secondary Ordovician condensate gas reservoirs were mainly formed by the late-stage gas invasion and gas washing of paleo-oil reservoirs. Chen et al. (2018) believed that the Cambrian natural gas in Central Tarim was less affected by the late-stage filling of kerogen cracking gas, and was mainly composed of the early-stage oil cracking gas. According to **Figures 8**, **9**, the Ordovician condensate gas in Central Tarim is distributed in the areas of kerogen cracking gas, oil cracking gas and the mixing zone, indicating the complex gas source, while the Cambrian condensate gas is mainly in the secondary cracking area of crude oil.

North Tarim Area

The methane content of Ordovician natural gas in the Halahatang area of North Tarim is fairly low among all the marine craton natural gas. The carbon isotope of methane is −53‰ ~ −45.2‰, and the carbon isotope of ethane is −41.1‰ ~ −34.3‰, which are also relatively low. Wu et al. (2016) and Zhu et al. (2019) believed that the Halahatang and Yingmai Ordovician natural gas in North Tarim is composed of both kerogen cracking gas and oil cracking gas, and comes mainly from Middle and Upper

Ordovician source rocks in the Aman transition zone in the south of Harahatang. **Figures 8**, **9** show that the points of associated gas samples in North Tarim mainly fall into the area of kerogen cracking gas, and some samples fall into the area between kerogen cracking gas and oil cracking gas. The methane content of Ordovician natural gas in the Lungu gas field of North Tarim is basically higher than 90%, and the isotopes of methane and ethane are about −34‰ and −35‰, respectively, which are different from that in Harahatang gas. Previous studies believed that the Lungu oil and gas reservoir could be characterized as "dry gas and heavy oil" and developed as a modified oil and gas reservoir by gas invasion (Wu, et al., 2016). **Figure 9** shows that the gas samples in the North Tarim gas reservoir are mainly located on the trend line of oil cracking gas, and the natural gas in the Lungu area is developed with the reversal of carbon isotope series as $\delta^{13}C_1 > \delta^{13}C_2$, which may be caused by the fractionation of carbon isotopes of methane and ethane during the interaction with crude oil during the gas invasion. This also shows that the source of natural gas in the Tarim marine craton is very complex, and the gas source analysis needs not only data on natural gas composition and isotopes, but also the actual geological conditions.

East Tarim Area

There are different views on the source of Ordovician natural gas in the Shunnan-Gucheng area of East Tarim. Wang et al. (2014) believed that the natural gas comes from Cambrian, Yun and Cao (2014) believed that the natural gas is mainly composed of kerogen cracking gas, while Zhou et al. (2019) believed that the natural gas is oil cracking gas. Based on the content of adamantane and thioadamantane, Ma et al. (2021) and Ma et al., 2021 believed that the Ordovician natural gas in the Shunnan-Gucheng area is oil cracking gas, and the cracking degree of oil can be 98%. **Figures 8**, **9** show that most gas samples in East Tarim are located in the area of oil cracking gas, indicating that the natural gas is mainly generated by oil cracking.

Shunbei Area

Wang et al., 2021 believed that the Ordovician natural gas in the Shunbei area is mainly kerogen cracking gas and is partly mixed with natural gas in the early stage of oil cracking. The gas-oil ratio of the Ordovician oil and gas reservoir in the Shunbei area is low, and the natural gas in this area is oil-associated gas. The oil has low content of methyladamantane, with a low cracking degree. The natural gas has similar maturity with oil, showing the same source from Cambrian source rocks. It is also mixed with a small amount of early-stage oil cracking gas. **Figures 8**, **9** show that the associated gas samples in Shunbei area mainly fall into the area of kerogen cracking gas area, and some fall into the middle part of kerogen and oil cracking gas, indicating the contribution of oil cracking gas.

Origin of CO_2

CO_2 origin identification is presented by effective index $\delta^{13}C_{CO2}$. Dai et al., 2018a found that the $\delta^{13}C_{CO2}$ value of organic CO_2 is less than −10‰, while the $\delta^{13}C_{CO2}$ value of inorganic CO_2 is greater than −8‰. The carbon isotope value of inorganic CO_2 generated from metamorphic carbonate rocks is close to the $\delta^{13}C_{CO2}$ value of carbonate rocks, showing a difference of 0 ± 3‰. The $\delta^{13}C_{CO2}$ values of inorganic CO_2 generated from volcanic magma and mantle sources are mostly distributed in −6‰ ± 2‰ range. Based on the identification chart, it can be seen that two Kuqa sandstone gas and Central Cambrian gas samples show the characteristics of organic CO_2, and most of the Ordovician natural gas in Halahatang, Shunbei and Central Tarim show the characteristics of inorganic CO_2 (**Figure 10**). The He isotope content of Tarim deep gas is low and shows no characteristics of mantle-derived gas. The ground temperature of Halahatang is lower than 160°C and that of Shunbei area is lower than 180°C. As a result, it is difficult to decompose carbonate rocks. The CO_2 is widely generated in deep gas of Tarim marine craton, and the CO_2 content in Central Tarim is up to 24.2%. The dissolution of CO_2 in water will make the formation water acidic, resulting in the dissolution of carbonate reservoirs and the production of CO_2 with high $\delta^{13}C_{CO2}$ value. Therefore, inorganic CO_2 is most likely to be generated from the dissolution of carbonate rocks under the acidic formation water.

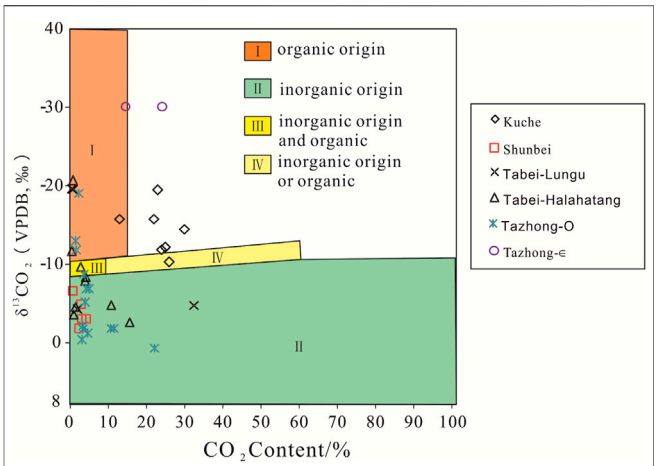

FIGURE 10 | CO_2 -$\delta^{13}C_{CO2}$ of deep natural gas in Tarim. (base map according to Dai et al., 2018b).

CONCLUSION

Natural gas in the foreland ultra-deep reservoirs and marine craton carbonate reservoirs in Kuqa, of the Tarim Basin, have distinct geochemical properties. Natural gas in the Kuqa foreland area is coal-derived gas, generated from the Triassic and Jurassic. Oil and gas vertically migrated and accumulated into Cretaceous reservoirs along the fault network; the natural gas in the marine craton area is oil-type gas with complex sources. There is a need to combine the geochemical identification charts of natural gas in North Tarim, Central Tarim and East Tarim with the actual geological conditions to identify gas sources. Even in the same structural belt, the sources of gas-reservoir gas, associated gas and condensate gas may be different. Natural gas includes kerogen

cracking gas, oil cracking gas and a mixture of the two. By comparing the different geochemical characteristics of the ultra-deep natural gas in the two oil-bearing systems, and combining the geochemical data with the actual geological conditions, we have a more comprehensive understanding of the ultra-deep natural gas in the Tarim in three-dimensional space, and also provide guidance for the further development of the Tarim Basin. Compared with other basins in China, natural gas and even crude oil have been continuously found in reservoirs deeper than 6000 m in the Tarim Basin due to the shallow burial in the early stage, rapid deep burial in the late stage and a low geothermal gradient. These allow the deep-buried source rocks in the Tarim Basin to continue to generate different kinds of hydrocarbons. Meanwhile, the structural evolution of the Tarim Basin is phased, resulting in a multi-stage evolution of source rocks and multi-stage oil cracking in craton marine area, leading to the complex origin of gas sources.

DATA AVAILABILITY STATEMENT

The original contributions presented in the study are included in the article/Supplementary Material, further inquiries can be directed to the corresponding author.

AUTHOR CONTRIBUTIONS

All authors listed have made a substantial, direct, and intellectual contribution to the work and approved it for publication.

FUNDING

This research was supported by the National Natural Science Foundation of China (41903062, 101019gj008001b24).

REFERENCES

Chen, F. R., Zhang, Y. J., Zhu, G. Y., and Zhang, B. S. (2018). Geochemistry and Accumulation Process of Deep Natural Gas in the Platform-Basin Region. *Tarim. Basin. Natur. Gas. Geo.* 29 (6), 880–891. doi:10.11764/j.issn.1672-1962.2018.05.022

Dai, J. X., Ni, Y. Y., Liu, Q. Y., Wu, X. Q., Gong, D. Y., Hong, F., et al. (2018b). Geochemical Characteristics of Natural Gas from Halahatang Sag in the TarimBasin. *Chemicalica* 43 (5), 477–488. doi:10.11698/PED.2018.04.05

Dai, J. X., Ni, Y. Y., Qin, S. F., Huang, S. P., Peng, W. L., and Han, W. X. (2018a). Geochemical Characteristics of Ultra-deep Natural Gas in the Sichuan Basin, SW China. *Petr. Exp. And Dev.* 45 (4). doi:10.1016/s1876-3804(18)30067-3

Dai, J. X., Ni, Y. Y., Zhang, W. Z., Huang, S. P., Gong, D. Y., Liu, D., et al. (2016). Relationships between Wetness and Maturity of Coal-Derived Gas in China. *Petr. Exp. And Dev.* 43 (5), 675–677. doi:10.11698/PED.2016.05.0110.1016/s1876-3804(16)30088-x

Ding, Z. W., Wang, R. J., Chen, F. F., Yang, J. P., Zhu, Z. Q., Yang, Z. M., et al. (2020). Origin, Hydrocarbon Accumulation and Oil-Gas Enrichment of Fault-Karst Carbonate Reservoirs: A Case Study of Ordovician Carbonate Reservoirs in South Tahe Area of HalahatangOilfield. *Tarim Basin. Petr. Exp. And Dev.* 47 (2). doi:10.1016/s1876-3804(20)60048-9

Han, J. F., Wu, G. H., Yang, H. J., Dai, L., and Su, Z. (2021). Type and Genesis of Condensate Gas Reservoir in the TazhongUplif of the Tarim Basin. *Natru. Gas. Ind.* 41 (7), 24–32. doi:10.3787/j.issn.1000-0976.2021.07.003

Huang, H., Zhang, S., and Su, J. (2016). Palaeozoic Oil-Source Correlation in the Tarim Basin, NW China: A Review. *Org. Geochem.* 94, 32–46. doi:10.1016/j.orggeochem.2016.01.008

Li, J., Li, J., Xie, Z. Y., Wang, C., Zhang, H. Z., Liu, M. C., et al. (2020). Oil and Gas Source and Accumulation of Zhongqiu 1 Trap in Qiulitage Structural Belt, Tarim Basin, NW China. *Petr. Exp. And Dev.* 47 (3). doi:10.1016/s1876-3804(20)60072-6

Li, J., Li, Z. S., Wang, X. B., Wang, D., Xie, Z., Li, J., et al. (2017). New Indexes and Charts for Genesis Identification of Multiple Natural Gases. *Petrol. Explor. Dev.* 44 (4), 503–512. doi:10.11698/PED.2017.040310.1016/s1876-3804(17)30062-9

Liu, G., Zeng, L., Zhu, R., Gong, L., Ostadhassan, M., and Mao, Z. (2021). Effective Fractures and Their Contribution to the Reservoirs in Deep Tight Sandstones in the Kuqa Depression, Tarim Basin, China. *Mar. Petroleum Geol.* 124, 104824. doi:10.1016/j.marpetgeo.2020.104824

Liu, Q., Jin, Z., Li, H., Wu, X., Tao, X., Zhu, D., et al. (2018). Geochemistry Characteristics and Genetic Types of Natural Gas in Central Part of the Tarim Basin, NW China. *Mar. Petroleum Geol.* 89, 91–105. doi:10.1016/j.marpetgeo.2017.05.002

Liu, Q., Jin, Z., Wang, X., Yi, J., Meng, Q., Wu, X., et al. (2018). Distinguishing Kerogen and Oil Cracked Shale Gas Using H, C-Isotopic Fractionation of Alkane Gases. *Mar. Petroleum Geol.* 91, 350–362. doi:10.1016/j.marpetgeo.2018.01.006

Liu, Q., Wu, X., Wang, X., Jin, Z., Zhu, D., Meng, Q., et al. (2019). Carbon and Hydrogen Isotopes of Methane, Ethane, and Propane: A Review of Genetic Identification of Natural Gas. *Earth-Science Rev.* 190, 247–272. doi:10.1016/j.earscirev.2018.11.017

Lorant, F., Prinzhofer, A., Behar, F., and Huc, A.-Y. (1998). Carbon Isotopic and Molecular Constraints on the Formation and the Expulsion of Thermogenic Hydrocarbon Gases. *Chem. Geol.* 147, 249–264. doi:10.1016/s0009-2541(98)00017-5

Ma, A. L., He, Y. L., Yun, L., Wu, X., Qiu, N., Chang, J., et al. (2021). The Geochemical Characteristics and Origin of Ordovician Ultra-deep Natural Gas in the North Shuntuoguole Area, Tarim Basin, NW China. *Natru. Gas. Geo.* 32 (7), 1047–1060. doi:10.1016/j.jnggs.2021.09.004

Ni, Y. Y., Liao, F. R., Gong, D. Y., Jiao, L. X., Gao, J. L., and Yao, L. M. (2019). Stable Carbon and Hydrogen Isotopic Characteristics of Natural Gas from Taibei Sag, Turpan-Hami Basin, NW China. *Petr. Exp. And Dev.* 46 (3). doi:10.1016/s1876-3804(19)60033-9

Wang, T. G., Song, D. F., Li, M. J., and Yang, C. (2014). Natural Gas Source and Deep Gas Exploration Potential of the Ordovician Yingshan Formation in the Shunnan-Gucheng Region, Tarim Basin. *Oil Gas Geol.* 35 (6), 753–762. doi:10.11743/ogg20140602

Wang, Z., Lv, X. X., Li, Y., Liang, H. T., Li, L., and He, T. (2021). Natural Fracture Opening Preservation and Reactivation in Deep Sandstones of the Kuqa Foreland Thrust Belt, Tarim Basin. *Mar. Petroleum Geol.* 127, 104956. doi:10.1016/j.marpetgeo.2021.104956

Wei, Q., Li, X., Liang, W. Q., Sun, K. X., Xie, Z. Y., Li, J., et al. (2019). Geochemical Characteristics and Genesis of Deep Tight Sandstone Gas in the Dabei-Keshen Zone, Kuqa Depression. *Bull. Min., Petr. And Geo.* 38 (2), 418–427. doi:10.19658/j.issn.1007-2802.2019.38.044

Wu, X., Han, J., Zhu, Y. F., and Liu, J. F. (2016). Analysis of Main Controlling Factors for Hydrocarbon Phases and Sturation in Eastern Lungu Area, Tarim Basin. *Nat. Gas. Geo.* 27 (1), 30–40. doi:10.11764/j.issn.1672-1926.2016.01.0030

Yan, L., Zhu, G. Y., Wang, S., Chen, Z. Y., Zhu, Y. F., Yang, M., et al. (2021). Accmulation Conditions and Favorable Areas for Natural Gas Accumulation in the 10000 Meters Ultra-deep Sinian-Cambrian in Tarim Basin. *ACTAPETR. Sin.* 42 (11), 1446–1457. doi:10.7623/syxb20211004

Yang, X. W., Wang, Z. M., He, W. Y., and Tian, J. (2019). *Practice and Innovation of Ultra-deep Oil and Gas Exploration in Tarim Basin*. Beijing: Petroleum Industry Press.

Yu, C., Huang, S. P., Gong, D. Y., Liao, F. R., Li, J., and Sun, Q. W. (2013). Partial Reversal Cause of Carbon and Hydrogen Isotope Compositions of Natural Gas: a Case Study in Sulige Gas Field, Ordos Basin. *ACTA PET. SIN.* 34 (1), 92–101. doi:10.7623/syxb2013S1011

Yun, L., and Cao, Z. C. (2014). Hydrocarbon Enrichment Pattern and Exploration Potential of the Ordovician in Shunnan Area, Tarim Basin. *Oil Gas Geol.* 35 (6), 788–797. doi:10.11743/ogg20140606

Zhang, Z. Y., Lin, C. S., Liu, Y. F., Liu, J. Y., Zhao, H. T., Li, H., et al. (2021). Lacustrine to Fluvial Depositional Systems: The Depositional Evolution of an Intracontinental Depression and Controlling Factors, Lower Cretaceous, Northern Tarim Basin, Northwest China. *Mar. Petro. Geo.* 126. doi:10.1016/j.marpetgeo.2021.104904

Zhao, X. X., Li, B., and Wu, G. H. (2022). Genesis and Enrichment Model of Ordovician Multi-phase Oil and Gas Reservoirs in Tazhong Block. *Tarim. Basin. Natru. Gas. Geo.* 33 (1), 36–48. doi:10.11764/j.jssn.1672-1926.2021.07.004

Zhou, X., Lü, X., Zhu, G., Cao, Y., Yan, L., and Zhang, Z. (2019). Origin and Formation of Deep and Superdeep Strata Gas from Gucheng-Shunnan Block of the Tarim Basin, NW China. *J. Petroleum Sci. Eng.* 177, 361–373. doi:10.1016/j.petrol.2019.02.059

Zhu, G., Li, J., Zhang, Z., Wang, M., Xue, N., He, T., et al. (2020). Stability and Cracking Threshold Depth of Crude Oil in 8000 M Ultra-deep Reservoir in the Tarim Basin. *Fuel* 282, 118777. doi:10.1016/j.fuel.2020.118777

Zhu, G., Milkov, A. V., Zhang, Z., Sun, C., Zhou, X., Chen, F., et al. (2019). Formation and Preservation of a Giant Petroleum Accumulation in Superdeep Carbonate Reservoirs in the Southern Halahatang Oil Field Area, Tarim Basin, China. *Bulletin* 103 (7), 1703–1743. doi:10.1306/11211817132

Zhu, G., Weng, N., Wang, H., Yang, H., Zhang, S., Su, J., et al. (2015). Origin of Diamondoid and Sulphur Compounds in the Tazhong Ordovician Condensate, Tarim Basin, China: Implications for Hydrocarbon Exploration in Deep-Buried Strata. *Mar. Petroleum Geol.* 62, 14–27. doi:10.1016/j.marpetgeo.2015.01.002

Zhu, G., Zhang, B., Yang, H., Su, J., and Han, J. (2014). Origin of Deep Strata Gas of Tazhong in Tarim Basin, China. *Org. Geochem.* 74, 85–97. doi:10.1016/j.orggeochem.2014.03.003

Zhu, G., Zhang, Z., Zhou, X., Li, T., Han, J., and Sun, C. (2019). The Complexity, Secondary Geochemical Process, Genetic Mechanism and Distribution Prediction of Deep Marine Oil and Gas in the Tarim Basin, China. *Earth-Science Rev.* 198, 102930. doi:10.1016/j.earscirev.2019.102930

Conflict of Interest: CY, YN, JD, YH, CF, and FL were employed by Research Institute of Petroleum Exploration and Development, Petrochina.

frontiers | Frontiers in Earth Science

ORIGINAL RESEARCH
published: 22 June 2022
doi: 10.3389/feart.2022.861040

Geochemical Characteristics and Origin of Shale Gases From Sichuan Basin, China

Yunyan Ni[1], Dazhong Dong[1]*, Limiao Yao[1], Jianping Chen[1], Xing Liang[2], Fei Liu[2], Jian Li[1], Jinhao Guo[1] and Jinliang Gao[1]*

[1]PetroChina Research Institute of Petroleum Exploration and Development, Beijing, China, [2]PetroChina Zhejiang Oilfield Company, Hangzhou, China

Natural gases from the Taiyang (shallow), Jiaoshiba (middle), and Weirong (deep) shale gas fields in the southern Sichuan Basin were analyzed for molecular and stable carbon isotopic compositions to investigate the geochemical characteristics and gas origins. All the gases belong to shale gas from the Upper Ordovician–Lower Silurian shale and are dominated by methane with gas wetness generally less than 0.83%. The $\delta^{13}C_1$ values are −28.5‰, −30.3‰, and −35.2‰ in Taiyang, Jiaoshiba, and Weirong shale gas fields, respectively. The extremely high thermal maturity is the controlling factor for the enrichment of ^{13}C in methane, with a minor contribution from the heavy carbon isotope of the organic matter in the Ordovician Wufeng Formation. Fischer–Tropsch-type synthesis of hydrocarbon gas from CO_2 and H_2 contributes to the increase of wet gas, which results in the offset from the $\delta^{13}C_1$~wetness linear trend in the Taiyang and Jiaoshiba gas fields. Methane, ethane, and propane in the Taiyang shale gas field have increasing $\delta^{13}C$ values with increasing burial depth, which is mainly caused by diffusive migration. All gases are characterized by a complete carbon isotopic reversal trend ($\delta^{13}C_1 > \delta^{13}C_2 > \delta^{13}C_3$), and it is mainly caused by the reversible free-radical reactions with the conversion from alkane to alkyl groups, with some contribution from the Fischer–Tropsch-type synthesis. The results of this study will improve our understanding of the geochemical characteristics of shale gases from different burial depths and have important implications for future shale gas exploration in the deep and shallow layers.

Keywords: shale gas, carbon isotope reversal, Wufeng–Longmaxi shale, Sichuan Basin, carbon isotope enrichment

OPEN ACCESS

Edited by:
Qingqiang Meng,
SINOPEC Petroleum Exploration and Production Research Institute, China

Reviewed by:
Xiaofeng Wang,
Northwest University, China
Haikuan Nie,
SINOPEC Petroleum Exploration and Production Research Institute, China

****Correspondence:***
Yunyan Ni
niyy@petrochina.com.cn
Dazhong Dong
ddz@petrochina.com.cn

Specialty section:
This article was submitted to Geochemistry, a section of the journal Frontiers in Earth Science

Received: *24 January 2022*
Accepted: *09 May 2022*
Published: *22 June 2022*

Citation:
Ni Y, Dong D, Yao L, Chen J, Liang X, Liu F, Li J, Guo J and Gao J (2022) Geochemical Characteristics and Origin of Shale Gases From Sichuan Basin, China. Front. Earth Sci. 10:861040. doi: 10.3389/feart.2022.861040

1 INTRODUCTION

Carbon isotopic compositions of methane and its homologs are important parameters to investigate the origin and generation history of natural gas (Tang et al., 2000; Ni et al., 2011; Dai et al., 2014a). Several studies have shown that the carbon isotope is dependent on the maturity of source rocks, the type and carbon isotope of source organic matter, and postgenetic processes (Stahl and Carey, 1975; Schoell, 1980; Dai, 1992; Tang et al., 2000; Dai et al., 2009; Ni et al., 2011; Curiale and Curtis, 2016; Ni et al., 2019a). Due to the kinetic isotopic fractionation effects (Lorant et al., 1998; Tang et al., 2000), primary gases are usually characterized by the normal carbon isotopic trend, that is, $\delta^{13}C_1 < \delta^{13}C_2 < \delta^{13}C_3$. However, recently, a number of studies have documented a depletion of ^{13}C in ethane and propane and an enrichment of ^{13}C in methane at high maturity, resulting in the carbon isotopic reversal between methane and ethane ($\delta^{13}C_1 > \delta^{13}C_2$) (Ferworn et al., 2008; Burruss and Laughrey,

2010; Rodriguez and Philp, 2010; Zumberge et al., 2012; Hao and Zou, 2013; Tilley and Muehlenbachs, 2013; Dai et al., 2014a, 2016b, 2017; Zhang et al., 2018b; Liu et al., 2018; Ni et al., 2018; Xia and Gao, 2018; Feng et al., 2020).

Zumberge et al. (2012) demonstrated a reversed carbon isotopic maturity trend in ethane and propane in gases from Barnett and Fayetteville shales, with thermal maturity (Ro%) over 1.5%. Dai et al. (2014b) explored this reversed trend to even higher thermal maturity and found the carbon isotopic maturity trend becomes positive again at stages with gas wetness (C_{2+}/C_{1+}, %) less than 1.4%. Ni et al. (2018) show such isotopic depletion of ^{13}C in thermogenic ethane and propane. One common feature of these carbon isotopic anomalies is that they occur at relatively high temperatures. To date, many studies have been carried out to investigate the mechanisms for the carbon isotopic characteristics of shale gases (Ferworn et al., 2008; Burruss and Laughrey, 2010; Rodriguez and Philp, 2010; Zumberge et al., 2012; Hao and Zou, 2013; Xia et al., 2013; Gao et al., 2014; Zhang et al., 2018b; Xia and Gao, 2018; Feng et al., 2020; Mi et al., 2022). Moreover, isotopic reversal may correlate with the gas generation potential, and the reversal magnitude may correspond to the amount of gas retained in the shale (Tilley et al., 2011; Feng et al., 2018; Wang et al., 2021; Zhao et al., 2021).

As the largest shale gas producer outside North America, after 10-years effort, China has achieved effective exploitation of marine shale gas resources in the Sichuan Basin and its surrounding areas with a middle burial depth of 2,000–3,500 m. In the Sichuan Basin, ultra-deep shale gas represents shale gas with a burial depth >4,500 m, deep shale gas means shale gas with a burial depth of 3,500–4,500 m, and shallow shale gas means shale gas with a burial depth <2,000 m. With the success of the burial depth of 2,000–3,500 m, recently, great efforts have been made in the shallow and deep layers. In the future, with the improvement of the technologies, shale gas exploration will extend to areas shallower than 2,000 m and deeper than 3,500 m. How about the geochemistry of shale gas from shallow and deep layers? Are there any differences among the shale gases from the shallow, middle, and deep layers? Here, we describe the molecular and stable carbon isotope geochemistry of natural gases from the Wufeng–Longmaxi shale in the Taiyang (vertical burial depth, 500–2,250 m), Jiaoshiba (vertical burial depth, 2,250–3,500 m) and Weirong (vertical burial depth, 3,550–3,880 m) shale gas fields in the Sichuan Basin. Two main objectives of this study will be addressed: 1) Investigating the origin of the shale gases from the three gas fields with different burial depths based on the molecular and stable carbon isotopic compositions and 2) demonstrating the geochemical differences among shale gases from these three gas fields and exploring the potential causes. The results presented in this study will improve our understanding of the geochemical differences among the shale gases with deep, middle, and shallow burial depths and interpretation of the carbon isotopic composition of shale gases in the future.

2 GEOLOGICAL SETTINGS

The Sichuan Basin, abundant in natural gas resources, is a large superimposed basin and covers an area of about 180×10^3 km^2 (**Figure 1**). The sedimentary strata are well-developed with thicknesses up to 12,000 m. It developed nine sets of gas source rocks and has found 25 conventional and tight gas-producing zones (18 being marine facies) and one marine facies shale gas–producing zone. The nine sets of gas source rocks include the Sinian Doushantuo and Dengying formations, Cambrian Qiongzhusi Formation, Upper Ordovician Wufeng–Lower Silurian Longmaxi formations, Permian Qixia, Maokou, Dalong, Longtan/Wujiaping formations, and Triassic Xujiahe Formation (**Figure 2**). The former seven sets belong to marine sapropelic source rocks. The Sinian Doushantuo and Dengying formations were deposited during a sea transgression. It is distributed mainly in the basin margins in the northwest, northeast, and southeast of the Sichuan Basin, with very thin thickness in the basin. The Cambrian Qiongzhusi Formation is characterized by black carbonaceous shale with an average thickness of 180 m in the basin. The organic matter is dominated by Type I and Type II_1 kerogen with total organic content (TOC) up to 6% in the southern and northern Sichuan, and the thermal maturity equivalent Ro% is 2%–5% (Xu et al., 2011). The Permian Qixia and Maokou formations are a set of carbonate deposits and are widely distributed in the basin with thickness between 150–400 m and TOC generally less than 2% (Huang et al., 2016). The Permian Dalong Formation is a set of black mudstone and siliceous mudstone. It is mainly distributed in the northern Sichuan Basin with a thickness up to 30 m (Xia et al., 2013). It has a TOC between 0.43%–21.2% (average = 8.3%, n = 38) and $\delta^{13}C$ values of kerogen from −24‰ to −29‰ (Chen et al., 2018). The Longtan Formation/Wujiaping Formation belongs to marine-continental transitional source rocks, where the Longtan Formation is a set of coal measure gas source rocks, similar to the Xujiahe Formation. Wujiaping Formation is contemporaneous with Longtan Formation, but mainly a set of marine sapropelic source rocks. The Triassic Xujiahe Formation is dominated by Type II_2 and Type III organic matter, which is a set of coal measure gas source rocks. The Wufeng–Longmaxi formations are the only industrial exploration and development strata of shale gas. The Wufeng Formation has a thickness of 2–11 m, and the Longmaxi hot shale is concentrated on the bottom 10–40 m of the Lower Longmaxi Formation. The Wufeng–Longmaxi hot shale has a burial depth of 500–5,500 m and is deposited in an environment of deep water shelf facies and stably distributed. By 2020, Jiaoshiba, Changning, Weiyuan, Huangjinba, Taiyang, Weirong, Yongchuan, and other shale gas fields have been discovered (**Figure 1**). In China, the cumulative proved geological reserves of shale gas were 2.0×10^{12} m^3, the completed production capacity was 300×10^8 m^3/year, and the annual shale gas output was 200.55×10^8 m^3 in 2020.

2.1 Taiyang Shale Gas Field

The Taiyang shale gas field is located in the south of Xuyong County, Sichuan Province, and is a part of the Zhaotong National Shale Gas Demonstration Zone (**Figure 1**). It belongs to the Taiyang anticline, which was a narrow and steep anticlinal structure cut and damaged by strike–slip faults. It has been uplifted continuously since the Late Jurassic, and

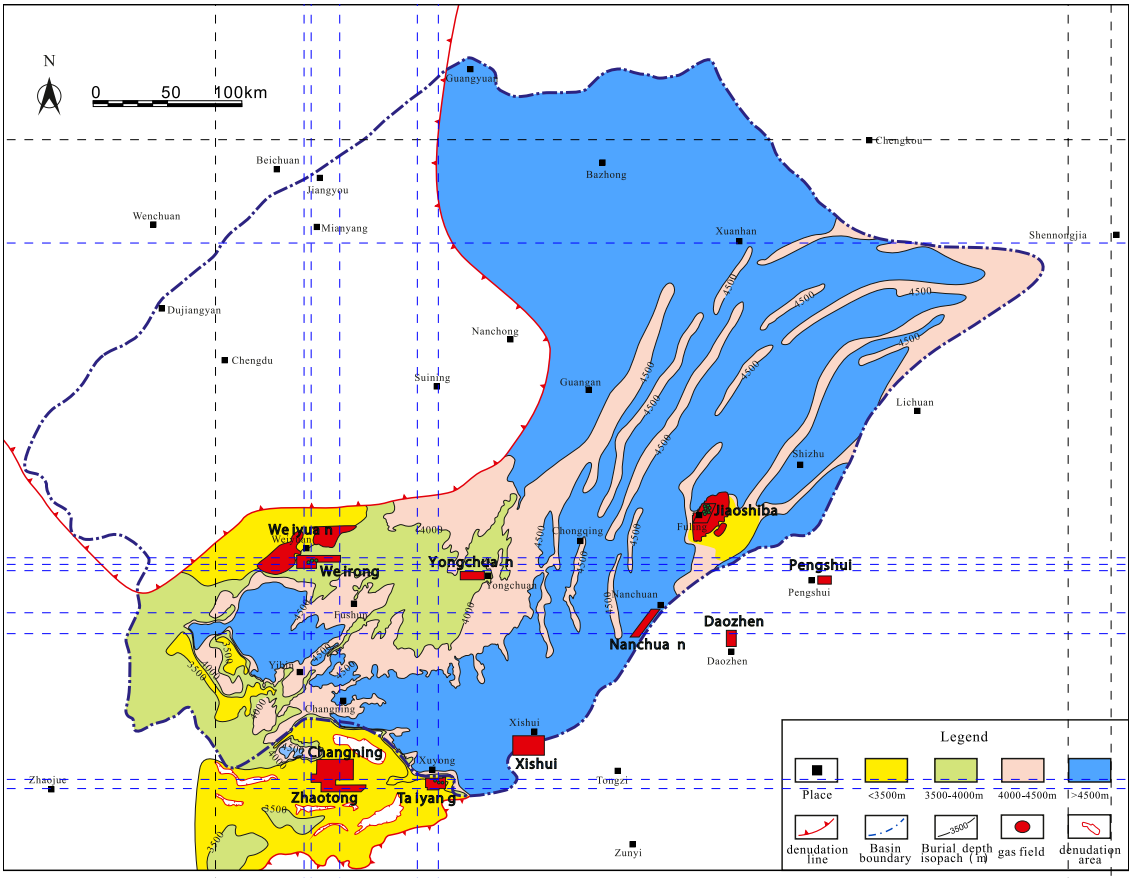

FIGURE 1 | Location map of the Taiyang, Jiaoshiba, and Weirong gas fields. Also shown are the actual vertical burial depths (excluding the horizontal portion) of the Upper Ordovician Wufeng–Lower Silurian Longmaxi formations in the Sichuan Basin.

the uplifted range is about 2,000 m, which resulted in the denudation of the strata above Permian and possible loss of free gas. The black organic-rich siliceous shale and carbonaceous shale of the Wufeng–Longmaxi formations are the main targets of the shale gas field development, with a vertical burial depth (excluding the horizontal portion) of 500–2,250 m and formation pressure coefficient of 1.2–1.47, which belongs to shallow, atmospheric-overpressure shale gas reservoirs. The high-quality reservoirs are 13–18 m thick and stable in distribution, with TOC content of 0.42%–9.05% with an average of 2.92%. The organic matter is dominated by Type II_1, and the equivalent Ro% ranges from 3.0% to 3.9% (average = 3.45%) (Wang et al., 2019; Liang et al., 2021; Zou et al., 2021). The shale porosity is 2.92%–8.01%, with an average of 4.98%. The average brittleness is 72%, the gas content is 3.3–5.51 m^3/t, and the average content of clay minerals is 24.7%. By the end of 2020, the accumulative proved reserves had been 1,365 × 10^8 m^3. The completed production capacity was 8 × 10^8 m^3/year, and the annual shale gas output was 4.0 × 10^8 m^3 in 2020.

2.2 Jiaoshiba Shale Gas Field

The Jiaoshiba shale gas field is located in the east of Chongqing and is a part of the Fuling National Shale Gas Demonstration Zone (**Figure 1**). It has an area of about 575.92 km^2. The main body the of Jiaoshiba gas field is a box anticlinal structure spreading NE–SW, with faults controlling the east and west sides and large-scale faults developing in the southeast. The uplift was late and large, about 3,000 m, and the limestone of the Triassic Jialingjiang Formation is exposed, but the gas reservoir is well-preserved. The Wufeng–Longmaxi organic-rich shale is the main target layer of the shale gas field. The optimal reservoir section has a burial depth (excluding the horizontal portion) of 2,250–3,500 m. It is stably distributed with a thickness of about 38–40 m and a pressure coefficient of 1.55. It is dominated by Type I organic matter with an average TOC of 3.76%, porosity of 4.87%, brittleness of 62.4%, gas content of 2.96 m^3/t, clay mineral content of 31.6%, and equivalent Ro% of 3.1% (2.6%–3.6%) (Dai et al., 2014a; Wang et al., 2019; Zou et al., 2021). By the end of 2020, the accumulative proved reserves had been 6008.14 × 10^8 m^3. The completed production capacity

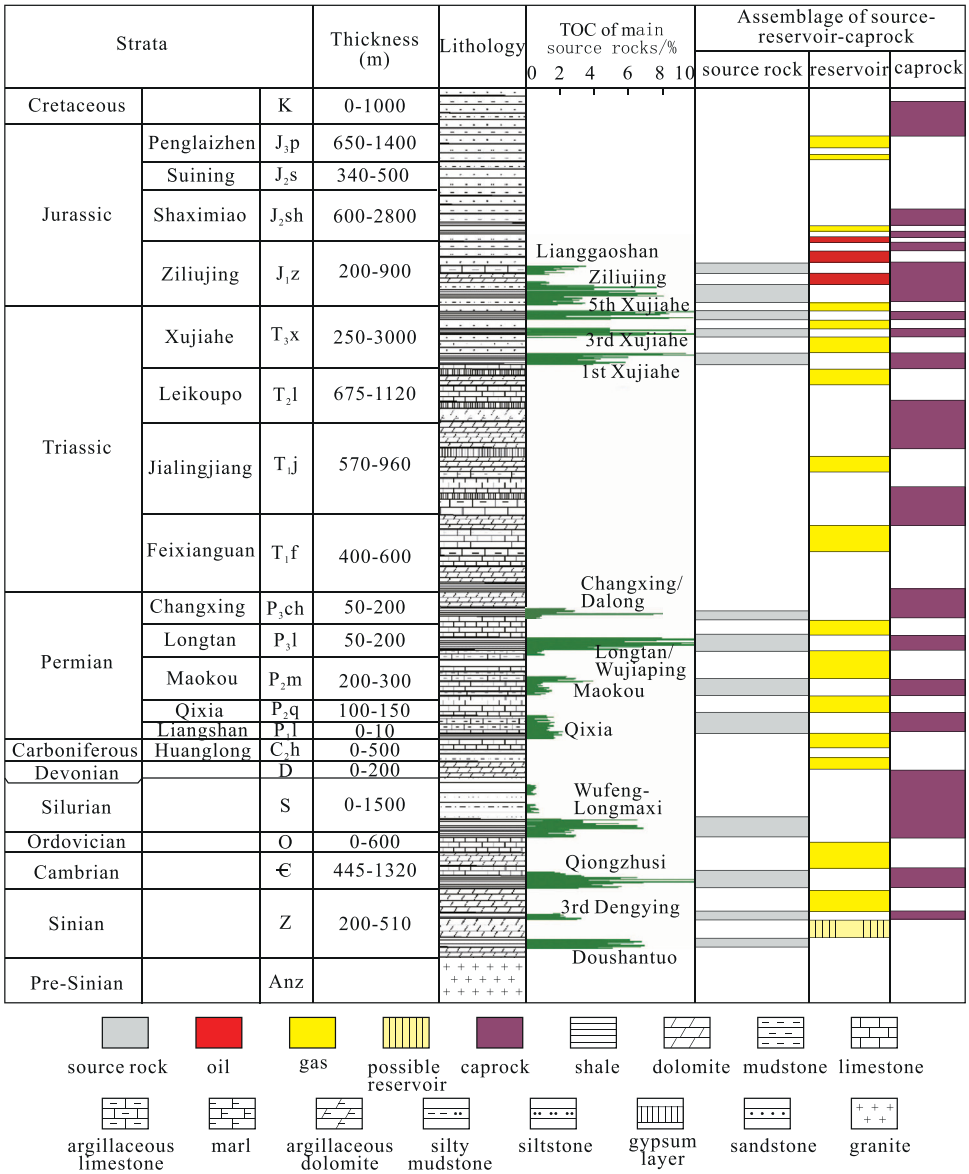

FIGURE 2 | Generalized stratigraphy of the Sichuan basin. Also shown are the TOC of main source rocks and the source-reservoir-caprock assemblage. Modified from Dai et al. (2021).

was 100×10^8 m^3/year, and the annual shale gas production was 67×10^8 m^3 in 2020.

2.3 Weirong Shale Gas Field

The Weirong shale gas field is located in Neijiang and Zigong counties of Sichuan Province and is a part of the Changning–Weiyuan National Shale Gas Demonstration Zone (**Figure 1**). The main body of the gas field belongs to the Baimazhen syncline of the low-fold structural belt in southwestern Sichuan. The structure is gentle, and the fault is not developed. Influenced by the uplift evolution of the Sichuan Basin in the Late Cretaceous, the Jurassic was exposed on the surface, and the burial depth (excluding the horizontal portion) of the gas layer was 3,550–3,880 m. The overall preservation condition of the gas layer is good, and the formation pressure is high, that is, 1.94–2.06. The high-quality reservoirs are 25–39 m thick and stable in distribution, with an average TOC of 2.80%, porosity of 6.07%, brittleness of 64%, gas content of 3.15 m^3/t, clay mineral content of 34%, and equivalent Ro% of 2.25% (1.8%–2.7%) (Wang et al., 2019; Zou et al., 2021). By the end of 2020, the cumulative proved reserves had been 1,247

$\times 10^8$ m^3. The completed production capacity was 10×10^8 m^3/year, and the annual shale gas output was 5.4×10^8 m^3 in 2020.

3 SAMPLES AND METHODS

Eleven shale gas samples from the Weirong shale gas field in the Changning–Weiyuan National Shale Gas Demonstration Zone (marked as Weirong), 10 shale gas samples from the Taiyang shale gas field in the Zhaotong National Shale Gas Demonstration Zone (marked as Taiyang), and 10 shale gas samples from the Jiaoshiba shale gas field in the Fuling National Shale Gas Demonstration Zone (marked as Jiaoshiba) were collected (**Figure 1**).

Samples were pure gases and collected directly from the wellheads or separators in the shale fields. Double-ended stainless steel bottles (10 cm diameter about 1,000 cm^3 volume) were used to collect the samples, which were equipped with shut-off valves with a maximum pressure of 22.5 MPa. The bottles and the lines were flushed with the sample gases for 15–20 min to remove air contamination. The pressure inside the bottle was kept above atmospheric pressure. Leakage tests by immersing bottles in a water bath were performed for all samples.

The molecular and isotopic compositions of the gas samples were determined at the PetroChina Research Institute of Petroleum Exploration and Development (RIPED). The molecular composition was determined using an Agilent 7890A gas chromatograph, which was equipped with a flame ionization detector and a thermal conductivity detector. Gas components were separated using six columns (2 Foot 12% UCW982 on PAW 80/100 mesh, 15 Foot 25% DC200 on PAW 80/100 mesh, 10 Foot Hayesep 80/100 mesh, 10 Foot Molecular Sieve 13X 45/60 mesh, 8 Foot Molecular Sieve 5A 60/80 mesh, and 3 Foot Hayesep Q 80/100 mesh). GC oven temperature was set at 85°C for 40 min. Immediately prior to the molecular composition analysis, the GC is calibrated by certified gas standards, which is also used to monitor the analytical drift by injecting them before, during, and after the analysis. The analytical precision and accuracy are typically better than 0.01% for methane, ethane, and propane.

Stable carbon isotopes were determined using a Thermo Delta V mass spectrometer, which was interfaced with a Thermo Trace GC Ultra gas chromatograph (GC). Methane, ethane, propane, and CO_2 were separated on a gas chromatograph using a fused silica capillary column (PLOT Q 27.5 m × 0.32 mm × 10 μm), converted into CO_2 in a combustion interface, and then injected into the mass spectrometer. The temperature programming of the GC oven was as follows: heated from 33°C to 80°C at 8°C/min, then to 250°C at 5°C/min, and maintained at 250°C for 10 min. An oil-related gas from the Tazhong gas field in the Tarim Basin in China is used as our laboratory working standard. More than 800 measurements including both online and offline of the compound-specific carbon isotopic compositions have been carried out by 10 laboratories (Dai et al., 2012b). International measurement standards (NBS19 and L-SVEC CO_2) are used to perform the two-point calibrations. The carbon isotopic values were reported in δ-notation per mil (‰) relative to VPDB. All analyses were duplicated, and the analytical precision and accuracy are better than ±0.3‰.

4 RESULTS

4.1 Molecular Composition

Methane is the dominant composition, which accounts for 98.82% (average, n = 10) in the Taiyang gas samples, 98.13% (average, n = 10) in the Jiaoshiba gas samples, and 96.91% (average, n = 11) in the Weirong gas samples (**Table 1**). The content of C_{2+} heavy hydrocarbon (mainly C_2H_6 and C_3H_8) is very small, generally less than 1%. It is 0.61% (average, n = 10) in the Taiyang gas samples, 0.58% (average, n = 10) in the Jiaoshiba gas samples, and 0.45% (average, n = 11) in the Weirong gas samples. In general, Taiyang shale gas has the highest content of both methane (98.82%) and C_{2+3} heavy hydrocarbon gases (0.59%), while Weirong gas samples have the lowest content of both methane (96.91%) and C_{2+3} heavy hydrocarbon gases (0.44%). All the gases have extremely low gas wetness, which has a value of 0.21%–0.83%, indicating they belong to dry gas. The content of nonhydrocarbon gases such as CO_2 and N_2 is also very less (**Table 1**). Both the Taiyang and Jiaoshiba gases have a trace amount of CO_2 and N_2, less than 1%. Weirong gas has similar content of N_2 (<1%) but a relatively higher content of CO_2, in which CO_2 is generally more than 1% with an average of 2.05% (average, n = 11) and is up to 6.64% in Well Wei 43-1HF.

4.2 Stable Carbon Isotopic Composition

Gas samples from the Taiyang, Jiaoshiba, and Weirong gas fields have distinct carbon isotopic values. Gases from the Taiyang gas field have the highest $\delta^{13}C_1$ values, −29.5‰ to −27.1‰, with an average of −28.5‰ (n = 10), followed by the gases from the Jiaoshiba gas field, −32.7‰ to −29.0‰, with an average of −30.3‰ (n = 10), and gases from the Weirong gas field have the lowest $\delta^{13}C_1$ values, −35.9‰ to −34.1‰, with an average of −35.2‰ (n = 11) (**Table 1**). The carbon isotopic compositions of ethane and propane are the highest in gas samples from the Taiyang gas field $\delta^{13}C_2$: −36.8‰ to −33.7‰, with an average of −35.4‰ (n = 10); $\delta^{13}C_3$: −37.6‰ to −34.6‰, with an average of −36.2‰ (n = 10), followed by gas samples from Jiaoshiba gas field [$\delta^{13}C_2$: −37.5‰ to −35.5‰, with an average of −36.4‰ (n = 10); $\delta^{13}C_3$: −39.5‰ to −37.7‰, with an average of −38.4‰ (n = 10)], and are the lowest in the gas samples from Weirong gas field ($\delta^{13}C_2$: −39.7‰ to −38.4‰, with an average of −38.9‰ (n = 11); $\delta^{13}C_3$: −42.0‰ to −38.7‰, with an average of −40.8‰ (n = 11) (**Table 1**).

5 DISCUSSION

In order to further explore the gas origin, published data about shale gas from the marine facies sapropelic organic matter (Type I and II_1 kerogen) of the Upper Ordovician Wufeng–Lower Silurian Longmaxi shale in the Changning–Weiyuan, Fuling,

TABLE 1 | Molecular and carbon isotopic composition of gas samples from the Upper Ordovician Wufeng–Lower Silurian Longmaxi formations in the Taiyang, Jiaoshiba, and Weirong shale gas fields in the Sichuan Basin, China.

Gas field	Well	Well depth	Burial depth	Composition (%)					Dryness	$\delta^{13}C$ (‰)		
		m	m	CH_4	C_2H_6	C_3H_8	CO_2	N_2	C_1/C_{1+}	CH_4	C_2H_6	C_3H_8
Taiyang	Yang102 H2-2	2204.86	919.9	98.81	0.60	0.01		0.58	0.994	−29.5	−36.2	−37.0
	Yang102 H2-6	2275.24	969.95	98.88	0.63	0.01		0.48	0.994	−29.4	−36.6	−37.6
	Yang102 H2-8	2589.82	995.82	99.03	0.66	0.01		0.30	0.993	−29.5	−36.8	−37.0
	Yang105 H3-2	3,426	2245.66	98.57	0.59	0.01	0.15	0.67	0.994	−27.1	−33.7	−34.9
	Yang105 H3-4	3,390	2140.76	98.88	0.59	0.01	0.14	0.37	0.994	−27.2	−33.7	−34.6
	Yang105 H3-6	3,325	2059.13	98.50	0.71	0.11	0.13	0.41	0.992	−27.2	−34.3	−34.8
	Yang105 H2-2	2,300	1544.28	98.94	0.57	0.02	0.05	0.40	0.994	−28.4	−35.7	−36.3
	Yang105 H2-4	2,400	1501.065	98.88	0.53	0.01	0.05	0.52	0.995	−29.1	−35.9	−36.3
	Yang105 H2-6	2,285	1414.845	98.76	0.49	0.01		0.45	0.995	−29.1	−35.4	−37.1
	Yang105 H2-8	2,300	1249.86	99.01	0.48	0.01		0.50	0.995	−28.7	−36.0	−36.5
Jiaoshiba	JY1-2HF	4,168	2416.215	98.09	0.62	0.03	0.31	0.84	0.993	−30.3	−35.5	−37.7
	JY2-3HF	4,518	2479.58	98.23	0.63	0.02	0.31	0.81	0.993	−29.0	−35.7	−38.1
	JY3-3HF	3,561	2428.855	97.98	0.61	0.02	0.35	0.95	0.994	−32.7	−37.5	−38.2
	JY4-2HF	4,312	2598.44	98.21	0.56	0.01	0.44	0.77	0.994	−30.2	−36.5	−38.2
	JY56-2HF	4,498	2818.265	98.09	0.52	0.01	0.57	0.81	0.995	−29.4	−36.1	−38.0
	JY18-5HF	4,650	2820.685	98.14	0.53	0.02	0.34	0.96	0.994	−30.0	−36.5	−38.9
	JY9-6HF	4,147	2310.17	98.26	0.64	0.02	0.21	0.87	0.993	−30.0	−36.2	−38.5
	JY39-7HF	5,410	2778.295	98.18	0.63	0.02	0.37	0.81	0.993	−30.4	−36.8	−39.5
	JY37-6HF	5,865	3139.72	98.09	0.47	0.01	0.60	0.83	0.995	−30.1	−36.6	−39.2
	JY61-2HF	4,770	3037.515	98.01	0.45	0.01	0.66	0.88	0.995	−30.3	−36.9	−38.1
Weirong	WY29-1HF	5,430	3,743	97.66	0.46	0.02	1.26	0.60	0.995	−35.4	−39.3	−41.9
	WY29-2HF	5,390	3,737	97.70	0.50	0.02	1.20	0.58	0.995	−35.9	−39.3	−42.0
	WY29-4 + 5 + 6		3,690	97.76	0.50	0.02	1.19	0.52	0.995	−35.4	−39.7	−41.8
	WY23-4HF	5,546	3,800	97.42	0.44	0.02	1.64	0.49	0.995	−35.2	−38.8	−41.1
	WY23-2HF	5,600	3830.22	97.23	0.42	0.01	1.72	0.61	0.996	−34.9	−38.4	−40.8
	WY23-6HF	5,596	3831.96	97.41	0.43	0.01	1.66	0.48	0.995	−34.9	−38.5	−40.7
	WY43-1HF	5,520	3,720	91.91	0.19	0.00	6.64	1.25	0.998	−34.1	−38.6	−38.8
	WY43-2HF	5,540	3,737	96.37	0.46	0.02	2.76	0.38	0.995	−35.1	−38.9	−38.9
	WY43-3HF	5,585	3,744	97.40	0.48	0.03	1.59	0.49	0.995	−35.6	−38.6	−38.7
	WY43-4HF	5,595	3,778	97.55	0.46	0.02	1.53	0.44	0.995	−35.4	−38.7	−41.9
	WY43-5HF	5,610	3,770	97.58	0.47	0.02	1.38	0.55	0.995	−35.4	−39.1	−42.0

Note: All the wells are horizontal and comprise vertical and horizontal portions. Well depth represents the depth including the actual vertical portion and the horizontal portion. Burial depth represents the actual vertical portion.

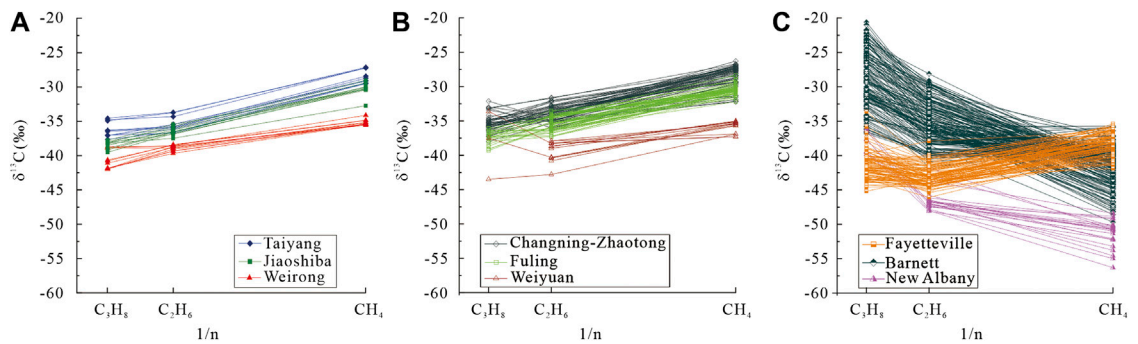

FIGURE 3 | Stable carbon isotopic compositions versus 1/n where n is the carbon number of methane, ethane, and propane from Taiyang, Jiaoshiba, and Weirong gas fields in the Sichuan Basin **(A)**. Gases from these three gas fields all have carbon isotopic reversal among the methane, ethane, and propane ($\delta^{13}C_1 > \delta^{13}C_2 > \delta^{13}C_3$). Also shown are published data about shale gases from the Changning-Zhaotong, Fuling, and Weiyuan national shale gas demonstration zones **(B)** and shale gases from the Barnett, New Albany, and Fayetteville shale (see text). **(C)** Modified from Chung et al. (1988).

and Zhaotong national shale gas demonstration zones, Pengshui and Yongchuan area in the Sichuan Basin, shale gas from the marine facies sapropelic organic matter of the Barnett shale in the Fort Worth Basin, Fayetteville shale in the Arkoma Basin, and New Albany shale in the Illinois Basin were also investigated (Cao et al., 2020; Chen et al., 2020; Dai et al., 2016b; Feng et al., 2019;

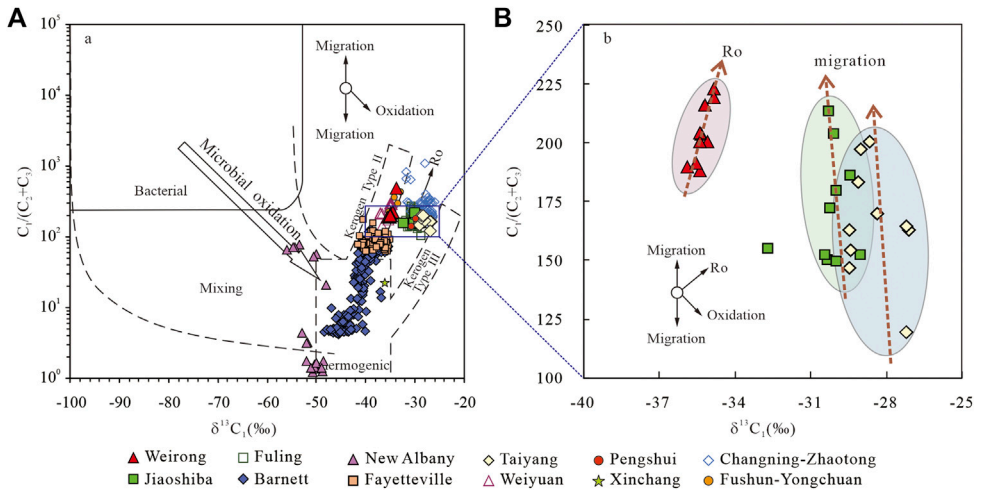

FIGURE 4 | Natural gas interpretative "Bernard" diagram (Bernard et al., 1976), showing gases from the Taiyang, Jiaoshiba, and Weirong gas fields are thermogenic gas **(A)** and the effects from migration and thermal maturation **(B)**. Also shown are shale gases from the published data (see text).

Feng et al., 2020; Feng et al., 2016; Lin et al., 2017; Wei et al., 2016; Wu et al., 2015; Zhang et al., 2018a; Martini et al., 2008; Rodriguez and Philp, 2010; Strąpoć et al., 2010; Zumberge et al., 2012).

5.1 Origin of the Gas

Carbon isotopic reversal occurs widely among the C_1–C_3 n-alkanes, that is, methane and its homologs get more depleted in ^{13}C with increasing carbon number ($\delta^{13}C_1 > \delta^{13}C_2 > \delta^{13}C_3$) (**Figure 3A**; **Table 1**). In general, this is consistent with previous studies of the shale gases from the Changning–Zhaotong, Weiyuan, and Fuling national shale gas demonstration zones (**Figure 3B**). In contrast, gas samples from the Barnett and New Albany shales mostly have a positive carbon isotopic distribution pattern among the C_1–C_3 alkane gases ($\delta^{13}C_1 < \delta^{13}C_2 < \delta^{13}C_3$), and those from the Fayetteville shale have similar carbon isotopic reversal (**Figure 3C**) (Martini et al., 2008; Rodriguez and Philp, 2010; Strąpoć et al., 2010; Zumberge et al., 2012).

Numerical studies have suggested a cut-off $\delta^{13}C_2$ value of −28‰ to distinguish the gases sourced from humic and sapropelic organic matter, that is, gases sourced from humic organic matter have $\delta^{13}C_2 > -28$‰, while gases sourced from sapropelic organic matter have $\delta^{13}C_2 < -28$‰ (Chen et al., 1995; Dai et al., 2009, Dai et al., 2012a; Dai et al., 2014b; Liang et al., 2002; Ni et al., 2014, Ni et al., 2015, Ni et al., 2019b). Gases from Taiyang, Jiaoshiba, and Weirong gas fields have $\delta^{13}C_2 < -33$‰, and should source from sapropelic organic matter according to the criterion of $\delta^{13}C_2$ value. However, such a distinguishing criterion is effective for gases with normal carbon isotopic distribution patterns which have not undergone secondary alteration but may not be applicable for gases with carbon isotopic reversal (Dai et al., 2013). Therefore, genetic information should be obtained from indexes and not only the $\delta^{13}C_2$ values.

"Bernard diagram," based on the carbon isotopic value of methane and the molecular composition of methane and ethane, was often used to determine the gas origin and later modifications (Bernard et al., 1976). This diagram differentiates the thermogenic and bacterial gases and shows the type of kerogen and later secondary alterations such as mixing between thermogenic and bacterial gases, migration, oxidation, and thermal maturation. Except gases from the New Albany in the Illinois Basin that have mixing effects, all other gases fall in the thermogenic gas area and have no impacts from bacterial gas (**Figure 4A**). **Figure 4B** demonstrates that gases from the Weirong gas field are mainly affected by the thermal maturation, but gases from the Jiaoshiba and Taiyang gas fields are likely affected by the migration effects.

In the $\delta^{13}C_1$ versus $\delta^{13}C_2$ and $\delta^{13}C_2$ versus $\delta^{13}C_3$ cross-plots, in general, the least mature gases lie in the lower left area and most mature gases lie in the upper right area. Theoretically, gases which have not undergone secondary alteration and are from the same source rocks but with different thermal maturation stages will lie on a straight line. Gases from the Taiyang, Jiaoshiba, and Weirong shale gas fields fall on the bottom right side of the diagram close to the area of sapropelic Type II kerogen and also in the area below the 1:1 line of $\delta^{13}C_1$ versus $\delta^{13}C_2$ (**Figure 5A**). This indicates gases from the Taiyang, Jiaoshiba, and Weirong gas fields were sourced from sapropelic organic matter. **Figure 5A** also shows a very low carbon isotopic composition of ethane, therefore demonstrating a carbon isotopic reversal between methane and ethane ($\delta^{13}C_1 > \delta^{13}C_2$). Similarly, in the plot of $\delta^{13}C_2$ versus $\delta^{13}C_3$, gases from the three gas fields fall in the area close to that of the sapropelic Type II kerogen (Berner and Faber, 1996) and demonstrate a carbon isotopic reversal between ethane and propane ($\delta^{13}C_2 > \delta^{13}C_3$) (**Figure 5B**).

Recently, new diagrams of $\delta^{13}C_1$ versus $\delta^{13}C_2$ and $\delta^{13}C_1$ versus Δ ($\delta^{13}C_2$–$\delta^{13}C_1$) were proposed to separate the shale-sourced and coal-sourced gases (Milkov, 2021). Both the $\delta^{13}C_1$ versus $\delta^{13}C_2$ and $\delta^{13}C_1$ versus Δ ($\delta^{13}C_2$–$\delta^{13}C_1$) diagrams can distinguish gases of primary microbial, secondary microbial, thermogenic, and abiotic origins, and the thermogenic gas includes mid-mature to late-mature shale-sourced and coal-sourced gases (**Figure 6**). Gases from the marine facies Taiyang, Jiaoshiba, and Weirong gas

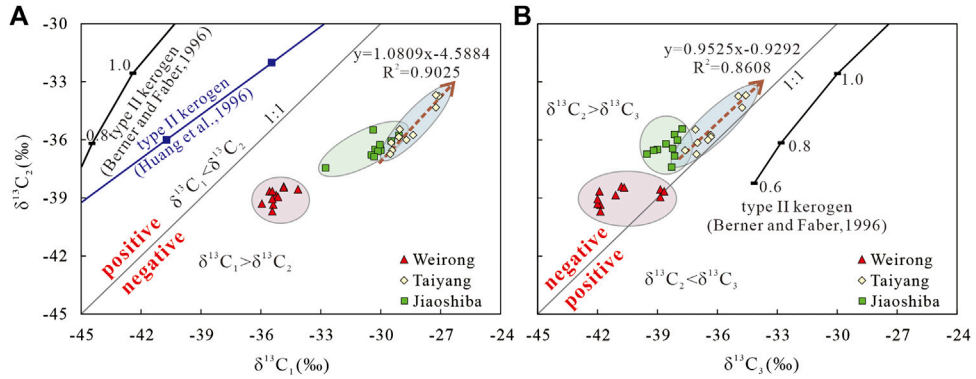

FIGURE 5 | $\delta^{13}C_1$ versus $\delta^{13}C_2$ **(A)** cross-plot and $\delta^{13}C_2$ versus $\delta^{13}C_3$ cross-plot **(B)** of gases from Taiyang, Jiaoshiba, and Weirong gas fields in the Sichuan Basin. Lines of Type II kerogen from Berner and Faber (1996) and Huang et al. (2016) are also shown. For the line from Berner and Faber (1996), the carbon isotope of the initial precursor is estimated to be −29‰.

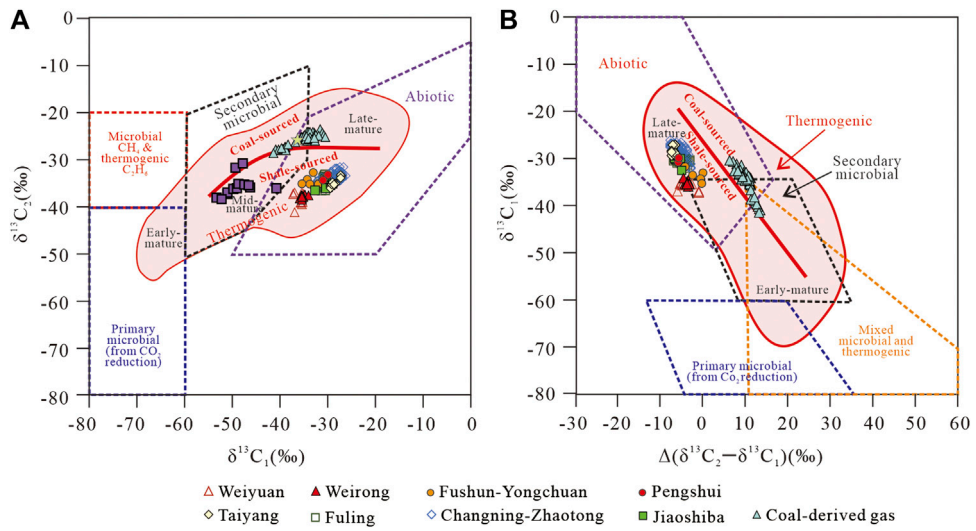

FIGURE 6 | Plots of $\delta^{13}C_1$ versus $\delta^{13}C_2$ **(A)** and $\delta^{13}C_1$ versus $\Delta(\delta^{13}C_2–\delta^{13}C_1)$ **(B)** of gases from the Taiyang, Jiaoshiba, and Weirong gas fields in the Sichuan Basin, China. Also shown are shale gases from the published data (see text). Modified from Milkov (2021).

fields fall in the area of shale-sourced thermogenic gas toward the late-mature thermal evolution stage, which is similar to the shale gases from the Weiyuan, Fuling, Changning–Zhaotong, Pengshui, and Yongchuan areas. Among the nine sets of source rocks in the Sichuan Basin, source rocks above the Wufeng–Longmaxi shale are impossible to have a contribution. The Qixia and Maokou source rocks are a set of carbonate deposits, the Longtan and Xujiahe source rocks are a set of coal measure deposit, and the Dalong source rocks are locally distributed in northern Sichuan. The Sinian source rocks are mainly distributed in the margins of the Basin and have little contribution. Though the Qiongzhusi shale is widely distributed, the Ordovician deposit is very thick, and the thickness can be up to 600 m. The hot shale in the Wufeng-Longmaxi formations is generally less than 50 m and concentrated in the Wufeng and the Lower Longmaxi formations. Hence, gases in the Taiyang, Jiaoshiba, and Weirong shale gas fields are shale gas reservoirs and sourced in the Wufeng–Longmaxi shale.

5.2 Carbon Isotope of Methane

When plotting the $\delta^{13}C_1$ versus gas wetness, gases from Weirong, Weiyuan, Barnett, and Fayetteville have a good linear relationship, while gases from Taiyang and Jiaoshiba are characterized by an enrichment of ^{13}C in methane and thus shift away from the linear maturity trend (**Figure 7A**). The ^{13}C-enriched methane was considered to be a late-stage methane and result from Rayleigh-type isotopic fractionation of ethane (Feng et al., 2020); however, such a mechanism may not satisfy the mass and isotopic balance requirements (Xia and Gao, 2018). In the southern Sichuan Basin, geological conditions are

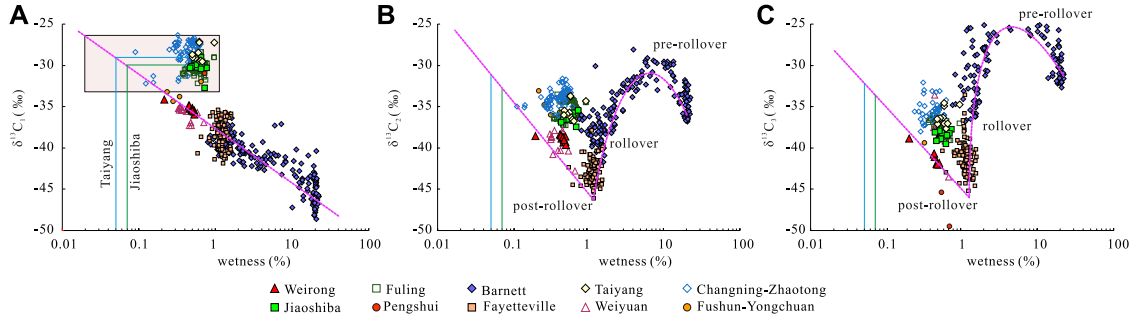

FIGURE 7 | Plots of wetness versus $\delta^{13}C_1$ **(A)**, $\delta^{13}C_2$ **(B)**, and $\delta^{13}C_3$ **(C)** of shale gases from Taiyang, Jiaoshiba, and Weirong gas fields. Also shown are shale gases from the published data (see text).

more complex than those in the Appalachian Basin. The Wufeng–Longmaxi shale has experienced very high geo-temperature and is at the over-mature stage at present and has suffered extensive uplifts locally. Considering these complex conditions, more influences should be considered in the southern Sichuan Basin. The offset of the $\delta^{13}C_1$ values in Taiyang and Jiaoshiba shale gas fields could be caused either by enrichment of ^{13}C in methane or by an increase in wetness. Compared to the Cambrian and Sinian conventional natural gas in the Weiyuan gas field (−32.7‰ to 32.0‰) (Dai, 2003; Wu et al., 2014), the Silurian Wufeng–Longmaxi shale gas in Taiyang and Jiaoshiba areas is clearly more enriched in ^{13}C.

5.2.1 Thermal Maturity of the Source Rocks

Various models have demonstrated the linear logarithmic relationship between the carbon isotopic composition of methane and the thermal maturity (Ro%) of source organic matter (Stahl and Carey, 1975; Schoell, 1980; Dai and Qi, 1989; Berner and Faber, 1996). In the oil window, methane is primarily generated from kerogen cracking. When thermal maturity still increases, wet gas cracking begins, which will increase methane but decrease in gas wetness (Prinzhofer and Huc, 1995). Hence, the carbon isotope of methane generally increases with increasing thermal maturity of the source rocks, and methane generated at higher thermal maturity normally has a higher carbon isotope and lower gas wetness.

Though the Wufeng–Longmaxi shale in the southern Sichuan Basin is generally all at the over-mature stage, differences still exist in different areas. Shale in the Weiyuan area has a relatively low equivalent Ro% of 2.25% (1.8%–2.7%) (Wang et al., 2019; Zou et al., 2021); correspondingly, its shale gas has the lowest $\delta^{13}C_1$ values (average = −35.2‰) and wetness of 0.47% (0.21%–0.53%), which falls on the linear maturity trend. Shale in the Taiyang area has the highest equivalent Ro% of 3.45% (3.0%–3.9%) (Wang et al., 2019; Liang et al., 2020a; Liang et al., 2020b; Zou et al., 2021); correspondingly, its shale gas has the highest $\delta^{13}C_1$ values (average = −28.5‰) and wetness of 0.61% (0.50%–0.83%), which falls off the linear maturity trend. Compared to the Weirong shale gas, the Taiyang shale gas should have lower gas wetness due to its higher thermal maturity. Similarly, shale in the Jiaoshiba area has an equivalent Ro% of 3.1% (2.6%–3.6%) (Dai et al., 2014a; Wang et al., 2019; Zou et al., 2021), which is higher than that in Weirong but lower than that in Taiyang. Correspondingly, its shale gas also has $\delta^{13}C_1$ values (average = −30.3‰) higher those that in Weirong but lower than those in Taiyang, and gas wetness of 0.59% (0.47%–0.67%), which also falls off the linear trend line (**Figure 7A**). Compared to the Weirong shale gas, the Jiaoshiba shale gas also should have lower gas wetness due to its higher thermal maturity. As shown in **Figure 7A**, if thermal maturity is the controlling factor, the Taiyang shale gas should have gas wetness around 0.05%, while the Jiaoshiba shale gas should have gas wetness around 0.07%, which is an order of magnitude lower than the actual determined wetness. According to such low gas wetness, the carbon isotopes of ethane and propane are relatively lower than expected (**Figures 7B, C**).

Carbon isotopic differences between methane and ethane [$\Delta(\delta^{13}C_2–\delta^{13}C_1)$] have been used to reflect the maturity influences on gases. As thermal maturity increases, the isotopic differences between methane and ethane decreases; therefore, the more mature gases normally will have smaller Δ ($\delta^{13}C_2–\delta^{13}C_1$) values (James, 1983; Clayton, 1991; Tang et al., 2000). Shale gases from Taiyang, Jiaoshiba, and Weirong gas fields generally demonstrate a good linear inversed relationship between the $\delta^{13}C_1$ value and $\Delta(\delta^{13}C_2–\delta^{13}C_1)$ value (R^2 = 0.9048). The $\delta^{13}C_1$ value increases from −36‰ to −27‰, correspondingly, and the Δ ($\delta^{13}C_2–\delta^{13}C_1$) value changes from −3‰ to −8‰ (**Figure 8A**). The carbon isotopic differences between methane and ethane get larger with increasing thermal maturity, which is opposite to the normal trend (**Figure 8A**). This is mainly caused by the depletion of ^{13}C in ethane with increasing thermal maturity. As the thermal maturity increases, methane becomes more enriched at ^{13}C, while ethane gets more depleted at ^{13}C; hence, the higher the thermal maturity, the larger the $\delta^{13}C$ differences between methane and ethane. This linear correlation implies that thermal maturity should be the controlling factor on the carbon isotopes of the shale gas. In addition to the thermal maturity of the source rocks, there should be a process that will increase the amount of wet gas but will not significantly impact the amount of methane (**Figures 8B, C**). As shown in **Figure 8**, methane content generally increases with increasing $\delta^{13}C_1$ values in the three gas fields, while shale gas in

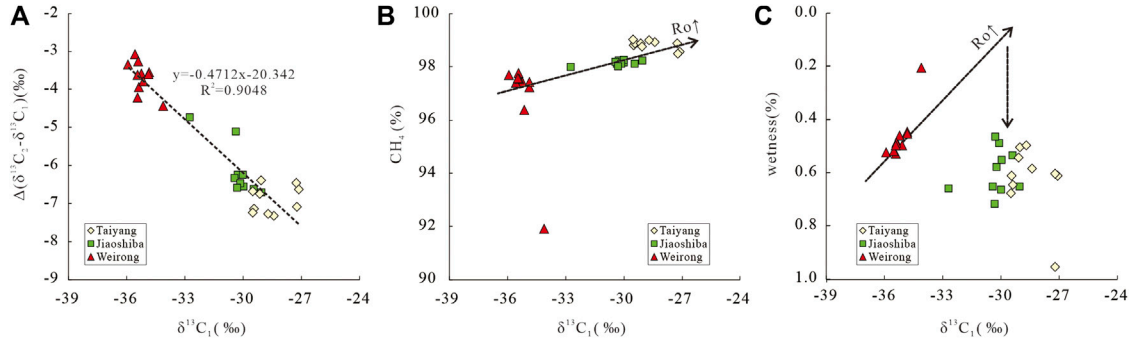

FIGURE 8 | Plots of $\delta^{13}C_1$ versus $\Delta(\delta^{13}C_2–\delta^{13}C_1)$, **(A)**, $\delta^{13}C_1$ versus CH_4 **(B)**, and $\delta^{13}C_1$ versus wetness **(C)** of gases from the Taiyang, Jiaoshiba, and Weirong gas fields in the Sichuan Basin, China.

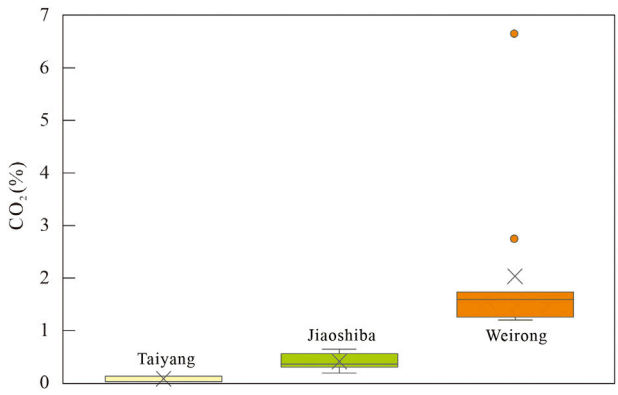

FIGURE 9 | Box plot of the CO_2 content in the shale gases from Taiyang, Jiaoshiba, and Weirong shale gas fields in the Sichuan Basin.

the Taiyang and Jiaoshiba gas fields apparently has higher wet gas.

5.2.2 Fischer-Tropsch-Type Synthesis of Hydrocarbon

Fischer–Tropsch-type synthesis of hydrocarbon from CO_2 and H_2 may have contributed to the increasing amount of wet gas and depletion of ^{13}C in hydrocarbon gas. The CO_2 content varies apparently in the Taiyang, Jiaoshiba, and Weirong shale gas fields. The CO_2 content is highest in the Weirong shale gas field, 1.19%–6.64% (average = 2.05%); followed by the Fuling shale gas field, 0.21%–0.66% (average = 0.42%); and the lowest in the Taiyang shale gas field, 0.05%–0.15% (average = 0.10%) (**Figure 9**). Among the 10 gas samples in Taiyang, CO_2 is detected only in five samples. From the Weirong gas field to the Taiyang gas field, the equivalent Ro% increases from 2.25% to 3.45% (Wang et al., 2019; Liang et al., 2021; Zou et al., 2021), while the CO_2 content decreases from 2.05% to 0.10%. The carbon isotope of CO_2 in the Jiaoshiba area varies from −5.8‰ to 10.4‰ (average = 3.7‰) (Feng et al., 2020), which was considered to be the product of thermal metamorphism of carbonate minerals (Dai et al., 2022). Carbonate minerals are abundant in the Wufeng–Longmaxi shale (Dai et al., 2014a; Dai et al., 2016b), and with increasing thermal maturity, thermal metamorphism will generate more CO_2. There must be a sink for CO_2 with increasing thermal maturity in the Jiaoshiba and Taiyang areas.

During the late cantagensis stage, water is likely involved in the generation of methane (Burruss and Laughrey, 2010). A Fischer–Tropsch-type synthesis of hydrocarbon from CO_2 and H_2 is expected to occur through the following two equations: CHx (organic matter) + $2H_2O \rightarrow CO_2 + (2 + x/2)\ H_2$ and $CO_2 + mH_2 \rightarrow xCH_4 + yC_2H_6 + ... + zH_2O$ (Tang and Xia, 2011). Among them, CO_2 could be from the thermal metamorphism of carbonate minerals in the shale and also from the water reforming reaction of organic matter. Higher thermal maturity represents longer reaction time and more consumption of CO_2 in the system, so the CO_2 content is the most in the Weirong shale gas field and the least in the Taiyang shale gas field. Such Fischer–Tropsch-type synthesis of hydrocarbon from CO_2 and H_2 has also been reported in the pyrolytic experiments of shale (Gao et al., 2014) and coal samples (Gao et al., 2018), and apparent carbon isotopic depletion in gaseous products has been documented.

With continuous cracking of wet gas, the amount of wet gas (mainly $C_2 + C_3$) will decrease, that is, the ethane content is less than 0.5% for Weirong shale gas. Due to the amount of CO_2 and H_2, the number of hydrocarbon gases generated *via* Fischer–Tropsch-type synthesis should be minimal. Hence, limited mixing between the late stage shale gas with the Fischer–Tropsch-type synthesized gas will significantly increase the wet gas content but have little impact on the methane content; similarly, the carbon isotopic depletion impact is little on methane, but to some extent significant on ethane and propane. This should be part of the reasons causing the isotopic depletion in ethane and propane.

5.2.3 $\delta^{13}C$ Value of the Source Organic Matter

In the southern Sichuan Basin, the $\delta^{13}C$ value of source organic matter may also have influenced on the $\delta^{13}C$ value of hydrocarbon gases. Generally, hgher $\delta^{13}C$ values of source rocks correspond to higher $\delta^{13}C$ values of gases generated

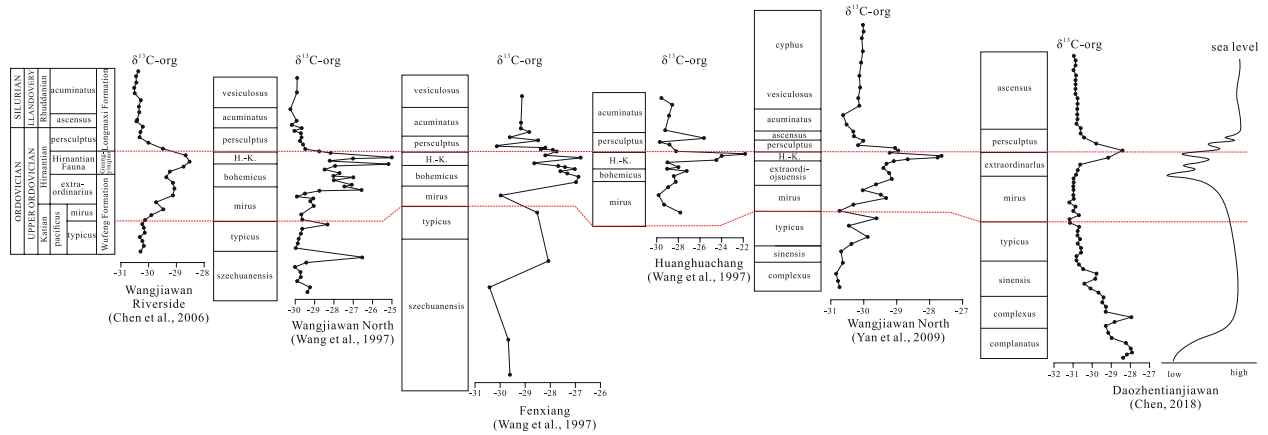

FIGURE 10 | Organic carbon isotopic curve of isolated kerogen at the Wangjiawan Riverside and North sections, Fenxiang, Huanghuachang, Nanbazi, and Tianjiawan sections in China (Wang et al., 1997; Fan et al., 2009; Yan et al., 2009; Chen, 2018). Also shown are the sea-level changes, the uppermost Ordovician systems, series stages, biozonations, and lithostratigraphic units. Modified from Fan et al. (2009).

from them, which is the inheritance effect of the carbon isotope (Dai et al., 1992).

A prominent positive carbon isotopic excursion of both shale and limestones has been recorded in the Late Ordovician Hirnantian stage (Middle and Upper Wufeng Formation in Sichuan Basin) in North America (Bergström et al., 2006; Orth et al., 1986), Europe (Brenchley et al., 1994; Marshall et al., 1997), and China (**Figure 10**) (Chen, 2018; Fan et al., 2009; Wang et al., 1993; Wang et al., 1997), which has been regarded as to be associated with the Gondwana glaciation. The positive carbon isotopic excursion is up to 5‰–7‰ in the Hirnantian limestones (Qing and Veizer, 1994; Marshall et al., 1997; Kump et al., 1999) and is up to −21.1‰ in the Tianjiawan shale in Daozhen county and −26.6‰ in the Nanbazi shale in Tongzi county (Chen, 2018). In addition to the positive carbon isotopic excursion of the organic matter during the Hirnantian stage, several studies have also demonstrated a significant positive carbon isotopic excursion (~8‰) of the organic matter in the early Katian (Lower Wufeng Formation in Sichuan Basin) or the Guttenberg stage in the late Middle Ordovician, which was caused by the decrease in surface-water CO_2 concentrations and the enrichment of microfossil *Gloeocapsomorpha Prisca* (Jacobson et al., 1988; Pancost et al., 1999; Pancost et al., 2013). Compounds exclusively from *Gloeocapsomorpha Prisca* may contribute a positive carbon isotopic shift of 3.5‰, indicating the significant contribution from source organic matter (Pancost et al., 2013). The $\delta^{13}C$ of shale decreased in the Rhuddanian stage (Lower Longmaxi Formation). Actually, the $\delta^{13}C$ value of kerogen is about −31.0‰ to −27.8‰ in the Changning–Zhaotong areas, −29.9‰ to −28.6‰ in the Jiaoshiba area (Lin et al., 2017), and −36.0‰ to −27.9‰ in the Weiyuan areas (Feng et al., 2018).

Gases sourced from the Wufeng shale are expected to be enriched in ^{13}C due to the positive carbon isotopic excursion. The continuous sedimentation and thin thickness of Wufeng–Longmaxi hot shale indicate that post-genetic processes such as migration and mixing in the shale layers are possible and contribution from the ^{13}C-enriched Wufeng shale cannot be ignored. The "sweet spot" of the Wufeng–Longmaxi shale gas is mainly concentrated in the Wufeng Formation and the lower part of the Longmaxi Formation, with a thickness of 15–50 m, and the Rhuddannian stage is the prime stage of the development of the Lower Silurian organic-enriched shale and also the key stage for the formation of "sweet spot" of shale gas (Zou et al., 2016, Zou et al., 2019). According to the graptolite occurrence, sedimentation from the Late Ordovician to the Early Silurian is continuous (Liang et al., 2018, Liang et al., 2020a; Rong et al., 2011, Rong et al., 2019). Particularly, in the Taiyang area, shale with TOC > 1% has a thickness of 50.3–57.0 m, and it is characterized by longitudinal continuous distribution without an interlayer in the middle (Liang et al., 2020b). Diffusive migration has been found in the Jiaoshiba area, where $\delta^{13}C_1$ values increased with proximity to the fault zone (Feng et al., 2020). In the Taiyang shale gas field, the linear relationship between burial depth and $\delta^{13}C$ values of methane, ethane, and propane also indicates possible influences from gas migration. However, the contribution from the carbon isotope of source organic matter cannot be the controlling factor on the enrichment of ^{13}C in methane. Though the Taiyang shale gas field is close to the Qianzhong paleo-uplift and located on the southern slope of the depression, the sea-level fall in the Hirnantian stage was significant, the positive carbon isotopic excursion should also be important, and TOC could even be up to 8%, while the thickness of the Hirnantian deposit is small, generally 2–3 m, so the contribution from the precursor organic matter should not be ignored but cannot be controlling.

5.2.4 Diffusion and Adsorption/Desorption

Shale gas from the Taiyang gas field shows a good linear correlation between $\delta^{13}C_1$ and $\delta^{13}C_2$ (R^2 = 0.9025) and between $\delta^{13}C_2$ and $\delta^{13}C_3$ (R^2 = 0.8608) (**Figure 5**). Such good

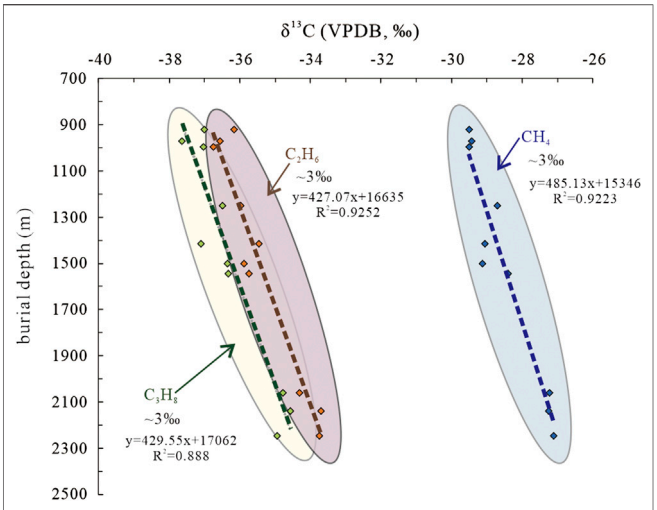

FIGURE 11 | Plot of $\delta^{13}C$ values of methane, ethane, and propane versus burial depth of gases from the Taiyang, shale gas field in the Sichuan Basin, China.

linear correlation is not necessarily caused by thermal maturity. When plotting the carbon isotope of shale gas from the Taiyang gas field versus their actual vertical burial depth, it is clear that methane, ethane, and propane become more enriched at ^{13}C, with increasing burial depth. When the burial depth changes from ~2300 to ~900 m, the carbon isotopic composition of methane, ethane, and propane all decreases by about ~3‰, and a linear correlation of such carbon isotopic changes exists for methane (R^2 = 0.9223), ethane (R^2 = 0.9252), and propane (R^2 = 0.888) (**Figure 11**). Due to the geothermal gradient, increasing burial depth usually represents the increase of geo-temperature and thus thermal maturity; hence, $\delta^{13}C$ values of hydrocarbon gases usually increase with increasing burial depth. However, the Wufeng–Longmaxi shale in the Taiyang area underwent deep burial from Triassic to Jurassic, resulting in the high thermal maturity, and began to uplift in the Cretaceous, so deep burial does not necessarily mean high geo-temperature and shale with different burial depths may have very similar thermal maturity. For example, the Longmaxi shale in Well Y109 has a burial depth of 2162–2202 m and equivalent Ro% of 3.1%, while the Longmaxi shale in Well Y102 has a much shallower burial depth (732–741 m) but still has similar equivalent Ro% (3.0%) (Liang et al., 2021). Therefore, there must be other post-genetic processes that cause the linear correlation between the burial depth and $\delta^{13}C$ values of hydrocarbon gases. Though the Wufeng–Longmaxi shale in the Taiyang area is typically characterized by shallow burial depth (can be less than 1,000 m), diffusive gas leakage might occur in these shallow layers. In the Taiyang area, the decreasing carbon isotopic compositions of hydrocarbon gas with decreasing burial depth cannot be caused by diffusive gas leakage. In general, diffusive gas leakage is more likely to occur in shallow layers. During the leakage, since ^{12}C-^{12}C bonds are weaker than ^{12}C-^{13}C bonds and leak faster, the leaking gas will be more enriched in methane and depleted in ^{13}C, and the residual gas which is still trapped in the reservoir will be more depleted in methane but enriched in ^{13}C. If gas leakage occurs in the shallow layers, gases in the shallow layers will be more enriched at ^{13}C compared to those of the deep layers. Apparently, this is opposite to the case in the Taiyang shale gas field.

Carbon isotopic fractionation of methane due to mass transport has been evaluated in many studies, especially in low-permeability shale. During gas transport, ^{12}C-^{12}C bonds are weaker than ^{12}C-^{13}C bonds and transport faster; thus, it caused a significant isotopically lighter carbon than the source (Pernaton et al., 1996; Zhang and Krooss, 2001). Previous studies documented a large isotopic fractionation during gas migration under a nonsteady state (Prinzhofer and Pernaton, 1997; Zhang and Krooss, 2001). Zhang and Krooss (2001) proposed that the magnitude of depletion in ^{13}C is the highest during the initial nonsteady state of the diffusion process and decreases to a constant difference when it approached the steady state. Canister desorption experimental study about the Longmaxi shale samples at reservoir temperatures showed a rapid enrichment of ^{13}C up to 13.7‰–16.2‰ in methane as desorption proceeds (Ma et al., 2020). Li et al. (2020) proposed to divide the gas transport process during a complete production into four stages and demonstrated that methane became depleted in ^{13}C during the transition stage (stage II) and became enriched in ^{13}C during the adsorbed gas desorption stage (stage III), while became depleted in ^{13}C again during the diffusion stage (stage IV). Carbon isotopic enrichment of methane due to adsorption/desorption during stage IV might contribute to the heavy carbon isotope of methane in Taiyang and Jiaoshiba shale gas fields. However, according to the analytical results and numerical calculations, it is suggested that under geological conditions, post-genetic coupled diffusion and adsorption/desorption due to gas transport normally cause isotopic fractionation of less than 5‰ (Xia and Tang, 2012). In the Taiyang shale gas field, once diffusive migration occurs, the separates will be more enriched in methane and depleted in ^{13}C, resulting in the relatively low $\delta^{13}C$ values in the shallow layer, while the residual will be more depleted in methane and enriched in ^{13}C, resulting in the relatively high $\delta^{13}C$ values in the deep layer. The $C_1/(C_2+C_3)$~$\delta^{13}C_1$ plot also shows that the Taiyang shale gas has a rapid change in molecular composition with burial depth, indicating potential effects from diffusive migration (**Figure 11**).

The geological conditions of the Taiyang gas field also support possible diffusive gas migration in this area. The main part of the Taiyang shale gas field is the Taiyang anticline, with a gas-bearing area of 580 km^2. It has suffered alteration from the superimposed multistage tectonic activities since the Caledonian period. The Taiyang anticline is characterized by "strong superimposed fold deformation and weak multistage fault reconstruction," and develops nearly east–west reverse faults and nearly south–north strike–slip faults. The nearly east–west faults are developed on the top and two wings of the anticline due to the north–south compression stress in the early stage. With continuous compression stress from north–south, the complex anticline gradually deforms and forms nearly north–south strike–slip faults. The uplift and denudation stage of extrusion

strike–slip in the Late Yanshanian-Himalayan period resulted in the shallow burial depth of Wufeng–Longmaxi formations, that is, 500–1,500 m in the main part of the anticlinal structure (Liang et al., 2021). The formation pressure coefficient is 1.22–1.47, natural micro-cracks are developed in the shale, and the porosity is 4%–9%, with an average of 5.67% (Liang et al., 2020a). Therefore, diffusive migration of shale gases is likely to occur during or after the uplift and denudation stages.

5.3 Depletion of ^{13}C in Ethane and Propane

At low mature and mature stages, $\delta^{13}C$ values of CH_4 are much lower than those of C_2H_6 and $\delta^{13}C$ values of C_2H_6 are much lower than those of C_3H_8, that is, $\delta^{13}C_1 > \delta^{13}C_2 > \delta^{13}C_3$. When the source rocks reach the oil window with Ro% of 1.5%, the carbon isotopic difference between methane and ethane and between ethane and propane will approach a similar value of −6‰ (Cesar et al., 2020). At this stage, isotopic effects of thermodynamic/equilibrium are predominant controlling factors, and isotopic exchange reactions occur under these conditions (Cesar et al., 2020). When the thermal maturity further increases, isotopic effects of thermodynamic/equilibrium are no longer the predominant controlling factors, and other processes may become more important; thus, carbon isotopic reversal first occurs in ethane and then in propane (Dai et al., 2016a; Cesar et al., 2020). In general, according to the published data, it is clear that with increasing thermal maturity, ethane and propane first become more enriched in ^{13}C, then become more depleted in ^{13}C, and finally become more enriched in ^{13}C again (Ferworn et al., 2008; Burruss and Laughrey, 2010; Rodriguez and Philp, 2010; Zumberge et al., 2012; Hao and Zou, 2013; Tilley and Muehlenbachs, 2013; Dai et al., 2014a; Dai et al., 2016b; Dai et al., 2017; Liu et al., 2018; Ni et al., 2018; Xia and Gao, 2018; Feng et al., 2020) (**Figures 7B, C**). The Wufeng–Longmaxi shale gases from the Taiyang, Jiaoshiba, and Weirong shale gas fields fall in the post-rollover area, where ethane and propane are still depleted at ^{13}C, but the carbon isotopic compositions get to be more positive again (**Figures 7B, C**).

Among the mechanisms which have been invoked to account for the carbon isotopic depletion in ethane and propane, most of them are related to high temperatures, for example, 1) *in situ* cracking of C_{2+} gas (Ferworn et al., 2008), *in situ* cracking of oil or gas (Rodriguez and Philp, 2010), simultaneous cracking of kerogen, oil, and gas in a closed system (Tilley et al., 2011), and cracking of kerogen-entrapped straight-chain aliphatic hydrocarbons (Ni et al., 2018); 2) water reacting with CH_4 to form isotopically light CO_2 and hydrogen and CO_2 and hydrogen, subsequently forming isotopically light ethane and propane (Zumberge et al., 2012); 3) Rayleigh fractionation of ethane and propane involving redox reactions with transition metals and water at temperatures on the order of 250°C–300°C (Burruss and Laughrey, 2010); 4) Diffusive migration during the stage with high maturity (Dai et al., 2016a). As discussed above, Fischer–Tropsch-type synthesis of hydrocarbon from CO_2 and H_2 has contributed to the carbon isotopic depletion in ethane and propane, but due to the limited amount of the reactant, it cannot be the controlling factor. In the southern Sichuan Basin, wet gas cracking cannot explain the depletion of ^{13}C in ethane and propane. C_{2+} wet gas cracking at elevated temperatures will increase C_2/C_3 ratio and thus a decrease in gas wetness (Prinzhofer and Huc, 1995). The Wufeng–Longmaxi shale gas is characterized by very low gas wetness, and the content of ethane and propane is generally less than 1. Wet gas cracking of pentanes and butanes will cause enrichment in ^{12}C in ethane and propane (Xia et al., 2013); however, under the over-mature dry gas stage, cracking of ethane and propane possibly occurs and the residual ethane and propane will become more enriched in ^{13}C due to the kinetic isotopic fractionation effects (Tang et al., 2000). Obviously, this is opposite to the phenomenon of the Wufeng–Longmaxi shale gas.

Actually, Xia and Gao (2018) stated that mechanisms such as mixing of primary and secondary products in source rocks (Rodriguez and Philp, 2010; Ni et al., 2018; Hao and Zou, 2013; Ferworn et al., 2008; Xia et al., 2013) and water-involved reactions (Burruss and Laughrey, 2010; Gao et al., 2014; Zhang et al., 2018b; Zumberge et al., 2012) cannot satisfy the isotopic and mass balance requirements and proposed that the depletion of ^{13}C in ethane and propane resulted from the reversible conversion from alkane to alkyl groups. The isotope effect is dependent on the rate and kinetic isotope effects of these reversible free-radical reactions catalyzed by minerals, and the isotopic depletion in ^{13}C is consistent with the extent of the decomposition (Xia and Gao, 2018). However, these free-radical reactions may proceed in very different ways in different locations since the free-radical concentrations may vary greatly in different geological environments. In the sandstone and limestone formations, there is no sufficient hydrogen donors, and the reversal reactions will be suppressed and the fractionation will proceed likely in a Rayleigh fractionation mode; while organic-rich shales have abundant hydrogen donor, so the reversible reaction is possible, and the isotopic reversal is commonly found in either conventional and unconventional natural gases at relatively high thermal mature stages (Xia and Gao, 2018). The Upper Ordovician Wufeng–Lower Silurian Longmaxi shale comprises black shale, siliceous shale, calcareous-siliceous shale, and argillaceous-siliceous shale (Zou et al., 2019). It is deposited in a deep water environment and dominated by Type I and II_1 organic matter and typically has TOC of around 3% in the Taiyang, Jiaoshiba, and Weirong areas (Dai et al., 2014a; Liang et al., 2020a; Liang et al., 2020b; Zou et al., 2021). During the Hirnantian Stage glacial interval (Middle and Upper Wufeng Formation), there was a rapid global fall in sea level, while the P_2O_5/TiO_2 ratio reached 0.84 and the southern Sichuan Basin still experienced plankton bloom, high paleo-productivity, and high burial rates of organic matter (Zou et al., 2019). During the Rhuddanian Stage (Lower Longmaxi Formation), sea level increased and plankton bloomed, resulting in the widespread deposition of back shale in deep, oxygen-poor conditions under high-productivity surface waters (Zou et al., 2019). In southern China, Silurian marine source rocks with restored hydrogen index greater than 600 mg/g TOC account for 43%, and samples with restored hydrogen index between 250–600 mg/g TOC account for 57% (Zhang et al., 2013). In addition, the Wufeng–Longmaxi shale reached over 180°C in Late Permian in the Taiyang area and reached over 200°C in Late Jurassic in the Jiaoshiba area (He et al., 2017; Liang et al., 2020b; Pang et al., 2019; Tenger et al., 2017; Xiong et al., 2021). In general, the Wufeng–Longmaxi shale has equivalent vitrinite reflectance Ro% of 2.73%–4.62% (Wang et al., 2019; Zou et al., 2021) and gas wetness between 0.09% and 0.97%. Therefore, the Wufeng–Longmaxi shale is abundant in hydrogen donors and at a high thermal maturation stage with a high conversion rate. When

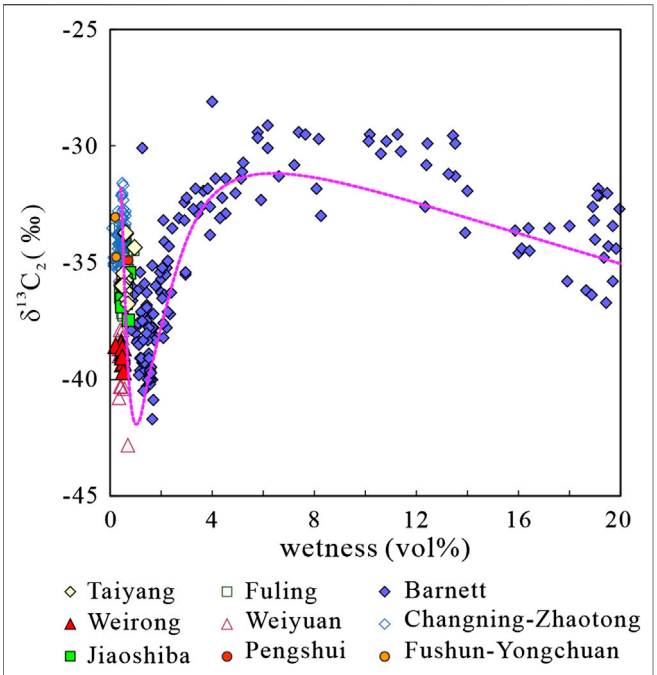

FIGURE 12 | Plot of wetness versus $\delta^{13}C_2$ of shale gases from Taiyang, Jiaoshiba, and Weirong gas fields. Also shown are shale gases from the published data (see text). The pink line was the calculated results by Xia and Gao (2018).

plotting the Wufeng–Longmaxi shale gases into the $\delta^{13}C_2$ value versus gas wetness plot of the Barnett shale gases by Xia and Gao (2018), the carbon isotopic fractionation of ethane of the Wufeng–Longmaxi shale gases agrees well with the calculated results (pink line in **Figure 12**), which mainly fall in the post-rollover stage and indicates high thermal maturity of the gas. As indicated by the reversible free-radical reactions, the isotopic compositions are positive at the stage of low conversion ratios and then become negative with increasing conversion ratios; When the conversion ratios get even higher and the remaining reactant becomes even less, the isotopic compositions become more positive again (Xia and Gao, 2018). As for the Wufeng–Longmaxi shale gas, the extremely low content of ethane and propane ($C_{2+3} < 1\%$) indicates high conversion ratios, so during the late catagenesis stage, decomposition of ethane and propane is accompanied by the depletion of ^{13}C in the residual ethane and propane, but in general, the isotopic composition becomes more positive again and falls in the post-rollover area. During this over-mature stage, reactions of free-radical decomposition are important controlling factors, resulting in the depletion of ^{13}C in ethane and propane, which prevail the thermal cracking reactions.

6 CONCLUSION

Molecular and stable carbon isotopic compositions of gases from the Wufeng–Longmaxi shale in the Taiyang (shallow), Jiaoshiba (middle), and Weirong (deep) shale gas fields in the Sichuan Basin have been investigated. All the gases are dominated by methane and have very low gas wetness (generally <0.83). Methane accounts for 98.82%, 98.13%, and 96.91% in the Taiyang, Jiaoshiba, and Weirong shale gas fields, respectively. The average carbon isotopic value of methane is −35.2‰ in Weirong, −30.3‰ in Jiaoshiba, and −28.5‰ in Taiyang shale gas fields. The enrichment of ^{13}C in methane is mainly caused by the extremely high thermal maturity. Shale gases from the Jiaoshiba and Taiyang gas fields fall offset from the $\delta^{13}C_1$~wetness linear trend line by the Weirong, Barnett, and Fayetteville shale gases, which is due to the contribution from the Fischer–Tropsch-type synthesis of hydrocarbon gas from CO_2 and H_2. When thermal cracking gas is mixed with the hydrocarbon gas generated by the Fischer–Tropsch-type synthesis, it will significantly increase the amount of wet gas, but has little impact on methane. In the Taiyang shale gas field, when burial depth changes from ~2300 to ~900 m, $\delta^{13}C_1$, $\delta^{13}C_2$, and $\delta^{13}C_3$ values decrease by ~3‰, and a linear correlation exists between carbon isotope and burial depth. This is mainly caused by diffusive migration. Shale gases from the Taiyang, Jiaoshiba, and Weirong gas fields are characterized by a complete carbon isotopic reversal trend among the C_1-C_3 alkane gases ($\delta^{13}C_1 > \delta^{13}C_2 > \delta^{13}C_3$). This is mainly caused by the reversible free-radical reactions with the conversion from alkane to alkyl groups with a minor contribution from the Fischer–Tropsch-type synthesis.

DATA AVAILABILITY STATEMENT

The original contributions presented in the study are included in the article/Supplementary Material; further inquiries can be directed to the corresponding authors.

AUTHOR CONTRIBUTIONS

YN: manuscript design and writing. DD: manuscript writing of geological information. LY and JC: data collection and manuscript revision. XL and FL: sample collection. JL: sample collection. JHG: sample analyses. JLG: data collection.

FUNDING

This study is funded by the National Key Research and Development Projects of China (Grant No. 2019YFC1805505) and the PetroChina Scientific Research and Technology Development Project (Grant Nos. 2021DJ05, 2017D-5008-08).

ACKNOWLEDGMENTS

We thank Prof. Jinxing Dai and Dr. Yuman Wang from the PetroChina Research Institute of Petroleum Exploration and Development for helpful and open discussion. We thank the reviewers for their thorough reviews and constructive suggestions, which improve the manuscript greatly.

REFERENCES

Bergström, S. M., Saltzman, M. M., and Schmitz, B. (2006). First Record of the Hirnantian (Upper Ordovician) $\delta^{13}C$ Excursion in the North American Midcontinent and its Regional Implications. *Geol. Mag.* 143, 657–678.

Bernard, B. B., Brooks, J. M., and Sackett, W. M. (1976). Natural Gas Seepage in the Gulf of Mexico. *Earth Planet. Sci. Lett.* 31, 48–54. doi:10.1016/0012-821x(76)90095-9

Berner, U., and Faber, E. (1996). Empirical Carbon Isotope/maturity Relationships for Gases from Algal Kerogens and Terrigenous Organic Matter, Based on Dry, Open-System Pyrolysis. *Org. Geochem.* 24, 947–955. doi:10.1016/s0146-6380(96)00090-3

Brenchley, P. J., Marshall, J. D., Carden, G. A. F., Robertson, D. B. R., Long, D. G. F., Meidla, T., et al. (1994). Bathymetric and Isotopic Evidence for a Short-Lived Late Ordovician Glaciation in a Greenhouse Period. *Geology* 22, 295–298. doi:10.1130/0091-7613(1994)022<0295:baiefa>2.3.co;2

Burruss, R. C., and Laughrey, C. D. (2010). Carbon and Hydrogen Isotopic Reversals in Deep Basin Gas: Evidence for Limits to the Stability of Hydrocarbons. *Org. Geochem.* 41, 1285–1296. doi:10.1016/j.orggeochem.2010.09.008

Cao, C., Zhang, M., Li, L., Wang, Y., Li, Z., Du, L., et al. (2020). Tracing the Sources and Evolution Processes of Shale Gas by Coupling Stable (C, H) and Noble Gas Isotopic Compositions: Cases from Weiyuan and Changning in Sichuan Basin, China. *J. Nat. Gas Sci. Eng.* 78, 103304. doi:10.1016/j.jngse.2020.103304

Cesar, J., Nightingale, M., Becker, V., and Mayer, B. (2020). Stable Carbon Isotope Systematics of Methane, Ethane and Propane from Low-Permeability Hydrocarbon Reservoirs. *Chem. Geol.* 558, 119907. doi:10.1016/j.chemgeo.2020.119907

Chen, C. (2018). *Research on Paleoceanography, Paleoclimate and Formation Mechanism of Source Rock during Geologic Transition Period from Late Ordovician to Early Silurian in Southern Sichuan Province - Northern Guizhou Province, South China*. Wuhan: China University of Geosciences (Wuhan. Ph.D thesis.

Chen, J., Li, W., Ni, Y., Dai, X., Liang, D., Deng, C., et al. (2018). The Permian Source Rocks in the Sichuan Basin and its Natural Gas Exploration Potential (Part 2): Geochemical Characteristics of Source Rocks and Latent Capacity of Natural Gas Resources. *Nat. Gas. Ind.* 38, 33–45.

Chen, J., Li, C., Shen, P., and Ying, G. (1995). Carbon and Hydrogen Isotopic Characteristics of Hydrocarbons in Coal Type Gas from China. *Sedimentol. Sin.* 13, 59–69.

Chen, Z., Chen, L., Wang, G., Zou, C., Jiang, S., Si, Z., et al. (2020). Applying Isotopic Geochemical Proxy for Gas Content Prediction of Longmaxi Shale in the Sichuan Basin, China. *Mar. Petroleum Geol.* 116, 104329. doi:10.1016/j.marpetgeo.2020.104329

Chung, H. M., Gormly, J. R., and Squires, R. M. (1988). Origin of Gaseous Hydrocarbons in Subsurface Environments: Theoretical Considerations of Carbon Isotope Distribution. *Chem. Geol.* 71, 97–104. doi:10.1016/0009-2541(88)90108-8

Clayton, C. (1991). Carbon Isotope Fractionation during Natural Gas Generation from Kerogen. *Mar. Petroleum Geol.* 8, 232–240. doi:10.1016/0264-8172(91)90010-x

Curiale, J. A., and Curtis, J. B. (2016). Organic Geochemical Applications to the Exploration for Source-Rock Reservoirs - A Review. *J. Unconv. Oil Gas Resour.* 13, 1–31. doi:10.1016/j.juogr.2015.10.001

Dai, J., Gong, D., Ni, Y., Huang, S., and Wu, W. (2014b). Stable Carbon Isotopes of Coal-Derived Gases Sourced from the Mesozoic Coal Measures in China. *Org. Geochem.* 74, 123–142. doi:10.1016/j.orggeochem.2014.04.002

Dai, J. (1992). Identification and Distinction of Various Alkane Gases. *Sci. China (Chem.)* 35, 1246–1257.

Dai, J., Liao, F., and Ni, Y. (2013). Discussions on the gas source of the Triassic Xujiahe Formation tight sandstone gas reservoirs in Yuanba and Tongnanba, Sichuan Basin: An answer to Yinfeng et al. *Pet. explor. Dev.* 40, 250–256. doi:10.1016/s1876-3804(13)60033-6

Dai, J., Ni, Y., Gong, D., Feng, Z., Liu, D., Peng, W., et al. (2017). Geochemical Characteristics of Gases from the Largest Tight Sand Gas Field (Sulige) and Shale Gas Field (Fuling) in China. *Mar. Petroleum Geol.* 79, 426–438. doi:10.1016/j.marpetgeo.2016.10.021

Dai, J., Ni, Y., Huang, S., Gong, D., Liu, D., Feng, Z., et al. (2016a). Secondary Origin of Negative Carbon Isotopic Series in Natural Gas. *J. Nat. Gas Geoscience* 1, 1–7. doi:10.1016/j.jnggs.2016.02.002

Dai, J., Ni, Y., Liu, Q., Wu, X., Yu, C., Gong, D., et al. (2022). Carbon Dioxide and its Carbon Isotopic Composition of Natural Gas in the Sichuan Basin, SW China. *Front. Earth Sci.* 10, 857876. doi:10.3389/feart.2022.857876

Dai, J., Ni, Y., and Zou, C. (2012a). Stable Carbon and Hydrogen Isotopes of Natural Gases Sourced from the Xujiahe Formation in the Sichuan Basin, China. *Org. Geochem.* 43, 103–111. doi:10.1016/j.orggeochem.2011.10.006

Dai, J., Ni, Y., Zou, C., Tao, S., Hu, G., Hu, A., et al. (2009). Stable Carbon Isotopes of Alkane Gases from the Xujiahe Coal Measures and Implication for Gas-Source Correlation in the Sichuan Basin, SW China. *Org. Geochem.* 40, 638–646. doi:10.1016/j.orggeochem.2009.01.012

Dai, J., Pei, X., and Qi, H. (1992). *Natural Gas Geology in China (Volume I)*. Beijing: Petroleum Industry Press.

Dai, J. (2003). Pool-forming Periods and Gas Sources of Weiyuan Gasfield. *Pet. Geol. exper.* 25 (5), 473–780.

Dai, J., and Qi, H. (1989). Relationship of $\delta^{13}C$-Ro of Coal-Derived Gas in China. *Chin. Sci. Bull.* 34, 690–692.

Dai, J. X., Ni, Y., Liu, Q., Wu, X., Gong, D., Hong, F., et al. (2021). Sichuan Super Gas Basin. *Pet. explor. Dev.* 48, 1–8. doi:10.1016/s1876-3804(21)60284-7

Dai, J., Xia, X., Li, Z., Coleman, D. D., Dias, R. F., Gao, L., et al. (2012b). Inter-laboratory Calibration of Natural Gas Round Robins for δ2H and δ13C Using Off-Line and On-Line Techniques. *Chem. Geol.* 310-311, 49–55. doi:10.1016/j.chemgeo.2012.03.008

Dai, J., Zou, C., Dong, D., Ni, Y., Wu, W., Gong, D., et al. (2016b). Geochemical Characteristics of Marine and Terrestrial Shale Gas in China. *Mar. Petroleum Geol.* 76, 444–463. doi:10.1016/j.marpetgeo.2016.04.027

Dai, J., Zou, C., Liao, S., Dong, D., Ni, Y., Huang, J., et al. (2014a). Geochemistry of the Extremely High Thermal Maturity Longmaxi Shale Gas, Southern Sichuan Basin. *Org. Geochem.* 74, 3–12. doi:10.1016/j.orggeochem.2014.01.018

Fan, J., Peng, P. a., and Melchin, M. J. (2009). Carbon Isotopes and Event Stratigraphy Near the Ordovician-Silurian Boundary, Yichang, South China. *Palaeogeogr. Palaeoclimatol. Palaeoecol.* 276, 160–169. doi:10.1016/j.palaeo.2009.03.007

Feng, Z., Dong, D., Tian, J., Qiu, Z., Wu, W., and Zhang, C. (2018). Geochemical Characteristics of Longmaxi Formation Shale Gas in the Weiyuan Area, Sichuan Basin, China. *J. Petroleum Sci. Eng.* 167, 538–548. doi:10.1016/j.petrol.2018.04.030

Feng, Z., Dong, D., Tian, J., Wu, W., Cai, Y., Shi, Z., et al. (2019). Geochemical Characteristics of Lower Silurian Shale Gas in the Changning-Zhaotong Exploration Blocks, Southern Periphery of the Sichuan Basin. *J. Petroleum Sci. Eng.* 174, 281–290. doi:10.1016/j.petrol.2018.11.022

Feng, Z., Hao, F., Dong, D., Zhou, S., Wu, W., Xie, C., et al. (2020). Geochemical Anomalies in the Lower Silurian Shale Gas from the Sichuan Basin, China: Insights from a Rayleigh-type Fractionation Model. *Org. Geochem.* 142, 103981. doi:10.1016/j.orggeochem.2020.103981

Feng, Z., Liu, D., Huang, S., Wu, W., Dong, D., Peng, W., et al. (2016). Carbon Isotopic Composition of Shale Gas in the Silurian Longmaxi Formation of the Changning Area, Sichuan Basin. *Petroleum Explor. Dev.* 43, 769–777. doi:10.1016/s1876-3804(16)30092-1

Ferworn, K., Zumberge, J., Reed, J., and Brown, S. (2008). *Gas Character Anomalies Found in Highly Productive Shale Gas Wells*. Houston, TX. http://www.zenzebra.net/quebec/Ferworn_et_al_2008.pdf.

Gao, J., Liu, J., and Ni, Y. (2018). Gas Generation and its Isotope Composition during Coal Pyrolysis: The Catalytic Effect of Nickel and Magnetite. *Fuel* 222, 74–82. doi:10.1016/j.fuel.2018.02.118

Gao, L., Schimmelmann, A., Tang, Y., and Mastalerz, M. (2014). Isotope Rollover in Shale Gas Observed in Laboratory Pyrolysis Experiments: Insight to the Role of Water in Thermogenesis of Mature Gas. *Org. Geochem.* 68, 95–106. doi:10.1016/j.orggeochem.2014.01.010

Hao, F., and Zou, H. (2013). Cause of Shale Gas Geochemical Anomalies and Mechanisms for Gas Enrichment and Depletion in High-Maturity Shales. *Mar. Petroleum Geol.* 44, 1–12. doi:10.1016/j.marpetgeo.2013.03.005

He, Z. L., Hu, Z. Q., Nie, H. K., Li, S. J., and Xu, J. (2017). Characterization of Shale Gas Enrichment in the Wufeng-Longmaxi Formation in the Sichuan Basin and its Evaluation of Geological Construction-Transformation Evolution Sequence. *Nat. Gas. Geosci.* 28, 724–733.

Huang, S. P., Jiang, Q. C., Wang, Z. C., Su, W., Feng, Q. F., and Feng, Z. Q. (2016). Differences between the Middle Permian Qixia and Maokou Source Rocks in the Sichuan Basin. *Nat. Gas. Ind.* 36, 26–34.

Jacobson, S. R., Hatch, J. R., Teerman, S. C., and Askin, R. A. (1988). Middle Ordovician Organic Matter Assemblages and Their Effect on Ordovician-Derived Oils. *AAPG Bull.* 72, 1090–1100. doi:10.1306/703c97c6-1707-11d7-8645000102c1865d

James, A. T. (1983). Correlation of Natural Gas by Use of Carbon Isotopic Distribution between Hydrocarbon Components. *Am. Assoc. Pet. Geol. Bull.* 67, 1176–1191. doi:10.1306/03b5b722-16d1-11d7-8645000102c1865d

Kump, L. R., Arthur, M. A., Patzkowsky, M. E., Gibbs, M. T., Pinkus, D. S., and Sheehan, P. M. (1999). A Weathering Hypothesis for Glaciation at High Atmospheric pCO2 during the Late Ordovician. *Palaeogeogr. Palaeoclimatol. Palaeoecol.* 152, 173–187. doi:10.1016/s0031-0182(99)00046-2

Li, W., Lu, S., Li, J., Zhang, P., Wang, S., Feng, W., et al. (2020). Carbon Isotope Fractionation during Shale Gas Transport: Mechanism, Characterization and Significance. *Sci. China Earth Sci.* 63, 674–689. doi:10.1007/s11430-019-9553-5

Liang, D., Zhang, S., Zhao, M., and Wang, F. (2002). Hydrocarbon Sources and Stages of Reservoir Formation in Kuqa depression,Tarim Basin. *Chin. Sci. Bull.* 47, 56–63. doi:10.1007/bf02902820

Liang, M., Tan, X., Chen, X., Wang, J., Ran, T., Wang, P., et al. (2018). Sequence Stratigraphy of Wufeng-Longmaxi Formation in the Southeastern Chongqing Area and its Geological Significance. *Coal Geol. Explor.* 46, 40–51.

Liang, X., Xu, Z., Zhang, Z., Wang, W., Zhang, J., Lu, H., et al. (2020b). Breakthrough of Shallow Shale Gas Exploration in Taiyang Anticline Area and its Significance for Resource Development in Zhaotong, Yunnan Province, China. *Pet. explor. Dev.* 47, 11–28. doi:10.1016/s1876-3804(20)60002-7

Liang, X., Xu, Z., Zhang, J., Zhang, Z., Li, Z., Jiang, P., et al. (2020a). Key Efficient Exploration and Development Technologies of Shallow Shale Gas: a Case Study of Taiyang Anticline Area of Zhaotong National Shale Gas Demonstration Zone. *Acta Pet. Sin.* 41, 1033–1048.

Liang, X., Shan, C., Zhang, Z., Xu, J., Wang, W., Zhang, J., et al. (2021). Three-dimensional Closed System" Accumulation Model of Taiyang Anticline Mountain Shallow Shale Gas in Zhaotong Demonstration Area. *Acta Geol. Sin.* 95, 1–20.

Lin, J., Hu, H., and Liang, Q. (2017). Geochemical Characteristics and Implications of Shale Gas in Jiaoshiba, Eastern China. *Earth Sci.* 42, 1124–1133.

Liu, Q., Jin, Z., Wang, X., Yi, J., Meng, Q., Wu, X., et al. (2018). Distinguishing Kerogen and Oil Cracked Shale Gas Using H, C-Isotopic Fractionation of Alkane Gases. *Mar. Petroleum Geol.* 91, 350–362. doi:10.1016/j.marpetgeo.2018.01.006

Lorant, F., Prinzhofer, A., Behar, F., and Huc, A.-Y. (1998). Carbon Isotopic and Molecular Constraints on the Formation and the Expulsion of Thermogenic Hydrocarbon Gases. *Chem. Geol.* 147, 249–264. doi:10.1016/s0009-2541(98)00017-5

Ma, Y., Zhong, N., Yao, L., Huang, H., Larter, S., and Jiao, W. (2020). Shale Gas Desorption Behavior and Carbon Isotopic Variations of Gases from Canister Desorption of Two Sets of Gas Shales in South China. *Mar. Petroleum Geol.* 113, 104127. doi:10.1016/j.marpetgeo.2019.104127

Marshall, J. D., Brenchley, P. J., Mason, P., Wolff, G. A., Astini, R. A., Hints, L., et al. (1997). Global Carbon Isotopic Events Associated with Mass Extinction and Glaciation in the Late Ordovician. *Palaeogeogr. Palaeoclimatol. Palaeoecol.* 132, 195–210. doi:10.1016/s0031-0182(97)00063-1

Martini, A. M., Walter, L. M., and McIntosh, J. C. (2008). Identification of Microbial and Thermogenic Gas Components from Upper Devonian Black Shale Cores, Illinois and Michigan Basins. *Bulletin* 92, 327–339. doi:10.1306/10180706037

Mi, J., He, K., Shuai, Y., and Guo, J. (2022). *Combination of Methyl from Methane Early Cracking: A Possible Mechanism for Carbon Isotopic Reversal of Overmature Natural Gas*. Geofluids, 9965046.

Milkov, A. V. (2021). New Approaches to Distinguish Shale-Sourced and Coal-Sourced Gases in Petroleum Systems. *Org. Geochem.* 158, 104271. doi:10.1016/j.orggeochem.2021.104271

Ni, Y., Gao, J., Chen, J., Liao, F., Liu, J., and Zhang, D. (2018). Gas Generation and its Isotope Composition during Coal Pyrolysis: Potential Mechanism of Isotope Rollover. *Fuel* 231, 387–395. doi:10.1016/j.fuel.2018.05.029

Ni, Y., Liao, F., Dai, J., Zou, C., Wu, X., Zhang, D., et al. (2014). Studies on Gas Origin and Gas Source Correlation Using Stable Carbon Isotopes - A Case Study of the Giant Gas Fields in the Sichuan Basin, China. *Energy Explor. Exploitation* 32, 41–74. doi:10.1260/0144-5987.32.1.41

Ni, Y., Liao, F., Gao, J., Chen, J., Yao, L., and Zhang, D. (2019a). Hydrogen Isotopes of Hydrocarbon Gases from Different Organic Facies of the Zhongba Gas Field, Sichuan Basin, China. *J. Petroleum Sci. Eng.* 179, 776–786. doi:10.1016/j.petrol.2019.04.102

Ni, Y., Liao, F., Yao, L., Gao, J., and Zhang, D. (2019b). Hydrogen Isotope of Natural Gas from the Xujiahe Formation and its Implications for Water Salinization in Central Sichuan Basin, China. *J. Nat. Gas Geoscience* 4, 215–230. doi:10.1016/j.jnggs.2019.08.003

Ni, Y., Ma, Q., Ellis, G. S., Dai, J., Katz, B., Zhang, S., et al. (2011). Fundamental Studies on Kinetic Isotope Effect (KIE) of Hydrogen Isotope Fractionation in Natural Gas Systems. *Geochimica Cosmochimica Acta* 75, 2696–2707. doi:10.1016/j.gca.2011.02.016

Ni, Y., Zhang, D., Liao, F., Gong, D., Xue, P., Yu, F., et al. (2015). Stable Hydrogen and Carbon Isotopic Ratios of Coal-Derived Gases from the Turpan-Hami Basin, NW China. *Int. J. Coal Geol.* 152, 144–155. doi:10.1016/j.coal.2015.07.003

Orth, C. J., Gilmore, J. S., Quintana, L. R., and Sheehan, P. M. (1986). Terminal Ordovician Extinction: Geochemical Analysis of the Ordovician/Silurian Boundary, Anticosti Island, Quebec. *Geol* 14, 433–436. doi:10.1130/0091-7613(1986)14<433:toegao>2.0.co;2

Pancost, R. D., Freeman, K. H., Herrmann, A. D., Patzkowsky, M. E., Ainsaar, L., and Martma, T. (2013). Reconstructing Late Ordovician Carbon Cycle Variations. *Geochimica Cosmochimica Acta* 105, 433–454. doi:10.1016/j.gca.2012.11.033

Pancost, R. D., Freeman, K. H., and Patzkowsky, M. E. (1999). Organic-matter Source Variation and the Expression of a Late Middle Ordovician Carbon Isotope Excursion. *Geol* 27, 1015–1018. doi:10.1130/0091-7613(1999)027<1015:omsvat>2.3.co;2

Pang, H. Q., Xiong, L., Wei, L., Shi, H., Dong, X., Zhang, T., et al. (2019). Analysis of Main Geological Factors for Enrichment and High Yield of Deep Shale Gas in Southern Sichuan: A Case Study of Weirong Shale Gas Field. *Nat. Gas. Ind.* 39, 78–84.

Pernaton, E., Prinzhofer, A., and Schneider, F. (1996). Reconsideration of Methane Isotope Signature as a Criterion for the Genesis of Natural Gas: Influence of Migration on Isotopic Signatures. *Rev. Inst. Fr. Pét.* 51, 635–651. doi:10.2516/ogst:1996042

Prinzhofer, A. A., and Huc, A. Y. (1995). Genetic and Post-genetic Molecular and Isotopic Fractionations in Natural Gases. *Chem. Geol.* 126, 281–290. doi:10.1016/0009-2541(95)00123-9

Prinzhofer, A., and Pernaton, É. (1997). Isotopically Light Methane in Natural Gas: Bacterial Imprint or Diffusive Fractionation? *Chem. Geol.* 142, 193–200. doi:10.1016/s0009-2541(97)00082-x

Qing, H., and Veizer, J. (1994). Oxygen and Carbon Isotopic Composition of Ordovician Brachiopods: Implications for Coeval Seawater. *Geochimica Cosmochimica Acta* 58, 4429–4442. doi:10.1016/0016-7037(94)90345-x

Rodriguez, N. D., and Philp, R. P. (2010). Geochemical Characterization of Gases from the Mississippian Barnett Shale, Fort Worth Basin, Texas. *Bulletin* 94, 1641–1656. doi:10.1306/04061009119

Rong, J., Chen, X., Wang, Y., Zhan, R., Liu, J., Huang, B., et al. (2011). Northward Expansion of Central Guizhou Oldland through the Ordovician and Silurian Transition: Evidence and Implication. *Sci. China* 41, 1407–1415.

Rong, J., Wang, Y., Zhan, R., Fan, J., Huang, B., Tang, P., et al. (2019). Silurian Integrative Stratigraphy and Timescale of China. *Sci. China Earth Sci.* 49, 93–114. doi:10.1007/s11430-017-9258-0

Schoell, M. (1980). The Hydrogen and Carbon Isotopic Composition of Methane from Natural Gases of Various Origins. *Geochimica Cosmochimica Acta* 44, 649–661. doi:10.1016/0016-7037(80)90155-6

Stahl, W. J., and Carey, B. D. (1975). Source-rock Identification by Isotope Analyses of Natural Gases from Fields in the Val Verde and Delaware Basins, West Texas. *Chem. Geol.* 16, 257–267. doi:10.1016/0009-2541(75)90065-0

Strąpoć, D., Mastalerz, M., Schimmelmann, A., Drobniak, A., and Hasenmueller, N. R. (2010). Geochemical Constraints on the Origin and Volume of Gas in the New Albany Shale (Devonian–Mississippian), Eastern Illinois Basin. *AAPG Bull.* 94, 1713–1740.

Tang, Y. C., and Xia, X. Y., (2011). *Quantitative Assessment of Shale Gas Potential Based on its Special Generation and Accumulation Processes*. Abstract, Search and Discovery Article #40819., American Association of Petroleum Geologist

Annual Meeting, Houston, p. <http://www.searchanddiscovery.com/documents/2011/40819tang/ndx_tang.pdf.

Tang, Y., Perry, J. K., Jenden, P. D., and Schoell, M. (2000). Mathematical Modeling of Stable Carbon Isotope Ratios in Natural Gases. *Geochimica Cosmochimica Acta* 64, 2673–2687. doi:10.1016/s0016-7037(00)00377-x

Tenger, B., Shen, B., Yu, L., Yang, Y., Zhang, W., Tao, C., et al. (2017). Mechanism of Shale Gas Generation and Accumulation in the Ordovician Wufeng-Longmaxi Formation, Sichuan Basin, SW China. *Pet. explor. Dev.* 44, 69–78.

Tilley, B., McLellan, S., Hiebert, S., Quartero, B., Veilleux, B., and Muehlenbachs, K. (2011). Gas Isotope Reversals in Fractured Gas Reservoirs of the Western Canadian Foothills: Mature Shale Gases in Disguise. *Bulletin* 95, 1399–1422. doi:10.1306/01031110103

Tilley, B., and Muehlenbachs, K. (2013). Isotope Reversals and Universal Stages and Trends of Gas Maturation in Sealed, Self-Contained Petroleum Systems. *Chem. Geol.* 339, 194–204. doi:10.1016/j.chemgeo.2012.08.002

Wang, G., Ma, Y., Zhao, Y., and Chen, W. (2021). Carbon Isotope Fractionation during Shale Gas Transport through Organic and Inorganic Nanopores from Molecular Simulations. *Energy fuels.* 35, 11992–12004. doi:10.1021/acs.energyfuels.1c01448

Wang, K., Chatterton, B. D. E., and Wang, Y. (1997). An Organic Carbon Isotope Record of Late Ordovician to Early Silurian Marine Sedimentary Rocks, Yangtze Sea, South China: Implications for CO2 Changes during the Hirnantian Glaciation. *Palaeogeogr. Palaeoclimatol. Palaeoecol.* 132, 147–158. doi:10.1016/s0031-0182(97)00046-1

Wang, K., Orth, C. J., Attrep, M., Chatterton, B. D. E., Wang, X., and Li, J.-j. (1993). The Great Latest Ordovician Extinction on the South China Plate: Chemostratigraphic Studies of the Ordovician-Silurian Boundary Interval on the Yangtze Platform. *Palaeogeogr. Palaeoclimatol. Palaeoecol.* 104, 61–79. doi:10.1016/0031-0182(93)90120-8

Wang, Y., Qiu, N., Yang, Y., Rui, X., Zhou, Y., Fang, G., et al. (2019). Thermal Maturity of Wufeng-Longmaxi Shale in Sichuan Basin. *Earth Sci.* 44, 953–971.

Wei, X., Guo, T., and Liu, R. (2016). Geochemical Features of Shale Gas and Their Genesis in Jiaoshiba Block of Fuling Shale Gasfield, Chongqing. *Nat. Gas. Geosci.* 27, 539–548.

Wu, W., Fang, C., Dong, D., and Liu, D. (2015). Shale Gas Geochemical Anomalies and Gas Source Identification. *Acta Pet. Sin.* 36, 1332–1340+1366.

Wu, W., Huang, S., Hu, G., and Gong, D. (2014). A Comparison between Shale Gas and Conventional Gas on Geochemical Characteristics in Weiyuan Area. *Nat. Gas. Geosci.* 25, 1994–2002.

Xia, X., Chen, J., Braun, R., and Tang, Y. (2013). Isotopic Reversals with Respect to Maturity Trends Due to Mixing of Primary and Secondary Products in Source Rocks. *Chem. Geol.* 339, 205–212. doi:10.1016/j.chemgeo.2012.07.025

Xia, X., and Gao, Y. (2018). Depletion of 13C in Residual Ethane and Propane during Thermal Decomposition in Sedimentary Basins. *Org. Geochem.* 125, 121–128. doi:10.1016/j.orggeochem.2018.09.003

Xia, X., and Tang, Y. (2012). Isotope Fractionation of Methane during Natural Gas Flow with Coupled Diffusion and Adsorption/desorption. *Geochimica Cosmochimica Acta* 77, 489–503. doi:10.1016/j.gca.2011.10.014

Xiong, L., Pang, H. Q., Zhao, Y., Wei, L. M., Zhou, H., and Cao, Q. (2021). Micro Pore Structure Characterization and Classification Evaluation of Reservoirs in Weirong Deep Shale Gas Field. *Reserv. Eval. Dev.* 11, 20–29.

Xu, S. L., Chen, H. D., Chen, A. Q., Lin, L. B., Li, J. W., and Yang, J. B. (2011). Source Rock Characteristics of Marine Strata, Sichuan Basin. *J. Jilin Univ. (Earth Sci. Ed.* 41, 343–350.

Yan, D., Chen, D., Wang, Q., Wang, J., and Wang, Z. (2009). Carbon and Sulfur Isotopic Anomalies across the Ordovician-Silurian Boundary on the Yangtze Platform, South China. *Palaeogeogr. Palaeoclimatol. Palaeoecol.* 274, 32–39. doi:10.1016/j.palaeo.2008.12.016

Zhang, M., Tang, Q., Cao, C., Lv, Z., Zhang, T., Zhang, D., et al. (2018a). Molecular and Carbon Isotopic Variation in 3.5 Years Shale Gas Production from Longmaxi Formation in Sichuan Basin, China. *Mar. Petroleum Geol.* 89, 27–37. doi:10.1016/j.marpetgeo.2017.01.023

Zhang, Q., Wang, H. Y., Bai, W. H., Lin, W., and Du, D. (2013). Restoration of Organic Matter Type in Silurian Marine Shale, South China. *Fault-Block Oil Gas Field* 20, 154–156.

Zhang, S., He, K., Hu, G., Mi, J., Ma, Q., Liu, K., et al. (2018b). Unique Chemical and Isotopic Characteristics and Origins of Natural Gases in the Paleozoic Marine Formations in the Sichuan Basin, SW China: Isotope Fractionation of Deep and High Mature Carbonate Reservoir Gases. *Mar. Petroleum Geol.* 89, 68–82. doi:10.1016/j.marpetgeo.2017.02.010

Zhang, T., and Krooss, B. M. (2001). Experimental Investigation on the Carbon Isotope Fractionation of Methane during Gas Migration by Diffusion through Sedimentary Rocks at Elevated Temperature and Pressure. *Geochimica Cosmochimica Acta* 65, 2723–2742. doi:10.1016/s0016-7037(01)00601-9

Zhao, S., Kang, S., Zheng, M., Lu, S., Yang, Y., Zhang, H., et al. (2021). Prediction of Decline in Shale Gas Well Production Using Stable Carbon Isotope Technique. *Front. Earth Sci.* 15, 849–859. doi:10.1007/s11707-021-0935-4

Zou, C. N., Zhao, Q., Cong, L., Wang, H., Shi, Z., Wu, J., et al. (2021). Development Progress, Potential and Prospect of Shale Gas in China. *Nat. Gas. Ind.* 41, 1–14.

Zou, C. N., Dong, D., Wang, Y., Li, X., Huang, J., Wang, S., et al. (2016). Shale Gas in China: Characteristics, Challenges and Prospects (II). *Pet. explor. Dev.* 43, 166–178. doi:10.1016/s1876-3804(16)30022-2

Zou, C., Zhu, R., Chen, Z.-Q., Ogg, J. G., Wu, S., Dong, D., et al. (2019). Organic-matter-rich Shales of China. *Earth-Science Rev.* 189, 51–78. doi:10.1016/j.earscirev.2018.12.002

Zumberge, J., Ferworn, K., and Brown, S. (2012). Isotopic Reversal ('rollover') in Shale Gases Produced from the Mississippian Barnett and Fayetteville Formations. *Mar. Petroleum Geol.* 31, 43–52. doi:10.1016/j.marpetgeo.2011.06.009

Conflict of Interest: Authors XL and FL are employed by PetroChina Zhejiang Oilfield Company.

The remaining authors declare that the research was conducted in the absence of any commercial or financial relationships that could be construed as a potential conflict of interest.

Publisher's Note: All claims expressed in this article are solely those of the authors and do not necessarily represent those of their affiliated organizations, or those of the publisher, the editors, and the reviewers. Any product that may be evaluated in this article, or claim that may be made by its manufacturer, is not guaranteed or endorsed by the publisher.

frontiers | Frontiers in Earth Science

ORIGINAL RESEARCH
published: 13 July 2022
doi: 10.3389/feart.2022.889112

Geochemical Characteristics and Gas Source Contributions of Noble Gases of the Sulige Large Tight Gas Field of Upper Paleozoic in Ordos Basin, China

Wang Xiaobo[1,2], Hou Lianhua[1,2], Li Jian[1,2], Yang Chunxia[1]*, Fan Liyong[3]*, Chen Jianfa[4], Zhang Chunlin[1,2], Guo Jianying[1,2], Tian Jixian[1,2], Zheng Yue[1,5] and Yang Chunlong[1,2]**

[1]PetroChina Research Institute of Petroleum Exploration & Development, Beijing, China, [2]Key Laboratory of Gas Reservoir Formation and Development of CNPC, Langfang, China, [3]Changqing Oilfield Company, PetroChina, Xi'an, China, [4]State Key Laboratory of Petroleum Resources and Prospecting, China University of Petroleum, Beijing, China, [5]College of Earth and Planetary Sciences, University of Chinese Academy of Sciences, Beijing, China

OPEN ACCESS

Edited by:
Maowen Li,
SINOPEC Petroleum Exploration and Production Research Institute, China

Reviewed by:
Peng Li,
SINOPEC Petroleum Exploration and Production Research Institute, China
Huiyuan Xu,
Sinopec, China

***Correspondence:**
Li Jian
lijian69@petrochina.com.cn
Yang Chunxia
yangcx83@petrochina.com.cn
Fan Liyong
lyfan123_cq@petrochina.com.cn
Yang Chunlong
yangchunlong69@petrochina.com.cn

Specialty section:
This article was submitted to Geochemistry, a section of the journal Frontiers in Earth Science

Received: 03 March 2022
Accepted: 27 May 2022
Published: 13 July 2022

Citation:
Xiaobo W, Lianhua H, Jian L, Chunxia Y, Liyong F, Jianfa C, Chunlin Z, Jianying G, Jixian T, Yue Z and Chunlong Y (2022) Geochemical Characteristics and Gas Source Contributions of Noble Gases of the Sulige Large Tight Gas Field of Upper Paleozoic in Ordos Basin, China. Front. Earth Sci. 10:889112. doi: 10.3389/feart.2022.889112

Tight gas is the fastest developing unconventional natural gas resource, becoming the principal part for gas reserves and production growth in China. The Sulige gas field is the largest gas field and also the typical low porosity and low permeability tight sandstone gas field discovered in China, with an annual natural gas output exceeding 300 billion and cumulative output exceeding 290 billion, playing an important role in ensuring national energy provision, helping China's energy transformation, and promoting green, low-carbon, environmental protection and high-quality development. Based on sample collection and laboratory analysis, natural gas compositions including hydrocarbons, non-hydrocarbons, light hydrocarbons, and noble gases of the Sulige gas field are systematically analyzed, their genetic identifications are identified, and finally gas source originations and contribution proportions are comprehensively discussed from the perspectives of noble gases and hydrocarbon gases. The main achievements are as follows: 1) natural gases in the Sulige gas field are mainly alkane gases, with high methane content, high drying coefficient, low heavy hydrocarbon contents, low non-hydrocarbon gas contents of CO_2 and N_2, and relatively low noble gas contents. The helium content is relative 2 order of magnitude higher than the atmospheric value, while neon, argon, krypton, and xenon are relatively about 1–2 orders of magnitudes lower than the atmospheric values. 2) The carbon and hydrogen isotopes of alkanes are generally positive sequence distributions with some part inversion. The $^{3}He/^{4}He$ values are mainly distributed in magnitude of 10^{-8}, the $^{40}Ar/^{36}Ar$ is ranged from 506 to 1940, the ^{129}Xe is relative loss, and the ^{132}Xe is relative surplus. 3) Natural gases in the Sulige gas field are typical coal-formed gases generated from a humic organic mother material with maturity from high mature to over mature according to C_7 and C_8 light hydrocarbons and alkane carbon isotopes. Noble gases are typical crustal genesis, mainly originating from the radioactive decay of crustal source materials. 4) The gas source correlations of noble gases and alkane gases and their quantitative evaluations on source contributions show that natural gases in the Sulige gas field are originated from Carboniferous-Permian coal measure source rocks in Ordos Basin, mainly contributed by coals and supplemented by mudstones, accounting for 55–60% and 40–45%, respectively.

Keywords: Ordos basin, Sulige gas field, tight gas, noble gases, C_7 and C_8 light hydrocarbon, genetic identification, gas source correlation

1 INTRODUCTION

Tight gas is a natural gas stored in overburden matrix permeability less than or equal to 0.1 md (air permeability less than 1 md) in tight sandstone formations. As an important unconventional gas resource, tight gas has played an important role in China's natural gas development and been in a leading position in the process of unconventional gas development in China, becoming a major growth point for increasing natural gas reserves and production. Accelerating the exploration and development of tight gas is strategically important for the development of natural gas and the adjustment of the energy structure in China. At present, tight gas in China is widely distributed in Sichuan, Ordos, Tuha, Songliao, and Junggar basins, and mainly accumulated in Ordos and Sichuan basins. As early as 1971, China discovered the Zhongba tight gas field in the western part of Sichuan Basin. Since the mid-1990s, great breakthroughs were made in the exploration of Upper Paleozoic gas in Ordos Basin, and a large number of tight gas fields such as Yulin, Sulige, Wushengqi, Mizhi, Shenmu, and Zizhou were discovered successively. The Sulige gas field is the largest onshore monoblock natural gas field and also the largest unconventional tight gas field in China. The proven (including basic proven) gas reserves is 4.77×10^{12} m^3 (Fu et al., 2019; Jia et al., 2021), the gas production is more than 300×10^8 m^3 in 2021 and the cumulative gas production is more than $2{,}900\times10^8$ m^3. It plays an important role in ensuring national energy provision security, helping China's energy transformation and promoting green, low-carbon and high-quality development. Noble gases are considered as valuable tracers for the studies of geological processes, having great effects on gas origins and migration, crustal–mantle interaction, geotectonic etc. (Xu et al., 1979, Xu et al., 1998; Allegre et al., 1983, 1993; Ballentine et al., 1992; Battani et al., 2000; Burnard et al., 2013; Clarke et al., 1976; Du, 1989; Honda et al., 1991, 1993; Hiyagon et al., 1992; Kennedy et al., 1990; Lee et al., 2006; Liu and Xu, 1987, 1993; Lupton, 1983; Lupton and Evans, 2004; Mamyrin et al., 1970, 1984; Mark et al., 2011; Ozima and Podesek, 1983; Poreda and Farley, 1992; Poreda et al., 1986; Prinzhofer, 2013; Sano et al., 2008; Sarda et al., 1988; Shen et al., 1995; Sun et al., 1991; Wang, 1989; Wang et al., 2013, Wang et al., 2015, Wang et al., 2016, Wang et al., 2018; Wei et al., 2014; Welhan and Craig, 1983; Welhan et al., 1983; Xu et al., 1996; Xu et al., 1996, 1997). A lot of researches have been done on the geochemical characteristics, genesis, and sources of natural gas in the Sulige gas field (Dai et al., 1997; Fu et al., 2000; He et al., 2003; Dai et al., 2005; Feng et al., 2007; Hu et al., 2007; Liu et al., 2007; Hu et al., 2008; Lin et al., 2009; Dai et al., 2012; Hu et al., 2012; Li et al., 2012; Fu et al., 2013; Liu et al., 2013; Wang et al., 2013; Yu et al., 2013; Dai et al., 2013; Dai, 2014; Dai, 2014; Yang et al., 2014; Dai et al., 2016; Jia et al., 2018; Fu et al., 2019; Guo et al., 2020; Dai et al., 2021; Jia et al., 2021), but relatively little work has been done on the genesis and sources of natural gases by using the full components and isotopes of noble gases and C_8 light hydrocarbons. Hence, the authors intend to systematically analyze the hydrocarbon, non-hydrocarbon, noble gas components, and isotopic characteristics of natural gases in the Sulige gas field based on a large amount of alkane gases, non-hydrocarbon gases, noble gases, and light hydrocarbons, to comprehensively identify the natural gas genesis in the largest tight gas field from the perspectives of alkane gases, noble gases, and C_8 light hydrocarbons, and finally to explore the natural gas sources and their contribution proportions in the Sulige tight sandstone gas field from various perspectives, such as comparison of noble gases and conventional hydrocarbon gases. This study aims to deepen the understandings of gas genesis and sources in the Sulige tight sandstone gas field, providing references for tight sandstone gas field exploration in China.

2 REGIONAL GEOLOGICAL BACKGROUND

The Ordos Basin is a multi-rotation evolutionary craton basin with stable subsidence and depressional migration, covering an area of about 37×10^4 km^2, which is ranked the second largest oil and gas-bearing basin in China after Tarim Basin (the distribution area of Paleozoic sedimentary rocks is about 25×10^4 km^2). In general, it has the characteristics of active surrounding structures, developed faults, stable internal structures, high in the West and low in the East, and gently inclined to the West. Tectonically, the Ordos Basin can be divided into six primary tectonic units (**Figure 1**), namely, Yimeng Uplift, Weibei Uplift, Western Shanxi Flexural Fold Belt, Yishan Slope, Tianhuan Depression, and the Western Margin Thrust Belt, and several secondary tectonic units. On the basis of Archean and Lower Proterozoic metamorphic rock basement, the basin has undergone five stages of tectonic evolution: Middle and Late Proterozoic Aula Valley, Early Paleozoic Shallow sea platform, Late Paleozoic Coastal Plain, Mesozoic Inland Basin, and Cenozoic Peripheral Fault Depression (Compilation group of petroleum geology of Changqing Oilfield, 1992; Yang and Pei, 1996; Kang et al., 2000; Liu et al., 2000; Yang et al., 2000; He et al., 2003; Yang et al., 2006; Hu, 2009).

The Ordos Basin is mostly developed from bottom to top with the Middle and Upper Paleozoic Changcheng and Jixian; Lower Paleozoic Cambrian and Ordovician; Upper Paleozoic Carboniferous Benxi Formation; Permian Taiyuan Formation; Shanxi Formation; Shihezi Formation and Shiqianfeng Formation; Mesozoic Triassic, Jurassic, and Cretaceous; Cenozoic Tertiary and Quaternary; missing Upper Ordovician; and Silurian and Devonian, and the average thickness of sedimentary rocks reaches 6000 m (Hu, 2009). Marine carbonate deposits are well developed in Lower Paleozoic, and fluvial and lacustrine clastic deposits are well developed in Upper Paleozoic and Mesozoic. The Shanxi Formation of Lower Permian is divided into Shan 2 and

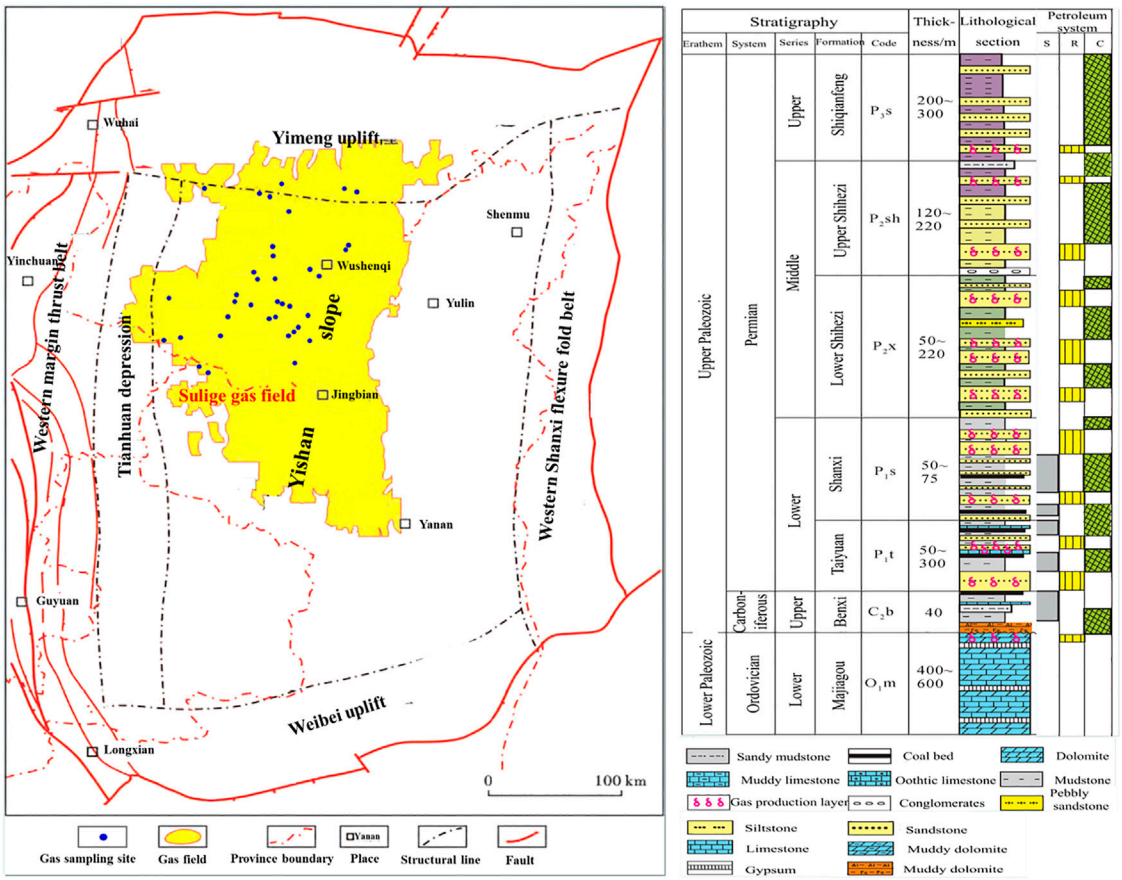

FIGURE 1 | Geological unit classification and the Sulige gas field distribution in Ordos Basin (Dai, 2014; Fu et al., 2019, Modifed).

Shan 1 members from bottom to top. The Shan 2 member which is a set of deltaic coal-formed clastic sediments, with lithology mostly of clastic sandstones or quartz sandstones, interspersed with thin layer of siltstones, mudstones, and coal seam, is one of the main gas layers in Upper Paleozoic. The Lower Shihezi Formation of Middle Permian is a set of stable distribution of fluvial–deltaic sediments and can be divided into He 8, He 7, He 6, and He 5 members. The He 8 member which is mostly composed of quartz sandstones and mudstones with unequal thickness alternate layer is one of the main gas layers in Upper Paleozoic. The Carboniferous-Permian coal measures hydrocarbon source rocks of Upper Paleozoic, with a thickness of 60–100 m, high organic matter content, high thermal evolution from high to over mature stage, and strong generation capacity are widely covered in the whole basin. The early Cretaceous is the main gas generation period for the Carboniferous-Permian coal measures hydrocarbon source rocks. The source rocks are in the high over mature stage and enter the peak of gas generation, which provides sufficient gas source for the formation of Paleozoic gas reservoir. The vertical superposition relationship between Permian-Carboniferous coal measures hydrocarbon source rocks and main reservoir such as He 8 and Shan 1 members of Permian are favorable for vertical migration and accumulation of natural gases generated in the peak of hydrocarbon generation of the source rocks. On the one hand, driven by the residual pressure of the source reservoir, the natural gases generated from the underlying Carboniferous-Permian coal measure source rocks accumulate and dissipate to the overlying Permian reservoir with the main mechanism of volumetric flow Darcy or non-Darcy seepage migration. On the other hand, due to the differences of hydrocarbon concentration caused by hydrocarbon generation, the natural gases generated in the source rock continuously diffuses to the overlying low porosity and permeability tight sandstone reservoir driven by concentration gradient (Wang et al., 2014; Wang et al., 2015). In addition, Upper Shihezi Formation has a stable distribution of fluvial and lacustrine mudstones with a thickness of about 60–120 m and constitutes the regional cover of Upper Paleozoic gas reservoir. The overlying mudstones and updip directional dense sandstones provide good direct covering and lateral sealing abilities (Yang and Pei, 1996; Kang et al., 2000; Yang et al., 2006; Hu, 2009).

The Sulige gas field is located in the north central part of Ordos Basin, tectonically in the northwestern part of the Yishan Slope, straddling three regional tectonic units: Yishan Slope, Yimeng Uplift, and Tianhuan Depression. Its administrative area is

located in the Inner Mongolia Autonomous Region and the Shaanxi Province, consisting of four blocks: Central, West, East, and South. The Paleozoic strata of the Sulige gas field are lack of middle and Upper Ordovician, Silurian, Devonian, and Lower Carboniferous. The Majiagou Formation of Lower Ordovician, Benxi Formation of Upper Carboniferous, Taiyuan Formation and Shanxi Formation of Lower Permian, Lower Shihezi Formation of Middle Permian, and Upper Shihezi Formation and Shiqianfeng Formation of Upper Permian are developed from bottom to top. The Sulige gas field is mostly developed in Upper Paleozoic, and its main reservoir is the He 8 member of Middle Permian Lower Shihezi Formation of Middle Permian and the Shan 1 member of Shanxi formation of Lower Permian, with a depth of 3,200–3,500 m and a thickness of 80–100 m, followed by Shan 2 member of Shanxi Formation of Lower Permian and Ma 5 member of Majiagou Formation of Lower Ordovician. The Sulige gas field is generally characterized by a large gas-bearing area, many formations, thin single layer thickness, poor reservoir properties, strong non-homogeneity, generally low porosity and permeability, low pressure coefficient, low reserve abundance, and low production. It is a typically large distributed dense sandstone gas reservoir with low permeability, low pressure, low abundance, and river sand body as the main reservoir. In 2000, the Su6 well obtained a high production rate of 120×10^4 m^3 per day in Shihezi Formation, which kicked off the large-scale exploration of the Sulige gas field and marked a major discovery (Dai, 2014). Since 2007, the Sulige gas field has insisted on the integration of exploration and development, and the scale of new gas reserves exceeded $5{,}000\times10^8$ m^3 per year for seven consecutive years (Yang and Liu, 2014). At present, the exploration area of the Sulige gas field is about 5.5×10^4 km^2, with total gas resources of 6×10^{12} m^3, proven gas-bearing area is 3.88×10^4 km^2, accumulated tertiary reserves reaches 4.77×10^{12} m^3, and the natural gas production reaches 2.7×10^{10} m^3 in 2020, which becomes a key area for increasing natural gas storage and production in the Changqing Oilfield and an important natural gas gathering area in China (Fu et al., 2019; Jia et al., 2018; Jia et al., 2021). It makes a significant contributions on guaranteeing a safe and stable gas supply in the Capital, North China, and areas around the field.

3 SAMPLES AND ANALYTICAL METHODS

The noble gas content in natural gas is low but relatively high in air (especially argon content is as high as 0.934%), so it can easily be contaminated, which can lead to experimental analysis data to severely deviate from the real value. In order to minimize the contamination of noble gases in air, special measures are required for sampling natural gases for noble gases analysis (Wang et al., 2013; Wang et al., 2016; Wang et al., 2018):① choose a double valve high pressure–resistant steel cylinder; ② evacuate a sampling steel cylinder to below 10^{-1} Pa using a mechanical pump; ③ repeatedly flush the steel cylinder with natural gas for 4–6 times during wellhead sampling and intercept the middle section of gas flow. For the aforementioned noble gas analysis and testing requirements, more than 50 gas samples were collected from the Sulige gas field in Ordos Basin using high-pressure cylinder sampling, involving Permian Taiyuan Formation, Shanxi Formation, Shihezi Formation, and Shiqianfeng Formation.

The sample collection tests were completed at the Key Laboratory of Gas Formation and Development of China National Petroleum Corporation (CNPC).

(1) The natural gas component analysis was performed using an Agilent 7890A gas chromatograph, separating components by using a PLOT Al_2O_3 capillary column with a specification of 50 m × 0.20 mm × 0.5 μm. The sample inlet temperature was 300°C, carrier gas was helium, flow rate was 1 ml/min, splitting ratio was 50:1, and the temperature program was set to keep 10 min from 30°C, then the temperature was increased to 260°C at the heating rate of 3°C/min.

(2) Noble gas components and isotopes were analyzed using a noble gas sampling system and a Noblesse isotope mass spectrometer. The high vacuum of the system was achieved by mechanical, molecular, and ion pumps, and the sample volume of natural gas samples was controlled by an injection control system; a zirconium-based furnace and a suction pump were used to purify hydrocarbon gas, nitrogen (N_2), oxygen (O_2), carbon dioxide (CO_2), hydrogen sulfide (H_2S), trace hydrogen (H_2), and other active gases in natural gas samples; enrich noble gases; measure the content of noble gas components; and further separate components according to different boiling points of noble gases. The noble gas isotope composition was determined based on the ion flow signal intensity peak height ratio method by sending it to the Noblesse noble gas isotope mass spectrometer for isotope analysis. The relative deviations of the noble gases helium, neon, argon, krypton, and xenon were ±3.36%, ±3.66%, ±1.32%, ±2.99%, and ±6.96%, respectively, and the relative deviations of the noble gases $^3He/^4He$, $^{20}Ne/^{22}Ne$, $^{21}Ne/^{22}Ne$, $^{40}Ar/^{36}Ar$, $^{38}Ar/^{36}Ar$, $^{129}Xe/^{130}Xe$, and $^{132}Xe/^{130}Xe$ isotopes were ±4.50%, ±1.32%, ±1.27%, ±1.39%, ±1.63%, ±1.84%, and ±2.13%, respectively.

(3) A natural gas carbon isotope analysis was performed using the Finnigan MAT Delta PLUS GC/C/IRMS isotope mass spectrometer. The gas was separated by gas chromatography, converted to CO_2, and then fed into IRMS for carbon isotope determination. The chromatographic column was PLOT Q (30 m × 0.32 mm × 20 mm). The temperature rise procedure of chromatographic column was heating up from 35°C to 80°C at the rate of 8°C/min, then to 260°C at the rate of 5°C/min, and finally, kept at a constant temperature for 10 min. Each sample was analyzed three times, and the analytical standard was VPDB with an analytical accuracy of ±0.5%.

(4) The chromatographic separation column was HP PLOT Q (30 m × 0.32 mm × 20 mm). The carrier gas was helium, and the temperature rise procedure of methane column was heating up from 35°C to 80°C at the rate of 8°C/min, then to 260°C at the rate of 5°C/min, and finally, kept at a constant temperature for 10 min. Each sample was analyzed three times, and the analytical standard was SMOW with an analytical accuracy of ±0.5%.

TABLE 1 | Data table of hydrocarbon, non-hydrocarbon, and noble gas components in some natural gas samples from the Sulige gas field in Ordos Basin.

Gas field	Well	Strata	CH_4 (%)	CO_2 (%)	N_2 (%)	H_2S (%)	C_2 (%)	C_3 (%)	C_1/C_1+	He (10^{-6})	Ne (10^{-6})	Ar (10^{-6})	Kr (10^{-6})	Xe (10^{-8})	References
Sulige	S47-44-37	P	89.07	2.76	6.72	0	1.12	0.19	0.984	679.3	7.68	80.3	0.0411	1.0567	This study
	S48-5-84	P	93.01	1.22	1.48	0	3.06	0.43	0.956	540.7	6.17	50.8	0.0211	0.6728	
	S53	P	83.77	1.12	0.78	0	7.93	2.45	0.854	563.3	6.59	62.4	0.0455	0.6714	
	S10-42-48	P	91.76	1.04	1.04	0	4.57	0.86	0.937	679.8	7.74	69.0	0.0278	0.9198	
	S20-16-16	P	91.4	0.74	1.05	0	4.85	0.95	0.931	371.9	4.69	43.5	0.0161	0.4743	
	S20-15-14	P	91.47	0.71	1.04	0	4.94	0.98	0.931	395.2	5.01	48.6	0.0187	0.5868	
	S14-5-52	P	93.8	1.46	0.69	0	3.24	0.48	0.959	360.1	4.32	51.7	0.0203	0.4780	
	S14-4-47	P	91.98	1.01	0.94	0	4.41	0.84	0.938	345.3	4.45	38.3	0.0164	0.4924	
	S14-17-34	P	92.96	0.93	0.96	0	3.92	0.64	0.948	345.0	4.71	40.6	0.0163	0.5432	
	S14-16-42	P	93.6	0.89	0.85	0	3.5	0.64	0.953	331.2	4.27	73.1	0.0239	0.5347	
	T7-9-2	P	87.95	1.02	5.6	0	4.03	0.76	0.942	228.8	4.30	29.9	0.0148	0.4513	
	S11-18-36	P	89.93	1.56	0.92	0	5.48	1.14	0.922	688.6	7.49	69.1	0.0210	0.7117	
	Z61	P	89.86	0.99	0.96	0	5.84	1.29	0.916	762.5	7.84	56.4	0.0224	0.9563	
	S75-79-34H	P	92.33	1.62	1.16	0	3.7	0.62	0.950	719.7	7.24	71.5	0.0212	0.7850	
	S38	P	89.89	2.09	1.64	0	4.66	0.88	0.934	465.4	5.57	47.3	0.0158	0.5721	
	S75	P	90.19	1.59	0.94	0	5.42	1.06	0.925	691.5	7.20	81.4	0.0235	0.7887	
	S95	P	92.3	1.67	1.08	0	3.77	0.62	0.949	675.9	7.05	76.3	0.0213	0.7238	
	S55	P	90.41	0.62	0.88	0	6.2	1.14	0.918	515.7	5.66	46.4	0.0149	0.5510	
	S148	P	93.46	2.17	2.79	0	1.31	0.15	0.983	742.7	7.57	67.2	0.0204	0.7767	
	S5-15-8	P	90.97	0.86	0.92	0	5.31	1.09	0.926	417.2	4.99	41.7	0.0135	0.5173	
	S76	P	85.95	0.16	1.3	0	8.3	2.42	0.872	718.6	7.74	20.2	0.0558	1.2329	
	S54-24-65	P	93.32	2.23	1.43	0	2.43	0.32	0.969	681.3	6.92	102.3	0.0363	0.9511	
	S77-4-6	P	93.87	0.30	1.2	0	3.48	0.6	0.953	512.7	5.71	50.5	0.0166	0.6699	
	S120-79-69	P	91.71	2.97	2.72	0	1.84	0.29	0.972	674.6	6.94	108.8	0.0371	0.8943	
	S48-2-86	P	93.06	1.47	0.6	0	3.79	0.61	0.950	401.9	4.80	26.5	0.0103	0.4313	
	S109	P	91.93	2.29	3.16	0	1.91	0.42	0.972	666.8	7.20	213.4	0.0496	0.9983	
	S77-70-13	P	91.11	1.75	0.9	0	4.74	0.86	0.936	651.0	6.56	60.3	0.0176	0.5690	
Changshen and Xushen	XS 6	K	95.22	0.40	1.30	0	2.39	0.38	0.968	151	3.1291	48.102	0.0149	0.2783	Wang et al. (2013); Dai, (2014)
	CS 2	K	1.57	97.45	0.71	0	0.01	0	0.9936	195	4.144	74.027	0.0154	0.4418	
	CSP 2	K	68.16	25.65	4.7	0	1.12	0.05	0.9831	453	6.179	331.313	0.0404	0.8632	
Weiyuan	W 2	Z	85.07	4.66	8.33	1.31	0.11	0	0.9987	2500		530			Dai et al. (2003)
	W 5	P	94.28		3.36		0.21	0.01	0.9976	1080		480			
	W 23	C-Z	85.44	4.75	8.14	1.25	0.15	0	0.9982	2620		150			
	W 27	Z	85.85	4.7	7.81	1.20	0.17	0	0.9980	2180		480			
	W 28	Pt	67.03	1.23	26.7	0.01	0.21	0.03	0.9964	2480		2050			
	W 30	Z	86.57	4.40	7.55	0.95	0.14	0	0.9984	3,420		460			
	W 39	Z	86.74	4.53	7.08	1.22	0.12	0	0.9986	2730		710			
	W 46	Z	85.66	4.66	8.11	1.17	0.11	0	0.9987	2520		490			
	W 100	Z	86.80	5.07	6.47	1.18	0.13	0	0.9985	2980		460			
	W 106	Z	86.54	4.82	6.26	1.32	0.07	0	0.9992	3,150		430			

(5) A natural gas light hydrocarbon analysis was performed by using a gas chromatograph 7890A with helium as the carrier gas and the PLOT Al_2O_3 capillary column of 50 m × 0.20 mm × 0.5 μm for component separation, the inlet temperature was 120°C, and liquid nitrogen cold trap for light hydrocarbon enrichment for 5 min. FID detector temperature was 320°C, the injection volume was 10–15 ml, and the ramp-up program was initiated. The initial temperature of the rise procedure was 30°C, kept at constant temperature for 15 min, and then the rise procedure was l.5°C/min to 70°C, 3°C/min to 160°C and 5°C/min to 300°C and kept at a constant temperature for 20 min, respectively.

4 RESULTS AND DISCUSSIONS

4.1 Distribution Characteristics of Alkane, Non-Hydrocarbon, and Noble Gas Components in the Sulige Gas Field

The alkane gas content of natural gas in the Sulige gas field occupies an absolute advantage. The highest methane content is mostly distributed in the range of 83.77%–93.87%, with an average of 91.15%. Ethane is mostly distributed in the range of 1.12%–8.30%, with an average of 4.21%. Propane is mostly distributed in the range of 0.15%–2.45%, with an average of

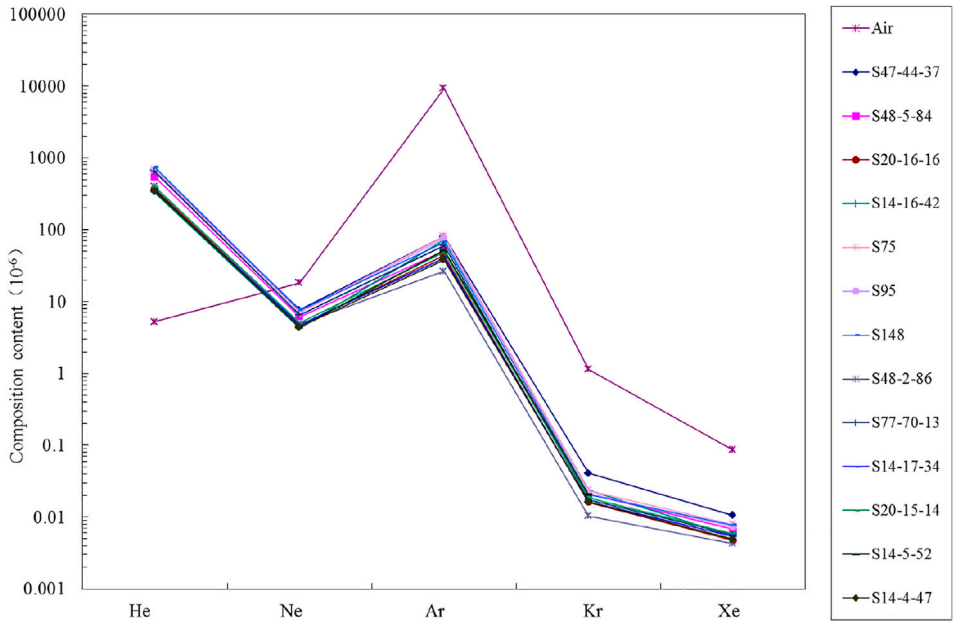

FIGURE 2 | Components abundance of noble gas He, Ne, Ar, Kr, and Xe of natural gases in the Sulige gas field in Ordos Basin.

0.84%. The drying factor (C_1/C_{1+}) is mostly distributed in the range of 0.854–0.984, with an average of 0.940 (**Table 1**). The non-hydrocarbon gas nitrogen (N_2) content was mostly distributed in the range of 0.60%–6.72%, with an average value of 1.62%, and carbon dioxide (CO_2) content was mostly distributed in the range of 0.30%–2.97%, with an average value of 1.38%, without H_2S.

Compared with hydrocarbon and non-hydrocarbon gases, the contents of noble gases in natural gas are relatively low. In general, the distribution of noble gas components in natural gases from the Sulige field in Ordos Basin has many characteristics (**Table 1**; **Figure 2**). 1) The helium content of natural gas samples is mostly distributed around $(228.8–762.5)\times10^{-6}$, with an average value of 549.1×10^{-6}, which is about two orders of magnitude higher than the atmospheric value of 5.24×10^{-6} in general. 2) The neon content in natural gas samples is around $(4.27–7.84)\times10^{-6}$, with an average value of 6.16×10^{-6}, which is about 1/3 of the atmospheric value of 18.18×10^{-6}. 3) The argon content in natural gas samples is around $(20.2–213.4)\times10^{-6}$, with an average value of 64.0×10^{-6}, which is about two orders of magnitude lower than the atmospheric value of 0.934%. 4) The krypton content in natural gas samples is around $(0.0103–0.0558)\times10^{-6}$, with an average value of 0.0244×10^{-6}, which is about two orders of magnitude lower than the atmospheric content value of 1.14×10^{-6}. 5) The xenon content in natural gas samples is around $(0.0043–0.0123)\times10^{-6}$, with an average value of 0.0070×10^{-6}, which is about one order of magnitude lower than the atmospheric content value of 0.078×10^{-6}. Compared with noble gases data of previous researchers on the Weiyuan gas field in Sichuan Basin and Changshen and Xushen gas fields in Songliao Basin (**Table 1**), the helium content of Sulige is obviously less than that of Weiyuan and relatively larger than Changshen and Xushen, while the argon content in Weiyuan is relatively larger than that of Sulige, Changshen, and Xushen.

4.2 Carbon Isotope Distribution Characteristics and Genesis Identifications of Alkane Gases and Carbon Dioxide in the Sulige Gas Field

The carbon isotope analysis data of alkane gas components in the Sulige gas field are shown in **Table 2**. The methane carbon isotope $\delta^{13}C_1$ values of natural gas samples are distributed in the range of −36.7‰ ~ −27.6‰, with main values ranging from −35‰ ~ −30‰ and an average value of −32.3‰. Ethane carbon isotope $\delta^{13}C_2$ values are distributed in the range of −27.9‰ ~ −22.4‰, with main values ranging from −26‰ ~ −23‰ and an average value of −24.1‰. Propane carbon isotope $\delta^{13}C_3$ values are distributed in the range of −28.9‰ ~ −21.9‰, with the main values ranging from −28‰ ~ −23‰ and an average value of −24.7‰. The *n*-butane carbon isotope δ^{13} nC_4 values are distributed in the range of −24.1‰ ~ −19.7‰, with main values ranging from −24‰ ~ −21‰ and an average value of −22.5‰. The isobutane carbon isotope δ^{13} iC_4 values are distributed in range of −24.2‰ ~ −20‰, with main values ranging from −23‰ ~ −20‰ and an average value of −21.6‰. The carbon dioxide isotope values of $\delta^{13}C_{CO2}$ in the Sulige gas field are mostly distributed in the range of −15.3‰ ~ −5‰, with an average value of about −10.3‰. For the hydrogen isotopes of alkane gases in the Sulige gas field, the δ^2H_1 values are generally distributed in the range of −203‰ ~ −171‰, with an average of −185.3‰; the δ^2H_2 values are usually distributed in the

TABLE 2 | Carbon isotope data of alkane gas components in some natural gas of the Sulige gas field.

Well	Strata	Hydrocarbon isotope value $\delta^{13}C$‰ (VPDB)					
		CO_2	C_1	C_2	C_3	iC_4	nC_4
S47-12-65	P_1s		−30.2	−24.8	−27.6		
S47-44-37	P_2x		−28.4	−24.7	−24.6		
S48-5-84	P_2x		−30.8	−22.8	−21.9	−20.2	−19.7
S53	P_1s-P_2x		−34.7	−24.5	−23.2	−23.3	−22.2
S20-16-16	P_1s-P_2x		−33.5	−23.8	−24.4	−21.7	−22.2
S20-15-14	P_1s-P_2x		−32.9	−23.2	−24.3	−21.5	−22.8
S14-5-52	P_1s		−32.5	−23.2	−26.0	−22.9	−24.1
S14-17-34	P_2x		−33.2	−24.3	−24.5	−21.9	−22.8
S14-16-42	P_2x		−33.1	−24.5	−24.7	−21.9	−22.7
T2-2-12	P_1s	−10.0	−33.0	−23.4	−24.3	−20.5	−22.8
T7-16-22X4	P_2x	−10.5	−34.0	−23.2	−23.7	−21.6	−22.3
S120-35-81C3	P_1s	−11.5	−32.9	−22.9	−23.3	−20.0	−21.4
T2-26-16	P_1s-P_2x	−11.5	−30.0	−24.4	−25.5	−20.6	−23.4
T2-26-2	P_2x	−10.4	−30.2	−23.0	−25.4	−21.1	−23.5
S47-17-61	P_2x	−8.4	−30.0	−27.9	−28.9		
S120-97-87	P_1s	−8.9	−27.6	−27.3	−27.4		
S47-36-43	P_1s	−5.0	−28.0	−24.2	−26.8		
S48-17-74	P_1s	−8.9	−30.3	−23.4	−24.5	−20.3	−22.0
S14-6-11H	P_2x	−8.6	−32.5	−23.8	−24.3	−21.2	−22.2
SD47-38	P_2x	−5.7	−34.8	−25.3	−25.6		
SD 47-35	P_1s	−10.4	−34.4	−24.2	−23.5	−21.1	−21.9
S5-9-8	P_1s	−11.5	−33.8	−22.4	−23.3	−21.6	−22.1
S63-09	P_2x	−13.7	−33.6	−23.8	−24.7	−22.0	−22.9
S66-1C1	P_1s	−10.6	−34.2	−23.7	−23.9	−21.5	−22.7
S77-32-37	P_1t	−15.3	−36.7	−26.5	−24.9	−24.2	−23.6
S36-16-15	P_1s	−8.1	−34.4	−23.5	−24.1	−21.9	−23.1
S36-16-12	P_2x	−11.8	−33.7	−24.5	−24.4	−21.9	−23.2
S54-35-113H2	P_2x	−13.6	−31.8	−23.6	−24.2	−21.3	−22.4
S54-22-80	P_2x	−11.9	−31.5	−23.2	−24.2	−21.9	−22.4
S11-17-35	P_1s	−10.1	−32.6	−23.7	−23.2	−21.8	−21.6

range of −168‰ ~ −151‰, with an average of −159.6‰; and the δ^2H_3 values are commonly distributed in the range of −165‰ ~ −150‰, with an average of −157.6‰ (**Table 3**).

The carbon isotopes of alkane gases of organic origin have the characteristic of increasing the $\delta^{13}C$ value with increasing carbon number ($\delta^{13}C_1<\delta^{13}C_2<\delta^{13}C_3<\delta^{13}C_4$), which is called a positive carbon isotope sequence of alkane gases; when the carbon isotope arrangement of alkane gases appears chaotic, it is called carbon isotope inversion; when $\delta^{13}C_i>\delta^{13}C_{i+1}$, it is called partial inversion of carbon isotope sequence; and when $\delta^{13}C_1>\delta^{13}C_2>\delta^{13}C_3>\delta^{13}C_4$ appears completely, it is called negative carbon isotope sequence of alkane gas (Dai, 2014). The carbon isotope sequence of alkane gases in Sulige gas samples generally show positive carbon isotope sequence of $\delta^{13}C_1<\delta^{13}C_2<\delta^{13}C_3<\delta^{13}C_4$, and some samples show $\delta^{13}C_2>\delta^{13}C_3$ inversion of carbon isotope sequence (**Figure 3A**).

Similarly, the hydrogen isotopes of alkane gas of organic origin also have the characteristics of increasing the δ^2H value with increasing carbon number ($\delta^2H_{CH4}<\delta^2H_{C2H6}<\delta^2H_{C3H8}$), which is called positive hydrogen isotope sequence of alkane gas; when the carbon isotope arrangement of alkane gas appears chaotic, it is called hydrogen isotope inversion; when $\delta^2H_{CiHi+2}>\delta^2H_{Ci+1\ H2i+4}$ appears, it is called partial inversion of hydrogen isotope sequence; and when $^2H_{CH4}>\delta^2H_{C2H6}>\delta^2H_{C3H8}$ appears completely, it is called negative carbon isotope sequence of alkane gas (Dai, 2014). The hydrogen isotopes of alkane in natural gas samples from the Sulige field generally show the characteristics of $\delta^2H_{CH4}<\delta^2H_{C2H6}<\delta^2H_{C3H8}$ positive hydrogen isotope sequence, and some of samples show $\delta^{13}C_2>\delta^{13}C_3$ inversion of alkane gas hydrogen isotopes (**Figure 3B**).

Stable carbon isotope values are the most reliable and commonly used methods for natural gas genesis, with methane isotope values generally ranging of −55‰ ~ −35‰ for oil-typed gas and −35‰ ~ −22‰ for coal-formed gas. Since methane carbon isotopes are strongly influenced by the degree of thermal evolution of source rocks, ethane isotopes are usually little influenced by the maturity of thermal evolution of source rocks and have good parent material inheritance effects, so the ethane carbon isotope value of $\delta^{13}C_2$ = −28.5‰ is generally used as the threshold for determining oil-typed gas and coal-formed gas (Dai et al., 1989; Dai, 1992, 2014). The $\delta^{13}C_2$ values of natural gas from the Sulige gas field in Ordos Basin are distributed in the range of −27.9‰ ~ −22.4‰, with main values ranging from −26‰ ~ −23‰ and an average value of −24.1‰. The natural gas $\delta^{13}C_2$ is significantly heavier than −28.5‰, which is significantly different from oil-typed gas, and can be identified as typical coal-formed gas based on ethane carbon isotopes. According to carbon isotopes of methane, ethane, and propane proposed by Dai (1993), the majority of the carbon isotope data points of the gas samples distribute in coal-formed gas area, and some of points fall in or near mixed carbon isotope inversion series area (**Figure 4**), indicating that natural gases from the Sulige gas field is generally coal-formed gas.

CO_2 is an important non-hydrocarbon gas component in natural gases. The CO_2 content in the Sulige gas field mostly distributes in the range of 0.30%–2.97%, and the average value is 1.38%. The $\delta^{13}C_{CO2}$ is mostly distributed in the range of −15.3‰ ~ −5‰, and the average value is −10.3‰. 1) When the CO_2 content is less than 15%, $\delta^{13}C_{CO2}$ < −10‰ is organic CO_2; 2) when $\delta^{13}C_{CO2} \geq$ −8‰, all are inorganic CO_2; and 3) when the CO_2 content is greater than 60%, all are inorganic CO_2 (Dai et al., 1989; Dai, 1992). According to the identification chart of different CO_2 genesis by Dai et al. (1992) (**Figure 5**), the CO_2 in the Sulige gas field is mostly organic in general with small part inorganic.

4.3 Noble Gases Isotope Distribution Characteristics and Genesis Identifications of the Sulige Gas Field

(1) The $^3He/^4He$ values (R) of He in natural gas samples from the Sulige gas field mostly distribute around (2.89–7.30)×10^{-8} (0.021–0.052Ra), with an average of 4.81×10^{-8} (0.034Ra). From the He-R/Ra genesis identifications of noble gases in natural gas, it can be found that the $^3He/^4He$ values of natural gas in the Sulige gas field generally distribute between 0.01<R/Ra<0.10, and the sample points all fall in a typical crust genesis area (**Table 4**; **Figure 6**). It indicates that noble gas helium in natural gas from the Sulige gas field is mostly of typical crustal genesis, and the proportion of crustal genesis helium is greater than 98.8%, originating from the decay of crustal genesis radioactive elements U and Th.

(2) From the noble gas Ne-$^{20}Ne/^{22}Ne$, $^{20}Ne/^{22}Ne$-$^{21}Ne/^{22}Ne$, and $^3He/^4He$-$^{20}Ne/^{22}Ne$ genesis identifications (**Figure 7**),

TABLE 3 | Hydrogen isotope data of alkane gas in some natural gas of the Sulige gas field.

Well	Strata	$\delta^{13}C$ (‰,VPDB)				$\delta^{2}H$ (‰, VSMOW)			References
		CH_4	C_2H_6	C_3H_8	C_4H_{10}	CH_4	C_2H_6	C_3H_8	
S11-18-36	P_2x	−33	−23.3	−22.3	−22.9	−180	−152	−152	Yu et al. (2013)
S120-42-84	P_1s-P_2x	−31.9	−23.6	−24.7	−22.7	−174	−152	−158	
S120-52-82	P_1s-P_2x	−31.1	−23.3	−25.6	−23.6	−176	−163	−164	
S139	P_1s-P_2x	−30.4	−24.2	−26.8	−23.7	−176	−165	−165	
S14-0-31	P_1s-P_2x	−32	−23.8	−24.7	−22	−180	−155	−157	
S14-11-09	P_2x	−31.6	−24	−24.2	−22.6	−172	−154	−158	
S336	P_1s-P_2x	−28.7	−22.6	−25.1	—	−173	−156	−153	
S48-14-76	P_1s-P_2x	−33.5	−22.8	−24.2	−22.2	−176	−159	−156	
S48-15-68	P_2x	−29.8	−23.4	−25	−22.6	−179	−157	−157	
S48-2-86	P_1s	−31.7	−23.2	−24.3	−22.3	−174	−159	−155	
S55	P_2x	−35.1	−24.6	−24.1	−24.8	−186	−151	−158	
S76-1-4	P_1s	−32.7	−23.6	−22.9	−23	−182	−155	−150	
S76-15-18	P_1s-P_2x	−35.7	−25.3	−24.8	−24.8	−189	−151	−152	
SN3-45	P_1s-P_2x	−31.3	−22.1	−22.8	−20.7	−172	−153	−154	
S48-13–79C3	P_1s-P_2x	−30.2	−22.9	−23.4	−21.9	−171	−158	−153	
S21	P_2x	−33.4	−23.4	−23.8	−22.7	−194	−167	−−163	Dai, 2014
S53	P_1s-P_2x	−35.6	−25.3	−23.7	−23.9	−202	−165	−160	
S75	P_1s-P_2x	−33.2	−23.8	−23.4	−22.4	−194	−−163	−157	
S95	P_1s-P_2x	−32.5	−23.9	−24	−22.7	−193	−167	−160	
S76	P_1s-P_2x	−35.1	−24.6	−24.4	−24.4	−203	−165	−161	
S53-78-46H	P_2x	−33.9	−23.9	−23	−23.2	−198	−165	−156	
S75-64-%X	P_1s-P_2x	−33.5	−24	−23.3	−22.8	−199	−167	−159	
S77-2-5	P_1s-P_2x	−30.8	−22.7	−23.3	−22.9	−−194	−168	−164	
S77-6-8	P_1s-P_2x	−33.6	−23.9	−24.1	−23.5	−201	−165	−165	
Z61	P_1s	−33.2	−23.5	−23.3	−23.2	−194	−159	−154	

it can be found that the $^{20}Ne/^{22}Ne$ values of natural gas samples from the Sulige gas field are mostly distributed in the range of 9.56–9.74, and $^{21}Ne/^{22}Ne$ values are mostly distributed in the range of 0.0295–0.0315. The ^{20}Ne is relatively deficient, while the ^{21}Ne and ^{22}Ne are relative excess. It indicates that neon in natural gas from the Sulige gas field is dominated by typical crustal genesis, which is a result of variable depositional environments of uranium, thorium, oxygen, and fluorine elements in crust. The $^{20}Ne/^{22}Ne$ ratios of Changshen and Xushen gas fields are larger than 9.8, reflecting the relative atmospheric excess of ^{20}Ne. It indicates that neon in natural gas from Changshen and Xushen fields has significant mantle genesis neon mixing characteristics.

(3) The $^{40}Ar/^{36}Ar$ values of natural gas samples from the Sulige gas field are relatively high and widely distributed, mostly in the range of 506–1940, with an average value of 1148, while the $^{38}Ar/^{36}Ar$ values are mostly distributed in range of 0.1709–0.1959, with an average value of 0.1909 (**Table 4**). According to the $^{3}He/^{4}He$–$^{40}Ar/^{36}Ar$ genesis identification chart, it can be found that the noble gas $^{3}He/^{4}He$ values in the Sulige gas field generally distribute around $(2.89–7.30)\times10^{-8}$, with an average value of 4.81×10^{-8}, and the $^{3}He/^{4}He$ and $^{40}Ar/^{36}Ar$ have an overall negative correlation growth. It shows that helium and argon in natural gases from the Sulige gas field have the characteristics of typical crustal origin genesis (**Figure 8**). In contrast to Yingcheng Formation in Changshen and Xushen gas fields, the $^{3}He/^{4}He$ is larger than 1.4×10^{-6} and the $^{3}He/^{4}He$ is positively correlated with $^{40}Ar/^{36}Ar$, indicating that the noble gases have significant mantle genesis mixing characteristics.

(4) The $^{129}Xe/^{130}Xe$ values of natural gas in the Sulige gas field are mostly distributed in the range of 6.362–6.479 with an average value of 6.436, while the $^{132}Xe/^{130}Xe$ values are mostly distributed in the range of 6.629–6.731 with an average value of 6.670 (**Table 4**). According to the noble gas $^{129}Xe/^{130}Xe$–$^{132}Xe/^{130}Xe$ genesis identification, it can found that the ^{129}Xe in the Sulige gas field is generally deficient relative to atmosphere and the ^{132}Xe is excess relative to atmosphere, and the gas sample points fall into a crustal genesis region (**Figure 9**), indicating that the noble gas xenon in natural gas is mostly of crustal genesis. While the ^{129}Xe in Changshen and Xushen gas fields in Songliao Basin is excess relative to the atmosphere, which has the characteristics of significant mantle genesis mixing.

4.4 Distribution Characteristics and Genesis Identifications of C_7 and C_8 Light Hydrocarbons

Light hydrocarbons are $C_{5–10}$ hydrocarbon compounds with a boiling point less than 200°C, including *n*-alkanes, isoalkanes, cycloalkanes, and aromatic compounds, which are very

important components of natural gas and crude oil and contain rich geochemical information. The geochemistry of light hydrocarbons can be used to study the parent material types and genesis, depositional environments, maturities, and secondary migration of natural gases. Some researchers have established genetic identification indexes and charts for the composition of C_7 light hydrocarbon series (*n*-heptane, methylcyclohexane, and dimethylcyclopentane), C_{5-7} aliphatic compositions (*n*-alkanes, isoalkanes, and cycloalkanes), light hydrocarbon monomer hydrocarbon carbon isotope ratios (benzene, toluene, cyclohexane, and methylcyclohexane), C_{6-7} aromatic and branched alkane combinations, benzene and toluene content, methylcyclohexane, and aromatic alkane—paraffin—to identify coal-formed and oil-typed gas (Leythauser et al., 1979; Leythauser et al., 1980; Hu et al., 1990; Dai, 1992; Dai, 1993; Jiang et al., 1999; Li et al., 2001; Li et al., 2003; Hu et al., 2007; Hu et al., 2010; Hu et al., 2012). At present, the studies of light hydrocarbons in natural gases have become a hot spot in the field of oil and gas geology. C_{5-7} and C_7 light hydrocarbon compositions have been widely used in oil and gas exploration and geological studies; however, few researches have been conducted on C_8 light hydrocarbon compounds. There is a lack of methods to identify the genesis and sources of coal-formed gas and oil-typed gas by using C_8 light hydrocarbon parameters. In this study, based on the researches of C_{5-7} and C_7 light hydrocarbons, the distribution characteristics and genetic identifications of C_8 light hydrocarbons were carried out.

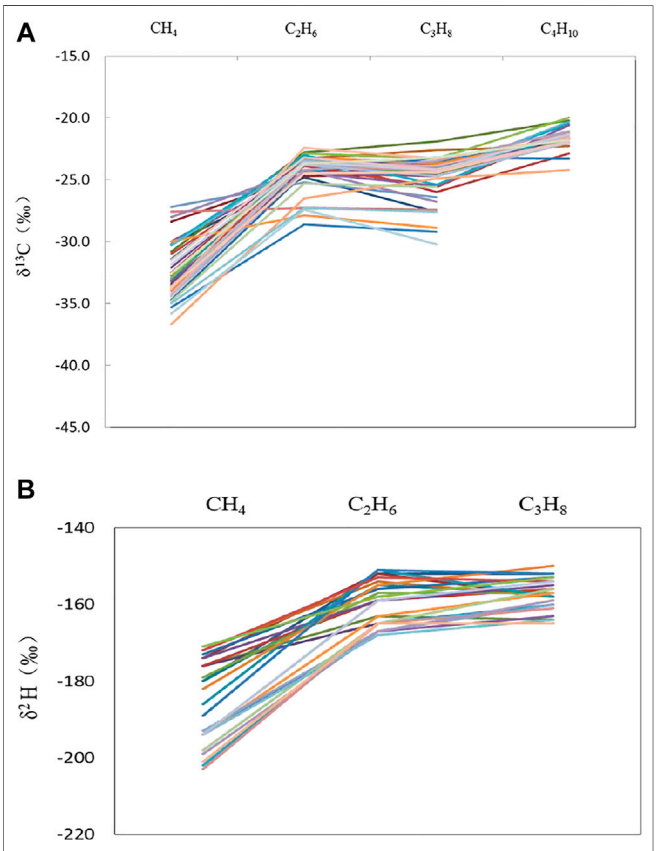

FIGURE 3 | Folding line of carbon **(A)** and hydrogen **(B)** isotope series of natural gas alkane from the Sulige gas field in Ordos Basin.

4.4.1 Distribution Characteristics and Genesis Identifications of C_7 Light Hydrocarbon Compounds

The C_7 light hydrocarbon compounds include *n*-heptane, methylcyclohexane, and dimethylcyclopentane. The *n*-heptane is mostly from algae and bacteria, which is a good maturity indicator. The methylcyclohexane is mostly from higher plant lignin and cellulose, which is a good parameter to reflect the type of terrestrial parent material. The dimethylcyclopentane is mostly from lipid-like compounds of aquatic organisms, which is a characteristic of oil-typed gas light hydrocarbons (Chung et al., 1998; Chung et al., 1991; Whiticar and Snowdon, 1999). Hu et al. (2007) analyzed 173 coal-formed gas samples in China and found that 92% of the gas samples had a methylcyclohexane volume fraction greater than 50%. Therefore, the dominant distribution of methylcyclohexane in a C_7 light hydrocarbon system is a major characteristic of coal-formed light hydrocarbons. According to the ternary diagram of relative content of the C_7 light hydrocarbon compounds system of natural gases from the Sulige gas field (**Figure 10A**), the methylcyclohexane is distributed in the range of 53.9%–77%, with an average of 66%; the *n*-heptane is distributed in the range of 9.6%–28.6%, with an average of 15%; the dimethylcyclopentane is distributed in the range of 11.5%–30%, with an average of 19%. All gas samples of the Sulige gas field is distributed in the lower left corner and show that methylcyclohexane content is dominant. So, the natural gases from the Sulige gas field are typical coal-formed gas mostly generated from humic parent material.

4.4.2 Distribution Characteristics and Genesis Identifications of C_{5-7} Light Hydrocarbon Aliphatic Compositions

The ternary diagram of relative contents of C_{5-7} aliphatic composition of *n*-alkanes, isoalkanes, and cycloalkanes is also commonly used to identify different types of natural gases. According to the ternary diagram of C_{5-7} aliphatic composition of *n*-alkanes, isoalkanes, and cycloalkanes of natural gases from the Sulige gas field (**Figure 10B**), it can be seen that *n*-alkane content of Sulige natural gas samples in the range of 12.2%–25.9%, with an average of 19.2%; isoalkane content in the range of 21%–62.1%, with an average of 49%; and cycloalkane content in the range of 14.5%–68%, with an average of 31.8%. The C_{5-7} aliphatic compositions show that natural gases from the Sulige gas field are rich in isoparaffins and cycloalkanes, indicating that natural gases from the Sulige gas field are typical coal-formed gases mostly originated from humic parent material.

4.4.3 Distribution Characteristics and Genesis Identifications of C_8 Light Hydrocarbon Aliphatic Compositions

Previous studies suggest that the light hydrocarbon fraction of humic parent material is rich in isoalkanes and aromatics (Leythaeuser et al., 1979; Leythaeuser et al., 1980), and the light hydrocarbon fraction of condensate from terrestrial parent material is rich in

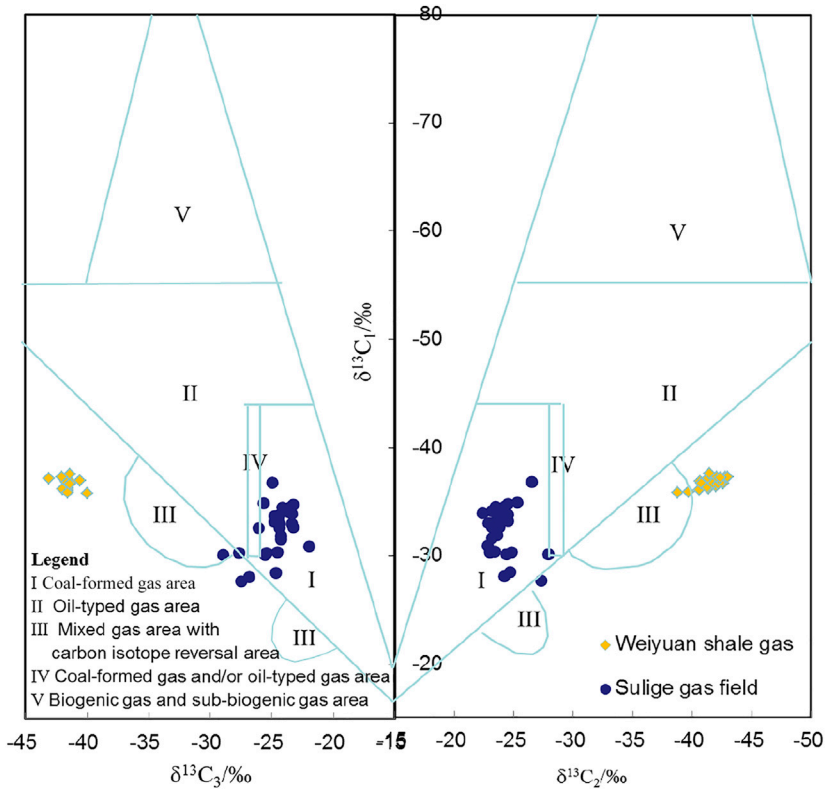

FIGURE 4 | Identification of $\delta^{13}C_1$-$\delta^{13}C_2$-$\delta^{13}C_3$ alkane gas genesis in the Sulige gas field, Ordos Basin (plate According to Dai, 1993; Modified).

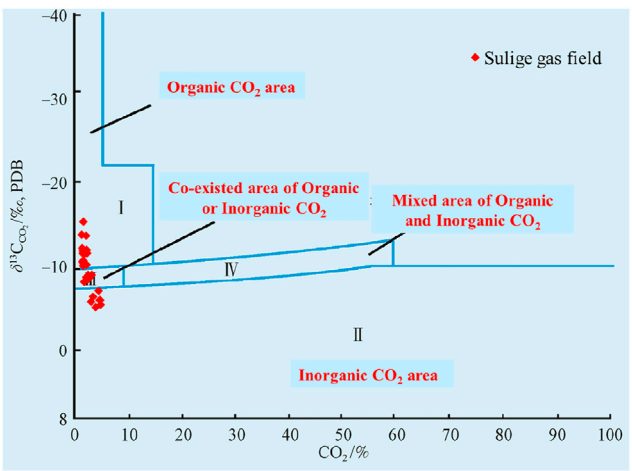

FIGURE 5 | Identification of organic and inorganic carbon dioxide in natural gases from the Sulige gas field (plate according to Dai, 1989).

cycloalkanes (Snowdon and Powell, 1982). Therefore, the relative content of C_8 aliphatic compositions of *n*-alkanes, isoalkanes, and cycloalkanes can also be used to identify natural gas genesis. In this study, based on a large number of experimental analysis and statistics of light hydrocarbons, the following indicators and ternary diagram were established for the identification of coal-formed gas and oil-typed gas by the relative contents of C_8 light hydrocarbon *n*-alkane, isoalkane, and cycloalkane compositions. 1) When $0 \le C_8$ *n*-alkane relative content $\le$ 20%, 20% $\le C_8$ cycloalkane relative content $\le$ 100%, and 0% $\le C_8$ isomeric alkane relative content $\le$ 70%, natural gas is generally coal-formed gas. 2) When 20% $\le C_8$ n-alkane relative content $\le$ 100%, $0 \le C_8$ cycloalkane relative content $\le$ 50%, and 20% $\le C_8$ isoalkane relative content $\le$ 60%, natural gas is generally oil-typed gas. According to the ternary diagram of C_8 aliphatic compositions for natural gases from the Sulige gas field (**Figure 11A**), *n*-alkane content of natural gas samples is in the range of 4%–18.2%, with an average of 7.9%; isoalkane content in the range of 10%–64.9%, with an average of 52.6%; and cycloalkane content in the range of 21.4%–86.3%, with an average of 39.5%. The C_8 aliphatic compositions show that natural gases from the Sulige gas field is rich in isoalkanes and cycloalkanes, indicating that natural gases from the Sulige gas field are typical coal-formed gases generated from humic parent material.

4.4.4 Distribution Characteristics and Genesis Identifications of C_8 Light Hydrocarbon Compounds

C_8 light hydrocarbon system compounds include cis-1,3-dimethylcyclohexane, *n*-octane, and 2-methylheptane. Dimethylcyclohexane is mostly derived from lignin and cellulose of higher plants, reflecting the characteristics of terrestrial parent material. While *n*-octane is mostly from algae and bacteria, 2-methylheptane is mostly from lipid-like compounds of aquatic

TABLE 4 | Some isotopic ratios of noble gases of natural gases in the Sulige gas field, Ordos Basin.

Gas field	Well	Strata	$^{3}He/^{4}He$ (10^{-8})	R/Ra	$^{20}Ne/^{22}Ne$	$^{21}Ne/^{22}Ne$	$^{40}Ar/^{36}Ar$	$^{38}Ar/^{36}Ar$	$^{129}Xe/^{130}Xe$	$^{132}Xe/^{130}Xe$
Sulige	S47-44-37	P	7.30	0.052	9.74	0.0295	610	0.1923		6.674
	S48-5-84	P	6.08	0.043	9.63	0.0309	1018	0.1959		6.639
	S53	P	7.12	0.051	9.66	0.0304	872	0.1908	6.460	6.694
	S10-42-48	P	4.55	0.032	9.68	0.0298	1093	0.1921	6.404	6.671
	S20-16-16	P	5.07	0.036	9.63		1190	0.1961		6.678
	S20-15-14	P	5.15	0.037	9.69	0.0301	1062	0.1935	6.362	6.696
	S14-5-52	P	4.37	0.031	9.56	0.0299	630	0.1919	6.437	6.642
	S14-4-47	P	4.48	0.032	9.64	0.0295	696	0.1904	6.404	6.660
	S14-17-34	P	5.52	0.039	9.62	0.0298	1163	0.1923	6.356	6.669
	S14-16-42	P	4.91	0.035			518	0.1890	6.469	6.652
	S11-18-36	P	6.74	0.048	9.63	0.0297	1197	0.1981	6.407	6.685
	Z61	P	4.48	0.032	9.67	0.0315	964	0.1918	6.462	6.638
	S75-79-34H	P	4.69	0.034	9.70		1786	0.1900	6.424	6.646
	S38	P	5.17	0.037			1391	0.1883	6.461	6.729
	S75	P	4.84	0.035			1030	0.1904	6.469	6.660
	S95	P	4.96	0.035			1195	0.1896	6.426	6.679
	S55	P	2.94	0.021			1289	0.1882	6.440	6.695
	S148	P	3.84	0.027			1940	0.1939	6.447	6.668
	S5-15-8	P	2.89	0.021			1327	0.1897	6.479	6.663
	S76	P	3.13	0.022			602	0.1836	6.422	6.649
	S54-24-65	P	4.59	0.033			1928	0.1926	6.477	6.642
	S77-4-6	P	3.06	0.022			1765	0.1923	6.431	6.629
	S120-79-69	P	5.58	0.040			1403	0.1959	6.417	6.634
	S48-2-86	P	3.72	0.027			1350	0.1918	6.464	6.731
	S109	P	5.28	0.038			506	0.1707	6.440	6.674
	S77-70-13	P	4.48	0.032			1316	0.1919	6.471	6.711
	T7-9-2	P	5.05	0.036						

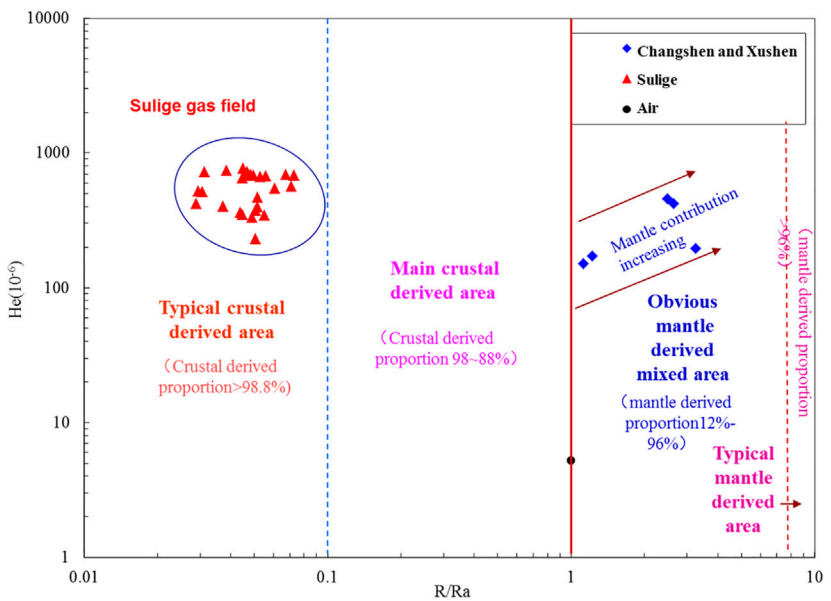

FIGURE 6 | Genesis identification chart of He and R/Ra of natural gases in the Sulige gas field, Ordos Basin (Plate according to Wang et al. 2013, Wang et al. 2016).

organisms, both reflecting the characteristics of oil-typed gas light hydrocarbons. Similarly, we also established a ternary diagram to identify coal-formed gas and oil-typed gas by the relative contents of cis-1,3-dimethylcyclohexane, *n*-octane, and 2-methylheptane of C_8 light hydrocarbon system compounds: 1) when 40% ≤ cis-1,3-dimethylcyclohexane relative content ≤ 100%, *n*-octane relative percentage content ≤ 40%, and 2-methylheptane relative percentage content ≤ 40%, natural gas is generally coal-formed gas. 2) When 0 ≤ cis-1,3-dimethylcyclohexane relative content ≤ 40%, 30% ≤ n-octane relative percentage ≤ 100%, and 0 ≤ 2-

methylheptane relative percentage ≤ 50%, natural gas is generally oil-typed gas. According to the ternary diagram of C_8 light hydrocarbon cis-1,3-dimethylcyclohexane, *n*-octane, and 2-methylheptane in the Sulige gas field, the relative contents of cis-1,3-dimethylcyclohexane, *n*-octane, and 2-methylheptane are 31.1%–92.2%, with an average of 56.6%; 2-methylheptane is 3.3%–36.3%, with an average of 20.1%; *n*-octane is 4.5%–46.9%, with an average of 23.3%; and *n*-octane is 4.5%–46.9%, with an average of 20.1%. The relative contents of 2-methylheptane is in the range of 3.3%–36.3%, with an average of 20.1%; the relative contents of *n*-octane is in the range of 4.5%–46.9%, with an average of 23.3%. Therefore, the aliphatic compositions of the C_8 light hydrocarbon compounds in the Sulige gas field is rich in cis-1,3-dimethylcyclohexane. The gas samples from the Upper Paleozoic tight gas field in the Sulige gas field fall into the coal-formed gas region (**Figure 11B**) and show typical coal-formed gas generated from humic parent material.

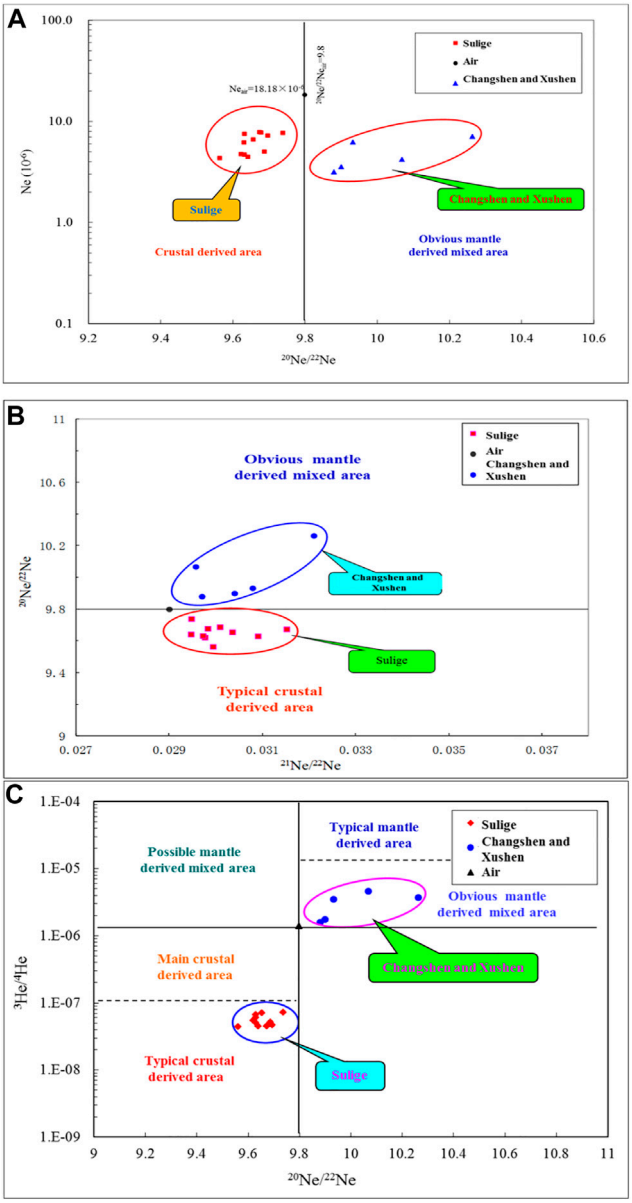

FIGURE 7 | Genesis identification chart of Ne and $^{20}Ne/^{22}Ne$ **(A)**, $^{20}Ne/^{22}Ne$ and $^{21}Ne/^{22}Ne$ **(B)**, and $^{3}He/^{4}He$ and $^{20}Ne/^{22}Ne$ **(C)** of natural gases in the Sulige gas field in Ordos Basin (Plate according to Wang et al. 2013, Wang et al. 2016).

5 GAS SOURCE CORRELATIONS OF THE SULIGE GAS FIELD IN ORDOS BASIN

5.1 Conventional Gas Source Correlations of the Sulige Gas Field

In total, two sets of source rocks are developed in Paleozoic of Ordos Basin: Carboniferous-Permian coal measure source rocks of Upper Paleozoic and marine carbonate source rocks of Lower Paleozoic. The Carboniferous-Permian coal measure source rocks are considered as the main source rocks in Ordos Basin (Chen et al., 1993; Dai et al., 1996; Dai et al., 2003; Dai et al., 2005). The coal measure source rocks of Carboniferous-Permian in Ordos Basin are widely distributed throughout the basin, mainly including coals and dark mudstones in Shanxi Formation, Taiyuan Formation, and Benxi Formation. The coals of Benxi, Taiyuan, and Shanxi Formations basically cover the whole basin and are main source rocks of Upper Paleozoic. The cumulative thickness of coals ranges from 4 to 40 m. Dark mudstones are developed in Benxi, Taiyuan, and Shanxi Formations, mainly in Taiyuan Formation and Shan2 member of Shanxi Formation, and widely distribute in upper Paleozoic with total thickness from 20 to 80 m. In Yan'an-Wuqi area in the southern part of Ordos Basin, the highest thermal evolution maturity of source rocks reach 2.8%, decreasing in a ring-like pattern toward north and south and basin margin. The thermal evolution maturity of most parts of the basin are above 1.5%, generally entering high mature to over mature stage.

According to the genetic identification, the natural gases of the Sulige gas field are typical coal-formed gas, mainly from coal measure source rocks of humic parent material. Combing the typical characteristics of existed Paleozoic source rocks in Ordos Basin, it is concluded that the natural gases of the Sulige gas field originate from Carboniferous-Permian coal measure source rocks. Furthermore, by calculating the natural gas maturity of the Sulige gas field, the calculated Ro values of natural gas maturity are mainly distributed from 1.0% to 2.0%, and the maturity of natural gas in southern part of the Sulige gas field is relative higher, while the maturity of natural gas in northern part is relative lower, having a similar trend with maturity of Carboniferous-Permian coal measure source rocks in Ordos Basin. It indicates that the natural gas in the Sulige gas field mainly originates from Carboniferous-Permian coal measure source rocks and also reflects that the natural gas in the Sulige gas field is mainly generated from near source rocks. The coal measure source rocks of Carboniferous-Permian in Ordos are characterized by widespread hydrocarbon generation, and the area with hydrocarbon generation intensity greater than 12×10^8 m^3/km^2 accounting for 71.6% of the total basin. The source rocks of the Sulige gas field and its nearby area have a

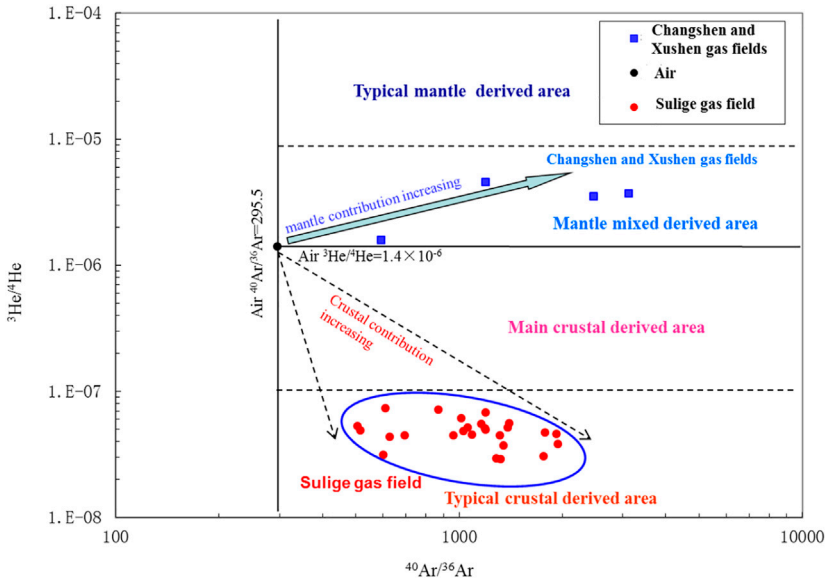

FIGURE 8 | Genesis identification chart of $^3He/^4He$ and $^{40}Ar/^{36}Ar$ of natural gases in the Sulige gas field in Ordos Basin (Plate according to Wang et al. 2013, Wang et al. 2016).

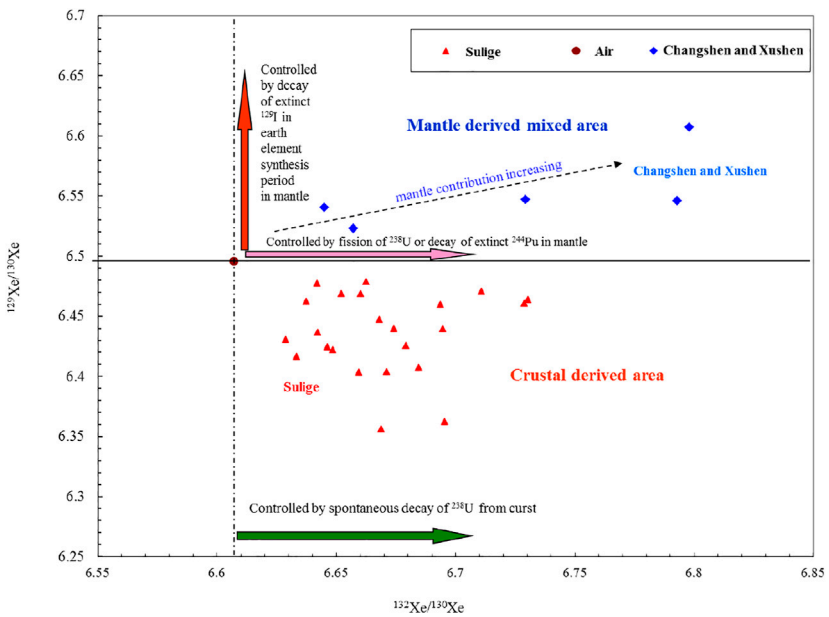

FIGURE 9 | Genesis identification chart of $^{129}Xe/^{130}Xe$ and $^{132}Xe/^{130}Xe$ of natural gases in the Sulige gas field in Ordos Basin (Plate according to Wang et al. 2013, Wang et al. 2016).

gas generation intensity of (12–30)×10^8 m^3/km^2 (Li et al., 2012; Zhao et al., 2013a).

Therefore, the natural gases from the Sulige gas field are typical coal-formed gas in high mature to over mature stage, mainly generating from coal measure source rocks of Upper Paleozoic Carboniferous-Permian in Ordos Basin.

5.2 Noble Gas Sources Correlation of the Sulige Gas Field

Based on the noble gas isotope analysis, the gas source comparison study of Ordos Sulige gas was further conducted by using helium and argon isotopes and argon isotope age accumulation effect. The $^3He/^4He$ values (R) of

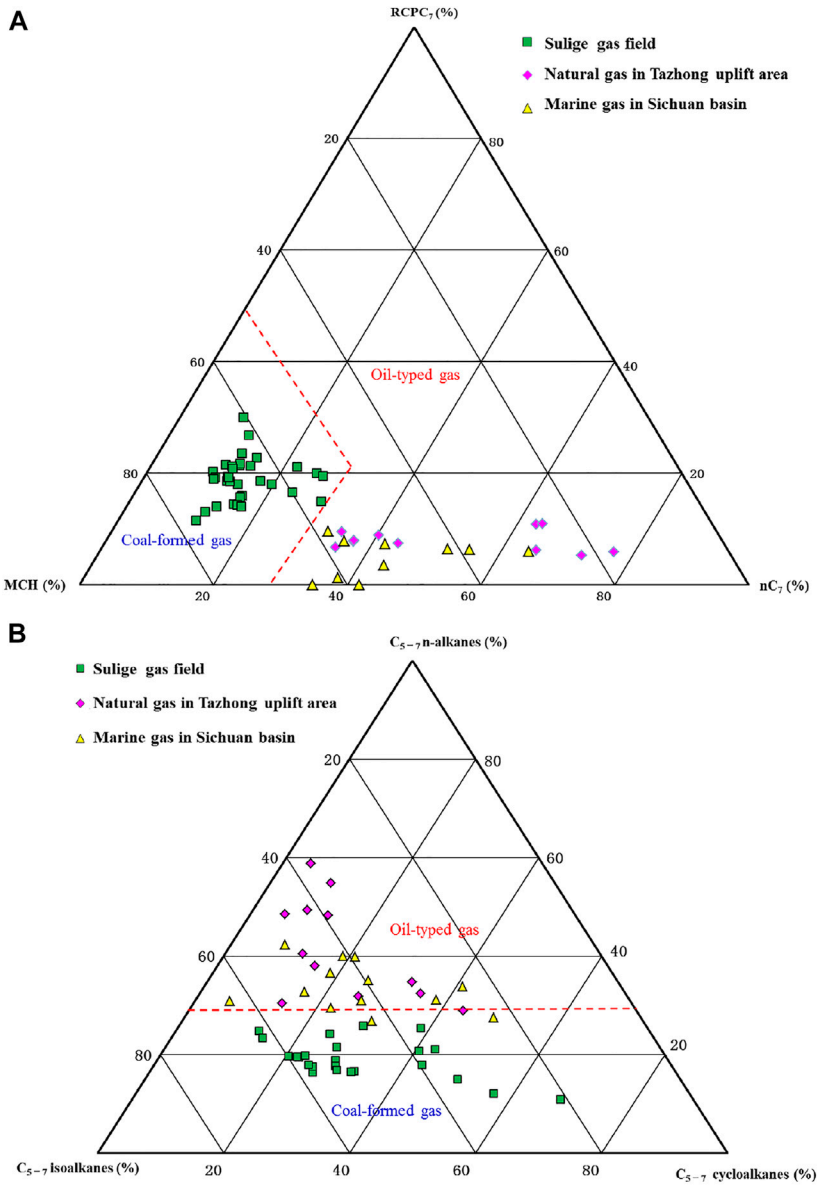

FIGURE 10 | Ternary diagram of the C_7 compositions **(A)** and C_{5-7} **(B)** light hydrocarbons system in the Sulige gas field (Plate according to Hu et al., 2007)

gas samples from the Sulige gas field mainly distribute around $(2.89–7.30)\times10^{-8}$ $(0.021\sim0.052R_a)$,with an average value of 4.81×10^{-8} $(0.034R_a)$, which is in the order of 10^{-8} with an overall distribution in $0.01<R/R_a<0.10$. It shows that noble gas helium in natural gas of the Sulige gas field is a typical crustal source genesis, and the proportion of crustal source contribution is more than 98.8%, mainly coming from decay of crustal source radioactive elements U and Th. Therefore, comparative gas source studies can be performed by using natural gas argon isotope age accumulation effect. The $^{40}Ar/^{36}Ar$ values of gas samples from the Sulige gas field are relatively high and widely distributed, mainly in the range of 506–1940, with an average value of 1148. The average value is in the range of 920–1450 for natural gas generated from Carboniferous-Permian source rocks (Shen et al., 1995). Furthermore, based on the relationship between argon isotopes of clastic strata and parent source stratigraphic age proposed by Xu et al. (1996), parent source stratigraphic age of natural gases in the Sulige gas field is estimated to be about 299 Ma, which is in the range of 250~355 Ma for Carboniferous-Permian coal measure source rocks in Upper Paleozoic of Ordos Basin. Therefore, the natural gases in the Sulige gas field mainly originate from Carboniferous-Permian coal measure source rocks of Upper Paleozoic. The comparative study of noble gas source correlations in the Sulige gas field by using age accumulation effect of argon isotopes of natural gas provides evidences for gas source correlation from a noble gas point of view, which is

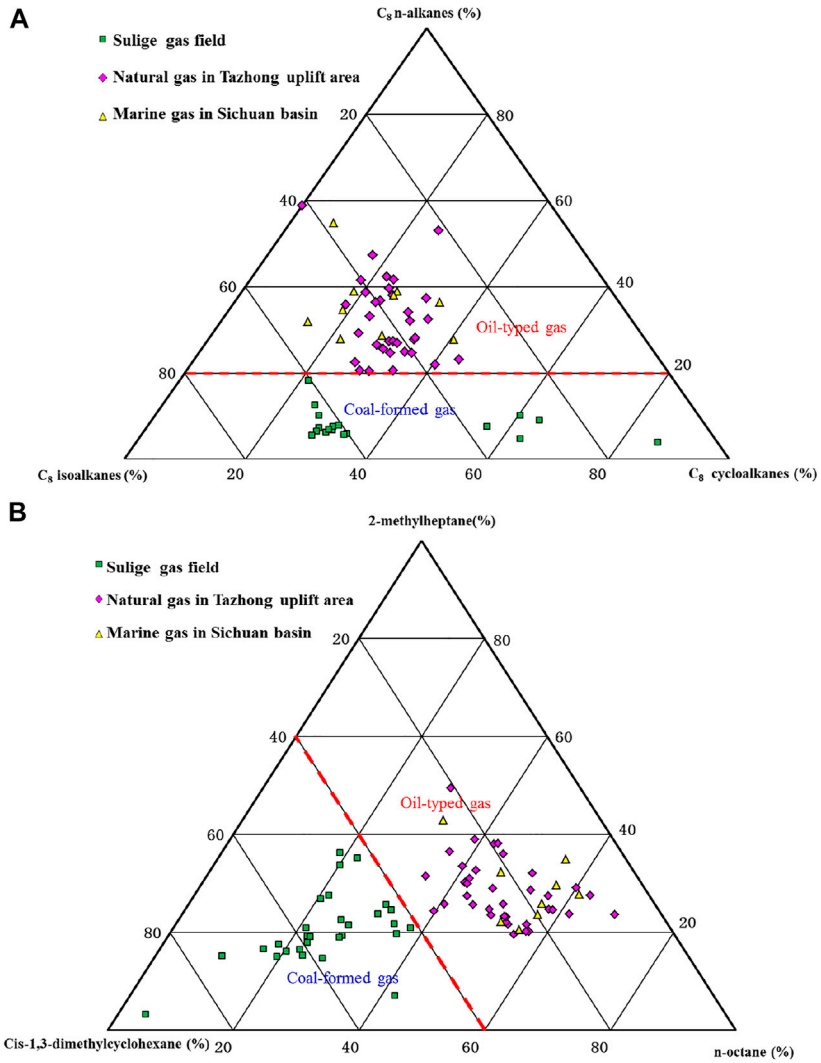

FIGURE 11 | Ternary diagram of C_8 light hydrocarbon aliphatic **(A)** and C_8 light hydrocarbon compounds **(B)** in natural gases from the Sulige gas field.

consistent with the results obtained by conventional gas source correlation methods by alkane gas isotopes, further deepening the understandings of gas sources in the Sulige gas field.

5.3 Quantitative Evaluation of Gas Sources Contributions From Noble Gas and Alkane Gas Isotopes for the Sulige Gas Field

Since coal measure source rocks usually contain coals and mudstones, the average content of K in Chinese coals is about 0.214% and the average content of potassium in Chinese mudstones is about 2.67%. Due to great differences on potassium content between coals and mudstones, the $^{40}Ar/^{36}Ar$ values in natural gas produced from coals is relatively low and in natural gas produced from mudstones in relatively high (Liu and Xu, 1987, 1993; Zhang et al., 2005). Therefore, the source contribution proportions of coals and mudstones can be quantitatively studied by the noble gas argon isotope $^{40}Ar/^{36}Ar$. The distribution of $^{40}Ar/^{36}Ar$ in the natural gases of the Sulige gas field ranges from 506 to 1940, and the average value is about 1148. The minimum value of $^{40}Ar/^{36}Ar$ in Upper Paleozoic natural gas samples of the Sulige gas field is approximated as the end element value of natural gas generated from coals, and the maximum value of $^{40}Ar/^{36}Ar$ in Upper Paleozoic natural gas samples of the Sulige gas field is approximated as the end element value of natural gas generated from mudstones. So, the source contribution proportions of coals and mudstones in Carboniferous-Permian coal measure source rocks are calculated as 55% and 45%, respectively, by using noble gas argon isotope of the $^{40}Ar/^{36}Ar$ method.

In addition, the contribution proportions of coals and mudstones in the coal measure source rocks of the Sulige gas field was also quantitatively investigated by using the alkane gas methane carbon isotope method. By comparing the data with previous analyses, the heaviest methane carbon isotope $\delta^{13}C_1$ of the positive sequence of alkane gases carbon isotopes in the Sulige gas field analyzed here is −28.4‰, which can be approximated as the methane carbon isotope end element value of natural gas from coals. The lightest methane

carbon isotope $\delta^{13}C_1$ with positive sequence of alkane gas isotope in Upper Paleozoic of Ordos Basin was found to be −38.1‰ (Dai, 2014), which can be used as the approximate end element value of methane carbon isotope for natural gas production from mudstones. In this study, the average value of methane carbon isotope $\delta^{13}C_1$ in the Sulige gas field is about −32.3‰, and the contribution of coals and mudstones in Carboniferous-Permian coal measure source rocks is calculated as 60% and 40% separately from the alkanes carbon isotope quantification.

Therefore, the Sulige gas field in Ordos Basin is mainly derived from coal measure source rocks of Carboniferous-Permian, and the contribution of coals mainly accounting for 55–60% and the contribution of mudstones accounting for 40–45%.

6 CONCLUSION

1. The Sulige gas field is mainly alkane gases with high methane content; low heavy hydrocarbon contents; high drying coefficient; low non-hydrocarbon gases contents, mainly CO_2 and N_2; and relatively low noble gas contents in general. The helium content is slightly higher than atmospheric content by about two orders of magnitude, while neon, argon, krypton, and exon contents are relatively lower than atmospheric values by about 1,2,2,1 orders of magnitude.
2. Natural gas alkane carbon and hydrogen isotopes are generally distributed in positive sequences, with a few parts inversion. The $^{3}He/^{4}He$ values are mainly distributed around $(2.89–7.30)\times10^{-8}$, with an average of 4.81×10^{-8}. The $^{40}Ar/^{36}Ar$ values are distributed in a wide range, from 506 to 1940, with an average value of 1148. The ^{129}Xe is relatively deficient, while the ^{132}Xe is relatively surplus.
3. The carbon isotopes of alkanes in the Sulige gas field indicate that the natural gases are high mature to over mature coal-formed gas. The genetic identification of C_7 and C_8 light hydrocarbons reflect that the natural gases are typical coal-formed gases, mainly originating from humic source rocks. The comprehensive identification of noble gas isotopes indicate that noble gases are typical crustal genesis, mainly generated from radioactive decay of U, Th, and other elements of crust. The CO_2 in the natural gases are mainly organic in general and partly inorganic.
4. The gas source correlations of noble gases and alkane gases and quantitative evaluation of gas source contributions show that the natural gases in the Sulige gas field mainly come from Carboniferous-Permian coal measure source rocks in Ordos Basin, where the contribution proportion of coals accounts for 55–60%, while the contribution proportion of mudstones accounts for 40–45%. The evaluation results of noble gas argon isotope and alkane gas carbon isotope are basically compatible, further deepening the understandings on gas sources of natural gases in the Sulige gas field.

DATA AVAILABILITY STATEMENT

The original contributions presented in the study are included in the article/Supplementary Material; further inquiries can be directed to the corresponding authors.

AUTHOR CONTRIBUTIONS

All authors listed have made a substantial, direct, and intellectual contribution to the work and approved it for publication.

FUNDING

This study was sponsored by the National Key Research & Development Plan Project (2021YFA0719004), the Program of PetroChina (2018D-500802, 2019B-0604, and 2016ycq03), the Major Project of National Special Science and Technology (2016ZX05007-003), and the Strategic Priority Research Program of the Chinese Academy of Sciences (XDA14010403). Thanks to reviewers for their constructive suggestions. We declare that all sources of funding received for the research being submitted in the manuscript.

REFERENCES

Allègre, C. J., Sarda, P., and Staudacher, T. (1993). Speculations about the Cosmic Origin of He and Ne in the Interior of the Earth. *Earth Planet. Sci. Lett.* 117, 229–233. doi:10.1016/0012-821x(93)90129-w

Allègre, C. J., Staudacher, T., Sarda, P., and Kurz, M. (1983). Constraints on Evolution of Earth's Mantle from Rare Gas Systematics. *Nature* 303, 762–766. doi:10.1038/303762a0

Ballentine, C. J., and O'Nions, R. K. (1992). The Nature of Mantle Neon Contributions to Vienna Basin Hydrocarbon Reservoirs. *Earth Planet. Sci. Lett.* 113, 553–567. doi:10.1016/0012-821x(92)90131-e

Battani, A., Sarda, P., and Prinzhofer, A. (2000). Basin Scale Natural Gas Source, Migration and Trapping Traced by Noble Gases and Major Elements: the Pakistan Indus Basin. *Earth Planet. Sci. Lett.* 181 (1/221), 229–249. doi:10.1016/s0012-821x(00)00188-6

Burnard, P., Zimmermann, L., and Sano, Y. (2013). "The Noble Gases as Geochemical Tracers: History and Background," in *The Noble Gases as Geochemical Tracers, Advances in Isotope Geochemistry*. Editor P. Burnard (New york Dordrecht London: Springer Berlin Heidelberg), 1–15. doi:10.1007/978-3-642-28836-4_1

Chen, A. D., Zhang, W. Z., and Xu, Y. C. (1993). Isotopic Characteristics and Application of Thermal Simulation Products of Hydrocarbon Generation in Sedimentary Rocks. *Chin. Sci. Part B* 23 (2), 9. CNKI: SUN: JBXK.0.1993-02-014.

Chung, E., Aldom, J. E., Chagla, A. H., Kostrzynska, M., Lee, H., and Palmateer, G. (1998). Detection of Cryptosporidium Parvum Oocysts in Municipal Water Samples by the Polymerase Chain Reaction. *J. Microbiol. Methods* 33 (2), 0–180. doi:10.1016/s0167-7012(98)00050-5

Chung, H. M., Rooney, M. A., and Claypool, G. E. (1991). "Thermal Maturity of Oils," in *Organic Geochemistry Advances and Applications in Energy and the Natural Environment, Organic Geochemistry. 15th Meeting of European Association of Organic Geochemists Poster Abstracts*. Editor D. Manning, 14.

Clarke, W. B., Jenkins, W. J., and Top, Z. (1976). Determination of Tritium by Mass Spectrometric Measurement of 3He. *Int. J. Appl. Radiat. Isotopes* 27, 515–522. doi:10.1016/0020-708x(76)90082-x

Compilation group of petroleum geology of Changqing Oilfield (1992). *Petroleum Geology of China (Volume 12) (Changqing Oilfield)*. Beijing: Petroleum Industry Press, 10–90. (in Chinese).

Dai, J., Ni, Y., Huang, S., Gong, D., Liu, D., Feng, Z., et al. (2016). Secondary Origin of Negative Carbon Isotopic Series in Natural Gas. *J. Nat. Gas Geoscience* 1 (1), 1–7. doi:10.1016/j.jnggs.2016.02.002

Dai, J. X., Chen, J. F., and Zhong, N. N. (2003). *Large Gas Fields in China and Their Gas Sources*. Beijing: Science Press, 83–163. (In Chinese).

Dai, J. X. (2014). *Coal-derived Large Gas Fields and Their Gas Sources in China*. Beijing: Science Press, 212–233.

Dai, J. X. (1993). Hydrocarbon Isotope Characteristics of Natural Gas and Identification of Various Natural Gases. *Nat. Gas. Geosci.* 4 (2), 1–40. (In Chinese with English abstract).

Dai, J. X. (1992). Identification and Distinction of Various Alkenes Gases. *Sci. China (Series B)* 35 (10), 1246–1257.

Dai, J. X., Li, J., Ding, W. W., Hu, G. Y., Luo, X., Tao, S. Z., et al. (2005). Geochemical Characters of the Giants Gas Accumulations with over One Hundred Billion Cubic Meters Reserves in China. *Pet. Explor. Dev.* 32 (4), 16–23. (In Chinese).

Dai, J. X., Ni, Y. Y., and Dong, D. Z. (2021). 2021-2025 Is a Period of Great Development of China's Natural Gas Industry: Suggestions on the Exploration and Development of Natural Gas during the 14th Five-Year Plan in China. *Nat. Gas. Geosci.* 32 (1), 1–16. doi:10.1016/j.jnggs.2021.08.001

Dai, J. X., Ni, Y. Y., and Wu, X. Q. (2012). Tight Gas in China and its Significance in Exploration and Exploitation. *Petroleum Explor. Dev.* 39 (3), 257–264. (In Chinese with English abstract). doi:10.1016/s1876-3804(12)60043-3

Dai, J. X., Ni, Y. Y., and Wu, X. Q. (2013). Tight Sandstone Gas in China and its Significance in Exploration and Development. *Petroleum Explor. Dev.* 39 (3), 257–264.

Dai, J. X., and Qi, H. F. (1989). The Relationship between $\delta^{13}C$ and Ro in Coal Derived Hydrocarbon in China. *Chin. Sci. Bull.* 34 (9), 690–692.

Dai, J. X., Song, Y., and Zhang, H. F. (1996). Main Controlling Factors for the Formation of Large and Medium-Sized Gas Fields in China. *Chin. Sci. Ser. D* 26 (6), 481–487. CNKI: SUN: JDXK.0.1996-06-000.

Dai, J. X., Song, Y., and Zhang, H. F. (1997). *Natural Gas Accumulation Zones in China*. Beijing: Science Press. (In Chinese).

Du, J. G. (1989). The Geochemistry of Light Noble Gases. *Geol. Geochem.* 4 (1), 56–59.

Feng, Q., Geng, A. S., Liao, Z. W., and Zhang, X. L. (2007). Carbon and Hydrogen Isotopic Compositions of Coal-Genetic Natural Gases and Their Applications in Accumulation in Upper Palezoic. *Ordos Basin* 36 (3), 261–266.

Fu, J. H., Duan, X. W., and Xi, S. L. (2000). Characteristics of Upper Paleozoic Gas Reservoirs in Ordos Basin. *Nat. Gas. Ind.* 20 (6), 17–19. (In Chinese with English abstract).

Fu, J. H., Fan, L. Y., Liu, X. S., and Huang, D. J. (2019). Gas Accumulation Conditions and Key Exploration & Development Technologies in Sulige Gas Field. *Acta Pet. Sin.* 40 (2), 240–256. doi:10.7623/syxb201902013

Fu, J. H., Guo, S. B., Liu, X. S., and Wang, Y. G. (2013). Shale Gas Accumulation Condition and Exploration and Exploration Potential of the Upper Paleozoic Shanxi Formation in Ordos Basin. *J. Jilin Univ. (Earth Sci. Ed.* 43 (2), 382–389. doi:10.13278/j.cnki.jjuese.2013.02.001

Guo, Q., Nie, J. W., Li, J. F., Li, J. F., Feng, X. P., and Xeng, Z. B. (2020). Research and Application Effect of Natural Gas Accumulation Model in Western Area of Sulige Gas Field. *Prog. Geophys. (in Chinese)* 35 (5), 1784–1791. doi:10.6038/pg2020DD0496

He, Z. X., Fu, J. H., and Xi, S. L. (2003). Geological Characteristics of Reservoir Formation in Sulige Atmospheric Field. *Journal of petroleum* 24 (2), 6–12. (In Chinese with English abstract).

Hiyagon, H., Ozima, M., Marty, B., and Zashu, S. (1992). Noble Gases in Submarine Glasses from Mid Oceanic Ridge and Loihi Seamount: Constraints on Early History of the Earth. *Gechim. Cosmochim. Acta* 56, 1301.

Honda, M., McDougall, I., Patterson, D. B., and Doulgeris, A. (1991). Possible Solar Noble-Gas Component in Hawaiian Basalts. *Nature* 349, 149–151. doi:10.1038/349149a0

Honda, M., Patterson, D. B., McDougall, I., and Falloon, T. J. (1993). Noble Gases in Submarine Pillow Basalt Glasses from the Lau Basin: Detection of a Solar Component in Back-Arc Basalts. *Earth Planet. Sci. Lett.* 120, 135. doi:10.1016/0012-821x(93)90235-2

Hu, A. P., Li, J., Zhang, W. Z., Li, Z. S., Hou, L., and Liu, Q. Y. (2008). Geochemical Characteristics and Origin of Gases from the Upper, Lower Paleozoic and the Mesozoic Reservoirs in the Ordos Basin, China. *Science in China Series D Earth Sciences* 51 (Suppl. 1), 183–194. doi:10.1007/s11430-008-5005-1

Hu, G. Y., Li, J., Ma, C. H., Li, Z. S., Zhang, M., and Zhou, Q. (2007). Characteristics and Implications of the Carbon Isotope Fractionation of Desorbed Coalbed Methane in Qinshui Coalbed Methane Field, China. *Earth Science Frontiers* 14 (6), 267–272. doi:10.1016/s1872-5791(08)60015-9

Hu, G. Y., Luo, X., and Li, Z. S. (2010). Geochemical Characteristics and Origin of Light Hydrocarbons in Biogenic Gas. *Science China (Earth Sciences)* 53 (6), 832–843. doi:10.1007/s11430-010-3072-6

Hu, G. Y., Wang, W. S., and Liao, F. R. (2012). Geochemical Characteristics and its Influencing Factors of Light Hydrocarbon in Coal-Derived Gas: A Case Study of Sichuan Basin. *Acta Petrologica Sinica* 28 (3), 905–916.

Hu, T. L., Ge, B. X., and Chang, Y. G. (1990). The Development and Application of Fingerprint Parameters for Hydrocarbons Absorbed by Source Rocks and Light Hydrocarbon in Natural Gas. *Petroleum Geology & Experiment* 12 (4), 375–379. (in Chinese).

Hu, W. R. (2009). *Introduction to Low Permeability Oil and Gas, Volume I, the Rapidly Rising Ordos Basin*. Beijing: Petroleum Industry Press. (In Chinese).

Jia, A. L., He, D. B., Wei, Y. S., and Li, Y. L. (2021). Predictions on Natural Gas Development Trend in China for the Next Fifteen Years. *Natural Gas Geoscience* 32 (1), 17–27. doi:10.1016/j.jnggs.2021.04.005

Jia, A. L., Wang, G. T., Meng, D. W., Guo, Z., Ji, G., and Chen, L. H. (2018). Well Pattern Infilling Stragergy to Enhance Oil Recovery of Giant Low-Permeability Tight Gas Field: a Case Study of Sulige Gas field,Ordos Basin. *Acta Petrolei Sinica* 39 (7), 802–813. doi:10.7623/syxb201807007

Jiang, Z. S., Hu, G. Y., Li, Z. S., Zhang, Y., and Xie, Z. Y. (1999). The Novel Approach of the Correlation between Paleozoic Natural Gas and Source Rock in Ordos Basin. *Acta Sedimentologica Sinica* 17 (Sup), 820–823.

Kang, Z. L., Fu, C. D., and Cui, S. F. (2000). *Introduction to Large and Medium-Sized Gas Fields in China*. Beijing: Petroleum Industry Press. (In Chinese).

Kennedy, B. M., Hiyagon, H., and Reynolds, J. H. (1990). Crustal Neon: A Striking Uniformity. *Earth Planet Science Letters* 98, 277–286. doi:10.1016/0012-821x(90)90030-2

Lee, J. Y., Marti, K., Severinghaus, J. P., Kawamura, K., Yoo, H. S., Lee, J. B., et al. (2006). A Redetermination of the Isotopic Abundances of Atmospheric Ar. *Geochim. Cosmochim. Acta* 70 (17), 4507–4512. doi:10.1016/j.gca.2006.06.1563

Leythaeuser, D., Schaefer, R. G., and Cornford, C. (1979). Generation and Migration of Light Hydrocarbon (C_2-C_7) in Sedimentary Basin. *Organic Geochemistry* 1, 191–204. doi:10.1016/0146-6380(79)90022-6

Leythaeuser, D., Schaefer, R. G., and Yükler, A. (1980). Diffusion of Light Hydrocarbons through Near-Surface Rocks. *Nature* 284 (5756), 522–525. doi:10.1038/284522a0

Li, J., Luo, X., Li, Z. S., Jiang, Z. S., Hu, G. Y., Xie, Z. Y., et al. (2003). New Issue of Carbon Isotope Composition of Toluene to Be as Index of Gas-Rock Correlation. *Natural Gas Geoscience* 14 (3), 177–180.

Li, J., Xie, Z. Y., Li, Z. S., Luo, X., Hu, G. Y., and Gong, S. (2001). Gas-Source Correlation of Natural Gas in Kuqa Depression, Tarim Basin. *Petroleum Exploration and Development* 28 (5), 29–32. CNKI:SUN:SKYK.0.2001-05-007.

Li, X. Q., Li, J., Wang, K. D., Kong, L. X., Feng, S. B., Huang, X. B., et al. (2012). Charging, Migration and Accumulation Characteristics of Natural Gas in the Sulige Low Permeability Sandstone Large Gas Field. *Geological Science and Technology Information* 31 (3), 55–62.

Lin, L. B., Lin, H. B., Hou, M. C., Chen, H. D., and Dong, G. Y. (2009). Geochemistry and Accumulation of the Upper Paleozoic Natural Gas in the Sulige Gas Field, Ordos Basin. *Sedimentary Geology and Tethyan Geology* 29 (2), 77–82.

Liu, G., Sun, M., and Zhao, Z. (2013). Characteristics and Accumulation Mechanism of Tight Sandstone Gas Reservoirs in the Upper Paleozoic, Northern Ordos Basin, China. *Petroleum Science* 10 (4), 442–449. doi:10.1007/s12182-013-0294-1

Liu, Q. Y., Liu, W. H., Xu, Y. C., Li, J., and Chen, M. J. (2007). Geochemistry of Natural Gas and Crude Composition of Gas-Generated Contribution for Various Source Rocks in Sulige Gas field,Ordos Basin. *Natrual Gas Geosicence* 18 (5), 697–705.

Liu, W. H., and Xu, Y. C. (1987). "Relationship between Argon in Natural Gas and Kalium-Argon in Source Rock," in *Lanzhou Institute of Geology, Chinese Academy of Science. Research Annual Report for Biology, Gas Geochemistry Laboratory* (Lanzhou: Gansu Science and Technology Press), 191–200.

Liu, W. H., and Xu, Y. C. (1993). The Significance of Helium and Argon Isotopic Composition in Natural Gases. *Chinese Science bulletin* 38 (9), 818–821.

Liu, X. S., Xi, S. L., and Fu, J. H. (2000). Natural Gas Generation of Upper Paleozoic in Ordos Basin. *Natural gas industry* 20 (6), 19–23. (In Chinese with English abstract).

Lupton, J. E., and Evans, L. (2004). The Atmospheric Helium Isotope Ratio: Is it Changing? *Geophys. Res. Lett.* 18 (3), 482–485.

Lupton, J. E. (1983). Terrestrial Inert Gases: Isotopic Tracer Studies and Clues to Primordia1 Components in the Mantle. *Annual Review Earth Plant Science* 11 (5), 371–414. doi:10.1146/annurev.ea.11.050183.002103

Mamyrin, B. A., Anufrriev, G. S., Kamenskii, I. L., and Tolstikhin, I. N. (1970). Determination of the Isotopic Composition of Air Helium. *Geochem. Int.* 7, 498–505.

Mamyrin, B. A., and Tolstikhin, I. N. (1984). *Helium Isotopes in Nature*. Amsterdam: Elsevier, 287. Developments in geochemistry 3.

Mark, D. F., Stuart, F. M., and Podesta, M. (2011). New High-Precision Measurements of the Isotopic Composition of Atmospheric Argon. *Geochim. Cosmochim. Acta* 75 (23), 7494–7501. doi:10.1016/j.gca.2011.09.042

Ozima, M., and Podesek, F. A. (1983). *Noble Gas Geochemistry*. London: Cambridge University Press, 1–252.

Poreda, R. J., and Farley, K. A. (1992). Noble Gases in Samoan Xenoliths. *Earth Planet. Sci. Lett.* 113, 129–144. doi:10.1016/0012-821x(92)90215-h

Poreda, R. J., Jenden, P. D., Kaplan, I. R., and Craig, H. (1986). Mantle Helium in Sacramento Basin Natural Gas Wells. *Geochimica et Cosmoehimiea Acta* 50 (12), 2 847. doi:10.1016/0016-7037(86)90231-0

Prinzhofer, A. (2013). "Noble Gas in Oil and Gas Accumulations," in *The Noble Gases as Geochemical Tracers, Advances in Isotope Geochemistry*. Editor P. Burnard (New york Dordrecht London: Springer Berlin Heidelberg), 225–247. doi:10.1007/978-3-642-28836-4_9

Sano, Y., Tominaga, T., and Takahata, N. (2008). Accurate Measurement of Atmospheric Helium Isotopes. *Anal. Sci.* 24 (4), 521–525. doi:10.2116/analsci.24.521

Sarda, P., Staudacher, T., and Allegre, C. J. (1988). Neon Isotopes in Submarine Basalts. *Earth Planet. Sci. Lett.* 91, 73–88. doi:10.1016/0012-821x(88)90152-5

Shen, P., Xu, Y. C., and Liu, W. H. (1995). Applied Models of Rare Gas Geochemistry in the Research of Natural Gases. *Acta Sedimentologica Sinica* 13 (2), 48–57.

Snowdon, L. R., and Powell, T. G. (1982). Immature Oil and Condensate-Modification of Hydrocarbon Generation Model for Terrestrial Organic Matter. *AAPG Bulletin* 66 (6), 755–788. doi:10.1306/03b5a313-16d1-11d7-8645000102c1865d

Sun, M. L., Xu, Y. C., and Wang, X. B. (1991). Mass Spectrometer Analysis for He Isotope in Natural Gases. *Journal of instrumental analysis* 10 (5), 50–55. (in Chinese with English abstract).

Wang, J., Zhang, X. B., and Chen, J. F. (2005). Evaluation of the Hydrocarbon-Generating Characteristic for Coal-Bearing Hydrocarbon-Source Rocks of Suligemiao Gas Field. *Coal Geology & Exploration* 33 (2), 26–29.

Wang, X. B., Chen, J. F., and Li, J. (2014). Analysis and Influencing Factors of Rock Diffusion Coefficient in High Temperature and High Pressure Tight Gas Reservoir. *Journal of China University of Petroleum (NATURAL SCIENCE EDITION)* 38 (3), 25–31. (In Chinese with English abstract).

Wang, X. B., Chen, J. F., and Li, J. (2015). Discussion on the Role and Contribution of Diffusion in the Formation of Low Porosity and Permeability Tight Sandstone Gas Reservoir. *Journal of China University of Petroleum (Natural Science Edition)* 39 (5), 58–64. (In Chinese with English abstract).

Wang, X. B., Chen, J. F., Li, Z. S., Li, J., Wang, D. L., Wang, Y. F., et al. (2016). Noble Gases Geochemical Characteristics and Gas Source Correlation for Dabei Gas Field in Kuche Depression, Tarim Basin. *Energy Exploration & Exploitation* 34 (1), 113–128. doi:10.1177/0144598715623673

Wang, X. B., Li, Z. S., Li, J., Wang, D. L., Chen, J. F., Xie, Z. Y., et al. (2013). Technique for Total Composition and Isotope Analyses of Noble Gases. *Acta Petrolei Sinica* 34 (S.1), 70–77. doi:10.7623/syxb2013S1008

Wang, X. B. (1989). *Noble Gas Isotope Geochemistry and Cosmochemistry*. Beijing: Science Press, 7–22.

Wang, X. B., Wei, G. Q., Li, J., Chen, J. F., Gong, S., Li, Z. S., et al. (2018). Geochemical Characteristics and Origins of Noble Gases of the Kela 2 Gas Field in the Tarim Basin, China. *Marine and Petroleum Geology* 89, 155–163. doi:10.1016/j.marpetgeo.2017.02.013

Wei, G. Q., Wang, D. L., Wang, X. B., Li, J., Li, Z. S., Xie, Z. Y., et al. (2014). Characteristics of Noble Gases in Gaoshiti—Moxi Large Gas Field in Sichuan Basin. *Petroleum Exploration and Development* 41 (5), 533–538. doi:10.1016/s1876-3804(14)60069-0

Welhan, J. A., and Craig, H. (1983). "Methane, Hydrogen and Helium in Hydrothermal Fluids at 21°N on the East Pacific Rise," in *Hydrothermal Processes at Seafloor Spreading Centers*. Editors P. A. Rona, K. Bostrom, and L. Laubier (New York: Plenum Press), 391–410. doi:10.1007/978-1-4899-0402-7_17

Welhan, J. A., Poreda, R. J., Rison, W., Poreda, R., and Craig, P. (1983). Geothermal Gases of the Mud Volcano Area, Yellowstone Park. *Eos (Transactions, American Geophysical Union)* 64, 882.

Whiticar, M. J., and Snowdon, L. R. (1999). Geochemical Characterization of Selected Western canada Oils by C_5-C_8 Compound Specific Isotope Correlation (CSIC). *Organic Geochemistry* 30 (7-8), 1127–1161. doi:10.1016/S0146-6380(99)00093-5

Xu, C., Shen, P., Liu, W. H., Tao, M. X., Sun, M. L., and Du, J. G. (1998). *Noble Gas Geochemistry Study in Natural Gas*. Beijing: Science Press, 1–231.

Xu, S., Xu, Y. C., Shen, P., Shun'ichi, N., and Hiroshi, W. (1997). Noble Gas Isotopes in Natural Gases from Central and Northwest China. *Chinese Science bulletin* 41 (12), 115–118. doi:10.1007/bf02882496

Xu, S., Xu, Y. C., Shen, P., Wang, X. B., Du, J. G., Shun'ichi, N., et al. (1996). The Isotopic Composition and its Geological Significance of Neon in Natural Gas of Eastern Basin in China. *Chinese Science bulletin* 41 (21), 970–l972.

Xu, Y. C., Wang, X. B., Wu, R. M., Shen, P., Wang, Y. X., and He, Y. P. (1979). Noble Gas Isotopic Composition of Natural Gases. *Geochimica* 8 (9), 271–282. (in Chinese).

Yang, H., and Liu, X. S. (2014). Progress of Paleozoic Coal-Derived Gas Exploration in Ordos Basin, West China. *Petroleum Exploration & Development* 41 (2), 129–137. doi:10.1016/s1876-3804(14)60017-3

Yang, H., Xi, S. L., and Wei, X. S. (2006). Analysis of Natural Gas Exploration Potential in Sulige Area. *Natural gas industry* 26 (12), 45–48. (In Chinese with English abstract).

Yang, H., Zhang, J., and Wang, F. Y. (2000). Characteristics of Paleozoic Gas Bearing System in Ordos Basin. *Natural gas industry* 20 (6), 7–11. (In Chinese with English abstract).

Yang, J. J., and Pei, X. G. (1996). *Natural Gas Geology in China (Volume IV): Ordos Basin*. Beijing: Petroleum Industry Press. (In Chinese).

Yu, C., Huang, S. P., Gong, D. Y., Liao, F. R., Li, J., and Sun, Q. W. (2013). Partial Reversal Cause of Carbon and Hydrogen Isotope Compositions of Natural Gas: a Case Study in Sulige Gas Field, Ordos Basin. *Acta Petrolei Sinica* 34 (Suppl. 1), 92–101. doi:10.7623/syxb2013s1011

Zhang, D. W., Liu, W. H., Zheng, J. J., Wang, X. F., and Nan, Q. Y. (2005). Identification of Main Gas Source in Kuqa Depression Using Argon Isotope Ratios. *Geochimica* 34 (4), 405–409. (in Chinese with English abstract).

Zhao, W. Z., Bian, C. S., and Xu, Z. H. (2013a). Similarities and Differences in Reservoir Formation between Sulige Gas Field and Xujiahe Formation Gas Field in Central Sichuan. *Petroleum exploration and development* 40 (4), 429–438. doi:10.1016/s1876-3804(13)60054-3

Zhao, W. Z., Hu, S. Y., and Wang, H. J. (2013b). Large Scale Accumulation and Distribution of Medium and Low Abundance Oil and Gas Resources in China. *Petroleum exploration and development* 40 (1), 1–14. doi:10.1016/s1876-3804(13)60001-4

Conflict of Interest: All authors are affiliated with Research Institute of Petroleum Exploration and Development/PetroChina, Changqing Oilfield/Petrochina, China University of Petroleum and University of Chinese Academy of Science. The authors declare that this study received funding from National Key Research & Development Plan Project, PetroChina Company Limited, Major Project of National Special Science and Technology, Chinese Academy of Science. The funders were involved in the study design, collection, analysis, interpretation of data, the writing of this article or the decision to submit it for publication.

frontiers | Frontiers in Earth Science

ORIGINAL RESEARCH
published: 19 July 2022
doi: 10.3389/feart.2022.891252

Genetic Type and Source Analysis of Natural Gas in the Leikoupo Formation of the Sichuan Basin in China

Shengfei Qin[1], Benjian Zhang[2], Chunhu Huang[3], Jiyuan Li[1,4], Jiamei Wang[1,4], Gang Tao[1,4] and Zheng Zhou[5]*

[1]Research Institute of Petroleum Exploration and Development (RIPED), PetroChina, Beijing, China, [2]Exploration and Development Research Institute, Southwest Oil and Gas Company, PetroChina, Chengdu, China, [3]Chuanzhong Gas Mine, Southwest Oil and Gas Company, PetroChina, Suining, China, [4]China University of Mining and Technology, Beijing, China, [5]Lancaster Environment Centre, Lancaster University, Lancaster, United Kingdom

The Middle Triassic Leikoupo Formation is largely extended through the Sichuan Basin, SW China. In this formation, several commercially exploited gas reservoirs have been discovered in western and central parts of the basin. Due to the complicated geochemical signatures of the natural gases in these reservoirs, there are contrasted interpretations about their sources, which hamper the evaluation and exploration for new gas resources in the area. To obtain complete understanding of the natural gas sources, the Leikoupo Formation gas reservoirs discovered so far in the Zhongba, Yuanba, Longgang, and Moxi gas fields were selected as the research object of this study. The genetic types and sources of the natural gases in the Leikoupo Formation are discussed based on gas geochemistry combined with their geological background. The natural gas in the top members of the Leikoupo Formation (T_2l^4 or T_2l^3) is partially originated from a humic kerogen contained in the source rocks from the overlying Upper Triassic Xujiahe Formation and from sapropel kerogen from the source rocks of the Leikoupo Formation itself. The natural gas of T_2l^1 member in the lower part of the Leikoupo Formation is mainly sapropel-type probably from the source rock of the Permian Wujiaping Formation, where the Permian Longtan Formation undergoes a phase change into the Wujiaping Formation The reversed $\delta^{13}C_1$ and $\delta^{13}C_2$ trend in the Leikoupo Formation of the Yuanba gas field is due to the more sapropelic source rocks and higher degree of maturity.

Keywords: Sichuan Basin, Leikoupo Formation, natural gases, geochemistry, genetic type, gas source

OPEN ACCESS

Edited by:
Maowen Li,
SINOPEC Petroleum Exploration and Production Research Institute, China

Reviewed by:
Shuai Yin,
Xi'an Shiyou University, China
Guodong Zheng,
Northwest Institute of Eco-Environment and Resources (CAS), China

****Correspondence:***
Shengfei Qin
qsf@petrochina.com.cn

Specialty section:
This article was submitted to Geochemistry, a section of the journal Frontiers in Earth Science

Received: *07 March 2022*
Accepted: *22 June 2022*
Published: *19 July 2022*

Citation:
Qin S, Zhang B, Huang C, Li J, Wang J, Tao G and Zhou Z (2022) Genetic Type and Source Analysis of Natural Gas in the Leikoupo Formation of the Sichuan Basin in China. Front. Earth Sci. 10:891252. doi: 10.3389/feart.2022.891252

1 INTRODUCTION

The Middle Triassic Leikoupo Formation is the latest set of marine strata developed in the Sichuan Basin, China, which is not the main strata for oil and gas exploration, and the exploration and research conducted for the Leikoupo Formation is relatively low. Back in the 1970s, small-scale gas pools were discovered in this set of strata, for example, the third member (T_2l^3) of the Leikoupo Formation in the Zhongba gas field in NW Sichuan (Qin et al., 2007), and the first member (T_2l^1) of the Leikoupo Formation in the Moxi gas field in central Sichuan. With the increasing natural gas exploration, commercial gas reservoirs have been found in the fourth section (T_2l^4) of the Leikoupo Formation in the Longgang and Yuanba gas fields successively in this century, showing that the Leikoupo Formation has good potential for gas exploration. Since the Leikoupo Formation is

dominated by evaporative platform facies as a whole, and evaporites mainly composed of gypsum and dolomite are deposited, it is doubtful whether the Leikoupo Formation formed in such an environment can develop effective source rocks. In addition, the geochemical characteristics of natural gas in the Leikoupo Formation are complex, and the types of natural gas origin are diverse. It is difficult to identify the gas sources, and there are different opinions on the source of natural gas. For example, in the Leikoupo Formation in the Zhongba gas field in western Sichuan, it was believed that all natural gas came from the underlying Permian hydrocarbon source rocks (Dai, 1980). It was also believed that the gas came from biogenic limestone and mudstone of the Leikoupo Formation (Li, 1993; Qin et al., 2007). Some studies suggested that the gas came from Permian sapropel source rock, mixed with a small amount of gas from coal measures (Liao et al., 2013), and some even thought that the gas mainly came from overlying coal measures (Wang, et al., 1989; Zheng, et al., 1990). In the central Sichuan Basin, recoverable gas reservoirs have been found in both the T_2l^4 and T_2l^1 members of the Leikoupo Formation, but the gas geochemical characteristics differ significantly between the reservoirs, and the gas source is highly controversial (Huang, 2014; Liu, et al., 2014; Zhou, et al., 2015; Liu, et al., 2019). Even within the T_2l^4 member, the gas' geochemical signatures are highly variable; the gas indicated to be not only humic-type gas but also sapropel-type, and it is difficult to explain the source of gas.

In this study, the gas reservoirs of the Leikoupo Formation in the Zhongba, Moxi, Longgang, and Yuanba gas fields that have been discovered so far are systematically analyzed using natural gas geochemical methods. The source of natural gas has been elucidated based on the comparative study of Triassic and Permian natural gas types and their source rocks, which in turn provides a basis for natural gas exploration in the Leikoupo Formation.

2 GEOLOGICAL BACKGROUND

The Indo-Chinese early episodic movement at the end of the Middle Triassic made the central Sichuan area rise to land, the seawater withdrew, and the large inland lake basin began to appear, which was an important turning period from marine sedimentation to lacustrine sedimentation in the Sichuan Basin as it ended the deposition of the carbonate platform in Sichuan. The uplift of the Sichuan Basin suffered from denudation, forming the erosion surface at the top of the Middle Triassic Leikoupo Formation. Since the Late Triassic, it has received continental deposits and developed multiple sets of coal-measure source rocks and multiple sets of interbedded sedimentary assemblages of sandstones.

2.1 Strata

There are many oil- and gas-bearing layers in the Sichuan Basin. This study focuses on the gas reservoir in the Leikoupo Formation. The related layers span the Triassic and the upper Permian. The strata from top to bottom are the Upper Triassic Xujiahe Formation (T_3x), Middle Triassic Leikoupo Formation (T_2l), Lower Triassic Jialingjiang Formation (T_1J) and Feixianguan Formation (T_1f), and Upper Permian Changxing Formation (P_3ch) and Longtan Formation (P_31) (**Figure 1**).

The Xujiahe Formation is a fluvial–swamp–lacustrine deposit developed in a humid environment (Luo, 1983, 2011; Li, 2011). Several sets of coal-measure source rocks and sandstone reservoirs are developed. The coal-measure source rocks and sandstones were stacked on top of each other. The Xujiahe Formation is subdivided into T_3x^1 to T_3x^6 members from bottom to top, in which T_3x^1, T_3x^3, and T_3x^5 are mainly coal-measure sources, and the organic matter is mainly kerogen-III type, which is a gas dominated source rock. The T_3x^2, T_3x^4, and T_3x^6 members are dominated by sandstone (Wang, et al., 1997; Yang, et al., 2005; Li et al., 2010) and are good reservoirs for gas storage.

The top of the Leikoupo Formation (T_2l) suffered from dissolution and contact with the overlying Xujiahe Formation in parallel unconformity. The T_2l is mainly composed of grayish-white medium-thick microcrystalline dolomite, argillaceous dolomite, and gray dolomite, with light gray gypsum and thin gray-black shale, which is a high-quality caprock in the whole area, in which the gray-black shale can be used as a hydrocarbon source rock. It is subdivided into T_2l^1 to T_2l^4 members from bottom to top, among which the natural gas reservoirs have been discovered in T_2l^1, T_2l^3, and T_2l^4 members.

The Jialingjiang Formation (T_1j) is composed of gray micrite limestone and dolomite interbedded with a gypsum layer, dolomitic gypsum, and argillaceous dolomite, which is not only a high-quality caprock in the whole area but also a gas reservoir in the Jialingjiang Formation. The top of the Feixianguan Formation (T_1f) consists of mudstone, dolomitic mudstone, gypsum, dolomicrite, micrite, and marlstone. The middle and lower part of the Feixianguan Formation is karst oolitic dolomite and limestone, which has good porosity and permeability and a regional high-quality reservoir rock (Wen, et al., 2012; Zhang, et al., 2013; Zhu, et al., 2013).

The Upper Permian (P_3) includes the Changxing Formation (P_3ch) and the Longtan Formation (P_31) from top to bottom. The Changxing Formation is mainly composed of bioclastic micrite limestone, reef limestone, and dolomite, which is also an important reservoir in central Sichuan (Peng, et al., 2011). The Longtan Formation is mainly composed of marine–continental transitional coal measures and marine biological limestone, which is an important regional hydrocarbon source rock series and the main source rock of Changxing and Feixianguan gas reservoirs such as Longgang and Yuanba gas fields. It should be pointed out that the coal-measure source rocks of the Longtan Formation have undergone phase transformation in some areas and become marine source rocks of the Wujiaping Formation (P_3w), and the hydrocarbon-generating material changed from humic to sapropel-type.

2.2 Gas Reservoir Types

The Leikoupo Formation gas reservoirs include T_2l^1, T_2l^3, and T_2l^4 members. A weathering crust and a karst reservoir are

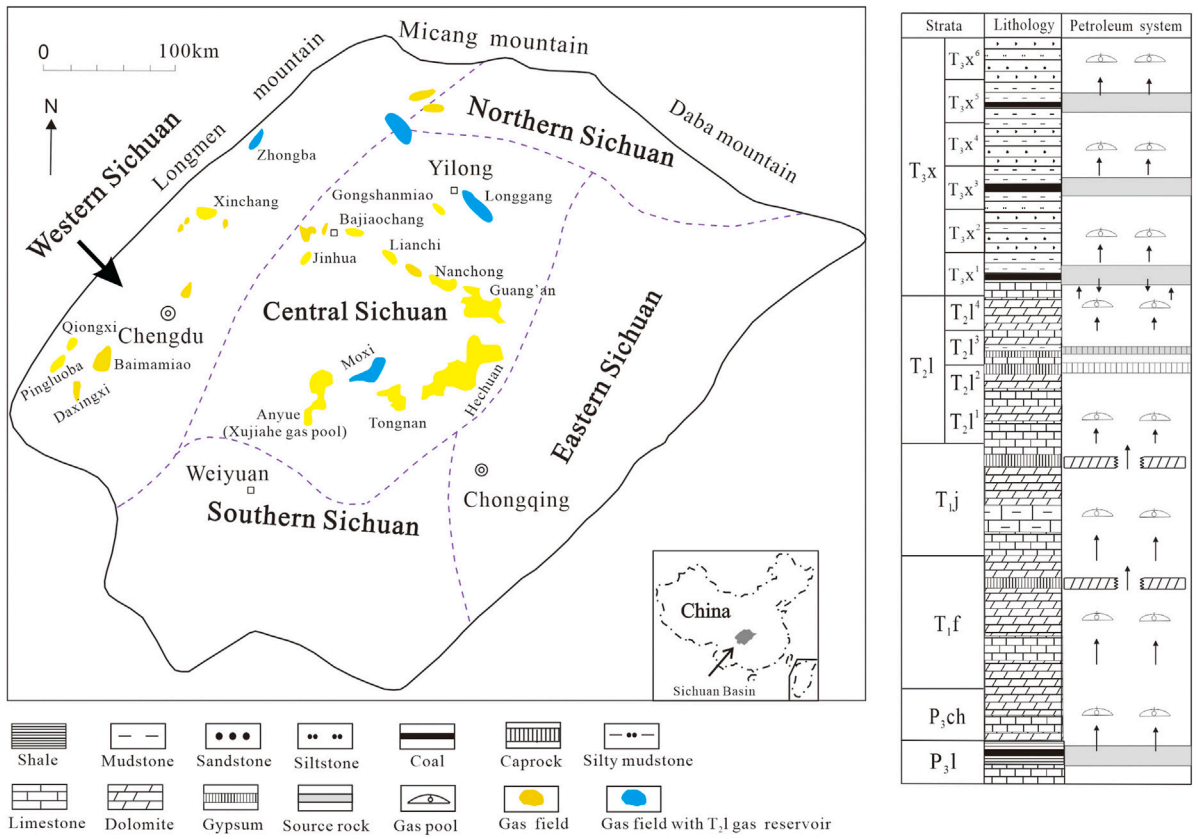

FIGURE 1 | Distribution of main gas fields and the Permian–Triassic petroleum system in the central and western Sichuan Basin.

developed at the top of the Leikoupo Formation, and their distribution are controlled by lithology and paleogeomorphology of exposed strata at the top (Bian, et al., 2019). The T_2l^3 gas reservoir of the Leikoupo Formation in the Zhongba gas field is distributed in the dolomite layer, which is an anticline reservoir type. The top is in an unconformable contact with the overlying Xujiahe Formation, missing the T_2l^4 member (Zeng, et al., 2007). The top surface of the Leikoupo Formation in the Yuanba gas field was affected by denudation and karstification, and a dolomite karst reservoir was formed in the T_2l^4 member. The reservoir is controlled by paleogeomorphology and has strong lateral heterogeneity (Fan, 2014), there is no unified gas–water interface, and natural gas tends to be distributed in structural highs (Liu, et al., 2019); therefore, the reservoir is a karst-controlled structural and lithologic gas reservoir. The reservoir of the T_2l^4 in the Longgang gas field is related to Indosinian denudation and karstification (Yang, et al., 2014), and the natural gas between different wells in the lateral direction is quite different, with obvious heterogeneity, which is a structural and lithologic gas reservoir. The T_2l^1 gas reservoir is currently mainly discovered in the Moxi gas field. This reservoir has a large trap area and is an anticline porous carbonate gas reservoir with a high degree of fullness. It has a unified gas–water interface and is a monolithic gas reservoir.

2.3 Possible Source Rocks

The reason why it is difficult to judge the source of natural gas in the Leikoupo Formation is that there are several sets of different types of source rocks developed in the Leikoupo Formation and it's overly and underlying strata, which may provide a gas source for the Leikoupo gas reservoirs under appropriate geological conditions. This increases the difficulty for identification of Leikoupo gas sources.

The natural gas generated by coal-measure source rocks of the Xujiahe Formation has formed many large- and medium-sized gas fields in the Sichuan Basin. The source rocks directly cover the unconformities of the Leikoupo Formation and might partly provide gas for the karst reservoirs of the Leikoupo Formation.

The Jialingjiang, Feixianguan, and Changxing formations under the Leikoupo Formation did not develop source rocks. Under the Changxing Formation, the marine–terrestrial transitional coal-measure source rocks developed in the Formation had acted as a source rock for many large gas reservoirs in Changxing and Feixianguan formations of Longgang, Yuanba, and Puguang gas fields (Hao, et al., 2008; Wu et al., 2015; Qin, et al., 2016a; Deng, et al., 2018). If conditions permitted, it might also be possible to indirectly supply gas sources to the Leikoupo gas reservoir through the Changxing, Feixianguan, and Jialingjiang formations.

The Leikoupo Formation was formed in a salinized evaporation environment. Many researchers questioned that such an environment could form high-quality source rocks. Theoretically, such a saline environment has weak hydrodynamics, limited seawater circulation, high salinity, and alternating deposition of gypsum salt and carbonate rocks, which is conducive to the preservation of organic matter, and some of the strata can develop high-quality source rocks. Early studies believed that the Leikoupo Formation in the western Sichuan Basin was an algae-rich carbonate rock deposited in deep-water lagoon facies on a confined-evaporative platform and had favorable conditions for forming the main source rock of large- and medium-sized gas fields (Xu et al., 2013). The gypsum-bearing carbonate samples of the Leikoupo Formation in the western Sichuan Basin have relatively high TOC, and the gypsum-dolomite flat and gypsum-bearing lagoon facies with more evaporative platform facies are deposited, which are favorable sedimentary facies belts and lithologic assemblages for the development of high-quality source rocks (Yang, 2016; Wang, et al., 2018b). Other studies have concluded that the TOC of organic-rich shale in the Leikoupo Formation in the Sichuan Basin is 0.49%–1.08%, with an average of 0.77%, and the Ro values are 2.36%–2.40% (Sun, et al., 2021). According to the evaluation standard of a highly mature source rock (Dai, et al., 2008), it is evaluated as a high-quality source rock. The source rock was formed in a dry heat, salt water, and anoxic environment. Drilling revealed that the actual drilling thickness of the Leikoupo Formation in the central and northern Sichuan area is 960 m, of which the T_2l^3 member is the most likely the source rock with a thickness of 530 m, and the lithology is argillaceous limestone, micrite limestone, organic-rich shale rock, salt rock, and gypsum. The T_2l^1, T_2l^2, and T_2l^4 members are dominated by dolomite and gypsum rock, and no source rocks have been found (Sun, et al., 2021).

In fact, it is not uncommon to form source rocks in evaporative environments. In both the Bohai Bay Basin and the tertiary of the Qaidam Basin, the symbiotic phenomenon of evaporite and the source rock had been found (Jin, et al., 2006). In the Junggar Basin (Yu, et al., 2018), Polish Basin (Krzywiec, et al., 2017), Mexico Basin (Xie, et al., 2019), and West Texas–New Mexico (Hussain, et al., 1991), source rocks had been found in an evaporative environment.

3 SAMPLING AND ANALYTICAL METHODS

3.1 Sample Collection

Natural gas samples were taken from the Xujiahe, Leikoupo, Jialingjiang, and Changxing formations in the central Sichuan Basin. To eliminate the interferences of external factors and ensure representativeness of the natural gas in these reservoirs, all samples were collected from wells with long-term normal production without application of de-foaming or any other chemical agents recently.

Gas samples from the reservoirs were taken at the wellheads by using double valve steel cylinders. To take such samples, the pressure gauge was dismantled before connecting the steel cylinder with the sampling tubing. Prior to taking samples, wellhead natural gas was used to flush the steel cylinder thoroughly for about 3 min. The sampling steel cylinder was then filled with natural gas equilibrated to the wellhead pressure.

3.2 Analytical Methods

Natural gas compositions were determined using an Agilent 6890N gas chromatograph (GC) with He and N_2 as the carrier gases. Double thermal conductivity detectors (TCD) and a 30 m × 0.25 mm × 0.25 μm quartz capillary column were used. The inlet temperature was 150 °C, and the TCD temperature was 200 °C. The initial oven temperature was maintained at 40 °C for 7.5 min isothermally, then rose from 40 °C to 90 °C at 15 °C/min, and finally rose from 90 °C to 180 °C at 6 °C/min.

An on-line analysis was conducted for the measurement of carbon isotopic compositions with a MAT 253 gas isotopic mass spectrometer. Natural gas samples were separated to methane, ethane, propane, butane, and CO_2 using the chromatography column of an SRI 8610C gas chromatograph, which were then transferred into a combustion furnace by the carrier gas (He) and oxidized into CO_2 by CuO at 850°C. All of the converted species were transferred by the carrier gas (He) into MS to measure the isotopic compositions. A dual inlet analysis was performed with the international measurement standard of NBS-19 CO_2 (δ^{13}CVPDB=1.95 ± 0.04‰, International Atomic Energy Agency, 1995), and the stable carbon isotopic values were reported in the δ notation in per mil (‰) relative to the Peedee belemnite standard (VPDB). Reproducibility and accuracy were estimated to be ± 0.2‰ with respect to the VPDB standard.

4 ANALYTICAL RESULTS

4.1 Natural Gas Components

The hydrocarbon gas contents of the 38 samples in this study range from 60.19% to 99.71%, with an average of 92.77%. Samples also contain a small amount of N_2, CO_2, and H_2S (**Table 1**). A small number of samples have N_2 content exceeding 10%; other samples have N_2 content of 0–3.8%, with an average of 1.01%. Most of the samples have low CO_2 content, less than 5%. A few samples have higher CO_2 content. The marine carbonate rocks in the reservoirs are accompanied by gypsum salt. This results in the gas reservoirs generally containing H_2S. Most of the natural gas containing H_2S in the world is distributed in such type of strata, and it is considered to be formed by TSR action (Krouse, et al., 1988; Worden, et al., 1995; Machel, 2001; Cross et al., 2004). The content of heavy hydrocarbon gas such as ethane in the hydrocarbon gas is very low, and the dry coefficient (C_1/C_{1+}) of natural gas is very high, ranging from 0.940 to 0.998, with an average of 0.983. Taking more than 0.95 as the criterion for dry gas, all the natural gas in the Leikoupo Formation is dry gas. Among them, the T_2l^1 gas reservoir in the Moxi gas field has the highest dry coefficient, with an average of 0.998, and the T_2l^3 gas reservoir in the Zhongba gas field is the lowest, with an average of 0.97. The T_2l^4 gas reservoirs in the Longgang and Yuanba gas

TABLE 1 | Composition and isotopic data of Permian and Triassic natural gas in the central Sichuan Basin.

Gas Field	Well	Strata	Main Molecular Composition (%)									$\delta^{13}C$ (VPDB)‰			References
			N_2	CO_2	H_2S	CH_4	C_2H_6	C_3H_8	iC_4H_{10}	nC_4H_{10}	$\delta^{13}C_1$	$\delta^{13}C_2$	$\delta^{13}C_3$	$\delta^{13}C_4$	
Zhongba	Zhong 29	T_3x^2	0.39	0.28	0.00	87.86	6.53	2.10	0.60	0.83	−36.7	−25.5	−23.3	−23.5	Qin et al. (2007)
	Zhong 34	T_3x^2	0.70	0.44	0.00	90.71	5.53	1.65	0.31	0.36	−36.1	−25.6	−23.2		Qin et al. (2007)
	Zhong 31	T_3x^2	0.22	0.47	0.00	90.49	6.00	1.62	0.32	0.35	−37.8	−23.0	−29.4	−22.5	Qin et al. (2007)
	Zhong 39	T_3x^2	0.03	0.32	0.00	87.82	6.36	2.70	0.93	1.38	−35.8	−26.0	−23.4	−23.7	Qin et al. (2007)
	Zhong 37	T_3x^2	0.21	0.48	0.00	90.44	5.83	1.62	0.33	0.37	−38.0	−24.4	−25.9	−22.3	Qin et al. (2007)
	Zhong 9	T_3x^2	0.20	0.44	0.00	90.65	5.91	1.61	0.31	0.35	−38.0	−23.9	−25.8	−22.4	Qin et al. (2007)
	Zhong 18	T_2l^3	1.69	4.86	3.30	86.88	1.66	0.53	0.39	0.00	−36.9	−27.7	−22.1	−29.6	Qin et al. (2007)
	Zhong 21	T_2l^3	1.78	3.65	1.78	87.92	1.82	0.54	0.39	0.00	−35.4	−31.1	−30.3	−29.8	Qin et al. (2007)
	Zhong 24	T_2l^3	0.22	4.69	4.11	87.78	1.88	0.56	0.40	0.00	−35.7	−30.3	−27.9		Qin et al. (2007)
Longgang	LG 3	T_3x^6	1.18	0.39	0	92.62	4.42	0.90	0.19	0.14	−37.1	−25.4	−23.8	−22.1	This study
	LG 12	T_3x^6	1.03	0.88	0	95.54	2.07	0.13	0.01	0.01	−37.8	−23.4	−22.2		This study
	LG 17	T_3x^6	0.45	0.43	0	92.16	5.38	0.84	0.19	0.14	−38.7	−25.1	−23.6	−21	This study
	LG 18	T_3x^6	0.5	0.38	0	93.83	4.4	0.55	0.09	0.06	−38.1	−23.6	−21.7	−23.6	This study
	LG 20	T_3x^6	0.87	0.39	0	87.65	7.42	2.15	0.49	0.38	−42.2	−25.6	−22	−21.8	This study
	LG 29	T_3x^6	0.23	0.08	0	97.24	2.13	0.17	0.03	0.02	−35.4	−20.8	−21.6	−18.3	This study
	LG172	T_3x^6	6.99	0.38	0	81.04	6.87	2.32	0.64	0.41	−38.6	−24.9	−23.3	−20.9	This study
	LG176	T_3x^6	0.29	0.54	0	91.32	5.88	1.19	0.21	0.18	−39.9	−24.7	−22.7	−21.5	This study
	LG 177	T_3x^6	0.34	0.54	0	92.64	4.99	0.9	0.17	0.14	−38.9	−25	−23.5	−22.5	This study
	LG 171	T_3x^4	0.19	0.43	0	91.07	6.1	1.37	0.28	0.23	−38.9	−24.2	−21.8	−20.3	This study
	LG 30	T_3x^2	0.26	0.55	0	95.28	3.07	0.43	0.09	0.07	−34.6	−23.5	−22.7	−20.6	This study
	LG176	T_3x^2	0.85	0.27	0	90.69	5.99	1.32	0.23	0.22	−37.9	−24.3	−22.2	−21.7	This study
	LG160	T_3x^2	12.2	0.19	0	77.09	6.81	1.78	0.66	0.36	−38.8	−24.2	−20.9	−21.3	This study
	LG3	T_2l^4	1.39	0.24	Nd*	92.81	4.28	0.83	0.16	0.12	−36.3	−25.1	−23.8	−21.7	This study
	LG7	T_2l^4	0.47	21.65	Nd	76.59	0.9	0.1	0.04	0.03	−37.2	−32.2	−24.3	−22.0	This study
	LG12	T_2l^4	0.31	8.65	Nd	88.1	2.2	0.37	0.06	0.04	−35.5	−26.2	−23.8	−21.7	This study
	LG17	T_2l^4	0.51	35.61	Nd	63.06	0.51	0.02	0	0.01	−35.8	−35.3			This study
	LG18	T_2l^4	0.12	4.59	0.01	94.34	0.79	0.07	0.01	0.01	−36.5	−35.5	−30.5	−27.1	This study
	LG20	T_2l^4	0.01	13.36	0.01	83.46	2.23	0.38	0.09	0.09	−38.4	−29.0	−25.5	−22.8	This study
	LG22	T_2l^4	0.39	1.76	Nd	95.78	1.72	0.19	0.04	0.03	−37.7	−30.8	−27.2		This study
	LG160	T_2l^4	1.27	1.84	Nd	94.18	2.14	0.32	0.06	0.06	−35.3	−26.6	−24.3	−23.8	This study
	LG172	T_2l^4	0.8	1.37	0.01	94.92	2.31	0.35	0.06	0.05	−36.3	−25.3	−24.4	−20.4	This study
	LG176	T_2l^4	0.34	2.42	Nd	95.16	1.71	0.23	0.02	0.02	−37.8	−32.5	−30.6		This study
	LG173	T_2l^4	2.87	0.15	Nd	92.01	2.96	0.65	0.14	0.15	−37.9	−28.5	−24.8		This study
	LG 022-H6	T_2l^4	0.84	0.71	Nd	92.25	4.41	0.83	0.17	0.14	−34.9	−26.5	−23.5	−21.4	This study
	LG 022-H2	T_2l^4	0.91	0.79	Nd	95.29	1.51	0.21	0.04	0.04	−37.2	−32.2	−27.9	−21.1	This study
	LG 022-H8	T_2l^4	1.70	0.24	Nd	91.50	4.33	0.79	0.16	0.13	−38.4	−26.7	−24.3	−21.4	This study
	LG 022-H3	T_2l^4	0.46	0.25	Nd	96.55	1.69	0.21	0.04	0.04	−36.7	−31.6	−26.7	−26.7	This study
	LG 1	T_1f	1.44	2.82	Nd	94.02	0.07	0.00	0.00	0.00	−29.5	−25.0	−20.6		This study
	LG 001–7	T_1f	1.1	2.37	Nd	94.49	0.08	0.01	0.00	0.00	−29.4	−25.2	−23.3	−24.1	This study
	LG 2	T_1f	0.2	4.77	3.06	91.90	0.05				−28.5	−24.3			Qin, et al. (2016a)
	LG 3	T_1f	1.76	15.84	0.04	81.96	0.11				−31.0	−22.8			Qin, et al. (2016a)
	LG 12	T_1f	2.84	1.12	Nd	95.70	0.09				−30.5	−27.3			Qin, et al. (2016a)
	LG 26	T_1f	0.59	7.09	2.75	89.48	0.06	0.01			−29.1	−25.8			Qin, et al. (2016a)
	LG 1	P_3ch	0.7	4.41	2.48	92.33	0.07				−29.4	−24.3			Qin, et al. (2016a)
	LG 2	P_3ch	0.31	6.07	4.52	89.03	0.06				−28.5	−21.7			Qin, et al. (2016a)
	LG 8	P_3ch	0.25	8.63	7.24	83.8	0.05				−29.0	−22.1			Qin, et al. (2016a)
	LG 11	P_3ch	0.17	6.08	9.09	84.56	0.07	0.01			−27.8	−27.0			Qin, et al. (2016a)
	LG 26	P_3ch	0.64	4.71	1.67	92.88	0.08				−29.4	−23.0			Qin, et al. (2016a)
	LG 28	P_3ch	0.58	2.48	0.7	96.15	0.07				−29.3	−24.7			Qin, et al. (2016a)
	LG 29	P_3ch	1.46	4.98	4.78	88.52	0.1	0.01			−29.3	−25.2			Qin, et al. (2016a)
	LG 001–2	P_3ch	0.25	4.36	Nd	92.04	0.07	0.00	0.00	0.00	−29.4	−25.3			This study
	LG 001–23	P_3ch	1.42	4.79	Nd	90.11	0.37	0.06	0.01	0.01	−28.8	−27.8	−26.6	−26.1	This study
Moxi	M 38-H	T_2l^1	2.28	0.00	Nd	96.90	0.39	0.08	0.02	0.02	−32.8	−29.7	−25.1	−24.1	This study
	Mo 30-24H	T_2l^1	3.80	0.25	Nd	94.70	0.23	0.01	0.00	0.00	−33.2	−33.0	−31.9	−31.0	This study
	M 030-H21	T_2l^1	1.36	0.11	Nd	97.23	0.20	0.01	0.00	0.00	−35.8	−33.8	−29.3	−29.4	This study
	Mo 140	T_2l^1	0.23	0.05	Nd	99.54	0.17				−35.0	−32.4			This study
	M 144	T_2l^1	0.75	0.16	Nd	98.90	0.18				−34.9	−32.1			This study
	M 004-H9	T_2l^1	0.59	0.13	Nd	99.12	0.16				−35.0	−32.8			This study
	MS 1	T_1j	2.31	0.46	Nd	96.71	0.28	0.01	0.00	0.00	−33.1	−34.0	−33.9	−28.7	This study
	MS 005–1	T_1j	1.47	0.21	Nd	97.30	0.21	0.01	0.00	0.00	−32.4	−32.9	−32.4	−29.0	This study
	M 150	T_1j	0.21	0.08	Nd	99.50	0.21				−34.7	−33.7			This study
	M 5	T_1j	0.80	0.18	Nd	98.85	0.17				−34.6	−33.2			This study
	M 005-H10	T_1j	0.44	0.10	Nd	99.24	0.21				−34.6	−34.6			This study

(Continued on following page)

TABLE 1 | (*Continued*) Composition and isotopic data of Permian and Triassic natural gas in the central Sichuan Basin.

Gas Field	Well	Strata	Main Molecular Composition (%)								$\delta^{13}C$ (VPDB)‰			References
			N_2	CO_2	H_2S	CH_4	C_2H_6	C_3H_8	iC_4H_{10}	nC_4H_{10}	$\delta^{13}C_1$	$\delta^{13}C_2$	$\delta^{13}C_3$	$\delta^{13}C_4$	
	M 005-H9	T_1j	0.81	0.18	Nd	99.12	0.16				−34.8	−33.6			This study
Yuanba	YB 222	T_3x^4	0.31	0.47	0	97.43	1.47	0.18	0.03	0.03	−3.98	−25.24			Hu, et al. (2014a)
	YB 2-CP1	T_3x^3	0.80	2.43	0	95.38	1.13	0.03	0	0.01	−30.9	−25.2	−24.4	−20.6	Hu, et al. (2014a)
	YB 3	T_3x^4	0.17	0.58	0	97.80	1.32	0.13			−31.4	−21.5	−23.9		Hu, et al. (2014a)
	YB2-C1	T_3x^1	0.48	0.29	0	98.07	1.01	0.09	0.01	0.01	−31.7	−30.2	−26.5		Hu, et al. (2014a)
	YL 1	T_3x^2	0.86	0.85	0	96.82	1.23	0.14	0.01	0.01	−32.1	−28.0			Hu, et al. (2014a)
	YL 3	T_3x^4	0	0.25	0.29	98.39	0.93	0.09	0	0.01	−30.6	−24.8			Hu, et al. (2014a)
	YL 10	T_3x^2	1.40	0.14	0	97.14	1.05	0.09			−31.8	−32.6	−32.7		Liu, et al. (2014)
	YB 05	T_3x^3	0	2.43	0	95.38	1.13	0.057	0.004	0.0071	−30.9	−25.2	−24.4		Liu, et al. (2011)
	YB 06	T_3x^2	0	0	0	96.6	2.39	0.35	0.04	0.04	−32.0	−27.0	−23.4		Liu, et al. (2011)
	YB 1	T_3x^2	0.58	0	0	96.6	2.39	0.35	0.04	0.04	−31.9	−28.5			Wu, et al. (2015)
	YL 10	T_3x^4	0.20	0.67	0	98.05	0.93	0.09	0.01	0.01	−32.0	−25.7	−27.3		Wu, et al. (2015)
	YL 9	T_3x^2	1.29	8.13	0	89.71	0.72	0.06	0.01	0.01	−30	−33	−33.6		Wu, et al. (2015)
	YB 27	T_3x^2	16.5	1.43	0	80.71	1.11	0.11			−31.8	−30.8			Yin, et al. (2013)
	YB 3	T_3x^1	1.12	0.59	0	95.56	2.36	0.28	0.03	0.03	−33.9	−24.4	−23.9		Yin, et al. (2013)
	YB 4	T_3x^4	0.68	0.35	0	97.46	1.25	0.14			−31.7	−28	−26.9		Yin, et al. (2013)
	YB 4	T_3x^2	0.53	0.53	0	97.86	0.91	0.08			−33.5	−29.7			Yin, et al. (2013)
	YB 11	T_3x^2	0.27	0	0	98.35	1.07	0.12	0.01	0.01	−30.3	−25.4			Yin, et al. (2013)
	YB 2	T_3x^3	0.8	2.43	0	95.38	1.13	0.06			−30.9	−25.2	−24.4		Yin, et al. (2013)
	YB 2	T_3x^1	0.48	0.29	0	98.07	1.01	0.09			−31.7	−30.2	−26.5		Yin, et al. (2013)
	YB 22	T_3x^2	0.36	0.67	0	98.21	0.67	0.04	0	0	−34.5	−35.4			Yin, et al. (2013)
	YL 6	T_3x^2	0.31	0.64	0	97.71	1.16	0.11	0.01	0.01	−31.3	−31.4	−31.7		Yin, et al. (2013)
	YB 221	T_2l^4	1.14		Nd	97.36	1.00	0.10			−33.2	−28.5	−27.5		Liu, et al. (2014)
	YB 223	T_2l^4	0.86	2.42	Nd	95.97	0.65	0.05			−35.6	−36.7			Liu, et al. (2014)
	YB 07	T_2l^4	0	2.07	Nd	96.41	0.63	0.05	0	0.01	−35.3	−36.0			Liu, et al. (2011)
	YB 10	T_2l^4	1.52	4.67	Nd	92.50	1.15	0.13	0.03		−33.6	−29.6	−29.4	−25.9	Qin, et al. (2016b)
	YB 13	T_2l^4	0.33	3.30	Nd	95.24	1.05	0.08	0		−31.7	−27.7			Qin, et al. (2016b)
	YB 17	T_2l^4	1.55	9.30	Nd	88.34	0.72	0.07	0.02		−32.11	−32.8	−33.41		Qin, et al. (2016b)
	YB 222	T_2l^4	0.27	1.04	Nd	97.65	0.93	0.09	0.02		−32.91	−28.6			Qin, et al. (2016b)
	YB 224	T_2l^4	13.7	26.14	Nd	59.79	0.37	0.03	0		−35.55	−36.23			Qin, et al. (2016b)
	YB 23	T_2l^4	0.37	0.77	Nd	98.08	0.73	0.05	0		−34.3	−35.1			Qin, et al. (2016b)
	YB 3	T_2l^4	0.74	3.28	Nd	95.38	0.58	0.02	0		−34.2	−36.5			Qin, et al. (2016b)
	YB 5	T_2l^4	0.86	2.42	Nd	96.02	0.65	0.05	0		−35.3	−36.0			Qin, et al. (2016b)
	YB 6	T_2l^4	2.69	5.89	Nd	90.88	0.50	0.04	0		−34.0	−34.5			Qin, et al. (2016b)
	YL 17	T_2l^4	1.07	0	Nd	98.02	0.81	0.08	0.02		−35.1	−32.7			Qin, et al. (2016b)
	YL 2	T_2l^4	11.3	21.77	Nd	66.48	0.42	0.04	0.02		−35.39	−36.61			Qin, et al. (2016b)
	YB 1	P3ch	30.2	3.04	13.33	53.25	0.09	0.09			−30.2	−27.6			Hu, et al. (2014b)
	YB 11	P3ch	11.8	0.23	7.37	80.55	0.05	0			−27.9	−25.2			Hu, et al. (2014b)
	YB 27	P3ch	3.12	0.83	5.14	90.71	0.04	0			−28.9	−26.6			Guo, et al. (2012)
	YB 221	P_3ch	15.1	22.09	Nd	61.98	0.04				−29.2	−28.6	−26.9		Wu, et al. (2015)
	YB 222	P_3ch	0.28	0.07	Nd	99.15	0.47	0.02			−30.9	−29.7	−29		Wu, et al. (2015)
	YB 224	P_3ch	0	4.68	6.85	88.46	0.06				−28.3	−25.9			Wu, et al. (2015)
	YB 273	P_3ch	0.84	6.04	0.45	92.57	0.05				−28.6	−25.4			Wu, et al. (2015)

*Nd = not determined.

fields are 0.971 and 0.991, respectively. Although both belong to T_2l^4 gas reservoir, the dry coefficient of the Yuanba gas field is slightly larger than that of the Longgang gas field, reflecting the difference in the maturity of the source rocks.

The natural gas in the upper and lower strata of the Leikoupo Formation is mainly hydrocarbon gas, the content of non-hydrocarbon gas is relatively low, and there are obvious differences in natural gas components between different strata.

The most important feature of natural gas in the Xujiahe Formation is that it does not contain H_2S; the content of N_2 is 0–16.5%, with an average of 1.36%, and the content of CO_2 is 0–8.13%, with an average of 0.78%. The content of ethane and other heavy hydrocarbon gas in alkane gas varies greatly for different gas reservoirs. The content of heavy hydrocarbon in the Zhongba gas field and the Longgang gas field is similar. The content in the Zhongba gas field and the Longgang gas field is between 2.22% and 11.37%, respectively, with an average of 7.32%, and the dry coefficient is between 0.89% and 0.98%, with an average of 0.92. There are both dry gas and wet gas in natural gas, indicating that the characteristics of gas source rocks are more complex. The content of heavy hydrocarbon gas in the Yuanba gas field is not only relatively low but also relatively concentrated, 0.71%–2.82%, with an average of 1.40%, and the dry coefficient is 0.97–0.99, with an average of 0.99. This shows that the source rock characteristics of natural gas in the Yuanba gas field are located under and adjacent to the T_2l^1 gas reservoir. The composition characteristics of natural gas are highly consistent with that of the T_2l^1 gas reservoir, and the dry

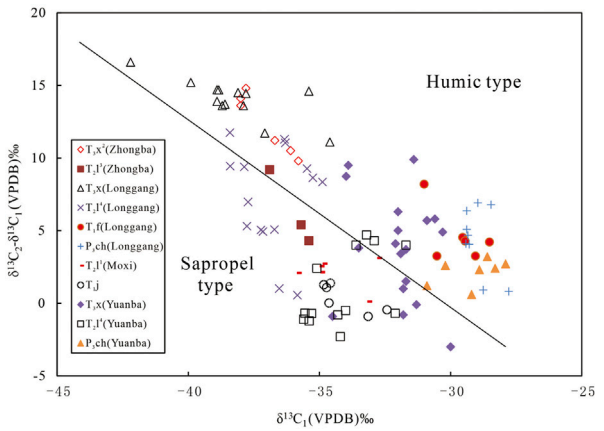

FIGURE 2 | Comparison of carbon isotope characteristics of Permian–Triassic natural gas in the Sichuan Basin.

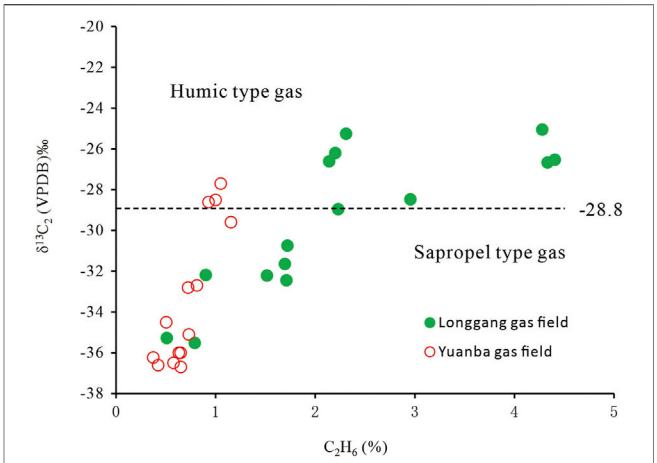

FIGURE 4 | Genetic types of natural gas in the T_2l^4 reservoir of the Sichuan Basin.

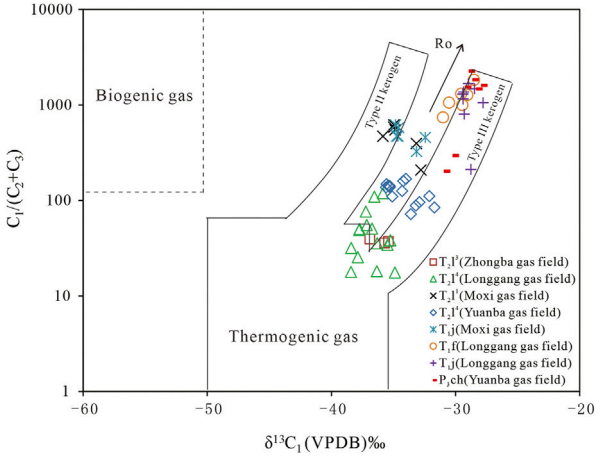

FIGURE 3 | Identification of natural gas from the Leikoupo Formation in the Sichuan Basin using Whitcar' identification Chart [(modified after Whiticar (1999)].

coefficient of natural gas is close to 1.0%. The average content of N_2 is 1.1% and that of CO_2 is 0.2% (**Table 1**).

The gas reservoirs of Feixuan and Changxing formations under the Jialingjiang Formation have the same source of natural gas (Qin, et al., 2016a), and the geochemical characteristics of natural gas are completely the same. The natural gas dry coefficient is close to 1; contains higher H_2S, nitrogen, and carbon dioxide content of most samples less than 5%; and also there are some samples have high content (**Table 1**).

4.2 Carbon Isotope of Natural Gas

The carbon isotopes of natural gas in the Leikoupo Formation are generally less negative, and the overall characteristics are that the $\delta^{13}C_1$ value is relative concentrated, ranging from −38.4‰ to −31.7‰, with an average of −35.4%, but the $\delta^{13}C_2$ values vary widely, ranging from −36.7‰ to −25.1‰, with an average of −31.4‰. As the propane content is very low, only part of the samples were detected, with the $\delta^{13}C_3$ values ranging from −33.4‰ to −22.1‰, with an average of −26.9‰.

The carbon isotopes of different gas reservoirs are obviously different. The carbon isotope values of the T_2l^1 gas reservoir in the Moxi gas field are the most concentrated, with $\delta^{13}C_1$ ranging from −35.8‰ to −32.8‰, with an average of −34.4‰, and $\delta^{13}C_2$ ranging from −33.8‰ to −29.7‰, with an average of −32.3‰. Although the $\delta^{13}C_1$ values are concentrated in the T_2l^3 gas reservoir in the Zhongba gas field and the T_2l^4 gas reservoir in Longgang and Yuanba gas fields, the range of the $\delta^{13}C_2$ value is widely distributed, ranging from −36.7‰ to −25.1‰. The carbon isotope characteristics of natural gas in the Jialingjiang Formation are consistent with those of the T_2l^1 reservoir, with $\delta^{13}C_1$ ranging from −34.8‰ to −32.4‰, with an average of −34.1‰, and $\delta^{13}C_2$ ranging from −34.6‰ to −32.9‰, with an average of −33.7‰.

The $\delta^{13}C_1$ of Changxing and Feixianguan formations in Yuanba and Longgang fields are the least negative in this area, and the variation range is relatively narrow, indicating the relatively consistent gas source rocks. The $\delta^{13}C_1$ ranges from −31‰ to −27.8‰, with an average of −29.2‰, and $\delta^{13}C_2$ ranges from −29.7‰ to −21.7‰, with an average of −25.8‰ (**Table 1**).

The $\delta^{13}C_1$ of the Xujiahe Formation gas reservoir ranges from −42.2‰ to −30.0‰, with an average of −34.7‰, and the $\delta^{13}C_2$ ranges from −35.4‰ to −20.8‰, with an average of −26.3‰. The carbon isotopes of natural gas vary widely, especially the ethane carbon isotopes that reflect the genetic types of natural gas. The natural gas of the Xujiahe Formation mainly comes from its own coal-measure source rocks, and its carbon isotopes vary greatly, which reflects that the source rock type of natural gas may not be single.

In addition, the natural gas in Leikoupo and Xujiahe gas reservoirs in the Yuanba gas field show the inversion of $\delta^{13}C_1$ and $\delta^{13}C_2$, that is, $\delta^{13}C_1 > \delta^{13}C_2$ (**Table 1**; **Figure 2**).

5 GENETIC TYPES OF NATURAL GAS

According to the carbon isotope distribution chart, it can be seen that among the natural gas in the Leikoupo Formation, the

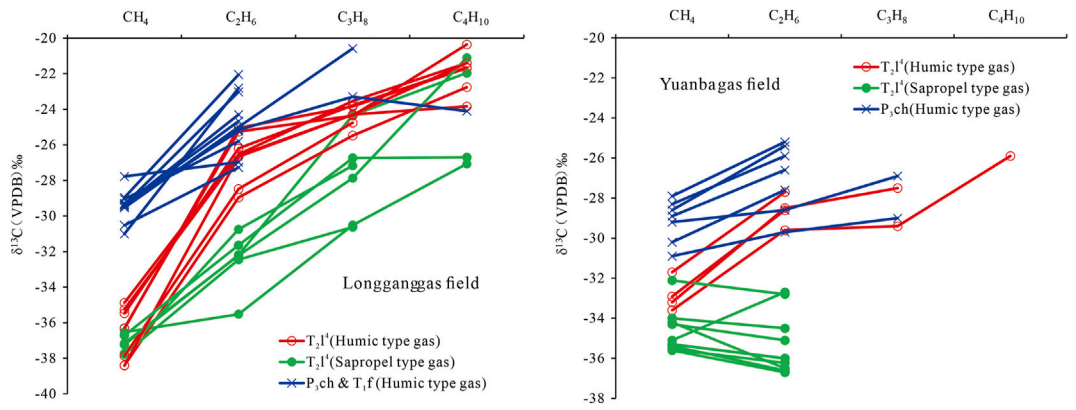

FIGURE 5 | Comparison of $\delta^{13}C$ of natural gas between the T_2l^4 reservoir and the P_3ch-T_1f reservoirs of the Sichuan Basin.

Longgang gas field is the most negative, followed by the Zhongba gas field. Yuanba and Moxi gas fields are relatively less negative (**Figure 2**). The source maturity of natural gas in the Leikoupo Formation of Longgang, Zhongba, Yuanba, and Moxi gas fields increases sequentially. The gas samples of T_1j and T_2l^1 gas reservoirs in the Moxi gas field completely overlap in Whiticar's chart. The natural gas of Changxing and Feixiangguan formations in Yuanba and Longgang gas fields also fall in the same area, and the maturity of their source rocks are much higher than that of the Leikoupo gas reservoir (**Figure 3**). In order to judge the genetic type of natural gas more precisely, this study adopts the identification standard of genetic type of natural gas proposed by Dai, that is, the value of $\delta^{13}C_2$ more negative than −28.8‰ indicate the sapropel-type gas (Dai, 1993).

It can be seen from **Table 1** that the $\delta^{13}C_2$ values of natural gas in the T_2l^1 reservoir of the Moxi gas field are more negative than −28.8‰, the genetic type is relatively simple, and all samples are sapropel gas. Among the three natural gas samples of the T_2l^3 member in the Zhongba gas field, two samples are sapropel gas and one is humic. The genesis of natural gas in the T_2l^4 reservoirs of Longgang and Yuanba gas fields is complicated; some samples are humic gas and some are sapropel-type, and the heterogeneity of the gas reservoir is very obvious. Half of the natural gas samples of the T_2l^4 gas reservoir in the Longgang gas field are humic-type, while only a few samples of the T_2l^4 gas reservoir in the Yuanba gas field are humic-type, and the natural gas is mainly sapropel-type (**Figure 4**). The carbon isotope of alkane gas series can better reflect the overall appearance of natural gas. Half of the samples of the T_2l^4 gas reservoir in the Longgang gas field are humic-type and the other half are sapropel-type, while the gas samples of the T_2l^4 gas reservoir in the Yuanba gas field are mainly sapropel-type, and only a few are humic gas (**Figure 5**).

6 DISCUSSION ON NATURAL GAS SOURCES

6.1 The T_2l^4 Gas Reservoir

The paleokarst on the top of the Leikoupo Formation developed and formed a good karst reservoir, which showed an unconformable contact with the coal-measure source rocks of the overlying Xujiahe Formation (Song, et al., 2012; Wang, et al., 2018a). Some corrosion ditches are formed in the Leikoupo Formation, and the corrosion ditches will be filled by the Xujiahe Formation. Theoretically, the natural gas generated by the source rocks of the Xujiahe Formation has the opportunity to migrate to the top reservoir of the Leikoupo Formation; therefore, the samples showing humic-type in T_2l^4 reservoir should come from the source rocks of the Xujiahe Formation.

It is researched that there is a close relationship between the $\delta^{13}C_2$ values and the C_2H_6 content in the T_2l^4 reservoir of Longgang and Yuanba gas fields. The higher the ethane content, the less negative of the carbon isotope, showing the characteristics of humic gas. Taking the Longgang gas field as an example, the samples with ethane content more than 2% in the T_2l^4 reservoir are humic gas, and on the contrary, those with the ethane content less than 2% are sapropel gas. A similar situation has occurred in the Yuanba gas field. Because the maturity of the source rocks is higher than that of the Longgang gas field, the ethane content is generally lower than that of the Longgang, but the $\delta^{13}C_2$ also tends to become less negative with the increase of the ethane content. The ethane content of several humic-type gas samples in T_2l^4 is more than 1%. The ethane content of sapropel gas samples is less than 1% (**Figure 4**). The $\delta^{13}C_2$ value can best reflect the type of source rock, and the content of ethane can often reflect the content of heavy hydrocarbon gas, which indirectly reflects the dry coefficient (or humidity coefficient) of natural gas; the higher value of the ethane content, the lower the dry coefficient (high humidity coefficient). The humidity coefficient is related to the maturity of source rocks. For the same type of source rocks, the smaller the humidity coefficient, the higher the maturity of source rocks (Dai, et al., 2016b). Under the same degree of evolution, different types of source rocks have different dry coefficients, the sapropel-type is lower than humic-type. The ethane content of sapropel gas is less than that of sapropel gas in T_2l^4, indicating that the maturity of sapropel gas of hydrocarbon source rocks is higher than that of humic gas.

According to the carbon isotope of the alkane gas series of the T_2l^4, there are obvious differences in carbon isotopes of heavy

hydrocarbons such as ethane between sapropel and humic gas; however, there is no obvious difference in the $\delta^{13}C_1$ values (**Figure 5**). Based on this, it is concluded that the sapropel gas in T_2l^4 can only come from the source rocks of the Leikoupo Formation or other underlying strata, mainly sapropel organic matter. Due to the fact that the $\delta^{13}C_1$ value generated by sapropelic source rocks is more negative than that generated by humic source rocks under the same maturity, the $\delta^{13}C_2$ value is highly related to the type of organic matter and does not change obviously with the increase of the maturity of source rocks, and the genetic type of natural gas is therefore often identified according to the ethane carbon isotope.

As the Xujiahe Formation is the first terrestrial strata deposited after the end of marine sedimentation in the Sichuan Basin, in addition to humic source rocks, the T_3x^1 member may also develop marine sapropel source rocks at some local area. It is unlikely that the sapropel gas in the T_2l^4 reservoir come from the sapropel source rocks that may undergo phase transformation corresponding to the T_3x^1 member in contact with it. If the sapropel gas in the T_2l^4 comes from the sapropel source rock in the T_3x^1 member, the maturity of this source rock should be similar to other humic hydrocarbon source rocks in the T_3x^1. As mentioned before, the $\delta^{13}C_1$ from rocks with the same maturity should be lighter than those from humic source rocks. In fact, the $\delta^{13}C_1$ of sapropel and humic gas in T_2l^4 are similar, but the $\delta^{13}C_2$ is quite different (**Figure 5**). The ethane content of sapropel gas in the T_2l^4 reservoir is less than that of humic gas (**Figure 4**). Therefore, it is judged that the sapropel gas in T_2l^4 comes from source rocks with higher maturity than the source rocks in the T_3x^1 member.

It is not possible that the sapropel gas in T_2l^4 came from the source rocks of the Longtan Formation below. This is because the hydrocarbon source rocks of the Longtan Formation and the T_2l^4 reservoir are separated by multiple sets of gypsum strata from the Jialingjiang Formation and T_2l^1 to T_2l^3 members, and there are many sealing layers, making it difficult for natural gas to migrate to the T_2l^4 reservoir. In addition, the natural gas from the Changxing and Feixianguan formations in Longgang and Yuanba gas fields all come from coal-measure source rock of the Longtan Formation; the carbon isotopes of methane and ethane are much less negative, and their characteristics are very different from those in T_2l^4 reservoirs, uncorrelated with the gas in T_2l^4 reservoir (**Figures 3**, **5**). Collectively, it is judged that the sapropel gas in T_2l^4 should come from the source rocks developed in the T_2l^3, and the humic gas comes from the Xujiahe coal-measure source rock.

6.2 The T_2l^3 Gas Reservoir

The forming condition of T_2l^3 gas reservoir is similar to that of the T_2l^4, in which the humic gas comes from the overlying Xujiahe Formation source rocks and the sapropel gas comes from the T_2l^3 source rocks. In this study, the T_2l^3 gas reservoir occurs in the Zhongba gas field, where the T_2l^4 member is depleted and the T_2l^3 section is in unconformity contact with the overlying Xujiahe Formation. The T_3x^2 gas reservoir develops above the T_3x^2 member in the gas field. The $\delta^{13}C_1$ of the gases in T_2l^3 and T_3x^2 reservoirs are similar, with the former

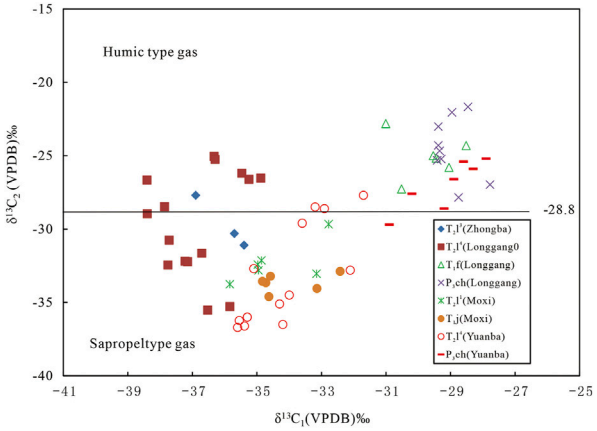

FIGURE 6 | Comparison of $\delta^{13}C_1$ and $\delta^{13}C_2$ in natural gas between the Leikoupo Formation and underlying gas reservoirs.

averaging −37‰ and the latter −36‰, but $\delta^{13}C_2$ are more different, with the Leikoupo Formation being more negative, averaging −29.7‰, and the T_3x^2 averaging −24.7‰, both of which are from different hydrocarbon source rocks. The T_2l^3 itself has source rock, and the sapropel-type gas should come from the T_2x^3 member source rock.

6.3 The T_2l^1 Gas Reservoir

In this study, all gas data of T_2l^1 come from the Moxi gas field, where the T_2l^1 gas reservoir is adjacent to the underlying Jialingjiang gas reservoir, and its geochemical characteristics are highly consistent with the natural gas in the Jialingjiang Formation based on the analysis of the samples in this study (**Figures 2**, **3**, **6**). The gas in both reservoirs should be from the same source, but it is difficult to determine which set of hydrocarbon source rocks the gas comes from. First, it is impossible for the gas to come from the coal-measure source rocks of the Xujiahe Formation because the gas characteristics of the T_2l^1 do not match the humic gas and there are effective interlayers between the Xujiahe Formation and T_2l^1, T_2l^2, T_2l^3, and T_2l^4 members, and it is difficult for the gas of the Xujiahe Formation to traverse downward through the multilayered gypsum rocks to reach the T_2l^1 reservoir.

Comparing the isotopic data of typical sapropel gas samples from the T_2l^4 section of the Longgang and Yuanba gas fields with the T_2l^1 gas reservoir, it is found that the T_2l^1 gas is closer to the sapropel gas of the T_2l^4 reservoir in Yuanba. The difference is that most of the sapropel gas samples from the T_2l^4 reservoir in Yuanba show carbon isotope inversion, while the carbon isotopes of gas from the T_2l^1 reservoir in Moxi do not. The $\delta^{13}C_2$ (average −32.3‰) is significantly less negative than that of sapropel gas (average 35.3‰) in the T_2l^4 gas reservoir in Yuanba (**Figure 7**), and the source rock may be relatively humic. Although there are some similarities between the carbon isotopes of T_2l^1 gas and T_2l^4, we cannot suggest that T_2l^1 gas may also come from T_2l^3 hydrocarbon source rocks because the direct caprock of the T_2l^1 gas reservoir is the gypsum layer and gypsum dolomite above the gas reservoir. There are

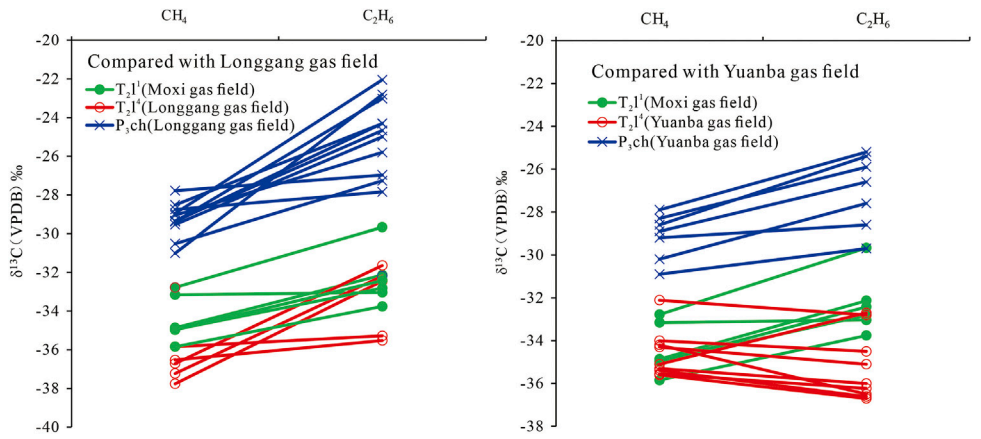

FIGURE 7 | Comparison of $\delta^{13}C_1$ and $\delta^{13}C_2$ of natural gas in the T_2l^1 reservoir with T_2l^4, P_3ch and T_1f reservoirs.

three layers of anhydrite layers with a total thickness of about 5 m on the gas reservoir, and 20 layers of anhydrite and gypsum dolomite are sandwiched up together with the T_2l^1 member, with a thickness of 160 m, which together constitute a good direct cover for the T_2l^1 gas reservoir (Dai, et al., 1996). Therefore, it is difficult for natural gas in the T_2l^3 member to migrate down to the T_2l^1 reservoir across such a thick high-quality caprock.

Earlier studies suggested that the natural gas in the T_2l^1 gas reservoir of the Moxi gas field was mainly from the coal-measure source rock of the Longtan Formation based on the less negative of $\delta^{13}C_2$ value in some drilled wells (Wang, et al., 1998). However, the average $\delta^{13}C_2$ value of T_2l^1 gas is −32.3‰, which is typical of sapropel gas (**Figure 6**). Its methane and ethane carbon isotopes are very different from the natural gas from the Longtan Formation coal-measure source rocks in the Changxing and Feixianguan formation gas reservoirs of the Longgang and Yuanba gas fields, and the carbon isotopes of the Changxing and Feixianguan natural gas are much less negative (**Figure 7**). Therefore, the natural gas in T_2l^1 gas reservoir does not come from the coal-measure rocks of the Longtan Formation. However, the coal-measure hydrocarbon source rocks of the Longtan Formation would have undergone a phase change in some areas of the Sichuan Basin and become marine hydrocarbon source rocks of the Wujiaping Formation (the Upper Permian), with a shift in organic matter type from humic to sapropelic. Compared with the coal measures of the Longtan Formation, the carbon isotope of the natural gas generated by the source rocks of the Wujiaping Formation would be relatively more negative, which can completely match the natural gas of the T_2l^1 member. Therefore, it is believed that the natural gas from the T_2l^1 member of the Moxi gas field comes from source rocks of the Wujiaping Formation.

6.4 Causes of Carbon Isotope Inversion in Natural Gas in T_2l^4 in the Yuanba Gas Field

The phenomenon of carbon isotope inversion in alkane gas has been reported for a long time (Stahl et al., 1975; Fuex, 1977; Burruss et al., 2010) and later studied by Tilley et al. (2011), Zumberge et al. (2012), and many others. This phenomenon is often found in major oil and gas basins in China, especially shale gas, where carbon isotopes are mostly in reverse order (Dai et al., 2016a). There are various explanations for the isotope inversion, but none is convincing. Most of the carbon isotope inversions in this study occurred in the T_2l^4 member of the Yuanba gas field, nine of the 14 samples have carbon isotope inversions of methane and ethane, that is, $\delta^{13}C_2<\delta^{13}C_1$. The inverted samples were nearly 65% (**Table 1**; **Figure 7**). Some samples from the Xujiahe Formation in the Yuanba gas field have carbon isotope inversions of methane and ethane, and the samples are all distributed in the T_3x^2 member, such as wells YL 9 and YL 10 (**Table 1**). No carbon isotope inversions were found in either T_2l^4 or Xujiahe Formation gas reservoirs in the Longgang gas field, and no carbon isotope inversions occurred in any of the other gas reservoirs.

First, we think that the carbon isotope inversion presented in this study can rule out the reason caused by mixing different natural gases. The natural gas generated from the Xujiahe Formation can migrate downward to the T_2l^4 gas reservoir, which is common in the Longgang gas field. Half of the samples from the T_2l^4 gas reservoir in the Longgang gas field are humic gas, while only a few samples from T_2l^4 gas reservoir in the Yuanba gas field are humic gas (**Figure 8**). This indicates that the scale of humic gas of the Xujiahe Formation mixed into the T_2l^4 gas reservoir in Longgang is larger than that in Yuanba. However, the natural gas of the Longgang T_2l^4 member does not appear reversed, while most samples of the Yuanba T_2l^4 member with little humic gas appear carbon isotope inversion. In addition, no sapropel gas samples were found in the Xujiahe Formation gas reservoir in the Longgang gas field, indicating that the natural gas in T_2l^4 member did not migrate upward obviously. However, more than half of the samples from the Xujiahe Formation gas reservoir in the Yuanba gas field are sapropel gas, indicating that the natural gas from the underlying T_2l^4 gas reservoir has massively upwardly migrated into the Xujiahe Formation gas reservoir (**Figure 9**). Only a few individual samples showed carbon isotope inversions in the case of large amounts of sapropel gas mixed into the Xujiahe Formation in the Yuanba gas field, and the inverted samples were all found in the T_3x^2 member,

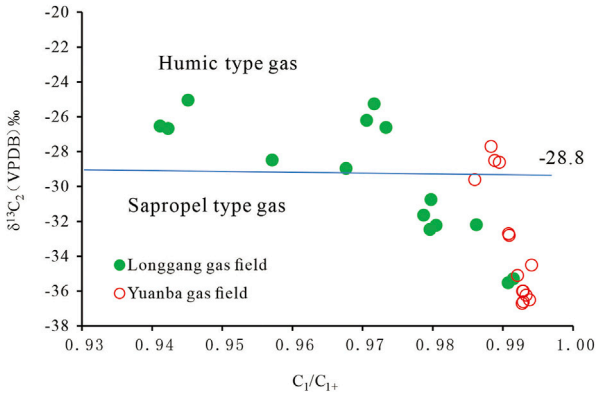

FIGURE 8 | Relationship between C_1/C_{1+} and $\delta^{13}C_2$ of T_2l^4 gas in Longgang and Yuanba gas fields.

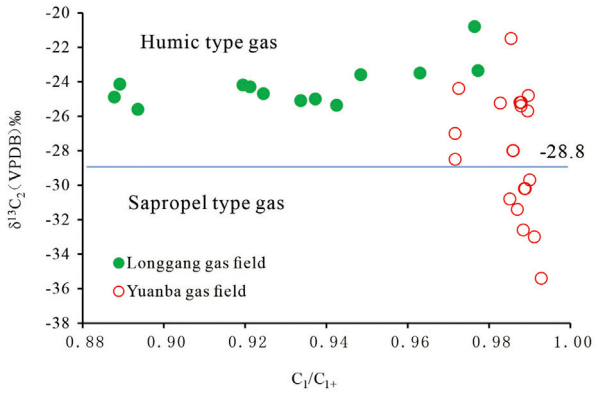

FIGURE 9 | Relationship between C_1/C_{1+} and $\delta^{13}C_2$ of T_3x gas in Longgang and Yuanba gas fields.

which is close to the T_2l^4 member, and showed typical sapropel gas, which had already inverted before leaving the T_2l^4 member and entering the Xujiahe Formation.

From the carbon isotope of sapropel gas in the T_2l^4 member of Longgang and Yuanba gas fields, the $\delta^{13}C_2$ in T_2l^4 member of Yuanba is 2‰ more negative than that of Longgang, while the methane carbon isotope is 2‰ less negative than that of Longgang. This indicates that the hydrocarbon source rock type in the T_2l^3 member of the Yuanba gas field is of a higher quality than that of Longgang gas field. The hydrocarbon source rock maturity is higher than Longgang. Therefore, it can be concluded that the carbon isotope inversion of natural gas in the Yuanba T_2l^4 member occurred because of its good hydrocarbon source rock type and higher maturity. Because the hydrocarbon source rock type is good and very favorable for oil generation, the ethane carbon isotope will be relatively more negative and will change less with increasing evolution, while methane carbon isotopes become less negative rapidly and become less negative than ethane as source rock maturity reaches a certain level. It is difficult for humic gas to have the carbon isotope inversion of methane and ethane. Because the $\delta^{13}C_2$ in humic gas is inherently much less negative, the carbon isotope of methane generated during the evolution of source rocks is difficult to be less negative than ethane. This also explains why the methane and ethane carbon isotopes in the Changxing and Feixianguan formation gas reservoirs did not reverse.

7 CONCLUSION

The natural gas of the Leikoupo Formation in the Sichuan Basin has complex genetic types and various gas sources. The natural gas in the T_2l^1 gas reservoir of the Moxi gas field is all sapropel-type, which comes from the sapropel source rock of the Upper Permian Wujiaping Formation. The natural gas in the T_2l^3 gas reservoir of the Zhongba gas field is mainly sapropel gas, which comes from hydrocarbon source rocks of T_2l^3 itself. Half of the natural gas in T_2l^4 gas reservoir of the Longgang gas field is humic gas from the humic source rocks of the Xujiahe Formation, and the other half is sapropel gas from the T_2l^3 source rocks. The gas in T_2l^4 gas reservoir of the Yuanba gas field is mainly sapropel gas from the T_2l^3 hydrocarbon source rocks, and a very small portion is humic gas from the Xujiahe Formation source rocks. The natural gas with inversed carbon isotopes of methane and ethane was formed from favorable quality source rocks at a higher evolution stage.

DATA AVAILABILITY STATEMENT

The original contributions presented in the study are included in the article/Supplementary Material; further inquiries can be directed to the corresponding author.

AUTHOR CONTRIBUTIONS

SQ put forward the opinion of article and wrote the manuscript. BZ compiled the diagrams. CH collected data. JL collected sample, performed analysis, and helped with manuscript translation. JW helped with sample analysis and manuscript translation. GT helped with sample analysis and manuscript translation. ZZ helped some data interpretation and manuscript revision.

ACKNOWLEDGMENTS

This study was jointly sponsored by the National Natural Science Foundation of China (Grant Nos. 41872162, 42141022). We thank Jamie Beagle for language correction. We are grateful to the editor for handling this manuscript and reviewers for helpful comments and suggestions that have improved the manuscript.

REFERENCES

Bian, C., Wang, Z., Jiang, Q., Chi, Y., and Xu, Z. (2019). Characteristics and Distribution of Karst Reservoirs in the Leikoupo Formation, Western Sichuan Basin. *China Pet. Explor.* 24 (1), 82–94. doi:10.3969/j.issn.1672-7703.2019.01.009

Burruss, R. C., and Laughrey, C. D. (2010). Carbon and Hydrogen Isotopic Reversals in Deep Basin Gas: Evidence for Limits to the Stability of Hydrocarbons. *Org. Geochem.* 41, 1285–1296. doi:10.1016/j.orggeochem.2010.09.008

Cross, M. M., Manning, D. A. C., Bottrell, S. H., and Worden, R. H. (2004). Thermochemical Sulphate Reduction (TSR): Experimental Determination of Reaction Kinetics and Implications of the Observed Reaction Rates for Petroleum Reservoirs. *Org. Geochem.* 35 (4), 393–404. doi:10.1016/j.orggeochem.2004.01.005

Dai, H., Huang, D., Liu, X., Yang, Y., He, X., Peng, H., et al. (2008). Characteristics and Evaluation of Marine Source Rock in Southwestern Shunan. *Nat. Gas. Geosci.* 19 (4), 503–508. doi:10.11764/j.issn.1672-1926.2008.04.503

Dai, J. (1993). Characteristics of Carbon and Hydrogen Isotopes of Natural Gases and Their Discriminations. *Nat. Gas. Geosci.* 2 (3), 1–40. doi:10.11764/j.issn.1672-1926.1993.02.1

Dai, J., Chen, J., Zhong, N., and Qin, S. (2003). *The Gas Fields and Their Origins in China*. Beijing: Science Press, 28–33.

Dai, J., Ni, Y., Huang, S., Gong, D., Liu, D., Feng, Z., et al. (2016a). Secondary Origin of Negative Carbon Isotopic Series in Natural Gas. *J. Nat. Gas Geoscience* 1 (1), 1–7. doi:10.1016/j.jnggs.2016.02.002

Dai, J., Ni, Y., Zhang, W., Huang, S., Gong, D., Liu, D., et al. (2016b). Relationships between Wetness and Maturity of Coal-Derived Gas in China. *Petroleum Explor. Dev.* 43 (5), 675–678. doi:10.1016/s1876-3804(16)30088-x

Dai, J., Pei, X., and Qi, H. (1996). *Natural Gas Geology in China Vol. 1*. Beijing: The Petroleum Industry Press, 14–15.

Dai, J. (1980). Preliminary Research on Natural Gas in Coal Series in China. *Acta Pet. Sin.* 1 (4), 27–37. doi:10.7623/syxb198004003

Deng, Y., Hu, G., and Zhao, C. (2018). Geochemical Characteristics and Origin of Natural Gas in Changxing-Feixianguan Formations from Longgang Gas Field in the Sichuan Basin, China. *Nat. Gas. Geosci.* 29 (6), 892–907. doi:10.11764/j.issn.1672-1926.2018.03.016

Fan, Z. (2014). Distribution of Ancient Ditches in Leikoupo Formation and its Control over Gas Accumulations in Yuanba Gas Field. *Petroleum Geol. Exp.* 36 (5), 562–566. doi:10.11781/sysydz201405562

Fuex, A. N. (1977). The Use of Stable Carbon Isotopes in Hydrocarbon Exploration. *J. Geochem. Explor.* 7, 155–188. doi:10.1016/0375-6742(77)90080-2

Guo, X., and Guo, T. (2012). *Theory and Practice of Exploration of Large Gas Fields at the Margin of the Puguang and Yuanba Carbonate Platforms*. Beijing: Science Press, 413.

Hao, F., Guo, T., Zhu, Y., Cai, X., Zou, H., and Li, P. (2008). Evidence for Multiple Stages of Oil Cracking and Thermochemical Sulfate Reduction in the Puguang Gas Field, Sichuan Basin, China. *Bulletin* 92 (5), 611–637. doi:10.1306/01210807090

Hu, G., Yu, C., Gong, D., Tian, X., and Wu, W. (2014a). The Origin of Natural Gas and Influence on Hydrogen Isotope of Methane by TSR in the Upper Permian Changxing and the Lower Triassic Feixianguan Formations in Northern Sichuan Basin, SW China. *Energy Explor. Exploitation* 32 (1), 139–158. doi:10.1260/0144-5987.32.1.139

Hu, W., Zhu, Y., Li, Y., Zou, H., and Guo, T. (2014b). Geochemical Characteristics and Origin of Natural Gases from Terrestrial Strata in Yuanba Area of the Northeastern Sichuan Basin. *J. Zhejiang Univ. Sci. Ed.* 41 (4), 468–476. doi:10.3785/j.issn.1008-9497.2014.04.020

Huang, R. (2014). Source and Accumulation of Natural Gas in Leikoupo Formation, Yuanba Area, Eastern-Northern Sichuan Basin. *Geoscience* 28 (2), 412–418. doi:10.3969/j.issn.1000-8527.2014.02.020

Hussain, M., and Warren, J. K. (1991). Source Rock Potential of Shallow-Water Evaporites: An Investigation in Holocenepleistocene Salt Flat Sabkah (Playa), West Texas-New Mexico. *Carbonates Evaporites* 6 (2), 217–224. doi:10.1007/BF03174424

Jin, Q., and Zhu, G. (2006). Progress in Research of Deposition of Oil Source Rocks in Saline Lake and Their Hydrocarbon Generation. *Geol. J. China Univ.* 12 (4), 483. doi:10.3969/j.issn.1006-7493.2006.04.009

Krouse, H. R., Viau, C. A., Eliuk, L. S., Ueda, A., and Halas, S. (1988). Chemical and Isotopic Evidence of Thermochemical Sulphate Reduction by Light Hydrocarbon Gases in Deep Carbonate Reservoirs. *Nature* 333, 415–419. doi:10.1038/333415a0

Krzywiec, P., Peryt, T. M., Kiersnowski, H., Pomianowski, P., Czapowski, G., and Kwolek, K. (2017). Permo-Triassic Evaporites of the Polish Basin and Their Bearing on the Tectonic Evolution and Hydrocarbon System, an Overview. *Permo-Triassic salt Prov. Eur. North Afr. Atl. Margins* 2017, 243–261. doi:10.1016/B978-0-12-809417-4.00012-4

Li, W. (2011). Formation of a Saline Enviroment and Evolution of a Sedimentary System in the Late Triassic of the Sichuan Basin. *Nat. Gas. Ind.* 31 (9), 31–38. doi:10.3787/j.issn.1000-0976.2011.09.006

Li, W., Zou, C., Yang, J., Wang, K., Yang, J., Wu, Y., et al. (2010). Types and Controlling Factors of Accumulation and High Productivity in the Upper Triassic Xujiahe Formation Gas Reservoirs, Sichuan Basin. *Acta Sedimentol. Sin.* 28 (5), 1037–1045. doi:10.14027/j.cnki.cjxb.2010.05.018

Li, Z. (1993). Surveying Gas Prospects of Leikoupo Formation in West Sichuan. *Nat. Gas. Ind.* 13 (2), 28–33. doi:10.11821/yj1983040003

Liao, F., Wu, X., Huang, S., and Yu, C. (2013). Geochemical Characeristics and Gas Source Correlation of Leikoupo Formation in Zhongba Field, Northwest Sichuan Basin. *Nat. Gas. Geosci.* 24 (1), 108–115. doi:10.11764/j.issn.1672-1926.2013.01.108

Liu, J., Liu, G., Wang, L., and Wu, X. (2014). Geochemical Characteritics and Origin of Permain and Triassic Natural Gas in Yuanba-Tongnanba Area, Northeastern Sichuan Basin. *Acta Pet. Sin.* 35 (3), 417–428. doi:10.7623/syxb201403002

Liu, R., Guo, T., and Shao, M. (2011). Source and Genetic Types of Gas in the Middle-Shallow Strata of the Yuanba Area, Northeast Sichuan Basin. *Nat. Gas. Ind.* 31 (6), 34–38. doi:10.3787/j.issn.1000-0976.2011.06.005

Liu, S., Sun, W., Song, J., Yong, Z., Wang, H., and Zhao, C. (2019). The Key Geological Promblems of Natural Gas Exploration in the Middle Triassic Formation in Sichuan Basin. *Nat. Gas. Geosci.* 30 (2), 151–167. doi:10.11764/j.issn.1672-1926.2018.12.011

Luo, Q. (1983). Discovery of Water-Transgression Cause Filling Sand-Bodies in Ancient Sediments-An Approach to the Genesis of Certain Upper Triassic Sand-Bodies in the Middle-Western Part of the Sichuan Basin and Discussion on Water-Transgression Delta. *Acta Sedimentol. Sin.* 1 (3), 59–67. CNKI:SUN:CJXB.0.1983-03-004.

Luo, Q. (2011). Understanding of the Upper Triassic Sedimentary Facies in the Sichuan Basin. *Nat. Gas. Ind.* 31 (9), 12–15. doi:10.3787/j.issn.1000-0976.2011.09.003

Machel, H. G. (2001). Bacterial and Thermochemical Sulfate Reduction in Diagenetic Settings-Old and New Insights. *Sediment. Geol.* 140 (1-2), l43–175. doi:10.1016/S0037-0738(00)00176-7

Peng, C., Liu, K., Zhang, Y., and Zhu, P. (2011). Seismic Sedim Entology of Organic Reef from the Changxing Form Ation of Central Sichuan. *Nat. Gas. Geosci.* 22 (3), 460–464. doi:10.11764/j.issn.1672-1926.2011.03.460

Qin, H., Pan, L., Yin, F., and Shen, J. (2016b). Discution on Source of Natural Gas and Causation of Reversed Orders of δ13C in Alkane Gas from Leikoupo Formation in Yuanba, Sichuan Basin, China. *J. Chengdu Univ. Technol. Sci. Technol. Ed.* 43 (5), 591–600. doi:10.3969/j.issn.1671-9727.2016.05.09

Qin, S., Tao, S., Tu, T., Wei, X., and Song, M. (2007). Characeristics of Natural Gas Geochemistry and Accumulation in Western Sichuan Depression. *Petroleum Explor. Dev.* 34 (1), 34–38. doi:10.3321/j.issn:1000-0747.2007.01.007

Qin, S., Yang, Y., Lü, F., Zhou, H., and Li, Y. (2016a). The Gas Origin in Changxing-Feixianguan Gas Pools of Longgang Gasfield in Sichuan Basin. *Nat. Gas. Geosci.* 27 (1), 40–48. doi:10.11764/j.issn.1672-1926.2016.01.0041

Song, W., Liu, L., Gan, X., Qin, Q., Su, P., and Fan, C. (2012). Weathering Crust Karstification in Leikoupo Formation in Central Sichuan Area. *Nat. Gas. Geosci.* 23 (6), 1019–1024. CNKI:SUN:TDKX.0.2012-06-007.

Stahl, W. J., and Carey, B. D. (1975). Source-rock Identification by Isotope Analyses of Natural Gases from Fields in the Val Verde and Delaware Basins, West Texas. *Chem. Geol.* 16, 257–267. doi:10.1016/0009-2541(75)90065-0

Sun, H., Luo, B., Wen, L., Wang, J., Zhou, G., Wen, H., et al. (2021). The First Discovery of Organic-Rich Shale in Leikoupo Formation and New Areas of Subsalt Exploration, Sichuan Basin. *Nat. Gas. Geosci.* 32 (2), 233–247. doi:10.11764/j.issn.1672-1926.2020.11.011

Tilley, B., McLellan, S., Hiebert, S., Quartero, B., Veilleux, B., and Muehlenbachs, K. (2011). Gas Isotope Reversals in Fractured Gas Reservoirs of the Western Canadian Foothills: Mature Shale Gases in Disguise. *Bulletin* 95 (8), 1399–1422. doi:10.1306/01031110103

Wang, S., Dai, H., Wang, T., and Lin, F. (1998). Gas Source and Migration of High-Mature Natural Gas in Moxi Gas Field. *Petroeum Explor.* 3 (2), 5–8. CNKI:SUN:KTSY.0.1998-02-002.

Wang, S., Luo, Q., and Wu, D. (1997). Organic Petrology of Source Rocks from the Upper Triassic Coal Measures in the Central and Western Sichuan Basin. *J. Mineral Pet.* 17 (1), 63–70.

Wang, T., Zhen, Y., Li, S., Zeng, Q., and He, J. (1989). From Geochemical Characteristics of Oil and Gas to Discuss the Gas Source of Lei-3 Reservoir, Zhongba Gas Field, in Northwest Sichuan. *Nat. Gas. Ind.* 9 (5), 20–26. CNKI:SUN:TRQG.0.1989-05-004.

Wang, W., Xu, G., Dan, Y., Song, X., Wang, Q., Feng, X., et al. (2018a). Unconformity Characeristics of the Top of Leikoupo Formation and Their Effect on Reservoirs in the Western Sichuan Basin. *Carsologica Sin.* 37 (4), 592–601. doi:10.11932/karst20180413

Wang, Y., Chen, Y., Hu, Y., Zeng, H., and Wu, X. (2018b). Discussion on Hydrocarbon Generation Ability of Evaporation Environment: A Case Study of Leikoupo Formation in West Sichuan Depression. *Fault-Block oil Gas Fied* 25 (4), 426–430. doi:10.6056/dkyqt201804004

Wen, L., Zhang, Q., Yang, Y., Liu, H., Che, Q., Liu, W., et al. (2012). Factors Controlling Reef-Bank Reservoirs in the Changxing-Feixianguan Formations in the Sichuan Basin and Their Play Fairways. *Nat. Gas. Ind.* 32 (1), 39–44. doi:10.3787/j.issn.1000-0976.2012.01.007

Whiticar, M. J. (1999). Carbon and Hydrogen Isotope Systematics of Bacterial Formation and Oxidation of Methane. *Chem. Geol.* 161 (1/2/3), 291–314. doi:10.1016/S0009-2541(99)00092-3

Worden, R. H., Smalley, P. C., and Oxtoby, N. H. (1995). Gas Souring by Thermochemical Sulfate Reduction at 140øC. *Bulletin* 79, 854–863. doi:10.1306/8d2b1bce-171e-11d7-8645000102c1865d

Wu, X., Liu, G., Liu, Q., Liu, J., and Yuan, X. (2015). Geochemical Characteristics and Genetic Types of Natural Gas in the Changxing-Feixianguan Formations from Yuanba Gasfield in the Sichuan Basin. *Nat. Gas. Geosci.* 26 (11), 460–464. doi:10.11764/j.issn.1672-1926.2015.11.2155

Xie, F., Wu, Q., Wang, L., Shi, Z., Zhang, C., Liu, B., et al. (2019). Passive Continental Margin Basins and the Controls on the Formation of Evaporites: A Case Study of the Gulf of Mexico Basin. *Carbonates Evaporites* 34 (2), 405–418. doi:10.1007/s13146-017-0404-z

Xu, G., Song, X., Feng, X., Long, K., Wang, Q., Shi, G., et al. (2013). Gas Potential of the Middle Triassic Leikoupo Fm in the Western Sichuan Basin. *Nat. Gas. Ind.* 33 (8), 8–14. doi:10.3787/j.issn.1000-0976.2013.08.002

Yang, G., Shi, X., Huang, D., Wang, H., and Ding, W. (2014). Characteristics and Major Controls of Weathering Crust Reservors in T2l43 in the Longgang Gas Field, Sichuan Basin. *Nat. Gas. Ind.* 34 (9), 17–24. doi:10.3787/j.issn.1000-0976.2014.09.003

Yang, K. (2016). Hydrocarbon Potential of Source Rocks in the Middle Triassic Leikoupo Formation in the Western Sichuan Depression. *Petroleum Geol. Exp.* 38 (3), 366–374. doi:10.11781/sysydz201603366

Yang, X., Zou, C., Tao, S., Wang, Z., Li, J., and Wang, S. (2005). Characteristics of Upper Triassic-Jurassic Oil and Gas System in Sichuan Basin and Oli and Gas Abundance Law. *China Pet. Explor.* 10 (2), 15–22. doi:10.3969/j.issn.1672-7703.2005.02.003

Yin, F., Liu, R., Wang, W., Zhang, Y., and Pan, L. (2013). Geochemical Characters of the Tight Sandstone Gas from Xujiahe Formation in Yuanba Gas Field and its Gas Source. *Nat. Gas. Geosci.* 24 (3), 621–627. doi:10.11764/j.issn.1672-1926.2013.03.621

Yu, K., Cao, Y., Qiu, L., and Sun, P. (2018). The Hydrocarbon Generation Potential and Migration in an Alkaline Evaporite Basin: The Early Permian Fengcheng Formation in the Junggar Basin, Northwestern China. *Mar. Petroleum Geol.* 98, 12–32. doi:10.1016/j.marpetgeo.2018.08.010

Zeng, D., Wang, X., Zhang, F., Song, Z., Zhang, R., Zhu, Y., et al. (2007). Study on Reservoir of the Leikoupo Formation of Middle Triassic in Northwestern Sichuan Basin. *J. Palaeogeogr.* 9 (3), 253–266. doi:10.3969/j.issn.1671-1505.2007.03.003

Zhang, J., Zhou, J., Pan, L., Wang, X., Wang, F., Hao, Y., et al. (2013). The Main Origins of High Quality Reservoir in Feixianguan Formation in Northeast Sichuan Basin: Atmospheric Water Eluviation and Seepage-Reflux Dolomitization. *Nat. Gas. Geosci.* 24 (1), 9–18.

Zheng, Y., Lin, F., Wang, T., and Yan, W. (1990). Geologic and Geochemical Conditions of Formation of Zhongba Condensate Gas Fields in Northwest Sichuan. *J. Southwest Petroleum Inst.* 12 (4), 18–30. doi:10.3863/j.issn.1000-2634.1990.04.003

Zhou, S., Wang, X., Zeng, D., He, B., and Zhou, X. (2015). Geochemistry and Accumulation Analysis of Gas Reservoir of Leikoupo 43 Sub-member of Middle Triassic in Longgang Area, Central Sichuan Basin. *Xinjiang Pet. Geol.* 36 (4), 415–422. doi:10.7657/XJPG20150407

Zhu, H., and Zhong, D. (2013). Characteristics and Formation Mechanism of the Triassic Feixianguan Formation Reservoir in Longgang Gas Field, Sichuan Basin. *J. Palaeogeogr.* 15 (2), 275–282. doi:10.7605/gdxh.2013.02.023

Zumberge, J., Ferworn, K., and Brown, S. (2012). Isotopic Reversal ('rollover') in Shale Gases Produced from the Mississippian Barnett and Fayetteville Formations. *Mar. Petroleum Geol.* 31, 43–52. doi:10.1016/j.marpetgeo.2011.06.009

Conflict of Interest: Authors SQ, BZ, and CH were employed by the company Southwest Oil and Gas Company, PetroChina.

The remaining authors declare that the research was conducted in the absence of any commercial or financial relationships that could be construed as a potential conflict of interest.

Publisher's Note: All claims expressed in this article are solely those of the authors and do not necessarily represent those of their affiliated organizations, or those of the publisher, the editors, and the reviewers. Any product that may be evaluated in this article, or claim that may be made by its manufacturer, is not guaranteed or endorsed by the publisher.

Advantages of publishing in Frontiers

OPEN ACCESS
Articles are free to read for greatest visibility and readership

FAST PUBLICATION
Around 90 days from submission to decision

HIGH QUALITY PEER-REVIEW
Rigorous, collaborative, and constructive peer-review

TRANSPARENT PEER-REVIEW
Editors and reviewers acknowledged by name on published articles

Frontiers
Avenue du Tribunal-Fédéral 34
1005 Lausanne | Switzerland

Visit us: www.frontiersin.org
Contact us: frontiersin.org/about/contact

REPRODUCIBILITY OF RESEARCH
Support open data and methods to enhance research reproducibility

DIGITAL PUBLISHING
Articles designed for optimal readership across devices

FOLLOW US
@frontiersin

IMPACT METRICS
Advanced article metrics track visibility across digital media

EXTENSIVE PROMOTION
Marketing and promotion of impactful research

LOOP RESEARCH NETWORK
Our network increases your article's readership